Chemistry of highly reactive group 5 and 6 transition metal compounds: Modeling aspects of the industrial hydrotreating process and synthesis of the first transition metal complexes that feature a [*CCC*] X_3-donor pincer ligand

Aaron Sattler

Submitted in partial fulfillment of the
requirements for the degree
of Doctor of Philosophy
in the Graduate School of Arts and Sciences

Columbia University
2012

ABSTRACT

Chemistry of highly reactive group 5 and 6 transition metal compounds: Modeling aspects of the industrial hydrotreating process and synthesis of the first transition metal complexes that feature a [*CCC*] X_3-donor pincer ligand

Aaron Sattler

Trimethylphosphine complexes of tungsten and molybdenum have been used to model the coordination chemistry and reactivity that may be observed on the surface of an industrial hydrotreating catalyst. Most notably, it was observed that $W(PMe_3)_4(\eta^2–CH_2PMe_2)H$ is capable of (*i*) the unprecedented cleavage of an aromatic carbon–carbon bond, and (*ii*) desulfurizing thiophene, benzothiophene, and dibenzothiophene. In addition to the group 6 chemistry, the first [*CCC*] X_3-donor pincer ligand for a transition metal was synthesized by two consecutive cyclometalations of a terphenyl complex of the group 5 metal tantalum.

Chapter 1 describes two new transformations that occur between $W(PMe_3)_4(\eta^2–CH_2PMe_2)H$ and haloarenes, namely the formation of (*i*) the alkylidene complex, $[W(PMe_3)_4(\eta^2–CHPMe_2)H]X$ (X = Br or I) and (*ii*) the phosphoniocarbyne complex, $W(PMe_3)_3Cl_2(CPMe_2Ph)$. Additionally, treatment of $[W(PMe_3)_4(\eta^2–CHPMe_2)H]X$ with $LiAlD_4$, allows for the isolation of the isotopomer $W(PMe_3)_4(\eta^2–CHDPMe_2)H$, thereby providing a means to measure the rate constant for the formation of the 16-electron species $[W(PMe_3)_5]$ from $W(PMe_3)_4(\eta^2–CH_2PMe_2)H$.

Chapter 2 describes the reactivity of trimethylphosphine complexes of molybdenum with phenazine and related N-heterocycles, in order to model aspects of hydrodenitrogenation. Several new coordination modes of phenazine to molybdenum

were observed. Studies also indicate that oxidative addition of H_2 is promoted by (*i*) incorporation of nitrogen substituents into the central ring and (*ii*) ring fusion. Furthermore, ring fusion promotes hydrogenation of the heterocyclic ligand.

Chapter 3 describes the novel aromatic carbon–carbon bond cleavage and dehydrogenation of quinoxaline by $W(PMe_3)_4(\eta^2\text{–}CH_2PMe_2)H$, giving the chelating *bis*-isocyanide complex, $[\kappa^2\text{-}C_2\text{-}C_6H_4(NC)_2]W(PMe_3)_4$.

Chapter 4 describes the reactivity of trimethylphosphine complexes of tungsten and molybdenum with thiophenes, in order to model aspects of hydrodesulfurization. $Mo(PMe_3)_4H_4$ desulfurizes thiophene and benzothiophene. Moreover, $W(PMe_3)_4(\eta^2\text{–}CH_2PMe_2)H$ is the first tungsten complex that is capable of desulfurization of thiophene, benzothiophene and dibenzothiophene.

Chapter 5 describes the reactivity of trimethylphosphine complexes of tungsten and molybdenum with furans, in order to model aspects of hydrodeoxygenation. Most notably, $Mo(PMe_3)_4H_4$ is capable of cleaving the C–C, C–O, and C–H bonds of furan, thereby producing propene and carbon monoxide.

Chapter 6 describes the synthesis of the first [*CCC*] X_3-donor pincer ligand for a transition metal. Specifically, addition of PMe_3 to $[Ar^{Tol_2}]TaMe_3Cl$ ($[Ar^{Tol_2}]$ = 2,6-di-*p*-tolylphenyl) induces elimination of methane and formation of the pincer complex, $[\kappa^3\text{-}Ar^{Tol'_2}]Ta(PMe_3)_2MeCl$ (Tol′ = C_6H_3Me). Reduction of $[\kappa^3\text{-}Ar^{Tol'_2}]Ta(PMe_3)_2Cl_2$ with KC_8 in benzene gives the arene complex $[\kappa^3\text{-}Ar^{Tol'_2}]Ta(PMe_3)_2(\eta^6\text{-}C_6H_6)$, which is the first structurally characterized benzene complex of tantalum. Deuterium labeling employing $Ta(PMe_3)_2(CD_3)_3Cl_2$ demonstrates that the pincer ligand is generated by a pair of Ar–H/Ta–Me sigma-bond metathesis transformations, rather than by a mechanism that involves α–H abstraction by a tantalum methyl ligand. The [*CCC*] pincer ligand ($[\kappa^3\text{-}Ar^{Tol'_2}]$) was also synthesized on niobium.

Chapter 7 describes the synthesis of a variety of other terphenyl complexes of tantalum, namely $[Ar^{Tol_2}]Ta(NMe_2)_3X$ (X = Me, Et, Pr^n, Bu^n, Np, BH_4, and $[Ar^{Tol_2}]$), all of

which cyclometalate under varying conditions to give $[\kappa^2\text{-}Ar^{Tol,Tol'}]Ta(NMe_2)_3$. The dialkyl complexes, $[Ar^{Tol_2}]Ta(NMe_2)_2R_2$ (R = Me, Et, Pr^n, Bu^n, and Np) have also been synthesized from the dichloride complex, $[Ar^{Tol_2}]Ta(NMe_2)_2Cl_2$. The *bis*-neopentyl complex, $[Ar^{Tol_2}]Ta(NMe_2)_2Np_2$, is not stable in solution at room temperature and converts to $[\kappa^2\text{-}Ar^{Tol,Tol'}]Ta(NMe_2)_2Np$ and neopentane, of which the former isomerizes to produce $[\kappa^2\text{-}Ar^{*Tol,Tol'}]Ta(NMe_2)_2Np$ (* indicates the new connectivity of the aryl ligand).

TABLE OF CONTENTS

ACKNOWLEDGEMENTS

First, I would like to thank my research advisor, Professor Gerard Parkin (whom I call Ged or G), for allowing me to join his research group in the spring of 2008. My graduate school experience over the past five years in your research group has been really, really, really great. Thank you for teaching me (*i*) how to become a synthetic inorganic chemist, (*ii*) how work with extremely air and water sensitive chemicals, (*iii*) how to be an X-ray crystallographer, (*iv*) how to analyze complex NMR spectra and (*v*) many other invaluable techniques in a chemistry laboratory. Besides for the physical techniques I've learned from you, you have taught me how to *think* critically about chemistry (*e.g.* why oxidation states are important and why not to use Green's Covalent Bond Classification method…joking). In addition to research, I was able to be a teaching assistant for you in General Chemistry three times, in addition to Structural Methods in Inorganic Chemistry; these experiences were not only enjoyable, but taught me a great deal about how to be an effective and superior teacher. Overall, it has been an unbelievably great five years, and so I thank you for allowing me to have this experience, for being my Ph.D. advisor, but most importantly, for being my friend.

I want to also thank the members of my graduate committee: Professor Jack Norton and Professor Scott Snyder. You have both been very supportive from the day we met, and I will always be appreciative for that. Jack, thank you for the advice and knowledge you have given me when I took your classes, and also when I would just show up at your office with questions, where you were more than willing to help. Scott, I also want to thank you for all your help and support over the past five years; I have stopped by your office numerous times and you have been nothing but very helpful with my questions concerning organic chemistry, in addition to my postdoctoral search and fellowships.

I would also like to thank my dissertation committee, Professor Jack Norton, Professor Jonathan Owen (Jon), Professor Jun Ho Shin, and Professor John Magyar, for taking the time to read my thesis and serving on my committee. Additionally, I want to thank Jon for his advice and support over the past three years concerning my research, postdoctoral search and fellowships, it has been really great getting to know you.

I want to also thank Professor Daniela Buccella of New York University. When I first met Daniela (who I also call DB or Deeb), she was a fifth year graduate student in the Parkin group and I was a new first year graduate student. For some reason, Daniela took me (and my twin Wes) under her wings, and taught me how to be a chemist. On my third day in lab, we synthesized "WP_5" together (well, mostly her doing and me watching) and I was fascinated with how confident and competent Daniela was with such reactive chemicals and foreign objects to me (Schlenk line, Schlenk tubes, ampoules, PMe_3, NaK…). I was inspired. I wanted to know as much as she did and luckily, Daniela didn't mind (too much) that I asked her around 50 questions per day. Even though Daniela was finishing up her thesis, preparing for her post-doc, making a talk for the Hammett Award, and more, she spent so much time teaching and training me and I will forever be grateful. Thank you for also teaching me your secrets and skills for solving crystals. Not only did she teach me chemistry and lab technique, but she also became one of my very good friends. Getting lunch together (you and the bodyguards, as "first-year" would say) was so much fun. You always looked out for me throughout your post-doc at MIT and your professorship at NYU. Our many skype chats and visits to Boston and NYU have all been great! Additionally, I had the privilege of meeting your husband, Dr. Collin Chan, who has answered many questions about organic chemistry, and has also become a great and very generous friend; thanks so much to you both!

I would also like to thank Professor Bruce Bursten. It was great having you come to group meetings and discussing interesting chemistry topics, such as molecular orbital

theory and group theory. Also, thanks for all your support and advice with my post-doc and fellowships.

Many thanks also go to my twin brother, Wesley Sattler (who I call: Wes, Wiz, The Wiz, and Wizzy). Wes has been an incredible labmate over the past five years, being extremely helpful with the physical techniques for synthesis and just talking about chemistry in general, always having good insight and advice. More importantly, he has been an unbelievable roommate, brother, twin, and friend to me for my whole life and I know that my experience here at Columbia would not be close to what it was without him. I am extremely lucky to have you as my brother and best friend. Thanks bro!

I want to also thank two of my very good friends who have been there for me for the past nine years: Johnny Gartiser (Dream) and Eric Harris (E). From the beginning of our friendship until now, you both have been nothing but helpful and supportive in all aspects of my life, including my chemistry aspirations. You are both family to me. Your numerous trips to the city to go out and have several social beverages with Wes and me helped keep us cheerful and I will miss this very much when I am in California. Good luck to you both in your teaching and coaching careers.

I need to also thank Ahmed Al-Harbi, informally known as Ack or Ack the Doc. Ahmed (my amigo) has been an unbelievable friend and labmate for four years. Thanks for your help with organic chemistry and teaching me how to run my first column. He has taught me a lot about life, staying calm, and being happy, and he truly wants the best for me. I am looking forward to seeing you become the best chemist that Saudi Arabia has and I am sure we will be close life-long friends. Thanks amigo.

I want to also thank Yi Rong (E) for being great! You are like my little sister and every time I see you, I smile. Your personality and sense of humor is great, and made the whole lab happier on a daily basis. I will miss you Yi.

I want to also thank Ashley Zuzek for being a great friend and labmate over the past three years. It has been a lot of fun working on the HDO project with you. I hope you get as lucky as I did with your next deskmate! Also, thank you very much for making sure my thesis was delivered to Prof. Shin.

I want to also thank Serge Ruccolo, a new member of the Parkin group. Serge worked with me when I first started research with $TaMe_3Cl_2$ during his six-month research experience before graduate school. I always liked French toast and French fries, and I'm glad I can now say that I like a French guy named Serge, who has become one of my good friends.

I want to also thank all of my labmates over the past five years: Ava Kreidler-Mueller (for being a great friend and always willing to get a coffee), Neena Chakrabarti (for always providing a needed laugh), Julia Oktawiec (the greatest Columbia undergraduate in the world and a pleasure to work with in lab), Dr. Joshua Palmer, Michelle Neary, Ben Kriegel, Greg Theophall, Dr. Victoria Landry , Dr. Keliang Pang, Dr. Kevin Yurkerwich, Ariel Schaap, Joseph Ulichny, and Douglas Villalta, who have made my graduate school experience what it was. Thanks to Yi, Ahmed, Ashley, Ava, Neena, Josh, and Serge for reading over my thesis for me. Good luck to the entire Parkin group!

Thanks to Dr. Dan Treitler (T-bone) for all your help and advice with organic chemistry over the past five years. Also, thanks for being a pivotal part in the birth of the "Wungsten Warriors", the greatest Columbia Chemistry intramural football team ever. Thanks for being a great friend these past five years and best of luck for your career at BMS.

Thank you Dr. Adel Elsohly. It has been great discussing chemistry with you, as you are so insightful. You have also been a great friend to me since I met you, so thanks! Good luck to you at Berkeley and with your beautiful wife and daughter, Donia and Iris.

Thank you Alex Brucks. It has been great getting to know you and becoming great friends. I will miss just hanging out watching TV and going to 1020.

Thank you Nate Wright. You have been nothing but kind and supportive since I met you, and I appreciate it. Thanks for being such a good friend.

I also want to thank: Dr. Chris Plummer, James Eagen, Jeff Bandar, Stephen Thomas, Dr. Brandi Cossairt, Steven Breazzano, Dr. Wes Chalifoux, Dan Griffith, Myles Smith, Alex Buitrago, Jessie Joussot (Jejo) and a special thanks to Andrea Wycoff; you have all contributed to my graduate school career in different ways and my experience here would not have been as incredibly great without you all. Thank you all for your friendship and support!

I also want to thank Jeffrey Lancaster for his help with Microsoft Word (*e.g.* Table of Contents, cross-references, captions etc…), which made writing this thesis easier (and also for always being a nice guy to me).

I would also like to thank Professor Gilbert Stork for allowing me to get to know you! It's an honor. Our interactions and discussions have been amazing. Also, thank you, Professor Stork and Dr. Ayako Yamashita, for your support, advice, kindness, and for a truly unforgettable lunch.

Many thanks also go to Dr. John Decatur for setting up so many NMR experiments, which were crucial for my research. Additionally, thanks for always being open to my questions about NMR concepts and taking the time to explain this difficult information to me. Thank you also to Michael Appel for helping to keep the NMR facility in great shape and always being friendly.

I also want to thank Dr. Yasuhiro Itagaki for all your help with my air-sensitive mass-specs and good conversation at happy hours.

I also want to thank Dr. Calman Lobel for keeping my calculations running over the past five years.

Thank you to Professor Nick Turro and Dr. Steffen Jockush for allowing me to use their photoreactor.

Thank you to Song Yu for helping me find research articles that were not readily accessible through the Columbia library services.

I would like to thank the entire chemistry department, for making Columbia such a great and special place to do my graduate research. Socky and Daisy (you are so supportive and great to Wes and me, I will miss my visits to your office), Carlos and Emilia (thanks for making sure I got paid and for good conversation), Alix and Dani (for all your help with registration and SSOL over the past five years, and also for booking room 209 for my defense), Jay (for keeping our lab working well and always being friendly and helpful), Robert, Chris, Bill, and Felix (for being great and friendly guys to me). You have all been so friendly since I met you, and this place would not work without you!

Thank you to Dr. Louis Avila for being so welcoming when I started graduate school and for organizing a great STAT program. Thank you also for your continued friendship and support.

Thank you Maria and Wallace for keeping out lab tidy!

I would also thank Mr. Walsh, from Ardsley Middle School, who first showed me how cool science was and how great it could be to be a scientist. I would also like to thank two professors from Binghamton University, Professor Wayne E. Jones and Professor James Dix, who inspired me to go to graduate school for chemistry. You both were nothing but extremely supportive during my years at Binghamton. I would also like to thank Justin Martin, the graduate student in Dr. Jones lab who I worked with, for spending many hours teaching me about research (and beer), and for being a supportive friend and colleague.

I also want to thank Ged's family, Rita, Lia and Catherine. It was great getting to know you and I've enjoyed our outings together very much. Lia and Catherine are great girls, you should be very proud!

I want to also thank my grandparents: Grandma Irma, Grandpa Harry, Poppy Paul and Grandma Florence (who we call Einstein or T-bone, and has been a lot of fun to hang out with and talk to, always providing good advice and a good laugh) and my great-grandma, G.G..

The last and most important thank you is for my Mom and Dad. You are truly the greatest parents a kid could have. You have taught me (and Wes) so much, and I am the person I am today because of you two. Since the day we were born, you chose to make us your number one priority and it shows. You have been nothing but loving and supportive in all aspects of my life, and I am truly grateful. All of my friends who meet you think you are the greatest because you are. Our family is the most important aspect of my life and always will be. Thank you and I love you so much!

For my Mom and Dad, I love you guys!

CHAPTER 1

Formation of a cationic alkylidene complex *via* formal hydride abstraction: Synthesis and structural characterization of $[W(PMe_3)_4(\eta^2–CHPMe_2)H]X$ (X = Br, I)

Table of Contents

Reproduced in part from:

Sattler, A.; Parkin, G. *Chem. Commun.* **2011**, *47*, 12828–12830.

1.1 Introduction

1.1.1 Trimethylphosphine compounds of transition metals

There are several examples of zerovalent homoleptic trimethylphosphine (PMe_3) complexes of transition metals that have been synthesized in the literature, examples of which are: $Mo(PMe_3)_6$,[1] $W(PMe_3)_6$,[2] $Fe(PMe_3)_5$,[3] $Os(PMe_3)_5$,[4] $Co(PMe_3)_4$,[5] $Ni(PMe_3)_4$,[6] $Pd(PMe_3)_4$,[7] and $Pt(PMe_3)_4$.[8] Trimethylphosphine is a ligand that has strong σ-donor properties combined with weak π-acceptor character, causing the aforementioned transition metal PMe_3 complexes, $M(PMe_3)_n$, to be deemed "electron rich". For this reason, oxidative addition reactions are often observed, as exemplified by the intramolecular C–H bond cyclometalation of the early transition metal complexes, $Mo(PMe_3)_6$ and $W(PMe_3)_6$, forming $Mo(PMe_3)_4(\eta^2\text{–}CH_2PMe_2)H$ and $W(PMe_3)_4(\eta^2\text{–}CH_2PMe_2)H$, respectively (Scheme 1). In the molybdenum system, the equilibrium (K_{eq} = 8.6 × 10^{-3} at 30 ˚C) favors $Mo(PMe_3)_6$, thus only a small amount of $Mo(PMe_3)_4(\eta^2\text{–}CH_2PMe_2)H$ and PMe_3 are detected in solution.[9] In contrast, the equilibrium for the tungsten system (K_{eq} = 17.8 at 30 ˚C) lies far towards the cyclometalated derivative, $W(PMe_3)_4(\eta^2\text{–}CH_2PMe_2)H$ (Scheme 1); thus, solutions of $W(PMe_3)_6$ convert to $W(PMe_3)_4(\eta^2\text{–}CH_2PMe_2)H$ and PMe_3 with a half life of *ca*. 2 hours.[2]

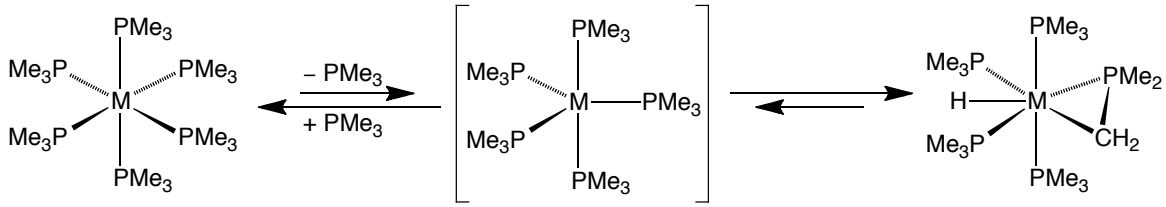

Scheme 1. Intramolecular cyclometalation of $M(PMe_3)_6$ (M = Mo and W) complexes.

1.1.2 $W(PMe_3)_4(\eta^2\text{–}CH_2PMe_2)H$

$W(PMe_3)_4(\eta^2\text{–}CH_2PMe_2)H$,[10] is an electron rich tungsten compound that exhibits diverse reactivity, producing molecules such as: $W(PMe_3)_6$,[2,11] $W(PMe_3)_4(SiH_3)_2H_2$,[12]

$W(PMe_3)_4(\eta^2–CH_2O)H_2$,[13] $W(PMe_3)_4H_2F(FHF)$,[14] $W(PMe_3)_4(Te)_2$,[15] $W(PMe_3)_5H_2$[12] and $W(PMe_3)_4H_4$,[12] as illustrated in Scheme 2. In many cases, the reactivity of $W(PMe_3)_4(\eta^2–CH_2PMe_2)H$ can be interpreted in terms of a pre-equilibrium with the 16-electron complex $[W(PMe_3)_5]$, although in some situations the reactions occur *via* direct attack at the W–C bond. For example, the formation of $W(PMe_3)_6$ upon treatment of $W(PMe_3)_4(\eta^2–CH_2PMe_2)H$ with PMe_3 proceeds *via* $[W(PMe_3)_5]$,[11] while the formation of $W(PMe_3)_4(\kappa^2–OC_6H_4)H_2$ upon treatment of $W(PMe_3)_4(\eta^2–CH_2PMe_2)H$ with phenol (PhOH) occurs *via* protonation of the W–C bond (Scheme 2).[11]

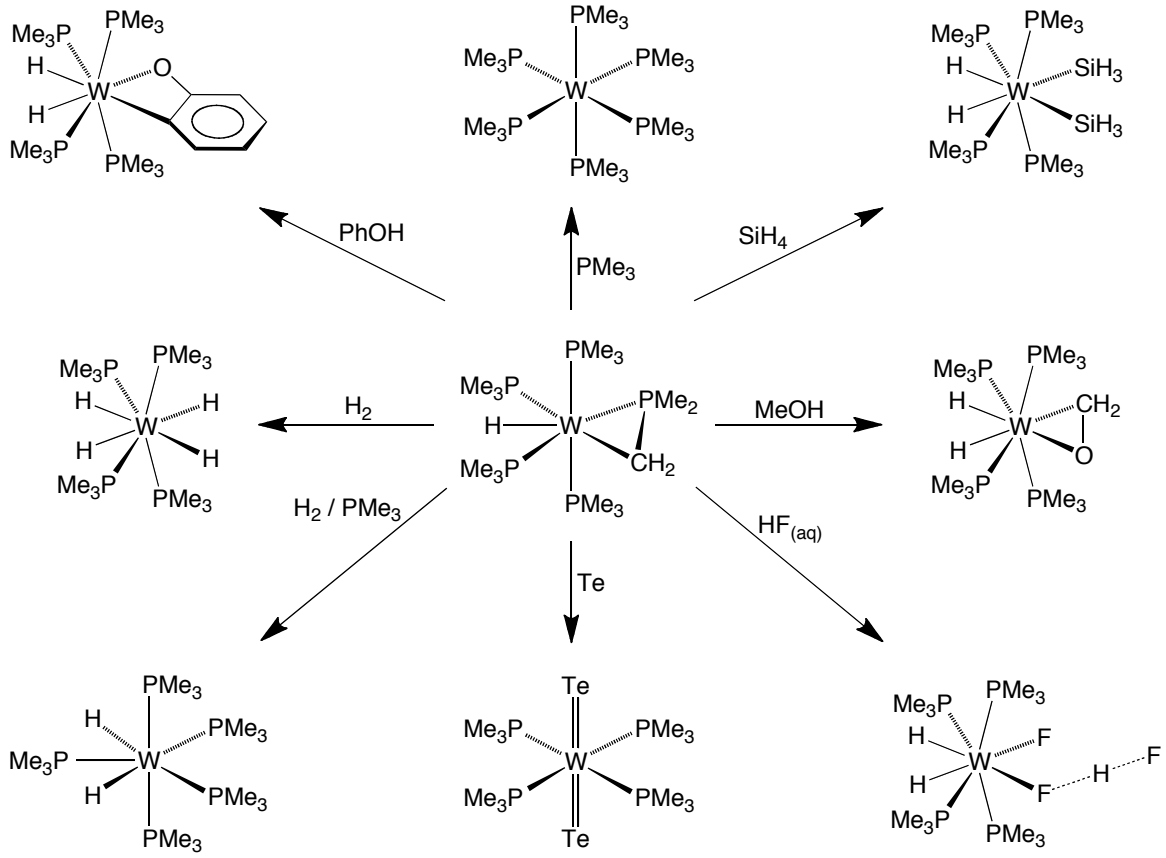

Scheme 2. Reactivity of $W(PMe_3)_4(\eta^2–CH_2PMe_2)H$.

1.1.3 $[W(PMe_3)_4(\eta^2–CHPMe_2)H]^+$: A cationic tungsten alkylidene

Interestingly, we have now observed a new reaction manifold for $W(PMe_3)_4(\eta^2–CH_2PMe_2)H$ that involves the overall formal abstraction of a hydride (H^-) by aryl

bromides and iodides. Specifically, a cationic alkylidene complex, $[W(PMe_3)_4(\eta^2–CHPMe_2)H]X$ (X = Br, I),[16] is produced and this research is described herein.

1.2 Synthesis of $[W(PMe_3)_4(\eta^2–CHPMe_2)H]X$ (X = Br, I)

Treatment of an unstirred yellow solution of $W(PMe_3)_4(\eta^2–CH_2PMe_2)H$ in benzene with either bromobenzene (PhBr) or iodobenzene (PhI) resulted in the deposition of large bright blue-purple crystalline needles, which were identified as $[W(PMe_3)_4(\eta^2–CHPMe_2)H]X$ (X = Br, I respectively) by X-ray diffraction (Scheme 3).[17] In order to obtain information concerning the fate of the aryl group, $W(PMe_3)_4(\eta^2–CH_2PMe_2)H$ was treated with *p*-bromotoluene (*p*-TolBr); the formation of toluene was observed as analyzed by ^1H NMR spectroscopy, thereby indicating that a formal hydride abstraction had taken place. A minor byproduct of the reaction was identified as $[Me_3PPh]X$ (X = Br, I); in the case of the iodide reaction, this was easily removed by washing with H_2O. On the other hand, the bromide derivative, $[W(PMe_3)_4(\eta^2–CHPMe_2)H]Br$, was appreciably soluble in H_2O;[18] thus, the $[Me_3PPh]Br$ could not be washed away with H_2O and was, therefore, not removed. Interestingly, extraction of the crystalline products with D_2O allowed us to obtain NMR spectroscopic data for aqueous $[W(PMe_3)_4(\eta^2–CHPMe_2)H]Br$, confirming that the bright blue-purple solution formed after addition of H_2O was actually $[W(PMe_3)_4(\eta^2–CHPMe_2)H]Br$, and not a "tungsten-blue" decomposition product.

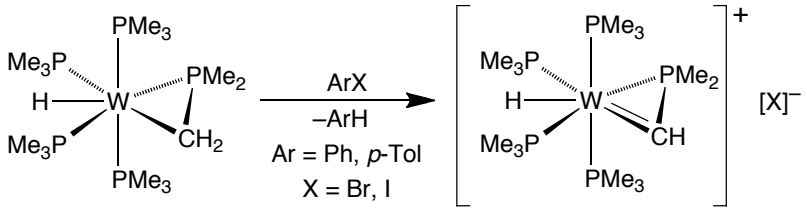

Scheme 3. Synthesis of $[W(PMe_3)_4(\eta^2–CHPMe_2)H]X$ (X = Br, I).

The most interesting feature of $[W(PMe_3)_4(\eta^2\text{–}CHPMe_2)H]^+$ is the presence of the η^2–$CHPMe_2$ alkylidene ligand, evidence for which is provided by both X–ray diffraction (Figure 1) and NMR spectroscopy (*vide infra*). While the oxidative addition of a single C–H bond of a PMe_3 ligand to generate an η^2–CH_2PMe_2 ligand is relatively common,[19,20] the cleavage of *two* C–H bonds to generate the η^2–$CHPMe_2$ alkylidene ligand has little precedent. Furthermore, the only structurally characterized compounds listed in the Cambridge Structural Database[21] that feature the η^2–$CHPMe_2$ ligand are tantalum derivatives, namely $Ta(PMe_3)_3(\eta^2\text{–}CH_2PMe_2)(\eta^2\text{–}CHPMe_2)$,[10] $Ta(PMe_3)_2(\eta^4\text{–}C_4H_6)(\eta^2\text{–}CHPMe_2)Cl$,[22] $Cp^*Ta(PMe_3)(\eta^2\text{-}CHPMe_2)H_2$[23] and $Cp^*Ta(PMe_3)(CH_2CH_2CMe_3)_2(\eta^2\text{–}CHPMe_2)$.[24,25]

1.3 Structural features of $[W(PMe_3)_4(\eta^2\text{–}CHPMe_2)H]X$ (X = Br, I)

The molecular structures of $[W(PMe_3)_4(\eta^2\text{–}CHPMe_2)H]X$ (X = Br, I) are shown in Figure 1 and are similar to that of $W(PMe_3)_4(\eta^2\text{–}CH_2PMe_2)H$,[26] which is shown in Figure 2. A notable distinction, however, pertains to the W–C bond lengths. Specifically, the W–C bond of $[W(PMe_3)_4(\eta^2\text{–}CHPMe_2)H]^+$ [1.978(3) Å for X = Br; 1.981(4) Å for X = I] is 0.33 Å shorter than that in $W(PMe_3)_4(\eta^2\text{–}CH_2PMe_2)H$ [2.312(2) Å]. The substantial shortening is in accord with the presence of a W=C double bond within $[W(PMe_3)_4(\eta^2\text{–}CHPMe_2)H]^+$. The average W=C bond length of 1.98 Å for the bromide and iodide derivatives is identical to the mean value for structurally characterized compounds with W=C double bonds listed in the Cambridge Structural Database,[21] and is respectively shorter and longer than the mean values for W–C single (2.22 Å) and W≡C triple (1.81 Å) bonds. While not as pronounced as the difference in W–C bond lengths, another interesting structural comparison is that the W–P bonds of $[W(PMe_3)_4(\eta^2\text{–}CHPMe_2)H]^+$ are 0.01 – 0.11 Å *longer* than those in $W(PMe_3)_4(\eta^2\text{–}CH_2PMe_2)H$ (Table 1).[27]

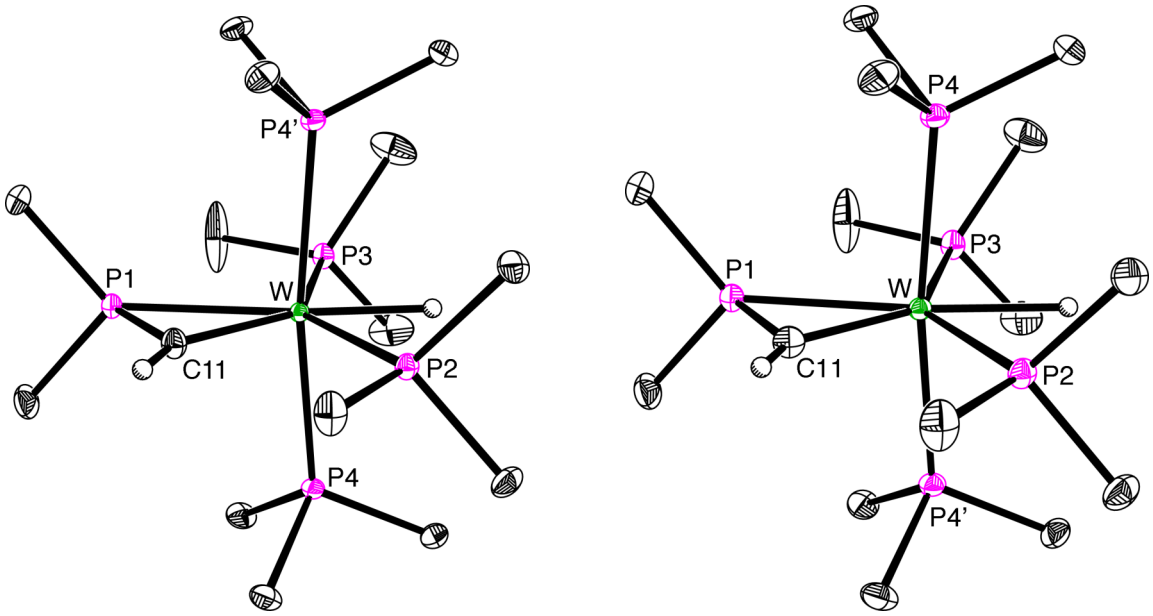

Figure 1. Molecular structures of $[W(PMe_3)_4(\eta^2\text{–}CHPMe_2)H]Br$ (left) and $[W(PMe_3)_4(\eta^2\text{–}CHPMe_2)H]I$ (right); only cations shown.

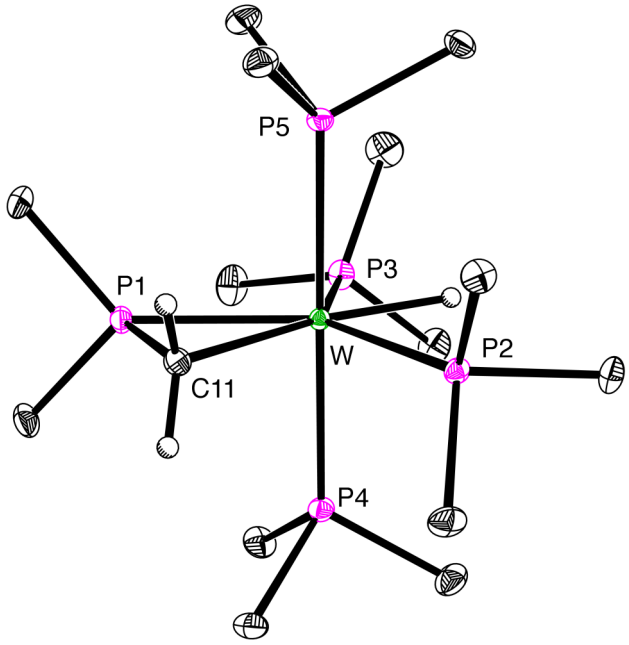

Figure 2. Molecular structure of $W(PMe_3)_4(\eta^2\text{–}CH_2PMe_2)H$.

Table 1. Selected bond lengths (Å) for $W(PMe_3)_4(\eta^2–CH_2PMe_2)H$ and $[W(PMe_3)_4(\eta^2–CHPMe_2)H]^+$.

	$W(PMe_3)_4(\eta^2–CH_2PMe_2)H$	$[W(PMe_3)_4(\eta^2–CHPMe_2)H]X$		Δ^a
		X = Br	X = I	
W–C11	2.312(2)	1.978(3)	1.981(4)	0.333
W–P1	2.3718(6)	2.4489(9)	2.446(1)	–0.076
W–P2	2.4465(5)	2.4556(9)	2.452(1)	–0.008
W–P3	2.4242(6)	2.5361(9)	2.532(1)	–0.110
W–P4	2.4156(6)	2.5049(8)	2.5034(8)	–0.089
W–P5(P4′)	2.4212(6)	2.5049(8)[b]	2.5034(8)[b]	–0.083
W–H	1.73(3)	1.72(3)	1.88(6)	–[c]

(a) $\Delta = d[W(PMe_3)_4(\eta^2–CH_2PMe_2)H] – d\{[W(PMe_3)_4(\eta^2–CHPMe_2)H]^+\}_{av}$.

(b) P5 = P4′.

(c) Δ is insignificant due to the large e.s.d.'s associated with the hydride position.

1.4 NMR spectroscopic features of $[W(PMe_3)_4(\eta^2–CHPMe_2)H]X$

Spectroscopic evidence for the presence of the alkylidene moiety in $[W(PMe_3)_4(\eta^2–CHPMe_2)H]^+$ is provided by the observation of a signal at 224.4 ppm in the ^{13}C NMR spectrum that exhibits coupling to all five phosphorus nuclei [$^1J_{P–C}$ = 50 Hz (d) and $J_{P–C}$ = 13 (quintet) Hz],[28] and hydrogen [$^1J_{C–H}$ = 174 (d) Hz]. The corresponding alkylidene signal in the ^1H NMR spectrum is observed as a doublet of quintets at 11.85 ppm, exhibiting coupling to the tungsten hydride [J_{H-H} = 13 (d) Hz] and the four PMe_3 ligands [J_{P-H} = 10 (quintet) Hz].[28] The experimental ^1H NMR spectrum, along with the simulated spectrum, are shown in Figure 3. These ^{13}C and ^1H NMR spectroscopic signals of the alkylidene moiety are shifted significantly downfield from the corresponding values of the methylene group of $W(PMe_3)_4(\eta^2–CH_2PMe_2)H$, which are observed at –11.7 ppm [$^1J_{C–H}$ = 144 Hz][29] and 0.43 ppm, respectively.[10] For comparison purposes, the ^1H and ^{13}C chemical shifts of other compounds with $\eta^2–CHPMe_2$ ligands are summarized in Table 2.[10,22,23,25]

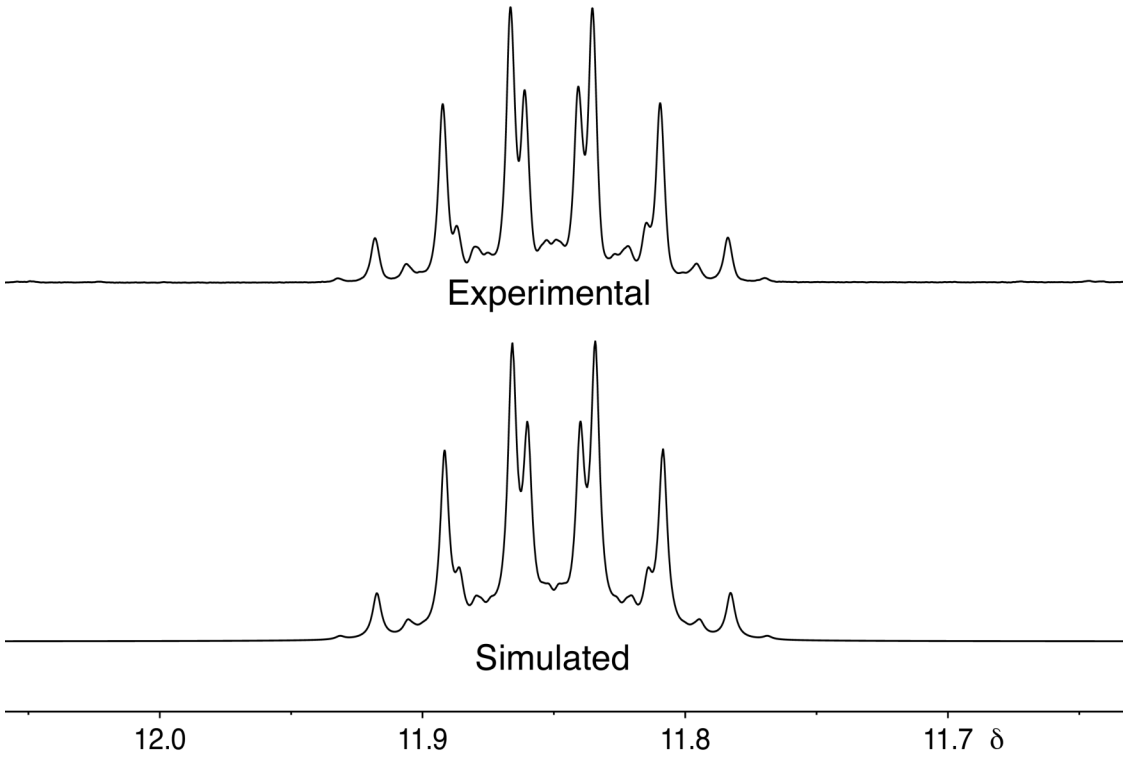

Figure 3. ^{1}H NMR spectra of the alkylidene hydrogen in $[W(PMe_3)_4(\eta^2\text{–}CHPMe_2)H]^+$ (simulated values: $J_{H\text{-}H}$ = 12.63 Hz, $J_{P\text{-}H}$ = 10.32 Hz, $J_{W\text{-}H}$ = 11.20 Hz).

Table 2. NMR Spectroscopic Data for η^2–$CHPMe_2$ Complexes.

	δ ^{13}C	**δ ^{1}H**	**δ ^{31}P**	**$^{1}J_{C\text{–}H}$ / Hz**	**$^{1}J_{P\text{–}C}$ / Hz**	**Ref.**
$[W(PMe_3)_4(\eta^2\text{–}CHPMe_2)H]^+$	224.4	11.85	–153.8	174	50	16
$Ta(PMe_3)_3(\eta^2\text{–}CH_2PMe_2)(\eta^2\text{–}CHPMe_2)$	193.5	9.46	–77.5	–[a]	78	10
$Ta(PMe_3)_2(\eta^4\text{–}C_4H_4)(\eta^2\text{–}CHPMe_2)Cl$	173.1	8.85	–118.2	158	50	22
$Ta(PMe_3)_4(\eta^2\text{–}CHPMe_2)Cl$	187.8	9.46	–139.6	161	73	22
$Ta(PMe_3)_2(\eta^2\text{–}CH_2PMe_2)(\eta^2\text{–}CHPMe_2)H_2$	170	8.10	–124.0	–[a]	–[a]	22
$Cp^*Ta(PMe_3)(\eta^2\text{–}CHPMe_2)H_2$	192.1	9.19	–[a]	171	53	23a
$Cp^*Ta(PMe_3)(\eta^2\text{–}CHPMe_2)HBr$	196.7	9.22	–[a]	–[a]	49	25
$Cp^*Ta(PMe_3)(\eta^2\text{–}CHPMe_2)HI$	202.1	9.53	–[a]	–[a]	50	25
$Cp^*Ta(PMe_3)(\eta^2\text{–}CHPMe_2)Br_2$	207.1	10.49	–28.4	–[a]	48	25

(a) Values not listed.

Another interesting feature of the ^{1}H NMR spectrum of $[W(PMe_3)_4(\eta^2–CHPMe_2)H]^+$ is that the hydride signal is observed as a doublet of doublet of quintets [J_{H-H} = 12 (d), J_{P-H} = 16 (d) and $^2J_{P-H}$ = 37 (quintet) Hz],[28] whereas the hydride signal of $W(PMe_3)_4(\eta^2–CH_2PMe_2)H$ is only a quintet [$^2J_{P-H}$ = 39 Hz].[10] Thus, while the hydride ligand of $[W(PMe_3)_4(\eta^2–CHPMe_2)H]^+$ couples to all phosphorus nuclei and the alkylidene hydrogen,[30] the hydride ligand of $W(PMe_3)_4(\eta^2–CH_2PMe_2)H$ exhibits coupling to only four of the five phosphorus nuclei, and does not couple to the methylene hydrogens.[10] The experimental and simulated spectra for the hydride signal of $[W(PMe_3)_4(\eta^2–CHPMe_2)H]^+$ are shown in Figure 4.

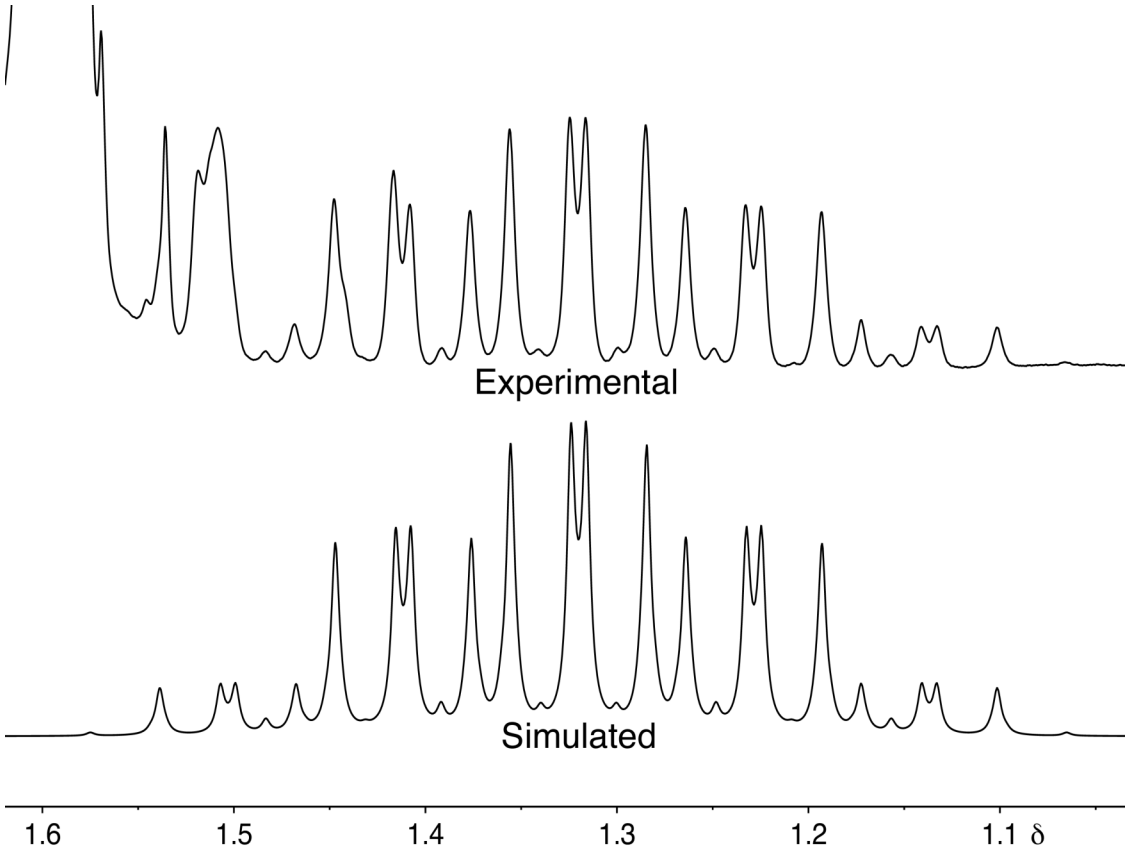

Figure 4. ^{1}H NMR spectra of the tungsten hydride in $[W(PMe_3)_4(\eta^2–CHPMe_2)H]^+$ (simulated values: J_{H-H} = 12.63 Hz, J_{P-H} = 15.81 Hz, $^2J_{P-H}$ = 36.63 Hz, J_{W-H} = 29.00 Hz). In the experimental spectrum, the hydride resonance of $[W(PMe_3)_4(\eta^2–CHPMe_2)H]^+$ is obscured by the PMe_3 resonances.

1.5 Bonding descriptions of η^2–$CHPMe_2$ ligands

The bonding in compounds that feature η^2-$CHPMe_2$ ligands has been discussed in the literature in terms of two resonance forms, namely alkylidene-phosphine (A) and phosphaalkyne (B) structures, that respectively feature M=C and P=C double bonds (Figure 5).[23,25,31] Therefore, we have investigated $[W(PMe_3)_4(\eta^2–CHPMe_2)H]^+$ computationally in order to evaluate which of these alternatives provides the better description for the bonding.

Firstly, the geometry optimized[32] structures of both $[W(PMe_3)_4(\eta^2–CHPMe_2)H]^+$ and $W(PMe_3)_4(\eta^2–CH_2PMe_2)H$ correspond closely to the experimental structures and reproduce the pronounced shortening of the W–C bond upon forming $[W(PMe_3)_4(\eta^2–CHPMe_2)H]^+$. Secondly, an analysis of the Fenske-Hall molecular orbitals[33] provides excellent evidence for the presence of a W–C π-bond (Figure 6) and hence an alkylidene-phosphine (A) description of the bonding. Thus, as illustrated in Figure 6, the HOMO-1 is a π-bonding molecular orbital derived from overlap of a tungsten d_{xz} orbital and a carbon p_z orbital,[34] while the HOMO corresponds to a nonbonding tungsten d_{yz} orbital, consistent with a d^2 configuration. In contrast, both the d_{xz} and d_{yz} orbitals are nonbonding for $W(PMe_3)_4(\eta^2–CH_2PMe_2)H$, in accord with the d^4 configuration of this molecule (Figure 7).

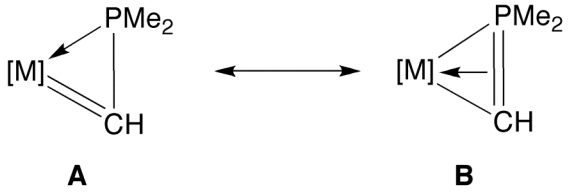

Figure 5. Bonding description of M(η^2–$CHPMe_2$) interaction (the phosphorus atom in resonance **B** is hypervalent).

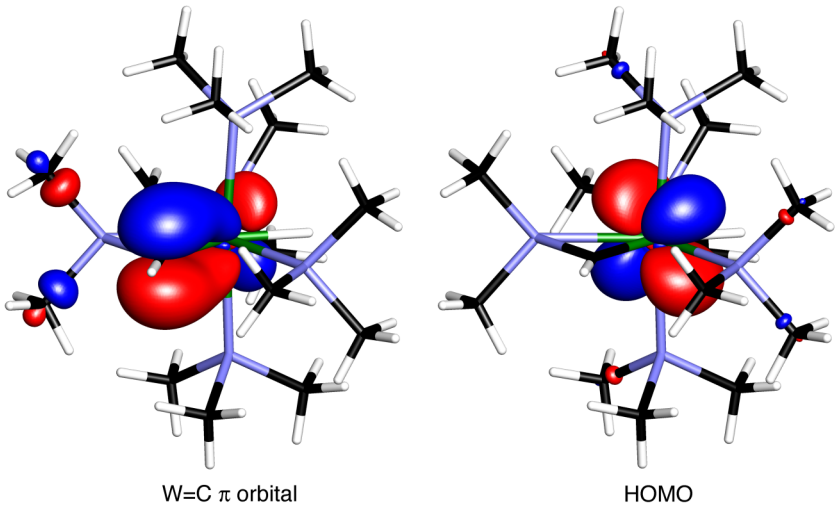

Figure 6. W=C π bonding molecular orbital (left) and HOMO (right) of $[W(PMe_3)_4(\eta^2\text{–}CHPMe_2)H]^+$.

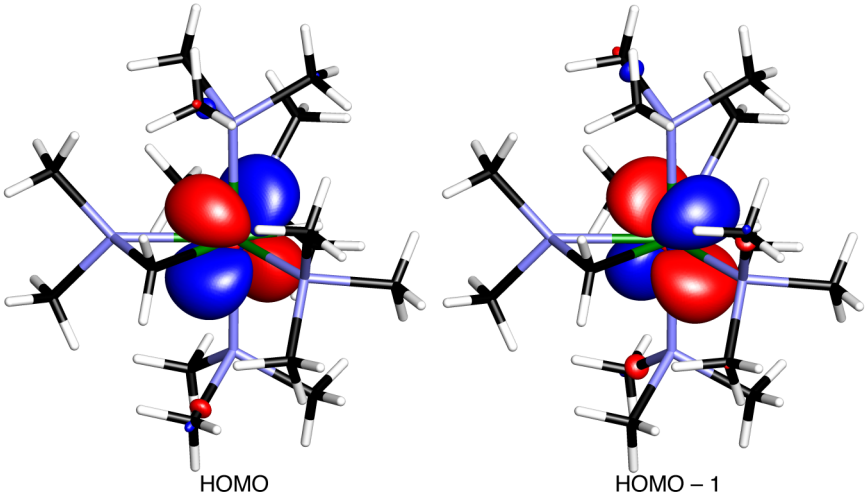

Figure 7. HOMO (left) and HOMO–1 (right) of $W(PMe_3)_4(\eta^2\text{–}CH_2PMe_2)H$.

In support of potential contributions from the alternative phosphaalkyne resonance structure (B), it has been noted that the P–C bond of the metallacycle in $[M(\eta^2\text{–}CHPMe_2)]$ complexes is shorter than the P–CH_3 bonds in PMe_3 ligands.[23,25] However, the P–C bond of the metallacycle within $W(PMe_3)_4(\eta^2\text{–}CH_2PMe_2)H$ [1.766(2) Å] is also shorter than the average value for PMe_3 ligands (1.819 Å)[21] and is only slightly longer than that in the cation, $[W(PMe_3)_4(\eta^2\text{–}CHPMe_2)H]^+$ [1.741(3) Å for X = Br; 1.739(4) Å for X = I]. Thus, it is evident that factors other than double bond character are

responsible for short P–C bonds in such ligands and that $[W(PMe_3)_4(\eta^2\text{–}CHPMe_2)H]^+$ is more appropriately described as an alkylidene-phosphine (A) derivative despite the presence of a short P–C bond.

1.6 Kinetics of the redistribution of deuterium in $W(PMe_3)_4(\eta^2\text{–}CHDPMe_2)H$

While the formation of $[W(PMe_3)_4(\eta^2\text{–}CHPMe_2)H]^+$ by treatment of $W(PMe_3)_4(\eta^2\text{–}CH_2PMe_2)H$ with ArX is irreversible, $W(PMe_3)_4(\eta^2\text{–}CH_2PMe_2)H$ can be regenerated from $[W(PMe_3)_4(\eta^2\text{–}CHPMe_2)H]^+$ by treatment with $LiAlH_4$ (Scheme 4). Interestingly, the corresponding reaction of $[W(PMe_3)_4(\eta^2\text{–}CHPMe_2)H]^+$ with $LiAlD_4$ proceeds such that the deuterium is incorporated regioselectively into the methylene group to form $W(PMe_3)_4(\eta^2\text{–}CHDPMe_2)H$. The ability to isolate this specific isotopomer is of note because subsequent migration of the deuterium label from the methylene site provides a means to probe the rate of forming the 16-electron species $[W(PMe_3)_5]$ by C–H reductive elimination (Scheme 4).

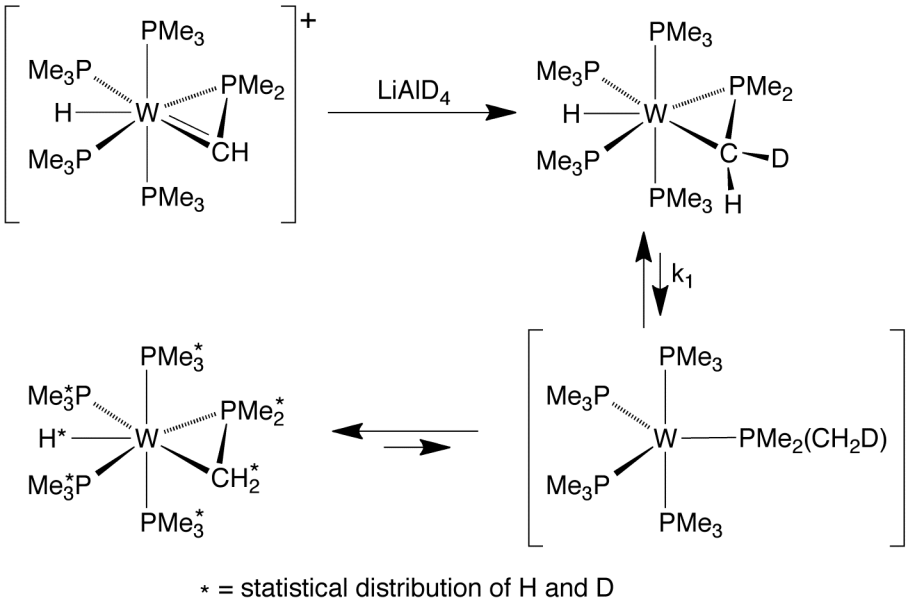

Scheme 4. Regioselective generation of $W(PMe_3)_4(\eta^2\text{–}CHDPMe_2)H$ form $[W(PMe_3)_4(\eta^2\text{–}CHPMe_2)H]^+$ and $LiAlD_4$.

The rate constant for the process (k_1) may be conveniently determined by monitoring the transfer of hydrogen (^{1}H) into the methylene group by using ^{1}H NMR spectroscopy (Figure 8), assuming that the PMe_3 ligands of the 16-electron species [$W(PMe_3)_5$] rapidly interconvert. As can be seen by the NMR spectra in Figure 8, the methylene resonance (δ = 0.40 ppm) increases in intensity with time, indicating the conversion of [CHD] to [CH_2], while there is a negligible change in the intensity of the hydride signal (δ = –3.75 ppm), due to only a statistical amount of deuterium incorporated into the W–H position. In addition to the methylene signal growing in intensity, the shape of the signal changes because the [CHD] and [CH_2] groups have slightly different chemical shifts. Significantly, at 30 ˚C, the derived free energy of activation, $\Delta G^{\ddagger}$ = 24.4(2) kcal mol^{-1}, compares favorably with the value of 24.5(3) kcal mol^{-1} that Rabinovich and Parkin previously determined by indirectly measuring the kinetics and equilibrium of the conversion of $W(PMe_3)_6$ to $W(PMe_3)_4(\eta^2\text{–}CH_2PMe_2)H$ and PMe_3,[2,11,35] thereby validating the original measurement.

In addition to the determination of $\Delta G^{\ddagger}$, monitoring the redistribution reaction of $W(PMe_3)_4(\eta^2\text{–}CHDPMe_2)H$ to a mixture of d_1-D-$W(PMe_3)_4(\eta^2\text{–}CH_2PMe_2)H$ isotopomers at different temperatures allowed for the determination of the activation parameters, $\Delta H^{\ddagger}$ = 24(2) kcal mol^{-1} and $\Delta S^{\ddagger}$ = –3(6) cal mol^{-1} K^{-1}. It should be noted that at 30 ˚C, the reaction was also monitored in the presence of free PMe_3 and there was a negligible effect on the reaction rate; these observation, therefore, indicate that PMe_3 dissociation is not occurring prior the rate determining step, consistent with the proposed mechanism. The rate constant data obtained can be seen in Table 3.

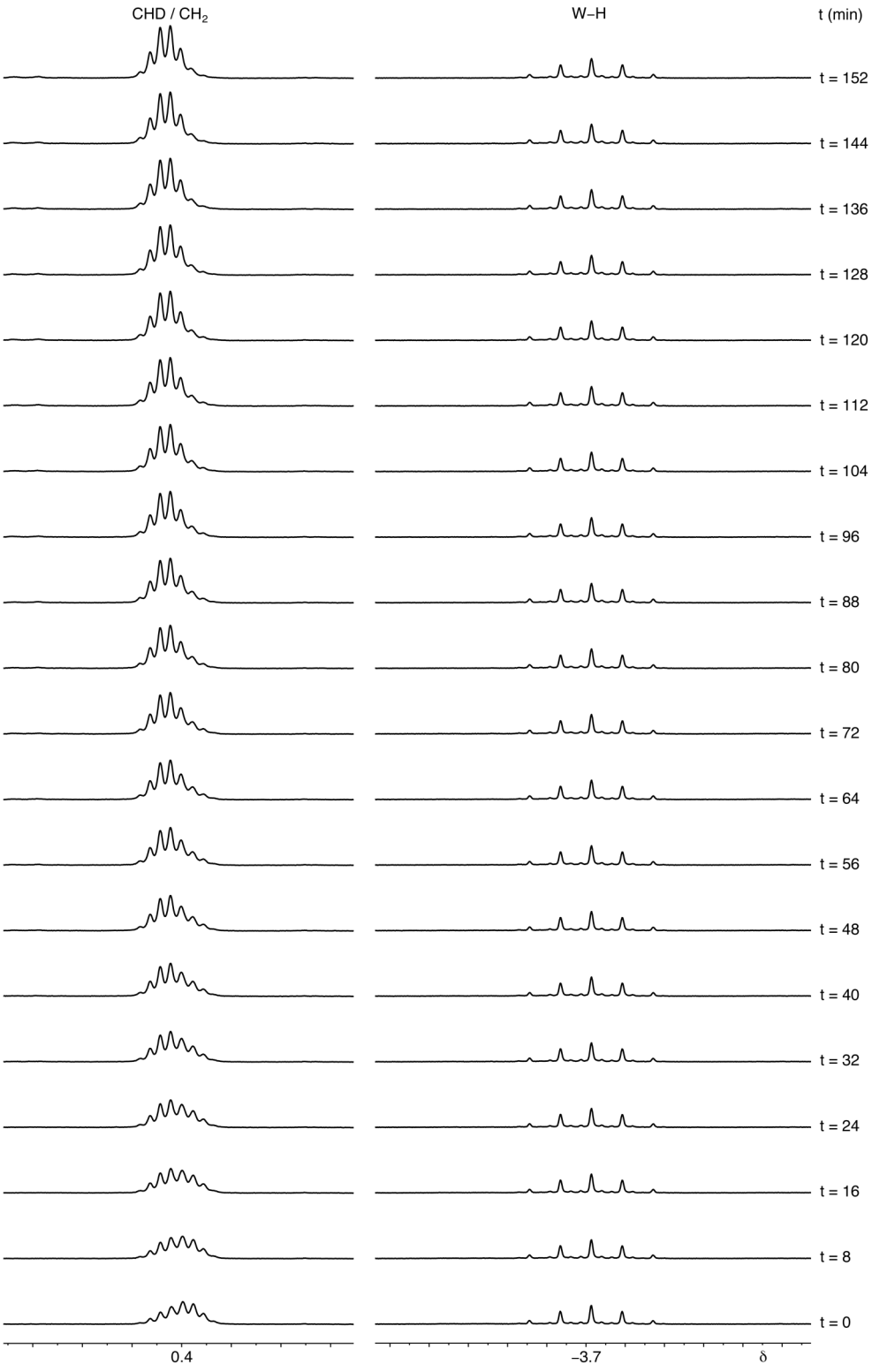

Figure 8. ^{1}H NMR spectra for isomerization of $W(PMe_3)_4(\eta^2\text{–}CHDPMe_2)H$ at 53°C (only every 5th spectrum shown).

Table 3. Rate constant data (k_1) for isomerization of $W(PMe_3)_4(\eta^2–CHDPMe_2)H$.[a]

Temperature (°C)	[PMe_3] (mM)	k_1 (s^{-1})
30	–	$1.6(5) \times 10^{-5}$
30	1.9	$2.0(2) \times 10^{-5}$ [b]
30	9.4	$1.3(4) \times 10^{-5}$
53	–	$2.08(8) \times 10^{-4}$
64	–	$9.9(5) \times 10^{-4}$

(a) Activation parameters: $\Delta H^{\ddagger} = 24(2)$ kcal mol^{-1}; $\Delta S^{\ddagger} = -3(6)$ cal mol^{-1} K^{-1}.

(b) The hydride signal of d_1-$W(PMe_3)_4(\eta^4$-$CH_2PMe_2)H$, rather than that of mesitylene, was used as the integration standard due to a small amount of decomposition during this experiment. In this regard, although deuterium is incorporated into the hydride site during the course of the reaction, the statistical variation in its intensity (from 1.00 to 0.98) is small compared to other sources of error in the experiment. Thus, any error introduced by using the hydride signal is considered to be negligible.

1.7 Mechanism of formation of $[W(PMe_3)_4(\eta^2–CHPMe_2)H]^+$

Isolation of $W(PMe_3)_4(\eta^2–CHDPMe_2)H$ also provides a means to obtain mechanistic information concerned with the formation of the alkylidene complex, $[W(PMe_3)_4(\eta^2–CHPMe_2)H]^+$. Specifically, the reaction of $W(PMe_3)_4(\eta^2–CHDPMe_2)H$ with *p*-TolBr is accompanied by the formation of toluene that possesses a significant quantity (*ca.* 40%) of deuterium in the *para* position (Scheme 5).[36] The formation of d_1-toluene signals a mechanism that is consistent with abstraction of a methylene hydrogen (deuterium), as opposed to a mechanism that involves abstraction of the tungsten hydride, followed by α–elimination (Scheme 5); additional details by which the hydrogen atom is abstracted, however, remain unknown.[37]

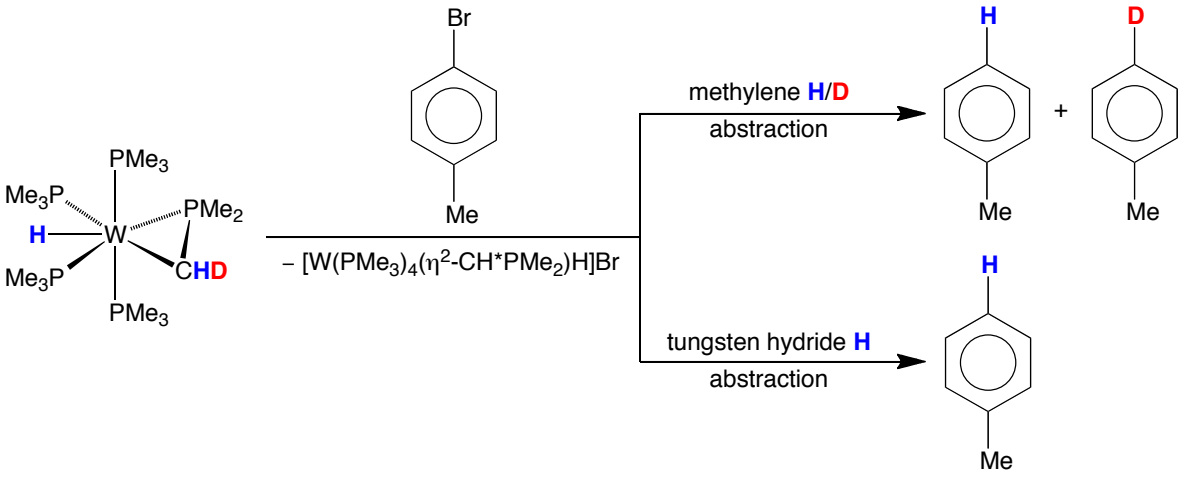

Scheme 5. Possible hydride abstraction pathways from $W(PMe_3)_4(\eta^2–CHDPMe_2)H$.

1.8 Reactivity of $W(PMe_3)_4(\eta^2–CH_2PMe_2)H$ towards chlorobenzene

Although treatment of $W(PMe_3)_4(\eta^2–CH_2PMe_2)H$ with bromobenzene and iodobenzene allowed for the isolation and characterization of $[W(PMe_3)_4(\eta^2–CHPMe_2)H]X$ (X = Br, I), the reaction of $W(PMe_3)_4(\eta^2–CH_2PMe_2)H$ with chlorobenzene proceeded differently. Specifically, a solution of $W(PMe_3)_4(\eta^2–CH_2PMe_2)H$ and chlorobenzene in benzene deposited, *inter alia*, large dark green crystals after sitting at room temperature for several weeks, which were identified as $W(PMe_3)_3Cl_2(CPMe_2Ph)$ (Scheme 6) by X-ray diffraction (Figure 9). Although the refinement of $W(PMe_3)_3Cl_2(CPMe_2Ph)$ converged well (R_1 [$I > 2\sigma(I)$] = 0.0470), because the structure is highly disordered, the proposed structure of $W(PMe_3)_3Cl_2(CPMe_2Ph)$ is tentative. Nevertheless, density functional geometry optimization calculations correspond closely with the experimental X-ray diffraction structure.[32,38]

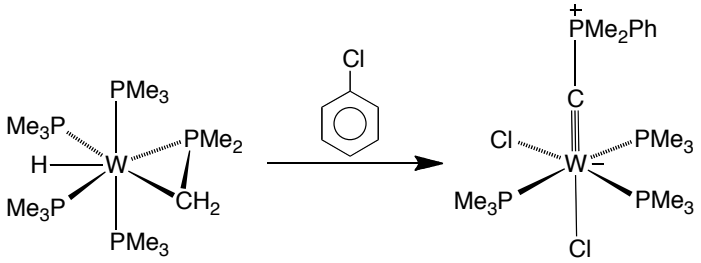

Scheme 6. Production of $W(PMe_3)_3Cl_2(CPMe_2Ph)$ from $W(PMe_3)_4(\eta^2–CH_2PMe_2)H$ and chlorobenzene.

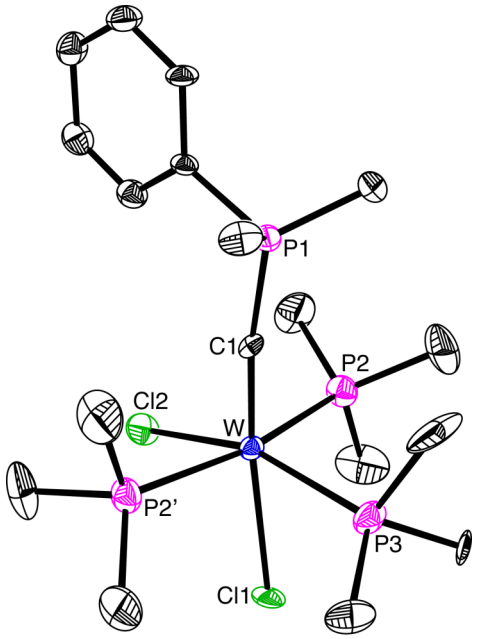

Figure 9. Molecular structure of $W(PMe_3)_3Cl_2(CPMe_2Ph)$ (disorder not shown).

The most interesting feature of $W(PMe_3)_3Cl_2(CPMe_2Ph)$ is the presence of the $W(CPMe_2Ph)$ moiety; similar $M(CPR_3)$ groups have been previously reported in the literature and named either phosphonio-methylidynes or phosphoniocarbynes.[39] The bonding in metal complexes that contain the (CPR_3) moiety have been described by two resonance structures,[39] which are shown in Figure 10 for $W(PMe_3)_3Cl_2(CPMe_2Ph)$, consisting of either a M≡C triple bond (A) or M=C double bond (B). The experimentally determined W–C [1.82(2) Å] bond length compares closely with that of the mean W≡C triple bond length (1.81 Å) and is significantly shorter than the mean W=C double bond length of 1.98 Å,[21] giving indication that resonance (A) is most appropriate. For comparison of the geometrical features of (CPR_3) ligands, the first isolated phosphonio-methylidyne, $[W_2(CPMe_3)_2(PMe_3)_4Cl_4][AlCl_4]_2$,[39a] has a W–C bond length of 1.83(3) Å and the second complex of this type, $WCl_2(CO)(PMePh_2)_2(CPMePh_2)$,[39g] has a W–C bond length of 1.823(7) Å, which are quite similar to $W(PMe_3)_3Cl_2(CPMe_2Ph)$ [1.82(2) Å]. However, the experimentally determined C–P bond length in the $(C–PR_3)$ fragment of

$W(PMe_3)_3Cl_2(CPMe_2Ph)$ [1.76(3) Å)] is significantly longer than those of $[W_2(CPMe_3)_2(PMe_3)_4Cl_4][AlCl_4]_2$ [1.71(3) Å)], and $WCl_2(CO)(PMePh_2)_2(CPMePh_2)$ [1.729(8) Å)]. The increased W–C bond length may be attributed to the disordered nature of the structure, which refined with a W–C–P bond angle of 170(10) °. The large e.s.d. gives indication to the low precision of the W–C–P bond angle and as such, small deviations in this angle can effect the W–C and C–P bond distances. In accord with this notion, the calculated geometry of $W(PMe_3)_3Cl_2(CPMe_2Ph)$ has a C–P bond length of 1.71 Å and W–C–P bond angle of 176.4, which is more in line with the previously determined structures.

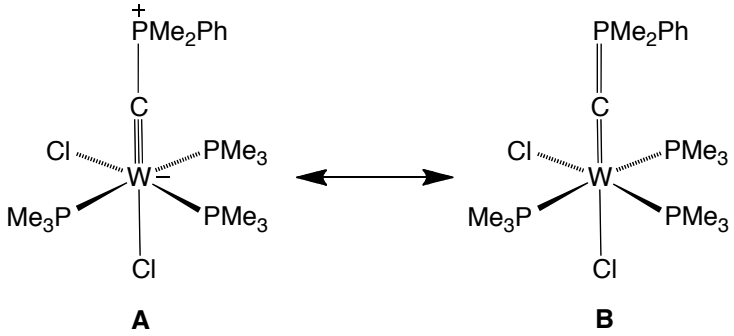

Figure 10. Resonance structures of $W(PMe_3)_3Cl_2(CPMe_2Ph)$ (the phosphorus atom in resonance **B** is hypervalent).

Additional support for resonance structure (A), in which there is substantial triple bond character in the W≡C fragment of $W(PMe_3)_3Cl_2(CPMe_2Ph)$, is provided by analysis of the Fenske-Hall molecular orbitals,[33] which are shown in Figure 11. Specifically, there are two π molecular orbitals derived from (*i*) overlap of the tungsten d_{yz} orbital and the carbon p_y orbital, and (*ii*) the tungsten d_{xz} orbital and the carbon p_x orbital.[40] In addition, the σ orbital of the W≡C interaction is shown, which is a component of a 3-center 2-electron interaction between tungsten, the carbyne carbon and the phosphorus of the PMe_2Ph unit (Figure 11).

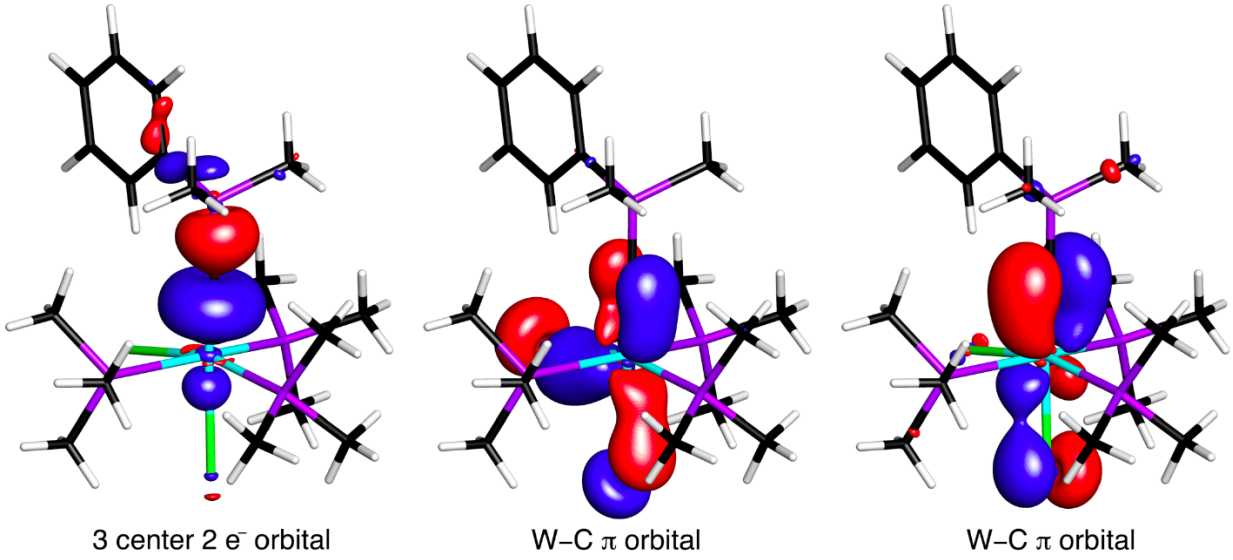

Figure 11. Molecular orbitals showing the σ and π components of the W≡C interaction.

1.9 Formation of $W(PMe_3)_3Cl_2(CPMe_2Ph)$

The mechanism of formation of $W(PMe_3)_3Cl_2(CPMe_2Ph)$ is intriguing because of the $(CPMe_2Ph)$ moiety produced. In this regard, in addition to isolating crystals of $W(PMe_3)_3Cl_2(CPMe_2Ph)$, we observed the deposition of a colorless solid, which has tentatively been identified as $[Me_3PPh]Cl$ by comparison of its ^1H and $^{31}P\{^1H\}$ NMR spectra with $[Me_3PPh]I$.[41] The synthesis of several other phosphoniocarbyne complexes[39d,e,f] (*e.g.* $CpTaCl_2(CPPh_3)$) used the phosphorane (phosphonium ylide) Ph_3PCH_2 as the active reagent, which results in the production of $[Ph_3PMe]Cl$ as a byproduct. Thus, in the reaction between $W(PMe_3)_4(\eta^2\text{–}CH_2PMe_2)H$ and chlorobenzene, we propose that $PhMe_2PCH_2$ is formed *in situ*, which then produces $W(PMe_3)_3Cl_2(CPMe_2Ph)$ and $[Me_3PPh]Cl$.

1.10 Summary and conclusions

In conclusion, the formal abstraction of a hydride to give the alkylidene complex $[W(PMe_3)_4(\eta^2\text{–}CHPMe_2)H]X$ (X = Br, I) represents a new type of reaction manifold for

$W(PMe_3)_4(\eta^2–CH_2PMe_2)H$. The latter compound may be regenerated by treatment of $[W(PMe_3)_4(\eta^2–CHPMe_2)H]^+$ with $LiAlH_4$, *via* a process that is regiospecific, such that $LiAlD_4$ gives selectively $W(PMe_3)_4(\eta^2–CHDPMe_2)H$. Isolation of $W(PMe_3)_4(\eta^2–CHDPMe_2)H$ allowed us to monitor, by using ^1H NMR spectroscopy, the migration of deuterium from the methylene group of $W(PMe_3)_4(\eta^2–CHDPMe_2)H$ to d_1-D-$W(PMe_3)_4(\eta^2–CH_2PMe_2)H$, thereby providing a means to measure the rate constant for accessing the 16-electron species $[W(PMe_3)_5]$. Additionally, treatment of $W(PMe_3)_4(\eta^2–CH_2PMe_2)H$ with chlorobenzene resulted in the formation of the phosphoniocarbyne complex, $W(PMe_3)_3Cl_2(CPMe_2Ph)$.

1.11 Experimental details

1.11.1 General considerations

All manipulations were performed using a combination of glovebox, high vacuum, and Schlenk techniques under an argon atmosphere unless otherwise specified.[42] Solvents were purified and degassed by standard procedures. ^1H NMR spectra were measured on Bruker 300 DRX, Bruker 300 DPX, Bruker 400 Avance III, Bruker 400 Cyber-enabled Avance III, and Bruker 500 DMX spectrometers. ^1H chemical shifts are reported in ppm relative to $SiMe_4$ ($\delta = 0$) and were referenced internally with respect to the protio solvent impurity (δ 7.16 for C_6D_5H; δ 3.31 for CD_2HOD, and δ 4.79 for HDO).[43] ^{13}C NMR spectra are reported in ppm relative to $SiMe_4$ ($\delta = 0$) and were referenced internally with respect to the solvent (δ 49.99 for CD_3OD).[43] ^{31}P chemical shifts are reported in ppm relative to 85% H_3PO_4 ($\delta = 0$) and were referenced using $P(OMe)_3$ ($\delta = 141.0$) as an external standard.[44] Coupling constants are given in hertz. Mass spectra were obtained on a LCMate JEOL ltd. Tokyo mass spectrometer using atmospheric pressure chemical ionization (APCI). $W(PMe_3)_4(\eta^2–CH_2PMe_2)H$ was prepared by the literature method.[12] $LiAlD_4$ was purchased commercially (Aldrich).

1.11.2 X-ray structure determinations

X-ray diffraction data were collected on a Bruker Apex II diffractometer. Crystal data, data collection and refinement parameters are summarized in Section 1.12, Table 4. The structures were solved using direct methods and standard difference map techniques, and were refined by full-matrix least-squares procedures on F^2 with SHELXTL (Version 6.10).[45]

1.11.3 Computational details

Calculations were carried out using DFT as implemented in the Jaguar 7.5 (release 207) suite of *ab initio* quantum chemistry programs.[46] Geometry optimizations were performed with the B3LYP density functional[47] using the 6-31G** (C, H, and P) and LACVP (W) basis sets.[48] The energies of the optimized structures were reevaluated by additional single point calculations on each optimized geometry using cc-pVTZ(-f) correlation consistent triple-ζ basis set for C, H, and P and LACV3P for W. Molecular orbital analyses were performed with the aid of JIMP2,[33] which employs Fenske-Hall calculations and visualization using MOPLOT.[49]

1.11.4 Synthesis of $[W(PMe_3)_4(\eta^2\text{–}CHPMe_2)H]I$

A solution of $W(PMe_3)_4(\eta^2\text{–}CH_2PMe_2)H$ (200 mg, 0.35 mmol) in benzene (3 mL) was treated with iodobenzene (145 mg, 0.71 mmol) giving rise to a dark yellow solution. The solution was allowed to stand overnight at room temperature, thereby depositing bright blue-purple crystals of $[W(PMe_3)_4(\eta^2\text{–}CHPMe_2)H]I$, together with colorless crystals of $[Me_3PPh]I$, as identified by comparison of the unit cell data with that of the literature [a = 24.831(6) Å, b = 7.399(2) Å, c = 12.782(3) Å; α = 90°, β = 90°, γ = 90°].[50,51] The mother liquor was decanted in air and the crystals were washed sequentially with pentane (3 × 5 mL), Et_2O (2 × 5 mL), and distilled water (3 × 5 mL) to remove the

colorless crystals of [Me_3PPh]I. The sample was then washed with Et_2O (2 × 5 mL) and pentane (2 × 5 mL) and dried *in vacuo* to give blue-purple crystals of [$W(PMe_3)_4(\eta^2$–$CHPMe_2)H$]I suitable for X-ray diffraction (120 mg, 49% yield). Anal. Calcd.: C, 26.1%, H, 6.4%. Found: C, 25.6%, H, 5.8%.

^1H NMR (CD_3OD): 1.32 [ddquint, J_{H-H} = 12, J_{P-H} = 16, $^2J_{P-H}$ = 37, $^1J_{W-H}$ = 29, 1H of $W(PMe_3)_4(\eta^2$–$CHPMe_2)\underline{H}$], 1.60 [d, $^2J_{P-H}$ = 10, 6H of $W(PMe_3)_4(\eta^2$–$CHP\underline{Me_2})H$], 1.68 [s, 36H of $W(P\underline{Me_3})_4(\eta^2$–$CHPMe_2)H$], 11.86 [dquint, J_{H-H} = 12, J_{P-H} = 11, J_{W-H} = 11, 1H of $W(PMe_3)_4(\eta^2$–$C\underline{H}PMe_2)H$]. $^{31}P\{^1H\}$ NMR (CD_3OD): –154.0 [quint, $^2J_{P-P}$ = 12, $^1J_{W-P}$ = 81, 1P of $W(PMe_3)_4(\eta^2$-$CH\underline{P}Me_2)H$], –34.9 [d, $^2J_{P-P}$ = 12, $^1J_{W-P}$ = 204, 4P of $W(\underline{P}Me_3)_4(\eta^2$–$CHPMe_2)H$]. $^{13}C\{^1H\}$ NMR (CD_3OD): 19.2 [d, $^1J_{P-C}$ = 27, 2C of $W(PMe_3)_4(\eta^2$–$CHP\underline{Me_2})H$], 26.9 [m, 12C of $W(P\underline{Me_3})_4(\eta^2$–$CHPMe_2)H$], 224.4 [dquint, $^1J_{P-C}$ = 51, J_{P-C} = 13, 1C of $W(PMe_3)_4(\eta^2$–$\underline{C}HPMe_2)H$].

1.11.5 Synthesis of $[W(PMe_3)_4(\eta^2$–$CHPMe_2)H]Br$

A solution of $W(PMe_3)_4(\eta^2$–$CH_2PMe_2)H$ (400 mg, 0.71 mmol) in benzene (5 mL) was treated with bromobenzene (250 mg, 1.60 mmol) giving rise to a dark yellow solution. The solution was allowed to stand overnight at room temperature, thereby depositing bright blue-purple crystals of $[W(PMe_3)_4(\eta^2$–$CHPMe_2)H]Br$, together with some colorless crystals (presumably [Me_3PPh]Br, *vide supra*). The mother liquor was decanted in air, and the crystals were washed sequentially with pentane (3 × 5 mL), Et_2O (2 × 5 mL), and pentane (2 × 5 mL) and dried *in vacuo* to give blue-purple crystals of $[W(PMe_3)_4(\eta^2$–$CHPMe_2)H]Br$ suitable for X-ray diffraction (260 mg, 57% yield).

^1H NMR (CD_3OD): 1.32 [ddquint, J_{H-H} = 13, J_{P-H} = 16, $^2J_{P-H}$ = 37, $^1J_{W-H}$ = 29, 1H of $W(PMe_3)_4(\eta^2$–$CHPMe_2)\underline{H}$], 1.59 [d, $^2J_{P-H}$ = 9, 6H of $W(PMe_3)_4(\eta^2$–$CHP\underline{Me_2})H$], 1.67 [s, 36H of $W(P\underline{Me_3})_4(\eta^2$–$CHPMe_2)H$], 11.85 [dquint, J_{H-H} = 13, J_{P-H} = 10, J_{W-H} = 11, $^1J_{C-H}$ = 174, 1H of $W(PMe_3)_4(\eta^2$–$C\underline{H}PMe_2)H$]. $^{31}P\{^1H\}$ NMR (CD_3OD): –153.8 [quint, $^2J_{P-P}$ = 12, $^1J_{W-P}$ = 82, 1P

of $W(PMe_3)_4(\eta^2\text{-}CH\underline{P}Me_2)H]$, –34.7 [d, $^2J_{P\text{-}P}$ = 12, $^1J_{W\text{-}P}$ = 204, 4P of $W(\underline{P}Me_3)_4(\eta^2$–$CHPMe_2)H]$. $^{13}C\{^1H\}$ NMR (CD_3OD): 19.2 [dquint, $^1J_{P\text{-}C}$ = 27, $^3J_{P\text{-}C}$ = 2, 2C of $W(PMe_3)_4(\eta^2$–$CHP\underline{Me}_2)H]$, 26.9 [m, 12C of $W(P\underline{Me}_3)_4(\eta^2$–$CHPMe_2)H]$, 224.4 [dquint, $^1J_{P\text{-}C}$ = 50, $^2J_{P\text{-}C}$ = 13, 1C of $W(PMe_3)_4(\eta^2$–$\underline{C}HPMe_2)H]$. ^{13}C NMR (CD_3OD): 19.2 [dq, $^1J_{P\text{-}C}$ = 27, $^1J_{H\text{-}C}$ = 129, 2C of $W(PMe_3)_4(\eta^2$–$CHP\underline{Me}_2)H]$, 26.9 [q, $^1J_{H\text{-}C}$ = 132, 12C of $W(P\underline{Me}_3)_4(\eta^2$–$CHPMe_2)H]$, 224.4 [dd, $^1J_{P\text{-}C}$ = 50, $^1J_{H\text{-}C}$ = 174, 1C of $W(PMe_3)_4(\eta^2$–$\underline{C}HPMe_2)H]$. ^1H NMR (D_2O): 0.23 [m, 1H of $W(PMe_3)_4(\eta^2$–$CHPMe_2)\underline{H}]$, 1.56 [d, $^2J_{P\text{-}H}$ = 10, 6H of $W(PMe_3)_4(\eta^2$–$CHP\underline{Me}_2)H]$, 1.62 [s, 36H of $W(P\underline{Me}_3)_4(\eta^2$–$CHPMe_2)H]$, 12.01 [sextet, $J_{P\text{-}H}$ = 11, $J_{H\text{-}H}$ = 11, $J_{W\text{-}H}$ = 11, 1H of $W(PMe_3)_4(\eta^2$–$C\underline{H}PMe_2)H]$. $^{31}P\{^1H\}$ NMR (D_2O): –154.6 [quint, $^2J_{P\text{-}P}$ = 12, $^1J_{W\text{-}P}$ = 84, 1P of $W(PMe_3)_4(\eta^2$–$CH\underline{P}Me_2)H]$, -35.7 [d, $^2J_{P\text{-}P}$ = 12, $^1J_{W\text{-}P}$ = 203, 4P of $W(\underline{P}Me_3)_4(\eta^2$–$CHPMe_2)H]$.

1.11.6 Reaction of $W(PMe_3)_4(\eta^2$–$CH_2PMe_2)H$ towards bromotoluene

A solution of $W(PMe_3)_4(\eta^2$–$CH_2PMe_2)H$ (60 mg, 0.11 mmol) in C_6D_6 (*ca*. 0.7 mL) was treated with *p*-bromotoluene (40 mg, 0.23 mmol) and allowed to stand at room temperature for 12 hours. After this period, the mixture was filtered, removing *inter alia* purple crystals of $[W(PMe_3)_4(\eta^2$–$CHPMe_2)H]Br$, and the filtrate was analyzed by ^1H NMR spectroscopy, thereby demonstrating the formation of toluene.

1.11.7 Reaction of $[W(PMe_3)_4(\eta^2$–$CHPMe_2)H]Br$ towards $LiAlH_4$

A suspension of $[W(PMe_3)_4(\eta^2$–$CHPMe_2)H]Br$ (12 mg, 0.02 mmol) in C_6D_6 (*ca*. 0.7 mL) was treated with $LiAlH_4$ (10 mg, 0.26 mmol). Et_2O (*ca*. 0.1 mL) was then added, thereby resulting in the formation of a bright yellow solution. The mixture was filtered and the filtrate was lyophilized and the solid obtained was extracted into C_6D_6 and analyzed by ^1H NMR spectroscopy, thereby demonstrating the formation of $W(PMe_3)_4(\eta^2$–$CH_2PMe_2)H$.

1.11.8 Reaction of $[W(PMe_3)_4(\eta^2–CHPMe_2)H]Br$ towards $LiAlD_4$

A suspension of $[W(PMe_3)_4(\eta^2–CHPMe_2)H]Br$ (50 mg, 0.08 mmol) in benzene (1 mL) was treated with a solution of $LiAlD_4$ (3 mg, 0.07 mmol) in Et_2O (*ca*. 0.2 mL). The resulting mixture was shaken for 1 minute and filtered. The filtrate was lyophilized and the yellow powder was extracted into C_6D_6 (*ca*. 0.7 mL) and analyzed by ^1H NMR spectroscopy, thereby demonstrating the formation of an isotopologue of $W(PMe_3)_4(\eta^2–CH_2PMe_2)H$ in which deuterium primarily resided in the methylene site, namely $W(PMe_3)_4(\eta^2–CHDPMe_2)H$.

1.11.9 Crystal Structure and Molecular Orbital Analysis of $W(PMe_3)_4(\eta^2–CH_2PMe_2)H$

Crystals of $W(PMe_3)_4(\eta^2–CH_2PMe_2)H$ suitable for X-ray diffraction were obtained from a solution in pentane at –15 ˚C.

1.11.10 Kinetics of isomerization of $W(PMe_3)_4(\eta^2–CHDPMe_2)H$

A suspension of $[W(PMe_3)_4(\eta^2–CHPMe_2)H]Br$ (100 mg, 0.16 mmol) in benzene (1 mL) was treated with a solution of $LiAlD_4$ (5 mg, 0.12 mmol) in Et_2O (*ca*. 0.2 mL). The resulting mixture was shaken for 1 minute and filtered. The filtrate was lyophilized and the yellow powder of $W(PMe_3)_4(\eta^2–CHDPMe_2)H$ obtained was extracted into C_6D_6 (*ca*. 2.1 mL) and filtered into a vial. Mesitylene (1 μL) was added as an internal integration standard, and the solution was divided evenly into 3 NMR tubes equipped with J. Young valves. Two of the samples were treated with PMe_3 and the kinetics of the isomerization of $W(PMe_3)_4(\eta^2–CHDPMe_2)H$ were measured at 30˚C by monitoring the increase in intensity of the methylene signal in the ^1H NMR spectrum. Using a similar procedure, the kinetics were also measured at 53˚C and 64˚C in the probe of the NMR spectrometer, as summarized in Table 3. Within experimental error, the rate constant data are not influenced by the presence of PMe_3.

1.11.11 Reaction of $W(PMe_3)_4(\eta^2–CHDPMe_2)H$ towards bromotoluene

A sample of $W(PMe_3)_4(\eta^2–CHDPMe_2)H$ was prepared by the above procedure employing $[W(PMe_3)_4(\eta^2–CHPMe_2)H]Br$ (200 mg, 0.31 mmol), benzene (1.5 mL) and a solution of $LiAlD_4$ (10 mg, 0.24 mmol) in Et_2O (*ca*. 0.4 mL). The resulting mixture was shaken for 1 minute and then filtered. The precipitate was extracted with benzene (1 mL), filtered and the filtrates were combined and lyophilized. The bright yellow powder was then extracted with d_6-benzene (*ca*. 0.7 mL), filtered into an NMR tube equipped with a J. Young valve and treated with *p*-bromotoluene (150 mg, 0.88 mmol). The sample was monitored by ^1H NMR spectroscopy, which demonstrated that the toluene formed contained *ca* 40% deuterium in the *para* position.

1.11.12 Synthesis of $[Ar^{(PhBr)_2}]H$

1,3-diiodobenzene (1.57 g, 4.74 mmol), 2-bromophenylboronic acid (2.00 g, 9.96 mmol), $Pd(PPh_3)_4$ (0.274 g, 0.24 mmol) and potassium carbonate (3.93 g, 28.44 mmol) were added to a large Schlenk equipped with a stirbar. THF (50 mL) was then added *via* cannula to the large Schlenk creating a yellow mixture. In a separate medium Schlenk, a mixture of H_2O (11 mL) and EtOH (11 mL) was subjected to 3 freeze pump thaw cycles, and then was cannulated into the large Schlenk. The Schlenk was then equipped with a reflux condenser, stirred vigorously and heated at 83 ˚C for 16 hours. After this period, the mixture was allowed to be exposed to air and was filtered. The filtrate was put into a separatory funnel and the organic layer was collected. The aqueous layer was extracted with Et_2O and the organic layers were then combined and pumped down under reduced pressure creating a thick orange waxy oil. This waxy oil was then dissolved in dichloromethane, and pre-absorbed onto silica gel, and purified by flash column chromatography (silica gel, hexanes) in air. The hexanes were then removed under reduced pressure resulting in a colorless to white wax. The wax was then

recrystallized by slow evaporation of a saturated pentane solution giving pure X-ray quality crystals of [$Ar^{(PhBr)_2}$]H (1.20 g, 65% yield). Anal. Calcd.: C, 55.7 %, H, 3.1 %. Found: C, 56.0 %, H, 3.2 . Mass Spec. (APCI+): m/z = 418.59 {M^+ + MeOH}.

^{1}H NMR (C_6D_6): 6.73 [dt, $^4J_{H-H}$ = 2, $^3J_{H-H}$ = 8, 2H of $Ar^{(PhBr)_2}$H], 6.92 [dt, $^4J_{H-H}$ = 1, $^3J_{H-H}$ = 8, 2H of $Ar^{(PhBr)_2}$H], 7.11 [dd, $^4J_{H-H}$ = 2, $^3J_{H-H}$ = 8, 2H of $Ar^{(PhBr)_2}$H], 7.19 [m, 1H of $Ar^{(PhBr)_2}$H], 7.31 [m, 2H of $Ar^{(PhBr)_2}$H], 7.39 [t, $^4J_{H-H}$ = 2, 1H of $Ar^{(PhBr)_2}$H], 7.48 [dd, $^4J_{H-H}$ = 1, $^3J_{H-H}$ = 8, 2H of $Ar^{(PhBr)_2}$H]. $^{13}C\{^1H\}$ NMR (C_6D_6): 123.1 [s, 2C of $Ar^{(PhBr)_2}$H], 127.6 [s, 2C of $Ar^{(PhBr)_2}$H], 128.1 [s, 1C of $Ar^{(PhBr)_2}$H], 129.0 [s, 2C of $Ar^{(PhBr)_2}$H], 129.0 [s, 2C of $Ar^{(PhBr)_2}$H], 130.9 [s, 1C of $Ar^{(PhBr)_2}$H], 131.7 [s, 2C of $Ar^{(PhBr)_2}$H], 133.4 [s, 2C of $Ar^{(PhBr)_2}$H], 141.3 [s, 2C of $Ar^{(PhBr)_2}$H], 142.8 [s, 2C of $Ar^{(PhBr)_2}$H].

1.11.13 Structural characterization of $W(PMe_3)_3Cl_2(CPMe_2Ph)$

A solution of $W(PMe_3)_4(\eta^2–CH_2PMe_2)H$ (100 mg, 0.18 mmol) in benzene (5 mL) was treated with chlorobenzene (70 mg, 0.62 mmol) giving rise to a dark yellow solution. The solution was allowed to stand at room temperature for *ca*. 3 weeks, thereby depositing a mixture of dark green crystals and a colorless white solid (10 mg). The green crystals were identified as $W(PMe_3)_3Cl_2(CPMe_2Ph)$ by X-ray diffraction.

1.12 Crystallographic data

Table 4. Crystal, intensity collection and refinement data.

	$[W(PMe_3)_4(\eta^2–CHPMe_2)H]I$	**$[W(PMe_3)_4(\eta^2–CHPMe_2)H]Br$**
lattice	Tetragonal	Tetragonal
formula	$C_{15}H_{44}IP_5W$	$C_{15}H_{44}BrP_5W$
formula weight	690.10	643.11
space group	$P4_2/m$	$P4_2/m$
a / Å	13.598(3)	13.476(3)
b / Å	13.598(3)	13.476(3)
c / Å	14.392(3)	14.118(4)
α / °	90	90
β / °	90	90
γ / °	90	90
V / Å^3	2661.3(11)	2563.8(11)
Z	4	4
temperature (K)	150(2)	125(2)
radiation (λ, Å)	0.71073	0.71073
ρ (calcd.) g cm^{-3}	1.722	1.666
μ (Mo Kα), mm^{-1}	5.799	6.373
θ max, deg.	31.50	31.76
no. of data collected	45502	44100
no. of data	4582	4516
no. of parameters	125	124
R_1 [$I > 2\sigma(I)$]	0.0220	0.0188
wR_2 [$I > 2\sigma(I)$]	0.0469	0.0410
R_1 [all data]	0.0295	0.0261
wR_2 [all data]	0.0497	0.0433
GOF	1.054	1.042

Table 4 (cont). Crystal, intensity collection and refinement data.

	$W(PMe_3)_4(\eta^2–CH_2PMe_2)H$	$[Ar^{(PhBr)_2}]H$
lattice	Monoclinic	Orthorhomic
formula	$C_{15}H_{45}P_5W$	$C_{18}H_{12}Br_2$
formula weight	564.21	388.10
space group	$P2_1/n$	$Pbca$
a / Å	14.8321(4)	7.2007(5)
b / Å	9.4806(3)	18.4482(13)
c / Å	18.0198(5)	22.2937(16)
α / °	90	90
β / °	106.6870(10)	90
γ / °	90	90
V / Å^3	2427.19(12)	2961.5(4)
Z	4	8
temperature (K)	125(2)	150(2)
radiation (λ, Å)	0.71073	0.71073
ρ (calcd.) g cm^{-3}	1.544	1.741
μ (Mo Kα), mm^{-1}	5.084	5.461
θ max, deg.	30.51	30.03
no. of data collected	14235	42597
no. of data	7349	4313
no. of parameters	208	181
R_1 [$I > 2\sigma(I)$]	0.0208	0.0287
wR_2 [$I > 2\sigma(I)$]	0.0461	0.0538
R_1 [all data]	0.0259	0.0582
wR_2 [all data]	0.0478	0.0627
GOF	1.011	1.032

Table 4 (cont). Crystal, intensity collection and refinement data.

	$W(PMe_3)_3Cl_2(CPMe_2Ph)$
lattice	Orthorhombic
formula	$C_{18}H_{38}Cl_2P_4W$
formula weight	633.11
space group	*Pmmn*
a / Å	10.2123(6)
b / Å	14.0712(8)
c / Å	9.2360(5)
α / °	90
β / °	90
γ / °	90
V / Å^3	1327.21(13)
Z	2
temperature (K)	225(2)
radiation (λ, Å)	0.71073
ρ (calcd.) g cm^{-3}	1.584
μ (Mo Kα), mm^{-1}	4.796
θ max, deg.	30.50
no. of data collected	20761
no. of data	2211
no. of parameters	148
R_1 [$I > 2\sigma(I)$]	0.0470
wR_2 [$I > 2\sigma(I)$]	0.1173
R_1 [all data]	0.0478
wR_2 [all data]	0.1177
GOF	1.200

1.13 References and notes

(1) (a) Cloke, F. G. N.; Cox, K. P.; Green, M. L. H.; Bashkin, J.; Prout, K. *J. Chem. Soc., Chem. Commun.* **1982**, 393-394.

(b) Brookhart, M.; Cox, K. P.; Cloke, F. G. N.; Green, J. C.; Green, M. L. H.; Hare, P. M.; Bashkin, J.; Derome, A. E.; Grebenik, P. D. *J. Chem. Soc., Dalton Trans.* **1985**, 423-433.

(2) Rabinovich, D.; Parkin, G. *J. Am. Chem. Soc.* **1990**, *112*, 5381-5383.

(3) Timms, P. L. *Angew. Chem. Int. Ed.* **1975**, *14*, 273-277.

(4) Ermer, S. P.; Shinomoto, R. S.; Deming, M. A.; Flood, T. C. *Organometallics* **1989**, *8*, 1377-1378.

(5) (a) Klein, H.–F. *Angew. Chem. Int. Ed.* **1971**, *10*, 343.

(b) Klein, H.–F.; Karsch, H. H. *Chem. Ber.* **1975**, *108*, 956-966.

(6) Klein, H.–F.; Schmidbaur, H. *Angew. Chem. Int. Ed.* **1970**, *9*, 903-904.

(7) Kuran, W.; Musco, A. *Inorg. Chim. Acta* **1975**, *12*, 187-193.

(8) Malatesta, L.; Cenini, S. *Zerovalent Compounds of Metals;* Academic Press, New York, 1974.

(9) Murphy, V. J.; Parkin, G. *J. Am. Chem. Soc.* **1995**, *117*, 3522-3528.

(10) Gibson, V. C.; Graimann, C. E.; Hare, P. M.; Green, M. L. H.; Bandy, J. A.; Grebenik, P. D.; Prout, K. *J. Chem. Soc. Dalton Trans.* **1985**, 2025-2035.

(11) Rabinovich, D.; Zelman, R.; Parkin, G. *J. Am. Chem. Soc.* **1992**, *114*, 4611-4621.

(12) Green, M. L. H.; Parkin, G.; Chen, M.; Prout, K. *J. Chem. Soc., Dalton Trans.* **1986**, 2227–2236.

(13) Green, M. L. H.; Parkin, G.; Moynihan, K. J.; Prout, K. *J. Chem. Soc., Chem. Commun.* **1984**, 1540.

(14) Murphy, V. J.; Rabinovich, D.; Hascall, T.; Klooster, W. T.; Koetzle, T. F.; Parkin, G. *J. Am. Chem. Soc.* **1998**, *120*, 4372-4387.

(15) (a) Rabinovich, D.; Parkin, G. *J. Am. Chem. Soc.* **1991**, *113*, 9421-9422.

(b) Rabinovich, D.; Parkin, G. *Inorg. Chem.* **1995**, *34*, 6341-6361.

(16) Sattler, A.; Parkin, G. *Chem. Commun.* **2011**, *47*, 12828–12830.

(17) $[W(PMe_3)_4(\eta^2\text{–}CHPMe_2)H]Br$ was first synthesized by treating $W(PMe_3)_4(\eta^2\text{–}CH_2PMe_2)H$ with $[Ar^{(PhBr)_2}]H$ (see Section 1.11.12) in an attempt to produce a [*CCC*] pincer ligand on tungsten.

(18) This was apparent by the observation that addition of H_2O resulted in the formation of bright blue-purple solution.

(19) For some early examples, see:

(a) Karsch, H. H.; Klein, H.-F.; Schmidbaur, H. *Angew. Chem. Int. Ed.* **1975**, *14*, 637.

(b) Rathke, J. W.; Muetterties, E. L. *J. Am. Chem. Soc.* **1975**, *97*, 3272.

(c) Klein, H.-F. *Angew. Chem. Int. Ed.* **1980**, *19*, 362.

(d) Werner, H.; Werner, R. *J. Organomet. Chem.* **1981**, *209*, C60.

(e) Werner, H.; Gotzig, J. *Organometallics* **1983**, *2*, 547.

(f) Mainz, V. V.; Andersen, R. A. *Organometallics* **1984**, *3*, 675.

(20) For some examples in molybdenum and tungsten chemistry, see:

(a) Murphy, V. J.; Parkin, G. *J. Am. Chem. Soc.* **1995**, *117*, 3522.

(b) Cloke, F. G. N.; Cox, K. P.; Green, M. L. H.; Bashkin, J.; Prout, K. *J. Chem. Soc., Chem. Commun.* **1982**, 393.

(c) Brookhart, M.; Cox, K.; Cloke, F. G. N.; Green, J. C.; Green, M. L. H.; Hare, P. M.; Bashkin, J.; Derome, A. E.; Grebenik, P. D. *J. Chem. Soc., Dalton Trans.* **1985**, 423.

(d) Janak, K. E.; Tanski, J. M.; Churchill, D. G.; Parkin, G. *J. Am. Chem. Soc.* **2002**, *124*, 4182.

(e) Kuiper, D. S.; Wolczanski, P. T.; Lobkovsky, E. B.; Cundari, T. R. *Inorg. Chem.* **2008**, *47*, 10542.

(f) Cotton, F. A.; Canich, J. A. M.; Luck, R. L.; Vidyasagar, K. *Organometallics* **1991**, *10*, 352.

(g) van der Eide, E. F.; Piers, W. E.; Parvez, M.; McDonald, R. *Inorg. Chem.* **2007**, *46*, 14.

(h) Baker, R. T.; Calabrese, J. C.; Harlow, R. L.; Williams, I. D. *Organometallics* **1993**, *12*, 830.

(21) Cambridge Structural Database (Version 5.32). *3D Search and Research Using the Cambridge Structural Database*, Allen, F. H.; Kennard, O. *Chemical Design Automation News* **1993**, *8* (1), pp 1 & 31-37.

(22) Green, M. L. H.; Hare, P. M.; Bandy, J. A. *J. Organomet. Chem.* **1987**, *330*, 61.

(23) (a) Gibson, V. C.; Kee, T. P.; Carter, S. T.; Sanner, R. D.; Clegg, W. *J. Organomet. Chem.* **1991**, *418*, 197.

(b) Kee, T. P.; Gibson, V. C.; Clegg, W. *J. Organomet. Chem.* **1987**, *325*, C14.

(24) Gibson, V. C.; Kee, T. P.; Clegg, W. *J. Chem. Soc., Chem. Commun.* **1990**, 313.

(25) For other examples of compounds with η^2–$CHPMe_2$ ligands, see: Anstice, H. M.; Fielding, H. H.; Gibson, V. C.; Housecroft, C. E.; Kee, T. P. *Organometallics* **1991**, *10*, 2183.

(26) The molecular structure of $W(PMe_3)_4(\eta^2–CH_2PMe_2)H$ as determined by X-ray diffraction has been previously reported (reference 10). However, the data were collected at room temperature and the tungsten hydride was not located and refined.

(27) A similar trend in longer M–P bond lengths for compounds with a greater positive charge has been observed for $[(dmpe)_3Mo]^q$ (q = 0, 1) and $[(dmpe)_3Re]^q$ (q = 1, 2). Roddick, D. M. personal communication to Gerard Parkin.

(28) The number of bonds (n) are not specified for ^nJ coupling constants for which more than one coupling pathway exists due to the presence of a ring system.

(29) The coupling constant was not reported in reference 10a.

(30) Coupling confirmed by $^1H\{^{31}P\}$ and ^1H homonuclear decoupling NMR experiments.

(31) While the dative interaction was not drawn for the phosphaalkyne structure (B) in references 23 and 25, it is implied on the basis that the ligand is described as a four electron donor.

(32) B3LYP using 6-31G** (C, H, and P) and LACVP (W) basis sets.

(33) (a) Hall, M. B.; Fenske, R. F. *Inorg. Chem.* **1972**, *11*, 768.

(b) Bursten, B. E.; Jensen, J. R.; Fenske, R. F. *J. Chem. Phys.* **1978**, *68*, 3320.

(c) Manson, J.; Webster, C. E.; Pérez, L. M.; Hall, M. B. http://www.chem.tamu.edu/jimp2/index.html.

(34) *z* is defined as perpendicular to the pentagonal plane, while *x* is defined as the W–C bond vector.

(35) This comparison assumes that the secondary kinetic isotope effect for reductive elimination of a C–H bond is small, as previously observed. See, for example: Parkin, G.; Bercaw, J. E. *Organometallics* **1989**, *8*, 1172-1179.

(36) The amount of d_1-toluene is < 50% because scrambling of the deuterium into other sites of $W(PMe_3)_4(\eta^2–CHDPMe_2)H$ occurs on a comparable timescale to the reaction with *p*-TolBr.

(37) One possibility is that $W(PMe_3)_4(\eta^2–CH_2PMe_2)H$ undergoes electrophilic attack by ArX to give a $[W(PMe_3)_n(CH_2PMe_2)(Ar)H]^+$ species that undergoes subsequent α–H abstraction by the aryl group.

(38) Singlet and triplet spin states were both calculated; the singlet state was chosen because of the significantly lower (> 25 kcal mol^{-1}) energy calculated.

(39) (a) Holmes, S. J.; Schrock, R. R.; Churchill, M. R.; Wasserman, H. J. *Organometallics* **1984,** *3*, 476-484.

(b) Hulley, E. B.; Bonanno, J. B.; Wolczanski, P. T.; Cundari, T. R.; Lobkovsky, E. B. *Inorg. Chem.* **2010,** *49*, 8524-8544.

(c) Jamison, G. M.; White, P. S.; Templeton, J. L. *Organometallics* **1991,** *10*, 1954-1959.

(d) Li, X.; Schopf, M.; Stephan, J.; Harms, K.; Sundermeyer, J. *Organometallics* **2002,** *21*, 2356-2358.

(e) Li, X.; Sun, H.; Harms, K.; Sundermeyer, J. *Organometallics* **2005,** *24*, 4699-4701.

(f) Li, X.; Wang, A.; Wang, L.; Sun, H.; Harms, K.; Sundermeyer, J. *Organometallics* **2007,** *26*, 1411-1413.

(g) List, A. K.; Hillhouse, G. L.; Rheingold, A. L. *Organometallics* **1989,** *8*, 2010-2016.

(40) *z* is defined as the W–C bond vector, *x* is defined as the P–W–P bond vector, and *y* is defined as the P–W–Cl bond vector .

(41) ^{1}H NMR of [Me_3PPh]Cl (D_2O): 2.21 [d, $^{2}J_{P\text{-}H}$ = 15, 9H of $\underline{Me}_3P$], 7.73 [m, 2H of P$\underline{Ph}$], 7.83 [m, 1H of P$\underline{Ph}$], 7.90 [m, 2H of P$\underline{Ph}$]. $^{31}P\{^{1}H\}$ NMR of [Me_3PPh]Cl (D_2O): 21.8 [s, 1P of Me_3PPh]. See reference 51 for NMR data on [Me_3PPh]I.

(42) (a) McNally, J. P.; Leong, V. S.; Cooper, N. J. in *Experimental Organometallic Chemistry*, Wayda, A. L.; Darensbourg, M. Y., Eds.; American Chemical Society: Washington, DC, 1987; Chapter 2, pp 6-23.

(b) Burger, B.J.; Bercaw, J. E. in *Experimental Organometallic Chemistry*; Wayda, A. L.; Darensbourg, M. Y., Eds.; American Chemical Society: Washington, DC, 1987; Chapter 4, pp 79-98.

(c) Shriver, D. F.; Drezdzon, M. A.; *The Manipulation of Air-Sensitive Compounds*, 2nd Edition; Wiley-Interscience: New York, 1986.

(43) Gottlieb, H. E.; Kotlyar, V.; Nudelman, A. *J. Org. Chem.* **1997**, *62*, 7512-7515.

(44) "Nuclear Magnetic Resonance Spectroscopy" Nelson, J. H. Prentice Hall, New Jersey (2003), p 79.

(45) (a) Sheldrick, G. M. SHELXTL, An Integrated System for Solving, Refining and Displaying Crystal Structures from Diffraction Data; University of Göttingen, Göttingen, Federal Republic of Germany, 1981.

(b) Sheldrick, G. M. *Acta Cryst.* **2008**, *A64*, 112-122.

(46) Jaguar 7.5, Schrödinger, LLC, New York, NY 2008.

(47) (a) Becke, A. D. *J. Chem. Phys.* **1993**, *98*, 5648-5652.

(b) Becke, A. D. *Phys. Rev. A* **1988**, *38*, 3098-3100.

(c) Lee, C. T.; Yang, W. T.; Parr, R. G. *Phys. Rev. B* **1988**, *37*, 785-789.

(d) Vosko, S. H.; Wilk, L.; Nusair, M. *Can. J. Phys.* **1980**, *58*, 1200-1211.

(e) Slater, J. C. *Quantum Theory of Molecules and Solids, Vol. 4: The Self-Consistent Field for Molecules and Solids*; McGraw-Hill: New York, 1974.

(48) (a) Hay, P. J.; Wadt, W. R. *J. Chem. Phys.* **1985**, *82*, 270-283.

(b) Wadt, W. R.; Hay, P. J. *J. Chem. Phys.* **1985**, *82*, 284-298.

(c) Hay, P. J.; Wadt, W. R. *J. Chem. Phys.* **1985**, *82*, 299-310.

(49) Version 2.0, June 1993; Lichtenberger, D. L. Department of Chemistry, University of Arizona, Tuscon, AZ 85721.

(50) Schüdel, H.; Näther, C.; Bock, H, *Acta Cryst.* **1995**, *C51*, 1841-1844.

(51) ^{1}H NMR of [Me_3PPh]I (D_2O): 2.21 [d, $^{2}J_{P\text{-}H}$ = 15, 9H of $\underline{Me_3}P$], 7.73 [m, 2H of P$\underline{Ph}$], 7.84 [m, 1H of P$\underline{Ph}$], 7.90 [m, 2H of P$\underline{Ph}$]. $^{31}P\{^{1}H\}$ NMR of [Me_3PPh]I (D_2O): 21.2 [s, 1P of Me_3PPh].

CHAPTER 2

Modeling aspects of hydrodenitrogenation: Reactivity of $Mo(PMe_3)_6$ towards phenazine and related heterocycles

Table of Contents

Reproduced in part from:

Sattler, A.; Zhu, G.; Parkin, G. *J. Am. Chem. Soc.* **2009**, *131*, 7828–7838.

2.1 Introduction

2.1.1 Hydrodenitrogenation (HDN)

Hydrodenitrogenation (HDN) is the industrial process whereby nitrogen containing impurities are removed from crude oil, which is important for minimizing toxic emissions of environmentally unfriendly gases, such as NO_2, during combustion.[1,2,3] HDN involves the cleavage of strong C–N bonds by using H_2, and is an energy intensive process performed at high temperatures and pressures, most commonly using a molybdenum sulfide catalyst supported on alumina (Scheme 1).[4] Aromatic nitrogen heterocycles are some of the most challenging compounds to process in crude oil because of their particularly strong C–N bonds. Therefore, studying the reactivity of these aromatic N-heterocycles with molybdenum can provide useful information concerning HDN. Specifically, inorganic compounds can serve as models for the HDN process providing insight into the transformations that may be involved.[2,5]

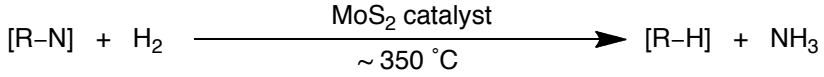

Scheme 1. Hydrodenitrogenation (HDN).

2.1.2 $Mo(PMe_3)_6$

As described in Chapter 1, there are several examples of homoleptic trimethylphosphine complexes of transition metals, one of which is $Mo(PMe_3)_6$. $Mo(PMe_3)_6$ was first synthesized in 1982 by Green *et al.* by using metal vapor synthesis techniques.[6] In 1995, Murphy and Parkin developed several new syntheses of $Mo(PMe_3)_6$, by either (*i*) reaction of the dihydride complex $Mo(PMe_3)_5H_2$[7] with neat PMe_3, (*ii*) reaction of the dinitrogen complex $Mo(PMe_3)_5N_2$[8] with neat PMe_3 or (*iii*) reaction of $MoCl_5$ with NaK alloy in neat PMe_3.[9] $Mo(PMe_3)_6$ has been a valuable synthetic reagent for a variety of interesting complexes, such as: $Mo(PMe_3)_4Se_2$,[7]

$Mo(PMe_3)_4(C_2H_4)_2$,[8] $Mo(PMe_3)_5N_2$,[6] $Mo(PMe_3)_2(C_4H_6)_2$,[6] $CpMo(PMe_3)_3H$,[6] and $Mo(PMe_3)_4(\eta^2\text{–}CH_2O)H_2$[10] (Scheme 2). It is also important to note that the reactivity of $Mo(PMe_3)_6$ is not simply analogous to that of $W(PMe_3)_4(\eta^2\text{–}CH_2PMe_2)H$.[11] For example, the reactivity of $Mo(PMe_3)_6$ with phenol or 2,4,6-trimethylphenol[12] (Scheme 2) differs significantly from the cyclometalation chemistry observed with $W(PMe_3)_4(\eta^2\text{–}CH_2PMe_2)H$ (see Chapter 1).[11]

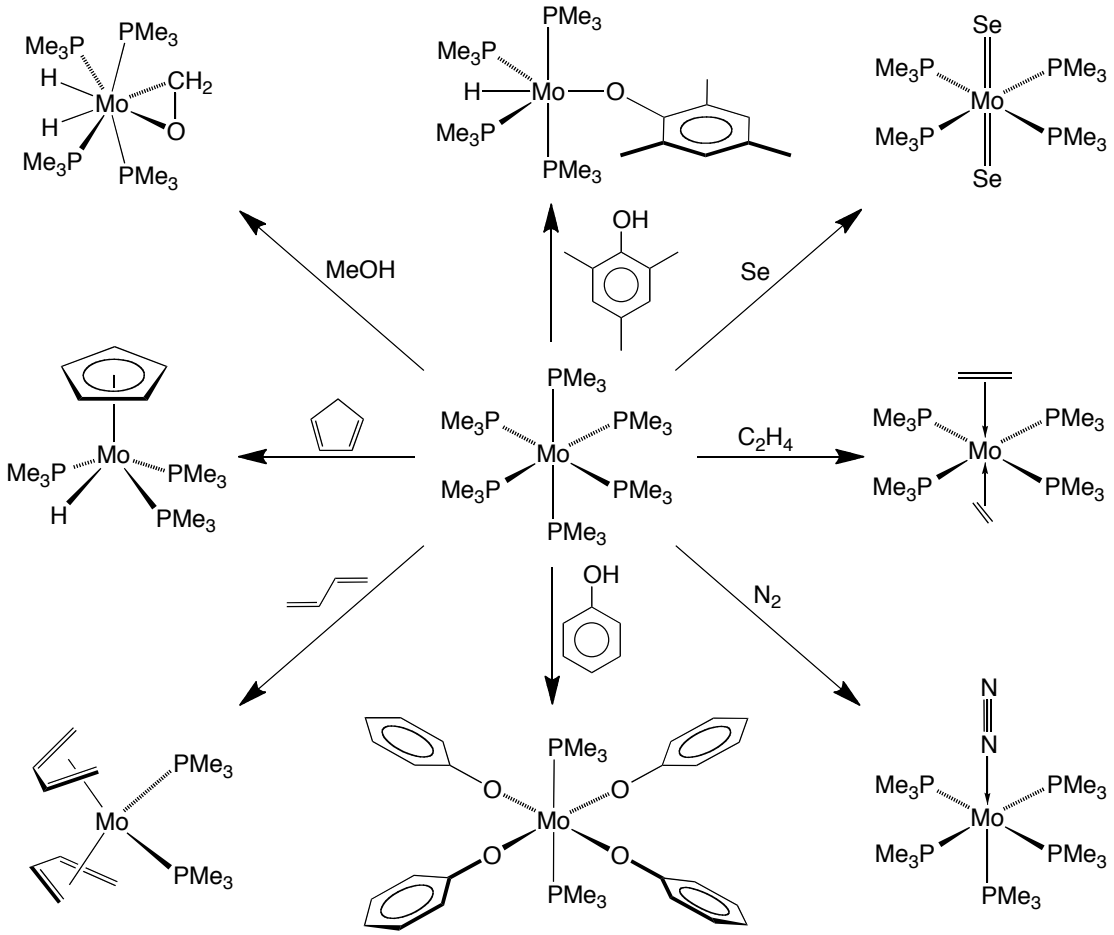

Scheme 2. Reactivity of $Mo(PMe_3)_6$.

2.1.3 Reactivity of $Mo(PMe_3)_6$ relevant to hydrodenitrogenation

In order to procure a more detailed understanding of the reactions involved in HDN, the Parkin group has studied the coordination chemistry of heterocyclic aromatic

nitrogen compounds with molybdenum, a key component of HDN catalysts.[13] For example, it was previously demonstrated that $Mo(PMe_3)_6$ reacts with quinoline (QH) (Figure 1) to form (η^6-C_5N-QH)$Mo(PMe_3)_3$ (Scheme 3), the first example of η^6-coordination of quinoline *via* the heterocyclic ring.[13c,14] Furthermore, it was found that quinoline may be catalytically hydrogenated to 1,2,3,4-tetrahydroquinoline by (η^6-C_5N-QH)$Mo(PMe_3)_3$ or $Mo(PMe_3)_4H_4$ (Scheme 3).

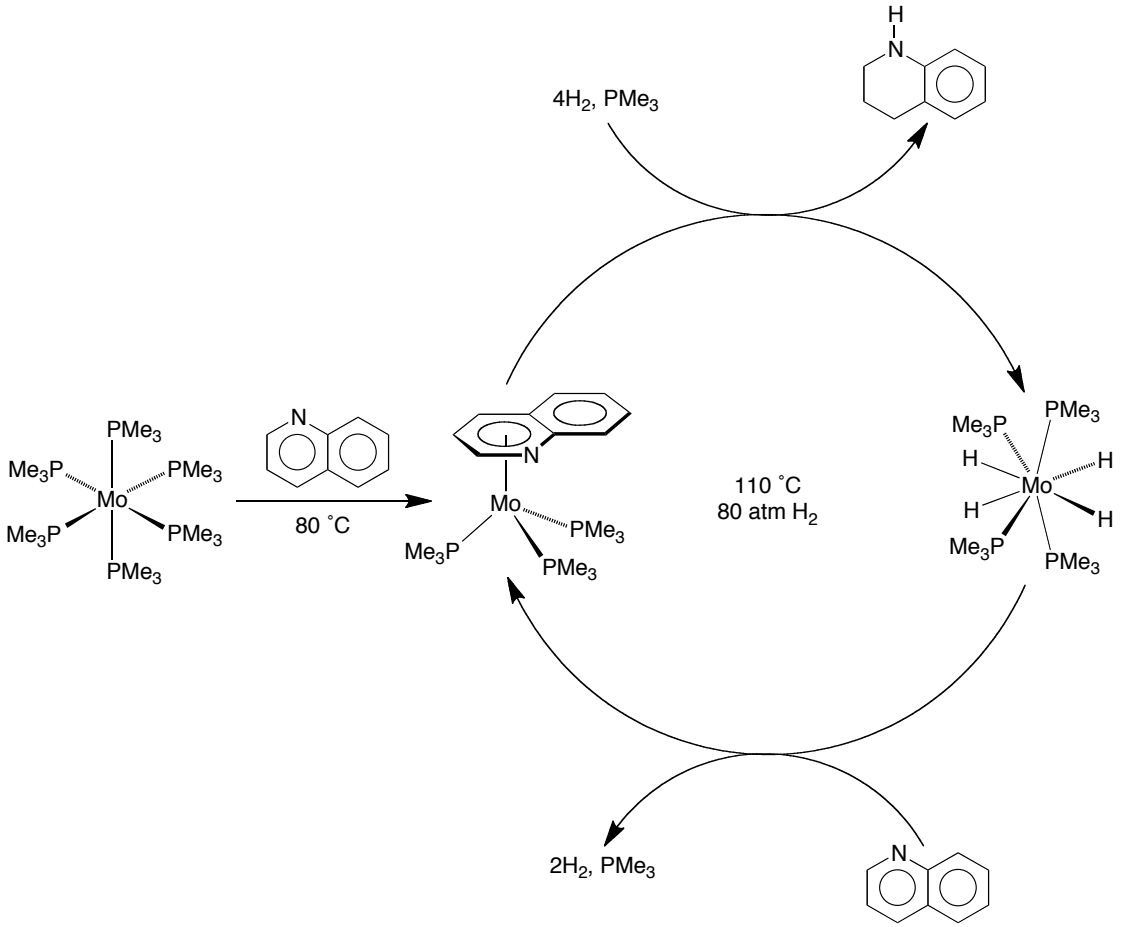

Scheme 3. Catalytic hydrogenation of quinoline by a molybdenum compound.

Recent studies have demonstrated that polynuclear aromatic compounds inhibit both hydrodenitrogenation and hydrodesulfurization,[15] and it is, therefore, important to investigate the means by which these compounds interact with molybdenum. Accordingly, the reactivity of $Mo(PMe_3)_6$ with the trinuclear aromatic compound

phenazine (PhzH) (Figure 1) is described in this chapter. Specifically, several molybdenum complexes of phenazine have been synthesized and structurally characterized, thereby demonstrating that phenazine may adopt a variety of unprecedented coordination modes to this metal. In addition, we investigated how ring fusion impacts the reactivity of heterocyclic aromatic nitrogen compounds of the type (η^6-NHetH)Mo(PMe_3)$_3$ towards oxidative addition of H_2 and subsequent hydrogenation, and this research is described herein.

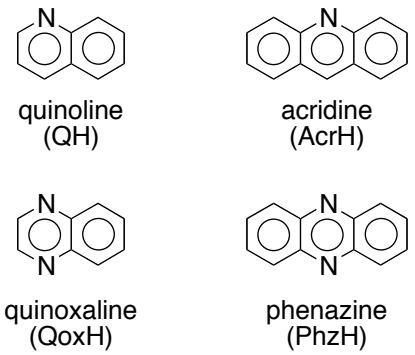

Figure 1. Binuclear and trinuclear aromatic nitrogen heterocycles.

2.2 Synthesis and structural characterization of molybdenum phenazine complexes

The Parkin group has previously demonstrated that anthracene (AnH) and acridine (AcrH) react with Mo(PMe_3)$_6$ to give (η^6-AnH)Mo(PMe_3)$_3$[16] and (η^6-C_6-AcrH)Mo(PMe_3)$_3$,[13a] respectively, in which the aromatic ligands coordinate in an η^6-manner *via* one of the outer rings (Scheme 4). The reaction of phenazine with Mo(PMe_3)$_6$ is considerably more complex and results in compounds that exhibit a variety of coordination modes.[17,18] Specifically, in addition to forming (η^6-C_6-PhzH)Mo(PMe_3)$_3$,[19] which is analogous to the reactivity observed for anthracene and acridine, Mo(PMe_3)$_6$ also reacts with phenazine to yield *(i)* (η^4-C_4-PhzH)$_2$Mo(PMe_3)$_2$, in which two phenazine ligands coordinate *via* η^4–coordination modes, and *(ii)* (μ-η^6,η^6-PhzH)[Mo(PMe_3)$_3$]$_2$, a dinuclear compound in which the phenazine ligand bridges two

metal centers (Scheme 5).[20] Thus, rather than only forming a complex in which phenazine coordinates to molybdenum in a 1:2 and 2:1 stoichiometries have also been isolated.

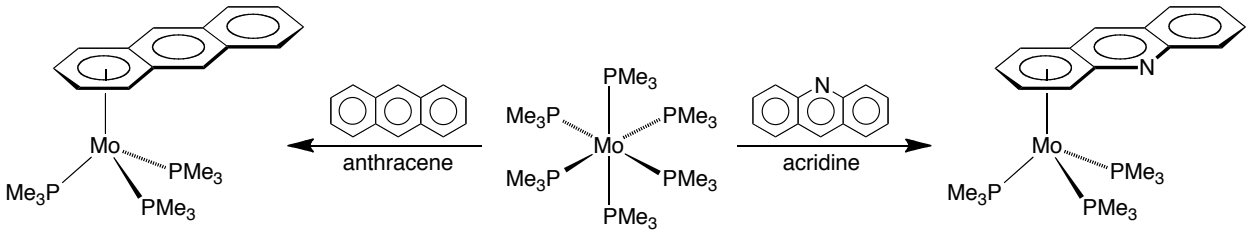

Scheme 4. Previously reported reactivity of $Mo(PMe_3)_6$ with anthracene and acridine.

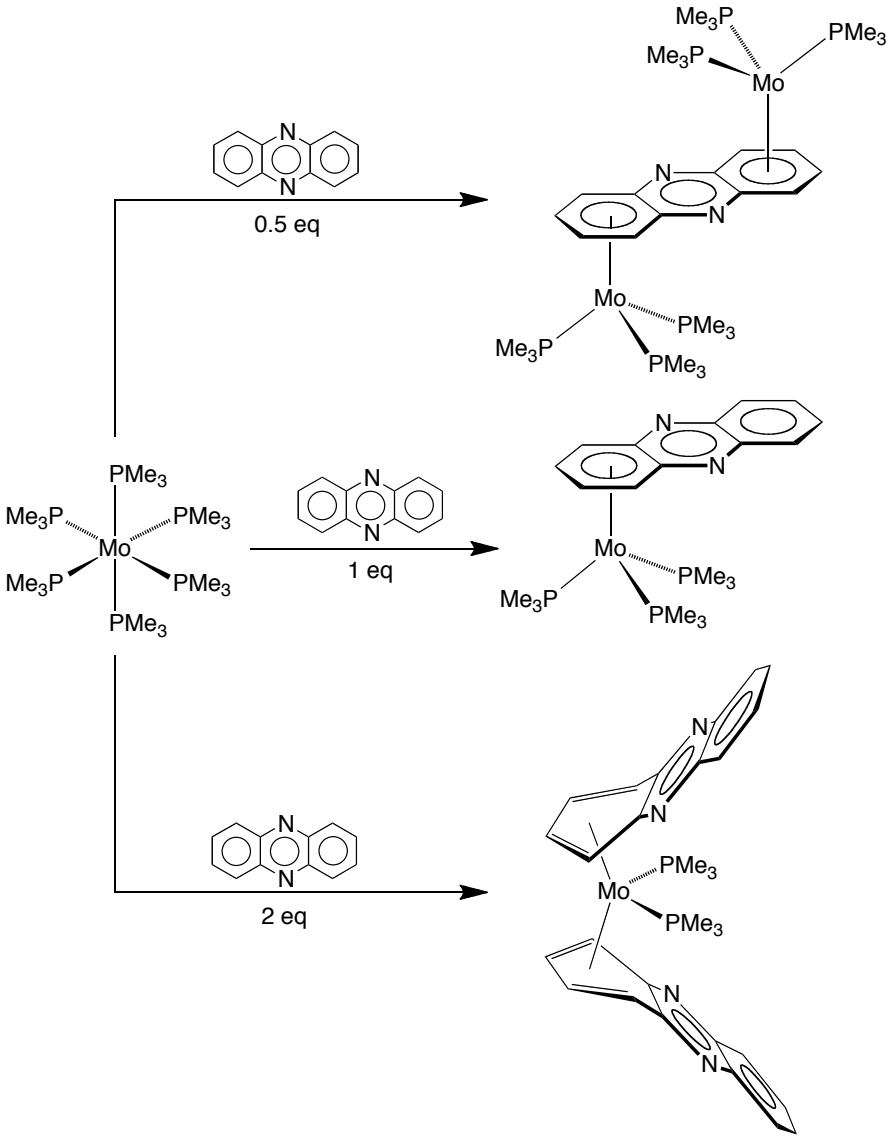

Scheme 5. Reactivity of $Mo(PMe_3)_6$ towards phenazine.

The molecular structures of (η^6-C_6-PhzH)Mo(PMe_3)$_3$,[21] (η^4-C_4-PhzH)$_2$Mo(PMe_3)$_2$, and (μ-η^6,η^6-PhzH)[Mo(PMe_3)$_3$]$_2$ have been determined by X-ray diffraction (Figures 2 – 4, respectively) and illustrate several interesting features. Firstly, the phenazine ligand in each compound coordinates by using *only the carbon atoms* of the carbocyclic rings, a previously unknown coordination mode for phenazine; in all other structurally characterized phenazine complexes, the ligand coordinates *via* its nitrogen atoms which, in many cases, are the *only* binding functionalities.[22,23] Another important feature of these compounds (discussed in more detail below) is that the phenazine ligands of (η^6-C_6-PhzH)Mo(PMe_3)$_3$ and (μ-η^6,η^6-PhzH)[Mo(PMe_3)$_3$]$_2$ adopt η^6-coordination modes, while those in (η^4-C_4-PhzH)$_2$Mo(PMe_3)$_2$ adopt η^4-coordination modes, such that the compound is closely analogous to the previously reported *bis*-butadiene complex (η^4-C_4H_6)$_2$Mo(PMe_3)$_2$[6] and the recently synthesized *bis*-crotonaldehyde complex, (η^4-OC_4H_6)$_2$Mo(PMe_3)$_2$ (see Chapter 5).

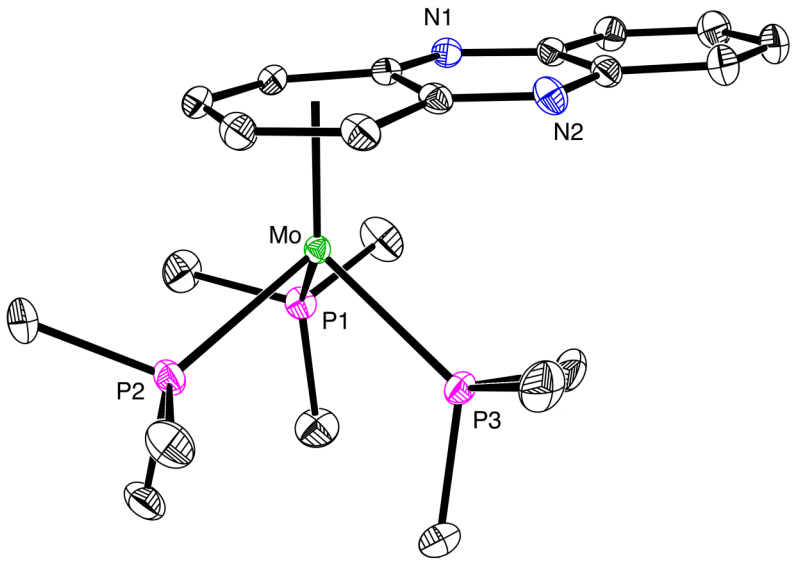

Figure 2. Molecular structure of (η^6-C_6-PhzH)Mo(PMe_3)$_3$.

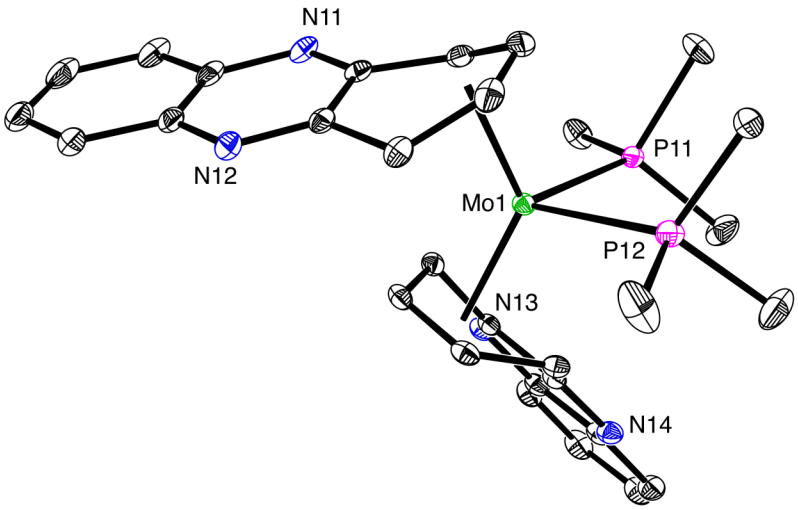

Figure 3. Molecular structure of $(\eta^4\text{-}C_4\text{-PhzH})_2Mo(PMe_3)_2$.

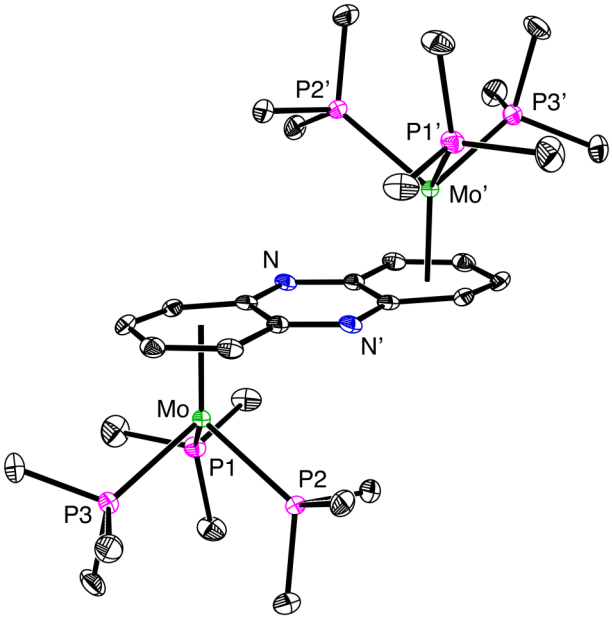

Figure 4. Molecular structure of $(\mu\text{-}\eta^6,\eta^6\text{-PhzH})[Mo(PMe_3)_3]_2$.

While the phenazine, acridine, and anthracene complexes $(\eta^6\text{-}C_6\text{-PhzH})Mo(PMe_3)_3$, $(\eta^6\text{-}C_6\text{-AcrH})Mo(PMe_3)_3$,[13a] and $(\eta^6\text{-AnH})Mo(PMe_3)_3$,[16] are structurally analogous, each exhibiting coordination *via* a terminal carbocyclic ring, the facility with which these complexes are obtained differs considerably. Thus, whereas the reaction of $Mo(PMe_3)_6$ with anthracene requires several days at 140 °C,[16] the corresponding reactions of

acridine and phenazine require less than 1 day, having half-lives of approximately 200 minutes and 10 minutes, respectively, at 80 ˚C. These observations indicate that the presence of nitrogen atoms in the central ring significantly promotes the reaction of the aromatic compound with $Mo(PMe_3)_6$, even though coordination of nitrogen is not observed in the final product. Although the mechanisms for the formation of these compounds are not known, it is possible that the nitrogen atom assists the initial coordination of acridine and phenazine to the metal center through the κ^1-*N* mode, thereby facilitating a subsequent transformation to the η^6-coordination compound.

In view of the fact that addition of excess $Mo(PMe_3)_6$ to phenazine resulted in the dinuclear complex $(\mu\text{-}\eta^6,\eta^6\text{-PhzH})[Mo(PMe_3)_3]_2$, it was attempted to synthesize dinuclear complexes of other aromatic N-heterocyles. Indeed, we were able to isolate dinuclear complexes of acridine and quinoxaline (QoxH) (Figure 1), namely $(\mu\text{-}\eta^6,\eta^6\text{-AcrH})[Mo(PMe_3)_3]_2$ and $(\mu\text{-}\eta^6,\eta^6\text{-QoxH})[Mo(PMe_3)_3]_2$,[24] and their molecular structures are shown in Figures 5 and 6, respectively.

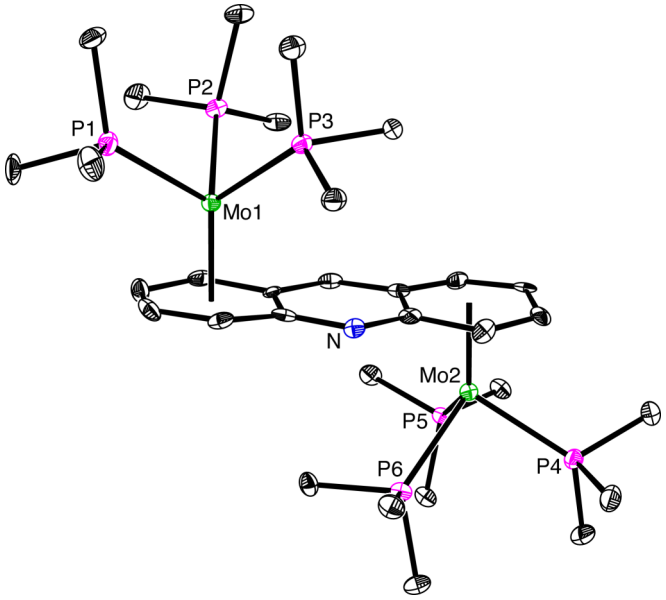

Figure 5. Molecular structure of $(\mu\text{-}\eta^6,\eta^6\text{-AcrH})[Mo(PMe_3)_3]_2$.

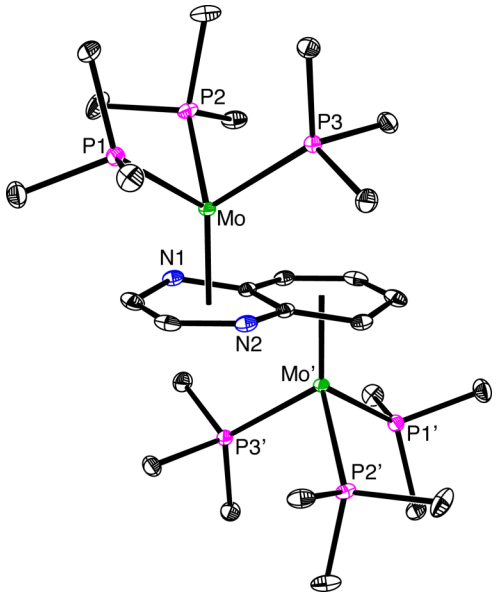

Figure 6. Molecular structure of (μ-η^6,η^6-QoxH)[Mo(PMe$_3$)$_3$]$_2$ (disorder of the quinoxaline ligand not shown).

2.3 Oxidative addition of H_2 to (η^6-NHetH)Mo(PMe$_3$)$_3$

Hydrogenation of the heterocyclic ring of polynuclear aromatic nitrogen compounds is considered to be an essential step that occurs prior to cleavage of the C–N bond during HDN.[3,25] For this reason, the reactivity of the above phenazine complexes towards H_2 has been examined. For example, while the *bis*(phenazine) complex (η^4-C_4-PhzH)$_2$Mo(PMe$_3$)$_2$ does not react with H_2 (*ca.* 1 atm) at room temperature, a green solution of (η^6-C_6-PhzH)Mo(PMe$_3$)$_3$ in benzene reacts instantaneously with H_2 (*ca.* 1 atm) to give an orange-brown solution of (η^4-C_4-PhzH)Mo(PMe$_3$)$_3$H$_2$ (Scheme 6). Although the reaction is reversible, we were able to determine the molecular structure of (η^4-C_4-PhzH)Mo(PMe$_3$)$_3$H$_2$ by crystallization at low temperature (–18 °C) in pentane in a sealed vial (Figure 7). As can be seen in Figure 7, the molecule has approximate C_s symmetry in which the mirror plane of the η^4-phenazine ligand is coincident with the plane comprising Mo, P1 and the two hydride ligands.[26,27]

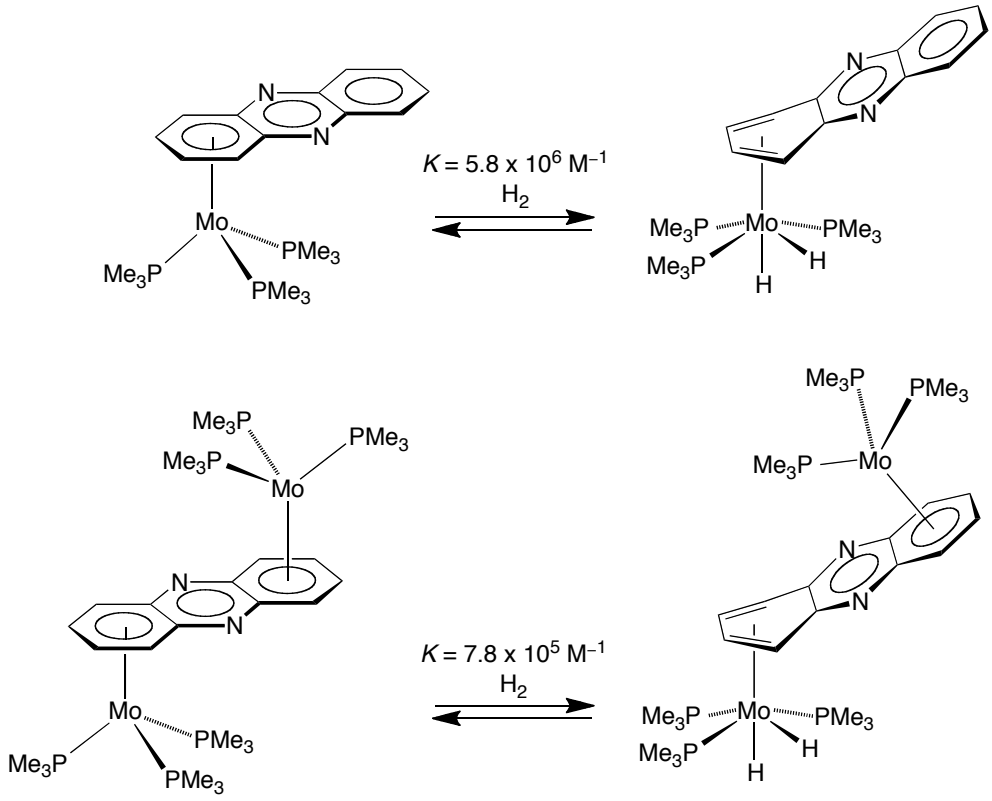

Scheme 6. Reactivity of (η^6-C_6-PhzH)Mo(PMe_3)$_3$ and (μ-η^6,η^6-PhzH)[Mo(PMe_3)$_3$]$_2$ towards H_2.

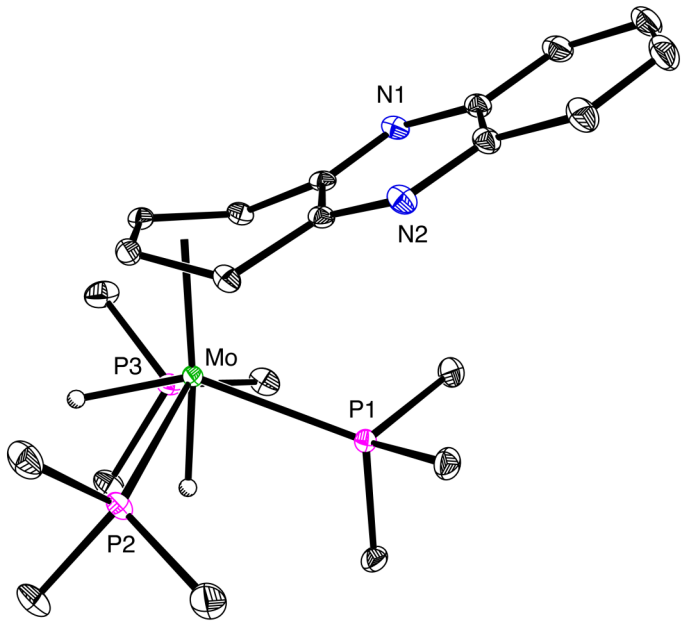

Figure 7. Molecular structure of (η^4-C_4-PhzH)Mo(PMe_3)$_3$$H_2$.

The dinuclear complex (μ-η^6,η^6-PhzH)[Mo(PMe$_3$)$_3$]$_2$ is likewise subject to oxidative addition of H_2, but the reaction occurs selectively with only *one* of the molybdenum centers to give (μ-η^6,η^4-PhzH)[Mo(PMe$_3$)$_3$][Mo(PMe$_3$)$_3$H$_2$] (Scheme 6). X-ray diffraction indicates that the coordination geometries of the two metal centers of (μ-η^6,η^4-PhzH)[Mo(PMe$_3$)$_3$][Mo(PMe$_3$)$_3$H$_2$] (Figure 8) are similar to the respective geometries of mononuclear (η^6-*C*$_6$-PhzH)Mo(PMe$_3$)$_3$ and (η^4-*C*$_4$-PhzH)Mo(PMe$_3$)$_3$H$_2$. Interestingly, while the molybdenum coordination environments of mononuclear (η^6-*C*$_6$-PhzH)Mo(PMe$_3$)$_3$ and dinuclear (μ-η^6,η^6-PhzH)[Mo(PMe$_3$)$_3$]$_2$ are similar, it is evident that coordination of the second molybdenum center does exert an influence on the ability of the other molybdenum center to undergo oxidative addition of H_2. For example, dinuclear (μ-η^6,η^4-PhzH)[Mo(PMe$_3$)$_3$][Mo(PMe$_3$)$_3$H$_2$] transfers H_2 to (η^6-*C*$_6$-PhzH)Mo(PMe$_3$)$_3$, giving (μ-η^6,η^6-PhzH)[Mo(PMe$_3$)$_3$]$_2$ and (η^4-*C*$_4$-PhzH)Mo(PMe$_3$)$_3$H$_2$ with K = 7.4 at 30°C (Scheme 7), thereby demonstrating that coordination of the second molybdenum center inhibits oxidative addition of H_2.

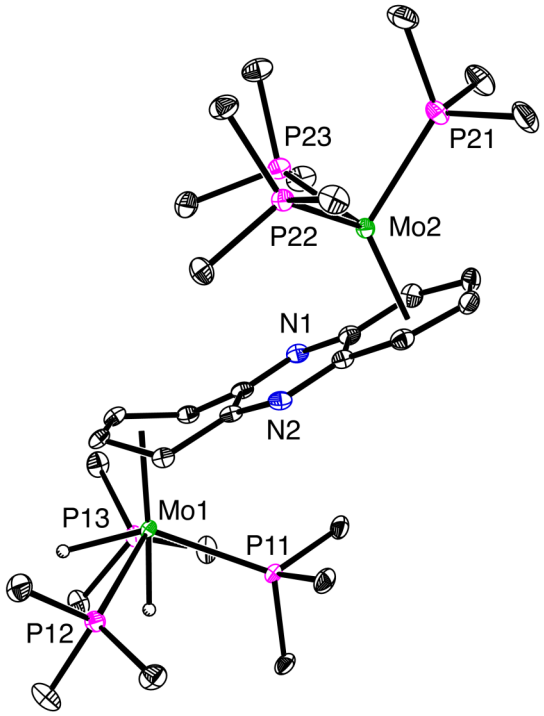

Figure 8. Molecular structure of (μ-η^6,η^4-PhzH)[Mo(PMe$_3$)$_3$][Mo(PMe$_3$)$_3$H$_2$].

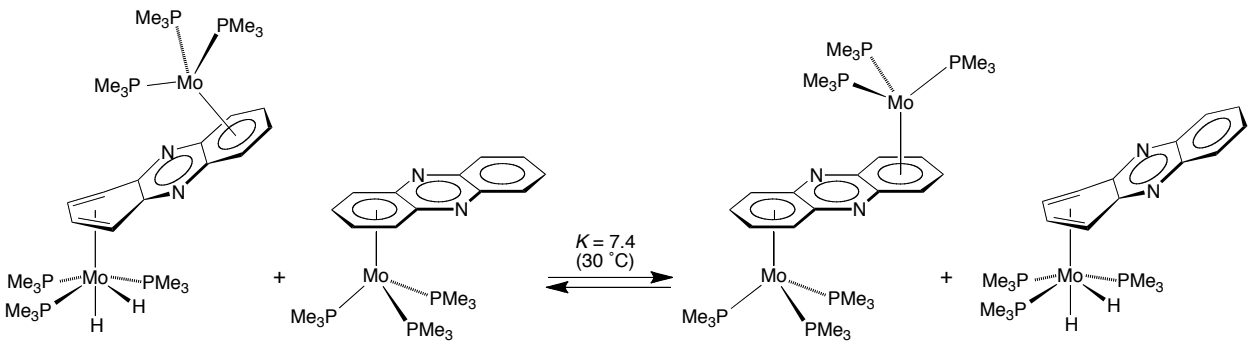

Scheme 7. H_2 transfer from (μ-η^6,η^4-PhzH)[Mo(PMe$_3$)$_3$][Mo(PMe$_3$)$_3$H$_2$] to (η^6-*C*$_6$-PhzH)Mo(PMe$_3$)$_3$.

2.4 Influence of nitrogen atom substituents on oxidative addition of H_2

Comparison of the reactivity of the phenazine, acridine and anthracene complexes (η^6-*C*$_6$-PhzH)Mo(PMe$_3$)$_3$, (η^6-*C*$_6$-AcrH)Mo(PMe$_3$)$_3$ and (η^6-AnH)Mo(PMe$_3$)$_3$, provides a means to identify how nitrogen atom substituents in an adjacent fused ring influence the ability of the metal center to undergo oxidative addition of H_2. Previously, the Parkin group reported that (η^6-AnH)Mo(PMe$_3$)$_3$ reacts reversibly with H_2 at room temperature to give (η^4-AnH)Mo(PMe$_3$)$_3$H$_2$.[16,28] Not surprisingly, the acridine counterpart, (η^6-*C*$_6$-AcrH)Mo(PMe$_3$)$_3$,[13a] also reacts rapidly with H_2 at room temperature to yield (η^4-*C*$_4$-AcrH)Mo(PMe$_3$)$_3$H$_2$ (Scheme 8). The molecular structure of (η^4-*C*$_4$-AcrH)Mo(PMe$_3$)$_3$H$_2$ has been determined by X–ray diffraction, using the same crystallization procedure as that for (η^4-*C*$_4$-PhzH)Mo(PMe$_3$)$_3$H$_2$ (Figure 9). Significantly, (η^4-*C*$_4$-AcrH)Mo(PMe$_3$)$_3$H$_2$ is the first structurally characterized complex that exhibits an η^4-coordination mode for acridine, which otherwise typically coordinates in a κ^1-*N* manner.[29,30] Also of note, the structure of (η^4-*C*$_4$-AcrH)Mo(PMe$_3$)$_3$H$_2$ differs from that of (η^4-*C*$_4$-PhzH)Mo(PMe$_3$)$_3$H$_2$ in that the long axis of the η^4-acridine ligand does not lie in the mirror plane of the [Mo(PMe$_3$)$_3$H$_2$] moiety. The solid state structure of (η^4-*C*$_4$-AcrH)Mo(PMe$_3$)$_3$H$_2$ is, nevertheless, in accord with that proposed for one of the configurations of (η^4-*C*$_4$-PhzH)Mo(PMe$_3$)$_3$H$_2$ observed in solution at low temperature (see reference 27). Furthermore, we also determined the molecular structure of the

anthracene complex, (η^4-AnH)Mo(PMe_3)$_3H_2$ (Figure 10), which exhibits the same configuration as that of (η^4-C_4-AcrH)Mo(PMe_3)$_3H_2$ in the solid state.

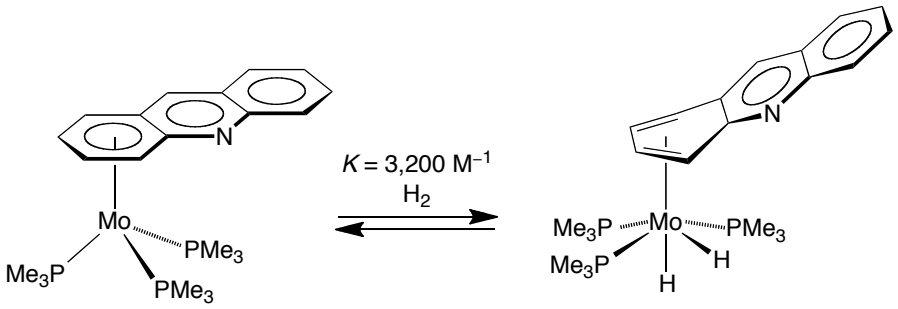

Scheme 8. Reversible reactivity of (η^6-C_6-AcrH)Mo(PMe_3)$_3$ with H_2.

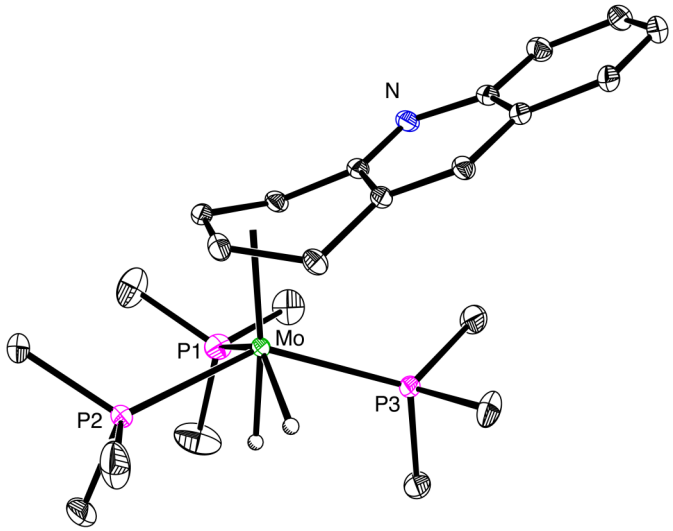

Figure 9. Molecular structure of (η^4-C_4-AcrH)Mo(PMe_3)$_3H_2$.

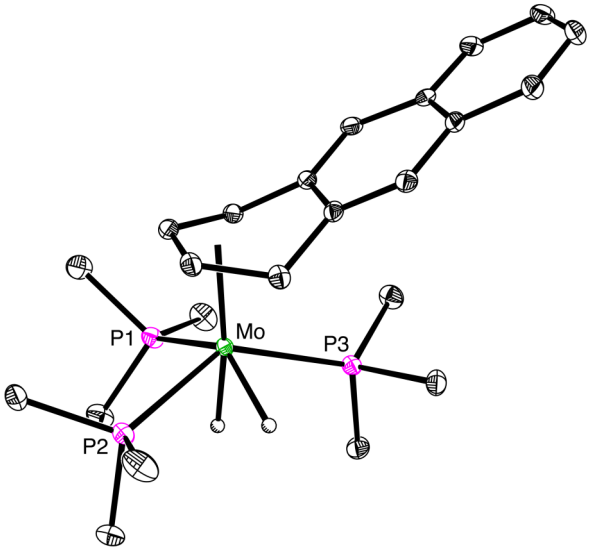

Figure 10. Molecular structure of (η^4-AnH)Mo(PMe_3)$_3H_2$.

As with (η^6-AnH)Mo(PMe_3)$_3$,[16,28] the oxidative addition of H_2 to (η^6-C_6-AcrH)Mo(PMe_3)$_3$ and (η^6-C_6-PhzH)Mo(PMe_3)$_3$ is reversible and a series of H_2 transfer experiments demonstrates that the equilibrium constant for oxidative addition increases in the sequence $K_{AnH} < K_{AcrH} < K_{PhzH}$ (Table 1). Specifically, (η^4-AnH)Mo(PMe_3)$_3H_2$ transfers H_2 to (η^6-C_6-AcrH)Mo(PMe_3)$_3$ giving (η^4-C_4-AcrH)Mo(PMe_3)$_3H_2$ and (η^6-AnH)Mo(PMe_3)$_3$ (K = 2.0 at 30˚C), while (η^4-C_4-AcrH)Mo(PMe_3)$_3H_2$ transfers H_2 to (η^6-C_6-PhzH)Mo(PMe_3)$_3$ giving (η^4-C_4-PhzH)Mo(PMe_3)$_3H_2$ and (η^6-C_6-AcrH)Mo(PMe_3)$_3$ (K = 1.8×10^2 at 30˚C), as illustrated in Scheme 9. From these equilibrium measurements, it is evident that the presence of nitrogen atoms in the central ring increases the ability of the metal center to undergo oxidative addition of H_2. In support of these observations, density functional theory (DFT) calculations also predict that the exothermicity for oxidative addition of H_2 increases with the number of nitrogen atoms in the central ring (Table 2).

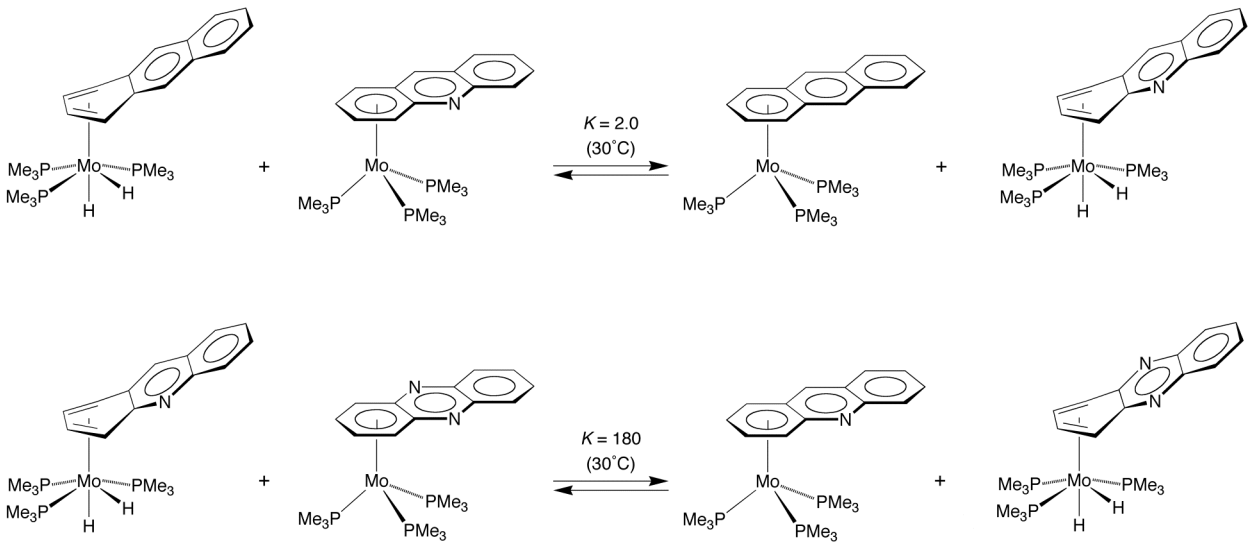

Scheme 9. H_2 transfer experiments [(η^4-AnH)Mo(PMe_3)$_3H_2$ transfers H_2 to (η^6-C_6-AcrH)Mo(PMe_3)$_3$ (top) and (η^4-C_4-AcrH)Mo(PMe_3)$_3H_2$ transfers H_2 to (η^6-C_6-PhzH)Mo(PMe_3)$_3$ (bottom)].

Table 1. Equilibrium constant data for oxidative addition of H_2 to (η^6-ArH)Mo(PMe_3)$_3$ in C_6D_6 at 30°C.

(η^6-ArH)Mo(PMe_3)$_3$	***K* (M^{-1})**
(η^6-AnH)Mo(PMe_3)$_3$[a]	1.6×10^4
(η^6-C_6-AcrH)Mo(PMe_3)$_3$[b]	3.2×10^4
(η^6-C_6-PhzH)Mo(PMe_3)$_3$[b]	5.8×10^6
(μ-η^6,η^6-PhzH)[Mo(PMe_3)$_3$]$_2$[b]	7.8×10^5
(η^6-C_6-QoxH)Mo(PMe_3)$_3$[c]	7.2×10^2

(a) Data taken from reference 28.

(b) Value determined from a thermodynamic cycle which couples experimentally measured values for H_2 exchange between the various metal centers (Schemes 7 and 9) with the oxidative addition of H_2 to (η^6-AnH)Mo(PMe_3)$_3$.

(c) Value at room temperature.

Table 2. Computational ΔH (kcal mol^{-1}) for oxidative addition of H_2 to (η^6-NHetH)Mo(PH_3)$_3$ giving two isomers of (η^4-NHetH)Mo(PH_3)$_3H_2$.

(η^6-ArH)Mo(PH_3)$_3$	**Symmetric (η^4-NHetH)Mo(PH_3)$_3H_2$**	**Asymmetric (η^4-NHetH)Mo(PH_3)$_3H_2$**
(η^6-AnH)Mo(PH_3)$_3$	-1.77	-4.19
(η^6-C_6-AcrH)Mo(PH_3)$_3$	-3.30	-5.67
(η^6-C_6-PhzH)Mo(PH_3)$_3$	-6.43	-8.04

2.5 Influence of ring fusion on oxidative addition of H_2

Previous experimental and computational studies concerned with the benzene, naphthalene and anthracene compounds, (η^6-PhH)Mo(PMe_3)$_3$, (η^6-NpH)Mo(PMe_3)$_3$ and (η^6-AnH)Mo(PMe_3)$_3$, have demonstrated that ring fusion also promotes oxidative addition of H_2.[16] In particular, the dihydride only becomes experimentally observable for the anthracene system. We have now extended this study to include heterocyclic aromatic compounds. Comparison of the reactivity of related mononitrogen heterocyclic systems, namely the quinoline (QH) and acridine derivatives, which

respectively possess two and three fused six-membered rings, demonstrates that ring fusion also promotes oxidative addition in this system. Thus, whereas (η^6-C_6-AcrH)Mo(PMe_3)$_3$ reacts with H_2 to give (η^4-C_4-AcrH)Mo(PMe_3)$_3H_2$ (Scheme 10), (η^6-C_6-QH)Mo(PMe_3)$_3$ is inert towards H_2 under comparable conditions.[13a]

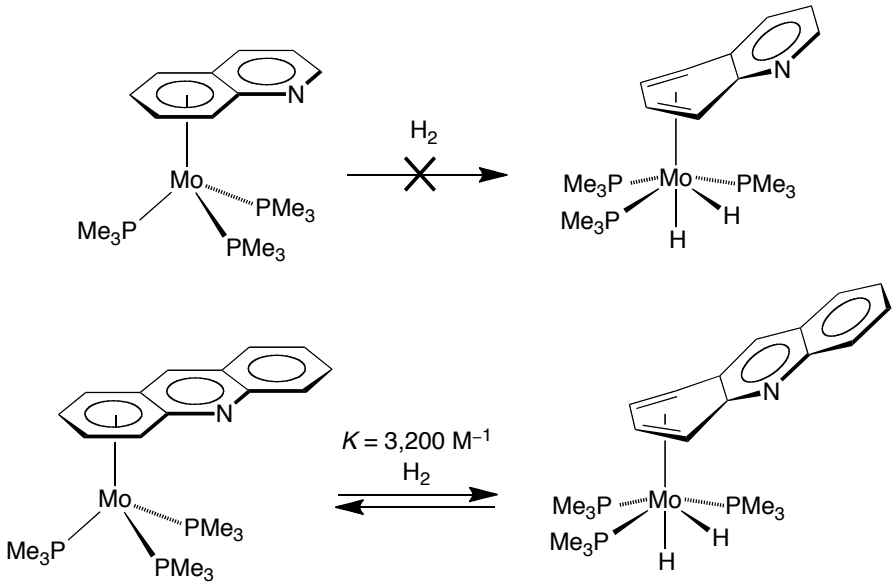

Scheme 10. Effects of ring fusion on oxidative addition of H_2.

A similar effect is observed upon comparison of the quinoxaline (QoxH) and phenazine compounds, (η^6-C_6-QoxH)Mo(PMe_3)$_3$[13c] and (η^6-C_6-PhzH)Mo(PMe_3)$_3$, both of which feature two nitrogen atoms in the adjacent fused ring. Thus, in contrast to the rapid reaction of (η^6-C_6-PhzH)Mo(PMe_3)$_3$ with H_2 to give (η^4-C_4-PhzH)Mo(PMe_3)$_3H_2$, the quinoxaline counterpart (η^6-C_6-QoxH)Mo(PMe_3)$_3$,[13c] with only two fused six-membered rings, requires several days to react and yields (η^4-C_4-QoxH)Mo(PMe_3)$_3H_2$ (Scheme 11) as only a component of an equilibrium mixture under 1 atmosphere of H_2 ($K = 7.2 \times 10^2$ M^{-1} at room temperature). As such, it demonstrates that, in this system, ring-fusion increases the reactivity of the metal center towards oxidative addition of H_2 by a factor of $\approx 10^4$ in equilibrium constant, an observation that may be viewed as a heterocyclic analogue of the "anthracene effect".[16]

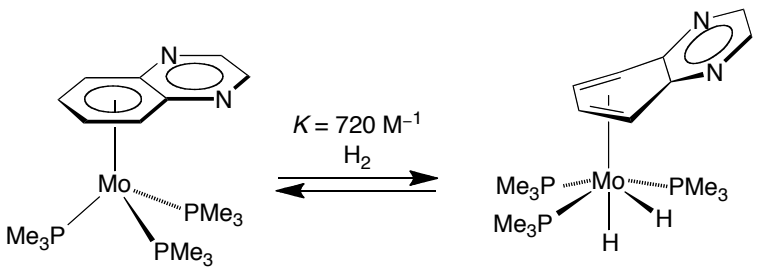

Scheme 11. Equilibrium between (η^6-C_6-QoxH)Mo(PMe_3)$_3$ and H_2 with (η^4-C_4-QoxH)Mo(PMe_3)$_3H_2$.

Despite the fact that (η^4-C_4-QoxH)Mo(PMe_3)$_3H_2$ is only observed as a component of an equilibrium mixture, the compound was successfully crystallized by cooling a solution in pentane at –18 ˚C in a sealed vial, and has been structurally characterized by X–ray diffraction. Most interestingly, the asymmetric unit consists of two molecules that differ by the orientation of the η^4-quinoxaline ligand relative to the [Mo(PMe_3)$_3H_2$] moiety (Figure 11). As such, it is evident that (η^4-C_4-QoxH)Mo(PMe_3)$_3H_2$ exhibits *both* of the configurations discussed above for the phenazine, acridine and anthracene compounds. In view of the fact that each of these compounds exhibits two conformations in solution at low temperature, it is possible that the different solid state structures may merely reflect crystal packing effects.

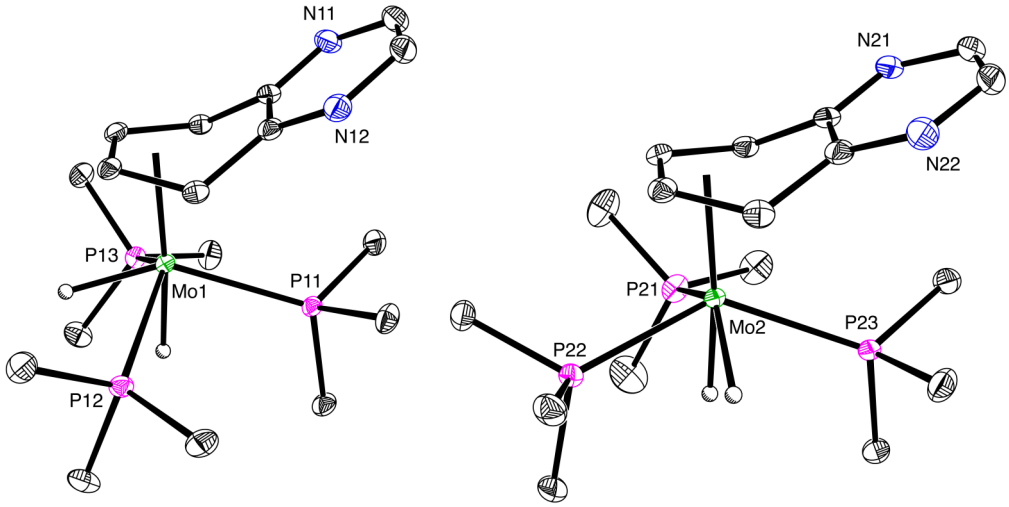

Figure 11. Molecular structure of (η^4-C_4-QoxH)Mo(PMe_3)$_3H_2$ (both isomers are in the asymmetric unit).

The ability to observe spectroscopically and structurally characterize (η^4-C_4-QoxH)Mo(PMe_3)$_3H_2$ is also noteworthy because the corresponding species were not observed for the quinoline and naphthalene derivatives. As such, it provides a further illustration that nitrogen substituents in an adjacent fused ring promote oxidative addition of H_2.

2.6 Hydrogenation of the N-heterocycles

While (η^6-C_6-PhzH)Mo(PMe_3)$_3$ and (η^6-C_6-AcrH)Mo(PMe_3)$_3$ only undergo oxidative addition of H_2 at room temperature, the phenazine and acridine ligands are hydrogenated at elevated temperatures. Accordingly, (η^6-C_6-PhzH)Mo(PMe_3)$_3$ releases a mixture of 5,10-dihydrophenazine and 1,2,3,4-tetrahydrophenazine upon treatment with H_2 in benzene at 95 °C,[31] while (η^6-C_6-AcrH)Mo(PMe_3)$_3$ releases 9,10-dihydroacridine under the same conditions; in both cases, the principal molybdenum containing product is (η^6-PhH)Mo(PMe_3)$_3$ (Scheme 12).

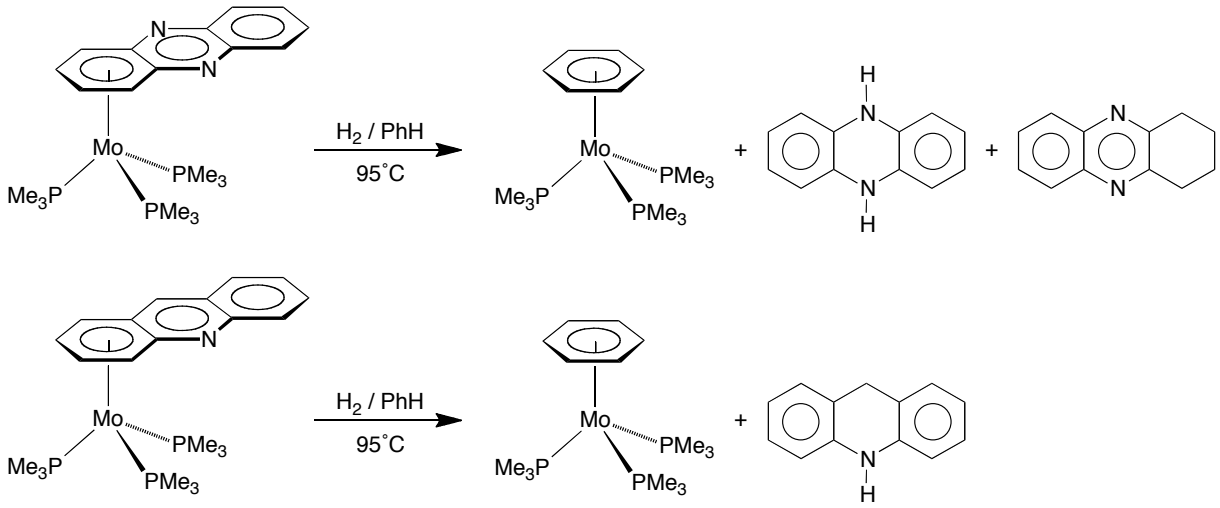

Scheme 12. Hydrogenation of phenazine and acridine by molybdenum.

In contrast to the hydrogenation of acridine, the quinoline counterpart (η^6-C_6-QH)Mo(PMe_3)$_3$ is stable under these conditions,[13a] from which it is evident that ring

fusion also promotes hydrogenation of the heterocyclic ligand in this system. Furthermore, although the turnover number is low (7.2 turnovers over a period of 21 days), acridine is catalytically hydrogenated in the presence of (η^6-C_6-AcrH)Mo(PMe_3)$_3$ and H_2 at 95 ˚C in cyclohexane. Under these conditions, the principal products are a *ca*. 2:3 mixture of 9,10-dihydroacridine and 1,2,3,4-tetrahydroacridine.[32] The formation of 1,2,3,4-tetrahydroacridine is noteworthy because several studies indicate that acridine is typically selectively hydrogenated at the central heterocyclic ring to give 9,10-dihydroacridine.[33] In fact, we are aware of only one catalyst that selectively hydrogenates the carbocyclic rings of acridine, namely $RuH_2(\eta^2\text{-}H_2)_2(PCy_3)_2$, as reported by Borowski and Sabo-Etienne.[30]

2.7 Structural comparison of η^6- and η^4-phenazine complexes

The phenazine complexes discussed above belong to two classes according to whether the ligand binds in an η^6 or η^4 manner *via* the carbon atoms, both of which are distinct from the previously reported modes for phenazine that involve coordination *via* the nitrogen atoms.[22,23] Thus, (η^6-C_6-PhzH)Mo(PMe_3)$_3$ and (μ-η^6,η^6-PhzH)[Mo(PMe_3)$_3$]$_2$ exhibit η^6-coordination, while (η^4-C_4-PhzH)Mo(PMe_3)$_3H_2$ and (η^4-C_4-PhzH)$_2$Mo(PMe_3)$_2$ possess η^4-coordination modes, and (μ-η^6,η^4-PhzH)[Mo(PMe_3)$_3$][Mo(PMe_3)$_3H_2$] exhibits both modes.

Despite the fact that (η^6-C_6-PhzH)Mo(PMe_3)$_3$ and (μ-η^6,η^6-PhzH)[Mo(PMe_3)$_3$]$_2$ both exhibit η^6-coordination, the phenazine ligands do not coordinate symmetrically. For example, the Mo–C bond distances for the carbocyclic ring of (η^6-C_6-PhzH)Mo(PMe_3)$_3$ increase in the sequence Mo–$C_{outer(av)}$ [2.28 Å] < Mo–$C_{central(av)}$ [2.30 Å] < Mo–$C_{ring\ junction(av)}$ [2.41 Å] (Table 3). As such, the phenazine ligand slips so that the ring junction becomes more distant from the metal. The displacement of the heterocycle from symmetric η^6–coordination may be expressed in terms of a slip parameter (Δ_{M-C}),

defined as the difference between *(i)* the average distance from the metal center to the two ring junction carbons and *(ii)* the average distance from the metal to the outer carbon atoms (Figure 12). In this regard, the slip parameters for (η^6-C_6-PhzH)Mo(PMe_3)$_3$ and (μ-η^6,η^6-PhzH)[Mo(PMe_3)$_3$]$_2$ are comparable to those of the acridine, quinoxaline and anthracene complexes, (η^6-C_6-AcrH)Mo(PMe_3)$_3$, (μ-η^6,η^6-AcrH)[Mo(PMe_3)$_3$]$_2$, (μ-η^6,η^6-QoxH)[Mo(PMe_3)$_3$]$_2$and (η^6-AnH)Mo(PMe_3)$_3$, as summarized in Table 3. Similar slippages are also observed for η^6-complexes of other fused-ring aromatic systems.[34]

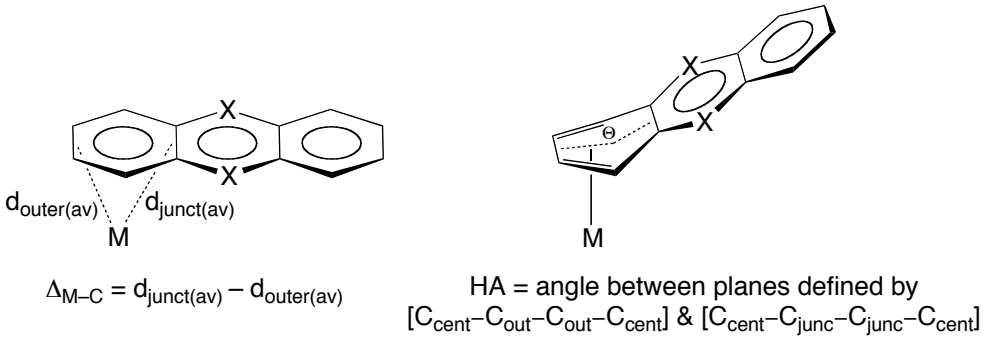

Figure 12. Definition of slip parameter (Δ_{M-C}) and hinge angle (HA).

Table 3. Average Mo–C bond lengths for the outer, central and ring junction carbon atoms of [(η^6–ArH)Mo] complexes, slip parameters (Δ_{M-C}) and hinge angles (HA) as determined by X–ray diffraction.

	***d*(Mo–C_{out})** **(Å)**	***d*(Mo–C_{cent})** **(Å)**	***d*(Mo–C_{junct})** **(Å)**	**(Δ_{M-C})** **(Å)**	**HA** **(°)**
(η^6-C_6-PhzH)Mo(PMe_3)$_3$	2.282	2.302	2.407	0.125	4.7
(μ-η^6,η^6-PhzH)[Mo(PMe_3)$_3$]$_2$	2.290	2.292	2.406	0.116	5.4
(μ-η^6,η^4-PhzH)[Mo(PMe_3)$_3$][Mo(PMe_3)$_3H_2$]	2.288	2.280	2.347	0.059	4.1
(η^6-C_6-AcrH)Mo(PMe_3)$_3$[a]	2.288	2.271	2.393	0.105	5.8
(μ-η^6,η^6-AcrH)[Mo(PMe_3)$_3$]$_2$	2.269	2.283	2.406	0.137	5.0
	2.285	2.294	2.4150	0.130	5.5
(μ-η^6,η^6-QoxH)[Mo(PMe_3)$_3$]$_2$	2.246	2.259	2.396	0.150	10.9
(η^6-C_6-AnH)Mo(PMe_3)$_3$[b]	2.273	2.283	2.416	0.143	6.0
	2.278	2.288	2.421	0.143	5.8

(a) Data taken from reference 13a.

(b) Data taken from reference 16 (values for two independent molecules).

The origin of the slippage may be traced to the nature of the highest occupied π molecular orbital (π–HOMO) of phenazine (Figure 13), obtained by analysis of the Fenske-Hall molecular orbitals.[35] In this regard, the bonding in transition metal compounds [M(η^6-arene)] is generally considered to involve π–donation from the arene HOMO, supplemented by δ–backbonding to the arene LUMO.[36,37] It was previously rationalized that the ring-slippage occurs in the naphthalene and anthracene compounds, (η^6-NpH)Mo(PMe_3)$_3$ and (η^6-AnH)Mo(PMe_3)$_3$, because of this former interaction.[16] Specifically, the π–HOMO of a ring-fused arene is localized on the outer carbon atoms, which causes the arene to slip in order to maximize the π–interaction with the metal *d* orbital. The π–HOMO of phenazine is also largely localized on the outer carbon atoms (Figure 13), thereby providing an explanation of the slippage in (η^6-C_6-PhzH)Mo(PMe_3)$_3$ and (μ-η^6,η^6-PhzH)[Mo(PMe_3)$_3$]$_2$.

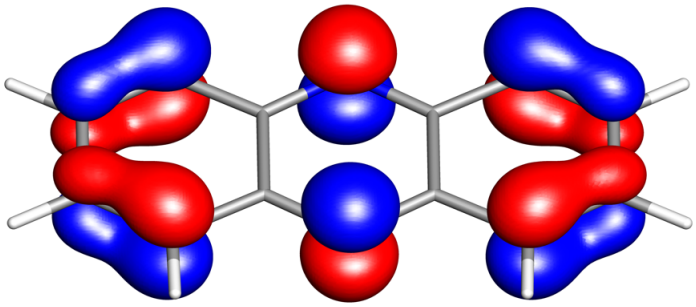

Figure 13. The highest occupied π molecular orbital of phenazine.

In contrast to the flat nature of the η^6-phenazine ligands in (η^6-C_6-PhzH)Mo(PMe_3)$_3$ and (μ-η^6,η^6-PhzH)[Mo(PMe_3)$_3$]$_2$, the η^4-phenazine ligands of (η^4-C_4-PhzH)Mo(PMe_3)$_3$H$_2$ and (η^4-C_4-PhzH)$_2$Mo(PMe_3)$_2$ exhibit a distinct fold at the central carbon atoms of the coordinated ring. The folding of the phenazine ligand may be expressed in terms of the hinge angle (HA), defined as the dihedral angle between the planes comprising *(i)* the η^4-diene component and *(ii)* the central and junction carbon atoms of the coordinated ring (Figure 12). In this regard, the phenazine ligand of (η^4-C_4-

PhzH)Mo(PMe_3)$_3H_2$ is folded by 34.5˚, while the phenazine ligands of the two crystallographically independent molecules of (η^4-C_4-PhzH)$_2$Mo(PMe_3)$_2$ exhibit hinge angles in the range 28.4 – 37.3˚. For comparison, the hinge angles of the η^6-phenazine complexes are only in the range 4.1 – 5.4˚. In addition to the hinge angle, another indication of the folding is provided by the slip parameter, which increases from 0.13 Å for (η^6-C_6-PhzH)Mo(PMe_3)$_3$ to 0.91 Å for (η^4-C_4-PhzH)Mo(PMe_3)$_3H_2$ (Tables 3 and 4).

Table 4. Average Mo–C bond lengths for the outer, central and ring junction carbon atoms of [(η^4–ArH)Mo] complexes, slip parameters (Δ_{M-C}) and hinge angles (HA) as determined by X–ray diffraction.

	***d*(Mo–C_{out})** **(Å)**	***d*(Mo–C_{cent})** **(Å)**	***d*(Mo–C_{junct})** **(Å)**	**(Δ_{M-C})** **(Å)**	**HA** **(˚)**
(η^4-C_4-PhzH)Mo(PMe_3)$_3H_2$	2.214	2.356	3.119	0.905	34.5
(μ-η^6,η^4-PhzH)[Mo(PMe_3)$_3$][Mo(PMe_3)$_3H_2$]	2.208	2.349	3.134	0.926	35.4
(η^4-C_4-AcrH)Mo(PMe_3)$_3H_2$	2.226	2.355	3.127	0.901	35.0
(η^4-AnH)Mo(PMe_3)$_3H_2$	2.251	2.352	3.167	0.916	39.2
(η^4-C_4-PhzH)$_2$Mo(PMe_3)$_2$[a]	2.220	2.360	3.152	0.932	37.3
	2.288	2.390	3.029	0.741	28.4
(η^4-C_4-PhzH)$_2$Mo(PMe_3)$_2$[a]	2.227	2.349	3.131	0.904	36.5
	2.296	2.358	3.045	0.749	33.1
(η^4-C_4-QoxH)Mo(PMe_3)$_3H_2$[b]	2.216	2.337	3.152	0.936	39.3
(η^4-C_4-QoxH)Mo(PMe_3)$_3H_2$[c]	2.251	2.355	3.098	0.847	35.1

(a) Two crystallographically independent molecules.

(b) Symmetric isomer of two crystallographically independent molecules.

(c) Asymmetric isomer of two crystallographically independent molecules.

For purpose of comparison, the slip parameters and hinge angles of the η^4-complexes of anthracene,[38] acridine, and quinoxaline complexes are also listed in Table 4. While a simple explanation of the bending of the aromatic ligands is to preserve an 18–electron configuration of the metal center, a more complete analysis indicates that folding serves to stabilize the orbital involved in the metal-to-ligand backbonding

interaction by minimizing the antibonding component between the metal and the two carbon atoms of the ring junction,[39] and this molecular orbital is shown in Figure 14.[35]

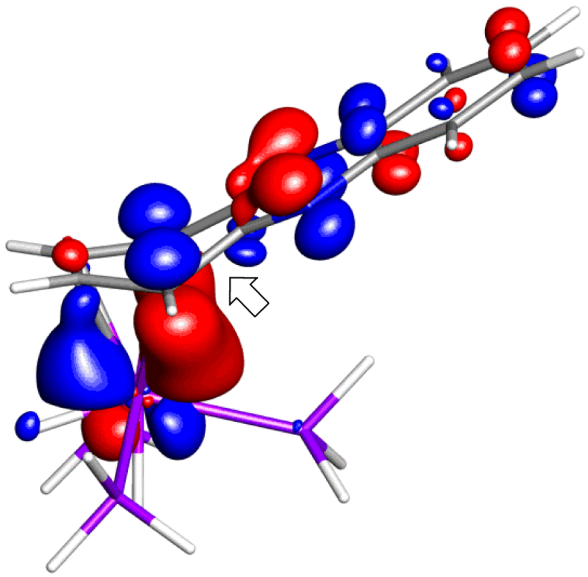

Figure 14. The occupied back-bonding molecular orbital of (η^4-C_4-PhzH)Mo(PH_3)$_3$$H_2$ for which the out-of-phase component with the d orbital (marked with an arrow) promotes folding of the heterocycle.

2.8 Summary and conclusions

In summary, phenazine reacts with Mo(PMe_3)$_6$ to give (η^6-C_6-PhzH)Mo(PMe_3)$_3$, (μ-η^6,η^6-PhzH)[Mo(PMe_3)$_3$]$_2$ and (η^4-C_4-PhzH)$_2$Mo(PMe_3)$_2$, in which the phenazine ligand exhibits previously unknown coordination modes *via* only the carbon atoms. Comparison of the reactivity of the phenazine, acridine and anthracene complexes, (η^6-C_6-PhzH)Mo(PMe_3)$_3$, (η^6-C_6-AcrH)Mo(PMe_3)$_3$ and (η^6-AnH)Mo(PMe_3)$_3$, demonstrates that incorporation of nitrogen substituents into the central ring promotes oxidative addition of H_2. The same conclusion is obtained by comparison of the reactivity of compounds that feature two fused rings, namely the quinoxaline and quinoline complexes, (η^6-C_6-QoxH)Mo(PMe_3)$_3$ and (η^6-C_6-QH)Mo(PMe_3)$_3$. Furthermore, comparison of the reactivity of *(i)* (η^6-C_6-PhzH)Mo(PMe_3)$_3$ and (η^6-C_6-QoxH)Mo(PMe_3)$_3$, and *(ii)* (η^6-C_6-AcrH)Mo(PMe_3)$_3$ and (η^6-C_6-QH)Mo(PMe_3)$_3$ demonstrate that ring fusion

promotes oxidative addition of H_2. Lastly, the phenazine and acridine ligands of (η^6-C_6-PhzH)Mo(PMe_3)$_3$ and (η^6-C_6-AcrH)Mo(PMe_3)$_3$ are hydrogenated when heated at 95 °C.

2.9 Experimental details

2.9.1 General considerations

All manipulations were performed using a combination of glovebox, high vacuum, and Schlenk techniques under an argon atmosphere unless otherwise specified.[40] Solvents were purified and degassed by standard procedures. ^{1}H NMR spectra were measured on Bruker 300 DRX, Bruker 400 DRX, and Bruker Avance 500 DMX spectrometers. ^{1}H chemical shifts are reported in ppm relative to $SiMe_4$ (δ = 0) and were referenced internally with respect to the protio solvent impurity (δ 7.16 for C_6D_6, 2.09 for C_7D_8, 1.38 for C_6D_{12}, and 7.26 for $CDCl_3$).[41,42] ^{13}C NMR spectra are reported in ppm relative to $SiMe_4$ (δ = 0) and were referenced internally with respect to the solvent (δ 128.06 for C_6D_6).[41] ^{31}P chemical shifts are reported in ppm relative to 85% H_3PO_4 (δ = 0) and were referenced using $P(OMe)_3$ (δ = 141.0) as an external standard.[43] Coupling constants are given in hertz. Infrared spectra were recorded on Nicolet Avatar 370 DTGS spectrometer and are reported in cm^{-1}. Mass spectra were obtained on a Micromass Quadrupole-Time-of-Flight mass spectrometer using fast atom bombardment (FAB). Mo(PMe_3)$_6$,[7] (η^6-AnH)Mo(PMe_3)$_3$,[16] (η^4-AnH)Mo(PMe_3)$_3H_2$,[16] (η^6-C_6-AcrH)Mo(PMe_3)$_3$,[13a] (η^6-C_6-QH)Mo(PMe_3)$_3$,[13a] (η^6-C_6-QoxH)Mo(PMe_3)$_3$,[13c] and (η^6-C_6-PhzH)Mo(PMe_3)$_3$,[18] were prepared by the literature methods.

2.9.2 X-ray structure determinations

X-ray diffraction data were collected on a Bruker Apex II diffractometer. Crystal data, data collection and refinement parameters are summarized in Section 2.10, Table 5. The structures were solved using direct methods and standard difference map techniques,

and were refined by full-matrix least-squares procedures on F^2 with SHELXTL (Version 6.10).[44]

2.9.3 Computational details

Calculations were carried out using DFT as implemented in the Jaguar 7.0 suite of *ab initio* quantum chemistry programs.[45] Geometry optimizations were performed with the B3LYP density functional[46] using the 6-31G** (C, H, N and P) and LACVP (Mo) basis sets.[47] The energies of the optimized structures were reevaluated by additional single point calculations on each optimized geometry using cc-pVTZ(-f) correlation consistent triple-ζ basis set for C, H, N, and P and LACV3P for Mo. Molecular orbital analyses were performed with the aid of Jimp 2,[35] which employs Fenske-Hall calculations and visualization using MOPLOT.[48]

2.9.4 Comparison of the reactivity of $Mo(PMe_3)_6$ towards phenazine and acridine

Two NMR tubes equipped with J. Young valves containing *(i)* a mixture of $Mo(PMe_3)_6$ (10 mg, 0.02 mmol) and phenazine (5 mg, 0.03 mmol) and *(ii)* a mixture of $Mo(PMe_3)_6$ (10 mg, 0.02 mmol) and acridine (5 mg, 0.03 mmol) were treated with a solution of C_6D_6 (*ca.* 0.7 mL), containing a trace amount of mesitylene as an internal standard. The samples were heated at 80˚C and monitored by ^{1}H NMR spectroscopy, thereby demonstrating that the reaction of $Mo(PMe_3)_6$ with phenazine to form (η^6-C_6-PhzH)$Mo(PMe_3)_3$ ($t_{½} \approx 10$ minutes) is more facile than the corresponding reaction with acridine to form (η^6-C_6-AcrH)$Mo(PMe_3)_3$ ($t_{½} \approx 200$ minutes) under the same conditions.

2.9.5 Synthesis of $(\eta^4$-C_4-PhzH)$_2Mo(PMe_3)_2$

A mixture of $Mo(PMe_3)_6$ (20 mg, 0.04 mmol) and phenazine (20 mg, 0.11 mmol) in benzene (*ca.* 0.7 mL) was heated at 95˚C for 4 days, over which period red crystals were

deposited. The crystals were isolated, washed with pentane (2 mL) and dried *in vacuo* to give (η^4-C_4-PhzH)$_2$Mo(PMe$_3$)$_2$ as a red solid (12 mg, 55% yield) suitable for X-ray diffraction. Anal. Calcd. for $C_{30}H_{34}N_4P_2Mo$: C, 59.2 %; H, 5.6 %; N, 9.2 %. Found: C, 59.3 %; H, 5.4 %; N, 9.1 %.

^{1}H NMR (C_6D_6): 0.42 [virtual triplet, PMe$_3$ (minor conformation)], 0.60 [d, $^2J_{P-H}$ = 7, PMe$_3$ (major conformation)], 2.97, 3.08, 3.21, 4.27, 4.82 [each broad singlet, 8H of 2 PhzH], 7.12 [m, 4H of 2 PhzH], 7.81 [m, 4H of 2 PhzH] (two conformations in the ratio 2:1 are observed in solution, but only the PMe$_3$ signals are distinct). IR Data (KBr disk, cm^{-1}): 3054 (w), 2964 (w), 2907 (w), 2851 (w), 1570 (w), 1506 (w), 1448 (w), 1410 (m), 1362 (vs), 1333 (m), 1287 (w), 1261 (w), 1217 (w), 1114 (w), 1018 (w), 948 (s), 808 (w), 759 (s), 714 (w), 668 (w).

2.9.6 Synthesis of (μ-η^6,η^6-PhzH)[Mo(PMe$_3$)$_3$]$_2$

A mixture of Mo(PMe$_3$)$_6$ (50 mg, 0.09 mmol) and phenazine (8 mg, 0.04 mmol) in d_{12}-cyclohexane (*ca.* 0.7 mL) was heated at 140˚C for 5 hours, after which period the volatile components were removed *in vacuo*. The residue was washed with benzene (*ca.* 0.5 mL) and with pentane (*ca.* 1 mL). Benzene (*ca.* 0.5 mL) was added and the mixture was lyophilized to give (μ-η^6,η^6-PhzH)[Mo(PMe$_3$)$_3$]$_2$ as a dark yellow solid (20 mg, 54% yield) which contains a small amount of 5,10-dihydrophenazine (< 5%). Crystals suitable for X-ray diffraction were grown by slow evaporation of a solution in pentane at –18 °C.

^{1}H NMR (C_6D_6): 1.17 [d, $^2J_{P-H}$ = 5, 54H of 6 PMe$_3$], 3.95 [s, 4H of PhzH], 4.98 [s, 4H of PhzH]. ^{13}C{^{1}H} NMR (C_6D_6): 25.7 [d, $^1J_{P-C}$ = 20, 18C of 6 PMe$_3$], 70.6 [s, 4C of PhzH], 75.5 [s, 4C of PhzH], 120.2 [s, 4C of PhzH (quaternary)]. ^{31}P{^{1}H} (C_6D_6): 10.08 [very br, PMe$_3$]. IR Data (KBr disk, cm^{-1}): 3058 (w), 2958 (m), 2895 (s), 2790 (w), 1506 (w), 1473

(w), 1452 (w), 1414 (m), 1362 (w), 1327 (w), 1315 (w), 1288 (w), 1271 (s), 1117 (w), 1080 (w), 939 (vs), 928 (vs), 869 (w), 831 (w), 778 (w), 691 (w), 649 (m).

2.9.7 Synthesis of (η^4-*C*$_4$-PhzH)Mo(PMe$_3$)$_3$H$_2$

(η^4-PhzH)Mo(PMe$_3$)$_3$H$_2$ was synthesized by a modified procedure.[18] A solution of (η^6-*C*$_6$-PhzH)Mo(PMe$_3$)$_3$ (10 mg) in C_6D_6 (*ca.* 0.7 mL) with mesitylene as an internal standard was placed in an NMR tube equipped with a J. Young valve and saturated with H_2 (1 atm), thereby resulting in a rapid color change (*ca.* 1 minute) from green to orange-brown. The reaction was monitored by ^{1}H and ^{31}P NMR spectroscopy, thereby demonstrating the conversion to (η^4-*C*$_4$-PhzH)Mo(PMe$_3$)$_3$H$_2$ (> 95%). The volatile components were removed by lyophilization giving an orange-brown solid and crystals suitable for X-ray diffraction were grown by slow evaporation of a solution in pentane at –18 ˚C.

2.9.8 Synthesis of (μ-η^6,η^4-PhzH)[Mo(PMe$_3$)$_3$][Mo(PMe$_3$)$_3$H$_2$]

A solution of (μ-η^6,η^6-PhzH)[Mo(PMe$_3$)$_3$]$_2$ (5 mg) in C_6D_6 (*ca.* 0.7 mL) with mesitylene as an internal standard was placed in an NMR tube equipped with a J. Young valve and saturated with H_2 (1 atm). The reaction was monitored by ^{1}H NMR spectroscopy, thereby demonstrating the conversion to (μ-η^6,η^4-PhzH)[Mo(PMe$_3$)$_3$][Mo(PMe$_3$)$_3$H$_2$] (> 95%) over a period of 30 minutes. The volatile components were removed by lyophilization giving a green solid and crystals suitable for X-ray diffraction were grown by slow evaporation of a solution in pentane at –18 °C.

^{1}H NMR (C_6D_6): -3.67 [br, 2H of MoH$_2$)], 1.00 [d, $^2J_{P-H}$ = 7, 27H of PMe$_3$], 1.37 [s, 27H of PMe$_3$], 2.97 [br, 2H of PhzH], 3.87 [br, 2H of PhzH], 4.65 [br, 2H of PhzH], 4.76 [br, 2H of PhzH]. ^{1}H NMR ($C_6D_5CD_3$ at -73°C, hydride region only), two species in the ratio *ca.* 2.5:1 are observed: -4.03 [t, $^2J_{P-H}$ = 41, 1H], -2.59 [dt, $^2J_{P-H}$ = 66, $^2J_{P-H}$ = 40, 1H]

(major species); -8.30 [t, $^{2}J_{P\text{-}H}$ = 54, 1H], -3.75 [m, 1H] (minor species). $^{13}C\{^{1}H\}$ NMR (C_6D_6): 24.7 [d, $^{1}J_{P-C}$ = 24, 9C of PMe_3], 26.9 [m, 9C of PMe_3], 60.2 [s, 2C of PhzH], 70.0 [s, 2C of PhzH], 72.4 [s, 2C of PhzH], 74.6 [s, 2C of PhzH], 102.0 [s, 2C of PhzH], 159.4 [s, 2C of PhzH]. $^{31}P\{^{1}H\}$ (C_6D_6): 7.1 [br, 6 P of PMe_3]. IR Data (KBr disk, cm^{-1}): 3046 (w), 3018 (w), 2957 (m), 2896 (s), 2797 (w), 1739 (br, m), 1556 (w), 1510 (m), 1418 (m), 1383 (w), 1361 (w), 1332 (m), 1280 (m), 1193 (w), 1097 (w), 1067 (w), 942 (vs), 845 (m), 718 (w), 689 (w), 657 (m).

2.9.9 Reactivity of (η^4-*C*$_4$-PhzH)$_2$Mo(PMe$_3$)$_2$ towards H_2

(a) A suspension of (η^4-*C*$_4$-PhzH)$_2$Mo(PMe$_3$)$_2$ (10 mg) in C_6D_6 (*ca.* 0.7 mL) was placed in an NMR tube equipped with a J. Young valve and saturated with H_2 (*ca.* 1 atm). The sample was left at room temperature and monitored by ^{1}H NMR spectroscopy, thereby demonstrating that (η^4-*C*$_4$-PhzH)$_2$Mo(PMe$_3$)$_2$ did not react after 2 days.

(b) A suspension of (η^4-*C*$_4$-PhzH)$_2$Mo(PMe$_3$)$_2$ (10 mg) in C_6D_6 (*ca.* 0.7 mL) was placed in an NMR tube equipped with a J. Young valve and saturated with H_2 (*ca.* 1 atm). The sample was heated at 95°C and monitored by ^{1}H NMR spectroscopy, thereby demonstrating that (η^4-*C*$_4$-PhzH)$_2$Mo(PMe$_3$)$_2$ remained largely unreacted after 5 days.

2.9.10 Synthesis of (η^4-*C*$_4$-AcrH)Mo(PMe$_3$)$_3$H$_2$

(η^4-AcrH)Mo(PMe$_3$)$_3$H$_2$ was synthesized by a modified procedure.[18] A solution of (η^6-*C*$_6$-AcrH)Mo(PMe$_3$)$_3$ (10 mg) in C_6D_6 (*ca.* 0.7 mL) with mesitylene as an internal standard was placed in an NMR tube equipped with a J. Young valve and saturated with H_2 (1 atm), thereby resulting in a rapid color change (*ca.* 30 minutes) from green to yellow. The reaction was monitored by ^{1}H and ^{31}P NMR spectroscopy, thereby demonstrating the conversion to (η^4-*C*$_4$-AcrH)Mo(PMe$_3$)$_3$H$_2$ (> 95%). The volatile components were

removed by lyophilization giving a yellow solid and crystals suitable for X-ray diffraction were grown by slow evaporation of a solution in pentane at –18 ˚C.

2.9.11 Synthesis of (η^4-*C*$_4$-QoxH)Mo(PMe$_3$)$_3$H$_2$

A solution of (η^6-*C*$_6$-QoxH)Mo(PMe$_3$)$_3$ (10 mg) in C_6D_6 (*ca.* 0.7 mL) with mesitylene as an internal standard was placed in an NMR tube equipped with a J. Young valve and saturated with H_2 (*ca.* 1 atm). The reaction was monitored by ^{1}H NMR spectroscopy, thereby demonstrating the conversion to an equilibrium mixture with (η^4-*C*$_4$-QoxH)Mo(PMe$_3$)$_3$H$_2$ over a period of 2 days ($K = 7.2 \times 10^2$ M^{-1} at room temperature). Crystals suitable for X-ray diffraction were grown by slow evaporation of a solution in pentane at –18 °C.

^{1}H NMR (C_6D_6): -4.0[very br, 2H of MoH_2], 1.01 [d, $^2J_{P–H} = 7$, 27H of PMe_3], 2.75 [s, 2H of QoxH], 4.83 [s, 2H of QoxH], 7.26 [s, 2H of QoxH]. ^{1}H NMR ($C_6D_5CD_3$ at -73°C, hydride region only), two species in the ratio *ca.* 3:1 are observed: -3.89 [ddt, $^2J_{P-H} = 41$, $^2J_{P-H} = 10$, $^2J_{H-H} = 10$, 1H], -2.42 [dt, $^2J_{P-H} = 67$, $^2J_{P-H} = 39$, 1H] (major species); -8.64 [ddt, $^2J_{P-H} = 57$, $^2J_{P-H} = 11$, $^2J_{H-H} = 11$, 1H], -3.61 [m, 1H] (minor species).

2.9.12 Structural characterization of (η^4-AnH)Mo(PMe$_3$)$_3$H$_2$

(η^4-AnH)Mo(PMe$_3$)$_3$H$_2$ was synthesized as previously reported *via* reaction of (η^6-AnH)Mo(PMe$_3$)$_3$ with H_2.[16] Crystals suitable for X-ray diffraction were obtained by slow evaporation of a pentane solution at –18 ˚C.

2.9.13 Hydrogenation of (η^6-*C*$_6$-PhzH)Mo(PMe$_3$)$_3$

A solution of (η^6-*C*$_6$-PhzH)Mo(PMe$_3$)$_3$ (5 mg) in C_6D_6 (*ca.* 0.7 mL) with mesitylene as an internal standard was placed in an NMR tube equipped with a J. Young valve and saturated with H_2 (*ca.* 1 atm), thereby resulting in a color change from green to orange-

brown over a period of *ca.* 1 minute due to the formation of (η^4-C_4-PhzH)Mo(PMe_3)$_3H_2$. The solution was then heated at 95˚C for 17 days and monitored by ^{1}H NMR spectroscopy, thereby demonstrating conversion to, *inter alia*, 5,10-dihydrophenazine[49] (*ca.* 50%) and 1,2,3,4-tetrahydrophenazine[50] (*ca.* 30%). The principal molybdenum containing species produced is (η^6–d_6-PhH)Mo(PMe_3)$_3$ (*ca.* 70%), together with trace amounts of (η^4-PhzH)$_2$Mo(PMe_3)$_2$.

2.9.14 Hydrogenation of (η^6-C_6-AcrH)Mo(PMe_3)$_3$

A solution of (η^6-C_6-AcrH)Mo(PMe_3)$_3$ (5 mg) in C_6D_6 (*ca.* 0.7 mL) with mesitylene as an internal standard was placed in an NMR tube equipped with a J. Young valve and saturated with H_2 (*ca.* 1 atm), thereby resulting in a color change from green to yellow over a period of ca. 30 minutes due to the formation of (η^4-C_4-AcrH)Mo(PMe_3)$_3H_2$. The solution was heated at 95 ˚C for 3 days and monitored by ^{1}H NMR spectroscopy, thereby demonstrating conversion to 9,10-dihydroacridine (*ca.* > 95%), which was identified by comparison of the ^{1}H NMR spectrum in $CDCl_3$ with that of an authentic sample.[51] The principal molybdenum containing species produced is (η^6-d_6-PhH)Mo(PMe_3)$_3$.

2.9.15 Internal comparison of the reactivity of (η^6-C_6-AcrH)Mo(PMe_3)$_3$ and (η^6-C_6-QH)Mo(PMe_3)$_3$ toward H_2

A solution of (η^6-C_6-AcrH)Mo(PMe_3)$_3$ (5 mg) and (η^6-C_6-QH)Mo(PMe_3)$_3$ (5 mg) in C_6D_6 (*ca.* 0.7 mL) with mesitylene as an internal standard was placed in an NMR tube equipped with a J. Young valve and saturated with H_2 (*ca.* 1 atm). The solution was heated at 95 ˚C and monitored by ^{1}H NMR spectroscopy, thereby demonstrating that (η^6-C_6-AcrH)Mo(PMe_3)$_3$ released 9,10-dihydroacridine over a period of 2 days, while (η^6-C_6-QH)Mo(PMe_3)$_3$ was stable with respect to hydrogenation over this period,

although a small amount of quinoline (*ca*. 25 %) dissociates due to conversion to (η^6-d_6-PhH)Mo(PMe_3)$_3$.

2.9.16 Hydrogenation of acridine in the presence of (η^6-C_6-AcrH)Mo(PMe_3)$_3$

A solution of (η^6-C_6-AcrH)Mo(PMe_3)$_3$ (4 mg) and acridine (7.4 equiv.) in d_{12}-cyclohexane (*ca.* 0.7 mL) with mesitylene as an internal standard was placed in an NMR tube equipped with a J. Young valve and saturated with H_2 (*ca.* 1 atm), thereby resulting in a change in color from green to yellow over a period of *ca*. 30 minutes, indicating the conversion to (η^4-C_4-AcrH)Mo(PMe_3)$_3H_2$. The solution was heated at 95 ˚C and monitored by ^{1}H NMR spectroscopy, thereby demonstrating the catalytic hydrogenation of 7.2 equivalents of acridine (in addition to the coordinated acridine) over a period of 21 days to a mixture of 9,10-dihydroacridine[51] and 1,2,3,4-tetrahydroacridine,[52] which were identified by ^{1}H NMR spectroscopy and mass spectrometry. Due to solubility differences in cyclohexane, the ratio of 9,10-dihydroacridine to 1,2,3,4-tetrahydroacridine (2:3) was determined by ^{1}H NMR spectroscopic analysis of the product mixture in $CDCl_3$. In addition to 9,10-dihydroacridine and 1,2,3,4-tetrahydroacridine, a small amount of insoluble 9,9′-biacridane was identified by X-ray diffraction. The latter compound has been reported to be generated *via* reaction between acridine and 9,10-dihydroacridine.[53] The hydrogenation reaction was repeated in the presence of elemental Hg, which was found to have no impact on the course of the reaction.

2.9.17 Measurement of the equilibrium constant for oxidative addition of H_2 to (η^6-C_6-QoxH)Mo(PMe_3)$_3$

A solution of (η^6-C_6-QoxH)Mo(PMe_3)$_3$ (5 mg) C_6D_6 (*ca.* 0.7 mL) with mesitylene as an internal standard was placed in an NMR tube equipped with a J. Young valve and

saturated with H_2 (1 atm). The reaction was monitored by ^{1}H NMR spectroscopy, thereby demonstrating the conversion to an equilibrium mixture with (η^4-C_4-QoxH)Mo(PMe_3)$_3H_2$ over a period 2 days ($K = 7.2 \times 10^2$ M^{-1} at room temperature). The concentration of H_2 was determined using reported solubility data.[54]

2.9.18 Measurement of the equilibrium constant for H_2 transfer from (μ-η^6,η^4-PhzH)[Mo(PMe_3)$_3$][Mo(PMe_3)$_3H_2$] to (η^6-C_6-PhzH)Mo(PMe_3)$_3$

A solution of (μ-η^6,η^4-PhzH)[Mo(PMe_3)$_3$][Mo(PMe_3)$_3H_2$] (7 mg, 0.008 mmol) and (η^6-C_6-PhzH)Mo(PMe_3)$_3$ (4 mg, 0.008 mmol) in C_6D_6 (*ca.* 0.7 mL) with mesitylene as an internal standard was placed in an NMR tube equipped with a J. Young valve. The sample was placed in a constant temperature bath at 30 ˚C and monitored for several days by ^{1}H NMR spectroscopy, thereby demonstrating the transfer of H_2 from (μ-η^6,η^4-PhzH)[Mo(PMe_3)$_3$][Mo(PMe_3)$_3H_2$] to (η^6-C_6-PhzH)Mo(PMe_3)$_3$, producing (μ-η^6,η^6-PhzH)[Mo(PMe_3)$_3$]$_2$ and (η^4-C_4-PhzH)Mo(PMe_3)$_3H_2$ as components of an equilibrium mixture ($K = 7.4$).

2.9.19 Measurement of the equilibrium constant for H_2 transfer from (η^4-AnH)Mo(PMe_3)$_3H_2$ to (η^6-C_6-AcrH)Mo(PMe_3)$_3$

A solution of (η^4-AnH)Mo(PMe_3)$_3H_2$ (5 mg) and (η^6-C_6-AcrH)Mo(PMe_3)$_3$ (5 mg) in C_6D_6 (*ca.* 0.7 mL) with mesitylene as an internal standard was placed in an NMR tube equipped with a J. Young valve. The sample was placed in a constant temperature bath at 30 ˚C and monitored for several days by ^{1}H NMR spectroscopy, thereby demonstrating the transfer of H_2 from (η^4-AnH)Mo(PMe_3)$_3H_2$ to (η^6-C_6-AcrH)Mo(PMe_3)$_3$, producing (η^6-AnH)Mo(PMe_3)$_3$ and (η^4-C_4-AcrH)Mo(PMe_3)$_3H_2$ as components of an equilibrium mixture ($K = 2.0$).

2.9.20 Measurement of the equilibrium constant for H_2 transfer from (η^4-C_4-AcrH)Mo(PMe_3)$_3H_2$ to (η^6-C_6-PhzH)Mo(PMe_3)$_3$

A solution of (η^4-C_4-AcrH)Mo(PMe_3)$_3H_2$ (5 mg) and (η^6-C_6-PhzH)Mo(PMe_3)$_3$ (5 mg) in C_6D_6 (*ca.* 0.7 mL) with mesitylene as an internal standard was placed in an NMR tube equipped with a J. Young valve. The sample was placed in a constant temperature bath at 30 ˚C and monitored for several days by ^{1}H NMR spectroscopy, thereby demonstrating the transfer of H_2 from (η^4-C_4-AcrH)Mo(PMe_3)$_3H_2$ to (η^6-C_6-PhzH)Mo(PMe_3)$_3$, producing (η^6-C_6-AcrH)Mo(PMe_3)$_3$ and (η^4-C_4-PhzH)Mo(PMe_3)$_3H_2$ as components of an equilibrium mixture ($K = 1.8 \times 10^2$).

2.9.21 Computational analysis of oxidative addition of H_2 to (η^6-NHetH)Mo(PMe_3)$_3$

A computational analysis of the oxidative addition of H_2 to (η^6-NHetH)Mo(PMe_3)$_3$ giving (η^4-NHetH)Mo(PMe_3)$_3H_2$ was performed for computationally simpler system in which the methyl groups of the PMe_3 ligands were replaced by hydrogen atoms. Furthermore, in each case, two isomers of (η^4-NHetH)Mo(PH_3)$_3H_2$ were considered on the basis of the X-ray diffraction and ^{1}H NMR spectroscopic studies[18] on (η^4-NHetH)Mo(PMe_3)$_3H_2$. The thermodynamics for formation of both isomers of (η^4-NHetH)Mo(PH_3)$_3H_2$ by oxidative addition of H_2 to (η^6-NHetH)Mo(PH_3)$_3$ were evaluated. Significantly, for each isomer, the calculations indicate that oxidative addition of H_2 becomes more exothermic in the sequence anthracene < acridine < phenazine, in accord with experimental observations.

2.10 Crystallographic data

Table 5. Crystal, intensity collection and refinement data.

	(μ-η⁶,η⁶-PhzH)[Mo(PMe$_3$)$_3$]$_2$	**(η⁴-*C*$_4$-PhzH)$_2$Mo(PMe$_3$)$_2$**
lattice	Monoclinic	Triclinic
formula	$C_{30}H_{62}Mo_2N_2P_6$	$C_{30}H_{34}MoN_4P_2$
formula weight	828.52	608.49
space group	$P2_1/n$	$P\text{-}1$
a/Å	14.5169(10)	13.4843(9)
b/Å	9.0962(6)	14.0854(10)
c/Å	16.3795(11)	15.9116(11)
α/°	90	76.5770(10)
β/°	115.4630(10)	70.9850(10)
γ/°	90	79.8950(10)
V/Å^3	1952.8(2)	2762.7
Z	2	4
temperature (K)	170(2)	125(2)
radiation (λ, Å)	0.71073	0.71073
ρ (calcd.) g cm^{-3}	1.409	1.463
μ (Mo Kα), mm^{-1}	0.910	0.617
θ max, deg.	30.54	30.51
no. of data collected	30537	44231
no. of data	5971	16778
no. of parameters	181	667
R_1 [$I > 2\sigma(I)$]	0.0467	0.0378
wR_2 [$I > 2\sigma(I)$]	0.0762	0.0879
R_1 [all data]	0.1027	0.0668
wR_2 [all data]	0.0911	0.1007
GOF	0.998	1.005

Table 5 (cont). Crystal, intensity collection and refinement data.

	(η^4-*C_4*-PhzH)Mo(PMe$_3$)$_3$H$_2$	**(μ-η^6,η^4-PhzH)[Mo(PMe$_3$)$_3$]-[Mo(PMe$_3$)$_3$H$_2$]**
lattice	Monoclinic	Monoclinic
formula	$C_{21}H_{37}MoN_2P_3$	$C_{45}H_{88}Mo_2N_2P_6$
formula weight	506.38	1034.87
space group	$P2_1/n$	$P2_1/c$
a/Å	9.2889(5)	18.1740(16)
b/Å	11.5097(6)	9.4426(8)
c/Å	23.4023(13)	26.621(2)
α/°	90	90
β/°	101.2140(10)	97.4800(10)
γ/°	90	90
V/Å^3	2454.2(2)	4529.5(7)
Z	4	4
temperature (K)	125(2)	125(2)
radiation (λ, Å)	0.71073	0.71073
ρ (calcd.) g cm^{-3}	1.370	1.518
μ (Mo Kα), mm^{-1}	0.739	0.801
θ max, deg.	30.54	30.52
no. of data collected	39614	71261
no. of data	7644	13827
no. of parameters	253	369
R_1 [$I > 2\sigma(I)$]	0.0310	0.0374
wR_2 [$I > 2\sigma(I)$]	0.0622	0.0801
R_1 [all data]	0.0406	0.0588
wR_2 [all data]	0.0665	0.0852
GOF	1.064	1.031

Table 5 (cont). Crystal, intensity collection and refinement data.

	(η^4-*C*$_4$-AcrH)Mo(PMe$_3$)$_3$H$_2$	**(η^4-AnH)Mo(PMe$_3$)$_3$H$_2$**
lattice	Monoclinic	Monoclinic
formula	$C_{24.5}H_{44}MoNP_3$	$C_{23}H_{39}MoP_3$
formula weight	541.46	504.39
space group	$P2_1/c$	$P2_1/n$
a/Å	9.7998(5)	10.1768(7)
b/Å	17.8776(9)	14.8140(10)
c/Å	16.1462(9)	16.9546(11)
α/°	90	90
β/°	100.4220(10)	103.3150(10)
γ/°	90	90
V/Å^3	2782.1(3)	2487.3(3)
Z	4	4
temperature (K)	125(2)	125(2)
radiation (λ, Å)	0.71073	0.71073
ρ (calcd.) g cm^{-3}	1.293	1.347
μ (Mo Kα), mm^{-1}	0.655	0.727
θ max, deg.	32.62	30.57
no. of data collected	47516	39767
no. of data	9744	7603
no. of parameters	253	252
R_1 [$I > 2\sigma(I)$]	0.0348	0.0367
wR_2 [$I > 2\sigma(I)$]	0.0804	0.0706
R_1 [all data]	0.0424	0.0652
wR_2 [all data]	0.0829	0.0791
GOF	1.066	1.002

Table 5 (cont). Crystal, intensity collection and refinement data.

	(η^4-*C*$_4$-QoxH)Mo(PMe$_3$)$_3$H$_2$	**(μ-η^6,η^6-AcrH)[Mo(PMe$_3$)$_3$]$_2$**
lattice	Monoclinic	Triclinic
formula	$C_{34}H_{70}Mo_2N_4P_6$	$C_{33.5}H_{69}Mo_2NP_6$
formula weight	912.64	863.60
space group	$P2_1/c$	$P\text{-}1$
a/Å	13.4943(11)	9.336(2)
b/Å	13.9119(11)	13.553(4)
c/Å	23.1706(19)	18.307(5)
α/°	90	97.988(4)
β/°	97.2630(10)	102.460(4)
γ/°	90	104.864(4)
V/Å^3	4314.9(6)	2139.2(9)
Z	4	2
temperature (K)	125(2)	125(2)
radiation (λ, Å)	0.71073	0.71073
ρ (calcd.) g cm^{-3}	1.405	1.341
μ (Mo Kα), mm^{-1}	0.832	0.833
θ max, deg.	32.71	26.37
no. of data collected	73761	26107
no. of data	15174	8740
no. of parameters	431	361
R_1 [$I > 2\sigma(I)$]	0.0251	0.0676
wR_2 [$I > 2\sigma(I)$]	0.0633	0.1337
R_1 [all data]	0.0306	0.1480
wR_2 [all data]	0.0669	0.1557
GOF	1.044	0.864

Table 5 (cont). Crystal, intensity collection and refinement data.

	(μ-η⁶,η⁶-QoxH)[Mo(PMe$_3$)$_3$]$_2$	**9,9′-biacridane**
lattice	Triclinic	Monoclinic
formula	$C_{26}H_{60}Mo_2N_2P_6$	$C_{26}H_{20}N_2$
formula weight	778.46	360.44
space group	*P-1*	$P2_1/n$
a / Å	9.0199(5)	12.5971(7)
b / Å	9.1656(5)	5.4794(3)
c / Å	13.0969(7)	12.6940(7)
α / °	71.8510(10)	90
β / °	89.2920(10)	96.5030(10)
γ / °	61.9120(10)	90
V / Å^3	895.99(8)	870.56(8)
Z	1	2
temperature (K)	125(2)	125(2)
radiation (λ, Å)	0.71073	0.71073
ρ (calcd.) g cm^{-3}	1.443	1.375
μ (Mo Kα), mm^{-1}	0.986	0.081
θ max, deg.	32.60	30.53
no. of data collected	15420	13405
no. of data	6083	2656
no. of parameters	166	135
R_1 [$I > 2\sigma(I)$]	0.0220	0.0434
wR_2 [$I > 2\sigma(I)$]	0.0525	0.1137
R_1 [all data]	0.0260	0.0575
wR_2 [all data]	0.0543	0.1248
GOF	1.039	1.026

2.11 References and notes

(1) Furimsky, E.; Massoth, F. E. *Catal. Rev.* **2005**, *47*, 297-489.

(2) Sanchez-Delgado, R. A. *Organometallic Modelling of the Hydrodesulfurization and Hydrodenitrogenation Reactions*, Kluwer Academic Publishers, Boston, 2002.

(3) (a) Angelici, R. J. *Polyhedron* **1997**, *16*, 3073-3088.

(b) Weller, K. J.; Fox, P. A.; Gray, S. D.; Wigley, D. E. *Polyhedron* **1997**, *16*, 3139-3163.

(c) Bianchini, C.; Meli, A.; Vizza, F. *Eur. J. Inorg. Chem.* **2001**, 43-68.

(d) Borowski, A. F. *Pol. J. Chem.* **2006**, *80*, 205-226.

(e) Laine, R. M. *Catal. Rev. - Sci. Eng.* **1983**, *25*, 459-474.

(4) Sánchez-Delgado, R. A. *Comprehensive Organometallic Chemistry III*; Crabtree, R. H., Mingos, D. M. P., Eds.; Elsevier: Oxford, U.K., **2006**; Vol. 1, Chapter 27.

(5) For examples, see:

(a) Fish, R. H.; Thormodsen, A. D.; Cremer, G. A. *J. Am. Chem. Soc.* **1982**, 104, 5234-5237.

(b) Borowski, A. F.; Sabo-Etienne, S.; Donnadieu, B.; Chaudret, B. *Organometallics* **2003**, *22*, 1630-1637.

(6) (a) Cloke, F. G. N.; Cox, K. P.; Green, M. L. H.; Bashkin, J.; Prout, K. *J. Chem. Soc., Chem. Commun.* **1982**, 393-394.

(b) Brookhart, M.; Cox, K. P.; Cloke, F. G. N.; Green, J. C.; Green, M. L. H.; Hare,

P. M.; Bashkin, J.; Derome, A. E.; Grebenik, P. D. *J. Chem. Soc., Dalton Trans.* **1985**, 423-433.

(7) (a) Gibson, V. C.; Grebenik, P. D.; Green, M. L. H. *J. Chem. Soc., Chem. Commun.* **1983**, 1101-1102.

(b) Gibson, V. C.; Graimann, C. E.; Hare, P. M.; Green, M. L. H.; Bandy, J. A.; Grebenik, P. D.; Prout, K. *J.Chem. Soc., Dalton Trans.* **1985**, 2025-2035.

(c) Lyons, D.; Wilkinson, G.; Thomton-Pett, M.; Hursthouse, M. B. *J. Chem. Soc., Dalton Trans.* **1984**, 695-700.

(8) Carmona, E.; Marin, J. M.; Poveda, M. L.; Atwood, J. L.; Rogers, R. D. *J. Am. Chem. Soc.* **1983**, *105*, 3014-3022.

(9) Murphy, V. J.; Parkin, G. *J. Am. Chem. Soc.* **1995**, *117*, 3522-3528.

(10) Hascall, T.; Murphy, V. J.; Janak, K. E.; Parkin, G. *J. Organomet. Chem.* **2002**, *652*, 37-49.

(11) Rabinovich, D.; Zelman, R.; Parkin, G. *J. Am. Chem. Soc.* **1992**, *114*, 4611-4621.

(12) Hascall, T.; Murphy, V. J.; Parkin, G. *Organometallics* **1996**, *15*, 3910-3912.

(13) (a) Zhu, G.; Tanski, J. M.; Churchill, D. G.; Janak, K. E.; Parkin, G. *J. Am. Chem. Soc.* **2002**, *124*, 13658-13659.

(b) Zhu, G.; Tanski, J. M.; Parkin, G. *Polyhedron* **2003**, *22*, 199-203.

(c) Zhu, G.; Pang, K.; Parkin, G. *J. Am. Chem. Soc.* **2008**, *130*, 1564-1565.

(d) Zhu, G.; Pang, K.; Parkin, G. *Inorg. Chim. Acta* **2008**, *361*, 3221-3229.

(14) Quinoline typically coordinates to a single transition metal in a κ^1-manner *via* the nitrogen atom, but examples of η^6-coordination *via* the carbocyclic ring are known. See: Sadimenko, A. P. *Adv. Heterocycl. Chem.* **2004**, *86*, 293-343.

(15) (a) Choudhary, T. V.; Parrott, S.; Johnson, B. *Catal. Commun.* **2008**, *9*, 1853-1857.

(b) Choudhary, T. V.; Parrott, S.; Johnson, B. *Environ. Sci. Technol.* **2008**, 42, 1944-1947.

(16) Zhu, G.; Janak, K. E.; Figueroa, J. S.; Parkin, G. *J. Am. Chem. Soc.* **2006**, *128*, 5452-5461.

(17) Sattler, A.; Zhu, G.; Parkin, G. *J. Am. Chem. Soc.* **2009**, *131*, 7828–7838.

(18) Zhu, G. "Transformations Relevant to Hydrodenitrogenation as Modeled by Reactions of Trimethylphosphine Molybdenum Compounds" – Dissertation, **2005**.

(19) $(\eta^6\text{-}C_6\text{-PhzH})Mo(PMe_3)_3$ was synthesized and characterized by Guang Zhu. See reference 18.

(20) For other dinuclear complexes that feature bridging fused polycyclic aromatic ligands, see: Ceccon, A.; Santi, S.; Orian, L.; Bisello, A. *Coord. Chem. Rev.* **2004**, *248*, 683-724.

(21) The molecular structure of $(\eta^6\text{-}C_6\text{-PhzH})Mo(PMe_3)_3$ was determined by Guang Zhu. See reference 18.

(22) (a) Althoff, A.; Jutzi, P.; Lenze, N.; Neumann, B.; Stammler, A.; Stammler, H. G. *Organometallics* **2002**, *21*, 3018-3022.

(b) Miyasaka, H.; Clérac, R.; Campos-Fernández, C. S.; Dunbar, K. R. *J. Chem. Soc., Dalton Trans.* **2001**, 858-861.

(c) Whiteford, J. A.; Stang, P. J.; Huang, S. D. *Inorg. Chem.* **1998**, *37*, 5595-5601.

(d) Munakata, M.; Kurodasowa, T.; Maekawa, M.; Honda, A.; Kitagawa, S. *J. Chem. Soc., Dalton Trans.* **1994**, 2771-2775.

(e) Cotton, F. A.; Felthouse, T. R. *Inorg. Chem.* **1981**, *20*, 600-608.

(f) Chesnut, D. J.; Plewak, D.; Zubieta, J. *J. Chem. Soc., Dalton Trans.* **2001**, 2567-2580.

(g) Batten, S. R.; Hoskins, B. F.; Robson, R. *New J. Chem.* **1998**, *22*, 173-175.

(h) Kurodasowa, T.; Munakata, M.; Matsuda, H.; Akiyama, S.; Maekawa, M. *J. Chem. Soc., Dalton Trans.* **1995**, 2201-2208.

(i) Cotton, F. A.; Kim, Y. M.; Ren, T. *Inorg. Chem.* **1992**, *31*, 2723-2726.

(23) Dinuclear complexes with bridging η^3,η^3-coordination modes are also known. See, for example:

(a) Evans, W. J.; Perotti, J. M.; Kozimor, S. A.; Champagne, T. M.; Davis, B. L.; Nyce, G. W.; Fujimoto, C. H.; Clark, R. D.; Johnston, M. A.; Ziller, J. W. *Organometallics* **2005**, *24*, 3916-3931.

(b) Evans, W. J.; Gonzales, S. L.; Ziller, J. W. *J. Am. Chem. Soc.* **1994**, *116*, 2600-2608.

(c) Scholz, J.; Scholz, A.; Weimann, R.; Janiak, C.; Schumann H. *Angew. Chem. Int. Ed. Engl.* **1994**, *33*, 1171-1174.

(24) The molecular structure lies on an inversion center causing a crystallographically imposed 50:50 disorder of the nitrogen atoms and C–H units in the quinoxaline ligand.

(25) However, it should be noted that there are examples of pyridine C-N bond cleavage, without prior hydrogenation, by metals other than molybdenum. See, for example:

(a) Kleckley, T. S.; Bennett, J. L.; Wolczanski, P. T.; Lobkovsky, E. *J. Am. Chem. Soc.* **1997**, *119*, 247-248.

(b) Gray, S. D.; Weller, K. J.; Bruck, M. A.; Briggs, P. M.; Wigley, D. E. *J. Am. Chem. Soc.* **1995**, *117*, 10678-10693.

(c) Weller, K. J.; Filippov, I.; Briggs, P. M.; Wigley, D. E. *Organometallics* **1998**, *17*, 322-329.

(d) Bailey, B. C.; Fan, H.; Huffman, J. C.; Baik, M.-H.; Mindiola, D. J. *J. Am. Chem. Soc.* **2006**, *128*, 6798-6799.

(26) The hydride ligands, which are in chemically reasonable positions, were located by X-ray diffraction and their positions were refined. Furthermore, their locations are supported by DFT geometry optimization calculations.

(27) NMR spectroscopic studies performed by Guang Zhu indicate that, in solution at low temperature, the molecule possesses two configurations (which rapidly interconvert at room temperature). Presumably, the two configurations differ according to the orientation of the η^4-phenazine ligand relative to that of the $[Mo(PMe_3)_3H_2]$ moiety. Thus, whereas one configuration has a structure in which the mirror plane of the η^4-phenazine ligand is coincident with the plane comprising Mo, P1 and the two hydride ligands, *i.e.* that of the solid state structure (Figure 7), the other configuration has a structure in which these planes are orthogonal to each other, like that of $(\eta^4\text{-}C_4\text{-AcrH})Mo(PMe_3)_3H_2$ (Figure 9). Support for this proposal is provided by (*i*) DFT calculations, finding energy minima for both symmetric and asymmetric forms of $(\eta^4\text{-}C_4\text{-PhzH})Mo(PMe_3)_3H_2$ (Table 2), and (*ii*) structural characterization of $(\eta^4\text{-}C_4\text{-QoxH})Mo(PMe_3)_3H_2$, which displays both isomeric forms in the crystallographic asymmetric unit (Figure 11).

(28) Zhu, G.; Janak, K. E.; Parkin, G. *Chem. Commun.* **2006**, 2501-2503.

(29) See, for example: Cotton, F. A.; Felthouse, T. R. *Inorg. Chem.* **1981**, *20*, 600-608.

(30) The η^4-acridine complex $(\eta^4\text{-AcrH})RuH_2(PCy_3)_2$ has been spectroscopically characterized. See: Borowski, A. F.; Sabo-Etienne, S.; Donnadieu, B.; Chaudret, B. *Organometallics* **2003**, *22*, 1630-1637.

(31) In this regard the hydrogenation of phenazine to 5,10-dihydrophenazine and 1,2,3,4-tetrahydrophenazine has been proposed to occur prior to hydrodenitrogenation. See: Nagai, M.; Sawahiraki, K.; Kabe, T. *Nippon Kagaku Kaishi* **1982**, *1*, 115-119.

(32) Catalytic hydrogenation of acridine by $Rh(PPh_3)_3Cl$ yields a similar mixture of 1,2,3,4-tetrahydroacridine and 9,10-dihydroacridine to that observed here. See: Fish, R. H.; Tan, J. L.; Thormodsen, A. D. *J. Org. Chem.* **1984**, *49*, 4500-4505.

(33) For examples of hydrogenation of acridine to 9,10-dihydroacridine, see:

(a) Rosales, M.; Castillo, S.; González, A.; González, L.; Molina, K.; Navarro, J.; Pacheco, I.; Perez, H. *Transition Met. Chem.* **2004**, *29*, 221-228.

(b) Fish, R. H.; Baralt, E.; Smith, S. J. *Organometallics* **1991**, *10*, 54-56.

(c) Fish, R. H.; Thormodsen, A. D.; Cremer, G. A. *J. Am. Chem. Soc.* **1982**, *104*, 5234-5237.

(d) Lee, C.; Steele, B. R.; Sutherland, R. G. *J. Organomet. Chem.***1980**, *186*, 265-270.

(e) Baralt, E.; Smith, S. J.; Hurwitz, J.; Horváth, I. T.; Fish, R. H. *J. Am. Chem. Soc.* **1992**, *114*, 5187-5196.

(f) Fish, R. H. *Ann. N. Y. Acad. Sci.* **1983**, *415*, 292-301.

(g) Chin, C. S.; Park, Y.; Lee, B. *Catal. Lett.* **1995**, *31*, 239-243.

(h) Rosales, M.; Navarro, J.; Sánchez, L.; González, A.; Alvarado, Y.; Rubio, R.; De La Cruz, C.; Rajmankina, T. *Transition Met. Chem.* **1996**, *21*, 11-15.

(i) Rosales, M.; Vallejo, R.; Soto, J. J.; Chacón, G.; González, A.; González, B. *Catal. Lett.* **2006**, *106*, 101-105.

(34) See, for example:

(a) Chen, J.; Angelici, R. J. *Organometallics* **1999**, *18*, 5721-5724.

(b) Vecchi, P. A.; Ellern, A.; Angelici, R. J. *Organometallics* **2005**, *24*, 3725-3730.

(c) Rudd, J. A., II; Angelici, R. J. *Inorg. Chim. Acta* **1995**, 240, 393-398.

(d) Hanic, F.; Mills, O. S. *J. Organomet. Chem.* **1968**, *11*, 151-158.

(35) (a) Hall, M. B.; Fenske, R. F. *Inorg. Chem.* **1972**, *11*, 768.

(b) Bursten, B. E.; Jensen, J. R.; Fenske, R. F. *J. Chem. Phys.* **1978**, *68*, 3320.

(c) Manson, J.; Webster, C. E.; Pérez, L. M.; Hall, M. B.
http://www.chem.tamu.edu/jimp2/index.html.

(36) Muetterties, E. L.; Bleeke, J. R.; Wucherer, E. J.; Albright, T. A. *Chem. Rev.* **1982**, *82*, 499-525.

(37) For calculations on (η^6–arene)ML_3 complexes, see:

(a) Howell, J. A. S.; Ashford, N. F.; Dixon, D. T.; Kola, J. C.; Albright, T. A.; Kwang, S. K. *Organometallics* **1991**, *10*, 1852-1864.

(b) Albright, T. A.; Hofmann, P.; Hoffmann, R.; Lillya, C. P.; Dobosh, P. A. *J. Am. Chem. Soc.* **1983**, *105*, 3396-3411.

(c) Byers, B. P.; Hall, M. B. *Organometallics* **1987**, *6*, 2319-2325.

(d) Rogers, R. D.; Atwood, J. L.; Albright, T. A.; Lee, W. A.; Rausch, M. D. *Organometallics* **1984**, *3*, 263-270.

(e) Albright, T. A.; Hofmann, P.; Hoffmann, R. *J. Am. Chem. Soc.* **1977**, *99*, 7546-7557.

(f) Albright, T. A.; Carpenter, B. K. *Inorg. Chem.* **1980**, *19*, 3092-3097.

(g) Cohen, R.; Weitz, E.; Martin, J. M. L.; Ratner, M. A. *Organometallics* **2004**, *23*, 2315-2325.

(h) Albright, T. A. *Acc. Chem. Res.* **1982**, *15*, 149-155.

(i) Asirvatham, V. S.; Gruhn, N. E.; Lichtenberger, D. L.; Ashby, M. T. *Organometallics*, **2000**, *19*, 2215-2227.

(38) For other examples of bent η^4–anthracene compounds, see:

(a) Brennessel, W. W.; Ellis, J. E.; Pomije, M. K.; Sussman, V. J.; Urnezius, E.; Young, V. G., Jr. *J. Am. Chem. Soc.* **2002**, *124*, 10258-10259.

(b) Brennessel, W. W.; Ellis, J. E.; Roush, S. N.; Strandberg, B. R.; Woisetschläger, O. E.; Young, V. G., Jr. *Chem. Commun.* **2002**, 2356-2357.

(c) Jilek, R. E.; Jang, M.; Smolensky, E. D.; Britton, J. D.; Ellis, J. E. *Angew. Chem. Int. Ed. Engl.* **2008**, *47*, 8692-8695.

(d) Sussman, V. J.; Ellis, J. E. *Angew. Chem. Int. Ed. Engl.* **2008**, *47*, 484-489.

(e) Brennessel, W. W.; Jilek, R. E.; Ellis, J. E. *Angew. Chem. Int. Ed. Engl.* **2007**, *46*, 6132-6136.

(f) Mashima, K.; Nakayama, Y.; Kaidzu, M.; Ikushima, N.; Nakamura, A. *J. Organomet. Chem.* **1998**, *557*, 3-12.

(g) Müller, J.; Gaede, P. E.; Hirsch, C.; Qiao, K. *J. Organomet. Chem.* **1994**, *472*, 329-335.

(h) Boese, R.; Stanger, A.; Stellberg, P.; Shazar, A. *Angew. Chem., Int. Ed. Engl.* **1993**, *32*, 1475-1477.

(i) Protasiewicz, J. D.; Bianconi, P. A.; Williams, I. D.; Liu, S.; Rao, C. P.; Lippard, S. J. *Inorg. Chem.* **1992**, *31*, 4134-4142.

(j) Bennett, M. A.; Bown, M.; Hockless, D. C. R. *Aust. J. Chem.* **2000**, *53*, 507-515.

(39) For a related example of folding to minimize this type of antibonding interaction in the anthracene compound, (η^6-AnH)Mo(PMe_3)$_3$, see reference 16.

(40) (a) McNally, J. P.; Leong, V. S.; Cooper, N. J. in *Experimental Organometallic Chemistry*, Wayda, A. L.; Darensbourg, M. Y., Eds.; American Chemical Society: Washington, DC, 1987; Chapter 2, pp 6-23.

(b) Burger, B.J.; Bercaw, J. E. in *Experimental Organometallic Chemistry*; Wayda, A. L.; Darensbourg, M. Y., Eds.; American Chemical Society: Washington, DC, 1987; Chapter 4, pp 79-98.

(c) Shriver, D. F.; Drezdzon, M. A.; *The Manipulation of Air-Sensitive Compounds*, 2nd Edition; Wiley-Interscience: New York, 1986.

(41) Gottlieb, H. E.; Kotlyar, V.; Nudelman, A. *J. Org. Chem.* **1997**, *62*, 7512-7515.

(42) Cambridge Isotope Laboratories, Inc., NMR Solvent Data Chart (www.isotope.com/cil/products/images/nmrchart.pdf).

(43) "Nuclear Magnetic Resonance Spectroscopy" Nelson, J. H. Prentice Hall, New Jersey (2003), p 79.

(44) (a) Sheldrick, G. M. SHELXTL, An Integrated System for Solving, Refining and Displaying Crystal Structures from Diffraction Data; University of Göttingen, Göttingen, Federal Republic of Germany, 1981.

(b) Sheldrick, G. M. *Acta Cryst.* **2008**, *A64*, 112-122.

(45) Jaguar 7.0, Schrödinger, LLC, New York, NY 2007.

(46) (a) Becke, A. D. *J. Chem. Phys.* **1993**, *98*, 5648-5652.

(b) Becke, A. D. *Phys. Rev. A* **1988**, *38*, 3098-3100.

(c) Lee, C. T.; Yang, W. T.; Parr, R. G. *Phys. Rev. B* **1988**, *37*, 785-789.

(d) Vosko, S. H.; Wilk, L.; Nusair, M. *Can. J. Phys.* **1980**, *58*, 1200-1211.

(e) Slater, J. C. *Quantum Theory of Molecules and Solids, Vol. 4: The Self-Consistent Field for Molecules and Solids*; McGraw-Hill: New York, 1974.

(47) (a) Hay, P. J.; Wadt, W. R. *J. Chem. Phys.* **1985**, *82*, 270-283.

(b) Wadt, W. R.; Hay, P. J. *J. Chem. Phys.* **1985**, *82*, 284-298.

(c) Hay, P. J.; Wadt, W. R. *J. Chem. Phys.* **1985**, *82*, 299-310.

(48) Version 2.0, June 1993; Lichtenberger, D. L. Department of Chemistry, University of Arizona, Tuscon, AZ 85721.

(49) (a) Sugimoto, A.; Kotani, T.; Tsujimoto, J.; Yoneda, S. *J. Heterocycl. Chem.* **1989**, *26*, 435-438.

(b) Bettinetti, G. F.; Maffei, S.; Pietra, S. *Synthesis* **1976**, 748-749.

(50) The formation of 1,2,3,4-tetrahydrophenazine was confirmed by removing all volatile components and recording the spectrum in $CDCl_3$ and comparing it with the literature data. See: Petukhov, P. A.; Tkachev, A. V. *Tetrahedron* **1997**, *53*, 9761-9768.

(51) Srikrishna, A.; Reddy, T. J.; Viswajanani, R. *Tetrahedron* **1996**, *52*, 1631-1636.

(52) Banwell, M. G.; Lupton, D. W.; Ma, X.; Renner, J.; Sydnes, M. O. *Org. Lett.* **2004**, *6*, 2741-2744.

(53) (a) Takano, J.; Kitahara, T.; Shihara, Y.; Shirai, K. *Proc. Fac. Sci. Tokai Univ.* **1985**, *20*, 111-116.

(b) Takano, J.; Kitahara, T.; Shihara, Y.; Shirai, K. *Nippon Kagaku Kaishi* **1983**, 400-404.

(54) Clever, H. L. in *Solubility Data Series*, Young, C. L., Ed.; Pergamon Press: Oxford, 1981; Volume 5/6: Hydrogen and Deuterium, p 159.

CHAPTER 3

Aromatic carbon–carbon bond cleavage by tungsten

Table of Contents

Reproduced in part from:

Sattler, A.; Parkin, G. *Nature* **2010**, *463*, 523–536.

3.1 Introduction

The cleavage of C–H and C–C bonds by transition metal centers is of fundamental interest and plays an important role in the synthesis of complex organic molecules from petroleum feedstocks.[1,2,3,4,5,6] While there are many examples for the oxidative addition of C–H bonds to a metal center, transformations that feature oxidative addition of C–C bonds are rare.[7] The paucity of transformations that involve the cleavage of C–C rather than C–H bonds is usually attributed to kinetic factors arising from (*i*) the greater steric hindrance and the directional nature of the sp^n hybrids that form the C–C bond, and (*ii*) the thermodynamic factors arising from the fact that M–C bonds are weaker than M–H bonds.[2,3,4,5] Not surprisingly, most examples of C–C bond cleavage thus either avoid the kinetic limitations by using metal compounds in which the C–C bond is held in close proximity to the metal center, or avoid the thermodynamic limitations by using organic substrates in which the cleavage is accompanied by either a relief of strain energy or the formation of an aromatic system.[2,3,4,5] In this chapter, we report that a tungsten center can be used to cleave a strong C–C bond that is a component of an unstrained 6-membered aromatic ring. The cleavage is enabled by the formation of an unusual chelating di(isocyanide) ligand, which raises the prospect that other metal centers with suitable ancillary ligands could also accomplish the cleavage of strong C–C bonds of aromatic substrates and thus provide new ways of functionalizing such molecules.

3.2 Reactivity of $W(PMe_3)_4(\eta^2\text{-}CH_2PMe_2)H$ towards quinoxaline

The Parkin group has been developing the coordination chemistry of molybdenum with respect to heterocyclic aromatic nitrogen compounds in order to acquire a more detailed understanding of the reactions involved in hydrodenitrogenation (HDN), the important process by which nitrogen is removed

from compounds in fossil fuels.[8,9,10,11] As part of these investigations, it was previously determined that quinoxaline (QoxH) (Figure 1) reacts with the electron-rich molybdenum complex, $Mo(PMe_3)_6$, at 25 ˚C to give (η^2-*N,C*-Qox)$Mo(PMe_3)_4H$ *via* oxidative addition of a C–H bond, which converts sequentially to (η^6-C_4N_2-QoxH)$Mo(PMe_3)_3$ and (η^6-C_6-QoxH)$Mo(PMe_3)_3$, upon heating at 80 ˚C and 130 ˚C, , respectively (Scheme 1).[9] Furthermore, we later found that (η^6-C_6-QoxH)$Mo(PMe_3)_3$ reacts with H_2 at room temperature to produce an equilibrium mixture with (η^4-C_4-QoxH)$Mo(PMe_3)_3H_2$ (see Chapter 2).

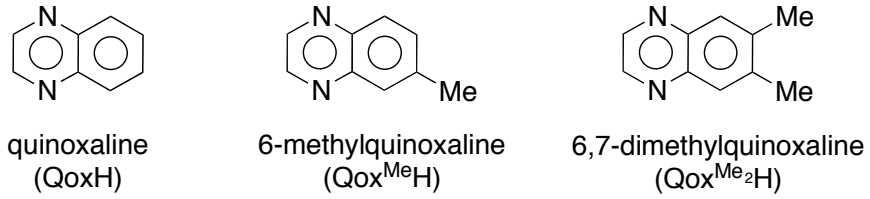

Figure 1. Quinoxaline (QoxH), 6-methylquinoxaline ($Qox^{Me}H$), and 6,7-dimethylquinoxaline ($Qox^{Me_2}H$).

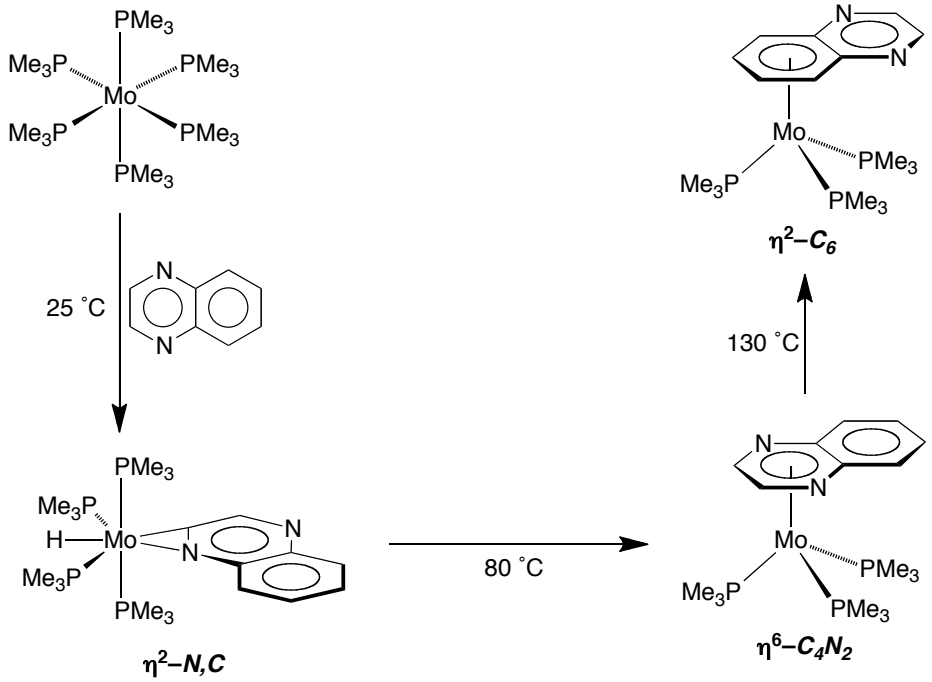

Scheme 1. Reactivity of $Mo(PMe_3)_6$ towards quinoxaline.

Seeking to discover a system that would achieve cleavage of a C–N bond of the aromatic ring, we explored tungsten compounds because of the greater ability of this metal to accomplish bond cleavage *via* oxidative addition than does molybdenum.[12] As illustrated in Scheme 2, the reaction of $W(PMe_3)_4(\eta^2\text{-}CH_2PMe_2)H$ with quinoxaline proceeds very differently compared with the molybdenum system. Thus, instead of tungsten simply coordinating quinoxaline in an η^6 manner, $W(PMe_3)_4(\eta^2\text{-}CH_2PMe_2)H$ reacts with quinoxaline to either (*i*) induce aromatic C–C bond cleavage and dehydrogenation to give $[\kappa^2\text{-}C_2\text{-}C_6H_4(NC)_2]W(PMe_3)_4$, or (*ii*) form the dihydride complex $(\eta^4\text{-}C_2N_2\text{-QoxH})W(PMe_3)_3H_2$. The latter compound does not convert to $[\kappa^2\text{-}C_2\text{-}C_6H_4(NC)_2]W(PMe_3)_4$ under the reaction conditions. The transformations observed for quinoxaline are also observed for 6-methylquinoxaline ($Qox^{Me}H$) and 6,7-dimethylquinoxaline ($Qox^{Me_2}H$) (Figure 1), thereby demonstrating the generality of the reactions.

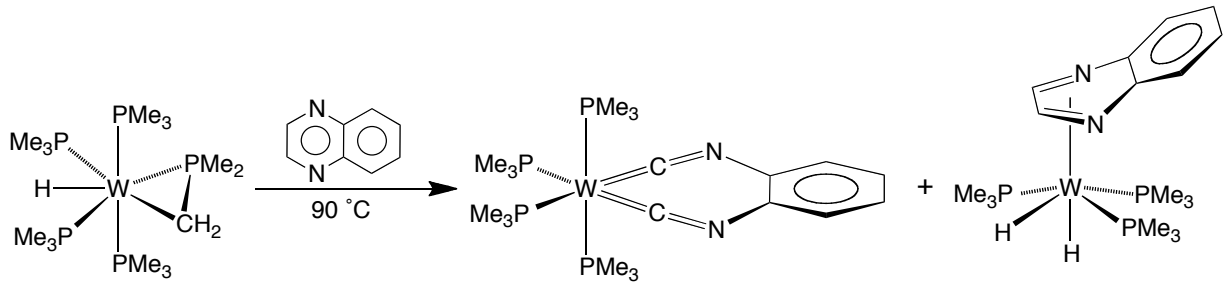

Scheme 2. Reactivity of $W(PMe_3)_4(\eta^2\text{-}CH_2PMe_2)H$ towards quinoxaline.

In addition to the dihydride $(\eta^4\text{-}C_2N_2\text{-QoxH})W(PMe_3)_3H_2$, the tetrahydride $W(PMe_3)_4H_4$ is also formed in low yield (< 5 %) during the course of the reaction. While an obvious source for the hydride ligands of these complexes is the H_2 that is liberated during the formation of $[\kappa^2\text{-}C_2\text{-}C_6H_4(NC)_2]W(PMe_3)_4$, we also observed conversion of QoxH to 2,2′-biquinoxaline, $(2,2'\text{-Qox})_2$ (identified by X–ray diffraction, Figure 2) which may also serve as a source of H_2. Not unexpectedly, the yield of $(\eta^4\text{-}C_2N_2\text{-QoxH})W(PMe_3)_3H_2$ (86 %), relative to that of $[\kappa^2\text{-}C_2\text{-}C_6H_4(NC)_2]W(PMe_3)_4$, increases

considerably if the reaction between $W(PMe_3)_4(\eta^2\text{-}CH_2PMe_2)H$ and quinoxaline is performed under an atmosphere of H_2.

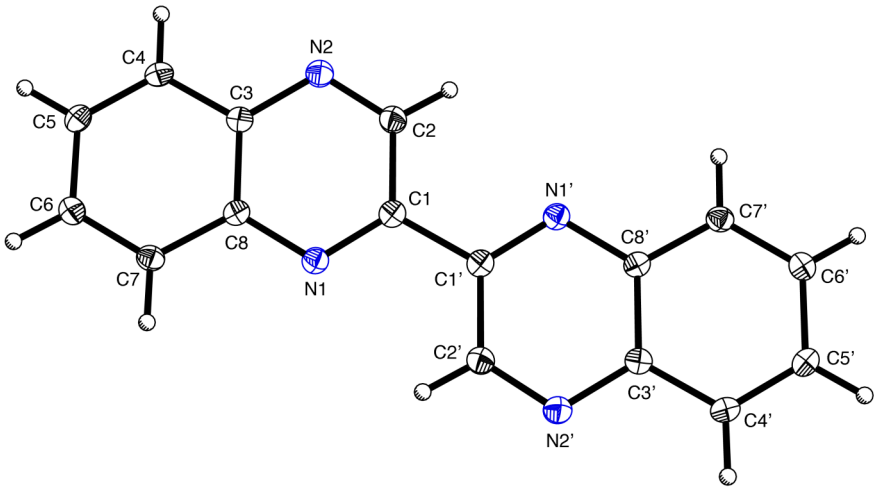

Figure 2. Molecular structure of 2,2′–Biquinoxaline, $(2,2'\text{–Qox})_2$.

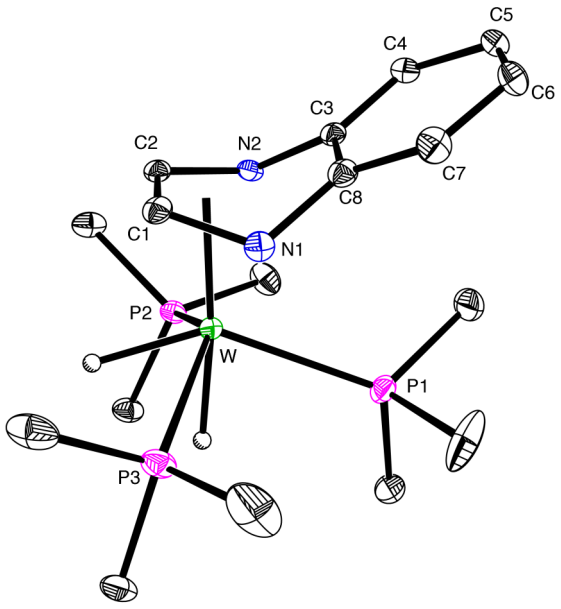

Figure 3. Molecular structure of $(\eta^4\text{-}C_2N_2\text{-QoxH})W(PMe_3)_3H_2$.

The dihydride complexes $(\eta^4\text{-}C_2N_2\text{-}Qox^{R_2}H)W(PMe_3)_3H_2$ (R_2 = H, H; Me, H; Me, Me) represent unprecedented examples of η^4-coordination of this dinuclear aromatic nitrogen compound *via* the heterocyclic ring and their molecular structures are shown

in Figures 3 – 5, respectively. As such, the (η^4-C_2N_2-Qox^{R_2}H)W(PMe$_3$)$_3$H$_2$ complexes provide important new structural motifs for the means by which heterocyclic nitrogen compounds may bind to the surface of hydrodenitrogenation catalysts.

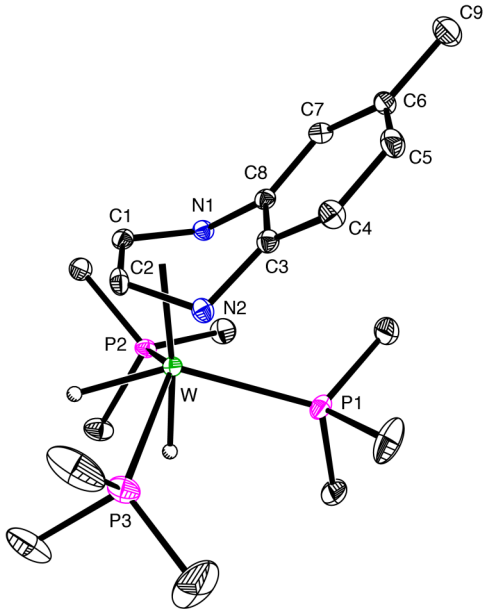

Figure 4. Molecular structure of (η^4-C_2N_2-Qox^{Me}H)W(PMe$_3$)$_3$H$_2$.

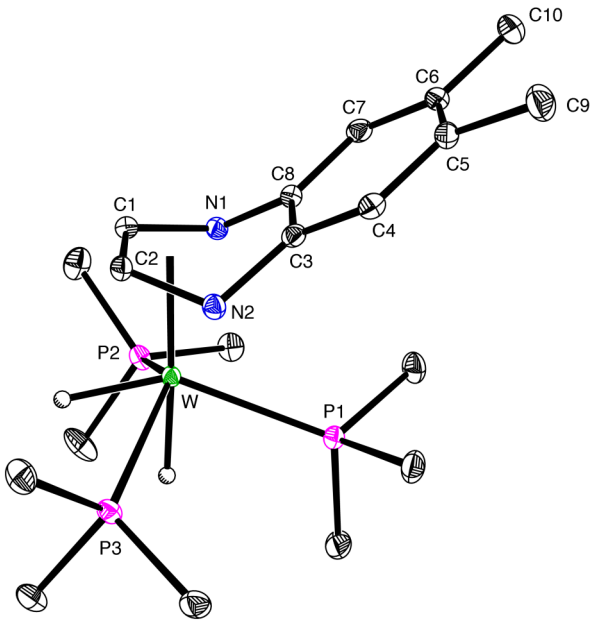

Figure 5. Molecular structure of (η^4-C_2N_2-Qox^{Me_2}H)W(PMe$_3$)$_3$H$_2$.

The most significant aspect of the reactions between $W(PMe_3)_4(\eta^2\text{-}CH_2PMe_2)H$ and $Qox^{R_2}H$, however, pertains to the formation of $[\kappa^2\text{-}C_2\text{-}C_6H_2R_2(NC)_2]W(PMe_3)_4$ (Scheme 2). As is evident from the molecular structures of $[\kappa^2\text{-}C_2\text{-}C_6H_4(NC)_2]W(PMe_3)_4$, $[\kappa^2\text{-}C_2\text{-}C_6H_3Me(NC)_2]W(PMe_3)_4$, and $[\kappa^2\text{-}C_2\text{-}C_6H_2Me_2(NC)_2]W(PMe_3)_4$ in Figures 6 – 8,[13,14] respectively, the formation of these compounds require the breaking of aromatic C–C bonds that are substantially stronger than a typical C–C single bond.[15] Remarkably, this unprecedented cleavage of the aromatic C–C bond takes place in preference to that of the C–N bond. The latter bond might have been expected to be more reactive because the cleavage of the C–N bond in pyridine[16] and its derivatives[17,18,19,20] has been achieved by various metal centers, thereby making the cleavage of the C–C bond in the present system all the more noteworthy.

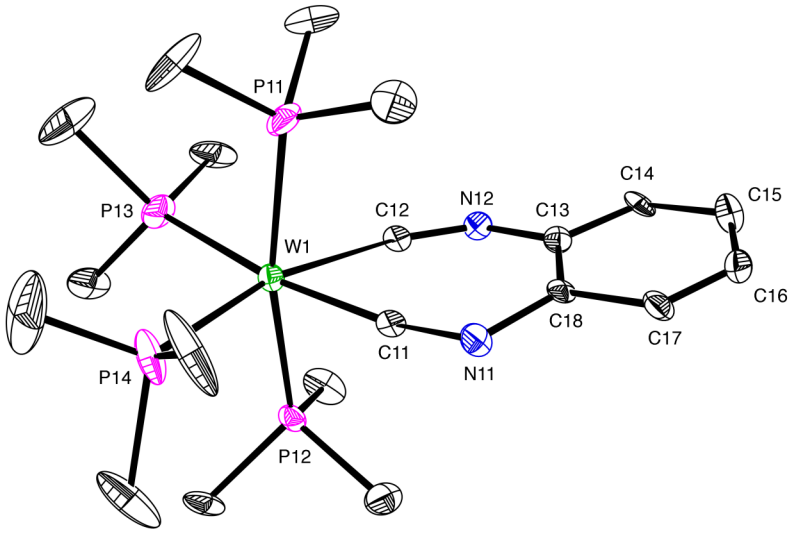

Figure 6. Molecular structure of $[\kappa^2\text{-}C_2\text{-}C_6H_4(NC)_2]W(PMe_3)_4$.

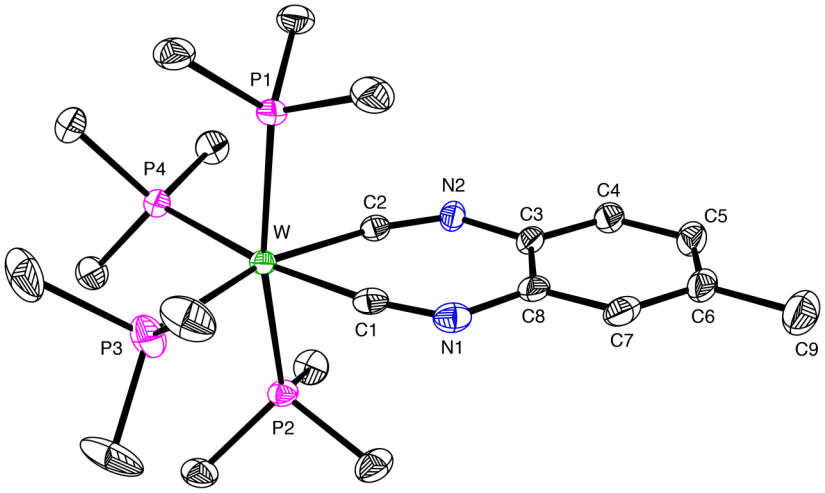

Figure 7. Molecular structure of $[\kappa^2\text{-}C_2\text{-}C_6H_3Me(NC)_2]W(PMe_3)_4$.

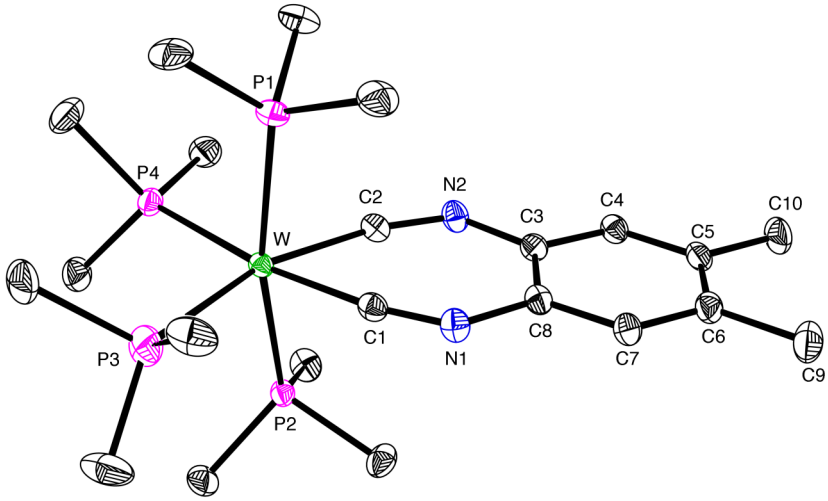

Figure 8. Molecular structure of $[\kappa^2\text{-}C_2\text{-}C_6H_2Me_2(NC)_2]W(PMe_3)_4$.

3.3 Structural and spectroscopic characterization of $[\kappa^2\text{-}C_2\text{-}C_6H_2R_2(NC)_2]W(PMe_3)_4$

The cleaved quinoxaline fragments within $[\kappa^2\text{-}C_2\text{-}C_6H_2R_2(NC)_2]W(PMe_3)_4$, *i.e.* $C_6H_2R_2(NC)_2$, correspond to known di(isocyanide) compounds.[21] As such, $[\kappa^2\text{-}C_2\text{-}C_6H_2R_2(NC)_2]W(PMe_3)_4$ may be viewed as simple transition metal isocyanide complexes of the type $ML_4(CNR)_2$, for which there is precedent. However, the $[\kappa^2\text{-}C_2\text{-}C_6H_2R_2(NC)_2]W(PMe_3)_4$ complexes exhibit several interesting structural features. Firstly,

whereas the majority of transition metal isocyanide compounds have almost linear C–N–C bond angles (the mean C–N–C bond angle for isocyanide compounds listed in the Cambridge Structural Database (Version 5.30) is 172°), the geometries at the nitrogen center in each of the $[\kappa^2\text{-}C_2\text{-}C_6H_2R_2(NC)_2]W(PMe_3)_4$ complexes are severely bent, having angles ranging from 125° to 128° (Table 1). Such bending, which has also been observed for some monodentate isocyanide complexes,[22] is consistent with considerable metal-to-ligand π–backbonding so that W=C=N–R is a better description of the interaction than is $W{\leftarrow}C^{-}{\equiv}N^{+}\text{–}R$.[23] Further evidence for the multiply bonded nature of the W–C interactions in $[\kappa^2\text{-}C_2\text{-}C_6H_2R_2(NC)_2]W(PMe_3)_4$ is the observed average W–C bond length of 1.93 Å (Table 1), which compares favorably with the mean value of 1.98 Å for structurally characterized compounds with $W{=}CR_2$ double bonds listed in the Cambridge Structural Database (Version 5.30), but is much shorter than the mean W–C single bond length of 2.23 Å.

Table 1. Bond lengths (Å) and angles (°) for the *bis*-isocyanide coordination to tungsten from molecular structures as determined by X-ray crystallography.

	***d*(W–C) (Å)**	***d*(C–N) (Å)**	**W–C–N (°)**	**C–N–C (°)**
$[\kappa^2\text{-}C_6H_4(NC)_2]W(PMe_3)_4$[a]	2.03(2), 2.01(2)	1.19(3), 1.21(2)	164.5(2), 166.0(2)	127(2), 125(2)
	1.78(2), 1.79(2)	1.39(3), 1.35(2)	169.2(2), 167.0(2)	127(2), 128(2)
$[\kappa^2\text{-}C_6H_4(NC)_2]W(PMe_3)_4$[b]	1.962, 1.973	1.237, 1.244	166.0, 162.5	128.4, 129.9
$[\kappa^2\text{-}C_6H_3Me(NC)_2]W(PMe_3)_4$	1.948(4), 1.947(3)	1.246(4), 1.253(4)	166.7(3), 165.9(3)	127.4(3), 127.7(3)
$[\kappa^2\text{-}C_6H_2Me_2(NC)_2]W(PMe_3)_4$	1.956(4), 1.966(4)	1.231(5), 1.257(5)	167.2(3), 164.6(3)	127.4(4), 128.0(4)

(a) The molecular structure of $[\kappa^2\text{-}C_2\text{-}C_6H_4NC)_2]W(PMe_3)_4$ was determined with a low quality data set. Therefore, bond lengths and angles have a significant error associated with them. Furthermore, pseudo-symmetry caused large deviations in bond lengths and angles for the two crystallographically independent molecules in the asymmetric unit.

(b) These bond lengths and angles are obtained from the calculated DFT geometry optimized structure, and are much more similar to $[\kappa^2\text{-}C_2\text{-}C_6H_3MeNC)_2]W(PMe_3)_4$ and $[\kappa^2\text{-}C_2\text{-}C_6H_2Me_2NC)_2]W(PMe_3)_4$.

A high degree of backbonding is also suggested by the ν(CN) stretching frequencies of [κ²-*C*₂-$C_6H_2R_2(NC)_2$]$W(PMe_3)_4$ ranging from 1698 – 1709 cm^{-1} (Table 2), which is at the low end for transition metal isocyanide complexes; for comparison, ν(CN) for isocyanide complexes span a range of at least 2310 cm^{-1} to 1670 cm^{-1}.[24,25] Similarly, the ^{13}C NMR spectroscopic signals of transition metal isocyanide compounds have a range of at least 151.8 – 238.7 ppm,[25,26] with the compound having the most downfield chemical shift, namely $[Fe(CNXyl)_4]^{2-}$, having the lowest ν(CN) stretching frequency and a highly bent C–N–C bond angle of 144(3)°.[25] The ^{13}C NMR chemical shift of 211.4 ppm for [κ²-*C*₂-$C_6H_3Me(NC)_2$]$W(PMe_3)_4$ is thus also consistent with considerable backbonding in this molecule.

Table 2. Isocyanide stretching frequencies of [κ²-*C*₂-$C_6H_2R_2(NC)_2$]$W(PMe_3)_4$ complexes.

	ν(CN) (cm^{-1})[a]
[κ²-*C*₂-$C_6H_4(NC)_2$]$W(PMe_3)_4$	1698
[κ²-*C*₂-$C_6H_3Me(NC)_2$]$W(PMe_3)_4$	1699
[κ²-*C*₂-$C_6H_2Me_2(NC)_2$]$W(PMe_3)_4$	1709

(a) Obtained using KBr disk.

An interesting point to note is that chelating isocyanide ligands are not common because M–C–N–R moieties prefer to adopt linear coordination at both nitrogen and carbon.[26] For this reason, while *o*-$(CN)_2C_6H_4$ has been employed as a ligand, it does not chelate but rather serves as a bridging ligand.[27] In accord with such behavior, the smallest ring size previously reported for a complex of a bidentate di(isocyanide) ligand is 12, as illustrated by [κ²-*C*₂-$CH_2\{OC_6H_4(NC)\}_2$]$Cr(CO)_4$.[28] The 7-membered ring of [κ²-*C*₂-$C_6H_4(NC)_2$]$W(PMe_3)_4$, featuring two W–C–N bond angles that are close to linear (165 – 169°), is thus exceptionally small for a transition metal complex of a bidentate di(isocyanide) ligand. The ability to isolate such a compound may result from the fact

that its mechanism of formation involves insertion of the tungsten center into the aromatic ring; indeed, treatment of $W(PMe_3)_4(\eta^2\text{-}CH_2PMe_2)H$ with *o*-$(CN)_2C_6H_4$ at room temperature results in the immediate formation of an unidentified precipitate, with no evidence for formation of $[\kappa^2\text{-}C_2\text{-}C_6H_4(NC)_2]W(PMe_3)_4$ by ^1H NMR spectroscopy.

3.4 Mechanism of C–C bond cleavage

Several different mechanisms could explain the observed formation of $[\kappa^2\text{-}C_2\text{-}C_6H_4(NC)_2]W(PMe_3)_4$. One involves the direct insertion of tungsten into the C–C bond followed by two α-hydrogen elimination steps. Such a process is in line with the observation that electron donating substituents on olefins promote C–C bond cleavage, as exemplified by the use of enetetramines to generate *N*–heterocyclic carbene compounds.[29,30] However, we favor the alternative mechanism outlined in Scheme 3 that comprises a series of C–H bond cleavage reactions to access a benzyne-type intermediate $[\eta^2\text{-}C_2\text{-}C_6H_4(NCCN)]W(PMe_3)_4H_2$, from which $[\kappa^2\text{-}C_2\text{-}C_6H_4(NC)_2]W(PMe_3)_4$ is then obtained *via* a sequence that involves reductive elimination of H_2 and C–C bond cleavage. The feasibility of this mechanism is supported by the report of the ruthenium benzyne complex $(\eta^2\text{-}C_6H_4)Ru(PMe_3)_4$,[31] a structural analogue of the proposed intermediate $[\eta^2\text{-}C_2\text{-}C_6H_4(NCCN)_2]W(PMe_3)_4$. Additionally, we were able to (*i*) observe the C–H activated complexes $(\eta^2\text{-}N,C\text{-Qox})W(PMe_3)_4H$ and $(\kappa^2\text{-}N,C\text{-Qox})W(PMe_3)_4H$ by ^1H NMR spectroscopy (Scheme 3), and (*ii*) isolate the mononuclear C–H activated complex, $(\eta^2\text{-}N,C\text{-Qox}^{Me2})W(PMe_3)_4H$ (Figure 9), and the dinuclear doubly C–H activated complex, $(\mu\text{–}\eta^2\text{-}N,C\text{-}\kappa^2\text{-}N,C\text{-Qox'})[W(PMe_3)_4H]_2$ (Figure 9), during the course of the reaction, providing evidence that C–H bond cleavage is facile in this system. The molecular structures of $(\eta^2\text{-}N,C\text{-Qox}^{Me2})W(PMe_3)_4H$ and $(\mu\text{–}\eta^2\text{-}N,C\text{-}\kappa^2\text{-}N,C\text{-Qox'})\text{-}[W(PMe_3)_4H]_2$ have been determined by X-ray diffraction, and are shown in Figures 10 and 11, respectively.

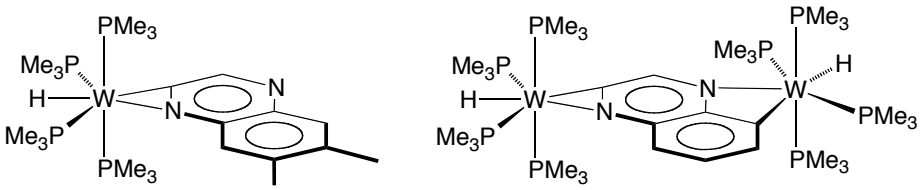

Figure 9. C–H activated complexes (η^2-*N,C*-Qox^{Me_2})W(PMe$_3$)$_4$H (left) and (μ–η^2-*N,C*-κ^2-*N,C*-Qox′)-[W(PMe$_3$)$_4$H]$_2$ (right).

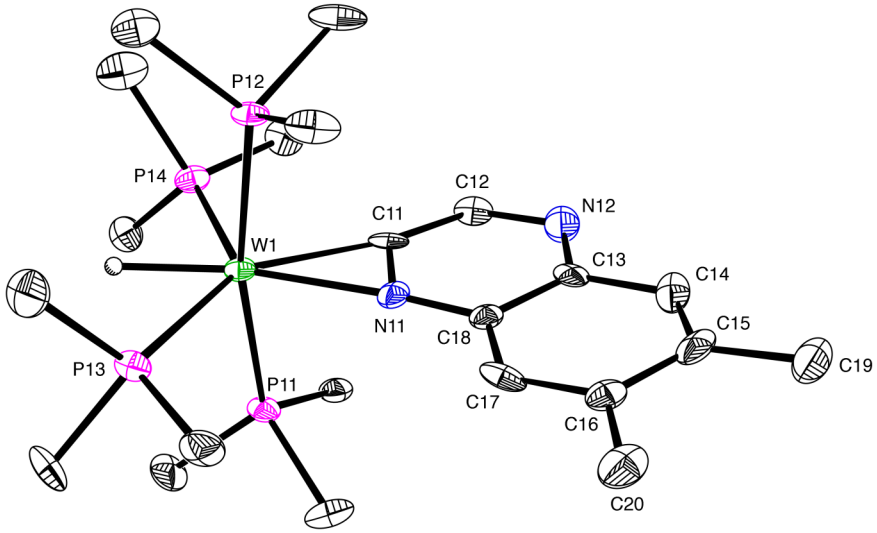

Figure 10. Molecular structure of (η^2-*N,C*-Qox^{Me_2})W(PMe$_3$)$_4$H.

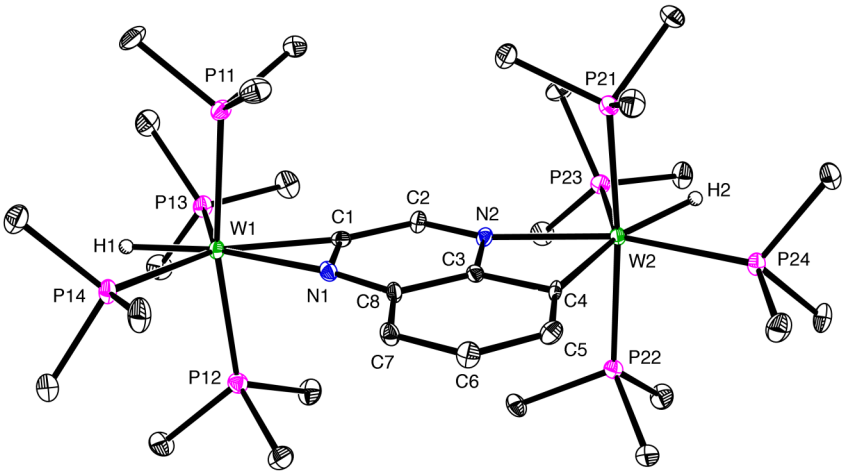

Figure 11. Molecular structure of (μ-η^2-*N,C*-κ^2-*N,C*-Qox′)[W(PMe$_3$)$_4$H]$_2$.

Importantly, C–H bond cleavage is reversible in this system and the observation of (η^2-*N,C*-Qox)W(PMe_3)$_4$H is thus not proof that this species is directly involved in the C–C bond cleavage process. It is, however, significant that a computational analysis of the reaction between W(PMe_3)$_4$(η^2-CH_2PMe_2)H and quinoxaline was recently performed, and was found to be in accord with our proposed reaction mechanism.[32,33] Specifically, the authors DFT calculations indicate that (η^2-*N,C*-Qox)W(PMe_3)$_4$H is directly involved in the formation of the doubly C–H activated benzyne-type complex [η^2-C_2-C_6H_4(NCCN)]W(PMe_3)$_4H_2$, which then eliminates H_2 to produce the final product, [κ^2-C_2-C_6H_4(NC)$_2$]W(PMe_3)$_4$.[32]

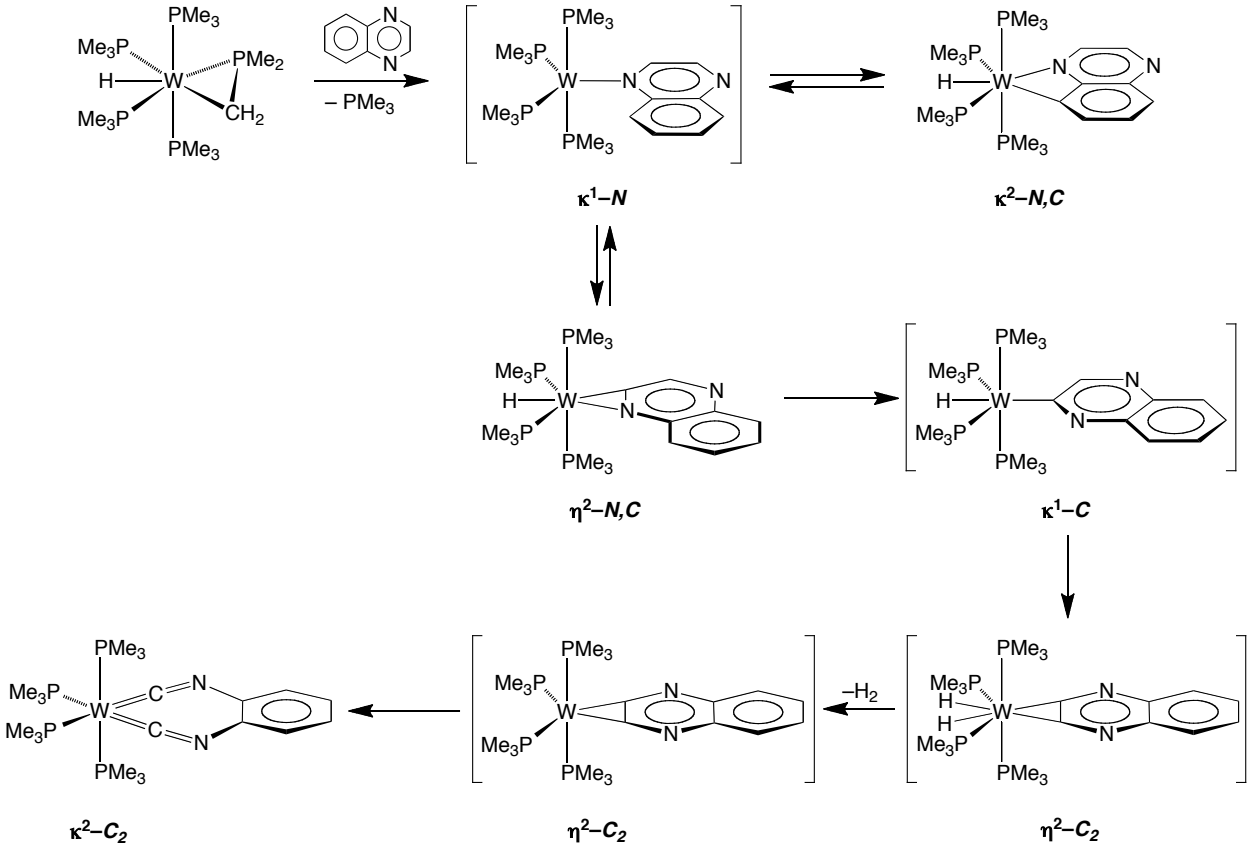

Scheme 3. Possible mechanism for formation of [κ^2-C_2-C_6H_4(NC)$_2$]W(PMe_3)$_4$.

We note that the overall cleavage of the C–C bond of the benzyne-type species proposed in this system resembles the formation of *bis*(isocyanide) compounds by base-induced cleavage of diaminoacetylene species,[34] a process that is the reverse of the well-known coupling reactions of isocyanides.[30,35,36] It is also worth noting that acetylenic C–C bonds have been successfully cleaved using metal-cluster complexes.[37]

3.5 Reactivity of $W(PMe_3)_4(\eta^2\text{-}CH_2PMe_2)H$ towards pyrazine

In view of the reactivity of quinoxaline with $W(PMe_3)_4(\eta^2\text{-}CH_2PMe_2)H$, we wanted to ascertain if the reactivity of the analogous mononuclear N-heterocycle, pyrazine (PyzH), was similar. In this regard, heating a solution of $W(PMe_3)_4(\eta^2\text{-}CH_2PMe_2)H$ and pyrazine in d_6-benzene at 90 °C (Scheme 4) allowed us to isolate crystals of $(\eta^2\text{-}N,C\text{-Pyz})W(PMe_3)_4H$ (Figure 12). However, we did not observe any C–C bond cleaved products by ^1H NMR spectroscopy. Thus, while C–H bond cleavage occurs, which is proposed to be a prerequisite step before C–C bond cleavage (see above), the absence of a fused phenylene ring clearly impacts further reactivity.

It is also interesting to note that the molecular structure of $(\eta^2\text{-}N,C\text{-Pyz})W(PMe_3)_4H$ (Figure 12) is highly disordered, and this is shown in Figure 13. Specifically, the tungsten center lies on a site that has *m* symmetry, such that a mirror plane exists based on the crystallographically imposed symmetry, even though the molecule (as it is oriented in the unit cell) does not. Therefore, the PART–1 command was used for every atom, excluding tungsten, in order to model the 50:50 disorder (Figure 13).

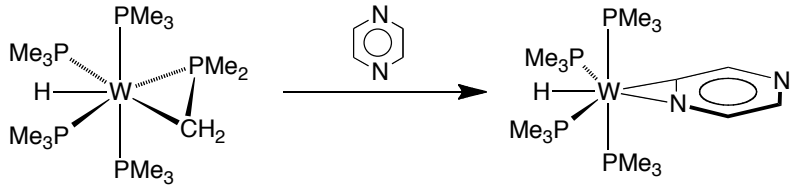

Scheme 4. Production of $(\eta^2\text{-}N,C\text{-Pyz})W(PMe_3)_4H$ from $W(PMe_3)_4(\eta^2\text{-}CH_2PMe_2)H$ and pyrazine.

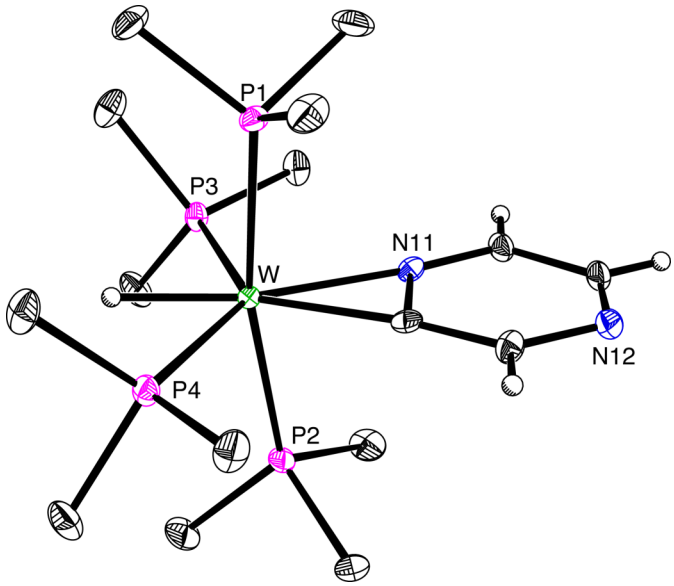

Figure 12. Molecular structure of (η^2-*N,C*-Pyz)W(PMe_3)$_4$H.

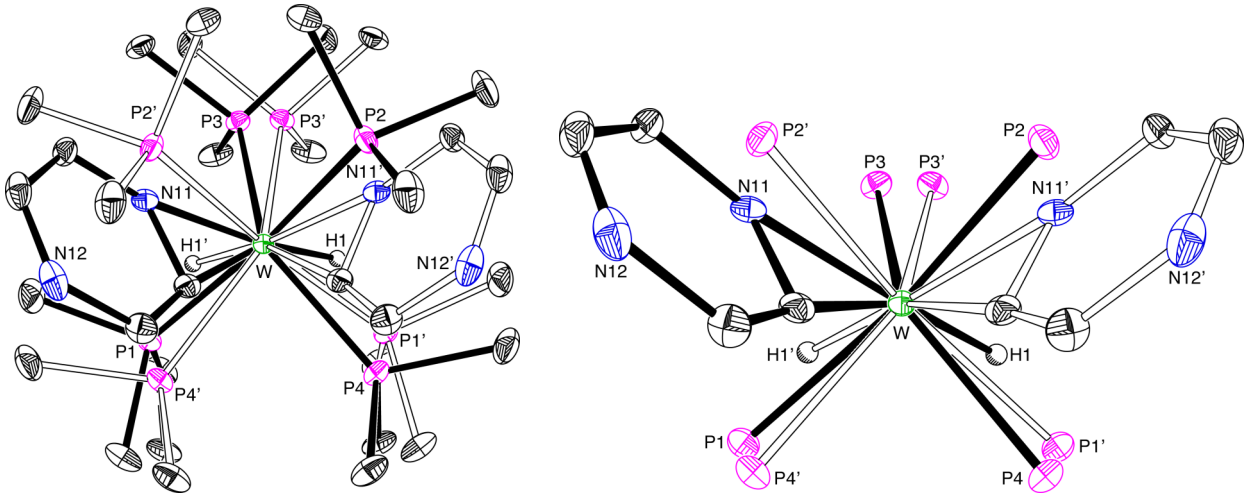

Figure 13. Disordered nature of (η^2-*N,C*-Pyz)W(PMe_3)$_4$H (solid lines represent one component of the disorder while hollow lines represent the other component. The figure on the right has removed all methyl groups from the PMe_3 ligands for clarity).

3.6 Summary and conclusions

In conclusion, we have observed the cleavage of an aromatic C–C bond by insertion of tungsten into an aromatic ring. The C–C bond cleavage enables a quinoxaline compound to be converted to an *o*-diisocyanobenzene derivative, a

transformation that may potentially be extended to other systems and thereby provide a new means for functionalizing aromatic molecules.

3.7 Experimental details

3.7.1 General considerations

All manipulations were performed using a combination of glovebox, high vacuum, and Schlenk techniques under an argon atmosphere unless otherwise specified.[38] Solvents were purified and degassed by standard procedures. ^{1}H NMR spectra were measured on Bruker 300 DRX, Bruker 400 DRX, and Bruker Avance 500 DMX spectrometers. ^{1}H chemical shifts are reported in ppm relative to $SiMe_4$ ($\delta = 0$) and were referenced internally with respect to the protio solvent impurity (δ 7.16 for C_6D_5H).[39] ^{13}C NMR spectra are reported in ppm relative to $SiMe_4$ ($\delta = 0$) and were referenced internally with respect to the solvent (δ 128.06 for C_6D_6).[39] ^{31}P chemical shifts are reported in ppm relative to 85% H_3PO_4 ($\delta = 0$) and were referenced using $P(OMe)_3$ ($\delta = 141.0$) as an external standard.[40] Coupling constants are given in hertz. Infrared spectra were recorded on Nicolet Avatar 370 DTGS spectrometer and are reported in cm^{-1}. Mass spectra were obtained on a Micromass Quadrupole-Time-of-Flight mass spectrometer using fast atom bombardment (FAB+). $W(PMe_3)_4(\eta^2\text{–}CH_2PMe_2)H$ was prepared by the literature method.[41]

3.7.2 X-ray structure determinations

X-ray diffraction data were collected on a Bruker Apex II diffractometer. Crystal data, data collection and refinement parameters are summarized in Section 3.8, Table 3. The structures were solved using direct methods and standard difference map techniques, and were refined by full-matrix least-squares procedures on F^2 with SHELXTL (Version 6.10).[42]

3.7.3 Computational details

Calculations were carried out using DFT as implemented in the Jaguar 7.5 suite of *ab initio* quantum chemistry programs.[43] Geometry optimizations were performed with the B3LYP density functional[44] using the 6-31G** (C, H, N and P) and LACVP (W) basis sets.[45] The energies of the optimized structures were reevaluated by additional single point calculations on each optimized geometry using cc-pVTZ(-f) correlation consistent triple-ζ basis set for C, H, N, and P and LACV3P for W.

3.7.4 Reaction between $W(PMe_3)_4(\eta^2\text{-}CH_2PMe_2)H$ and quinoxaline

A mixture of $W(PMe_3)_4(\eta^2\text{-}CH_2PMe_2)H$ (23 mg, 0.04 mmol), quinoxaline (5 mg, 0.04 mmol) and mesitylene (1.0 μL) as an internal integration standard was placed in an NMR tube equipped with a J. Young valve and treated with d^6-benzene (*ca.* 0.7 mL). The sample was heated at 90 ˚C for 18 hours and monitored by ^1H NMR spectroscopy, thereby demonstrating the conversion to $[\kappa^2\text{-}C_2\text{-}C_6H_4(NC)_2]W(PMe_3)_4$ (15% yield based on quinoxaline) and $(\eta^4\text{-}C_2N_2\text{-QoxH})W(PMe_3)_3H_2$ (24% yield); in addition some $W(PMe_3)_4H_4$ is also formed. The volatile components were removed *via* lyophilization and the residue was extracted into pentane (1 mL) and filtered. Red crystals of $[\kappa^2\text{-}C_2\text{-}C_6H_4(NC)_2]W(PMe_3)_4$ suitable for X–ray diffraction were obtained by slow evaporation of the filtrate at –18 ˚C.

^1H NMR (C_6D_6): 1.03 [d, $^2J_{P\text{-}H}$ = 5, 18H of $W(P\underline{Me}_3)_4$], 1.73 [vt, $|\,^2J_{P\text{-}H} + {}^6J_{P\text{-}H} = 5\,|$, 18H of $W(P\underline{Me}_3)_4$], 6.50 [m, 2H of $\kappa^2\text{–}C_6\underline{H}_4(NC)_2$], 6.72, [m, 2H of $\kappa^2\text{–}C_6\underline{H}_4(NC)_2$]. $^{31}P\{^1H\}$ (C_6D_6): -37.0 [t, $^2J_{P\text{-}P}$ = 14, 2P of $W(\underline{P}Me_3)_4$], -30.4 [t, $^2J_{P\text{-}P}$ = 14, 2P of $W(\underline{P}Me_3)_4$]. IR Data (KBr disk, cm^{-1}): 3047 (w), 2965 (m), 2901 (m), 2800 (w), 1698 (s) [ν(CN)], 1624 (w), 1592 (w), 1565 (w), 1495 (m), 1451 (m), 1416 (s), 1374 (m), 1329 (s), 1295 (s), 1275 (s), 1230 (m), 1197 (m), 1117 (m), 1023 (w), 936 (vs), 849 (s), 746 (s), 711 (s), 664 (s) (sample contains ca. 10 % $(\eta^4\text{-}C_2N_2\text{-QoxH})W(PMe_3)_3H_2$).

Monitoring of the reaction by ^{1}H NMR spectroscopy demonstrated the formation of (κ^2-*N,C*-Qox)W(PMe_3)$_4$H and (η^2-*N,C*-Qox)W(PMe_3)$_4$H during early stages of the reaction, while a reaction performed in the presence of excess W(PMe_3)$_4$(η^2-CH_2PMe_2)H generated (μ–η^2-*N,C*-κ^2-*N,C*-Qox')[W(PMe_3)$_4$H]$_2$, which was characterized by X–ray diffraction. In addition, X–ray diffraction was used to identify the formation of 2,2'–biquinoxaline, (2,2'–Qox)$_2$, which has been previously reported.[46]

^{1}H NMR data for (κ^2-*N,C*-QoxH)W(PMe_3)$_4$H (C_6D_6): -6.89 [ddt, $^2J_{P\text{-}H}$ = 95, $^2J_{P\text{-}H}$ = 89, $^2J_{P\text{-}H}$ = 13, 1H of W-H], 1.22 [m, 18H of W(PMe_3)$_4$], obscured [18H of W(PMe_3)$_4$], 6.95 [m, 1H of Qox], 7.25 [m, 1H of Qox], 7.51 [m, 1H of Qox], 7.70 [d, $^3J_{H\text{-}H}$ = 3, 1H of Qox]. ^{1}H NMR data for (η^2-*N,C*-Qox)W(PMe_3)$_4$H (C_6D_6): -6.05 [ddt, $^2J_{P\text{-}H}$ = 84, $^2J_{P\text{-}H}$ = 65, $^2J_{P\text{-}H}$ = 9, 1H of W-H], 1.30 [m, 27H of W(PMe_3)$_4$], 1.44 [m, 9H of W(PMe_3)$_4$], 6.34 [m, 2H of Qox], 6.75 [m, 1H of Qox], 7.48 [m, 1H of Qox], 7.62 [s, 1H of Qox].

3.7.5 Reaction between W(PMe_3)$_4$(η^2-CH_2PMe_2)H and quinoxaline in the presence of H_2

A mixture of W(PMe_3)$_4$(η^2-CH_2PMe_2)H (23 mg, 0.04 mmol), quinoxaline (5 mg, 0.04 mmol) and mesitylene (1.0 μL) as an internal integration standard was placed in an NMR tube equipped with a J. Young valve and treated with d^6-benzene (*ca.* 0.7 mL). The sample was charged with H_2 (*ca.* 1 atm) and heated at 90 ˚C for 2 hours. The reaction was monitored by ^{1}H NMR spectroscopy, thereby demonstrating the conversion to (η^4-C_2N_2-QoxH)W(PMe_3)$_3$H$_2$ (86% yield based on quinoxaline); in addition some W(PMe_3)$_4$H$_4$ is also formed. After this period, the volatile components were removed *via* lyophilization and the residue obtained was extracted into pentane (1 mL) and filtered. Dark yellow crystals of (η^4-C_2N_2-QoxH)W(PMe_3)$_3$H$_2$ suitable for X–ray diffraction were obtained by slow evaporation of the extract at –18 ˚C.

^{1}H NMR (C_6D_6): -6.32 [t, $^{2}J_{P\text{-}H}$ = 49, 1H of W-H], -0.28 [dt, $^{2}J_{P\text{-}H}$ = 44, $^{2}J_{P\text{-}H}$ = 59, 1H of W-H], 1.23 [br, 9H of $W(PMe_3)_3$], 1.30 [d, $^{2}J_{P\text{-}H}$ = 3, 18H of $W(PMe_3)_3$], 6.03 [s, 2H of QoxH], 6.65, [m, 2H of QoxH], 6.93 [m, 2H of QoxH]. $^{13}C\{^{1}H\}$ NMR (C_6D_6): 22.4 [m ,3C of $W(PMe_3)_3$], 24.2 [m, 6C of $W(PMe_3)_3$], 92.4 [s, 2C of QoxH], 121.0 [s, 2C of QoxH], 122.0 [s, 2C of QoxH], 161.8 [s, 2C of QoxH]. $^{31}P\{^{1}H\}$ (C_6D_6): -28.2 [m, 1P of $W(\underline{P}Me_3)_3$], -19.3 [t, $^{2}J_{P\text{-}P}$ = 8, 2P of $W(\underline{P}Me_3)_3$]. Mass Spectrum (FAB+): m/z = 545.2 {M+1}.

3.7.6 Reaction between $W(PMe_3)_4(\eta^2\text{-}CH_2PMe_2)H$ and 6-methylquinoxaline

A mixture of $W(PMe_3)_4(\eta^2\text{-}CH_2PMe_2)H$ (23 mg, 0.04 mmol), 6-methylquinoxaline (5 μl, 0.04 mmol) and mesitylene (1.0 μL) as an internal integration standard was placed in an NMR tube equipped with a J. Young valve and treated with d^6-benzene (*ca.* 0.7 mL). The sample was heated at 90 ˚C for 6 hours and monitored by ^{1}H NMR spectroscopy, thereby demonstrating the conversion to $[\kappa^2\text{-}C_2\text{-}C_6H_3Me(NC)_2]W(PMe_3)_4$ (15% yield based on 6-methylquinoxaline) and $(\eta^4\text{-}C_2N_2\text{-}Qox^{Me}H)W(PMe_3)_3H_2$ (17% yield); in addition, some $W(PMe_3)_4H_4$ is also formed. The volatile components were removed *via* lyophilization and the residue was extracted into pentane (1 mL) and filtered. Dark green crystals of $[\kappa^2\text{-}C_2\text{-}C_6H_3Me(NC)_2]W(PMe_3)_4$ suitable for X–ray diffraction were obtained by slow evaporation of the extract at –18 ˚C. Anal. Calcd. for $C_{21}H_{42}N_2P_4W$: C, 40.0 %; H, 6.7 %; N, 4.4 %. Found: C, 39.75 %; H, 6.45 %; N, 4.32 %.

^{1}H NMR (C_6D_6): 1.04 [dd, $^{2}J_{H\text{-}P}$ = 5, $^{2}J_{H\text{-}P}$ = 2, 18H of $W(PMe_3)_4$], 1.73 [t, $^{2}J_{H\text{-}P}$ = 3, 18H of $W(PMe_3)_4$], 1.97 [s, 3H of κ^2–$C_6H_3Me(NC)_2$], 6.36 [d, $^{4}J_{H\text{-}H}$ = 2, 1H of κ^2–$C_6H_3Me(NC)_2$, (part of an ABC pattern)], 6.45 [d, $^{3}J_{H\text{-}H}$ = 8, 1H of κ^2–$C_6H_3Me(NC)_2$ (part of an ABC pattern)], 6.54 [dd, $^{3}J_{H\text{-}H}$ = 8, $^{4}J_{H\text{-}H}$ = 2 1H of κ^2–$C_6H_3Me(NC)_2$ (part of an ABC pattern)]. $^{13}C\{^{1}H\}$ NMR (C_6D_6): 21.1 [s, 1C of κ^2–$C_6H_3\underline{Me}(NC)_2$], 25.6 [m, 12C of $W(P\underline{Me}_3)_4$], 122.8 [s, 1C of κ^2–$\underline{C}_6H_3Me(NC)_2$], 123.6 [s, 1C of κ^2–$\underline{C}_6H_3Me(NC)_2$], 123.8 [s, 1C of κ^2–$\underline{C}_6H_3Me(NC)_2$], 130.9 [s, 1C of κ^2–$\underline{C}_6H_3Me(NC)_2$], 131.7 [s, 1C of κ^2–$\underline{C}_6H_3Me(NC)_2$],

211.4 [m, 2C of κ^2–$C_6H_3Me(N\underline{C})_2$], 1C not observed. $^{31}P\{^1H\}$ (C_6D_6): -36.8 [m, 2P of $W(PMe_3)_4$], -30.6 [t, $^2J_{P\text{-}P}$ = 13, $^1J_{P\text{-}W}$ = 273, 2P of $W(PMe_3)_4$]. IR Data (KBr disk, cm^{-1}): 2968 (w), 2907 (m), 2850 (w), 1699 (m) [ν(CN)], 1616 (w), 1496 (m), 1418 (m), 1291 (m), 1090 (m), 949 (vs), 820 (w).

3.7.7 Reaction between $W(PMe_3)_4(\eta^2\text{-}CH_2PMe_2)H$ and 6-methylquinoxaline in the presence of H_2

A mixture of $W(PMe_3)_4(\eta^2\text{-}CH_2PMe_2)H$ (23 mg, 0.04 mmol), 6-methylquinoxaline (5 μl, 0.04 mmol) and mesitylene (1.0 μL) as an internal integration standard was placed in an NMR tube equipped with a J. Young valve and treated with d^6-benzene (*ca.* 0.7 mL). The sample was charged with H_2 (*ca.* 1 atm) and heated at 90 °C. The reaction was monitored by ^1H NMR spectroscopy, thereby demonstrating the conversion to (η^4-C_2N_2-$Qox^{Me}H$)$W(PMe_3)_3H_2$ (49% yield based on 6-methylquinoxaline) over a period of 4 hours; in addition, some $W(PMe_3)_4H_4$ is also formed. After this period, the volatile components were removed *via* lyophilization and the residue obtained was extracted into pentane (1 mL) and filtered. Colorless crystals of (η^4-C_2N_2-$Qox^{Me}H$)$W(PMe_3)_3H_2$ suitable for X–ray diffraction were obtained by slow evaporation of the extract at –18 °C.

^1H NMR (C_6D_6): -6.31 [t, $^2J_{P\text{-}H}$ = 49, 1H of W-H], -0.28 [dt, $^2J_{P\text{-}H}$ = 35, $^2J_{P\text{-}H}$ = 63, 1H of W-H], 1.26 [d, $^2J_{P\text{-}H}$ = 7, 9H of $W(PMe_3)_3$], 1.31 [br, 18H of $W(PMe_3)_3$], 2.15 [s, 3H of $Qox^{Me}H$], 6.03 [s, 2H of $Qox^{Me}H$], 6.44, [d, $^3J_{H\text{-}H}$ = 7, 1H of $Qox^{Me}H$], 6.72 [s, 1H of $Qox^{Me}H$], 6.83 [d, $^3J_{H\text{-}H}$ = 7, 1H of $Qox^{Me}H$].

3.7.8 Reaction between $W(PMe_3)_4(\eta^2\text{-}CH_2PMe_2)H$ and 6,7-dimethylquinoxaline

A mixture of $W(PMe_3)_4(\eta^2\text{-}CH_2PMe_2)H$ (25 mg, 0.04 mmol), 6,7-dimethylquinoxaline (6 mg, 0.04 mmol) and mesitylene (1.0 μL) as an internal integration standard was placed in an NMR tube equipped with a J. Young valve and treated with d^6-benzene (*ca.* 0.7

mL). The sample was heated at 90 ˚C for 2 days and monitored by ^{1}H NMR spectroscopy, thereby demonstrating the conversion to [κ^2-C_2-$C_6H_2Me_2(NC)_2$]W(PMe_3)$_4$ (18 % yield) and (η^4-C_2N_2-Qox^{Me2}H)W(PMe_3)$_3H_2$ (9% yield). The volatile components were removed *via* lyophilization and the residue was extracted into pentane (1 mL) and filtered. Red crystals of [κ^2-C_2-$C_6H_2Me_2(NC)_2$]W(PMe_3)$_4$ suitable for X–ray diffraction were obtained by slow evaporation of the filtrate at –18 ˚C.

^{1}H NMR (C_6D_6): 1.06 [d, $^2J_{P\text{-}H}$ = 5, 18H of W(PMe_3)$_4$], 1.74 [m, 18H of W(PMe_3)$_4$], 1.89 [s, 6H of κ^2–$C_6H_2Me_2(NC)_2$], 6.35, [s, 2H of κ^2–$C_6H_2Me_2(NC)_2$]. ^{31}P{^{1}H} (C_6D_6): -36.7 [t, $^2J_{P\text{-}P}$ = 13, 2P of W(PMe_3)$_4$], -30.5 [t, $^2J_{P\text{-}P}$ = 13, 2P of W(PMe_3)$_4$]. IR Data (KBr disk, cm^{-1}): 2964 (m), 2900 (s), 1709 (m) [ν(CN)], 1418 (m), 1328 (w), 1292 (m), 1272 (m), 1189 (w), 936 (vs), 848 (m), 705 (m), 656 (m). Monitoring of the reaction by ^{1}H NMR spectroscopy demonstrated the formation of (η^2-*N,C*-Qox^{Me2})W(PMe_3)$_4$H during early stages of the reaction, which was also characterized by X–ray diffraction. ^{1}H NMR (C_6D_6, partial data): -5.67 [ddt, $^2J_{P\text{-}H}$ = 84, $^2J_{P\text{-}H}$ = 67, $^2J_{P\text{-}H}$ = 8, 1H of W-H], 1.98 [s, 6H of Me_2], 6.44 [s, 1H of Qox^{Me2}], 7.36 [s, 1H of Qox^{Me2}], 7.74 [s, 1H of Qox^{Me2}].

3.7.9 Reaction between W(PMe_3)$_4$(η^2-CH_2PMe_2)H and 6,7-dimethylquinoxaline in the presence of H_2

A mixture of W(PMe_3)$_4$(η^2-CH_2PMe_2)H (23 mg, 0.04 mmol), 6,7-dimethylquinoxaline (6 mg, 0.04 mmol) and mesitylene (1.0 μL) as an internal integration standard was placed in an NMR tube equipped with a J. Young valve and treated with d^6-benzene (*ca.* 0.7 mL). The sample was charged with H_2 (*ca.* 1 atm) and heated at 90 ˚C. The reaction was monitored by ^{1}H NMR spectroscopy, thereby demonstrating the conversion to (η^4-C_2N_2-Qox^{Me2}H)W(PMe_3)$_3H_2$ (38 % yield) over a period of 5 hours. After this period, the volatile components were removed *via* lyophilization and the residue obtained was extracted into pentane (1 mL) and filtered. Colorless crystals of (η^4-C_2N_2-

$Qox^{Me_2}H)W(PMe_3)_3H_2$ suitable for X–ray diffraction were obtained by slow evaporation of the extract at –18 ˚C.

^1H NMR (C_6D_6): -6.30 [t, $^2J_{P\text{-}H}$ = 50, 1H of W-H], -0.30 [dt, $^2J_{P\text{-}H}$ = 41, $^2J_{P\text{-}H}$ = 62, 1H of W-H], 1.33 [d, $^1J_{P\text{-}H}$ = 6, 27H of $W(PMe_3)_3$], 2.06 [s, 6H of Me_2], 6.05 [s, 2H of $Qox^{Me_2}H$], 6.77 [s, 2H of $Qox^{Me_2}H$].

3.8 Crystallographic data

Table 3. Crystal, intensity collection and refinement data.

	[κ²-*C*₂-C₆H₄(NC)₂]W(PMe₃)₄	**(η⁴-*C*₂*N*₂-QoxH)W(PMe₃)₃H₂**
lattice	Monoclinic	Monoclinic
formula	$C_{20}H_{40}N_2P_4W$	$C_{17}H_{35}N_2P_3W$
formula weight	616.27	544.23
space group	$P2_1$	$P2_1/c$
a/Å	14.122(3)	9.0173(11)
b/Å	13.278(3)	15.1314(18)
c/Å	14.879(3)	16.403(2)
α/°	90	90
β/°	105.295(3)	104.366(2)
γ/°	90	90
V/Å³	2691.1(9)	2168.1(5)
Z	4	4
temperature (K)	125(2)	125(2)
radiation (λ, Å)	0.71073	0.71073
ρ (calcd.) g cm^{-3}	1.521	1.667
μ (Mo Kα), mm^{-1}	4.539	5.551
θ max, deg.	26.37	32.71
no. of data collected	32499	36560
no. of data	10985	7576
no. of parameters	476	225
R_1 [$I > 2\sigma(I)$]	0.0756	0.0279
wR_2 [$I > 2\sigma(I)$]	0.1143	0.0509
R_1 [all data]	0.1660	0.0466
wR_2 [all data]	0.1374	0.0560
GOF	1.027	1.001

Table 3 (cont). Crystal, intensity collection and refinement data.

	[κ²-*C*₂-C₆H₃Me(NC)₂]W(PMe₃)₄	**(η⁴-*C*₂*N*₂-Qox^{Me}H)-W(PMe₃)₃H₂**
lattice	Monoclinic	Monoclinic
formula	$C_{21}H_{42}N_2P_4W$	$C_{18}H_{37}N_2P_3W$
formula weight	630.30	558.26
space group	*C2/c*	$P2_1/n$
a / Å	34.364(4)	10.4986(12)
b / Å	9.7012(10)	10.2558(12)
c / Å	19.2762(19)	21.635(3)
α / °	90	90
β / °	121.9860(10)	98.726(2)
γ / °	90	90
V / Å^3	5450.5(10)	2302.5(5)
Z	8	4
temperature (K)	125(2)	125(2)
radiation (λ, Å)	0.71073	0.71073
ρ (calcd.) g cm^{-3}	1.536	1.610
μ (Mo Kα), mm^{-1}	4.484	5.229
θ max, deg.	32.30	30.94
no. of data collected	45947	35741
no. of data	9537	7250
no. of parameters	297	235
R_1 [$I > 2\sigma(I)$]	0.0344	0.0261
wR_2 [$I > 2\sigma(I)$]	0.0635	0.0508
R_1 [all data]	0.0631	0.0410
wR_2 [all data]	0.0713	0.0553
GOF	1.004	1.094

Table 3 (cont). Crystal, intensity collection and refinement data.

	[κ²-*C*₂-C₆H₂Me₂(NC)₂]W(PMe₃)₄	**(η⁴-*C*₂*N*₂-Qox^{Me_2}H)W(PMe₃)₃H₂**
lattice	Monoclinic	Monoclinic
formula	$C_{22}H_{44}N_2P_4W$	$C_{19}H_{39}N_2P_3W$
formula weight	644.32	572.28
space group	*C2/c*	$P2_1/n$
a / Å	34.669(3)	10.0850(8)
b / Å	9.8900(10)	10.8134(8)
c / Å	19.7025(19)	21.8990(16)
α / °	90	90
β / °	122.3070(10)	95.5850(10)
γ / °	90	90
V / Å^3	5709.8(10)	2376.8(3)
Z	8	4
temperature (K)	125(2)	125(2)
radiation (λ, Å)	0.71073	0.71073
ρ (calcd.) g cm^{-3}	1.499	1.599
μ (Mo Kα), mm^{-1}	4.282	5.068
θ max, deg.	32.72	30.51
no. of data collected	48380	36946
no. of data	10028	7257
no. of parameters	307	245
R_1 [$I > 2\sigma(I)$]	0.0421	0.0207
wR_2 [$I > 2\sigma(I)$]	0.1087	0.0297
R_1 [all data]	0.0571	0.0323
wR_2 [all data]	0.1159	0.0432
GOF	1.209	1.032

Table 3 (cont). Crystal, intensity collection and refinement data.

	[μ-η²-*N,C*-κ²-*N,C*-Qox′][W(PMe$_3$)$_4$H]$_2$	**(η²-*N,C*-Qox^{Me_2})W(PMe$_3$)$_4$H**
lattice	Monoclinic	Triclinic
formula	$C_{32}H_{78}N_2P_8W_2$	$C_{22}H_{46}N_2P_4W$
formula weight	1106.42	646.34
space group	*C2/c*	*P-1*
a / Å	38.217(4)	12.560(2)
b / Å	9.4018(9)	14.272(3)
c / Å	26.655(3)	17.057(3)
α / °	90	71.072(3)
β / °	104.7300(10)	78.423(3)
γ / °	90	87.254(3)
V / Å^3	9262.7(15)	2832.9(9)
Z	8	4
temperature (K)	125(2)	125(2)
radiation (λ, Å)	0.71073	0.71073
ρ (calcd.) g cm^{-3}	1.587	1.515
μ (Mo Kα), mm^{-1}	5.263	4.315
θ max, deg.	32.62	26.37
no. of data collected	78993	34419
no. of data	16288	11597
no. of parameters	428	557
R_1 [$I > 2\sigma(I)$]	0.0454	0.0647
wR_2 [$I > 2\sigma(I)$]	0.0597	0.1404
R_1 [all data]	0.0949	0.1520
wR_2 [all data]	0.0687	0.1859
GOF	1.013	0.860

Table 3 (cont). Crystal, intensity collection and refinement data.

	(η^2-*N,C*-PyzH)W(PMe_3)$_4$H	**2,2′–Biquinoxaline**
lattice	Orthorhombic	Monoclinic
formula	$C_{16}H_{41}N_2P_4W$	$C_{16}H_{10}N_4$
formula weight	569.24	258.28
space group	*Cmca*	$P2_1/n$
a/Å	15.5462(14)	5.7903(6)
b/Å	9.7978(9)	5.3489(5)
c/Å	31.488(3)	18.7694(18)
α/°	90	90
β/°	90	91.350(2)
γ/°	90	90
V/Å^3	4796.2(7)	581.16(10)
Z	8	2
temperature (K)	125(2)	125(2)
radiation (λ, Å)	0.71073	0.71073
ρ (calcd.) g cm^{-3}	1.577	1.476
μ (Mo Kα), mm^{-1}	5.086	0.092
θ max, deg.	32.65	28.27
no. of data collected	40128	2662
no. of data	4428	1305
no. of parameters	221	91
R_1 [$I > 2\sigma(I)$]	0.0237	0.0455
wR_2 [$I > 2\sigma(I)$]	0.0390	0.1420
R_1 [all data]	0.0348	0.0614
wR_2 [all data]	0.0412	0.1552
GOF	1.032	1.073

3.9 References and notes

(1) Jones, W. D. Advances in carbon–hydrogen activation. *Comprehensive Organometallic Chemistry III*, Volume 1, Chapter 1.25; Crabtree, R. H. and Mingos, D. M. P. (Eds), Elsevier, Oxford, 2006.

(2) Jones, W. D. *Nature* **1994**, *364*, 676-677.

(3) Jun, C. H. *Chem. Soc. Rev.* **2004**, *33*, 610-618.

(4) van der Boom, M.E.; Milstein, D. *Chem. Rev.* **2003**, *103*, 1759-1792.

(5) Crabtree, R. H. *Chem. Rev.* **1985**, *85*, 245-269.

(6) Rybtchinski, B.; Milstein, D. *Angew. Chem. Int. Ed.* **1999**, *38*, 870-883.

(7) For other examples of C–C bond cleavage, see:

(a) Li, H. R.; Li, W. J.; Liu, W. P.; He, Z. H.; Li, Z. P. *Angew. Chem. Int. Ed.* **2011,** *50*, 2975-2978.

(b) Huang, L. H.; Cheng, K.; Yao, B. B.; Xie, Y. J.; Zhang, Y. H. *J. Org. Chem.* **2011,** *76*, 5732-5737.

(c) Chaplin, A. B.; Green, J. C.; Weller, A. S. *J. Am. Chem. Soc.* **2011,** *133*, 13162-13168.

(d) Summerscales, O. T.; Jimenez-Halla, J. O. C.; Merino, G.; Power, P. P. *J. Am. Chem. Soc.* **2011,** *133*, 180-183.

(e) Gerfaud, T.; Wei, H. L.; Neuville, L.; Zhu, J. P. *Org. Lett.* **2011,** *13*, 6172-6175.

(f) Zhang, C.; Xu, Z. J.; Shen, T.; Wu, G. L.; Zhang, L. R.; Jiao, N. *Org. Lett.* **2012,** *14*, 2362-2365.

(g) Wu, X. X.; Lia, L.; Zhang, J. L. *Chem. Commun.* **2011,** *47*, 7824-7826.

(h) Wang, T.; Zhang, J. L. *Chem. Eur. J.* **2011,** *17*, 86-90.

(i) Ellis, D.; McKay, D.; Macgregor, S. A.; Rosair, G. M.; Welch, A. J. *Angew. Chem. Int. Ed.* **2010,** *49*, 4943-4945.

(8) Zhu, G.; Tanski, J. M.; Churchill, D. G.; Janak, K. E.; Parkin, G. *J. Am. Chem. Soc.* **2002**, *124*, 13658-13659.

(9) Zhu, G.; Pang, K.; Parkin, G. *J. Am. Chem. Soc.* **2008**, *130*, 1564-1565.

(10) Sattler, A.; Zhu, G.; Parkin, G. *J. Am. Chem. Soc.* **2009**, *131*, 7828-7838.

(11) See Chapter 2.

(12) Buccella, D.; Parkin, G. *J. Am. Chem. Soc.* **2006**, *128*, 16358-16364.

(13) Due to the fact that the crystals of $[\kappa^2\text{-}C_2\text{-}C_6H_4(NC)_2]W(PMe_3)_4$ were very small and not single, the crystallographic dataset collected was of low quality.

(14) All of the molecular structures were subjected to density functional geometry optimization calculations, and the calculated structures are in good agreement with the experimentally determined structures (see Section 3.7.3).

(15) Cyranski, M. K. *Chem. Rev.* **2005**, *105*, 3773-3811.

(16) Kleckley, T. S.; Bennett, J. L.; Wolczanski, P. T.; Lobkovsky, E. B. *J. Am. Chem. Soc.* **1997**, *119*, 247-248.

(17) Bonanno, J. B.; Veige, A. S.; Wolczanski, P. T.; Lobkovsky, E. B. *Inorg. Chim. Acta* **2003**, *345*, 173-184.

(18) Gray, S. D.; Weller, K. J.; Bruck, M. A.; Briggs, P. M.; Wigley, D. E. *J. Am. Chem. Soc.* **1995**, *117*, 10678-10693.

(19) Weller, K. J.; Filippov, I.; Briggs, P. M.; Wigley, D. E. *Organometallics* **2008**, *17*, 322-329.

(20) Bailey, B. C.; Fan, H.; Huffman, J. C.; Baik, M. H.; Mindiola, D. J. *J. Am. Chem. Soc.* **2006**, *128*, 6798-6799.

(21) Ito, Y.; Ohnishi, A.; Ohsaki, H.; Murakami, M. *Synthesis* **1998**, 714-715.

(22) Wagner, N. L.; Laib, F. E.; Bennett, D. W. *J. Am. Chem. Soc.* **2000**, *122*, 10856-10867.

(23) Kuznetsov, M. L. T *Russ. Chem. Rev.* **2002**, *71*, 265-282.

(24) Strauch, H. C.; Wibbeling, B.; Fröhlich, R.; Erker, G. *Organometallics* **1999**, *18*, 3802-3812.

(25) Brennessel, W. W.; Ellis, J. E. *Angew. Chem. Int. Ed.* **2007**, *46*, 598-600.

(26) Hahn, F. E. *Angew. Chem. Int. Ed.* **1993**, *32*, 650-665.

(27) Espinet, P.; Soulantica, K.; Charmant, J. P. H.; Orpen, A. G. *Chem. Commun.* **2000**, 915-916.

(28) Hahn, F. E.; Tamm, M.; Imhof, L.; Lugger, T. *J. Organomet. Chem.* **1996**, *526*, 149-155.

(29) Lappert, M. F. *J. Organomet. Chem.* **2005**, *690*, 5467-5473.

(30) Wilker, C. N.; Hoffmann, R.; Eisenstein, O. *Nouv. J. Chim.* **1983**, *7*, 535-544.

(31) Hartwig, J. F.; Bergman, R. G.; Andersen, R. *J. Am. Chem. Soc.* **1991**, *113*, 3404-3418.

(32) Miscione, G. P.; Carvajal, M. A.; Bottoni, A. *Organometallics* **2011**, *30*, 4924-4934.

(33) An additional study was performed and found that the first intermediate to react with quinoxaline is a tungsten compound that has lost *two* PMe_3 ligands, namely $W(PMe_3)_2(\eta^2\text{-}CH_2PMe_2)H$. However, the authors also conclude that two C–H activation occurs with subsequent formation of a benzyne intermediate and then loss of H_2, which is closely analogous to our proposed mechanism. See: Li, J.; Yoshizawa, K. *Chem. Eur. J.* **2012**, *18*, 783-787.

(34) Pombeiro, A. J. L.; da Silva, M.; Michelin, R. A. *Coord. Chem. Rev.* **2001**, *218*, 43-74.

(35) Carnahan, E. M.; Protasiewicz, J. D.; Lippard, S. J. *Acc. Chem. Res.* **1993**, *26*, 90-97.

(36) Ito, Y.; Ihara, E.; Hirai, M.; Ohsaki, H.; Ohnishi, A.; Murakami, M. *J. Chem. Soc., Chem. Commun.* **1990**, 403-405.

(37) Clauss, A. D.; Shapley, J. R.; Wilker, C. N.; Hoffmann, R. *Organometallics* **1984**, *3*, 619.

(38) (a) McNally, J. P.; Leong, V. S.; Cooper, N. J. in *Experimental Organometallic Chemistry*, Wayda, A. L.; Darensbourg, M. Y., Eds.; American Chemical Society: Washington, DC, 1987; Chapter 2, pp 6-23.

(b) Burger, B.J.; Bercaw, J. E. in *Experimental Organometallic Chemistry*; Wayda, A. L.; Darensbourg, M. Y., Eds.; American Chemical Society: Washington, DC, 1987; Chapter 4, pp 79-98.

(c) Shriver, D. F.; Drezdzon, M. A.; *The Manipulation of Air-Sensitive Compounds*, 2nd Edition; Wiley-Interscience: New York, 1986.

(39) Gottlieb, H. E.; Kotlyar, V.; Nudelman, A. *J. Org. Chem.* **1997**, *62*, 7512-7515.

(40) "Nuclear Magnetic Resonance Spectroscopy" Nelson, J. H. Prentice Hall, New Jersey (2003), p 79.

(41) Green, M. L. H.; Parkin, G.; Chen, M.; Prout, K. *J. Chem. Soc., Dalton Trans.* **1986**, 2227–2236.

(42) (a) Sheldrick, G. M. SHELXTL, An Integrated System for Solving, Refining and Displaying Crystal Structures from Diffraction Data; University of Göttingen, Göttingen, Federal Republic of Germany, 1981.

(b) Sheldrick, G. M. *Acta Cryst.* **2008**, *A64*, 112-122.

(43) Jaguar 7.0, Schrödinger, LLC, New York, NY 2007.

(44) (a) Becke, A. D. *J. Chem. Phys.* **1993**, *98*, 5648-5652.

(b) Becke, A. D. *Phys. Rev. A* **1988**, *38*, 3098-3100.

(c) Lee, C. T.; Yang, W. T.; Parr, R. G. *Phys. Rev. B* **1988**, *37*, 785-789.

(d) Vosko, S. H.; Wilk, L.; Nusair, M. *Can. J. Phys.* **1980**, *58*, 1200-1211.

(e) Slater, J. C. *Quantum Theory of Molecules and Solids, Vol. 4: The Self-Consistent Field for Molecules and Solids*; McGraw-Hill: New York, 1974.

(45) (a) Hay, P. J.; Wadt, W. R. *J. Chem. Phys.* **1985**, *82*, 270-283.

(b) Wadt, W. R.; Hay, P. J. *J. Chem. Phys.* **1985**, *82*, 284-298.

(c) Hay, P. J.; Wadt, W. R. *J. Chem. Phys.* **1985**, *82*, 299-310.

(46) Fitchett, C. M.; Richardson, C.; Steel, P. J. *Org. Biomol. Chem.* **2005**, 3, 498-502.

CHAPTER 4

Carbon–sulfur bond cleavage and hydrodesulfurization of thiophenes by molybdenum and tungsten trimethylphosphine compounds

Table of Contents

Reproduced in part from:

Sattler, A.; Janak, K. E.; Parkin, G. *Inorg. Chim. Acta* **2011**, *369*, 197–202.

Sattler, A.; Parkin, G. *J. Am. Chem. Soc.* **2011**, *133*, 3748–3751.

4.1 Introduction

4.1.1 Hydrodesulfurization (HDS)

Hydrodesulfurization (HDS) is the important industrial process by which sulfur-containing impurities are removed from crude petroleum feedstocks prior to their use, in order to obtain *(i)* cleaner fuels that minimize environmental pollution and *(ii)* cleaner chemical feedstocks that are less likely to poison the catalysts that are used for subsequent transformations (Scheme 1).[1,2,3,4,5,6] The catalysts employed for HDS are largely composed of molybdenum and tungsten sulfides (MoS_2 and WS_2, respectively) supported on alumina and also contain smaller quantities of other transition metals, common examples of which are Co and Ni, which are called promoter metals.[7] Much effort has been directed towards enhancing the efficiency of this process, however, the heterogeneous nature of the catalyst makes it difficult to achieve a molecular level understanding of the catalytic cycle.[7] As such, considerable effort has been directed towards obtaining an understanding of this process at a mechanistic level by investigating the reactivity of various sulfur-containing compounds, and thiophenes (Figure 1) in particular, towards various metal centers.[8,9]

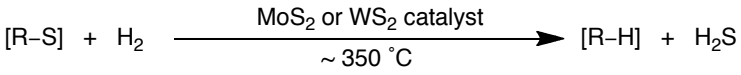

Scheme 1. Hydrodesulfurization.

Despite the fact that molybdenum and tungsten are the most universal components of the industrial HDS catalysts,[1,5,6] the majority of these studies has focused on precious metals such as Rh, Ir, Pd and Pt.[8,9] In this chapter, we describe (*i*) the reactivity of several molybdenum hydride compounds with thiophenes[10] and (*ii*) the first report of desulfurization of thiophenes by molecular tungsten compounds.[11]

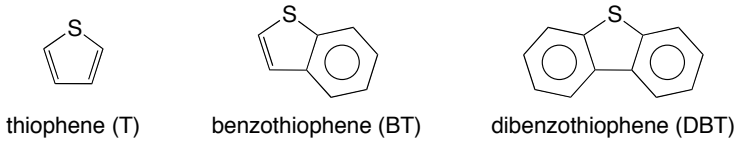

Figure 1. Thiophene (T), benzothiophene (BT), and dibenzothiophene (DBT).

4.1.2 Previous studies: HDS and molecular molybdenum compounds

Molybdenum is a major component of the hydrodesulfurization catalysts used in industry.[3] In this regard, the Parkin group has studied the reactivity of thiophenes with molecular molybdenum complexes, in order to gain insight concerning the coordination chemistry and reactivity that may be observed on the surface of a MoS_2 catalyst. For example, Parkin and his graduate students reported reactivity studies concerning the *ansa*-metallocene complex, $[Me_2Si(C_5Me_4)_2]MoH_2$,[12,13] with thiophenes, as illustrated in Scheme 2. The most notable feature of this study was the observation of C–S bond cleavage of thiophene and benzothiophene (Scheme 2), which was first time that a molybdenum complex had displayed this type of reactivity. The Parkin group also reported on the reactivity of $Mo(PMe_3)_6$ towards thiophene[14] and benzothiophene,[15] observing several interesting products emanating from C–S bond cleavage (Scheme 3).

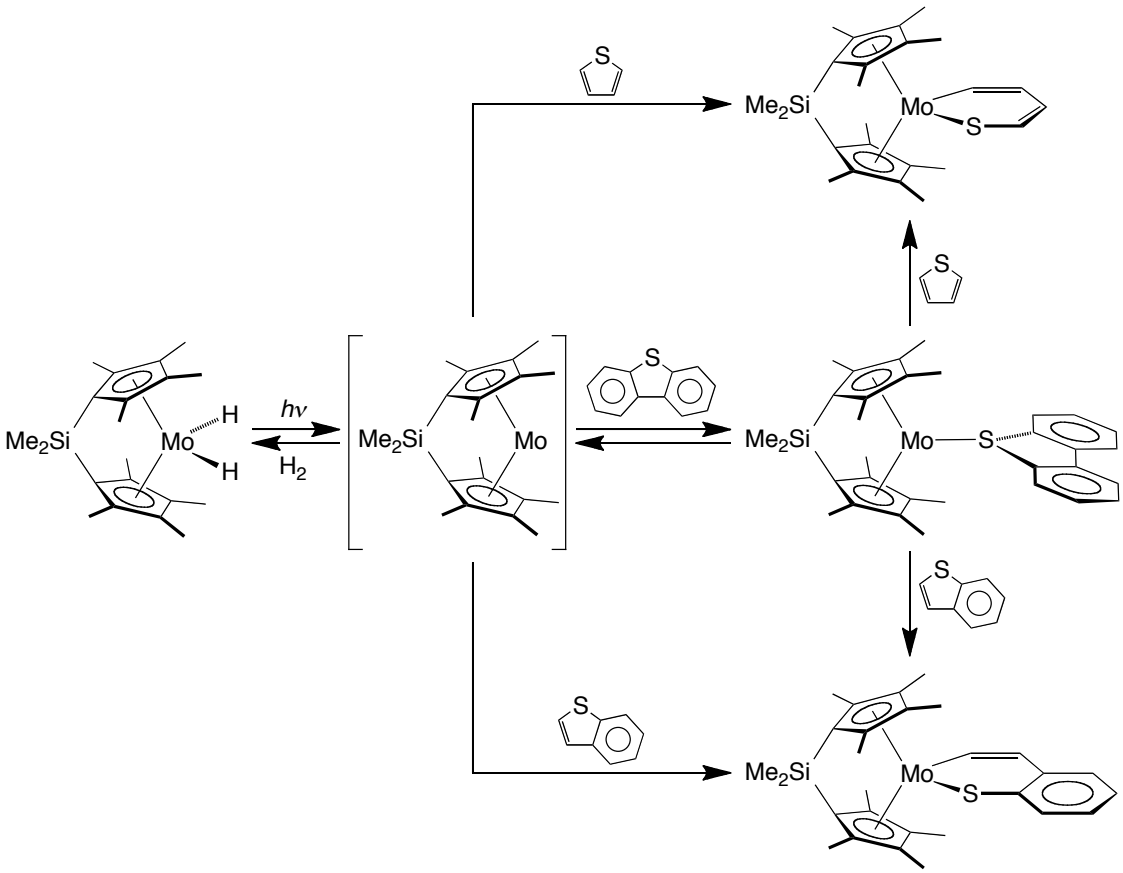

Scheme 2. Reactivity of $[Me_2Si(C_5Me_4)_2]MoH_2$ towards thiophenes.

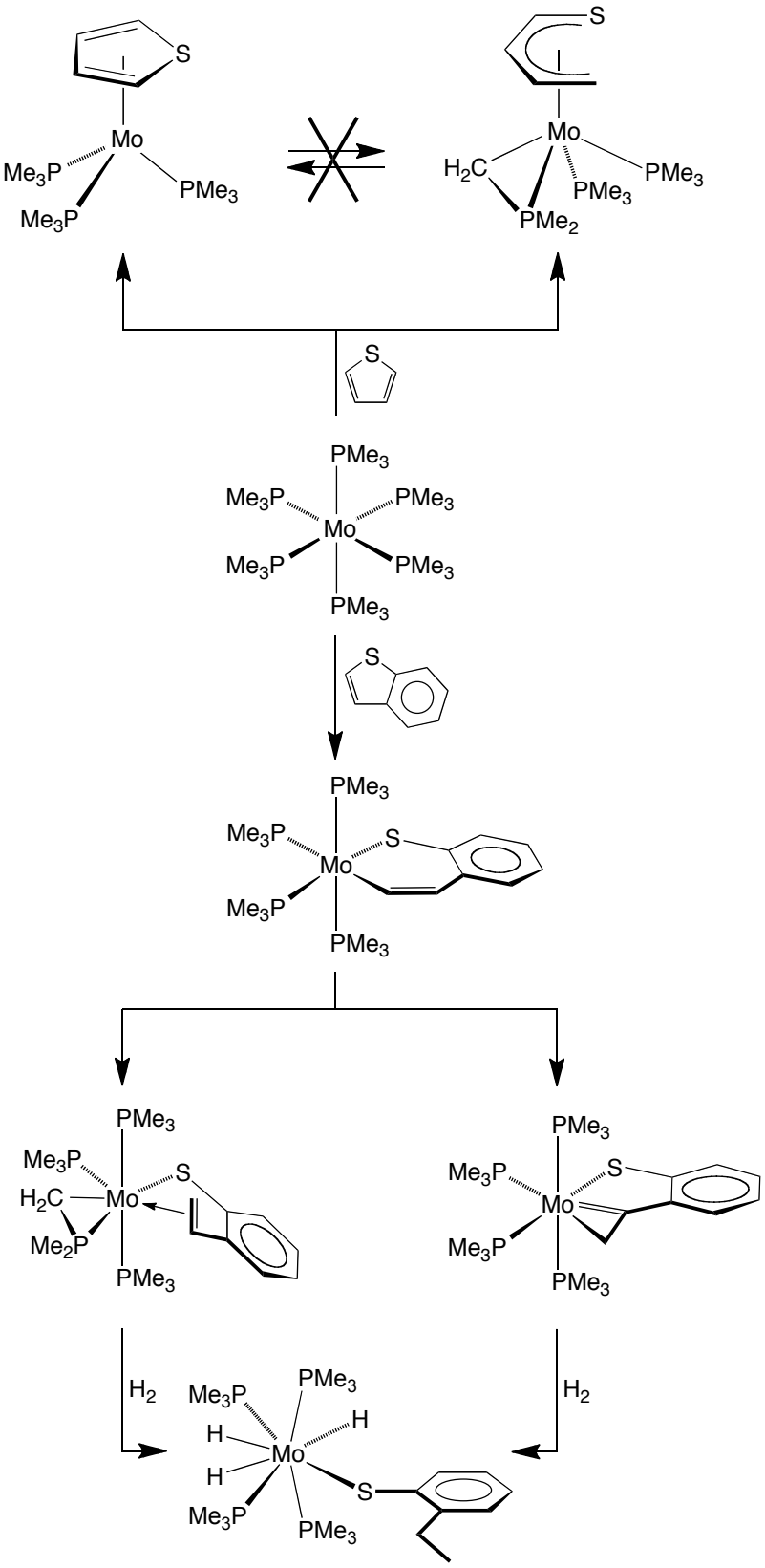

Scheme 3. Reactivity of $Mo(PMe_3)_6$ towards thiophene and benzothiophene.

4.2 Reactivity of $Mo(PMe_3)_5H_2$ towards thiophene

As shown in Scheme 3, $Mo(PMe_3)_6$ reacts with thiophene to give (*i*) the η^5–thiophene complex, $(\eta^5\text{–}C_4H_4S)Mo(PMe_3)_3$, and (*ii*) the butadiene–thiolate complex, $(\eta^5\text{–}C_4H_5S)Mo(PMe_3)_2(\eta^2\text{–}CH_2PMe_2)$.[14] We have now observed that $(\eta^5\text{–}C_4H_4S)Mo(PMe_3)_3$ and $(\eta^5\text{–}C_4H_5S)Mo(PMe_3)_2(\eta^2\text{–}CH_2PMe_2)$ can also be obtained *via* the reaction of $Mo(PMe_3)_5H_2$ with thiophene (Scheme 4). Furthermore, $Mo(PMe_3)_5H_2$ reacts with benzothiophene at 60 °C to give, *inter alia*, the 1–metallacyclopropene-thiophenolate complex $(\kappa^1,\eta^2\text{–}CH_2CC_6H_4S)Mo(PMe_3)_4$ (Scheme 4), a complex that is also obtained from the reaction of $Mo(PMe_3)_6$ with benzothiophene (Scheme 3).[15]

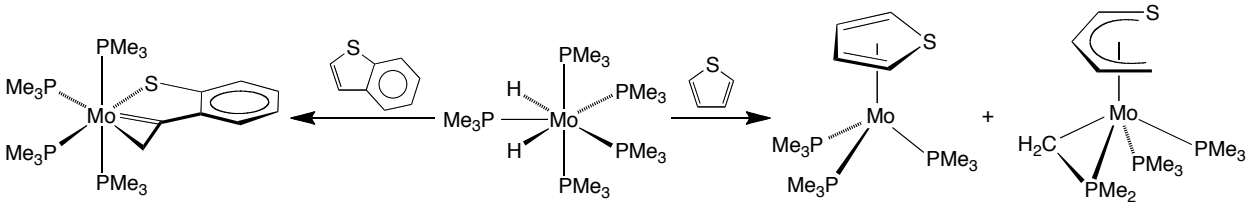

Scheme 4. Reactivity of $Mo(PMe_3)_5H_2$ towards thiophene and benzothiophene.

When monitoring of the reaction between $Mo(PMe_3)_5H_2$ and thiophene by ^1H NMR spectroscopy, signals for a paramagnetic intermediate were observed prior to formation of $(\eta^5\text{–}C_4H_4S)Mo(PMe_3)_3$ and $(\eta^5\text{–}C_4H_5S)Mo(PMe_3)_2(\eta^2\text{–}CH_2PMe_2)$. The same intermediate can also be observed in the reaction between $Mo(PMe_3)_6$ and thiophene (Scheme 5), and since the reaction with $Mo(PMe_3)_6$ is much faster than the corresponding reaction with $Mo(PMe_3)_5H_2$, the intermediate can be isolated by crystallization if the reaction mixture is immediately cooled to –15 °C before it has the opportunity to convert to $(\eta^5\text{–}C_4H_4S)Mo(PMe_3)_3$ and $(\eta^5\text{–}C_4H_5S)Mo(PMe_3)_2(\eta^2\text{–}CH_2PMe_2)$.

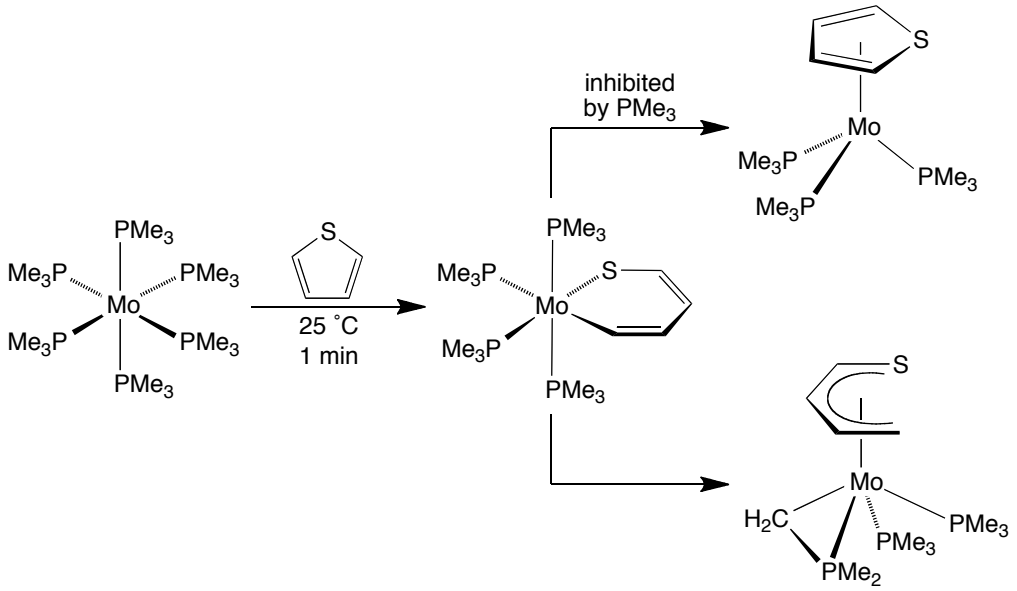

Scheme 5. Isolation of the paramagnetic intermediate, $(\kappa^2\text{–}C_4H_4S)Mo(PMe_3)_4$.

Significantly, the intermediate has been identified as the octahedral 16 electron paramagnetic complex $(\kappa^2\text{–}C_4H_4S)Mo(PMe_3)_4$ by X–ray diffraction (Figure 2). In accord with $(\kappa^2\text{–}C_4H_4S)Mo(PMe_3)_4$ being an intermediate, it rapidly converts to $(\eta^5\text{–}C_4H_4S)Mo(PMe_3)_3$ and $(\eta^5\text{–}C_4H_5S)Mo(PMe_3)_2(\eta^2\text{–}CH_2PMe_2)$ at room temperature (Scheme 5), with the predominant isomer depending on the reaction conditions. Specifically, the η^5–thiophene complex $(\eta^5\text{–}C_4H_4S)Mo(PMe_3)_3$ is favored (> 95 %) in the absence of PMe_3, whereas the η^5–butadiene–thiolate complex is the favored product in the presence of PMe_3. It is, therefore, suggested that conversion of $(\kappa^2\text{–}C_4H_4S)Mo(PMe_3)_4$ to $(\eta^5\text{–}C_4H_4S)Mo(PMe_3)_3$ occurs *via* initial reversible dissociation of PMe_3, while dissociation of PMe_3 occurs after (or possibly during) the rate determining step in the transformation that gives the η^5–butadiene–thiolate complex. This mechanistic scenario is consistent with the substantial temperature dependence of the product distribution,[14] in which the relative amount of $(\eta^5\text{–}C_4H_4S)Mo(PMe_3)_3$ increases with temperature due to a favorable entropy term resulting from dissociation of PMe_3 prior to the rate determining step.

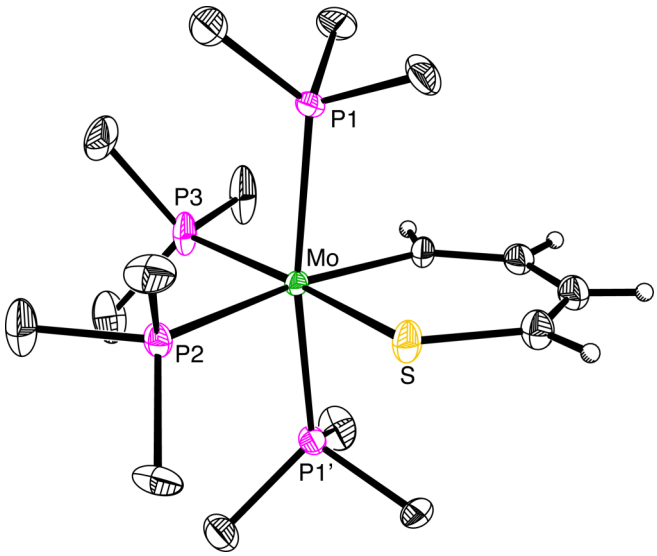

Figure 2. Molecular structure of (κ^2–C_4H_4S)Mo(PMe_3)$_4$.

Another interesting feature of this system is that the formation of the η^5–thiophene complex by treatment of Mo(PMe_3)$_6$ with thiophene does not simply proceed by displacement of PMe_3 ligands by thiophene, but rather occurs *via* a more complex mechanism that involves reversible C–S bond cleavage. Thus, C–S bond cleavage of thiophene precedes η^5–coordination, a counter-intuitive result that may be of relevance to other systems.[16] Also of note, in the presence of protiothiophene (C_4H_4S), the d_4–isotopologue (κ^2–C_4D_4S)Mo(PMe_3)$_4$ converts selectively to (η^5–C_4D_4S)Mo(PMe_3)$_3$, thereby demonstrating that the transformation to the η^5–thiophene complex does not involve complete reductive elimination (*i.e.* C–S bond coupling *and* release of thiophene) (Scheme 6). Thus, it is postulated that reductive coupling of the C–S bond leads directly to an η^x–thiophene adduct that subsequently transforms to the η^5–thiophene derivative.

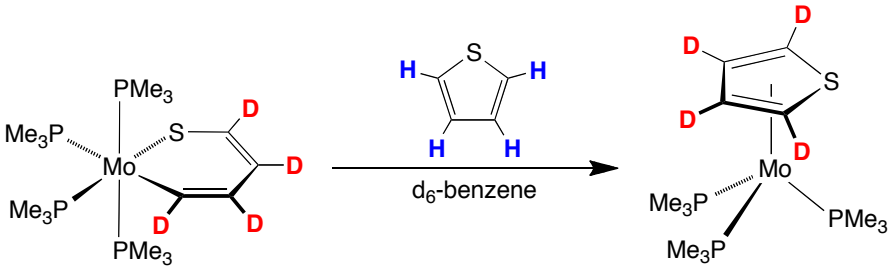

Scheme 6. Reactivity of (κ^2–C_4D_4S)Mo(PMe_3)$_4$ in the presence of protiothiophene (C_4H_4S).

While the reactivity of $Mo(PMe_3)_6$ and $Mo(PMe_3)_5H_2$ towards thiophene are similar, there are some interesting differences. For example, the reaction of $Mo(PMe_3)_6$ with d_4-thiophene is accompanied by the formation of an isotopomer of (η^5–C_4D_4HS)$Mo(PMe_3)_2$(η^2–CH_2PMe_2) in which the hydrogen from the PMe_3 ligand is transferred selectively to the carbon adjacent to the sulfur of the η^5–butadiene–thiolate ligand (Scheme 7).[14] The corresponding reaction of $Mo(PMe_3)_5H_2$ is accompanied by hydrogen (^1H) incorporation into other sites of the η^5–butadiene–thiolate ligand (Scheme 7). Furthermore, ^1H incorporation (mainly into the α-site)[17] is also observed for the η^5–thiophene ligand of (η^5–C_4H_4S)$Mo(PMe_3)_3$ obtained from the reaction of $Mo(PMe_3)_5H_2$ with d_4-thiophene, whereas there is negligible incorporation for the corresponding reaction of $Mo(PMe_3)_6$. Another aspect is that the reaction between $Mo(PMe_3)_5H_2$ and d_4-thiophene is accompanied by incorporation of hydrogen into the α-position of free thiophene,[18] thereby suggesting the existence of an additional pathway that involves reversible α-C–H bond cleavage prior to formation of either (η^5–C_4H_4S)$Mo(PMe_3)_3$ or (η^5–C_4H_5S)$Mo(PMe_3)_2$(η^2–CH_2PMe_2).

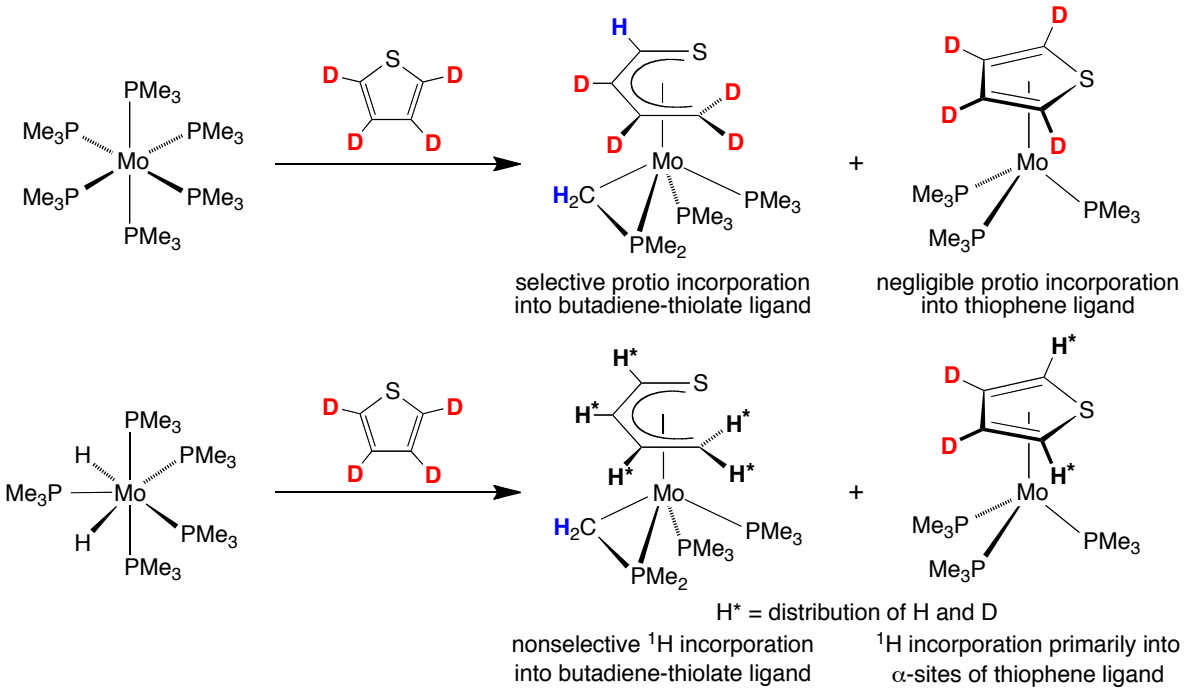

Scheme 7. Deuterium distribution in reactions of d_4-thiophene towards molybdenum compounds.

The above observations suggest that there are mechanistic differences pertaining to the reactions of thiophene with $Mo(PMe_3)_6$ and $Mo(PMe_3)_5H_2$. While $Mo(PMe_3)_6$ can generate $[Mo(PMe_3)_5]$ as a viable 16–electron intermediate, $Mo(PMe_3)_5H_2$ can generate both $[Mo(PMe_3)_5]$ and the dihydride $[Mo(PMe_3)_4H_2]$ *via* reductive elimination of H_2 and dissociation of PMe_3, respectively. For example, the conversion of $Mo(PMe_3)_5H_2$ to $Mo(PMe_3)_6$ upon treatment with PMe_3 is an example of reductive elimination of H_2,[19] while the conversion of $Mo(PMe_3)_5H_2$ to $Mo(PMe_3)_4H_4$ upon treatment with H_2 is an example of a reaction that occurs *via* dissociation of PMe_3.[20] The subtle differences in the reactivity of $Mo(PMe_3)_6$ and $Mo(PMe_3)_5H_2$ towards thiophene are, therefore, suggested to be a consequence of the ability of the latter to access $[Mo(PMe_3)_4H_2]$. The intermediate $[Mo(PMe_3)_4H_2]$ provides a simple means by which facile ^1H incorporation into the α-position of deuterothiophene can be achieved, *via* reversible C–H(D) oxidative addition and reductive elimination, thereby resulting in different selectivities for the ^1H incorporation into the η^5–thiophene and η^5–butadiene–thiolate ligands of the products derived from the reactions with d_4-thiophene, as compared to that for $Mo(PMe_3)_6$. The reactivity of $W(PMe_3)_5H_2$ with thiophene was also studied and compared to that of $Mo(PMe_3)_5H_2$, and this is described in Section 4.5.

4.3 Reactivity of $Mo(PMe_3)_4H_4$ towards thiophenes

In contrast to the facile reaction between $Mo(PMe_3)_5H_2$ and thiophene, the tetrahydride $Mo(PMe_3)_4H_4$ does not react with thiophene under mild conditions. However, treatment of $Mo(PMe_3)_4H_4$ with d_4-thiophene does result in incorporation of hydrogen into the α-position of free thiophene at 100 °C,[21] analogous to the reaction with $Mo(PMe_3)_5H_2$. Furthermore, at higher temperatures (120 °C), $Mo(PMe_3)_4H_4$ converts thiophene to, *inter alia*, 1-butene (Scheme 8),[22] thereby demonstrating that the system is capable of C–S bond cleavage of thiophene and hydrogen transfer, which are two key steps in the hydrodesulfurization of thiophene. It should be noted that C_4

hydrocarbons are the principal products of thiophene hydrodesulfurization and that the formation of butenes has also been observed upon reaction of thiophene with a molecular molybdenum-cobalt-sulfide cluster in the presence of H_2.[23,24] Although the molybdenum containing compounds formed from the thermal reaction between $Mo(PMe_3)_4H_4$ and thiophene have not been identified,[25] $Mo(PMe_3)_4H_4$ reacts with thiophene under photochemical activation to generate $(\eta^5\text{–}C_4H_4S)Mo(PMe_3)_3$ and $(\eta^5\text{–}C_4H_5S)Mo(PMe_3)_2(\eta^2\text{–}CH_2PMe_2)$ as two components of a mixture of products (Scheme 9).

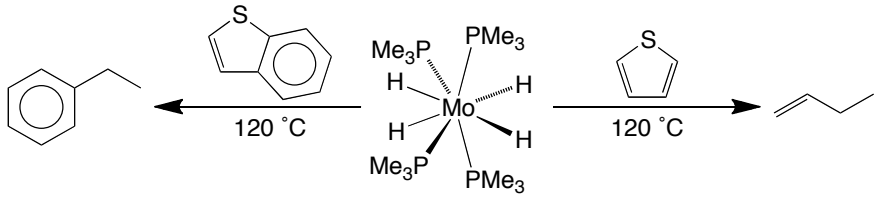

Scheme 8. Desulfurization of thiophene and benzothiophene by $Mo(PMe_3)_4H_4$.

Similar to the reaction of thiophene, $Mo(PMe_3)_4H_4$ cleaves both C–S bonds of benzothiophene at 120 ˚C to liberate ethylbenzene (Scheme 8)[26] which is a principal product of hydrodesulfurization.[27] The desulfurization of thiophene and benzothiophene described here is noteworthy because such transformations are not well precedented in homogeneous systems,[24,28,29,30,31,32,33,34] and are unknown for mononuclear molybdenum compounds. Similar to the reaction with thiophene, the molybdenum containing compounds from the thermal reaction between $Mo(PMe_3)_4H_4$ and benzothiophene have not been identified; however, the photochemical reaction generates, *inter alia*, the arylthiolate complex, $Mo(PMe_3)_4(SC_6H_4Et)H_3$,[15] the formation of which is improved in the presence of H_2 (Scheme 9). The molecular structure of $Mo(PMe_3)_4(SC_6H_4Et)H_3$ is shown in Figure 3.

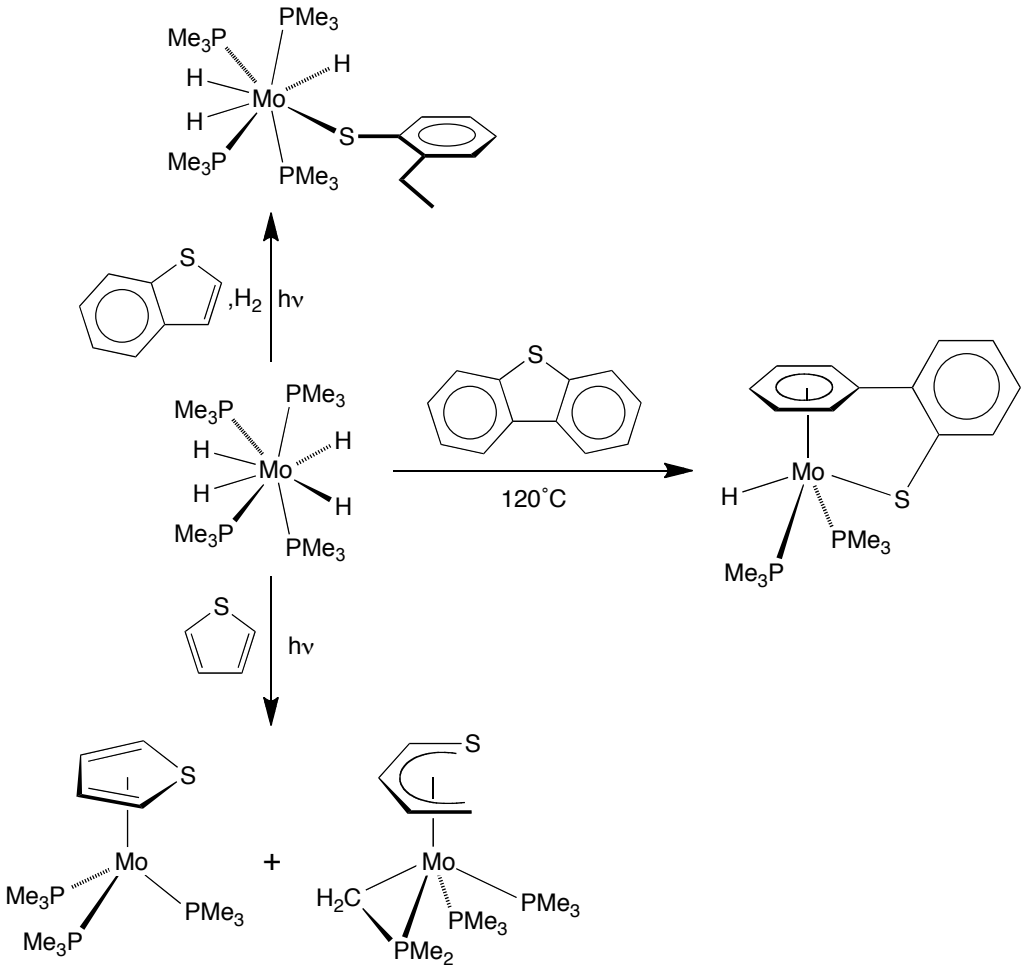

Scheme 9. Reactivity of $Mo(PMe_3)_4H_4$ towards thiophenes.

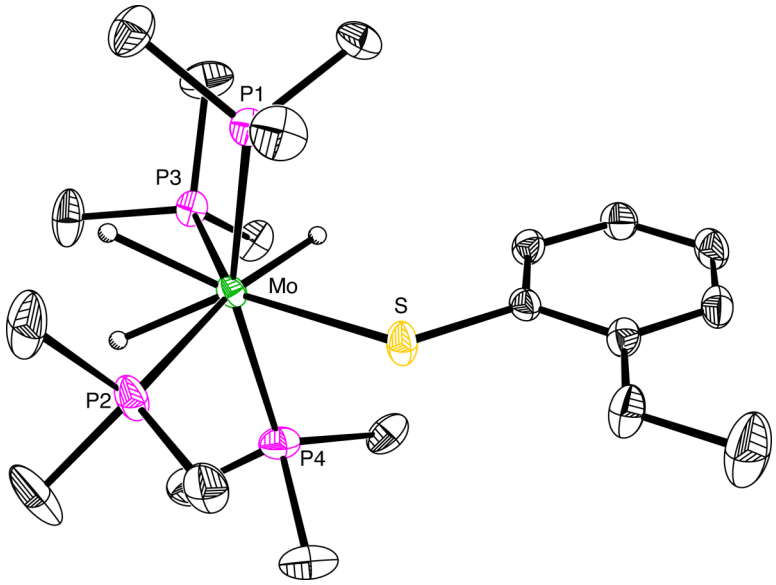

Figure 3. Molecular structure of $Mo(PMe_3)_4(SC_6H_4Et)H_3$.

$Mo(PMe_3)_4H_4$ also reacts with dibenzothiophene to give $[\eta^6,\kappa^1\text{-}C_6H_5C_6H_4S]\text{-}Mo(PMe_3)_2H$, which results from C–S bond cleavage and hydrogen transfer (Scheme 9). The molecular structure of $[\eta^6,\kappa^1\text{-}C_6H_5C_6H_4S]Mo(PMe_3)_2H$ has been determined by X–ray diffraction, as illustrated in Figure 4. The formation of $[\eta^6,\kappa^1\text{-}C_6H_5C_6H_4S]\text{-}Mo(PMe_3)_2H$ is noteworthy because it represents the first example of cleavage of the C–S bond of dibenzothiophene by a molybdenum compound. As shown above in Scheme 2, although $[Me_2Si(C_5Me_4)_2]MoH_2$ is capable of cleaving the C–S bonds of thiophene and benzothiophene, $[Me_2Si(C_5Me_4)_2]MoH_2$ reacts with dibenzothiophene to give only the κ^1–adduct, $[Me_2Si(C_5Me_4)_2]Mo(\kappa^1\text{–DBT})$.[12] It should be noted that C–S bond cleavage of dibenzothiophene has been observed for other metals but is not typically accompanied by subsequent hydrogen transfer.[35,36,37,38,39,40,41,42]

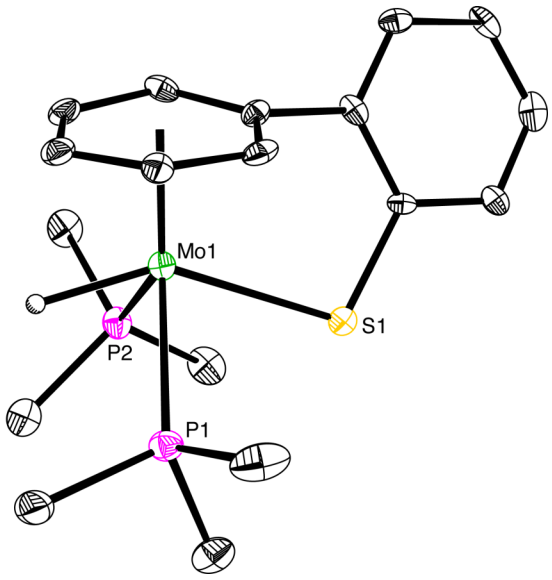

Figure 4. Molecular structure of $[\eta^6,\kappa^1\text{-}C_6H_5C_6H_4S]Mo(PMe_3)_2H$.

For comparison purposes, there are no other examples of structurally characterized complexes listed in the Cambridge Structural database[43] that feature $[\eta^6,\kappa^1\text{-}C_6H_5C_6H_4S]$ ligands, although there are several examples of molybdenum compounds that possess related $[\eta^6,\kappa^1\text{-}C_6H_5ArS]$ ligands. These compounds, however,

are not obtained *via* C–S bond cleavage of dibenzothiophene derivatives, but are rather obtained *via* reactions with the arylthiolate ligand.[44,45,46,47] Previously the Parkin group synthesized the closely related aryloxide complex $[\eta^6,\kappa^1\text{-}C_6H_5C_6H_3(Ph)O]Mo(PMe_3)_2H$ *via* reaction of $Mo(PMe_3)_6$ with 2,6–$Ph_2C_6H_3OH$.[48] The most notable difference in the structures of $[\eta^6,\kappa^1\text{-}C_6H_5C_6H_4S]Mo(PMe_3)_2H$ and $[\eta^6,\kappa^1\text{-}C_6H_5C_6H_3(Ph)O]Mo(PMe_3)_2H$ is that the longer Mo–S and C–S *versus* Mo–O and C–O bonds allow the arylthiolate group to lie closer to the plane of the η^6-arene moiety, as illustrated in Figure 5. Thus, the *ipso* carbon of the η^6-arene moiety of $[\eta^6,\kappa^1\text{-}C_6H_5C_6H_4S]Mo(PMe_3)_2H$ is closer to planarity ($\Sigma_{C\text{–}C\text{–}C}$ = 359.8° and 360.0° for two crystallographically independent molecules) than is that in $[\eta^6,\kappa^1\text{-}C_6H_5C_6H_3(Ph)O]Mo(PMe_3)_2H$ ($\Sigma_{C\text{–}C\text{–}C}$ = 357.4°). Correspondingly, the η^6–$C_{6(centroid)}$–C_{ipso}–C_{aryl} angle for $[\eta^6,\kappa^1\text{-}C_6H_5C_6H_4S]Mo(PMe_3)_2H$ (171.4° and 173.2° for two crystallographically independent molecules) is closer to 180° than is the value for $[\eta^6,\kappa^1\text{-}C_6H_5C_6H_3(Ph)O]Mo(PMe_3)_2H$ (164.3°).

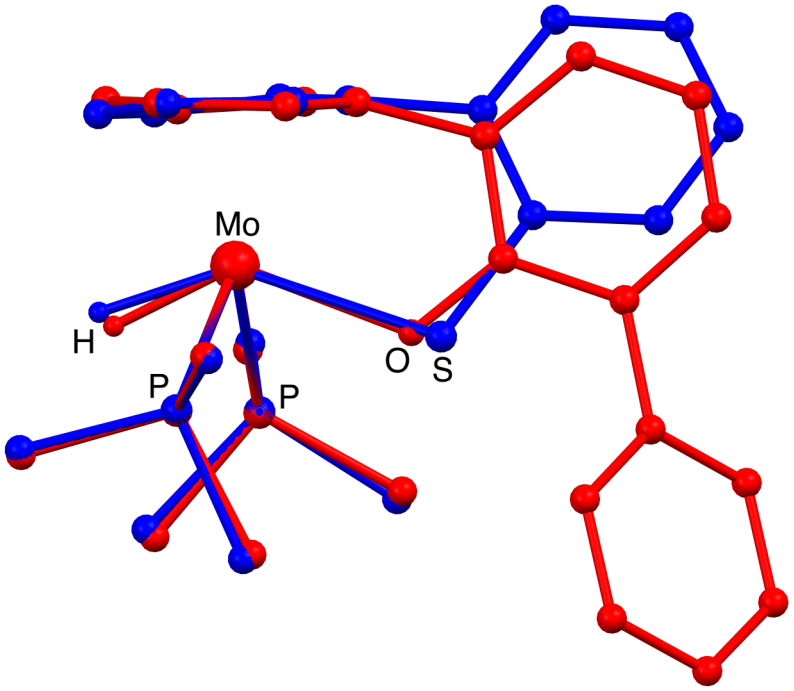

Figure 5. Structural overlay of $[\eta^6,\kappa^1\text{-}C_6H_5C_6H_4S]Mo(PMe_3)_2H$ (blue) and $[\eta^6,\kappa^1\text{-}C_6H_5C_6H_3(Ph)O]Mo(PMe_3)_2H$ (red).

4.4 Reactivity of $W(PMe_3)_4(\eta^2–CH_2PMe_2)H$ towards thiophene

Tungsten is also a prevalent component of HDS catalysts and so we also investigated the reactivity of $W(PMe_3)_4(\eta^2–CH_2PMe_2)H$[49] towards thiophenes, and have discovered that it is capable of cleaving the C–S bonds of thiophene, benzothiophene and dibenzothiophene. For example, $W(PMe_3)_4(\eta^2–CH_2PMe_2)H$ reacts with thiophene at 60 ˚C to give the butadiene-thiolate complex $(\eta^5–C_4H_5S)W(PMe_3)_2(\eta^2–CH_2PMe_2)$,[50] which has been structurally characterized by X-ray diffraction (Figure 6), representing the first example of thiophene C–S bond cleavage and hydrogen transfer by a tungsten compound (Scheme 10).[51] Furthermore, the butadiene-thiolate ligand of $(\eta^5–C_4H_5S)W(PMe_3)_2(\eta^2–CH_2PMe_2)$ may be hydrogenated at 60 ˚C to give the butanethiolate complex $W(PMe_3)_4(SBu^n)H_3$, as illustrated in Scheme 10.[52,53] These observations demonstrate that a single tungsten center is capable of achieving two of the key steps in the hydrodesulfurization of thiophene, namely C–S bond cleavage and hydrogenation. It should be noted that, to date, crystals of $W(PMe_3)_4(SBu^n)H_3$ have not been obtained. However, evidence for $W(PMe_3)_4(SBu^n)H_3$ is provided by: (*i*) ^1H, $^{31}P\{^1H\}$ and $^{13}C\{^1H\}$ NMR spectroscopic data (Section 4.12.24) (*ii*) the reaction of $W(PMe_3)_4(SBu^n)H_3$ towards benzoic acid, which produces $HSBu^n$, thereby confirming the presence of the sulfur atom in the (SBu^n) ligand (Section 4.12.25), and (*iii*) structural characterization of the selenium analogue, namely $W(PMe_3)_4(SeBu^n)H_3$,[54] which is shown in Figure 7.

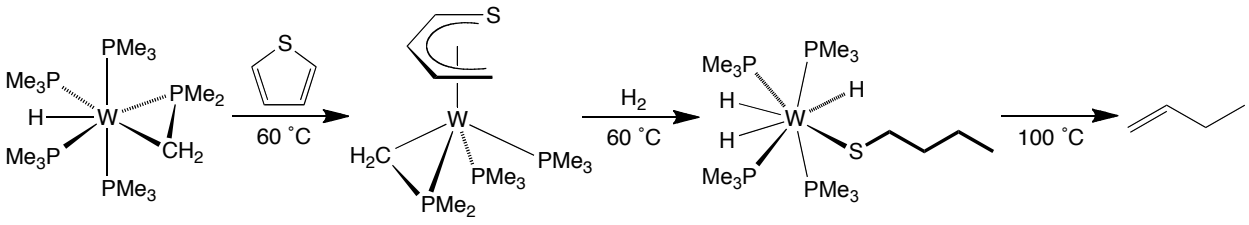

Scheme 10. Reactivity of $W(PMe_3)_4(\eta^2–CH_2PMe_2)H$ towards thiophene.

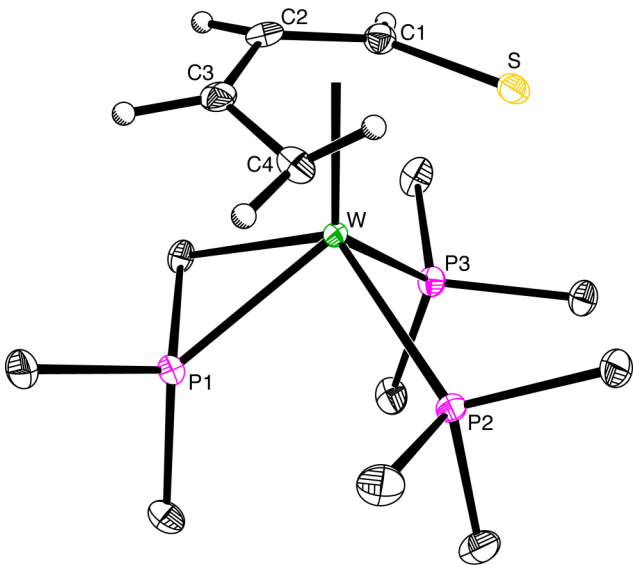

Figure 6. Molecular structure of $(\eta^5\text{–}C_4H_5S)W(PMe_3)_2(\eta^2\text{–}CH_2PMe_2)$.

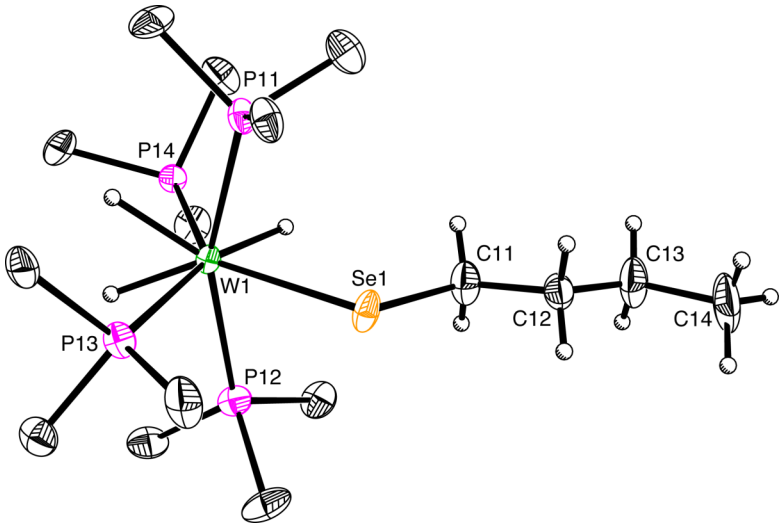

Figure 7. Molecular structure of $W(PMe_3)_4(SeBu^n)H_3$.

It is useful to compare the reactivity of $W(PMe_3)_4(\eta^2\text{–}CH_2PMe_2)H$ towards thiophene with that of the corresponding molybdenum system because there are some distinct differences.[10,14,15,55] For example, whereas only the butadiene-thiolate complex $(\eta^5\text{–}C_4H_5S)W(PMe_3)_2(\eta^2\text{–}CH_2PMe_2)$ has been isolated for the tungsten system, the reaction of $Mo(PMe_3)_6$ proceeds readily at room temperature to give the

metallathiacycle, (κ^2–*C*,*S*–C_4H_4S)Mo(PMe_3)$_4$, which rapidly converts to the butadiene-thiolate complex (η^5–C_4H_5S)Mo(PMe_3)$_2$(η^2–CH_2PMe_2) *and* the η^5–thiophene derivative (η^5–C_4H_4S)Mo(PMe_3)$_3$ (see Scheme 5 above).[10,14] Another interesting difference is that whereas the tungsten butadiene-thiolate complex (η^5–C_4H_5S)W(PMe_3)$_2$(η^2–CH_2PMe_2) is readily hydrogenated to the butanethiolate complex W(PMe_3)$_4$(SBu^n)H_3 at 60 °C, the molybdenum counterpart (η^5–C_4H_5S)Mo(PMe_3)$_2$(η^2–CH_2PMe_2) does not react with H_2 under the same conditions.

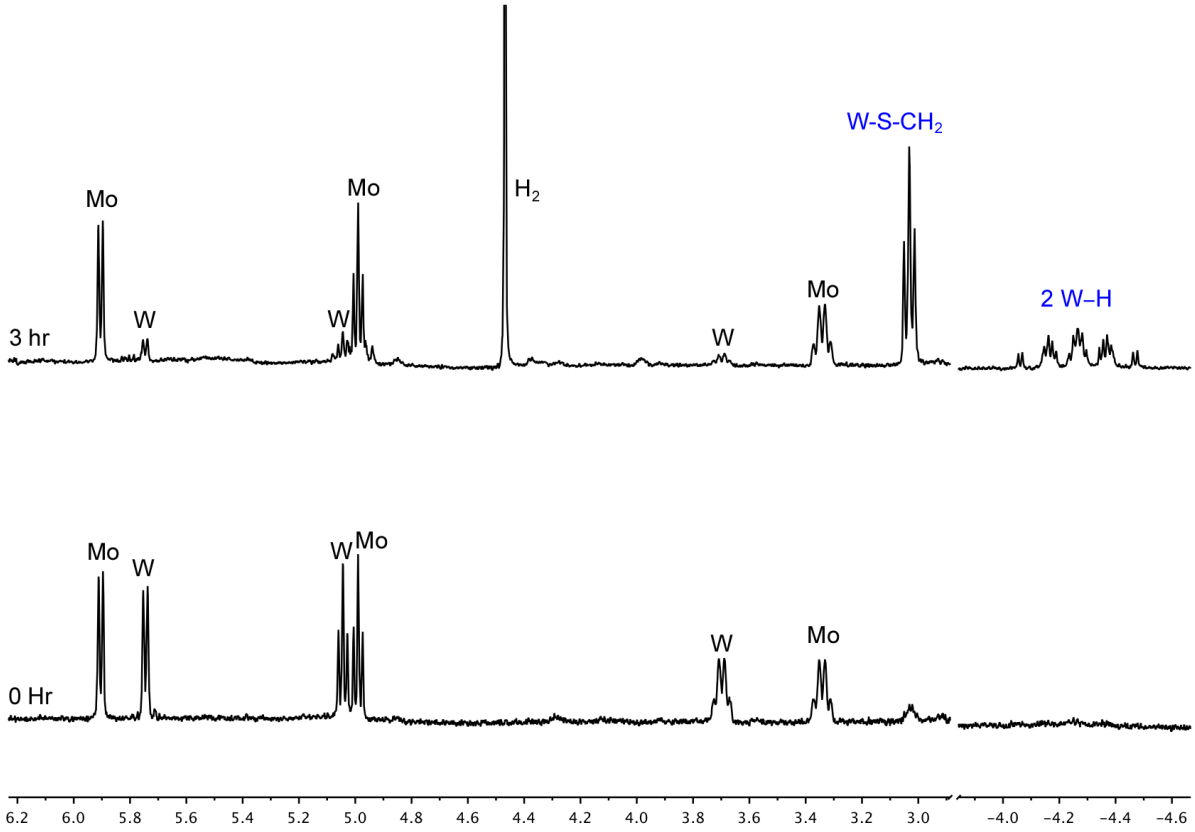

Figure 8. ^{1}H NMR spectrum of 1:1 mixture of (η^5–C_4H_5S)W(PMe_3)$_2$(η^2–CH_2PMe_2) and (η^5–C_4H_5S)Mo(PMe_3)$_2$(η^2–CH_2PMe_2) (bottom). H_2 (*ca.* 1 atm) was added, and the solution was heated at 60 °C for 3 hours and analyzed by ^{1}H NMR spectroscopy (top) (W = (η^5–C_4H_5S)W(PMe_3)$_2$(η^2–CH_2PMe_2), Mo = (η^5–C_4H_5S)Mo(PMe_3)$_2$(η^2–CH_2PMe_2), **W-S-CH$_2$** = methylene adjacent to sulfur of W(PMe_3)$_4$(SBu^n)H_3, **2W-H** = 2 hyrdrides of W(PMe_3)$_4$(SBu^n)H_3).

The dissimilar reactivity was demonstrated by heating a 1:1 mixture of (η^5–C_4H_5S)W(PMe_3)$_2$(η^2–CH_2PMe_2) and (η^5–C_4H_5S)Mo(PMe_3)$_2$(η^2–CH_2PMe_2) in the presence of H_2 at 60 °C (see Section 4.12.34), and monitoring the reaction by using ^{1}H NMR spectroscopy (Figure 8). As is illustrated in Figure 8, after the reaction mixture was heated at 60 °C for 3 hours, the (η^5–C_4H_5S)W(PMe_3)$_2$(η^2–CH_2PMe_2) has largely converted to W(PMe_3)$_4$(SBu^n)H_3, while the (η^5–C_4H_5S)Mo(PMe_3)$_2$(η^2–CH_2PMe_2) remains unreacted. Thus, although the formation of the butadiene-thiolate complex from the reaction of thiophene with the molybdenum complex Mo(PMe_3)$_6$ is more facile than that for the reaction of W(PMe_3)$_4$(η^2–CH_2PMe_2)H, hydrogenation of the butadiene-thiolate ligand occurs more readily for the tungsten system.

4.5 Reactivity of tungsten hydrides towards thiophene

In view of the fact that hydrogenation is an important component of hydrodesulfurization, we have also investigated the reactivity of the series of tungsten hydride complexes, W(PMe_3)$_5H_2$, W(PMe_3)$_4H_4$ and W(PMe_3)$_3H_6$, towards thiophene (Schemes 11 – 13, respectively). Significantly, these hydride complexes exhibit very different reactivity to that of W(PMe_3)$_4$(η^2–CH_2PMe_2)H. For example, W(PMe_3)$_5H_2$ reacts with thiophene (Scheme 11) to give the κ^1-thienyl complex, W(PMe_3)$_4$(κ^1-C_α-C_4H_3S)H_3, which has been structurally characterized by X-ray diffraction (Figure 9).[56] W(PMe_3)$_4$(κ^1-C_α-C_4H_3S)H_3 is also generated by the photochemical reaction of thiophene with W(PMe_3)$_4H_4$ (Scheme 12).[57,58] In contrast, thiophene reacts with W(PMe_3)$_3H_6$ to give the butanethiolate complex W(PMe_3)$_4$(SBu^n)H_3, as illustrated in Scheme 13.[59]

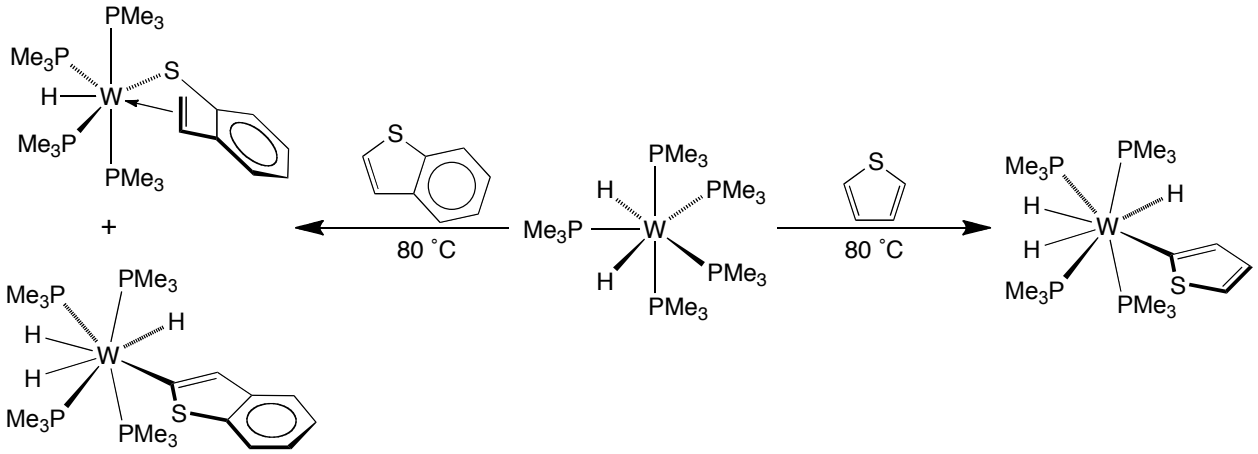

Scheme 11. Reactivity of $W(PMe_3)_5H_2$ towards thiophene and benzothiophene.

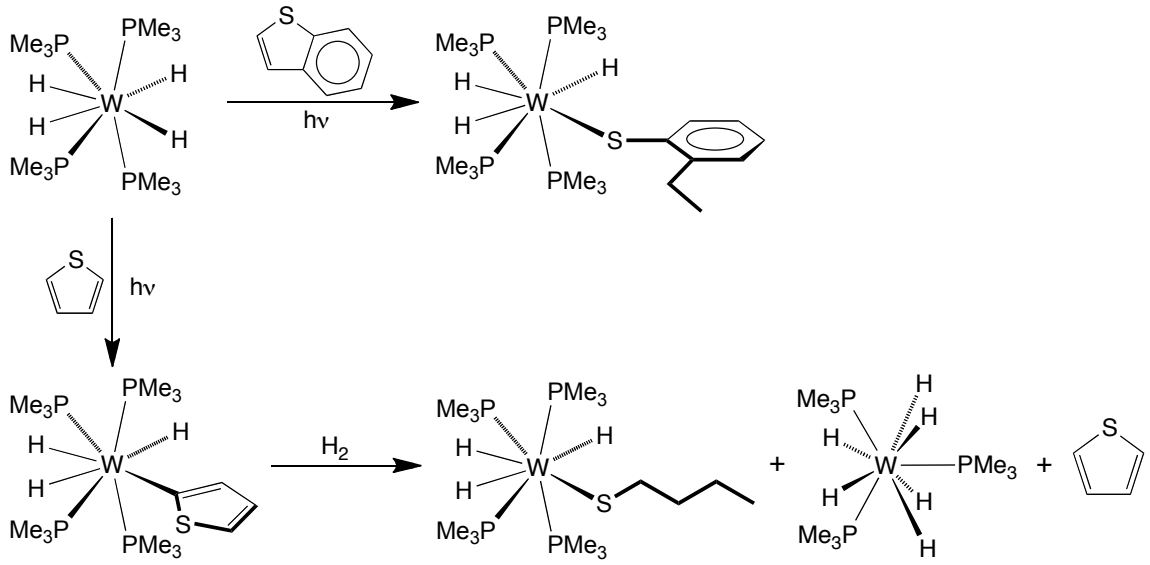

Scheme 12. Reactivity of $W(PMe_3)_4H_4$ towards thiophene and benzothiophene.

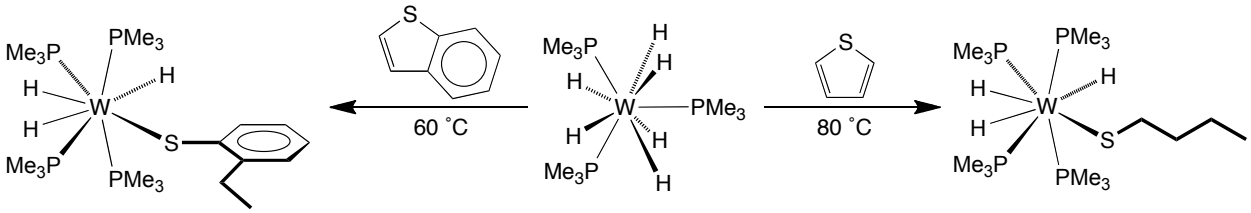

Scheme 13. Reactivity of $W(PMe_3)_3H_6$ towards thiophene and benzothiophene.

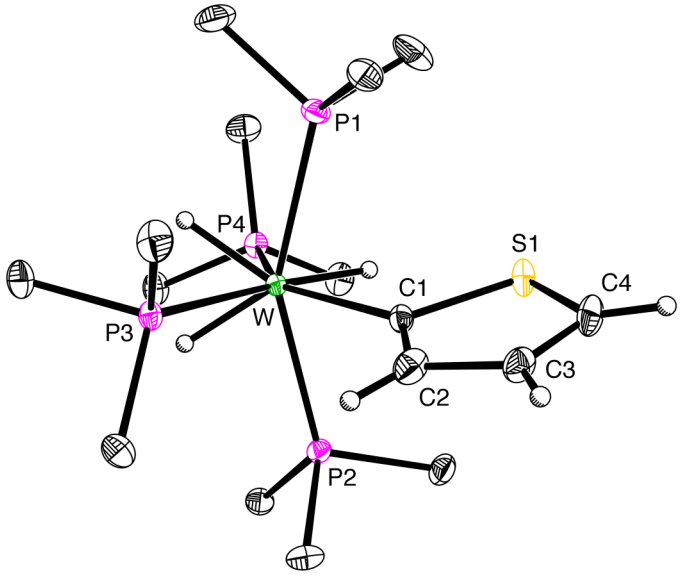

Figure 9. Molecular structure of $W(PMe_3)_4(\kappa^1\text{-}C_\alpha\text{-}C_4H_3S)H_3$ (the thienyl ligand exhibits a two-fold rotational disorder and only the major configuration is shown).

The fact that $W(PMe_3)_4(\eta^2\text{–}CH_2PMe_2)H$ and $W(PMe_3)_5H_2$ behave differently towards thiophene suggests that the reactions do not occur *via* a common $[W(PMe_3)_5]$ intermediate (see above for similar reactivity differences between $Mo(PMe_3)_6$ and $Mo(PMe_3)_5H_2$). We postulate that whereas the reaction of $W(PMe_3)_4(\eta^2\text{–}CH_2PMe_2)H$ proceeds *via* $[W(PMe_3)_5]$, the reaction of $W(PMe_3)_5H_2$ involves initial dissociation of PMe_3 to give 16–electron $[W(PMe_3)_4H_2]$, followed by oxidative addition of a thiophene C–H bond. This suggests that cleavage of the C–S bond, relative to a C–H bond, is favored for the lower valent metal center.

The formation of the κ^1-thienyl complex $W(PMe_3)_4(\kappa^1\text{-}C_\alpha\text{-}C_4H_3S)H_3$ is also noteworthy because the corresponding reaction of the molybdenum counterpart $Mo(PMe_3)_5H_2$ with thiophene does not yield $Mo(PMe_3)_4(\kappa^1\text{-}C_\alpha\text{-}C_4H_3S)H_3$, but rather gives a mixture of the η^5–thiophene and butadiene-thiolate complexes, $(\eta^5\text{–}C_4H_4S)Mo(PMe_3)_3$ and $(\eta^5\text{–}C_4H_5S)Mo(PMe_3)_2(\eta^2\text{–}CH_2PMe_2)$ (Scheme 4).[10] Thus, the molybdenum system exhibits a greater propensity to cleave the C–S bond of thiophene than does the

tungsten system. We propose that the origin of this difference is that the tungsten κ^1-thienyl complex $W(PMe_3)_4(\kappa^1\text{-}C_\alpha\text{-}C_4H_3S)H_3$ represents a kinetic product that is also of sufficient thermodynamic stability to inhibit access to the intermediate that is capable of achieving C–S bond cleavage.

As stated above, treatment of $Mo(PMe_3)_5H_2$ with d_4-thiophene is accompanied by incorporation of hydrogen into the α-position of free thiophene prior to formation of the η^5–thiophene and butadiene-thiolate complexes,[10] whereas no such exchange is observed for $W(PMe_3)_5H_2$. Furthermore, $W(PMe_3)_4(\kappa^1\text{-}C_\alpha\text{-}C_4H_3S)H_3$ does not react with PMe_3 to regenerate $W(PMe_3)_5H_2$. These observations, therefore, are consistent with facile reversible oxidative addition of the C–H bond of thiophene to molybdenum, but irreversible (on the time-scale of the experiment) oxidative addition to tungsten.

Although the evidence presented above indicates that $W(PMe_3)_4(\kappa^1\text{-}C_\alpha\text{-}C_4H_3S)H_3$ does not undergo facile reductive elimination of thiophene, elimination of thiophene may be induced by treatment of $W(PMe_3)_4(\kappa^1\text{-}C_\alpha\text{-}C_4H_3S)H_3$ with H_2, a reaction that is also accompanied by the formation of $W(PMe_3)_3H_6$ and the butanethiolate complex, $W(PMe_3)_4(SBu^n)H_3$, as illustrated in Scheme 12. Relative to $W(PMe_3)_4(SBu^n)H_3$, the formation of $W(PMe_3)_3H_6$ and thiophene is inhibited by PMe_3, thereby suggesting a reversible dissociation of PMe_3 prior to the rate determining step. As such, reductive elimination of thiophene presumably occurs *via* a higher valent species such as $W(PMe_3)_3(\kappa^1\text{-}C_\alpha\text{-}C_4H_3S)H_5$, obtained by dissociation of PMe_3 and oxidative addition of H_2. The formation of the butanethiolate complex $W(PMe_3)_4(SBu^n)H_3$ in this reaction is interesting because it demonstrates that although $W(PMe_3)_5H_2$ itself does not allow isolation of a product derived from C–S bond cleavage (Scheme 11), such a species may be achieved upon treatment with H_2 (Scheme 12).[60]

4.6 Structural characterization of $W(PMe_3)_3H_6$

Although not related to hydrodesulfurization, it is important to note that the molecular structure of $W(PMe_3)_3H_6$ has now been determined by X-ray diffraction. $W(PMe_3)_3H_6$ was first synthesized by Lyons and Wilkinson by the reaction of $WCl_4(PMe_3)_3$ and $LiAlH_4$, followed by treatment with methanol;[61,62] ^1H and ^{31}P NMR spectroscopic studies indicate that $W(PMe_3)_3H_6$ is fluxional in solution and that all six hydrides are equivalent [$\delta = -2.61$, $^2J_{P-H} = 37.6$ (q) Hz], as are the PMe_3 ligands [$\delta = 1.57$, $J_{P-H} = 8.2$ (vt) Hz].[61] The molecular geometry of $W(PMe_3)_3H_6$ was proposed to have one of two high symmetry idealized structures.[61] The first has D_{3h} symmetry, in which the hydride ligands make up a trigonal prism with the phosphorus atoms of the PMe_3 ligands capping the square faces (Figure 10, right), as predicted for other $W(PR_3)_3H_6$ complexes.[63,64] The second has C_{2v} symmetry, also having a tricapped trigonal prism geometry, but instead has only one phosphorus atom in a capping position, while the other two occupy eclipsed positions on opposite prism faces (Figure 10, left), as was found for $W(PPhPr^i_2)_3H_6$.[65,66]

We have now determined the molecular structure of $W(PMe_3)_3H_6$ (Figure 11), and the data indicate that is best described as having an approximate C_{2v} symmetric structure (Figure 10, left).[67] For example, whereas a D_{3h} structure is expected to have idealized P–W–P angles of 120°, the bond angles in $W(PMe_3)_3H_6$ deviate significantly from 120° [P1–W–P2: 128.567(16)°; P1–W–P2′: 128.567(16)°; P2–W–P2′: 102.49(3)°]. Furthermore, the W–P bond lengths [W–P1: 2.4156(8) Å, W–P2: 2.4706(6) Å, W–P2′: 2.4706(6) Å] are significantly different (0.055 Å), also indicating that $W(PMe_3)_3H_6$ does not have D_{3h} symmetry, as a D_{3h} symmetric structure is expected to have three equal W–P bond lengths. Thus, $W(PMe_3)_3H_6$ is best described as having a tricapped trigonal prismatic structure with approximate C_{2v} symmetry in which the [P2, H1, H2] and [P2′, H1′, H2′] faces forming the top and bottom faces of the trigonal prism, while P1 caps

the [H1, H2, H1′, H2′] square face and H3 and H4 cap the [P2, H2, H2′, P2′] and [P2, H1, H1′, P2′] square faces, respectively (Figure 11, right). In accord with the experimental structure, a density functional geometry optimization calculation predicts P–W–P angles of 128.4°, 129.8° and 101.4°, and W–P bond lengths of 2.460 Å, 2.522 Å, and 2.536 Å, clearly deviating from a structure with D_{3h} symmetry.[68]

The geometry is similar to that of the related hexahydride triphosphine complex, namely $W(PPhPr^{i}_{2})_3H_6$ [P–W–P angles: P1–W–P2: 125.4(1)°; P2–W–P3: 126.6(1)°; P1–W–P3: 107.9(1)°. W–P bond lengths: W–P1: 2.528(1) Å, W–P2: 2.427(1) Å, W–P3: 2.524(1) Å].[65,66]

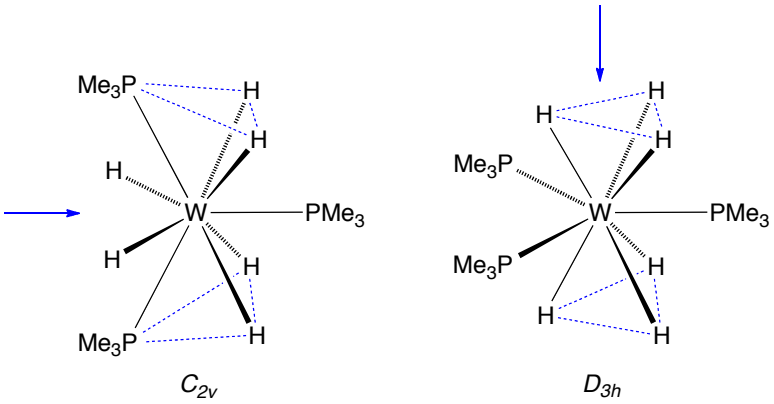

Figure 10. High symmetry structures for $W(PMe_3)_3H_6$ (blue dashed lines show the trigonal prism and the blue arrows represent the primary symmetry axis).

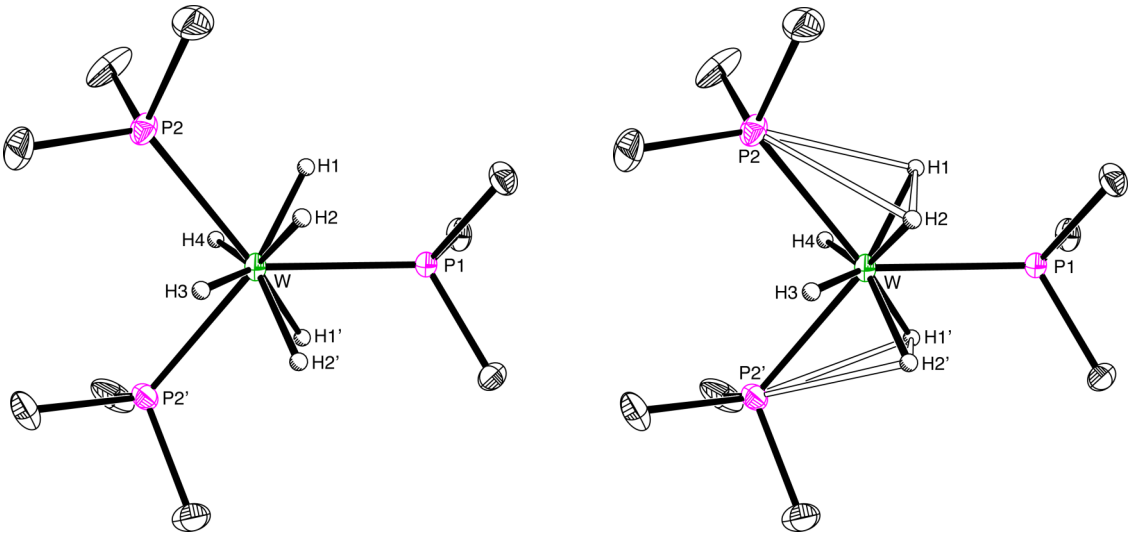

Figure 11. Molecular structure of $W(PMe_3)_3H_6$ (left) and view showing the trigonal prism geometry with hollow lines (right). W, P1, H3 and H4 lie on the crystallographic mirror plane.

4.7 Reactivity of tungsten complexes towards benzothiophene

The reactivity of $W(PMe_3)_4(\eta^2\text{–}CH_2PMe_2)H$, $W(PMe_3)_5H_2$, $W(PMe_3)_4H_4$ and $W(PMe_3)_3H_6$ towards benzothiophene has also been investigated. $W(PMe_3)_4(\eta^2\text{–}CH_2PMe_2)H$ reacts with benzothiophene to give a mixture of products that include isomeric $(\kappa^1,\eta^2\text{–}CH_2CHC_6H_4S)W(PMe_3)_3(\eta^2\text{–}CH_2PMe_2)$ and $(\kappa^1,\eta^2\text{–}CH_2CC_6H_4S)W(PMe_3)_4$ (Scheme 14), both of which are the result of C–S bond cleavage. Interestingly, the corresponding reaction of $W(PMe_3)_5H_2$ with benzothiophene gives a different pair of isomers, $(\kappa^1,\eta^2\text{–}CH_2CHC_6H_4S)W(PMe_3)_4H$ and $W(PMe_3)_4(\kappa^1\text{-}C_\alpha\text{-}CCHSC_6H_4)H_3$ (Scheme 11), that feature two more hydrogen atoms than the products obtained from $W(PMe_3)_4(\eta^2\text{–}CH_2PMe_2)H$.[69] Thus, $(\kappa^1,\eta^2\text{–}CH_2CHC_6H_4S)W(PMe_3)_4H$ is formally different from $(\kappa^1,\eta^2\text{–}CH_2CHC_6H_4S)W(PMe_3)_3(\eta^2\text{–}CH_2PMe_2)$ by addition of H_2 across the W–C bond, but is otherwise structurally very similar (Figure 12). $W(PMe_3)_4(\kappa^1\text{-}C_\alpha\text{-}CCHSC_6H_4)H_3$, which has been structurally characterized by X-ray diffraction (Figure 13), displays a similar coordination environment to the thienyl compound, $W(PMe_3)_4(\kappa^1\text{-}C_\alpha\text{-}C_4H_3S)H_3$, (Figure 9).

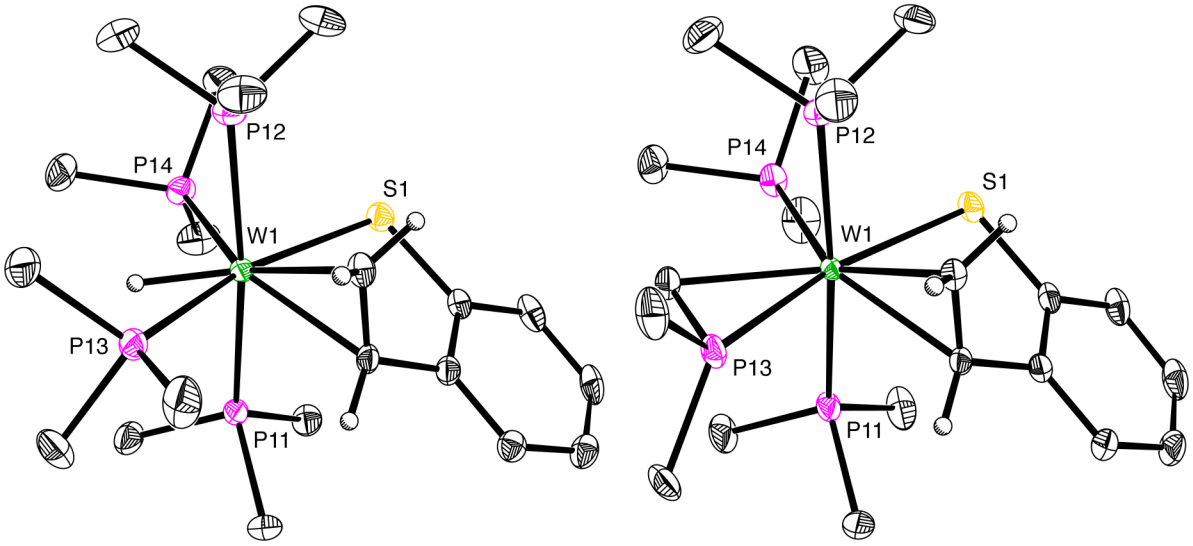

Figure 12. Molecular structures of $(\kappa^1,\eta^2\text{–}CH_2CHC_6H_4S)W(PMe_3)_4H$ (left) and $(\kappa^1,\eta^2\text{–}CH_2CHC_6H_4S)$-$W(PMe_3)_3(\eta^2\text{–}CH_2PMe_2)$ (right).

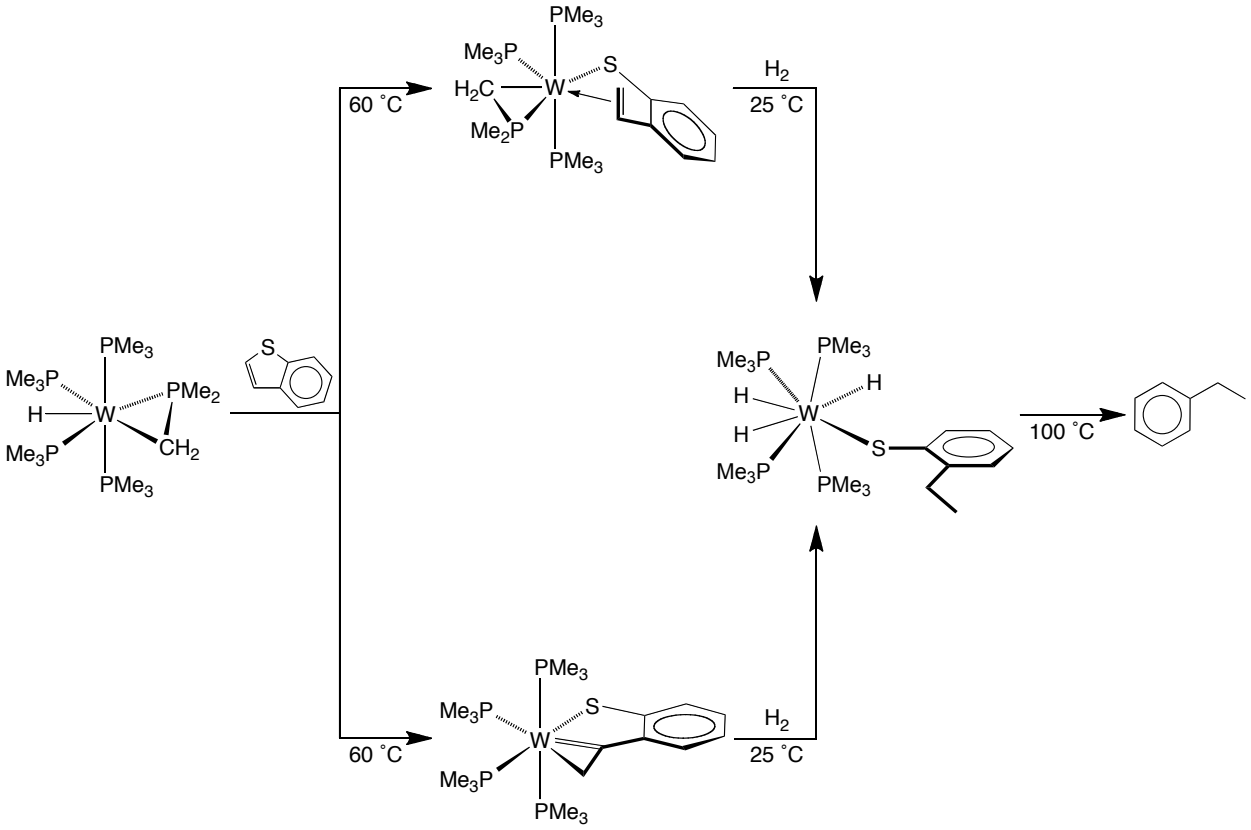

Scheme 14. Reactivity of $W(PMe_3)_4(\eta^2–CH_2PMe_2)H$ towards benzothiophene.

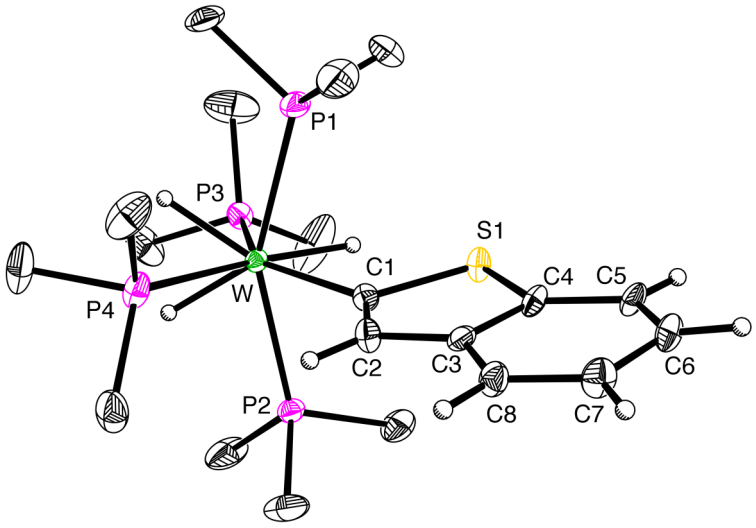

Figure 13. Molecular structure of $W(PMe_3)_4(\kappa^1–C_\alpha–CCHSC_6H_4)H_3$ (the benzothienyl ligand exhibits a two-fold rotational disorder and only the major configuration is shown).

$(\kappa^1,\eta^2\text{–}CH_2CHC_6H_4S)W(PMe_3)_3(\eta^2\text{–}CH_2PMe_2)$, $(\kappa^1,\eta^2\text{–}CH_2CC_6H_4S)W(PMe_3)_4$ and $(\kappa^1,\eta^2\text{–}CH_2CHC_6H_4S)W(PMe_3)_4H$ all react with H_2 at room temperature to give the arylthiolate $W(PMe_3)_4(SC_6H_4Et)H_3$ (Scheme 14), which has been structurally characterized by X-ray diffraction (Figure 14). Furthermore, $W(PMe_3)_4(SC_6H_4Et)H_3$ is also obtained upon treatment of benzothiophene with $W(PMe_3)_4H_4$ and $W(PMe_3)_3H_6$, although the latter requires photochemical activation (Schemes 12 and 13, respectively).[70] Of most interest, however, upon heating, $W(PMe_3)_4(SC_6H_4Et)H_3$ eliminates ethylbenzene (Scheme 14), a principal product of benzothiophene hydrodesulfurization.[71,72] As such, the reactivity exhibited by this tungsten system provides a series of steps by which benzothiophene may be hydrodesulfurized by a single tungsten center.[53]

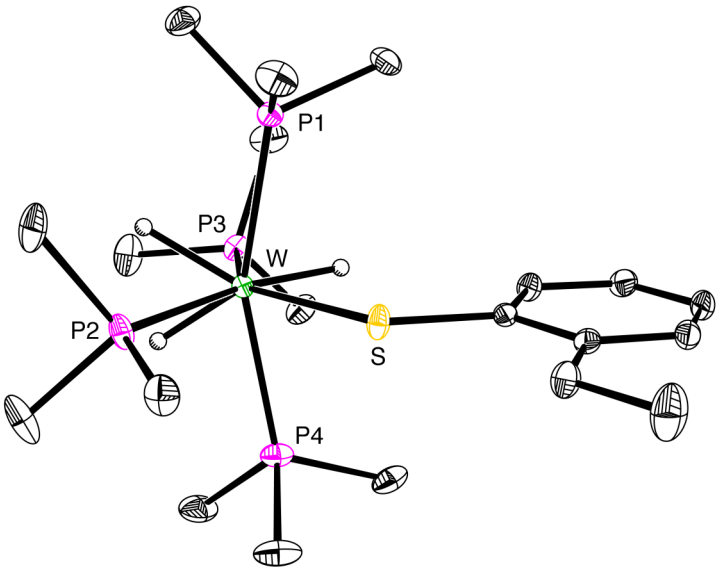

Figure 14. Molecular structure of $W(PMe_3)_4(SC_6H_4Et)H_3$.

4.8 Reactivity of $W(PMe_3)_4(\eta^2\text{–}CH_2PMe_2)H$ towards dibenzothiophene

$W(PMe_3)_4(\eta^2\text{–}CH_2PMe_2)H$ is also capable of desulfurizing dibenzothiophene, one of the compounds that is most resistant to hydrodesulfurization.[9] Specifically, $W(PMe_3)_4(\eta^2\text{–}CH_2PMe_2)H$ reacts with dibenzothiophene to give the dinuclear

dibenzometallacyclopentadiene complex, [(κ^2-$C_{12}H_8$)W(PMe_3)](μ-S)(μ-CH_2PMe_2)(μ-PMe_2)[W(PMe_3)$_3$] (Scheme 15),[73] which has been structurally characterized by X-ray diffraction (Figure 15). While C–S bond cleavage of dibenzothiophene is precedented, reactions that involve desulfurization are rare.[9,74,75] Indeed, there is only one other structurally characterized complex listed in the Cambridge Structural Database[43] that features a κ^2-biphenylene ligand derived from dibenzothiophene, a nickel compound synthesized by Jones.[74,76] In addition, treatment of [(κ^2-$C_{12}H_8$)W(PMe_3)](μ-S)(μ-CH_2PMe_2)(μ-PMe_2)[W(PMe_3)$_3$] with H_2 (*ca.* 1 atm) at 60 ˚C liberates biphenyl (Scheme 15).

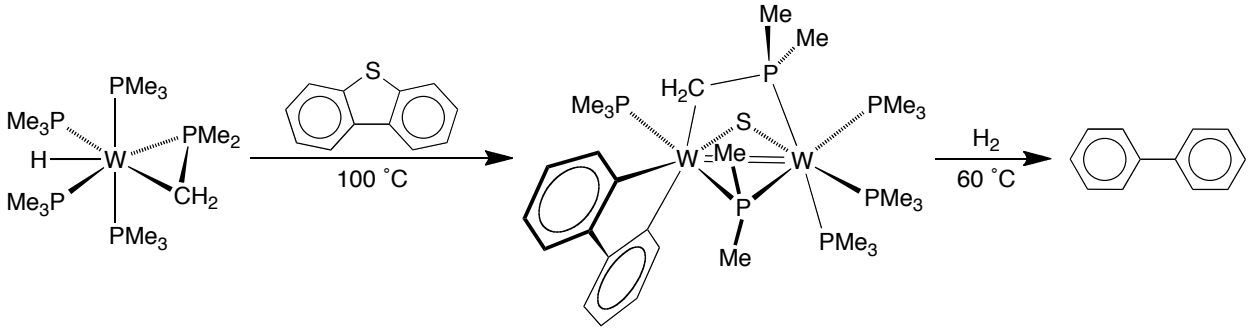

Scheme 15. Reactivity of W(PMe_3)$_4$(η^2–CH_2PMe_2)H towards dibenzothiophene.

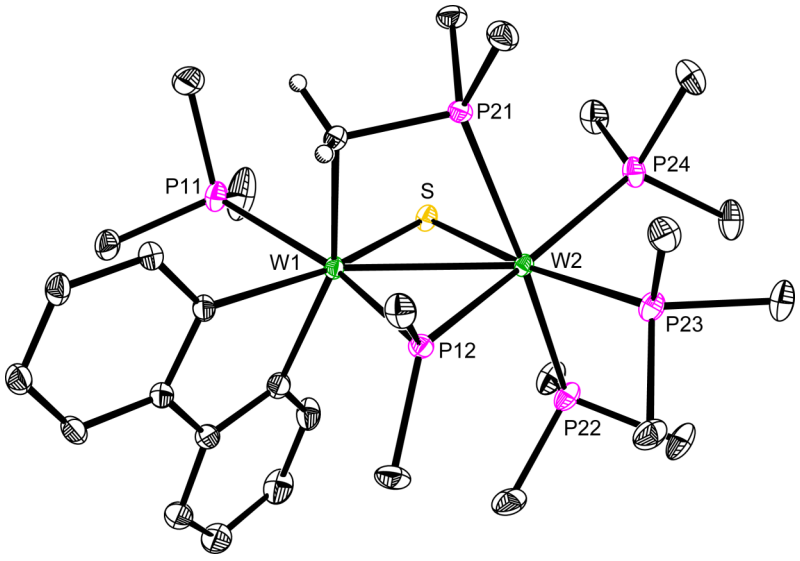

Figure 15. Molecular structure of [(κ^2-$C_{12}H_8$)W(PMe_3)](μ-S)(μ-CH_2PMe_2)(μ-PMe_2)[W(PMe_3)$_3$].

Although we have not isolated any products from the reactions of either $W(PMe_3)_5H_2$, $W(PMe_3)_4H_4$ or $W(PMe_3)_3H_6$ with dibenzothiophene, the latter two are effective catalysts for the exchange of deuterium and hydrogen between dibenzothiophene and C_6D_6.[77] For example, $W(PMe_3)_3H_6$ catalyzes the H/D exchange into dibenzothiophene's α positions at 60 ˚C and the β and γ positions at 80 ˚C, while the δ site remains undeuterated under these conditions.[78,79]

4.9 Bonding description of $[(\kappa^2\text{-}C_{12}H_8)W(PMe_3)](\mu\text{-}S)(\mu\text{-}CH_2PMe_2)(\mu\text{-}PMe_2)[W(PMe_3)_3]$

The bonding description of $[(\kappa^2\text{-}C_{12}H_8)W(PMe_3)](\mu\text{-}S)(\mu\text{-}CH_2PMe_2)(\mu\text{-}PMe_2)\text{-}[W(PMe_3)_3]$ is ambiguous because of (*i*) the presence of the bridging $\mu\text{-}PMe_2$ ligand, an LX ligand, and (*ii*) the presence of two tungsten centers. Specifically, it is unclear what is the metal–metal bond order; three probable resonance structures that have W–W bond orders of 0, 1 and 2 are shown in Figure 16. Only resonance structures in which both metal centers have even numbers of electrons are considered because the molecule is diamagnetic (see Section 4.12.46). Additionally, although the W–W bond length [2.7770(3) Å] compares favorably with the mean W–W single bond length (2.769 Å) listed in the Cambridge Structural Database,[43] and is approximately 0.2 Å longer than the mean W=W double bond length (2.574 Å), there is ambiguity because of the presence of three bridging ligands, which can influence the metal–metal bond distances.[80,81,82] For this reason, we have analyzed the Fenske-Hall molecular orbitals (Figure 17).[83] Examination of the molecular orbitals in Figure 17 indicates that there are two bonding orbitals between the two tungsten atoms (σ and π). Furthermore, the HOMO is a nonbonding d_{xy} orbital largely based on the tungsten atom of the $[W(PMe_3)_3]$ unit, indicating a d^2 configuration for that metal center. Therefore, $[(\kappa^2\text{-}C_{12}H_8)W(PMe_3)](\mu\text{-}S)(\mu\text{-}CH_2PMe_2)(\mu\text{-}PMe_2)[W(PMe_3)_3]$ is best described as having a W=W double bond (Figure 16).

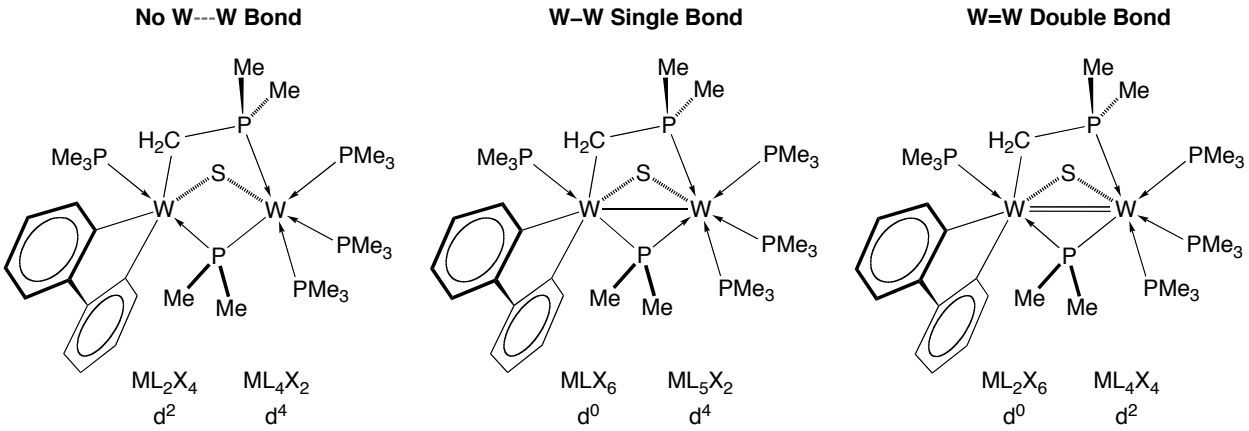

Figure 16. Possible metal–metal bonding in $[(\kappa^2\text{-}C_{12}H_8)W(PMe_3)](\mu\text{-}S)(\mu\text{-}CH_2PMe_2)(\mu\text{-}PMe_2)[W(PMe_3)_3]$.

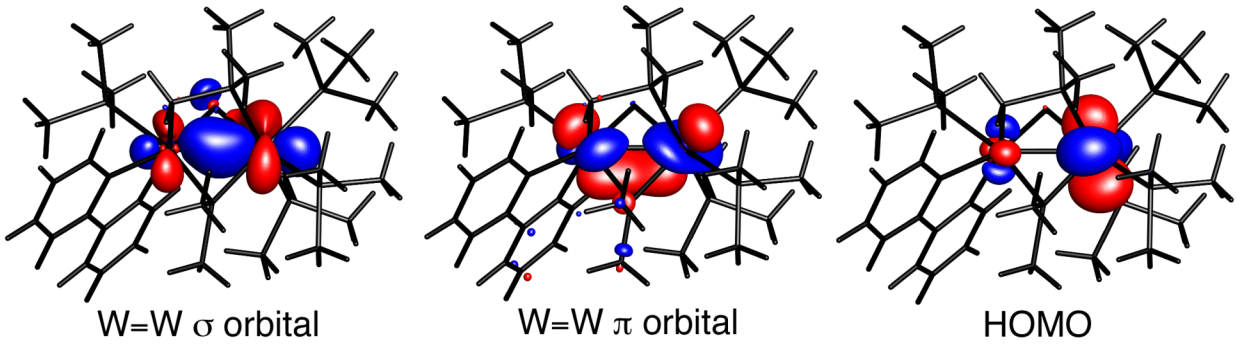

Figure 17. Molecular orbitals showing the σ and π components of the W=W interaction and the HOMO.

4.10 Cluster chemistry

The ability of the previously synthesized transition metal terminal sulfido compounds, $W(PMe_3)_4S_2$[84,85] and $Mo(PMe_3)_4S_2$,[19] to serve as homogeneous models of a hydrotreating catalyst was also explored. In this regard, thermolysis (80 ˚C) of a solution of $W(PMe_3)_4S_2$ in benzene deposited black needle-shaped crystals of the C_i symmetric tungsten sulfide cluster, $W_8S_{16}(PMe_3)_{10}$ (Scheme 16). The molecular structure of $W_8S_{16}(PMe_3)_{10}$ is shown in Figure 18.

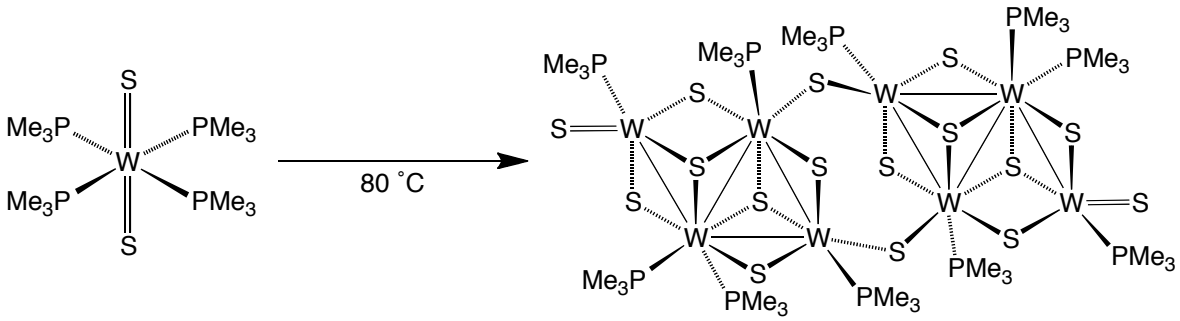

Scheme 16. Synthesis of $W_8S_{16}(PMe_3)_{10}$.

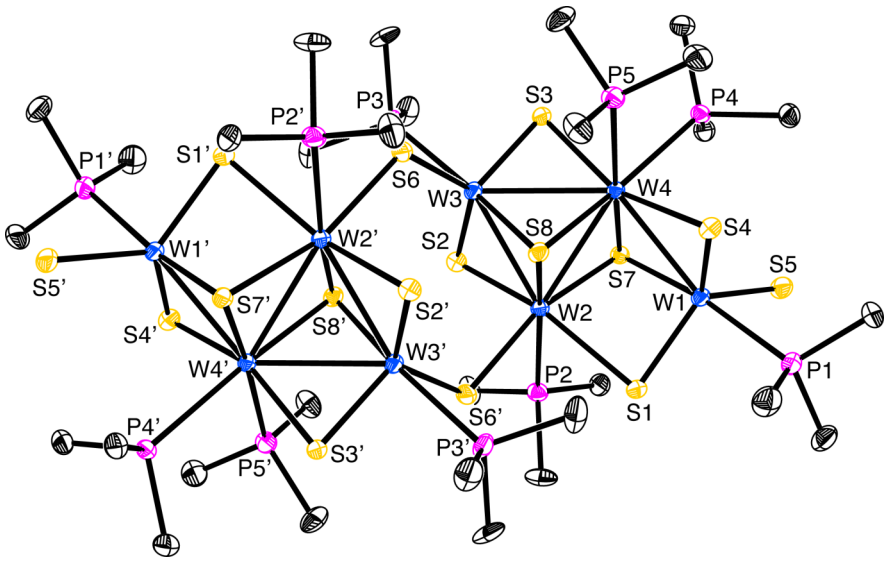

Figure 18. Molecular structure of $W_8S_{16}(PMe_3)_{10}$.

$W_8S_{16}(PMe_3)_{10}$ has inversion symmetry, and as such, can be described as a symmetric dimer with two equivalent halves. Each half consists of: 3 $W(PMe_3)$ fragments, 1 $W(PMe_3)_2$ fragment, 4 (μ-S) bridging sulfides, 2 (μ_3-S) bridging sulfides, 1 terminal sulfide (W=S), and a (μ*-S) bridging sulfide, in which (μ*-S) is defined as a ligand that bridges the two monomeric units, *i.e.* S6 and S6′ of the solid state structure (Figure 18). Thus, $W_8S_{16}(PMe_3)_{10}$ is more precisely described by the formula $[W_4(\mu\text{-}S)_4(\mu_3\text{-}S)_2(\mu^*\text{-}S)(=S)(PMe_3)_5]_2$ and its symmetrical nature is illustrated in Figure 19.

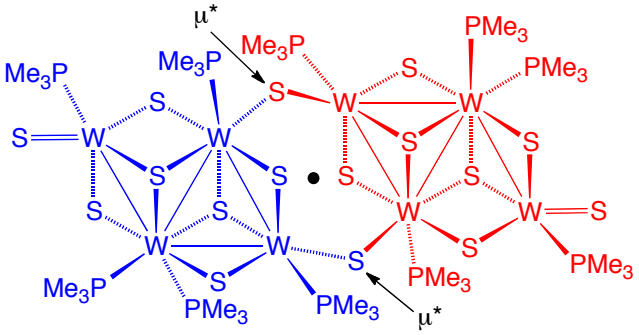

Figure 19. Dimeric nature of $W_8S_{16}(PMe_3)_{10}$, *i.e.* $[W_4(\mu\text{-}S)_4(\mu_3\text{-}S)_2(\mu^*\text{-}S)(=S)(PMe_3)_5]_2$ (μ^* indicates a sulfide that bridges the two monomeric units, • indicates the molecular inversion center).

The terminal sulfido ligand of $W_8S_{16}(PMe_3)_{10}$ has a W–S bond length of 2.214(2) Å; evidence that it is, in fact, a terminal sulfide and not a terminal hydrosulfido is provided by comparison with the other W–S bond lengths in $W_8S_{16}(PMe_3)_{10}$ (Table 1). For example, the W–S bond length of the W=S moiety is 0.155 Å shorter than the average W–S bond length of the (μ-S) ligands[86] and 0.193 Å shorter than the average bond length of the (μ_3-S) ligands. It is also prudent to compare the W–S bond length of the W=S moiety of $W_8S_{16}(PMe_3)_{10}$ to the W=S moieties listed in the Cambridge Structural Database (2.155 Å).[43] In this regard, although 2.214 Å is 0.059 Å longer than the average W–S bond length of terminal W=S moieties (Table 1), it is considerably shorter (0.189 Å) than the mean W–S bond length for molecules with a W–S(R/H) fragment (2.403 Å). Most notably, the W=S bond length of $W_8S_{16}(PMe_3)_{10}$ (2.214 Å) is very similar to the other terminal sulfido complexes of tungsten that contain PMe_3 ligands, namely $W(PMe_3)_4S_2$, $W(PMe_3)_2(CNBu^t)_2S_2$, and $W(PMe_3)_2(\eta^2\text{-}PhCHO)S_2$, which have an average W–S bond length of 2.229 Å (Table 2).

Furthermore, there are several structurally characterized compounds with terminal hydrosulfido ligands (W–SH), two of which are $Cp^*W(CO)_3SH$[87] and $[\mu\text{-}(C_5H_4)_2][W(CO)_3SH]_2$,[88] having W–S bond lengths that are *ca.* 0.3 Å longer [2.522(2) Å and 2.513(2) Å, respectively] than the W–S bond of $W_8S_{16}(PMe_3)_{10}$. The most relevant comparison, however, is that with the previously reported tetranuclear tungsten cluster

$W_4S_6(PMe_2Ph)_6(SH)_2$, *i.e.* $[W_4(\mu\text{-}S)_4(\mu_3\text{-}S)_2(PMe_2Ph)_6(SH)_2]$ (Figure 20), having a terminal hydrosulfido moiety (W–SH) with a W–S bond length of 2.390(2),[89] which is 0.176 Å longer that the W–S bond of $W_8S_{16}(PMe_3)_{10}$ (Table 1).

Table 1. Average experimental W–S bond lengths (Å) of $W_8S_{16}(PMe_3)_{10}$ and $W_4S_6(PMe_2Ph)_6(SH)$.

	***d*[W–(μ-S)]/Å**	***d*[W–(μ_3-S)/Å**	***d*(W=S)/Å**	***d*[W–S(R/H)]/Å**
$W_8S_{16}(PMe_3)_{10}$	2.369	2.407	2.214	–
$W_4S_6(PMe_2Ph)_6(SH)_2$	2.356	2.382	–	2.390
C.S.D.[a]	2.311	2.418	2.155	2.403

(a) C.S.D. = Average bond lengths listed in the Cambridge Structural Database.

Table 2. Average experimental terminal W–S bond lengths (Å) in tungsten PMe_3 terminal sulfido complexes.

	***d*(W=S)/Å**	**Reference**
$W_8S_{16}(PMe_3)_{10}$	2.214	this work
$W(PMe_3)_4S_2$	2.253	85
$W(PMe_3)_2(CNBu^t)_2S_2$	2.247	84,85
$W(PMe_3)_2(\eta^2\text{-}PhCHO)S_2$	2.186	84,85

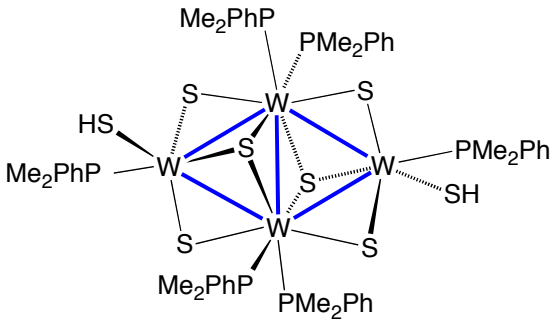

Figure 20. Previously synthesized electron-precise cluster $W_4S_6(PMe_2Ph)_6(SH)_2$ (see reference 89).

It is interesting to compare the structure of $W_8S_{16}(PMe_3)_{10}$ with that of $W_4S_6(PMe_2Ph)_6(SH)_2$,[89] and the major differences are illustrated in Figure 21 (colored

blue). Thus, $W_8S_{16}(PMe_3)_{10}$ can be formally viewed as the product of condensation of two molecules $W_4S_6(PMe_2Ph)_6(SH)_2$, the PMe_3 counterpart of $W_4S_6(PMe_2Ph)_6(SH)_2$, accompanied by dissociation of two phosphine ligands and elimination of two molecules of H_2.

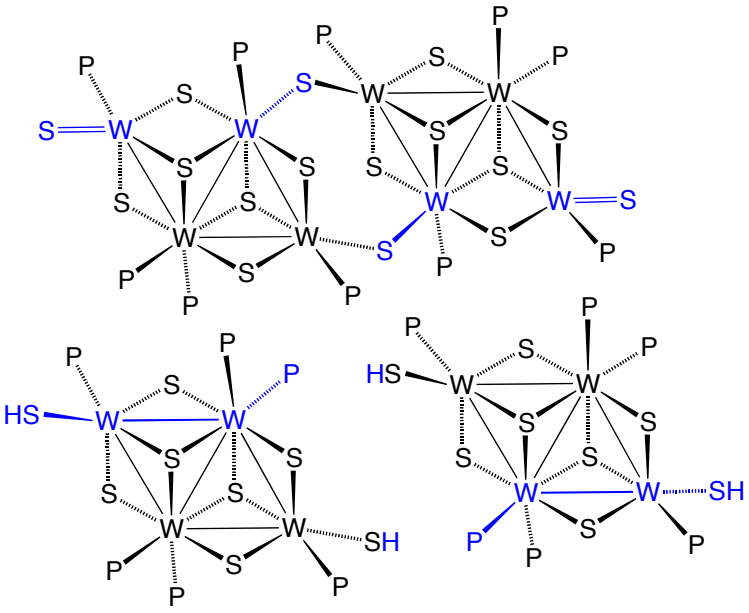

Figure 21. Comparison of $W_8S_{16}(PMe_3)_{10}$ (top) and two molecules of $W_4S_6(PMe_2Ph)_6(SH)_2$ (bottom) [blue fragments are highlighted to illustrate the major differences]. PMe_3 and PMe_2Ph ligands are represented by P in this figure.

The bonding in $W_8S_{16}(PMe_3)_{10}$ is also of interest but is complicated due to the complex nature of the molecule (*e.g.* 8 tungsten atoms and 4 (μ_3-S) LX_2 ligands). Metal–metal bonding in transition metal clusters has been previously described and is commonly classified in three categories, namely: (*i*) electron-precise clusters, (*ii*) electron-rich clusters, and (*iii*) electron-deficient clusters.[90,91] In an electron-precise cluster, exemplified by $W_4S_6(PMe_2Ph)_6(SH)_2$ (Figure 20),[89] the number of skeletal valence electron pairs is equal to the number of metal–metal single bonds. Thus, in $W_4S_6(PMe_2Ph)_6(SH)_2$, there are 14 total X-type interactions[92] and there are four tungsten atoms (each free tungsten atom has 6 valence electrons for a total of 24), such that there

are 5 skeletal valence electron pairs [½(24 – 14)]. As illustrated by the blue bonds in Figure 20, there are also five possible W–W contacts, and the cluster is, therefore, electron-precise, as each metal–metal bond can simply be described as 2-center 2-electron interaction. In accord with each W–W interaction consisting of equivalent single bonds, the bond W–W bond distances [2.8373(8) Å, 2.8114(7) Å, 2.8118(6) Å, 2.8114(7) Å, and 2.8118(6) Å] are all very similar with the narrow range of 0.0259 Å.

On the other hand, $W_8S_{16}(PMe_3)_{10}$ is an electron-deficient cluster [32 X-type interactions, 8 tungsten atoms, each with 6 valence electrons: ½(48 – 32) = 8], having 12 plausible W–W contacts but only 8 skeletal valence electron pairs. In this regard, analysis of the W–W bond lengths of $W_8S_{16}(PMe_3)_{10}$ indicate that the W–W interactions are not equivalent. Specifically, there are two W–W interatomic distances [W1–W2: 3.2441(4) Å, W2–W3': 4.1440(4) Å] that are significantly longer than the other four [W1–W4: 2.7569(4) Å, W2–W3: 2.7501(4) Å, W2–W4: 2.8844(4) Å, W3–W4: 2.8489(4) Å] (Table 2, see Figure 18 for atom labels). Indeed, the mean W–W single bond length listed in the Cambridge Structure Database is 2.772 Å,[43] such that the large W–W interatomic distances of 3.2441(4) Å and 4.1440(4) Å for W1–W2 and W2–W3' are not indicative of bonding interactions. Thus, it is postulated that only 8 W–W bonds exist in $W_8S_{16}(PMe_3)_{10}$, as illustrated in Figure 22 (blue bonds), which is in accord with the presence of only 8 skeletal valence electron pairs.

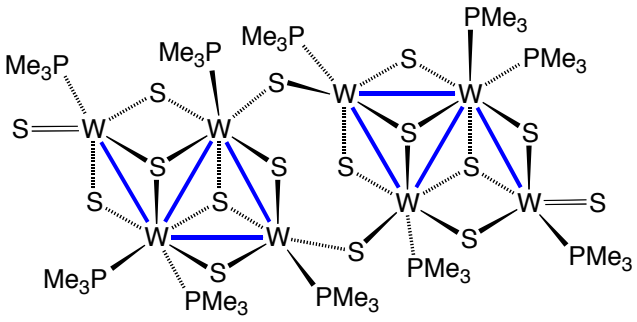

Figure 22. $W_8S_{16}(PMe_3)_{10}$ illustrating the proposed metal–metal bonding (blue).

Table 3. W–W bond lengths (Å) of $W_8S_{16}(PMe_3)_{10}$ as determined by X-ray diffraction.

	***d*(W–W)/Å**
W2–W3	2.7501(4)
W1–W4	2.7569(4)
W2–W4	2.8844(4)
W3–W4	2.8489(4)
W1–W2	3.2441(4)
W2–W3'	4.1440(4)
C.S.D.[a]	2.772

(a) C.S.D. = Average W–W single bond length listed in the Cambridge Structural Database (1989 hits).

Additional evidence for the presence of 8 W–W bonds is provided by DFT calculations. In this regard, the computationally simpler cluster $W_8S_{16}(PH_3)_{10}$, in which the methyl groups of the PMe_3 ligands have been replaced by hydrogen atoms, was geometry optimized with imposed C_i symmetry. First, it should be noted that the overall calculated geometry reproduces the experimental structure well. After convergence, a simpler model (Figure 24) comprised of $W_4(\mu\text{-}S)_4(\mu_3\text{-}S)_2(SH)_2(=S)(PH_3)_5$, in which the two (μ*-S) bridging sulfide ligands were replaced by SH moieties, was employed to derive Fenske-Hall molecular orbitals.[83] Examination of the molecular orbitals indicates that there are six molecular orbitals (Figure 23) that contribute to the 4 W–W σ-bonds.[93] Furthermore, there are no orbitals that (*i*) contribute to a fifth W–W bond (*i.e.* between W1 and W2) or (*ii*) have any localized metal character, indicating that all of the tungsten centers have a d^0 configuration. Figure 25 illustrates a plausible resonance structure for $W_8S_{16}(PMe_3)_{10}$, giving each tungsten center a d^0 configuration (*i.e.* every tungsten has 6 X-type interactions).

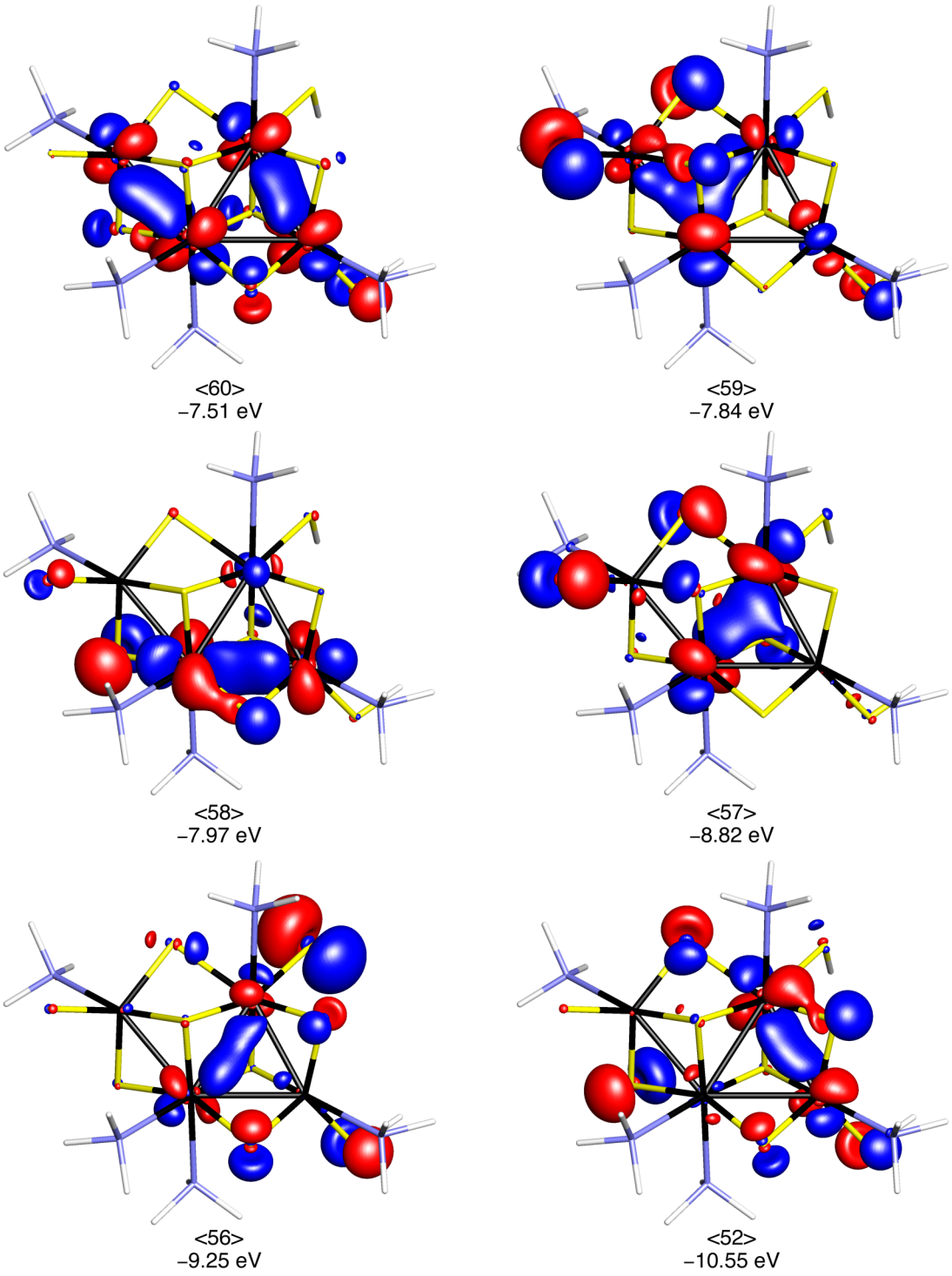

Figure 23. Molecular orbitals of $W_4(\mu\text{-}S)_4(\mu_3\text{-}S)_2(SH)_2(=S)(PH_3)_5$ showing the major σ–bonding components of the W–W interactions. Orbital <60> is the HOMO (black: tungsten, yellow: sulfur, magenta: phosphorus, white: hydrogen).

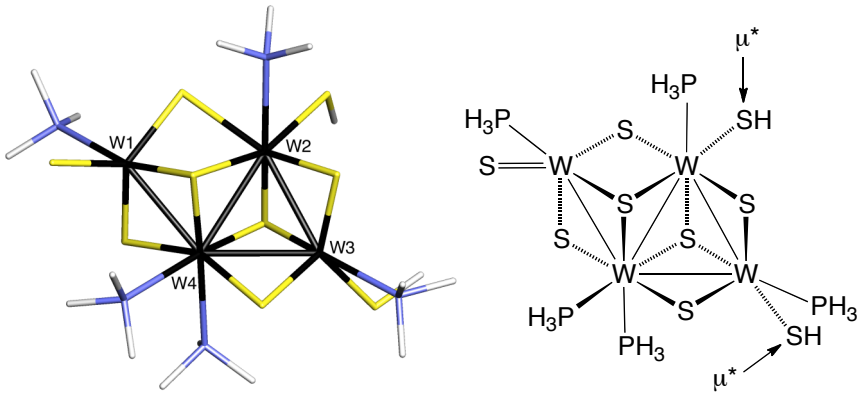

Figure 24. Illustration of the geometry of $W_4(\mu\text{-}S)_4(\mu_3\text{-}S)_2(SH)_2(=S)(PH_3)_5$ used for the molecular orbitals in Figure 23 (left) and the replacement of SH moieties for the (μ*-S) bridging sulfide ligands (right).

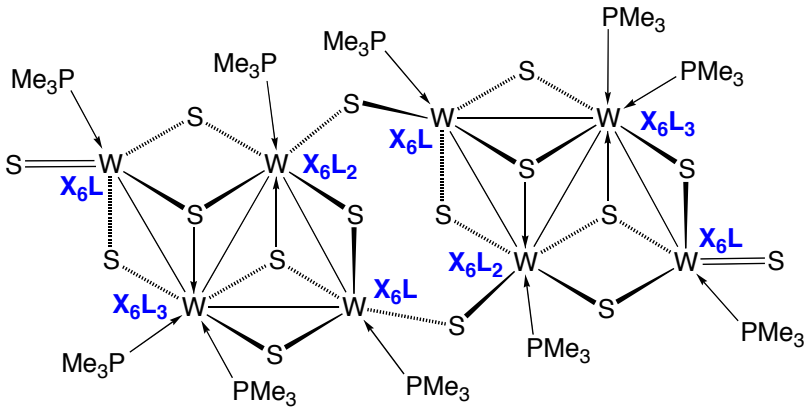

Figure 25. Illustration of the MLX description of each tungsten center; each tungsten has 6 X-type interactions, thus each tungsten has a d^0-configuration.

The synthesis of other chalcogenide clusters from the known tungsten terminal selenido and tellurido compounds, $W(PMe_3)_4Se_2$[94,85] and $W(PMe_3)_4Te_2$,[95,85] was also attempted but unfortunately, single crystals of sufficient quality for X-ray diffraction were not obtained.

A C_i symmetric molybdenum sulfide cluster has also been synthesized by treating a suspension of $Mo(PMe_3)_6$ in benzene with hydrogen sulfide, thereby depositing crystals of $Mo_4S_6(PMe_3)_6(SH)_2$ (Figure 26) after standing at room temperature for *ca.* 1 day (Scheme 17).[96,97] $Mo_4S_6(PMe_3)_6(SH)_2$ has been previously reported first by

Saito,[98] and then later by Rauchfuss.[99] It should be noted that $Mo_4S_6(PMe_3)_6(SH)_2$ is isostructural with $W_4S_6(PMe_2Ph)_6(SH)_2$ (Figure 20).[89]

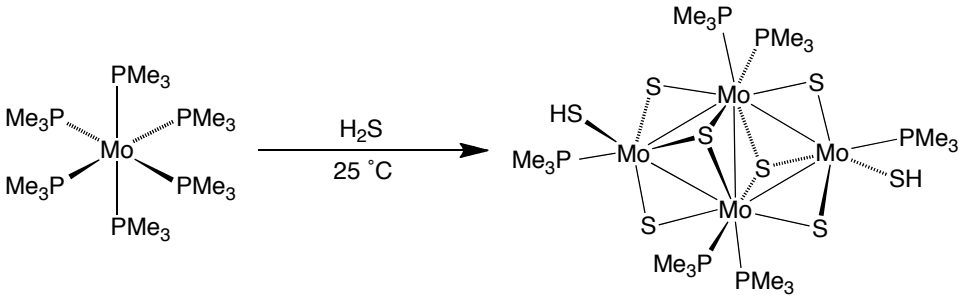

Scheme 17. Synthesis of $Mo_4S_6(PMe_3)_6(SH)_2$.

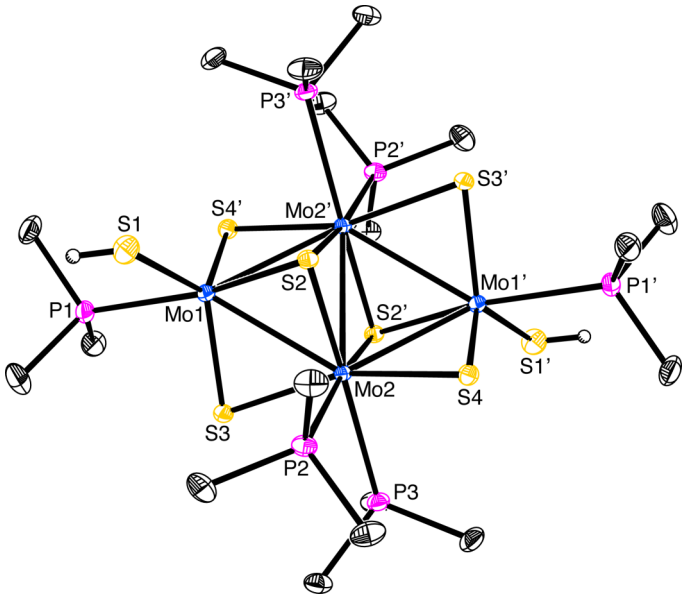

Figure 26. Molecular structure of $Mo_4S_6(PMe_3)_6(SH)_2$.

Two new trinuclear molybdenum clusters[100] were produced by heating solutions of *in situ* generated $Mo(PMe_3)_4Se_2$ and $Mo(PMe_3)_4Te_2$ in benzene, thereby depositing black, block-shaped crystals of $Mo_3Se_5(PMe_3)_6$[101] and $Mo_3Te_5(PMe_3)_6$,[102] respectively (Schemes 18 and 19). $Mo_3Se_5(PMe_3)_6$ and $Mo_3Te_5(PMe_3)_6$ are analogous to the previously synthesized cluster, $Mo_3S_5(PMe_3)_6$.[103,104] The molecular structures of the pseudo D_{3h} symmetric $Mo_3Se_5(PMe_3)_6$ and $Mo_3Te_5(PMe_3)_6$ were determined by X-ray diffraction and are shown in Figures 27 and 28, respectively.[105] The E (E = S, Se, and Te) and PMe_3

ligands of $Mo_3E_5(PMe_3)_6$ form an approximate octahedral geometry about each molybdenum center, while the Mo–Mo bonds bisect the (μ_2-E)-(μ_3-E)-(μ_3-E) faces (Figure 29).

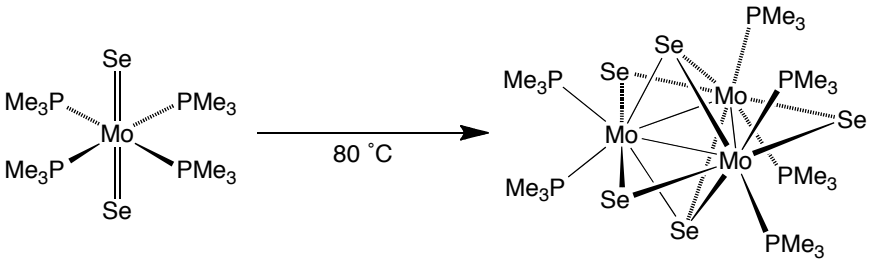

Scheme 18. Synthesis of $Mo_3Se_5(PMe_3)_6$.

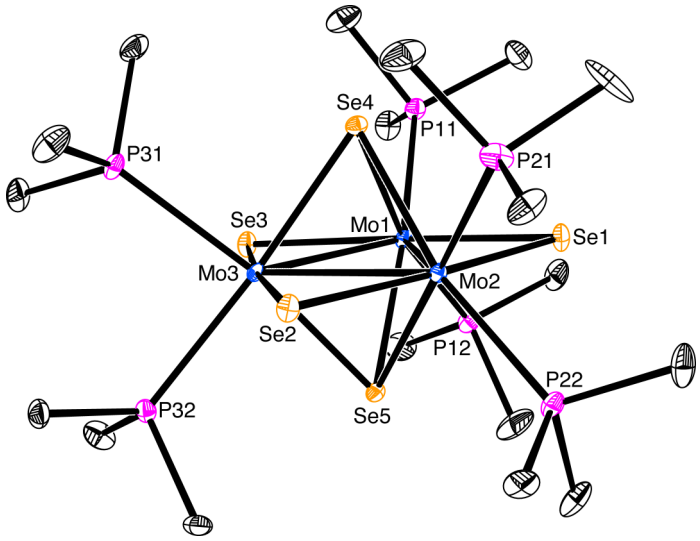

Figure 27. Molecular structure of $Mo_3Se_5(PMe_3)_6$.

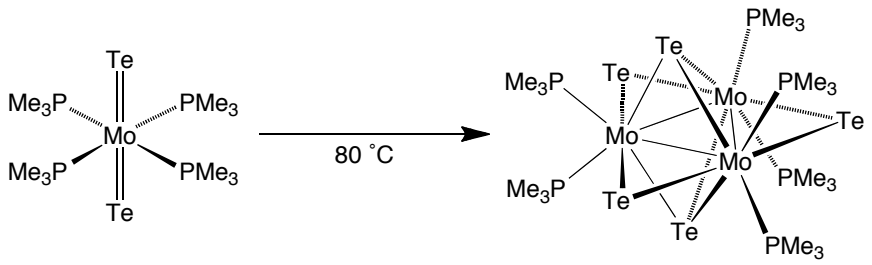

Scheme 19. Synthesis of $Mo_3Te_5(PMe_3)_6$.

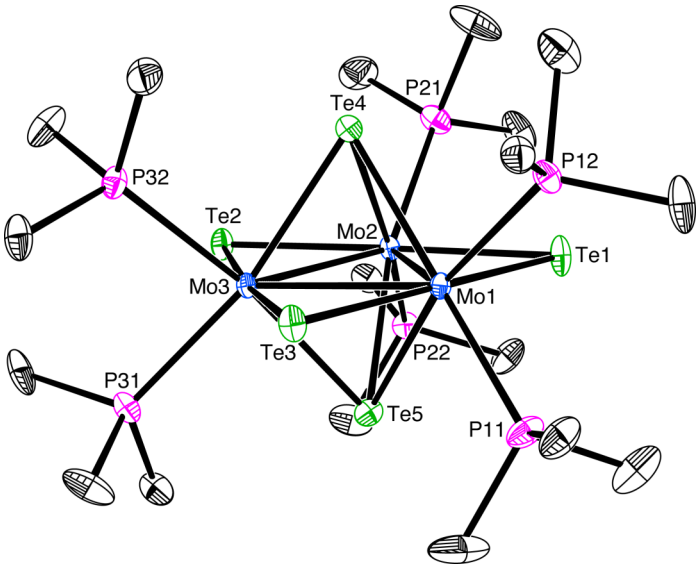

Figure 28. Molecular structure of $Mo_3Te_5(PMe_3)_6$.

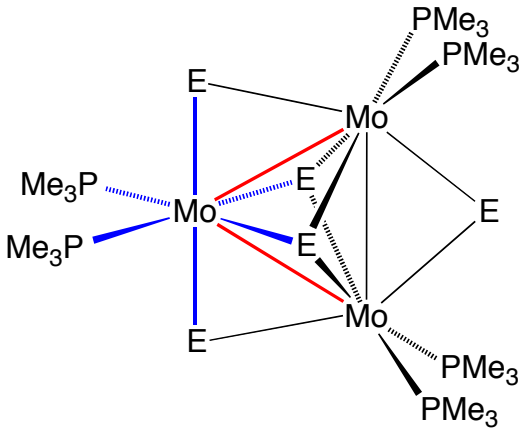

Figure 29. Representation of $Mo_3E_5(PMe_3)_6$ (E = S, Se or Te) clusters exemplifying the octahedral coordination, shown in blue, of the six ligands around molybdenum. The red lines represent the Mo–Mo bonds, which bisect the (μ_2-E)-(μ_3-E)-(μ_3-E) faces.

Unlike $Mo_4S_6(PMe_3)_6(SH)_2$, which is an electron-precise cluster,[90,91] or $W_8S_{16}(PMe_3)_{10}$, which is an electron-deficient cluster, $Mo_3Se_5(PMe_3)_6$ and $Mo_3Te_5(PMe_3)_6$ are electron-rich clusters. Specifically, the $Mo_3E_5(PMe_3)_6$ (E = S, Se and Te) clusters each have 4 skeletal valence electron pairs (10 X-type interactions and 3 molybdenum atoms) but only 3 Mo–Mo contacts, thus having an excess of 1 electron pair, causing the bonding description to be ambiguous. For example, the extra pair of electrons could (*i*)

contribute to a Mo–Mo double bond, (*ii*) be a localized "lone pair" on one molybdenum atom, (*iii*) be a delocalized non-bonding orbital on two or three molybdenum atoms, or (*iv*) cause a Mo–Mo bond to break, as Mingos predicts.[91] Furthermore, although the $Mo_3E_5(PMe_3)_6$ (E = S, Se and Te) clusters are isostructural, the identity of the chalcogenide does, nevertheless, effect the Mo–Mo interactions, as indicated by the increase in the average Mo–Mo bond lengths of $Mo_3S_5(PMe_3)_6$, $Mo_3Se_5(PMe_3)_6$, and $Mo_3Te_5(PMe_3)_6$ (2.714 Å,[103] 2.781 Å, and 2.910 Å, respectively) as the chalcogen increases size (Table 4).[106]

Table 4. Average Mo–Mo bond lengths (Å) and Mo–E–Mo angles (°) of $Mo_3E_5(PMe_3)_6$ (E = S, Se, and Te) complexes, as determined by X-ray diffraction.

	***d*(Mo-Mo)/Å**	***d*[Mo-(μ-E)]/Å**	***d*[Mo-(μ-E)]/Å**	**Mo-(μ-E)-Mo/°**	**Mo-(μ_3-E)-Mo/°**
$Mo_3S_5(PMe_3)_6$	2.714	2.393	2.421	69.10	68.18
$Mo_3Se_5(PMe_3)_6$	2.781	2.508	2.541	67.08	66.36
$Mo_3Te_5(PMe_3)_6$	2.910	2.695	2.716	65.37	64.79
C.S.D.[a]	2.738	–	–	–	–

(a) C.S.D. = Average Mo–Mo single bond lengths listed in the Cambridge Structural Database (5104 hits).

In order to understand better the $Mo_3E_5(PMe_3)_6$ (E = S, Se, and Te) clusters, DFT geometry optimization calculations were carried out on the computationally simpler $Mo_3E_5(PH_3)_6$ clusters, in which the methyl groups of the PMe_3 ligands were replaced by hydrogen atoms. First, it should be noted that the overall calculated geometries reproduce the experimental structures well. Interestingly, although the Mo-Mo bond lengths increase as the chalcogen increases size, the Mo–Mo orbital interactions in the three clusters are very similar, which is illustrated by comparison of Figures 30–32, for $Mo_3S_5(PH_3)_6$, $Mo_3Se_5(PH_3)_6$ and $Mo_3Te_5(PH_3)_6$, respectively. Thus, the $Mo_3E_5(PH_3)_6$ clusters each possess 3 occupied orbitals [*i.e.* <45>, <46>, <47> for $Mo_3S_5(PH_3)_6$, <67>, <71>, <72> for $Mo_3Se_5(PH_3)_6$, and <65>, <71>, <72> for $Mo_3Te_5(PH_3)_6$] that contribute to

the Mo–Mo σ-bonds, giving a metal-metal bond order of 1 for each Mo–Mo interaction (Figures 30–32). Furthermore, the HOMO's of the $Mo_3E_5(PH_3)_6$ clusters [*i.e.* <48> for $Mo_3S_5(PH_3)_6$, <73> for $Mo_3Se_5(PH_3)_6$, and <73> for $Mo_3Te_5(PH_3)_6$] are localized only on the three Mo centers, and can, therefore, be described as a delocalized nonbonding pair, consistent with the presence of 3 metal-metal bonds and 10 X-type ligands.

In view of the similar molecular orbital interactions for the $Mo_3E_5(PH_3)_6$ clusters that contribute to the metal-metal bonding, it is postulated that the increase in Mo–Mo bond length is due to the increased atomic radius of the heavier chalcogen, which essentially pushes the metal centers apart. Thus, if we make the simple assumption that the Mo–(μ_2-E)–Mo angles are equal, as the chalcogen increases size, the metal–metal bond distance will increase, which is illustrated in Figure 33. The average Mo–E bond lengths and Mo–(μ_2-E)–Mo angles listed in the Cambridge Structural Database are listed in Table 5 and it is apparent that the average Mo–E bond length does increase significantly in the order S < Se < Te but the average Mo–(μ_2-S)–Mo and Mo–(μ_2-Se)–Mo angles are quite similar, while the average Mo–(μ_2-Te)–Mo angle is *ca*. 5 ° smaller. Moreover, the experimental Mo–E bond lengths also increase significantly in the order S < Se < Te in $Mo_3E_5(PMe_3)_6$ (E = S, Se, and Te, Table 4) while the Mo–(μ_2-E)–Mo angles have a small range of ~ 4° (Table 5). Thus, despite the fact that $Mo_3Te_5(PMe_3)_6$ has the smallest Mo–(μ_2-E)–Mo angle (65.37 °), the Mo–Mo bond lengths are still the longest because of the increased Mo–Te bond distances.

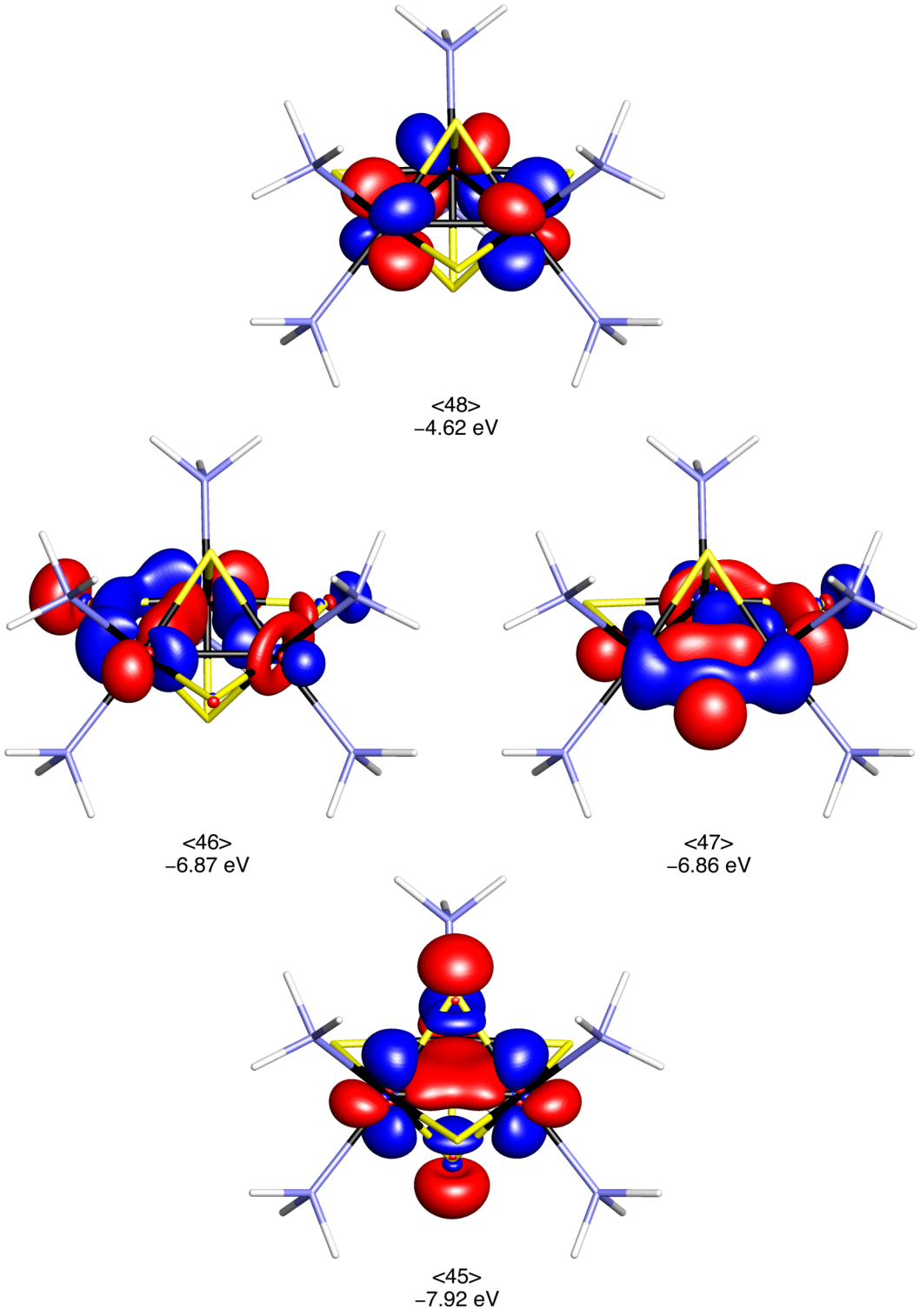

Figure 30. Molecular orbitals of $Mo_3S_5(PH_3)_6$ showing the major σ–bonding components of the Mo–Mo interactions. Orbital <48> is the HOMO, which is delocalized over the three Mo centers (black: tungsten, yellow: sulfur, magenta: phosphorus, white: hydrogen).

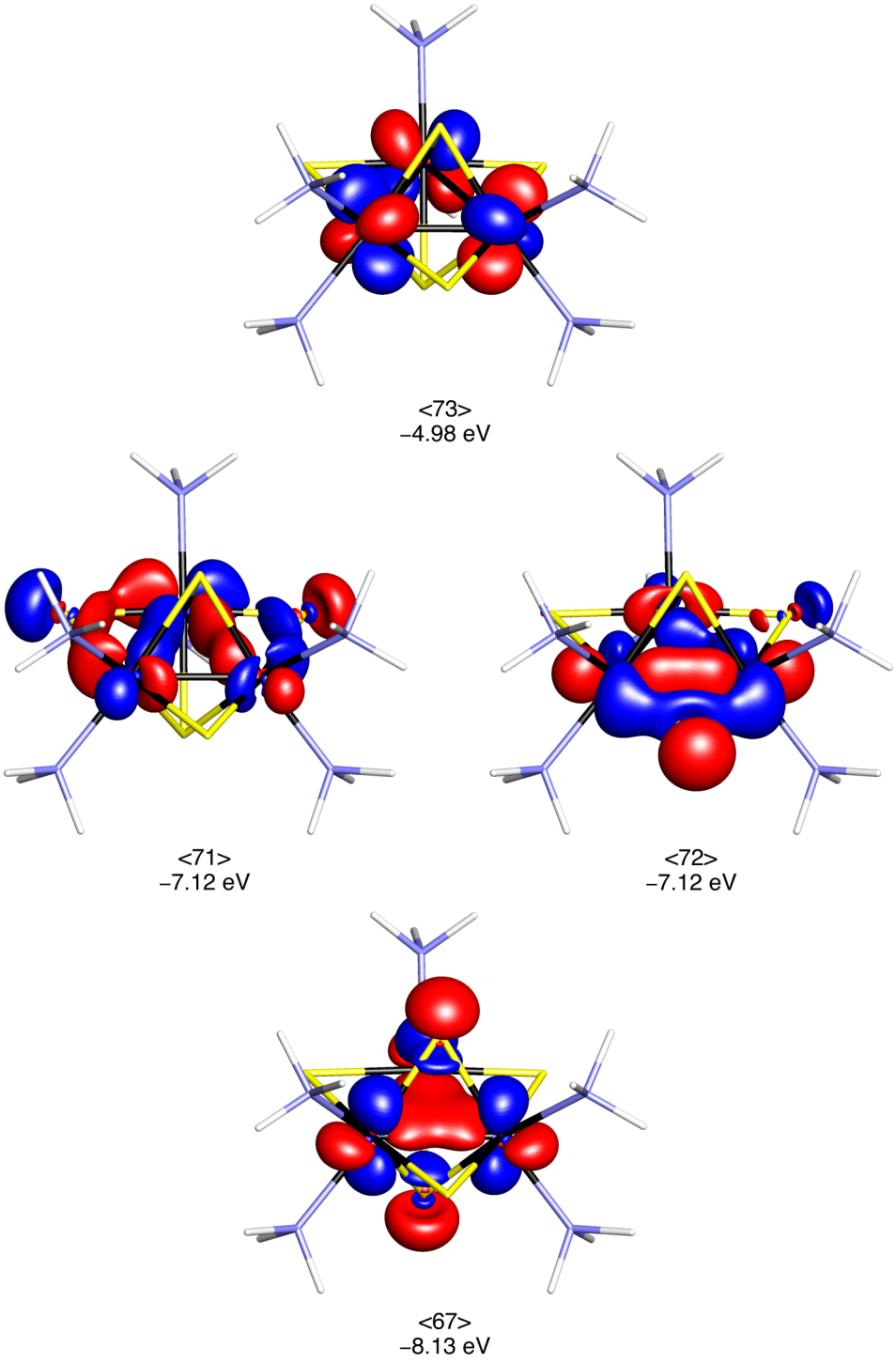

Figure 31. Molecular orbitals of $Mo_3Se_5(PH_3)_6$ showing the major σ–bonding components of the Mo–Mo interactions. Orbital <73> is the HOMO, which is delocalized over the three Mo centers (black: tungsten, yellow: selenium, magenta: phosphorus, white: hydrogen).

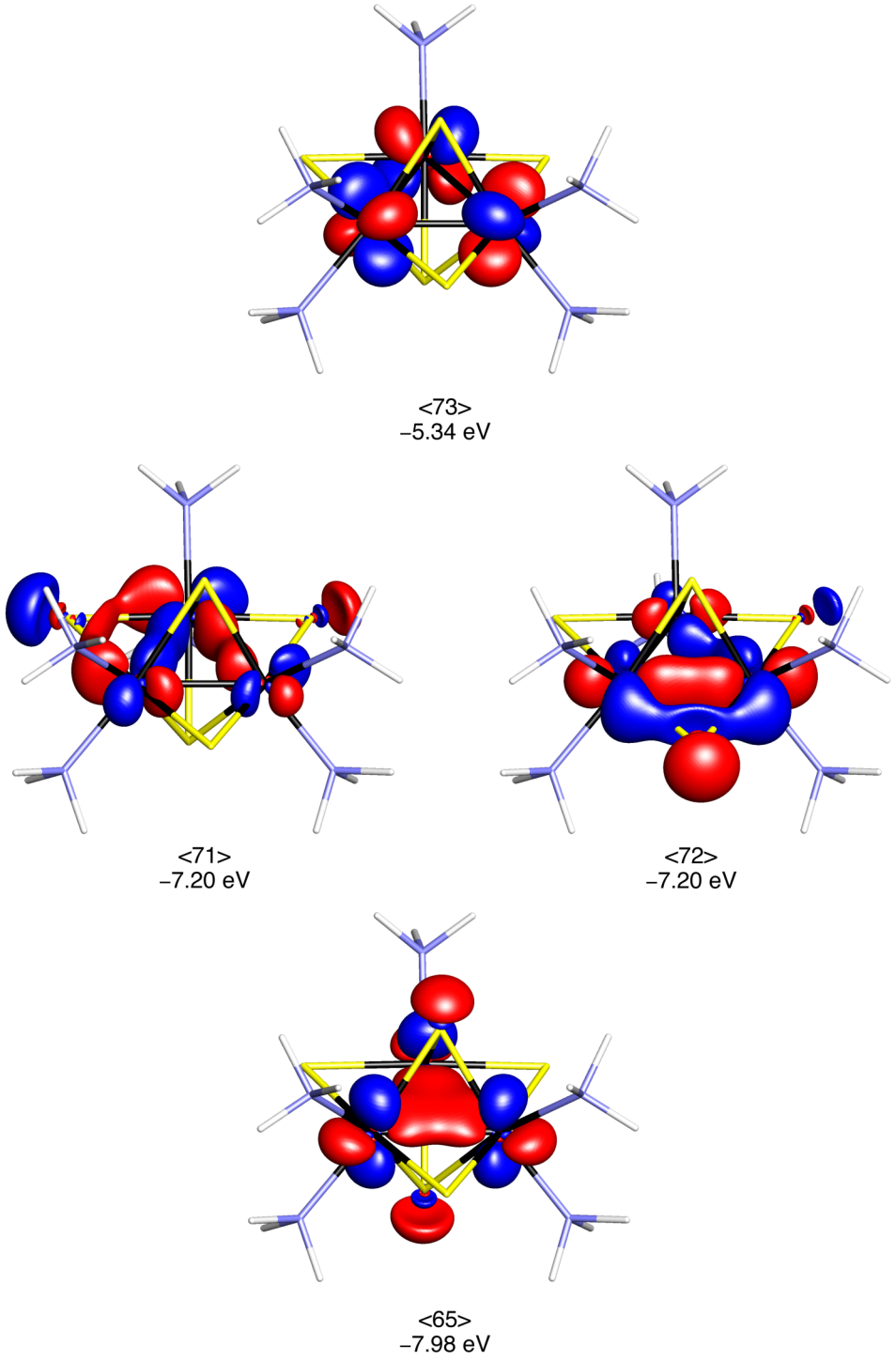

Figure 32. Molecular orbitals of $Mo_3Te_5(PH_3)_6$ showing the major σ–bonding components of the Mo–Mo interactions. Orbital <73> is the HOMO, which is delocalized over the three Mo centers (black: tungsten, yellow: tellurium, magenta: phosphorus, white: hydrogen).

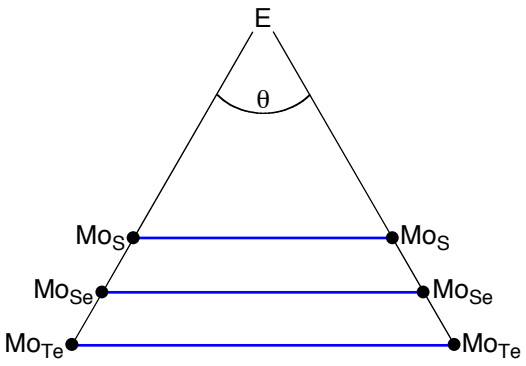

Figure 33. Illustration of how the Mo–Mo bond length increases as a function of chalcogenide atomic radius, assuming that the Mo–E–Mo angle (θ) is constant.

Table 5. Average Mo–E (E = S, Se, and Te) bond lengths (Å) and Mo–(μ_2-E)–Mo angles (°) listed in the Cambridge Structural Database[a] and the average Mo–(μ_2-E)–Mo angles in the experimental structures of $Mo_3E_5(PMe_3)_6$.

	Cambridge Structural Database			**$Mo_3E_5(PMe_3)_6$**
	***d*[Mo–(μ_2-E)]/Å**	***d*[Mo–(μ_3-E)]/Å**	**Mo–(μ_2-E)–Mo/°**	**Mo–(μ_2-E)–Mo/°**
S	2.316	2.366	75.06	69.10
Se	2.439	2.504	75.71	67.08
Te	2.665	2.675	69.74[b]	65.37

(a) Searches constrained for Mo–Mo single bonds and 2-coordinate chalcogenides (E = S, Se and Te).
(b) There are only a limited number (< 10) of structures with (μ_2-Te) ligands and most contain other (μ_2-X) bridges such as (μ_2-S). These were excluded from the search for the average Mo–(μ_2-E)–Mo angle. If these structures are included, the average Mo–(μ_2-E)–Mo angle is 64.45°.

For comparison, a series of complexes have been reported with Mo–(μ_2-E)–Mo (E = S, Se, and Te) bridging ligands, namely the *syn* isomers of $[Cp^*MoO(\mu\text{-}S)]_2$,[107] $[Cp^*MoO(\mu\text{-}Se)]_2$,[108] $[Cp^*MoO(\mu\text{-}Te)]_2$,[109] in addition to the *anti* isomers (Figure 34).[109,110] In line with the $Mo_3E_5(PMe_3)_6$ (E = S, Se, and Te) clusters, the Mo–Mo bond distances in $[Cp^*MoO(\mu\text{-}E)]_2$ increase in the order E = S < Se < Te, while the Mo–E–Mo angles are similar, and decrease slightly as the chalcogen increases size (Table 6).

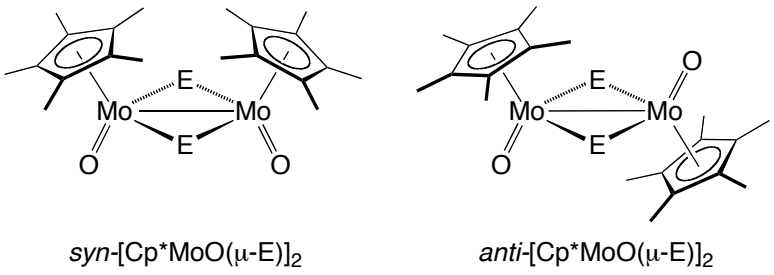

syn-[Cp*MoO(μ-E)]$_2$ *anti*-[Cp*MoO(μ-E)]$_2$

Figure 34. *Syn* and *Anti* isomers of [Cp*MoO(μ-E)]$_2$ (E = S, Se, and Te).

Table 6. Average experimental Mo–Mo bond lengths (Å) and Mo–E–Mo angles (°) of [Cp*MoO(μ-E)]$_2$ (E = S, Se, and Te) complexes, as determined by X-ray diffraction.

	***d*(Mo–Mo)/Å**		**Mo–E–Mo/°**	
	syn	***anti***	***syn***	***anti***
[Cp*MoO(μ-S)]$_2$	2.868	2.904	76.535	77.682
[Cp*MoO(μ-Se)]$_2$	2.938	2.984	74.553	75.255
[Cp*MoO(μ-Te)]$_2$	3.073	3.154	71.285	72.766

Although no more studies have been carried out with the clusters described above, it is possible that they may be able to serve as model systems for the hydrotreating catalysts, because they have structural similarities to tungsten and molybdenum sulfide.[111]

4.11 Summary and conclusions

In summary, the molybdenum hydride complexes $Mo(PMe_3)_5H_2$ and $Mo(PMe_3)_4H_4$ are capable of cleaving the C–S bonds of thiophene, benzothiophene and dibenzothiophene under varying conditions. Of particular note, $Mo(PMe_3)_4H_4$ is capable of desulfurizing thiophene and benzothiophene to liberate 1-butene and ethylbenzene, respectively, while it cleaves the C–S bond of dibenzothiophene to give $[\eta^6,\kappa^1\text{-}C_6H_5C_6H_4S]Mo(PMe_3)_2H$. These results demonstrate the ability of molybdenum compounds to serve as models for the hydrodesulfurization process.

The reactivity of $W(PMe_3)_4(\eta^2–CH_2PMe_2)H$, $W(PMe_3)_5H_2$, $W(PMe_3)_4H_4$ and $W(PMe_3)_3H_6$, towards thiophenes has demonstrated that tungsten centers are capable of achieving a variety of transformations relevant to hydrodesulfurization. $W(PMe_3)_4(\eta^2–CH_2PMe_2)H$ cleaves the C–S bond of thiophene to give the butadiene-thiolate complex, $(\eta^5–C_4H_5S)W(PMe_3)_2(\eta^2–CH_2PMe_2)$, that may be subsequently hydrogenated to the butanethiolate complex $W(PMe_3)_4(SBu^n)H_3$. $W(PMe_3)_4(\eta^2–CH_2PMe_2)H$ also cleaves the C–S bond of benzothiophene to give isomeric $(\kappa^1,\eta^2–CH_2CHC_6H_4S)W(PMe_3)_3(\eta^2–CH_2PMe_2)$ and $(\kappa^1,\eta^2–CH_2CC_6H_4S)W(PMe_3)_4$, that may be hydrogenated at room temperature to give the arylthiolate $W(PMe_3)_4(SC_6H_4Et)H_3$ which, upon heating, liberates the hydrodesulfurization product, ethylbenzene. Finally, $W(PMe_3)_4(\eta^2–CH_2PMe_2)H$ is also capable of desulfurizing dibenzothiophene to form the dinuclear dibenzometallacyclopentadiene complex, $[(\kappa^2\text{-}C_{12}H_8)W(PMe_3)](\mu\text{-}S)(\mu\text{-}CH_2PMe_2)\text{-}[W(PMe_3)_3]$. The structural characterization of these compounds, together with their interconversions, provide a foundation for analyzing the reactions that occur on tungsten based HDS catalysts.

4.12 Experimental details

4.12.1 General considerations

All manipulations were performed using a combination of glovebox, high vacuum, and Schlenk techniques under an argon atmosphere unless otherwise specified.[112] Solvents were purified and degassed by standard procedures. ^1H NMR spectra were measured on Bruker 300 DRX, Bruker 300 DPX, Bruker 400 Avance III, Bruker 400 Cyber-enabled Avance III, and Bruker 500 DMX spectrometers. ^1H chemical shifts are reported in ppm relative to $SiMe_4$ ($\delta = 0$) and were referenced internally with respect to the protio solvent impurity (δ 7.16 for C_6D_5H; δ 2.09 for C_7D_7H).[113] ^{13}C NMR spectra are reported in ppm relative to $SiMe_4$ ($\delta = 0$) and were referenced internally with respect to the solvent (δ

128.06 for C_6D_6).[113] ^{31}P chemical shifts are reported in ppm relative to 85% H_3PO_4 ($\delta = 0$) and were referenced using $P(OMe)_3$ ($\delta = 141.0$) as an external standard.[114] Coupling constants are given in hertz. $Mo(PMe_3)_6$,[19] $Mo(PMe_3)_5H_2$[115] and $Mo(PMe_3)_4H_4$[116] were prepared by the literature methods. $W(PMe_3)_4(\eta^2\text{–}CH_2PMe_2)H$, $W(PMe_3)_5H_2$ and $W(PMe_3)_4H_4$ were prepared by the literature methods.[117] $W(PMe_3)_3H_6$ was obtained *via* the photochemical reaction of $W(PMe_3)_4H_4$ with H_2.[118] $W(PMe_3)_4(SH)_2H_2$,[84] $Mo(PMe_3)_4Se_2$,[19] and $Mo(PMe_3)_4Te_2$,[19] were prepared by the literature methods. Thiophene was purchase from Aldrich and dried over molecular sieves prior to use. Benzothiophene and dibenzothiophene were purchased from Aldrich. d_4-Thiophene was purchased from CDN Isotopes and dried over molecular sieves prior to use.

4.12.2 X-ray structure determinations

X-ray diffraction data were collected on a Bruker Apex II diffractometer. Crystal data, data collection and refinement parameters are summarized in Section 4.13, Table 7. The structures were solved using direct methods and standard difference map techniques, and were refined by full-matrix least-squares procedures on F^2 with SHELXTL (Version 6.10).[119]

4.12.3 Computational details

Calculations were carried out using DFT as implemented in the Jaguar 7.5 (release 207) suite of *ab initio* quantum chemistry programs.[120] Geometry optimizations were performed with the B3LYP density functional[121] using the 6-31G** (C, H, P and S) and LACVP (Mo and W) basis sets.[122] The energies of the optimized structures were reevaluated by additional single point calculations on each optimized geometry using cc-pVTZ(-f) correlation consistent triple-ζ basis set for C, H, P, and S and LACV3P for

Mo and W. Molecular orbital analyses were performed with the aid of JIMP2,[83] which employs Fenske-Hall calculations and visualization using MOPLOT.[123]

4.12.4 Reaction of $Mo(PMe_3)_5H_2$ towards thiophene

$Mo(PMe_3)_5H_2$ (50 mg, 0.10 mmol) was placed in an NMR tube equipped with a J. Young valve and treated sequentially with d_6-benzene (*ca*. 0.7 mL) and thiophene (*ca*. 25 μL, 0.31 mmol). The sample was monitored by ^{1}H NMR spectroscopy, thereby demonstrating the formation of small quantities of paramagnetic (κ^2–C_4H_4S)$Mo(PMe_3)_4$ (see below for synthesis). The sample was heated at 60 ˚C for 1 hour and the formation of (η^5–C_4H_4S)$Mo(PMe_3)_3$ and (η^5–C_4H_5S)$Mo(PMe_3)_2(\eta^2$–$CH_2PMe_2)$ was demonstrated by comparison of the ^{1}H NMR spectra with authentic samples.[14]

4.12.5 Reaction of $Mo(PMe_3)_5H_2$ towards d_4-thiophene

(a) A sample of $Mo(PMe_3)_5H_2$ (50 mg, 0.10 mmol) was placed in an NMR tube equipped with a J. Young valve and treated sequentially with d_6-benzene (*ca*. 0.7 mL) and d_4-thiophene (*ca*. 20 μL, 0.24 mmol). The sample was heated at 60 ˚C for 1 hour and monitored by ^{1}H NMR spectroscopy, thereby demonstrating that (*i*) hydrogen was incorporated into the thiophene ring of (η^5–$C_4D_xH_{4-x}S$)$Mo(PMe_3)_3$, (*ii*) hydrogen was incorporated nonselectively into the η^5–butadiene–thiolate ligand of (η^5–$C_4D_{5-x}H_xS$)$Mo(PMe_3)_2(\eta^2$–$CH_2PMe_2)$, and (*iii*) hydrogen is incorporated into the α-position of free thiophene prior to formation of either (η^5–$C_4D_xH_{4-x}S$)$Mo(PMe_3)_3$ or (η^5–$C_4D_{5-x}H_xS$)$Mo(PMe_3)_2(\eta^2$–$CH_2PMe_2)$. The sample was lyophilized, dissolved in d_8-toluene and examined by ^{1}H NMR spectroscopy at –70 ˚C (which increases the chemical shift separation of the α and β-sites), thereby demonstrating that the majority (> 90%) of hydrogen incorporation occurred in the α-position of the thiophene ring.

(b) $Mo(PMe_3)_5H_2$ (15 mg, 0.03 mmol) was placed in an NMR tube equipped with a J. Young valve and treated with protio benzene, C_6H_6, (*ca*. 0.7 mL) followed by addition of d_4-thiophene (*ca*. 10 μL, 0.12 mmol). The sample was heated at 60 ˚C for 1 hour and monitored by ^2H NMR spectroscopy, demonstrating (*i*) that deuterium was incorporated into the PMe_3 ligands (*ii*) and deuterium was incorporated into the hydride site of the $Mo(PMe_3)_4H_4D_{4-x}$ produced in the reaction.

4.12.6 Reaction of $Mo(PMe_3)_6$ towards 2-D-d_1-thiophene

A solution of 2-D-d_1-thiophene in C_6D_6 (*ca*. 0.7 mL, see below) was added to a sample of $Mo(PMe_3)_6$ (10 mg, 0.02 mmol) in an NMR tube equipped with a J. Young valve. The mixture was heated at 60 ˚C for 0.5 hours and monitored by ^1H NMR spectroscopy, thereby demonstrating the formation of $(\eta^5\text{–}C_4H_3DS)Mo(PMe_3)_3$. The sample was lyophilized, dissolved in d_8-toluene and examined by ^1H NMR spectroscopy at –70 ˚C (which increases the chemical shift separation of the α and β-sites), thereby demonstrating that the α-position of the η^5-thiophene ligand was the signal further upfield (α_H: δ = 3.83, β_H: δ = 3.90).

Synthesis of 2-D-d_1-Thiophene. A solution of thiophene (1 mL, 0.0125 mol) in pentane (5 mL) was treated slowly with Bu^nLi (3.7 mL of 2.5 M solution in hexanes, 0.0093 mol, 0.75 equivalents). The solution was stirred for 1.5 hours and then the volatile components were removed *in vacuo* to give a yellow oil. The oil was cooled with an ice bath and D_2O (104 μL, 0.0057 mol, 0.38 equivalents) was added dropwise. After the addition was complete, the mixture was cooled in a dry ice bath (–78 ˚C) and the volatile components were removed *in vacuo*. The mixture was then allowed to thaw and warm to room temperature and the volatile components were vacuum transferred into an ampoule (25 mL) and were treated with d_6-benzene (3 mL). The solution was

examined by ^{1}H NMR spectroscopy which demonstrated the formation of 2-D-d_1-thiophene. ^{1}H NMR (C_6D_6): 6.82 [m, 2H of β-positions of $C_4\underline{H}_3DS$], 6.93 [m, 1H of α-position of $C_4\underline{H}_3DS$].

4.12.7 Synthesis of $(\kappa^2–C_4H_4S)Mo(PMe_3)_4$

A sample of $Mo(PMe_3)_6$ (20 mg, 0.04 mmol) in pentane (*ca*. 1 mL) was treated with thiophene (*ca*. 40 μL, 0.50 mmol), stirred for *ca*. 1 minute and filtered. The filtrate was immediately placed in the freezer (–15 ˚C), thereby depositing dark green needle shaped crystals of $(\kappa^2–C_4H_4S)Mo(PMe_3)_4$ after *ca*. 30 minutes. The mother liquor was decanted and the X–ray diffraction quality crystals were washed with cold (–15 ˚C) pentane (3 × 1 mL), and dried *in vacuo* (3 mg, 17 % yield).

^{1}H NMR (C_6D_6): -17.1 [very broad, 18H of *trans* PMe_3], 8.7 [very broad, 9H of *cis* PMe_3], 10.6 [very broad, 9H of *cis* PMe_3] (due to its facile conversion to $(\eta^5–C_4H_4S)Mo(PMe_3)_3$ and $(\eta^5–C_4H_5S)Mo(PMe_3)_2(\eta^2–CH_2PMe_2)$, $(\kappa^2–C_4H_4S)Mo(PMe_3)_4$ was characterized directly in the reaction mixture; assignment tentative due to paramagnetic nature of the complex).

4.12.8 Conversion of $(\kappa^2–C_4H_4S)Mo(PMe_3)_4$ to $(\eta^5–C_4H_4S)Mo(PMe_3)_3$ and $(\eta^5–C_4H_5S)Mo(PMe_3)_2(\eta^2–CH_2PMe_2)$

(a) A solution of freshly synthesized $(\kappa^2$-$C_4H_4S)Mo(PMe_3)_4$ in d_6-benzene (*ca*. 0.7 mL) was placed in an NMR tube equipped with a J. Young valve. The sample was monitored by ^{1}H NMR spectroscopy, thereby demonstrating that $(\kappa^2$-$C_4H_4S)Mo(PMe_3)_4$ converts rapidly (> 95 % conversion within 5 minutes) to $(\eta^5–C_4H_4S)Mo(PMe_3)_3$ (> 95 %), together with a negligible amount of $(\eta^5–C_4H_5S)Mo(PMe_3)_2(\eta^2–CH_2PMe_2)$.

(b) A sample of freshly synthesized (κ^2-C_4H_4S)$Mo(PMe_3)_4$ was dissolved in a pre-made solution of PMe_3 in d_6-benzene and placed in an NMR tube equipped with a J. Young valve. The sample was monitored by ^1H NMR spectroscopy, thereby demonstrating that, in the presence of PMe_3, (κ^2-C_4H_4S)$Mo(PMe_3)_4$ converts rapidly (*ca*. 75% within 5 minutes, > 95% after 1 hour) to (η^5–C_4H_5S)$Mo(PMe_3)_2(\eta^2$–CH_2PMe_2), together with a small amount of thiophene and $Mo(PMe_3)_6$. Under these conditions, no (η^5–C_4H_4S)$Mo(PMe_3)_3$ could be detected in the ^1H NMR spectrum.

4.12.9 Synthesis of (κ^2–C_4D_4S)$Mo(PMe_3)_4$

A sample of $Mo(PMe_3)_6$ (15 mg, 0.03 mmol) in pentane (*ca*. 1 mL) was treated with d_4-thiophene (*ca*. 20 μL, 0.24 mmol), stirred for *ca*. 1 minute and filtered. The filtrate was immediately placed in the freezer (–15 ˚C), thereby depositing dark green needle shaped crystals of (κ^2–C_4D_4S)$Mo(PMe_3)_4$ after *ca*. 30 minutes. The mother liquor was decanted and the crystals were washed with cold (–15 ˚C) pentane (3 × 1 mL), and dried *in vacuo*.

4.12.10 Conversion of (κ^2–C_4D_4S)$Mo(PMe_3)_4$ to (η^5–C_4D_4S)$Mo(PMe_3)_3$ and (η^5–C_4D_4HS)$Mo(PMe_3)_2(\eta^2$–CH_2PMe_2)

(a) A sample of freshly synthesized crystals of (κ^2-C_4D_4S)$Mo(PMe_3)_4$ was dissolved in a pre-made solution of thiophene (*ca*. 10 μL, 0.13 mmol) in d_6-benzene (*ca*. 0.7 mL) and placed in an NMR tube equipped with a J. Young valve. The sample was monitored by ^1H NMR spectroscopy, thereby demonstrating that (κ^2-C_4D_4S)$Mo(PMe_3)_4$ converts rapidly (> 95 % conversion within 5 minutes) to (η^5–C_4D_4S)$Mo(PMe_3)_3$ (> 95 %), with no indication of any formation of (η^5–C_4H_4S)$Mo(PMe_3)_3$.

(b) A sample of freshly synthesized crystals of (κ^2-C_4D_4S)Mo(PMe_3)$_4$ was dissolved in a pre-made solution of PMe_3 in d_6-benzene (*ca*. 0.7 mL) and placed in an NMR tube equipped with a J. Young valve. The sample was monitored by ^{1}H NMR spectroscopy, thereby demonstrating that, in the presence of PMe_3, (κ^2-C_4D_4S)Mo(PMe_3)$_4$ converts rapidly (*ca*. 75% within 5 minutes, > 95% after 1 hour) to (η^5–C_4D_4HS)Mo(PMe_3)$_2$(η^2–CH_2PMe_2), in which the ^{1}H emanating from the PMe_3 is solely incorporate in the site adjacent to the sulfur.

4.12.11 Reaction of Mo(PMe_3)$_5H_2$ towards benzothiophene

A mixture of Mo(PMe_3)$_5H_2$ (20 mg, 0.04 mmol) and benzothiophene (10 mg, 0.07 mmol) was placed in an NMR tube equipped with a J. Young valve and treated with d_6-benzene (*ca*. 0.7 mL). The sample was heated at 60 ˚C for 1.5 hour and monitored by ^{1}H NMR spectroscopy, thereby demonstrating the formation of (κ^1,η^2–$CH_2CC_6H_4S$)Mo(PMe_3)$_4$, as identified by comparison with that of an authentic sample.[15]

4.12.12 Reaction of Mo(PMe_3)$_4H_4$ towards thiophene

A sample of Mo(PMe_3)$_4H_4$ (50 mg, 0.12 mmol) was placed in an NMR tube equipped with a J. Young valve and treated sequentially with d_6-benzene (*ca*. 0.7 mL) and thiophene (*ca*. 20 μL, 0.25 mmol). The sample was heated at 120 ˚C for *ca*. 2 hours and monitored by ^{1}H NMR spectroscopy, thereby demonstrating the production of 1-butene, together with a small amount of (η^5–C_4H_5S)Mo(PMe_3)$_2$(η^2–CH_2PMe_2).

4.12.13 Reaction of Mo(PMe_3)$_4H_4$ towards d_4-thiophene

(a) A sample of Mo(PMe_3)$_4H_4$ (10 mg, 0.02 mmol) was placed in an NMR tube equipped with a J. Young valve and treated sequentially with d_6-benzene (*ca*. 0.7 mL) and d_4-thiophene (*ca*. 10 μL, 0.12 mmol). The sample was heated at 100 ˚C for 2 hours and

monitored by ^{1}H NMR spectroscopy, thereby demonstrating the incorporation of hydrogen into the α-position of free thiophene.

(b) A sample of $Mo(PMe_3)_4H_4$ (10 mg, 0.02 mmol) was placed in an NMR tube equipped with a J. Young valve and treated sequentially with protio benzene, C_6H_6 (*ca*. 0.7 mL) and d_4-thiophene (*ca*. 10 μL, 0.12 mmol). The sample was heated at 100 ˚C for 2 hour and monitored by ^{2}H NMR spectroscopy, thereby demonstrating that deuterium was incorporated into the PMe_3 ligands and the hydride sites of the $Mo(PMe_3)_4H_4D_{4-x}$.

4.12.14 Reaction of $Mo(PMe_3)_4H_4$ towards thiophene in the presence of mercury

A sample of $Mo(PMe_3)_4H_4$ (20 mg, 0.05 mmol) was placed in a vial and treated sequentially with d_6-benzene (*ca*. 1.4 mL) and thiophene (*ca*. 20 μL, 0.25 mmol). This solution was transferred equally to two NMR tubes equipped with J. Young valves, one of which was treated with a drop of mercury. Both samples were heated at 120 ˚C for *ca*. 12 hours and monitored by ^{1}H NMR spectroscopy, thereby demonstrating that 1-butene was produced in both samples.

4.12.15 Photochemical reaction of $Mo(PMe_3)_4H_4$ towards thiophene

A sample of $Mo(PMe_3)_4H_4$ (10 mg, 0.02 mmol) was placed in an NMR tube equipped with a J. Young valve and treated sequentially with d_6-benzene (*ca*. 0.7 mL) and thiophene (*ca*. 10 μL, 0.12 mmol). The sample was photolyzed (λ_{max} = 350 nm) for 2.5 hours, and monitored by ^{1}H NMR spectroscopy, thereby demonstrating the formation of $(\eta^5\text{–}C_4H_4S)Mo(PMe_3)_3$ and $(\eta^5\text{–}C_4H_5S)Mo(PMe_3)_2(\eta^2\text{–}CH_2PMe_2)$.

4.12.16 Reaction of $Mo(PMe_3)_4H_4$ towards benzothiophene

A mixture of $Mo(PMe_3)_4H_4$ (10 mg, 0.02 mmol) and benzothiophene (5 mg, 0.04 mmol) was placed in an NMR tube equipped with a J. Young valve and treated with d_6-benzene (*ca*. 0.7 mL). The sample was heated at 120 ˚C for *ca*. 2 hours and monitored by ^1H NMR spectroscopy, thereby demonstrating the formation of ethylbenzene.

4.12.17 Reaction of $Mo(PMe_3)_4H_4$ towards benzothiophene in the presence of mercury

A mixture of $Mo(PMe_3)_4H_4$ (20 mg, 0.05 mmol) and benzothiophene (10 mg, 0.07 mmol) was placed in a vial and treated with d_6-benzene (*ca*. 1.4 mL). This solution was transferred equally to two NMR tubes equipped with J. Young valves, one of which was treated with a drop of mercury. Both samples were heated at 120 ˚C for *ca*. 2 hours and monitored by ^1H NMR spectroscopy, thereby demonstrating that ethylbenzene was produced in both samples.

4.12.18 Photochemical reaction of $Mo(PMe_3)_4H_4$ towards benzothiophene

A mixture of $Mo(PMe_3)_4H_4$ (20 mg, 0.05 mmol) and benzothiophene (11 mg, 0.08 mmol) in a small vial was treated with d_6-benzene (*ca*. 1.4 mL). This solution was transferred equally to two NMR tubes equipped with J. Young valves. One sample was then frozen, degassed, allowed to thaw and then charged with H_2 (*ca*. 1 atm). Both samples were then photolyzed (λ_{max} = 350 nm) for 3 hours, demonstrating the formation of $Mo(PMe_3)_4(SC_6H_4Et)H_3$, as identified by comparison with the ^1H NMR spectrum of an authentic sample.[15] The sample charged with H_2 gave $Mo(PMe_3)_4(SC_6H_4Et)H_3$ in greater yield.

4.12.19 Reaction of $Mo(PMe_3)_4H_4$ towards dibenzothiophene

A mixture of $Mo(PMe_3)_4H_4$ (20 mg, 0.05 mmol) and dibenzothiophene (12 mg, 0.07 mmol) was placed in an NMR tube equipped with a J. Young valve and treated with d_6-benzene (*ca*. 0.7 mL). The sample was heated at 120 ˚C for *ca*. 24 hours and monitored by ^1H NMR spectroscopy, thereby demonstrating the formation of $[\eta^6,\kappa^1\text{-}C_6H_5C_6H_4S]Mo(PMe_3)_2H$. Crystals of $[\eta^6,\kappa^1\text{-}C_6H_5C_6H_4S]Mo(PMe_3)_2H$ were obtained by slow evaporation of a pentane solution at –15 ˚C.

^1H NMR (C_6D_6): -4.91 [t, $^2J_{P\text{-}H}$ = 61, 1H of Mo<u>H</u>], 1.23 [d, $^3J_{P\text{-}H}$ = 7, 18H of Mo(P<u>Me</u>$_3$)$_2$], 3.27 [t, $^3J_{H\text{-}H}$ = 5, 1H of η^6-<u>Ph</u>], 4.27 [t, $^3J_{H\text{-}H}$ = 5, 2H of η^6-<u>Ph</u>], 4.45 [d, $^3J_{H\text{-}H}$ = 5, 2H of η^6-<u>Ph</u>], 6.87 [dt, $^5J_{H\text{-}H}$ = 1, $^3J_{H\text{-}H}$ = 7, 1H of $C_6\underline{H}_4$], 6.97 [dt, $^5J_{H\text{-}H}$ = 1, $^3J_{H\text{-}H}$ = 7, 1H of $C_6\underline{H}_4$], 7.26 [dd, $^5J_{H\text{-}H}$ = 1, $^3J_{H\text{-}H}$ = 7, 1H of $C_6\underline{H}_4$], 7.78 [d, $^3J_{H\text{-}H}$ = 7, 1H of $C_6\underline{H}_4$]. $^{31}P\{^1H\}$ NMR (C_6D_6): 6.9 [part of AB quartet, $^2J_{P\text{-}P}$ = 42, 1P of Mo(<u>P</u>Me$_3$)$_2$], 7.4 [part of AB quartet, $^2J_{P\text{-}P}$ = 42, 1P of Mo(<u>P</u>Me$_3$)$_2$].

4.12.20 Synthesis of $(\eta^5\text{–}C_4H_5S)W(PMe_3)_2(\eta^2\text{–}CH_2PMe_2)$

A solution of $W(PMe_3)_4(\eta^2\text{–}CH_2PMe_2)H$ (50 mg, 0.09 mmol) in d_6-benzene (*ca.* 0.7 mL) in an NMR tube equipped with a J. Young valve was treated with thiophene (*ca.* 0.1 mL, 1.2 mmol). The sample was heated at 60 ˚C for 16 hours and monitored by ^1H NMR spectroscopy, thereby demonstrating conversion to $(\eta^5\text{–}C_4H_5S)W(PMe_3)_2(\eta^2\text{–}CH_2PMe_2)$ in *ca.* 20 % yield. The solution was lyophilized giving a dark black solid residue that was extracted into pentane (*ca.* 2 mL). The extract was placed at –15 ˚C for 1 week, thereby depositing yellow crystals of $(\eta^5\text{-}C_4H_5S)W(PMe_3)_2(\eta^2\text{-}CH_2PMe_2)$. The mother liquor was decanted and the crystals were washed with cold pentane (*ca*. 2 × 1 mL) and dried *in vacuo* (6 mg, 14% yield). Crystals of $(\eta^5\text{–}C_4H_5S)W(PMe_3)_2(\eta^2\text{–}CH_2PMe_2)$ suitable for X-ray diffraction were obtained from pentane at –15 ˚C.

^{1}H NMR (C_6D_6): 0.23 [br m, 2H of (η^2-C$\underline{H}_2$PMe$_2$)], 0.82 [d, $^2J_{P\text{-}H}$ = 9, 3H of (η^2-CH$_2$P$\underline{Me}_2$)], 1.16 [d, peak under adjacent peak so can not report coupling, 3H of (η^2-CH$_2$P$\underline{Me}_2$)], 1.19 [d, $^2J_{P\text{-}H}$ = 6, 9H of (P$\underline{Me}_3$)$_2$], 1.32 [d, $^2J_{P\text{-}H}$ = 8, 9H of (P$\underline{Me}_3$)$_2$], 1.92 [d, $^3J_{H\text{-}H}$ = 6, 1H of SCHCHCHC$\underline{H}_2$], 2.67 [br, 1H of SCHCHCHC$\underline{H}_2$], 3.70 [d, $^3J_{H\text{-}H}$ = 8, 1H of SCHCHC$\underline{H}$CH$_2$], 5.04 [t, $^3J_{H\text{-}H}$ = 6, 1H of SCHC$\underline{H}$CHCH$_2$], 5.74 [d, $^3J_{H\text{-}H}$ = 6, 1H of SC$\underline{H}$CHCHCH$_2$] (the assignments are supported by HSQC spectroscopy). ^{31}P{^{1}H} NMR (C_6D_6): -75.3 [dd, $^2J_{P\text{-}P}$ = 65, $^2J_{P\text{-}P}$ = 6, 1P of W(η^2-CH$_2$PMe$_2$)], -29.5 [dd, $^2J_{P\text{-}P}$ = 19, $^2J_{P\text{-}P}$ = 6, 1P of W(PMe$_3$)$_2$], -15.4 [dd, $^2J_{P\text{-}P}$ = 63, $^2J_{P\text{-}P}$ = 19, 1P of W(PMe$_3$)$_2$] (the assignments are supported by ^{31}P–^{1}H HMBC spectroscopy). ^{13}C{^{1}H} NMR (C_6D_6): -15.7 [m, 1C of (η^2-$\underline{C}$H$_2$PMe$_2$)], 10.1 [d, $^1J_{P\text{-}C}$ = 15, 1C of (η^2-CH$_2$P$\underline{Me}_2$)], 19.2 [d, $^1J_{P\text{-}C}$ = 25, 1C of (η^2-CH$_2$P$\underline{Me}_2$)], 21.5 [d, $^1J_{P\text{-}C}$ = 23, 3C of (P$\underline{Me}_3$)$_2$], 24.8 [dd, $^1J_{P\text{-}C}$ = 29, $^1J_{P\text{-}C}$ = 7, 3C of (P$\underline{Me}_3$)$_2$], 49.1 [t, $^2J_{P\text{-}C}$ = 10, 1C of SCHCHCH$\underline{C}$H$_2$], 88.1 [s, 1C of SCHCH$\underline{C}$HCH$_2$], 88.3 [s, 1C of S$\underline{C}$HCHCHCH$_2$], 111.9 [s, 1C of SCH$\underline{C}$HCHCH$_2$] (the assignments are supported by HSQC spectroscopy).

4.12.21 Reaction of W(PMe$_3$)$_4$(η^2–CH$_2$PMe$_2$)H towards d$_4$-thiophene

A solution of W(PMe$_3$)$_4$(η^2–CH$_2$PMe$_2$)H (10 mg, 0.02 mmol) in C_6D_6 (*ca.* 0.7 mL) in an NMR tube equipped with a J. Young valve was treated with d$_4$-thiophene (*ca.* 20 μL, 0.24 mmol). The sample was heated at 60 ˚C for 21 hours and monitored by ^{1}H NMR spectroscopy, thereby demonstrating the formation of (η^5–C$_4$D$_4$HS)W(PMe$_3$)$_2$(η^2–CH$_2$PMe$_2$), in which the hydrogen (^{1}H) derived from the cyclometallated PMe$_3$ is incorporated only into the CH group adjacent to sulfur. The sample was lyophilized, dissolved in C_6H_6 (*ca.* 0.7 mL) and analyzed by ^{2}H NMR spectroscopy, thereby providing additional evidence that there was no deuterium (^{2}H) incorporation into the CH group adjacent to sulfur.

4.12.22 Synthesis of $W(PMe_3)_4(\kappa^1\text{-}C_\alpha\text{-}C_4H_3S)H_3$

A solution of $W(PMe_3)_5H_2$ (20 mg, 0.04 mmol) in d_6-benzene (*ca*. 0.7 mL) in an NMR tube equipped with a J. Young valve was treated with thiophene (*ca*. 20 μL, 0.25 mmol) and heated at 80 ˚C. The reaction was monitored by ^1H NMR spectroscopy, thereby demonstrating the formation of $W(PMe_3)_4(\kappa^1\text{-}C_\alpha\text{-}C_4H_3S)H_3$ after a period of 6 hours. The solution was lyophilized and the solid obtained was extracted into pentane (2 mL) and placed at –15 ˚C, thereby depositing colorless crystals of $W(PMe_3)_4(\kappa^1\text{-}C_\alpha\text{-}C_4H_3S)H_3$ suitable for X–ray diffraction. The crystals were isolated, washed with cold pentane (-15 ˚C) and dried *in vacuo* giving $W(PMe_3)_4(\kappa^1\text{-}C_\alpha\text{-}C_4H_3S)H_3$ (15 mg, 74% yield). Anal. calcd. for $W(PMe_3)_4(\kappa^1\text{-}C_\alpha\text{-}C_4H_3S)H_3$: C, 33.5 %, H, 7.4 %. Found: C, 33.0 %, H, 6.9 %.

^1H NMR (C_6D_6): –3.98 [br m, 2H of $W\underline{H}_3$], -0.56 [br d, $^2J_{P\text{-}H}$ = 74, 1H of $W\underline{H}_3$], 1.24 [vt, $^2J_{P\text{-}H}$ =6, 18H of $W(P\underline{Me}_3)_4$], 1.53 [d, $^2J_{P\text{-}H}$ = 7, 18H of $W(P\underline{Me}_3)_4$], 7.20 [m, 2H of $C_4\underline{H}_3S$], 7.59 [d, $^3J_{H\text{-}H}$ = 2, 1 H of $C_4\underline{H}_3S$]. $^{31}P\{^1H\}$ NMR (C_6D_6): -43.4 [br, 1P of $W(\underline{P}Me_3)_4$], -30.8 [t, $^2J_{P\text{-}P}$ = 19, $^1J_{W\text{-}P}$ = 178, 2P of $W(\underline{P}Me_3)_4$], -18.4 [br, 1P of $W(\underline{P}Me_3)_4$].

4.12.23 Reaction of $W(PMe_3)_5H_2$ towards d_4-thiophene

A solution of $W(PMe_3)_5H_2$ (20 mg, 0.04 mmol) in d_6-benzene (*ca*. 0.7 mL) in an NMR tube equipped with a J. Young valve was treated with d_4-thiophene (*ca*. 20 μL, 0.25 mmol). The sample was heated at 60 ˚C for 18 hours, and monitored by ^1H NMR spectroscopy, thereby indicating that there was no hydrogen (^1H) incorporation into free d_4-thiophene.

4.12.24 Synthesis of $W(PMe_3)_4(SBu^n)H_3$

A solution of $W(PMe_3)_4(\eta^2\text{–}CH_2PMe_2)H$ (60 mg, 0.11 mmol) in benzene (5 mL) in an ampoule was treated with thiophene (*ca.* 0.2 mL, 2.5 mmol). The mixture was treated with H_2 (*ca*. 1 atm) and heated at 60 ˚C for 1 day. After this period, the sample was

lyophilized to give a dark black solid (53 mg) which, on the basis of ^{1}H NMR spectroscopy consists of $W(PMe_3)_4(SBu^n)H_3$ (85%), $W(PMe_3)_3H_6$ (5%) and $W(PMe_3)_4H_4$ (10%). Correspondingly, the yield of $W(PMe_3)_4(SBu^n)H_3$ is 76%.

^{1}H NMR (C_6D_6): –4.26 [m, 2H of W$\underline{H}_3$], –0.46 [m, 1H of W$\underline{H}_3$], 1.01 [t, $^3J_{H\text{-}H}$ = 8, 3H of $SCH_2CH_2CH_2C\underline{H}_3$], 1.36 [d, $^2J_{P\text{-}H}$ = 7, 9H of W(P$\underline{Me}_3)_4$], 1.52 [d, $^2J_{P\text{-}H}$ = 8, 9H of W(P$\underline{Me}_3)_4$], 1.60 [vt, $^2J_{P\text{-}H}$ = 6, 18H of W(P$\underline{Me}_3)_4$], 1.67 [m, 2H of $SCH_2CH_2C\underline{H}_2CH_3$], 1.96 [m, 2H of $SCH_2C\underline{H}_2CH_2CH_3$], 3.01 [t, $^3J_{H\text{-}H}$ = 8, 2H of $SC\underline{H}_2CH_2CH_2CH_3$]. ^{31}P{^{1}H} NMR ($C_6D_6$): -36.7 [dt, $^2J_{P\text{-}P}$ = 28, $^2J_{P\text{-}P}$ = 16, 1P of $W(PMe_3)_4$], -33.7 [t, $^2J_{P\text{-}P}$ = 17, $^1J_{W\text{-}P}$ = 182, 2P of $W(PMe_3)_4$], -16.6 [dt, $^2J_{P\text{-}P}$ = 28, $^2J_{P\text{-}P}$ = 17, 1P of $W(PMe_3)_4$]. ^{13}C{^{1}H} NMR (C_6D_6): 14.6 [s, 1C of $SCH_2CH_2CH_2\underline{C}H_3$], 23.2 [s, 1C of $SCH_2CH_2\underline{C}H_2CH_3$], 24.5 [vt, $^1J_{P\text{-}C}$ = 24, 6C of W(P$\underline{Me}_3)_4$], 25.3 [d, $^1J_{P\text{-}C}$ = 23, 3C of W(P$\underline{Me}_3)_4$], 32.3 [d, $^1J_{P\text{-}C}$ = 30, 3C of W(P$\underline{Me}_3)_4$], 40.2 [s, 1C of $SCH_2\underline{C}H_2CH_2CH_3$], 44.1 [dd, $^3J_{P\text{-}C}$ = 16, $^3J_{P\text{-}C}$ = 5, 1C of $S\underline{C}H_2CH_2CH_2CH_3$] (the assignments are supported by HSQC spectroscopy).

4.12.25 Reactivity of $W(PMe_3)_4(SBu^n)H_3$ towards benzoic acid

A solution of $W(PMe_3)_4(SBu^n)H_3$ (10 mg, 0.02 mmol) in d_6-benzene (*ca*. 0.7 mL) was added to a sample of benzoic acid (8 mg, 0.07 mmol) in an NMR tube equipped with a J. Young valve. The solution was analyzed by ^{1}H NMR spectroscopy, thereby demonstrating the immediate liberation of Bu^nSH, which was identified by comparison of the ^{1}H NMR spectrum with that of an authentic sample.

4.12.26 Elimination of 1-butene from $W(PMe_3)_4(SBu^n)H_3$

A solution of $W(PMe_3)_4(SBu^n)H_3$ (5 mg, 0.01 mmol) in d_6-benzene (*ca*. 0.7 mL) in an NMR tube equipped with a J. Young valve was heated at 100 °C and monitored by ^{1}H NMR spectroscopy, thereby demonstrating that $W(PMe_3)_4(SBu^n)H_3$ produces, *inter alia*,

1-butene over a period of 18 hours. The presence of 1-butene was confirmed by comparison of the ^{1}H NMR spectrum with that of an authentic sample.

4.12.27 Reaction of $W(PMe_3)_3H_6$ towards thiophene: formation of $W(PMe_3)_4(SBu^n)H_3$

A solution of $W(PMe_3)_3H_6$ (5 mg, 0.01 mmol) in d_6-benzene (*ca*. 0.7 mL) in an NMR tube equipped with a J. Young valve was treated with thiophene (*ca*. 20 μL, 0.25 mmol). The sample was heated at 80 ˚C for 5 hours and monitored by ^{1}H NMR spectroscopy, thereby demonstrating the formation of $W(PMe_3)_4(SBu^n)H_3$. Furthermore, ^{1}H NMR spectroscopy demonstrated the incorporation of deuterium into both the α and β sites of free thiophene.

4.12.28 Reaction of $W(PMe_3)_3H_6$ towards thiophene in the presence of PMe_3

A solution of $W(PMe_3)_3H_6$ (5 mg, 0.01 mmol) in d_6-benzene (*ca*. 0.7 mL) in an NMR tube equipped with a J. Young valve was treated with thiophene (*ca*. 20 μL, 0.25 mmol) and PMe_3 (*ca*. 0.05 mL). The sample was heated at 80 ˚C monitored by ^{1}H NMR spectroscopy, thereby demonstrating the formation of $W(PMe_3)_4H_4$ over a period of 4 hours. $W(PMe_3)_4(SBu^n)H_3$ was not observed under these conditions.

4.12.29 Photochemical reaction of $W(PMe_3)_4H_4$ with thiophene: H/D exchange between thiophene and C_6D_6

A solution of $W(PMe_3)_4H_4$ (5 mg, 0.01 mmol) in d_6-benzene (*ca*. 0.7 mL) in an NMR tube equipped with a J. Young valve was treated with thiophene (*ca*. 20 μL, 0.25 mmol). The sample was photolyzed (λ_{max} = 350 nm) for 2.5 hours and monitored by ^{1}H NMR spectroscopy, thereby demonstrating the incorporation of deuterium into both the α and β sites of free thiophene. In addition, $W(PMe_3)_4H_4$ converted to $W(PMe_3)_3H_6$ and $W(PMe_3)_4(\kappa^1\text{-}C_\alpha\text{-}C_4H_3S)H_3$ (*ca*. 5:1).

4.12.30 Photochemical reaction of $W(PMe_3)_4H_4$ towards thiophene in the presence of PMe_3

A solution of $W(PMe_3)_4H_4$ (10 mg, 0.02 mmol) in d_6-benzene (*ca*. 1.4 mL) was treated with thiophene (*ca*. 40 μL, 0.50 mmol) and divided equally into two NMR tubes equipped with J. Young valves, one of which was treated with PMe_3 (*ca*. 0.05 mL). Both samples were photolyzed (λ_{max} = 350 nm) for 2.5 hours, and analyzed by ^1H NMR spectroscopy, thereby demonstrating that PMe_3 inhibited the incorporation of deuterium into free thiophene.

4.12.31 Reaction of $(\eta^5\text{-}C_4H_5S)W(PMe_3)_2(\eta^2\text{-}CH_2PMe_2)$ towards H_2: formation of $W(PMe_3)_4(SBu^n)H_3$

A solution of $(\eta^5\text{-}C_4H_5S)W(PMe_3)_2(\eta^2\text{-}CH_2PMe_2)$ (5 mg, 0.01 mmol) in d_6-benzene (*ca*. 0.7 mL) in an NMR tube equipped with a J. Young valve was treated with H_2 (*ca*. 1 atm). The sample was then heated at 60 °C and monitored by ^1H NMR spectroscopy, thereby demonstrating the formation of $W(PMe_3)_4(SBu^n)H_3$ after *ca*. 18 hours.

4.12.32 Reaction of $(\eta^5\text{-}C_4H_5S)W(PMe_3)_2(\eta^2\text{-}CH_2PMe_2)$ towards H_2 in the presence of PMe_3

A solution of $(\eta^5\text{-}C_4H_5S)W(PMe_3)_2(\eta^2\text{-}CH_2PMe_2)$ (5 mg, 0.01 mmol) in d_6-benzene (*ca*. 0.7 mL) in an NMR tube equipped with a J. Young valve was treated with PMe_3 (*ca*. 0.05 mL) and then was charged with H_2 (*ca*. 1 atm). The sample was then heated at 80 °C for 3 hours, and monitored by ^1H NMR spectroscopy, indicating that the formation of $W(PMe_3)_4(SBu^n)H_3$ is not prevented by PMe_3.

4.12.33 Reactivity of $(\eta^5\text{-}C_4H_5S)Mo(PMe_3)_2(\eta^2\text{-}CH_2PMe_2)$ towards H_2

A solution of $(\eta^5\text{-}C_4H_5S)Mo(PMe_3)_2(\eta^2\text{-}CH_2PMe_2)$ (5 mg, 0.01 mmol) in d_6-benzene (*ca*. 0.7 mL) in an NMR tube equipped with a J. Young valve was treated with H_2 (*ca*. 1 atm). The sample was monitored by ^1H NMR spectroscopy, which indicated that no hydrogenation occurs after 60 ˚C for 3 hours, 80 ˚C for 3 hours, 100 ˚C for 3 hours, and 120 ˚C for 12 hours.

4.12.34 Reaction of $(\eta^5\text{-}C_4H_5S)M(PMe_3)_2(\eta^2\text{-}CH_2PMe_2)$ [M = W and Mo] towards H_2

A mixture of $(\eta^5\text{-}C_4H_5S)W(PMe_3)_2(\eta^2\text{-}CH_2PMe_2)$ (6 mg, 0.01 mmol) and $(\eta^5\text{-}C_4H_5S)Mo(PMe_3)_2(\eta^2\text{-}CH_2PMe_2)$ (5 mg, 0.01 mmol) was placed in an NMR tube equipped with a J. Young valve and treated with d_6-benzene (*ca*. 0.7 mL) and mesitylene (*ca*. 1 μL) as an internal integration standard. The sample was charged with H_2 (*ca*. 1 atm) and heated at 80 ˚C. The reaction was monitored by ^1H NMR spectroscopy, thereby indicating that, under identical conditions, the tungsten complex, $(\eta^5\text{-}C_4H_5S)W(PMe_3)_2(\eta^2\text{-}CH_2PMe_2)$, converts to $W(PMe_3)_4(SBu^n)H_3$ while the molybdenum compound $(\eta^5\text{-}C_4H_5S)Mo(PMe_3)_2(\eta^2\text{-}CH_2PMe_2)$ is inert to hydrogenation.

4.12.35 Reactivity of $W(PMe_3)_4(\kappa^1\text{-}C_\alpha\text{-}C_4H_3S)H_3$ towards PMe_3

A sample of $W(PMe_3)_4(\kappa^1\text{-}C_\alpha\text{-}C_4H_3S)H_3$ (10 mg, 0.02 mmol) in an NMR tube equipped with a J. Young valve was treated with PMe_3 (*ca*. 0.1 mL) and heated at 80 ˚C for 2 hours. After this period, the volatile components were removed *in vacuo* and the solid obtained was dissolved in d_6-benzene (*ca*. 0.7 mL) and analyzed by ^1H NMR spectroscopy, thereby demonstrating that no $W(PMe_3)_5H_2$ had formed.

4.12.36 Reactivity of $W(PMe_3)_4(\kappa^1\text{-}C_\alpha\text{-}C_4H_3S)H_3$ towards H_2

A solution of $W(PMe_3)_4(\kappa^1\text{-}C_\alpha\text{-}C_4H_3S)H_3$ (5 mg, 0.01 mmol) in d_6-benzene (*ca*. 0.7 mL) in an NMR tube equipped with a J. Young valve was treated with H_2 (*ca*. 1 atm). The sample was heated at 80 ˚C for 3 hours and monitored by ^1H NMR spectroscopy, thereby demonstrating the formation of a mixture of $W(PMe_3)_4(SBu^n)H_3$ (*ca*. 60%), $W(PMe_3)_3H_6$ (*ca*. 40%), and free thiophene.

4.12.37 Reactivity of $W(PMe_3)_4(\kappa^1\text{-}C_\alpha\text{-}C_4H_3S)H_3$ towards H_2 in the presence of PMe_3

A solution of $W(PMe_3)_4(\kappa^1\text{-}C_\alpha\text{-}C_4H_3S)H_3$ (10 mg, 0.02 mmol) in d_6-benzene (*ca*. 1.4 mL) was transferred equally to two NMR tubes equipped with J. Young valves, one of which was treated with PMe_3 (*ca*. 0.05 mL). The samples were charged with H_2 (*ca*. 1 atm) and heated at 80 ˚C. The reactions were monitored by ^1H NMR spectroscopy, thereby indicating that, in the absence of PMe_3, $W(PMe_3)_4(\kappa^1\text{-}C_\alpha\text{-}C_4H_3S)H_3$ converted completely to $W(PMe_3)_4(SBu^n)H_3$ and $W(PMe_3)_3H_6$, whereas in the presence of PMe_3, the production of $W(PMe_3)_4(SBu^n)H_3$ is inhibited (*ca*. 30% conversion), and there is no formation of $W(PMe_3)_3H_6$.

4.12.38 Photochemical reaction of $W(PMe_3)_4(\kappa^1\text{-}C_\alpha\text{-}C_4H_3S)H_3$ towards H_2

$W(PMe_3)_4(\kappa^1\text{-}C_\alpha\text{-}C_4H_3S)H_3$ (5 mg, 0.01 mmol) was added to an NMR tube equipped with a J. Young valve and treated with d_6-benzene (*ca*. 0.7 mL). The sample was treated with H_2 (*ca*. 1 atm) and photolyzed (λ_{max} = 350 nm) for 2.5 hours. The reaction was monitored by ^1H NMR spectroscopy, indicating that $W(PMe_3)_3H_6$, free thiophene, and $W(PMe_3)_4(SBu^n)H_3$ formed.

4.12.39 Synthesis of $(\kappa^1,\eta^2\text{–}CH_2CHC_6H_4S)W(PMe_3)_3(\eta^2\text{–}CH_2PMe_2)$

$W(PMe_3)_4(\eta^2\text{–}CH_2PMe_2)H$ (30 mg, 0.05 mmol) and benzothiophene (10 mg, 0.07 mmol) was added to an NMR tube equipped with a J. Young valve. The sample was heated at 60 ˚C for 3 hrs. After this period, the tube was pumped down *in vacuo* and the residue was extracted with pentane (2 mL), and filtered into a small vial. The filtrate was allowed to evaporate slowly over a period of 2 days, thereby depositing orange X-ray quality crystals of $(\kappa^1,\eta^2\text{–}CH_2CHC_6H_4S)W(PMe_3)_3(\eta^2\text{–}CH_2PMe_2)$. The crystals were washed with cold pentane (–15 ˚C) and dried *in vacuo*, giving pure $(\kappa^1,\eta^2\text{–}CH_2CHC_6H_4S)W(PMe_3)_3(\eta^2\text{–}CH_2PMe_2)$ (5 mg, 15 % yield). Mass Spectrum (FAB+): m/z = 622.01 $\{M^+\}$.

^1H NMR (C_6D_6): 0.60 [very br, 1H of $W(\eta^2\text{-}C\underline{H}_2PMe_2)$], 0.94 [d, $^2J_{P\text{-}H}$ = 8, 6H of $W(\eta^2\text{-}CH_2P\underline{Me}_2)$], 1.09 [very br, 9H of $W(P\underline{Me}_3)$], 1.30 [d, $^2J_{P\text{-}H}$ = 7, 9H of $W(P\underline{Me}_3)$], 1.33 [br d, $^2J_{P\text{-}H}$ = 4, 9H of $W(P\underline{Me}_3)$], 1.80 [br m, 1H of $(\kappa^1,\eta^2\text{-}C\underline{H}_2CHC_6H_4S)$], 2.08 [br m, 1H of $(\kappa^1,\eta^2\text{-}C\underline{H}_2CHC_6H_4S)$], 3.76 [br m, 1H of $(\kappa^1,\eta^2\text{-}CH_2C\underline{H}C_6H_4S)$], 6.91 [m, 2H of $(\kappa^1,\eta^2\text{-}CH_2CHC_6\underline{H}_4S)$], 7.40 [d, $^3J_{H\text{-}H}$ = 7, 1H of $(\kappa^1,\eta^2\text{-}CH_2CHC_6\underline{H}_4S)$], 7.60 [d, $^3J_{H\text{-}H}$ = 7, 1H of $(\kappa^1,\eta^2\text{-}CH_2CHC_6\underline{H}_4S)$], 1H of $W(\eta^2\text{-}C\underline{H}_2PMe_2)$ not observed. $^{31}P\{^1H\}$ NMR (C_6D_6): -87.7 [br, 1P of $W(\eta^2\text{-}CH_2\underline{P}Me_2)$], -45.6 [br, 1P of $W(\underline{P}Me_3)_3$], -34.5 [br, 1P of $W(\underline{P}Me_3)_3$], -33.8 [br, 1P of $W(\underline{P}Me_3)_3$].

4.12.40 Synthesis of $(\kappa^1,\eta^2\text{–}CH_2CC_6H_4S)W(PMe_3)_4$

A mixture of $W(PMe_3)_4(\eta^2\text{–}CH_2PMe_2)H$ (30 mg, 0.05 mmol) and benzothiophene (10 mg, 0.07 mmol) in an NMR tube equipped with a J. Young valve and treated with d_6-benzene (*ca*. 0.7 mL). The sample was heated at 60 ˚C for 18 hours and analyzed by ^1H NMR spectroscopy, thereby demonstrating the formation of, *inter alia*, $(\kappa^1,\eta^2\text{–}CH_2CC_6H_4S)W(PMe_3)_4$, on the basis based on similarity of the ^1H and ^{31}P NMR spectra to those of the molybdenum counterpart, $(\kappa^1,\eta^2\text{–}CH_2CC_6H_4S)Mo(PMe_3)_4$.[15] $(\kappa^1,\eta^2\text{–}$

$CH_2CHC_6H_4S)W(PMe_3)_3(\eta^2–CH_2PMe_2)$ was only observed in small quantities under these conditions.

4.12.41 Synthesis of $(\kappa^1,\eta^2–CH_2CHC_6H_4S)W(PMe_3)_4H$ and $W(PMe_3)_4(\kappa^1\text{-}C_\alpha\text{-}CCHSC_6H_4)H_3$

(a) A mixture of $W(PMe_3)_5H_2$ (20 mg, 0.04 mmol) and benzothiophene (6 mg, 0.04 mmol) was placed in an NMR tube equipped with a J. Young valve and treated with d_6-benzene (*ca*. 0.7 mL). The sample was heated at 80 ˚C for 6 hours and monitored by ^{1}H NMR spectroscopy, thereby demonstrating the formation of $(\kappa^1,\eta^2–CH_2CHC_6H_4S)W(PMe_3)_4H$ and $W(PMe_3)_4(\kappa^1\text{-}C_\alpha\text{-}CCHSC_6H_4)H_3$ (the approximate ratio of products is 9:1). After this period, the solution was lyophilized, extracted into pentane (2 mL), filtered and placed at –15 ˚C, thereby depositing orange crystals suitable for X–ray diffraction. The crystals were washed with cold pentane (–15 ˚C) and dried *in vacuo* giving $(\kappa^1,\eta^2–CH_2CHC_6H_4S)W(PMe_3)_4H$ (6 mg, 27% yield). Mass spectrum (FAB+): *m*/*z* = 549.06 $\{M^+ + 1 – PMe_3\}$.

^{1}H NMR (C_6D_6): –4.05 [ddt, $^2J_{P\text{-}H}$ = 105, $^2J_{P\text{-}H}$ = 76, $^2J_{P\text{-}H}$ = 14, 1H of W–H], 0.98 [d, $^2J_{P\text{-}H}$ = 6, 9H of $W(P\underline{Me}_3)_4$], 1.27 [very br, 9H of $W(P\underline{Me}_3)_4$], 1.40 [d, $^2J_{P\text{-}H}$ = 7, 9H of $W(P\underline{Me}_3)_4$], 1.47 [d, $^2J_{P\text{-}H}$ = 5, 9H of $W(P\underline{Me}_3)_4$], 1.47 [1H of $(\kappa^1,\eta^2\text{-}C\underline{H}_2CHC_6H_4S)$; coincident with a PMe_3 signal and located *via* a 2D COSY experiment], 1.86 [m, 1H of $(\kappa^1,\eta^2\text{-}C\underline{H}_2CHC_6H_4S)$], 3.02 [m, 1H of $(\kappa^1,\eta^2\text{-}CH_2C\underline{H}C_6H_4S)$], 6.84 [dt, $^4J_{H\text{-}H}$ = 1, $^3J_{H\text{-}H}$ = 7, 1H of $(\kappa^1,\eta^2\text{-}CH_2CHC_6\underline{H}_4S)$], 6.90 [dt, $^4J_{H\text{-}H}$ = 1, $^3J_{H\text{-}H}$ = 7, 1H of $(\kappa^1,\eta^2\text{-}CH_2CHC_6\underline{H}_4S)$], 7.32 [dd, $^4J_{H\text{-}H}$ = 1, $^3J_{H\text{-}H}$ = 7, 1H of $(\kappa^1,\eta^2\text{-}CH_2CHC_6\underline{H}_4S)$], 7.62 [dd, $^4J_{H\text{-}H}$ = 1, $^3J_{H\text{-}H}$ = 7, 1H of $(\kappa^1,\eta^2\text{-}CH_2CHC_6\underline{H}_4S)$]. $^{31}P\{^1H\}$ NMR (C_6D_6): –39.5 [m, 1P of $W(\underline{P}Me_3)_4$], –34.0 [m, 2P of $W(\underline{P}Me_3)_4$], –33.0 [m, 1P of $W(\underline{P}Me_3)_4$].

(b) A mixture of $W(PMe_3)_5H_2$ (20 mg, 0.04 mmol) and benzothiophene (6 mg, 0.04 mmol) was placed in an NMR tube equipped with a J. Young valve and treated with PMe_3 (*ca*. 0.2 mL). The sample was heated at 80 ˚C for 18 hours, after which period the volatile components were removed *in vacuo*. The residue was dissolved in d_6-benzene and analyzed by ^1H NMR spectroscopy, thereby demonstrating the formation of a *ca*. 2:1 mixture of $W(PMe_3)_4(\kappa^1\text{-}C_\alpha\text{-}CCHSC_6H_4)H_3$ and $(\kappa^1,\eta^2\text{–}CH_2CHC_6H_4S)W(PMe_3)_4H$, in addition to unreacted $W(PMe_3)_5H_2$ and benzothiophene (*ca.* 30%). The solution was lyophilized and the solid obtained was extracted into pentane (1 mL) and placed at –15 ˚C, thereby depositing large orange X-ray quality crystals of $(\kappa^1,\eta^2\text{–}CH_2CHC_6H_4S)W(PMe_3)_4H$ and several small colorless X-ray quality crystals of $W(PMe_3)_4(\kappa^1\text{-}C_\alpha\text{-}CCHSC_6H_4)H_3$, which were separated by hand and used for X-ray diffraction.

^1H NMR of $W(PMe_3)_4(\kappa^1\text{-}C_\alpha\text{-}CCHSC_6H_4)H_3$ (C_6D_6): –3.97 [m, 2H of $W\underline{H}_3$], –0.48 [br d, $^2J_{P\text{-}H}$ = 70, 1H of $W\underline{H}_3$], 1.22 [vt, $^2J_{P\text{-}H}$ = 6, 18H of $W(P\underline{Me}_3)_4$], 1.53 [under $W(PMe_3)_5H_2$ signal, 18H of $W(P\underline{Me}_3)_4$], 7.05 [t, $^3J_{H\text{-}H}$ = 7, 1H of $(\kappa^1\text{-}C_\alpha\text{-}CCHSC_6\underline{H}_4)$], 7.25 [t, $^3J_{H\text{-}H}$ = 7, 1H of $(\kappa^1\text{-}C_\alpha\text{-}CCHSC_6\underline{H}_4)$], 7.79 [d, $^3J_{H\text{-}H}$ = 8, 1H of $(\kappa^1\text{-}C_\alpha\text{-}CCHSC_6\underline{H}_4)$], 7.89 [d, $^3J_{H\text{-}H}$ = 7, 1H of $(\kappa^1\text{-}C_\alpha\text{-}CCHSC_6\underline{H}_4)$], 1H of $(\kappa^1\text{-}C_\alpha\text{-}CC\underline{H}SC_6H_4)$ not identified (assignments are tentative because the compound was only obtained in significant quantities as a component of a mixture).

4.12.42 Synthesis of $W(PMe_3)_4(SC_6H_4Et)H_3$

(a) A mixture of $W(PMe_3)_4(\eta^2\text{–}CH_2PMe_2)H$ (50 mg, 0.09 mmol) and benzothiophene (12 mg, 0.09 mmol) in an ampoule was treated with benzene (3 mL) and charged with H_2 (*ca*. 1 atm). The mixture was heated at 80 ˚C for 12 hours. After this period, the solution was lyophilized to give a light green solid (27 mg) which, on the basis of ^1H NMR spectroscopy consists of $W(PMe_3)_4(SC_6H_4Et)H_3$, $W(PMe_4)_4H_4$ and benzothiophene (*ca*.

5:4:1 ratio). Correspondingly, the yield of $W(PMe_3)_4(SC_6H_4Et)H_3$ is 31%. Colorless X-ray quality crystals of $W(PMe_3)_4(SC_6H_4Et)H_3$ were obtained from a solution in pentane at -15 ˚C. $W(PMe_3)_4(SC_6H_4Et)H_3$ can also be obtained quantitatively by addition of H_2 to $(\kappa^1,\eta^2\text{–}CH_2CHC_6H_4S)W(PMe_3)_3(\eta^2\text{–}CH_2PMe_2)$ (*vide infra*).

^{1}H NMR (C_6D_6): –4.12 [quintet, $^2J_{P\text{-}H}$ = 41, 2H of W$\underline{H}_3$], –0.12 [dt, $^2J_{P\text{-}H}$ = 89, $^2J_{P\text{-}H}$ = 22, 1H of W$\underline{H}_3$], 1.39 [m, 27H of W(P$\underline{Me}_3)_4$], 1.53 [t, $^3J_{H\text{-}H}$ = 8, 3H of $SC_6H_4\underline{Et}$], 1.55 [d, $^3J_{P\text{-}H}$ = 7, 9H of W(P$\underline{Me}_3)_4$], 3.38 [q, $^3J_{H\text{-}H}$ = 7, 2H of $SC_6H_4\underline{Et}$], 7.00 [t, $^3J_{H\text{-}H}$ = 8, 1H of $SC_6\underline{H}_4Et$], 7.23 [m, 2H of $SC_6\underline{H}_4Et$], 8.66 [d, $^3J_{H\text{-}H}$ = 8, 1H of $SC_6\underline{H}_4Et$]. $^{31}P\{^1H\}$ NMR (C_6D_6): -36.7 [dt, $^2J_{P\text{-}P}$ = 29, $^2J_{P\text{-}P}$ = 15, 1P of $W(PMe_3)_4$], -31.1 [t, $^2J_{P\text{-}P}$ = 17, $^1J_{W\text{-}P}$ = 182, 2P of $W(PMe_3)_4$], -15.5 [dt, $^2J_{P\text{-}P}$ = 30, $^2J_{P\text{-}P}$ = 18, 1P of $W(PMe_3)_4$]. Mass Spectrum (FAB+): m/z = 629.1 $\{M^+ + 1\}$.

(b) A mixture of $W(PMe_3)_3H_6$ (5 mg, 0.01 mmol) and benzothiophene (5 mg, 0.04 mmol) was placed in an NMR tube equipped with a J. Young valve and treated with d_6-benzene (*ca*. 0.7 mL). The sample was heated at 60 ˚C for 18 hours and monitored by ^{1}H NMR spectroscopy, thereby indicating the formation of $W(PMe_3)_4(SC_6H_4Et)H_3$.

(c) A mixture of $W(PMe_3)_4H_4$ (10 mg, 0.02 mmol) and benzothiophene (5 mg, 0.04 mmol) was placed in an NMR tube equipped with a J. Young valve and treated with d_6-benzene (*ca*. 0.7 mL). The sample was photolyzed (λ_{max} = 350 nm) for 3 hours, and monitored by ^{1}H NMR spectroscopy, thereby indicating the formation of $W(PMe_3)_4(SC_6H_4Et)H_3$ and $(\kappa^1,\eta^2\text{–}CH_2CHC_6H_4S)W(PMe_3)_4H$ (in a ratio of *ca*. 1:1), together with a small quantity of $W(PMe_3)_3H_6$ (< 10%). The sample was then charged with H_2 (*ca*. 1 atm), and $(\kappa^1,\eta^2\text{–}CH_2CHC_6H_4S)W(PMe_3)_4H$ converted to $W(PMe_3)_4(SC_6H_4Et)H_3$ over a period of several hours at room temperature.

4.12.43 Reactivity of $(\kappa^1,\eta^2\text{–}CH_2CHC_6H_4S)W(PMe_3)_3(\eta^2\text{–}CH_2PMe_2)$ and $(\kappa^1,\eta^2\text{-}CH_2CC_6H_4S)W(PMe_3)_4$ towards H_2

(a) A solution of $(\kappa^1,\eta^2\text{–}CH_2CHC_6H_4S)W(PMe_3)_3(\eta^2\text{–}CH_2PMe_2)$ (5 mg, 0.01 mmol) in d_6-benzene (*ca*. 0.7 mL) in an NMR tube equipped with a J. Young valve was treated with H_2 (*ca*. 1 atm). The sample was monitored by ^1H NMR spectroscopy, thereby demonstrating that $(\kappa^1,\eta^2\text{–}CH_2CHC_6H_4S)W(PMe_3)_3(\eta^2\text{–}CH_2PMe_2)$ converts to $W(PMe_3)_4(SC_6H_4Et)H_3$ over a period of *ca*. 30 minutes at room temperature.

(b) Although $(\kappa^1,\eta^2\text{-}CH_2CC_6H_4S)W(PMe_3)_4$ has not been isolated in pure form (*vide supra*), a sample in d_6-benzene that contains $(\kappa^1,\eta^2\text{-}CH_2CC_6H_4S)W(PMe_3)_4$ was prepared *via* the reaction of $W(PMe_3)_4(\eta^2\text{–}CH_2PMe_2)H$ with benzothiophene, and was treated with H_2 (*ca*. 1 atm.). The sample was monitored by ^1H NMR spectroscopy, thereby demonstrating that $(\kappa^1,\eta^2\text{-}CH_2CC_6H_4S)W(PMe_3)_4$ converts to $W(PMe_3)_4(SC_6H_4Et)H_3$ over a period of *ca*. 30 minutes at room temperature.

4.12.44 Reaction of $(\kappa^1,\eta^2\text{-}CH_2CHC_6H_4S)W(PMe_3)_4H$ towards H_2

A solution of $(\kappa^1,\eta^2\text{-}CH_2CHC_6H_4S)W(PMe_3)_4H$ (5 mg, 0.01 mmol) in d_6-benzene (*ca*. 0.7 mL) in an NMR tube equipped with a J. Young valve was treated with H_2 (*ca*. 1 atm). The sample was monitored by ^1H NMR spectroscopy, thereby demonstrating that $(\kappa^1,\eta^2\text{-}CH_2CHC_6H_4S)W(PMe_3)_4H$ converts to $W(PMe_3)_4(SC_6H_4Et)H_3$ over a period of *ca*. 30 minutes at room temperature.

4.12.45 Elimination of ethylbenzene from $W(PMe_3)_4(SC_6H_4Et)H_3$

A solution of $W(PMe_3)_4(SC_6H_4Et)H_3$ (5 mg, 0.01 mmol) in d_6-benzene (*ca*. 0.7 mL) in an NMR tube equipped with a J. Young valve was heated at 100 °C and monitored by ^1H NMR spectroscopy, thereby demonstrating that $W(PMe_3)_4(SC_6H_4Et)H_3$ produces, *inter*

alia, ethylbenzene over a period of 20 hours. The presence of ethylbenzene was confirmed by comparison of the ^{1}H NMR spectrum with that of an authentic sample.

4.12.46 Synthesis of $[(\kappa^2\text{-}C_{12}H_8)W(PMe_3)](\mu\text{-}S)(\mu\text{-}CH_2PMe_2)(\mu\text{-}PMe_2)[W(PMe_3)_3]$

A mixture of $W(PMe_3)_4(\eta^2\text{–}CH_2PMe_2)H$ (50 mg, 0.09 mmol) and dibenzothiophene (15 mg, 0.08 mmol) was placed in an NMR tube equipped with a J. Young valve. The sample was heated at 100 ˚C for 18 hours, after which period the volatile components were removed *in vacuo*. The black solid residue was extracted with pentane (2 mL), filtered and the filtrate was cooled at –15 ˚C for 3 days. Several different amorphous solids were deposited after this period, one of which was a dark green solid. The dark green solid was hand separated (in air) and returned to an argon glove box. The sample was extracted into pentane (1 mL), filtered, and cooled at –15 ˚C for 1 day, thereby depositing dark green X-ray quality crystals of $[(\kappa^2\text{-}C_{12}H_8)W(PMe_3)](\mu\text{-}S)(\mu\text{-}CH_2PMe_2)(\mu\text{-}PMe_2)[W(PMe_3)_3]$ (2 mg, 5% yield). Mass spectrum (FAB+): m/z = 992.0 $\{M^+\}$, 916.0 $\{M^+ - PMe_3\}$, 840.0 $\{M^+ - 2PMe_3\}$.

^{1}H NMR (C_6D_6): –2.33 [br m, $^2J_{H\text{-}H}$ = 13, 1H of (μ-C$\underline{H}_2$PMe$_2$)], –1.52 [br m, $^2J_{H\text{-}H}$ = 13, 1H of (μ-C$\underline{H}_2$PMe$_2$)], 0.39 [d, $^2J_{P\text{-}H}$ = 5, 3H of (μ-P$\underline{Me}_2$)], 0.50 [d, $^2J_{P\text{-}H}$ = 6, 3H of (μ-P$\underline{Me}_2$)], 0.63 [d, $^2J_{P\text{-}H}$ = 6, 9H of (P$\underline{Me}_3$)], 1.49 [d, $^2J_{P\text{-}H}$ = 6, 9H of (P$\underline{Me}_3$)], 1.49 [3H of (μ-P$\underline{Me}_2$); coincident with a PMe_3 signal; assignment is based on integration and is tentative], 1.58 [d, $^2J_{P\text{-}H}$ = 6, 9H of (P$\underline{Me}_3$)], 1.66 [d, $^2J_{P\text{-}H}$ = 8, 9H of (P$\underline{Me}_3$)], 1.99 [d, $^2J_{P\text{-}H}$ = 8, 3H of (μ-P$\underline{Me}_2$)], 6.11 [d, $^3J_{H\text{-}H}$ = 6, 1H of (κ^2-$C_{12}\underline{H}_8$)], 6.29 [t, $^3J_{H\text{-}H}$ = 7, 1H of (κ^2-$C_{12}\underline{H}_8$)], 7.16 [1H of (κ^2-$C_{12}\underline{H}_8$); coincident with the C_6D_5H signal and located *via* a 2D COSY experiment], 7.45 [t, $^3J_{H\text{-}H}$ = 7, 1H of (κ^2-$C_{12}\underline{H}_8$)], 7.50 [dt, $^4J_{H\text{-}H}$ = 1, $^3J_{H\text{-}H}$ = 7, 1H of (κ^2-$C_{12}\underline{H}_8$)], 7.56 [d, $^3J_{H\text{-}H}$ = 7, 1H of (κ^2-$C_{12}\underline{H}_8$)], 7.79 [d, $^3J_{H\text{-}H}$ = 8, 1H of (κ^2-$C_{12}\underline{H}_8$)], 8.23 [dd, $^4J_{H\text{-}H}$ = 1, $^3J_{H\text{-}H}$ = 7, 1H of (κ^2-$C_{12}\underline{H}_8$)].

4.12.47 Elimination of biphenyl from $[(\kappa^2\text{-}C_{12}H_8)W(PMe_3)](\mu\text{-}S)(\mu\text{-}CH_2PMe_2)(\mu\text{-}PMe_2)\text{-}[W(PMe_3)_3]$ in the presence of H_2

A sample of freshly crystallized $[(\kappa^2\text{-}C_{12}H_8)W(PMe_3)](\mu\text{-}S)(\mu\text{-}CH_2PMe_2)(\mu\text{-}PMe_2)[W(PMe_3)_3]$ (5 mg, 0.01 mmol) was treated with d_6-benzene (*ca*. 0.7 mL) and placed in an NMR tube equipped with a J. Young valve. The sample was charged with H_2 (*ca*. 1 atm) and heated at 60 ˚C. The reaction was monitored by ^{1}H NMR spectroscopy, thereby demonstrating that $[(\kappa^2\text{-}C_{12}H_8)W(PMe_3)](\mu\text{-}S)(\mu\text{-}CH_2PMe_2)(\mu\text{-}PMe_2)[W(PMe_3)_3]$ produces biphenyl over a period of 1.5 hours. The presence of biphenyl was confirmed by comparison of the ^{1}H NMR spectrum with that of an authentic sample. Further confirmation that the sample contained biphenyl was obtained by lyophilizing the sample and analyzing the ^{1}H NMR spectrum in $CDCl_3$.

4.12.48 Reactivity of $W(PMe_3)_3H_6$ towards dibenzothiophene

A mixture of $W(PMe_3)_3H_6$ (5 mg, 0.01 mmol) and dibenzothiophene (5 mg, 0.03 mmol) was placed in an NMR tube equipped with a J. Young valve and treated with d_6-benzene (*ca*. 0.7 mL). The sample was heated at 60 ˚C and monitored by ^{1}H NMR spectroscopy, thereby demonstrating that deuterium was fully incorporated into the 4 and 6 positions of free dibenzothiophene after a period of 2 hours. The sample was then heated at 80 ˚C for 2 more hours, thereby demonstrating that deuterium was fully incorporated into the 2, 3, 7 and 8 positions of dibenzothiophene. The sample was lyophilized, dissolved in C_6H_6 (*ca*. 0.7 mL) and analyzed by ^{2}H NMR spectroscopy, thereby confirming the incorporation of deuterium into the 2, 3, 4, 6, 7 and 8 positions.[124]

4.12.49 Photochemical reaction of $W(PMe_3)_4H_4$ towards dibenzothiophene

A mixture of $W(PMe_3)_4H_4$ (5 mg, 0.01 mmol) and dibenzothiophene (5 mg, 0.03 mmol) was placed in an NMR tube equipped with a J. Young valve and treated with d_6-

benzene (*ca*. 0.7 mL). The sample was photolyzed (λ_{max} = 350 nm) for 2.5 hours, and monitored by ^{1}H NMR spectroscopy, thereby demonstrating that deuterium was incorporated into the 2, 3, 4, 6, 7 and 8 positions of free dibenzothiophene.

4.12.50 Synthesis of $W_8S_{16}(PMe_3)_{10}$

$W(PMe_3)_4S_2$ (50 mg, 0.09 mmol) and benzene (*ca*. 0.7 mL) were added to an NMR tube equipped with a J. Young valve and heated at 80 ˚C for *ca*. 18 hours, thereby depositing black needle shaped crystals of $W_8S_{16}(PMe_3)_{10}$, which were of sufficient quality for an X-ray diffraction study. The mixture was diluted with pentane (2 mL) and shaken, and the crystals were allowed to settle to the bottom of the NMR tube. The mother liquor was then decanted and the crystals were washed with pentane (3 × 2 mL), and then dried *in vacuo* giving $W_8S_{16}(PMe_3)_{10}\bullet(C_6H_6)_{0.1667}$ as dark black needle-shaped crystals (8 mg, 26% isolated yield).[125] Anal. calcd. for $W_8S_{16}(PMe_3)_{10}\bullet(C_6H_6)_{0.1667}$: C, 13.50 %, H, 3.33 %. Found: C, 13.68 %, H, 3.10 %.

IR Data (KBr disk, cm^{-1}): 2969 (m), 2901 (s), 2796 (w), 2539 (w), 2360 (w), 2340 (w), 2237 (w), 1997 (w), 1942 (w), 1613 (w), 1412 (s), 1298 (s), 1277 (s), 949 (vs), 848 (m), 729 (m), 670 (m), 615 (w), 443 (s) [ν(W=S)], 423 (s) [ν(W=S)]. *When trying to obtain ^{1}H NMR spectroscopic data for $W_8S_{16}(PMe_3)_{10}$ in C_6D_6, a doublet (28 Hz) at 3.66 ppm was observed, which is similar to the doublet observed for the SH signal in $Mo_4S_6(PMe_3)_6(SH)_2$. Thus, it is possible that this signal corresponds to a small impurity present, but the molecular assignment of $W_8S_{16}(PMe_3)_{10}$ is, therefore, tentative.*

4.12.51 Structural characterization of $Mo_4S_6(PMe_3)_6(SH)_2$

$Mo(PMe_3)_6$ (250 mg, 0.45 mmol) and benzene (*ca*. 10 mL) were added to an ampoule. The suspension was frozen at –198 ˚C, degassed and allowed to thaw. H_2S (*ca*. 1 atm) was then added, and the suspension was stirred for 1 hour, after which period the H_2S

atmosphere was removed and replaced by argon. The green mixture was allowed to sit at room temperature for 1 day, thereby depositing large black crystals of $Mo_4S_6(PMe_3)_6(SH)_2$, which were of sufficient quality for an X-ray diffraction study.

^{1}H NMR (C_6D_6): 1.46 [m, 36H of 2 Mo(P<u>Me</u>$_3$)$_2$], 1.78 [d, $^2J_{P\text{-}H}$ = 8, 18H of 2 Mo(P<u>Me</u>$_3$)], 2.74 [d, $^3J_{P\text{-}H}$ = 28, 2H of 2 Mo(S<u>H</u>)$_2$, coupling supported by a selective heteronuclear decoupling (^{1}H{^{31}P}) experiment]. ^{31}P{^{1}H} NMR (C_6D_6): –24.0 [t, $J_{P\text{-}P}$ = 6, 4P of 2 Mo(<u>P</u>Me$_3$)$_2$], 2.2 [quint, $J_{P\text{-}P}$ = 6, 2P of 2 Mo(<u>P</u>Me$_3$)]. IR Data (KBr disk, cm^{-1}): 2968 (m), 2901 (s), 2797 (w), 2515 (w) [ν(SH)], 2501 (w) [ν(SH)], 2002 (w), 1477 (w), 1416 (m), 1297 (m), 1278 (s), 950 (vs), 847 (w), 724 (m), 670 (m), 457 (w), 422 (m).

4.12.52 Synthesis of $Mo_3Se_5(PMe_3)_6$

$Mo(PMe_3)_6$ (50 mg, 0.09 mmol), selenium powder (18 mg, 0.23 mmol) and d_6-benzene (*ca*. 0.7 mL) were mixed in a vial for *ca*. 5 minutes, and then allowed to stand at room temperature for *ca*. 2 hours. The mixture was then filtered into an NMR tube equipped with a J. Young valve and analyzed by ^{1}H NMR spectroscopy, thereby demonstrating the formation of $Mo(PMe_3)_4Se_2$.[19] The sample was then heated at 80 ˚C for *ca*. 18 hours, thereby depositing black crystals of $Mo_3Se_5(PMe_3)_6$, which were of sufficient quality for an X-ray diffraction study. The mother liquor was decanted and the crystals were washed with pentane (3 × 2 mL), and then dried *in vacuo* giving $Mo_3Se_5(PMe_3)_6$ as dark black block-shaped crystals (18 mg, 52% isolated yield). Anal. calcd. for $Mo_3Se_5(PMe_3)_6$: C, 18.98 %, H, 4.78 %. Found: C, 18.94 %, H, 4.36 %.

^{1}H NMR (C_6D_6): 1.54 [s, 54H of (P<u>Me</u>$_3$)$_6$]. ^{1}H NMR ($CDCl_3$): 1.59 [br s, 54H of (P<u>Me</u>$_3$)$_6$]. *The assignment is tentative due to the quick decomposition observed in the $CDCl_3$ solvent. The ^{1}H NMR spectrum was obtained immediately (< 5 min) after $CDCl_3$ was added to the $Mo_3Se_5(PMe_3)_6$ crystals, but it is possible that the 1.59 ppm signal corresponds to another species in solution. It should be noted that the ^{1}H NMR spectrum of $Mo_3S_5(PMe_3)_6$ was reported*

as a broad singlet at 1.4 ppm in $CDCl_3$.[103] $^{31}P\{^1H\}$ NMR (C_6D_6): –15.0 [s, 6P of $(\underline{P}Me_3)_6$]. [IR Data (KBr disk, cm^{-1}): 2962 (m), 2895 (s), 2791 (w), 2359 (w), 2335 (w), 2214 (w), 1995 (w), 1939 (w), 1410 (s), 1295 (s), 1273 (s), 943 (s), 846 (m), 719 (s), 665 (s).

4.12.53 Structural characterization of $Mo_3Te_5(PMe_3)_6$

$Mo(PMe_3)_6$ (50 mg, 0.09 mmol), tellurium powder (28 mg, 0.22 mmol), PMe_3 (*ca*. 0.05 mL) and d_6-benzene (*ca*. 0.7 mL) were mixed in a vial for *ca*. 5 minutes, and then allowed to stand at room temperature for *ca*. 2 hours. The mixture was then filtered into an NMR tube equipped with a J. Young valve and analyzed by ^1H NMR spectroscopy, thereby demonstrating the formation of $Mo(PMe_3)_4Te_2$.[19] The sample was then heated at 80 ˚C for *ca*. 18 hours, thereby depositing black block-shaped crystals of $Mo_3Te_5(PMe_3)_6$, which were of sufficient quality for an X-ray diffraction study. The mother liquor was decanted and the crystals were washed with pentane (3 × 2 mL), and then dried *in vacuo* giving $Mo_3Te_5(PMe_3)_6$ as dark black block-shaped crystals, in addition to needle-shaped crystals, the molecular structure of which have not yet been identified (6 mg total).

4.13 Crystallographic data

Table 7. Crystal, intensity collection and refinement data.

	(κ^2–C_4H_4S)Mo(PMe_3)$_4$	**[η^6,κ^1-$C_6H_5C_6H_4S$]Mo(PMe_3)$_2$H**
lattice	Tetragonal	Monoclinic
formula	$C_{16}H_{40}MoP_4S$	$C_{18}H_{28}MoP_2S$
formula weight	484.36	434.34
space group	$P4_2nm$	$P2_1/c$
a/Å	15.815(6)	10.3741(12)
b/Å	15.815(6)	28.891(3)
c/Å	9.552(4)	12.8569(15)
α/°	90	90
β/°	90	92.947(2)
γ/°	90	90
V/Å^3	2389.1(16)	3848.4(8)
Z	4	8
temperature (K)	150(2)	125(2)
radiation (λ, Å)	0.71073	0.71073
ρ (calcd.) g cm^{-3}	1.347	1.499
μ (Mo Kα), mm^{-1}	0.901	0.951
θ max, deg.	29.12	30.52
no. of data collected	9774	61434
no. of data	3332	11726
no. of parameters	122	416
R_1 [$I > 2\sigma(I)$]	0.0639	0.0542
wR_2 [$I > 2\sigma(I)$]	0.1435	0.0656
R_1 [all data]	0.1042	0.2142
wR_2 [all data]	0.1625	0.0954
GOF	1.009	0.673

Table 7 (cont). Crystal, intensity collection and refinement data.

	$(\eta^5\text{-}C_4H_5S)W(PMe_3)_2(\eta^2\text{-}CH_2PMe_2)$	$W(PMe_3)_4(\kappa^1\text{-}C_\alpha\text{-}C_4H_3S)H_3$
lattice	Orthorhombic	Orthorhombic
formula	$C_{13}H_{31}P_3SW$	$C_{16}H_{42}P_4SW$
formula weight	496.20	574.29
space group	*Pna2₁*	*Pccn*
a / Å	21.784(3)	16.282(3)
b / Å	10.1799(13)	32.499(6)
c / Å	8.4941(10)	9.1520(16)
α / °	90	90
β / °	90	90
γ / °	90	90
V / Å^3	1883.6(4)	4842.9(15)
Z	4	8
temperature (K)	125(2)	149(2)
radiation (λ, Å)	0.71073	0.71073
ρ (calcd.) g cm^{-3}	1.750	1.575
μ (Mo Kα), mm^{-1}	6.483	5.118
θ max, deg.	32.66	30.51
no. of data collected	31414	74148
no. of data	6622	7388
no. of parameters	185	237
R_1 [$I > 2\sigma(I)$]	0.0264	0.0276
wR_2 [$I > 2\sigma(I)$]	0.0430	0.0535
R_1 [all data]	0.0391	0.0386
wR_2 [all data]	0.0456	0.0568
GOF	1.001	1.042

Table 7 (cont). Crystal, intensity collection and refinement data.

	(κ^1,η^2-$CH_2CHC_6H_4S$)-$W(PMe_3)_3(\eta^2$–CH_2PMe_2)	**(κ^1,η^2–$CH_2CHC_6H_4S$)-$W(PMe_3)_4H$**
lattice	Monoclinic	Monoclinic
formula	$C_{20}H_{42}P_4SW$	$C_{20}H_{44}P_4SW$
formula weight	622.33	624.34
space group	$P2_1/c$	$P2_1/n$
a/Å	14.6865(16)	18.507(2)
b/Å	19.500(2)	15.220(2)
c/Å	18.620(2)	19.118(3)
α/°	90	90
β/°	105.020(2)	98.724(2)
γ/°	90	90
V/Å^3	5150.4(10)	5322.9(12)
Z	8	8
temperature (K)	150(2)	150(2)
radiation (λ, Å)	0.71073	0.71073
ρ (calcd.) g cm^{-3}	1.605	1.558
μ (Mo Kα), mm^{-1}	4.820	4.664
θ max, deg.	31.00	30.03
no. of data collected	59799	82546
no. of data	16375	15571
no. of parameters	491	500
R_1 [$I > 2\sigma(I)$]	0.0420	0.0514
wR_2 [$I > 2\sigma(I)$]	0.0994	0.1065
R_1 [all data]	0.0514	0.0786
wR_2 [all data]	0.1050	0.1178
GOF	1.046	1.038

Table 7 (cont). Crystal, intensity collection and refinement data.

	$W(PMe_3)_4(SC_6H_4Et)H_3$	$W(PMe_3)_4(\kappa^1\text{-}C_\alpha\text{-}CCHSC_6H_4)H_3$
lattice	Triclinic	Triclinic
formula	$C_{20}H_{48}P_4SW$	$C_{20}H_{44}P_4SW$
formula weight	628.37	624.34
space group	*P-1*	*P-1*
a/Å	9.6343(11)	8.9970(13)
b/Å	12.1821(14)	10.0679(15)
c/Å	13.5960(15)	15.782(2)
α/°	85.772(2)	80.769(2)
β/°	72.371(2)	73.792(2)
γ/°	68.5870(10)	84.386(2)
V/Å^3	1414.6(3)	1352.8(3)
Z	2	2
temperature (K)	125(2)	150(2)
radiation (λ, Å)	0.71073	0.71073
ρ (calcd.) g cm^{-3}	1.475	1.533
μ (Mo Kα), mm^{-1}	4.387	4.587
θ max, deg.	30.63	30.51
no. of data collected	22975	21808
no. of data	8664	8217
no. of parameters	260	285
R_1 [$I > 2\sigma(I)$]	0.0239	0.0434
wR_2 [$I > 2\sigma(I)$]	0.0493	0.0685
R_1 [all data]	0.0290	0.0688
wR_2 [all data]	0.0508	0.0750
GOF	1.013	1.022

Table 7 (cont). Crystal, intensity collection and refinement data.

	[(κ²-$C_{12}H_8$)W(PMe_3)](μ-S)(μ-CH_2PMe_2)(μ-PMe_2)[W(PMe_3)$_3$]	**W(PMe_3)$_4$(SeBu^n)H_3**
lattice	Monoclinic	Triclinic
formula	$C_{29}H_{58}P_6SW_2$	$C_{16}H_{48}P_4SeW$
formula weight	992.33	627.23
space group	$P2_1/n$	$P\text{-}1$
a / Å	10.2637(11)	9.7057(19)
b / Å	21.784(2)	16.128(3)
c / Å	16.7801(18)	17.245(3)
α / °	90	91.621(3)
β / °	94.326(2)	99.820(3)
γ / °	90	92.254(3)
V / Å^3	3741.0(7)	2656.2(9)
Z	4	4
temperature (K)	150(2)	150(2)
radiation (λ, Å)	0.71073	0.71073
ρ (calcd.) g cm^{-3}	1.762	1.568
μ (Mo Kα), mm^{-1}	6.475	5.958
θ max, deg.	31.50	30.03
no. of data collected	63207	41389
no. of data	12439	15463
no. of parameters	366	442
R_1 [$I > 2\sigma(I)$]	0.0253	0.0599
wR_2 [$I > 2\sigma(I)$]	0.0517	0.0629
R_1 [all data]	0.0371	0.1748
wR_2 [all data]	0.0556	0.0816
GOF	1.017	0.944

Table 7 (cont). Crystal, intensity collection and refinement data.

	$W_8S_{16}(PMe_3)_{10}$	$Mo_4S_6(PMe_3)_6(SH)_2$
lattice	Rhombohedral	Monoclinic
formula	$C_{35.06}H_{95.06}P_{10}S_{16}W_8$	$C_{30}H_{68}Mo_4P_6S_8$
formula weight	2810.32	1254.90
space group	*R-3*	$P2_1/n$
a / Å	39.2644(17)	11.4556(4)
b / Å	39.2644(17)	13.7281(5)
c / Å	14.7948(6)	16.5880(6)
α / °	90	90
β / °	90	98.6920(10)
γ / °	120	90
V / Å^3	19753.2(15)	2578.73(16)
Z	9	2
temperature (K)	125(2)	200(2)
radiation (λ, Å)	0.71073	0.71073
ρ (calcd.) g cm^{-3}	2.126	1.616
μ (Mo Kα), mm^{-1}	11.020	1.482
θ max, deg.	30.53	30.60
no. of data collected	53019	41259
no. of data	13418	7915
no. of parameters	311	231
R_1 [$I > 2\sigma(I)$]	0.0378	0.0232
wR_2 [$I > 2\sigma(I)$]	0.0955	0.0485
R_1 [all data]	0.0639	0.0314
wR_2 [all data]	0.1053	0.0519
GOF	1.123	1.044

Table 7 (cont). Crystal, intensity collection and refinement data.

	$Mo_3Se_5(PMe_3)_6$	$Mo_3Te_5(PMe_3)_6$
lattice	Monoclinic	Monoclinic
formula	$C_{18}H_{54}Mo_3P_6Se_5$	$C_{18}H_{54}Mo_3P_6Te_5$
formula weight	1139.05	1382.25
space group	*C2/c*	*C2/c*
a / Å	19.5484(17)	20.219(5)
b / Å	11.1863(10)	11.559(3)
c / Å	51.077(4)	50.748(12)
α / °	90	90
β / °	90.3430(10)	90.208(3)
γ / °	90	90
V / Å^3	11168.9(17)	11861(5)
Z	12	12
temperature (K)	200(2)	200(2)
radiation (λ, Å)	0.71073	0.71073
ρ (calcd.) g cm^{-3}	2.032	2.322
μ (Mo Kα), mm^{-1}	6.151	4.806
θ max, deg.	28.28	28.28
no. of data collected	75153	60884
no. of data	13826	14734
no. of parameters	461	461
R_1 [$I > 2\sigma(I)$]	0.0648	0.0598
wR_2 [$I > 2\sigma(I)$]	0.1257	0.1124
R_1 [all data]	0.0720	0.0876
wR_2 [all data]	0.1277	0.1211
GOF	1.375	1.113

4.14 References and notes

(1) (a) Stirling, D. *The Sulfur Problem: Cleaning up Industrial Feedstocks*; RSC Clean Technology Monographs (2000).

(b) Brunet, S.; Mey, D.; Pérot, G.; Bouchy, C.; Diehl, F. *Appl. Catal., A: General* **2005**, *278*, 143-172.

(c) Mochida, I.; Choi, K.-H. *J. Jap. Pet. Inst.* **2004**, *47*, 145-163.

(d) Choudhary, T. V. *Ind. Eng. Chem. Res.* **2007**, *46*, 8363-8370.

(e) Startsev, A. N. *Catal. Today* **2009**, *144*, 350–357.

(f) Startsev, A. N. *Catal. Rev. Sci. Eng.* **1995**, *37*, 353-423.

(2) Sánchez–Delgado, R. A. *Organometallic Modelling of the Hydrodesulfurization and Hydrodenitrogenation Reactions*, Kluwer Academic Publishers, Boston, 2002.

(3) Sánchez–Delgado, R. A. *Comprehensive Organometallic Chemistry III*, Volume 1, Chapter 27; Crabtree, R. H. and Mingos, D. M. P. (Eds), Elsevier, Oxford, 2006.

(4) Angelici, R. J. *Organometallics* **2001**, *20*, 1259-1275.

(5) (a) Topsøe, H.; Clausen, B. S.; Massoth, F. E. *Hydrotreating Catalysis* in *Catalysis: Science and Technology;* Anderson, J. R.; Boudart, M. (eds.) Vol 11, Springer-Verlag, New York, 1996.

(b) Furimsky, E. *Catal Rev. Sci. Eng.* **1980**, *22*, 371-400.

(c) Ancheyta, J.; Rana, M. S.; Furimsky, E. *Catal. Today* **2005**, *109*, 3-15.

(6) (a) Rao, K. S.; Dhar, G. M. *J. Catal.* **1989**, *115*, 277-281.

(b) Lee, D. K.; Lee, I. C.; Park, S. K.; Bae, S. Y.; Woo, S. I. *J. Catal.* **1996**, *159*, 212-218.

(c) Lee, D. K.; Lee, H. T.; Lee, I. C.; Park, S. K.; Bae, S. Y.; Kim, C. H.; Woo, S. I. *J. Catal.* **1996**, *159*, 219-229.

(d) Alonso, G.; Chianelli, R. R. *J. Catal.* **2004**, *221*, 657-661.

(7) Startsev, A. N.; Zakharov, I. I. *Russ. Chem. Rev.* **2003**, *72*, 517-536.

(8) Sadimenko, A. P. *Adv. Heterocyclic Chem.* **2001**, *78*, 1-64.

(9) For review articles concerned with modeling HDS, see:

(a) Angelici, R. J. *Polyhedron* **1997**, *16*, 3073-3088.

(b) Bianchini, C.; Meli, A.; Vizza, F. *J. Organomet. Chem.* **2004**, *689*, 4277-4290.

(c) Bianchini, C.; Meli, A. *Acc. Chem. Res.* **1998**, *31*, 109-116.

(d) Brorson, M.; King, J. D.; Kiriakidou, K.; Prestopino, F.; Nordlander, E. *Metal Clusters in Chemistry* **1999**, *2*, 741-781.

(e) References 2,3 and 4.

(10) Sattler, A.; Janak, K. E.; Parkin, G. *Inorg. Chim. Acta* **2011**, *369*, 197-202.

(11) Sattler, A.; Parkin, G. *J. Am. Chem. Soc.* **2011**, *133*, 3748-3751.

(12) Churchill, D. G.; Bridgewater, B. M.; Parkin, G. *J. Am. Chem. Soc.* **2000**, *122*, 178-179.

(13) Churchill, D. G.; Bridgewater, B. M.; Zhu, G.; Pang, K.; Parkin, G. *Polyhedron* **2006**, *25*, 499-512.

(14) Janak, K. E.; Tanski, J. M.; Churchill, D. G.; Parkin, G. *J. Am. Chem. Soc.* **2002**, *124*, 4182-4183.

(15) Buccella, D.; Janak, K. E.; Parkin, G. *J. Am. Chem. Soc.* **2008**, *130*, 16187-16189.

(16) C–S Cleavage of 2-cyanothiophene has been shown to occur prior to isomerization to a thienyl–cyanide derivative, thereby providing another example of facile reversibility of the C–S cleavage of thiophenes. See: Grochowski, M. R.; Li, T.; Brennessel, W. W.; Jones, W. D. *J. Am. Chem. Soc.* **2010**, *132*, 12412–12421.

(17) The identification of the ^{1}H NMR spectroscopic signals of the α- and β-sites of the η^5–thiophene ligand of $(\eta^5\text{–}C_4H_4S)Mo(PMe_3)_3$ were identified by using 2-D-d_1-thiophene.

(18) ^{2}H NMR spectroscopy demonstrates that deuterium is incorporated into the PMe_3 ligands, in addition to the hydride site of $Mo(PMe_3)_4H_4$, which is also formed during the reaction.

(19) Murphy, V. J.; Parkin, G. *J. Am. Chem. Soc.* **1995**, *117*, 3522-3528.

(20) Gibson, V. C.; Graimann, C. E.; Hare, P. M.; Green, M. L. H.; Bandy, J. A.; Grebenik, P. D.; Prout, K. *J. Chem. Soc., Dalton Trans.* **1985**, 2025-2035.

(21) The deuterium is incorporated into both hydride and PMe_3 sites.

(22) The formation of 1-butene is not prevented if the reaction is carried out in the presence of mercury.

(23) Curtis, M. D. *Appl. Organomet. Chem.* **1992**, *6*, 429-436.

(24) Riaz, U.; Curnow, O.; Curtis, M. D. *J. Am. Chem. Soc.* **1991**, *113*, 1416-1417.

(25) Small quantities (< 5%) of (η^5–C_4H_5S)Mo(PMe_3)$_2$(η^2–CH_2PMe_2) have been observed by ^{1}H NMR spectroscopy.

(26) The formation of ethylbenzene is not prevented in the presence of mercury.

(27) Daly, F. P. *J. Catal.* **1978**, *51*, 221-228.

(28) Jones, W. D.; Chin, R. M. *J. Am. Chem. Soc.* **1994**, *116*, 198-203.

(29) Arce, A. J.; Arrojo, P.; Deeming, A. J.; De Sanctis, Y. *J. Chem. Soc. Dalton Trans.* **1992**, 2423-2424.

(30) Chen, J. B.; Daniels, L. M.; Angelici, R. J. *J. Am. Chem. Soc.* **1991**, *113*, 2544-2552.

(31) Ogilvy, A. E.; Draganjac, M.; Rauchfuss, T. B.; Wilson, S. R. *Organometallics* **1988**, *7*, 1171-1177.

(32) Vicic, D. A.; Jones, W. D. *Organometallics* **1997**, *16*, 1912-1919.

(33) Bianchini, C.; Jiménez, M. V.; Mealli, C.; Meli, A.; Moneti, S.; Patinec, V.; Vizza, F. *Angew. Chem. Int. Edit. Engl.* **1996**, *35*, 1706-1708.

(34) Bianchini, C.; Herrera, V.; Jimenez, M. V.; Meli, A.; Sánchez-Delgado, R.; Vizza, F. *J. Am. Chem. Soc.* **1995**, *117*, 8567-8575.

(35) Jones, W. D.; Dong, L. *J. Am. Chem. Soc.* **1991**, *113*, 559-564.

(36) Vicic, D. A.; Jones, W. D. *J. Am. Chem. Soc.* **1999**, *121*, 7606-7617.

(37) Vicic, D. A.; Jones, W. D. *J. Am. Chem. Soc.* **1997**, *119*, 10855-10856.

(38) Jones, W. D.; Chin, R. M. *J. Am. Chem. Soc.* **1992**, *114*, 9851-9858.

(39) Vicic, D. A.; Jones, W. D. *Organometallics* **1998**, *17*, 3411-3413.

(40) Jones, W. D.; Chin, R. M. *J. Organomet. Chem.* **1994**, *472*, 311-316.

(41) Schaub, T.; Backes, M.; Plietzsch, O.; Radius, U. *Dalton Trans.* **2009**, 7071-7079.

(42) Garcia, J. J.; Maitlis, P. M. *J. Am. Chem. Soc.* **1993**, *115*, 12200-12201.

(43) Cambridge Structural Database (Version 5.32). *3D Search and Research Using the Cambridge Structural Database*, Allen, F. H.; Kennard, O. *Chemical Design Automation News* **1993**, *8* (1), pp 1 & 31-37.

(44) Bishop, P. T.; Dilworth, J. R.; Nicholson, T.; Zubieta, J. *J. Chem. Soc. Dalton Trans.* **1991**, 385-392.

(45) Bishop, P. T.; Dilworth, J. R.; Zubieta, J. A. *J. Chem. Soc. Chem. Commun.* **1985**, 257-259.

(46) Buyuktas, B. S.; Olmstead, M. M.; Power, P. P. *Chem. Commun.* **1998**, 1689-1690.

(47) Komuro, T.; Matsuo, T.; Kawaguchi, H.; Tatsumi, K. *J. Am. Chem. Soc.* **2003**, *125*, 2070-2071.

(48) Hascall, T.; Baik, M. H.; Bridgewater, B. A.; Shin, J. H.; Churchill, D. G.; Friesner, R. A.; Parkin, G. *Chem. Commun.* **2002**, 2644-2645.

(49) For an introduction to $W(PMe_3)_4(\eta^2\text{–}CH_2PMe_2)H$ and reactivity studies, see Chapters 1 and 3.

(50) Isotope labeling studies employing d_4-thiophene indicate that the molybdenum and tungsten butadiene-thiolate compounds $(\eta^5\text{–}C_4H_5S)M(PMe_3)_2(\eta^2\text{–}CH_2PMe_2)$ are formed *via* a common mechanism, with the hydrogen from the PMe_3 ligand terminating in the site adjacent to sulfur.

(51) Furthermore, even examples of simple coordination[a-e] and C–S bond cleavage[f,g] of thiophenes are rare for tungsten. See:

(a) Reynolds, M. A.; Guzei, I. A.; Logsdon, B. C.; Thomas, L. M.; Jacobson, R. A.; Angelici, R. J. *Organometallics* **1999**, *18*, 4075-4081.

(b) Delafuente, D. A.; Myers, W. H.; Sabat, M.; Harman, W. D. *Organometallics* **2005**, *24*, 1876-1885.

(c) Schultz, R. H. *Organometallics* **2004**, *23*, 4349-4356.

(d) Wasserman, H. J.; Kubas, G. J.; Ryan, R. R. *J. Am. Chem. Soc.* **1986**, *108*, 2294-2301.

(e) Stolz, I. W.; Haas, H.; Sheline, R. K. *J. Am. Chem. Soc.* **1965**, *87*, 716-718.

(f) Jones, W. D.; Chin, R. M.; Crane, T. W.; Baruch, D. M. *Organometallics* **1994**, *13*, 4448-4452.

(g) Mills, R. C.; Abboud, K. A.; Boncella, J. M. *Chem. Commun.* **2001**, 1506-1507.

(52) For other examples of hydrogenation of thiophene and benzothiophene to bridging butanethiolate and ethylphenylthiolate ligands, see: Vicic, D. A.; Jones, W. D. *Organometallics* **1997**, *16*, 1912-1919.

(53) For examples of desulfurization of thiophene and benzothiophene by other metals, see reference 10.

(54) Analogous to $W(PMe_3)_4(SBu^n)H_3$, $W(PMe_3)_4(SeBu^n)H_3$ is produced from the reaction of $W(PMe_3)_4(\eta^2\text{–}CH_2PMe_2)H$ with selenophene in the presence of H_2.

(55) For related studies, see references 12 and 13.

(56) For another example of selective C–H bond cleavage of thiophene by tungsten, see: Sakaba, H.; Yumoto, T.; Watanabe, S.; Kabuto, C.; Kabuto, K. *Chem. Lett.* **2003**, *32*, 14-15.

(57) The reaction is also accompanied by the formation of $W(PMe_3)_3H_6$, due to the reaction of $W(PMe_3)_4H_4$ with the H_2 that is liberated.

(58) $W(PMe_3)_4H_4$ also serves as a catalyst for the photochemical exchange of hydrogen and deuterium between both the α- and β-positions of thiophene and C_6D_6. The isotopic exchange, however, is inhibited by PMe_3, which implies that the reaction occurs *via* reversible oxidative addition of benzene and thiophene C–H(D) bonds to 16-electron $[W(PMe_3)_3H_4]$, rather than to $[W(PMe_3)_4H_2]$.

(59) This transformation is necessarily accompanied by ligand redistribution. In an attempt to increase the yield of $W(PMe_3)_4(SBu^n)H_3$, the reaction between $W(PMe_3)_3H_6$ and thiophene was performed in the presence of PMe_3. However, under these conditions, only $W(PMe_3)_4H_4$ (which is thermally unreactive towards thiophene) was obtained.

(60) Among other mechanisms, the formation of $W(PMe_3)_4(SBu^n)H_3$ could possibly take place *via* C–S bond cleavage of the κ^1–thienyl ligand. For an example of such cleavage of a κ^1–thienyl ligand at a ditungsten center, see: Chisholm, M. H.; Haubrich, S. T.; Huffman, J. C.; Streib, W. E. *J. Am. Chem. Soc.* **1997**, *119*, 1634-1647.

(61) Lyons, D.; Wilkinson, G. *J. Chem. Soc., Dalton Trans.* **1985**, 587-590.

(62) For related hexahydrides, see:

(a) Moss, J. R.; Shaw, B. L. *J. Chem. Soc., Dalton Trans.* **1972**, 1910-1911.

(b) Crabtree, R. H.; Hlatky, G. G. *J. Organomet. Chem.* **1982,** *238*, C21-C23.

(63) Meakin, P.; Guggenberger, L. J.; Peet, W. G.; Muetterties, E. L.; Jesson, J. P. *J. Am. Chem. Soc.* **1973,** *95*, 1467-1474.

(64) The D_{3h} symmetry does not include the methyl groups of the PMe_3 ligands, instead only looking at the coordination geometry of the 9 atoms around tungsten.

(65) Gregson, D.; Howard, J. A. K.; Nicholls, J. N.; Spencer, J. L.; Turner, D. G. *J. Chem. Soc., Chem. Commun.* **1980**, 572-573.

(66) Gregson, D.; Mason, S. A.; Howard, J. A. K.; Spencer, J. L.; Turner, D. G. *Inorg. Chem.* **1984,** *23*, 4103-4107.

(67) $W(PMe_3)_3H_6$ is oriented in the unit cell such that there is crystallographically imposed mirror plane (molecular C_s symmetry) comprising W, P1, H3, and H4.

(68) A DFT calculation in which the geometry of $W(PMe_3)_3H_6$ was constrained to be C_{3v} symmetric (the P–W–P bond angles are all 120˚), indicates that this conformation is *ca*. 3 kcal mol^{-1} higher in energy.

(69) The formation of $(\kappa^1,\eta^2\text{–}CH_2CHC_6H_4S)W(PMe_3)_4H$ and $W(PMe_3)_4(\kappa^1\text{-}C_\alpha\text{-}CCHSC_6H_4)H_3$ also provides another interesting contrast with the molybdenum system, for which $Mo(PMe_3)_5H_2$ reacts with benzothiophene to give $(\kappa^1,\eta^2\text{–}CH_2CC_6H_4S)Mo(PMe_3)_4$. See Section 4.2 and reference 10.

(70) $W(PMe_3)_4(SC_6H_4Et)H_3$ (**8**) can also be formed directly by reaction of $W(PMe_3)_4(\eta^2\text{–}CH_2PMe_2)H$ with benzothiophene in the presence of H_2.

(71) Daly, F. P. *J. Catal.* **1978**, *51*, 221-228.

(72) The tungsten and sulfur containing products are presently unknown.

(73) The formation of $[(\kappa^2\text{-}C_{12}H_8)W(PMe_3)](\mu\text{-}S)(\mu\text{-}CH_2PMe_2)(\mu\text{-}PMe_2)[W(PMe_3)_3]$ requires cleavage of both P–C and C–H bonds of PMe_3 and elimination of methane. For an example of P–C cleavage of PMe_3, see: Shin, J. H.; Parkin, G. *J. Chem. Soc., Chem. Commun.* **1998**, 1273-1274.

(74) (a) Vicic, D. A.; Jones, W. D. *J. Am. Chem. Soc.* **1999**, *121*, 7606-7617.

(b) Vicic, D. A.; Jones, W. D. *Organometallics* **1998**, *17*, 3411-3413.

(75) (a) Garcia, J. J.; Maitlis, P. M. *J. Am. Chem. Soc.* **1993**, *115*, 12200-12201.

(b) Garcia, J. J.; Mann, B. E.; Adams, H.; Bailey, N. A.; Maitlis, P. M. *J. Am. Chem. Soc.* **1995**, *117*, 2179-2186.

(c) Matsubara, K.; Okamura, R.; Tanaka, M.; Suzuki, H. *J. Am. Chem. Soc.* **1998**, *120*, 1108-1109.

(76) For a ruthenium complex derived from dibenzothiophene in which the biphenyldiyl fragment coordinates to two metal centers, see: Chehata, A.; Oviedo, A.; Arévalo, A.; Bernès, S.; García, J. J. *Organometallics* **2003**, *22*, 1585-1587.

(77) $W(PMe_3)_4H_4$ requires photochemical activation to catalyze the exchange.

(78) The α site is closest to the sulfur atom.

(79) In support of these observations, DFT calculations on the computationally simpler system in which the methyl groups of the PMe_3 ligands are replaced by hydrogen atoms, indicate that the δ isomer of $W(PH_3)_4(\kappa^1\text{-}C\text{–dibenzothienyl})H_3$ is more than 10 kcal mol^{-1} less stable than the α, β and γ isomers.

(80) Parkin, G. *Stuct. Bond.* **2010**, *136*, 113-146.

(81) Vahrenkamp, H. *Angew. Chem. Int. Ed.* **1978,** *17*, 379-392.

(82) Cotton, F. A.; Daniels, L. M.; Murillo, C. A.; Zhou, H.-C. *Inorg. Chim. Acta* **2000**, *300-302*, 319-327.

(83) (a) Hall, M. B.; Fenske, R. F. *Inorg. Chem.* **1972**, *11*, 768.

(b) Bursten, B. E.; Jensen, J. R.; Fenske, R. F. *J. Chem. Phys.* **1978**, *68*, 3320.

(c) Manson, J.; Webster, C. E.; Pérez, L. M.; Hall, M. B. http://www.chem.tamu.edu/jimp2/index.html.

(84) Rabinovich, D.; Parkin, G. *J. Am. Chem. Soc.* **1991**, *113*, 5904-5905.

(85) Rabinovich, D.; Parkin, G. *Inorg. Chem.* **1995**, *34*, 6341-6361.

(86) It should be noted that there is a large range for the W–S bond lengths of the (μ-S) ligands (2.254(2) Å – 2.575(2) Å). However, this has been observed previously. See:

(a) Secheresse, F.; Lefebvre, J.; Daran, J. C.; Jeannin, Y. *Inorg. Chem.* **1982**, *21*, 1311-1314.

(b) Reference 89.

(87) Bauer, A.; Capps, K. B.; Wixmerten, B.; Abboud, K. A.; Hoff, C. D. *Inorg. Chem.* **1999,** *38*, 2136-2142.

(88) Capps, K. B.; Whitener, G. D.; Bauer, A.; Abboud, K. A.; Wasser, I. M.; Vollhardt, K. P. C.; Hoff, C. D. *Inorg. Chem.* **2002,** *41*, 3212-3217.

(89) (a) Kuwata, S.; Mizobe, Y.; Hidai, M. *J. Chem. Soc., Dalton Trans.* **1997**, 1753-1758.

(b) Kuwata, S.; Mizobe, Y.; Hidai, M. *J. Chem. Soc., Chem. Commun.* **1995**, 1057-1058.

(90) (a) Wade, K. *J. Chem. Soc. D: Chem. Commun.* **1971**, 792-793.

(b) Wade, K. *Nature Physical Science* **1972**, *240*, 71.

(91) Mingos, D. M. P. *Nature Physical Science* **1972**, *236*, 99-102.

(92) (a) Green, M. L. H. *J. Organomet. Chem.* **1995**, *500*, 127-148.

(b) Parkin, G. in *Comprehensive Organometallic Chemistry III*, Volume 1, Chapter 1.01; Crabtree, R. H. and Mingos, D. M. P. (Eds), Elsevier, Oxford, 2006.

(93) The major σ-components that contribute to the W–W bonding interactions are:

orbital	**W1–W4**	**W2–W3**	**W2–W4**	**W3–W4**
<52>	–	20%	–	–
<56>	–	–	8%	–
<57>	–	–	33%	–
<58>	–	–	–	38%
<59>	12%	–	9%	–
<60>	23%	23%	–	–
Total	35%	43%	50%	38%

(94) Rabinovich, D.; Parkin, G. *Inorg. Chem.* **1994**, *33*, 2313-2314.

(95) Rabinovich, D.; Parkin, G. *J. Am. Chem. Soc.* **1991**, *113*, 9421-9422.

(96) For other molybdenum sulfide phosphine cluster compounds, see:

(a) Saito, T.; Yamamoto, N.; Yamagata, T.; Imoto, H. *J. Am. Chem. Soc.* **1988,** *110*, 1646-1647.

(b) Amari, S.; Imoto, H.; Saito, T. *Chem. Lett.* **1997**, 967-968.

(97) For a review on transition metal hydrosulfido compounds, see: Kuwata, S.; Hidai, M. *Coord. Chem. Rev.* **2001**, *213*, 211-305.

(98) Tsuge, K.; Imoto, H.; Saito, T. *Inorg. Chem.* **1992,** *31*, 4715-4716.

(99) Schwarz, D. E.; Rauchfuss, T. B.; Wilson, S. R. *Inorg. Chem.* **2003**, *42*, 2410-2417.

(100) For related studies on trinuclear molybdenum systems, see:

(a) Cotton, F. A. *Polyhedron* **1986**, *5*, 3-14.

(b) Chisholm, M. H.; Folting, K.; Huffman, J. C.; Kirkpatrick, C. C. *J. Am. Chem. Soc.* **1981,** *103*, 5967-5968.

(c) Jiang, Y.; Tang, A.; Hoffmann, R. *Organometallics* **1985**, *4*, 27-34.

(d) Chisholm, M. H.; Folting, K.; Huffman, J. C.; Kirkpatrick, C. C. *Inorg. Chem.* **1984**, *23*, 1021-1037.

(e) Bursten, B. E.; Cotton, F. A.; Hall, M. B.; Najjar, R. C. *Inorg. Chem.* **1982**, *21*, 302-307.

(f) Müller, A.; Jostes, R.; Cotton, F. A. *Angew. Chem. Int. Ed.* **1980**, *19*, 875-882.

(101) For related molybdenum selenide clusters, see:

(a) Avarvari, N.; Kiracki, K.; Llusar, R.; Polo, V.; Sorribes, I.; Vicent, C. *Inorg. Chem.* **2010,** *49*, 1894-1904.

(b) Feliz, M.; Llusar, R.; Uriel, S.; Vicent, C.; Humphrey, M. G.; Lucas, N. T.; Samoc, M.; Luther-Davies, B. *Inorg. Chim. Acta* **2003,** *349*, 69-77.

(c) Llusar, R.; Uriel, S.; Vicent, C. *J. Chem. Soc., Dalton Trans.* **2001**, 2813-2818.

(102) For related molybdenum telluride clusters, see:

(a) Gushchin, A. L.; Sokolov, M. N.; Vicent, C.; Virovets, A. V.; Peresypkina, E. V.; Fedin, V. P. *Polyhedron* **2009,** *28*, 3479-3484.

(b) Lin, X.; Chen, H.-Y.; Chi, L.-S.; Lu, C.-Z.; Zhuang, H.-H. *Polyhedron* **2000,** *19*, 925-929.

(c) Lin, X.; Chen, H.-Y.; Chi, L.-S.; Zhuang, H.-H. *Polyhedron* **1998,** *18*, 217-223.

(103) (a) Tsuge, K.; Yajima, S.; Imoto, H.; Saito, T. *J. Am. Chem. Soc.* **1992,** *114*, 7910-7912.

(b) Tsuge, K.; Imoto, H.; Saito, T. *Inorg. Chem.* **1995,** *34*, 3404-3409.

(104) For a related molybdenum sulfide cluster, see: Petrov, P. A.; Virovets, A. V.; Alberola, A.; Llusar, R.; Konchenko, S. N. *Dalton Trans.* **2010,** *39*, 8875-8877.

(105) It should be noted that $Mo_3S_5(PMe_3)_6$ (reference 103) crystallizes in a hexagonal unit cell with unit cell parameters [*a*=11.112(1) and *c*=53.507(10)] very similar to those of the reduced primitive cells of $Mo_3Se_5(PMe_3)_6$ and $Mo_3Te_5(PMe_3)_6$. However, we were not able to solve $Mo_3Se_5(PMe_3)_6$ and $Mo_3Te_5(PMe_3)_6$ in a hexagonal space group and found that the structure refined best in a monoclinic C centered unit cell.

(106) The average Mo–P bond length of $Mo_3Te_5(PMe_3)_6$ is only 0.007 Å longer than that of $Mo_3Se_5(PMe_3)_6$, thus indicating that the chalcogenide has a negligible effect on the Mo–PMe_3 bonding.

(107) Lundmark, P.; Kubas, G.; Butcher, R. *J. Chem. Crystallogr.* **1997,** *27*, 377-379.

(108) Endrich, K.; Guggolz, E.; Serhadle, O.; Ziegler, M. L.; Korswagen, R. P. *J. Organomet. Chem.* **1988,** *349*, 323-351.

(109) Chakrahari, K. K. V.; Dhayal, R. S.; Ghosh, S. *Polyhedron* **2011,** *30*, 1048-1054.

(110) Rakowski DuBois, M.; DuBois, D. L.; VanDerveer, M. C.; Haltiwanger, R. C. *Inorg. Chem.* **1981,** *20*, 3064-3071.

(111) Wyckoff, R. W. G. "Crystal Structures" **1963**, *1*, p.280–281, 2nd Ed. Interscience Publishers, New York, New York.

(112) (a) McNally, J. P.; Leong, V. S.; Cooper, N. J. in *Experimental Organometallic Chemistry*, Wayda, A. L.; Darensbourg, M. Y., Eds.; American Chemical Society: Washington, DC, 1987; Chapter 2, pp 6-23.

(b) Burger, B.J.; Bercaw, J. E. in *Experimental Organometallic Chemistry*; Wayda, A. L.; Darensbourg, M. Y., Eds.; American Chemical Society: Washington, DC, 1987; Chapter 4, pp 79-98.

(c) Shriver, D. F.; Drezdzon, M. A.; *The Manipulation of Air-Sensitive Compounds*, 2nd Edition; Wiley-Interscience: New York, 1986.

(113) Gottlieb, H. E.; Kotlyar, V.; Nudelman, A. *J. Org. Chem.* **1997**, *62*, 7512-7515.

(114) "Nuclear Magnetic Resonance Spectroscopy" Nelson, J. H. Prentice Hall, New Jersey (2003), p 79.

(115) Lyons, D.; Wilkinson, G.; Thomton-Pett, M.; Hursthouse, M. B. *J. Chem. Soc., Dalton Trans.* **1984**, 695-700.

(116) Brookhart, M.; Cox, K.; Cloke, F. G. N.; Green, J. C.; Green, M. L. H.; Hare, P. M.; Bashkin, J.; Derome, A. E.; Grebenik, P. D. *J. Chem. Soc., Dalton Trans.* **1985**, 423-433.

(117) Green, M. L. H.; Parkin, G.; Chen, M.; Prout, K. *J. Chem. Soc., Dalton Trans.* **1986**, 2227–2236.

(118) Parkin, G. *Rev. Inorg. Chem.* **1985**, *7*, 251-297.

(119) (a) Sheldrick, G. M. SHELXTL, An Integrated System for Solving, Refining and Displaying Crystal Structures from Diffraction Data; University of Göttingen, Göttingen, Federal Republic of Germany, 1981.

(b) Sheldrick, G. M. *Acta Cryst.* **2008**, *A64*, 112-122.

(120) Jaguar 7.5, Schrödinger, LLC, New York, NY 2008.

(121) (a) Becke, A. D. *J. Chem. Phys.* **1993**, *98*, 5648-5652.

(b) Becke, A. D. *Phys. Rev. A* **1988**, *38*, 3098-3100.

(c) Lee, C. T.; Yang, W. T.; Parr, R. G. *Phys. Rev. B* **1988**, *37*, 785-789.

(d) Vosko, S. H.; Wilk, L.; Nusair, M. *Can. J. Phys.* **1980**, *58*, 1200-1211.

(e) Slater, J. C. *Quantum Theory of Molecules and Solids, Vol. 4: The Self-Consistent Field for Molecules and Solids*; McGraw-Hill: New York, 1974.

(122) (a) Hay, P. J.; Wadt, W. R. *J. Chem. Phys.* **1985**, *82*, 270-283.

(b) Wadt, W. R.; Hay, P. J. *J. Chem. Phys.* **1985**, *82*, 284-298.

(c) Hay, P. J.; Wadt, W. R. *J. Chem. Phys.* **1985**, *82*, 299-310.

(123) Version 2.0, June 1993; Lichtenberger, D. L. Department of Chemistry, University of Arizona, Tuscon, AZ 85721.

(124) Campaigne, E.; Ashby, J. *Journal of Heterocyclic Chemistry* **1969**, 6, 517 – 522.

(125) C_6H_6 co-crystallizes with $W_8S_{16}(PMe_3)_{10}$.

CHAPTER 5

Modeling aspects of hydrodeoxygenation by using tungsten and molybdenum trimethylphosphine complexes

Table of Contents

5.1 Introduction

Aspects of hydrodesulfurization (HDS) and hydrodenitrogenation (HDN) have been discussed in Chapters 2 – 4. Hydrodeoxygenation (HDO) is another component of the hydrotreating process, which removes oxygen impurities from crude feedstocks (Scheme 1).[1,2,3,4] In conventional crude oil, there is approximately 5 wt. % sulfur, < 1 wt. % nitrogen and < 2 wt. % oxygen;[5,6] thus a majority of the research in this area has focused on HDS because of (*i*) the greater percentage of sulfur in feedstocks and (*ii*) the deleterious effects combustion of mercaptans has on the environment. HDO receives the least attention, compared with HDS and HDN, most likely because of (*i*) the low percentage of oxygen compounds in conventional crudes and (*ii*) the fact that burning oxygenated compounds produces water (Scheme 1), which is environmentally benign.[1] However, in synthetic feeds derived from biomass, the concentration of oxygen is significantly higher, sometimes reaching almost 50 wt. %,[6] which introduces new problems in the refining process. For example, some oxygen compounds can cause catalyst deactivation in refineries and can also lead to low quality fuels for combustion.[6]

Analogous to our previous research concerning HDS[7,8] and HDN[9,10] detailed in Chapters 2 – 4, and previous studies performed by the Parkin group,[11,12,13] we were interested in studying the reactivity of trimethylphosphine complexes of molybdenum and tungsten with oxygenated compounds. In this regard, this chapter describes new research concerning the reactivity of furans (Figure 1) with trimethylphosphine complexes of molybdenum and tungsten in order to serve as models for the type of reactivity that oxygenated organic compounds may have with the surface of an industrial catalyst.

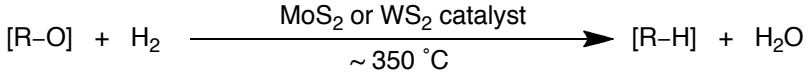

Scheme 1. Hydrodeoxygenation (HDO).

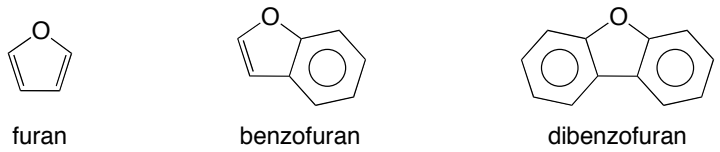

Figure 1. Furan, benzofuran and dibenzofuran.

5.2 Reactivity of $W(PMe_3)_4(\eta^2–CH_2PMe_2)H$ towards furan

$W(PMe_3)_4(\eta^2–CH_2PMe_2)H$ reacts with furan at 60 ˚C in benzene to produce two major species, namely $(\eta^5–C_4H_5O)W(PMe_3)_2(\eta^2–CH_2PMe_2)$ and $(\kappa^1,\eta^2\text{-}C_4H_3O)(\kappa^1\text{-}O\text{-}C_4H_5O)W(PMe_3)_3$ (Scheme 2). The former compound, which can be considered a butadiene-alkoxide derivative, is the oxygen analogue of the thiolate product obtained from the reaction between $W(PMe_3)_4(\eta^2–CH_2PMe_2)H$ and thiophene, namely $(\eta^5–C_4H_5S)W(PMe_3)_2(\eta^2–CH_2PMe_2)$.[8] It should be noted that C–O bond cleavage in furan followed by hydrogen transfer has been previously observed by Felkin, when furan was allowed to react with $(Ph_3P)_2ReH_7$, thereby producing $(\eta^5–C_4H_5O)Re(PPh_3)_2CO$.[14]

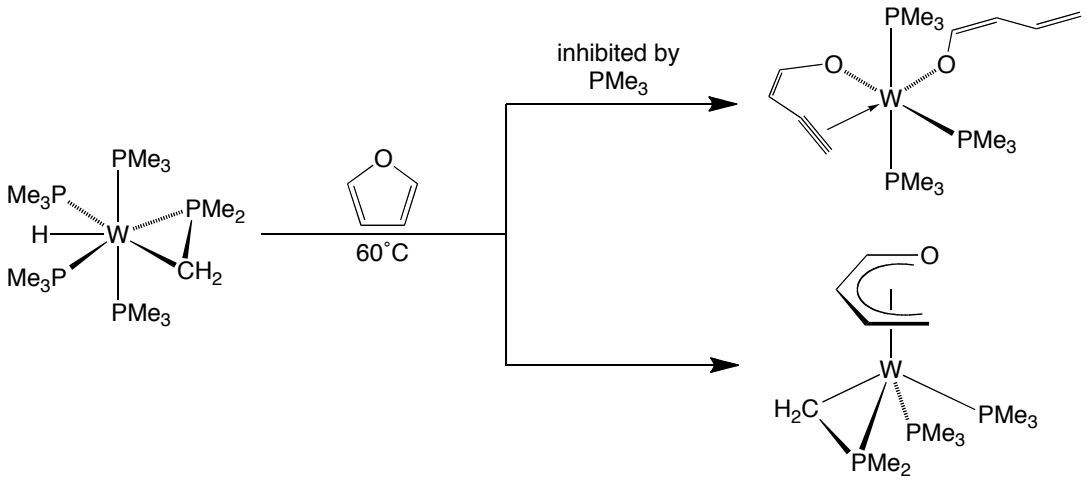

Scheme 2. Reactivity of $W(PMe_3)_4(\eta^2–CH_2PMe_2)H$ towards furan.

The other major product of the reaction between $W(PMe_3)_4(\eta^2–CH_2PMe_2)H$ and furan, $(\kappa^1,\eta^2\text{-}C_4H_3O)(\kappa^1\text{-}O\text{-}C_4H_5O)W(PMe_3)_3$, contains two different ligands emanating from C–O bond cleavage of furan, and its molecular structure is shown in Figure 2. The

most interesting aspect of $(\kappa^1,\eta^2\text{-}C_4H_3O)(\kappa^1\text{-}O\text{-}C_4H_5O)W(PMe_3)_3$ is the $(\kappa^1,\eta^2\text{-}C_4H_3O)$ ligand, which is a butyne-enolate and is formally the result of C–O bond cleavage and hydrogen atom elimination from the β-position of furan.[15] It is key to note that similar types of transformations with yttrium and rare-earth furyl complexes have been previously observed.[16] For example, it was demonstrated that upon heating, $Cp^*_2Y(\kappa^1\text{-}C_\alpha\text{-}C_4H_3O)$ converts to $[Cp^*_2Y]_2(\mu\text{-}OC_4H_2)$ and furan, in which the $(\mu\text{-}OC_4H_2)$ is a ring opened bridging butynyl-enolate ligand.[16a]

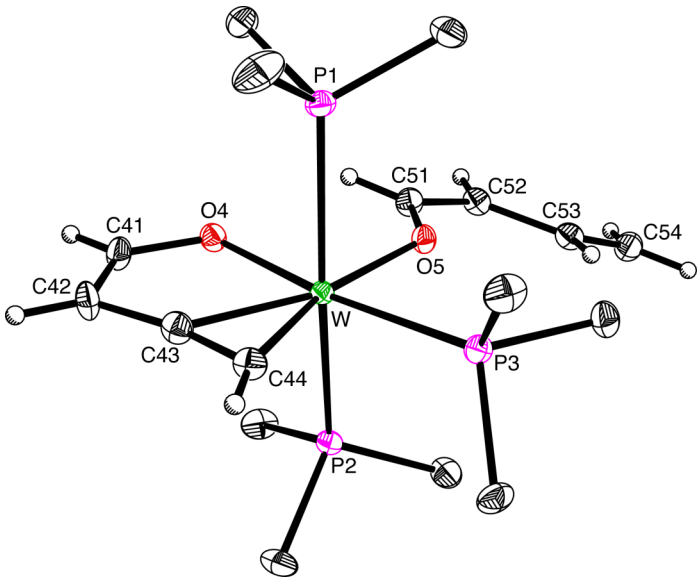

Figure 2. Molecular structure of $(\kappa^1\text{-}O,\eta^2\text{-}C_2\text{–}C_4H_3O)(\kappa^1\text{-}O\text{–}C_4H_5O)W(PMe_3)_3$.

The relative amounts of $(\eta^5\text{–}C_4H_5O)W(PMe_3)_2(\eta^2\text{–}CH_2PMe_2)$ and $(\kappa^1,\eta^2\text{-}C_4H_3O)(\kappa^1\text{-}O\text{-}C_4H_5O)W(PMe_3)_3$ in the product mixture are dependent on the reaction conditions, with the latter being favored in the presence of a large excess of furan. However, if the reaction between $W(PMe_3)_4(\eta^2\text{–}CH_2PMe_2)H$ and furan is performed in the presence of PMe_3, negligible amounts of $(\kappa^1,\eta^2\text{-}C_4H_3O)(\kappa^1\text{-}O\text{-}C_4H_5O)W(PMe_3)_3$ are formed. Thus, the inhibitory effect of PMe_3 on the formation $(\kappa^1,\eta^2\text{-}C_4H_3O)(\kappa^1\text{-}O\text{-}C_4H_5O)W(PMe_3)_3$ indicates

that its production presumably involves a reversible dissociation of PMe_3 prior to the rate determining step.

In view of the similarity of $(\eta^5\text{–}C_4H_5O)W(PMe_3)_2(\eta^2\text{–}CH_2PMe_2)$ to the analogous compound obtained from reaction between $W(PMe_3)_4(\eta^2\text{–}CH_2PMe_2)H$ and thiophene, namely $(\eta^5\text{–}C_4H_5S)W(PMe_3)_2(\eta^2\text{–}CH_2PMe_2)$,[8] it is of interest to ascertain if the mechanisms of their formations are similar. In this regard, when d_4-furan is allowed to react with $W(PMe_3)_4(\eta^2\text{–}CH_2PMe_2)H$, the hydrogen atom emanating from the PMe_3 ligand terminates on the methylene group of the (η^5-OCDCDCDCDH) ligand (Scheme 3), whereas in the thiophene system, the hydrogen atom from the PMe_3 ligand ends up on the position adjacent to the sulfur atom (η^5-SCHCDCDCD$_2$) (Scheme 3). Thus, the divergent distributions of hydrogen atoms indicate that the mechanisms of formation for the aforementioned compounds are different, even though they are structural analogues.

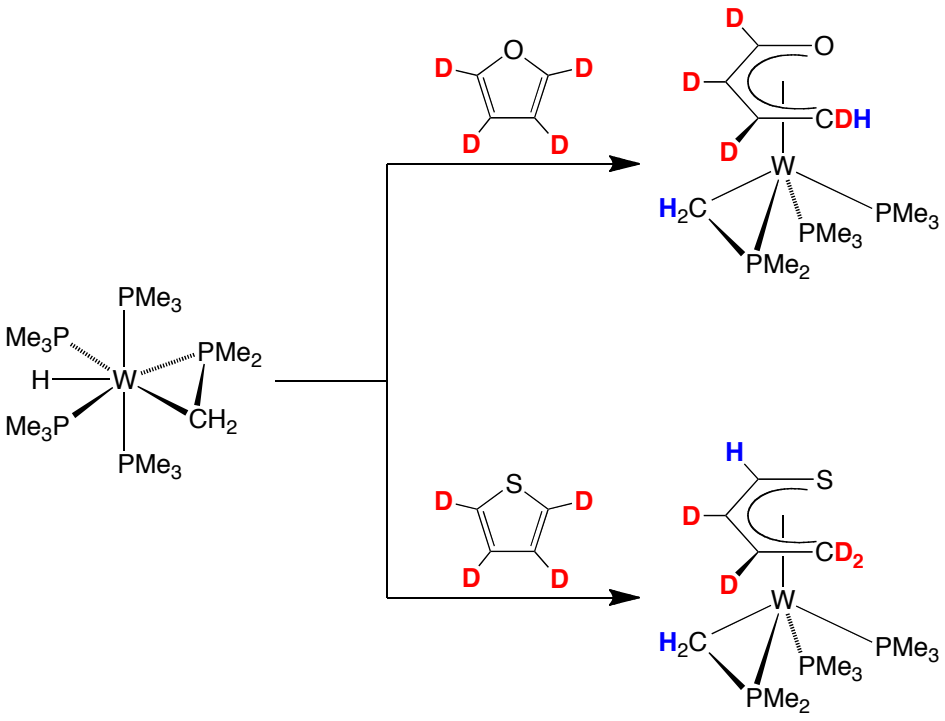

Scheme 3. Deuterium distribution of d_4-furan and d_4-thiophene reactivity towards $W(PMe_3)_4(\eta^2\text{–}CH_2PMe_2)H$.

The mechanism of formation of $(\kappa^1,\eta^2\text{-}C_4H_3O)(\kappa^1\text{-}O\text{-}C_4H_5O)W(PMe_3)_3$ was also studied. Although it may be obvious, there are two observations that should be noted. One, the $(\kappa^1\text{-}O\text{-}C_4H_5O)$ ligand is also a butadiene-alkoxide fragment as in $(\eta^5\text{–}C_4H_5O)W(PMe_3)_2(\eta^2\text{–}CH_2PMe_2)$, but instead of coordinating in an η^5 manner, it coordinates through a κ^1 mode using only the oxygen atom. Two, $(\kappa^1,\eta^2\text{-}C_4H_3O)(\kappa^1\text{-}O\text{-}C_4H_5O)W(PMe_3)_3$ is formally related to $(\eta^5\text{–}C_4H_5O)W(PMe_3)_2(\eta^2\text{–}CH_2PMe_2)$ by the addition of one equivalent of furan. Thus, $(\eta^5\text{–}C_4H_5O)W(PMe_3)_2(\eta^2\text{–}CH_2PMe_2)$ might be an intermediate in the production of $(\kappa^1,\eta^2\text{-}C_4H_3O)(\kappa^1\text{-}O\text{-}C_4H_5O)W(PMe_3)_3$. However, treatment of $(\eta^5\text{–}C_4H_5O)W(PMe_3)_2(\eta^2\text{–}CH_2PMe_2)$ with furan in d_6-benzene, a reaction performed by graduate student Ashley Zuzek, resulted in a negligible amounts of $(\kappa^1,\eta^2\text{-}C_4H_3O)(\kappa^1\text{-}O\text{-}C_4H_5O)W(PMe_3)_3$ being produced, thereby indicating that $(\eta^5\text{–}C_4H_5O)W(PMe_3)_2(\eta^2\text{–}CH_2PMe_2)$ is not the active intermediate towards the production of $(\kappa^1,\eta^2\text{-}C_4H_3O)(\kappa^1\text{-}O\text{-}C_4H_5O)W(PMe_3)_3$. In this regard, density functional theory calculations[17] were carried out to ascertain if the reaction of $(\eta^5\text{–}C_4H_5O)W(PMe_3)_2(\eta^2\text{–}CH_2PMe_2)$ with furan to produce $(\kappa^1,\eta^2\text{-}C_4H_3O)(\kappa^1\text{-}O\text{-}C_4H_5O)W(PMe_3)_3$ is thermodynamically favorable; indeed, the computational ΔH was found to be *ca.* –30 kcal mol^{-1}, thereby indicating that $(\kappa^1,\eta^2\text{-}C_4H_3O)(\kappa^1\text{-}O\text{-}C_4H_5O)W(PMe_3)_3$ is not formed due to kinetic factors.

Two other complexes were isolated from the reaction between $W(PMe_3)_4(\eta^2\text{–}CH_2PMe_2)H$ and furan by crystallization (Figure 3). One is an alkylidene derivatitve, $[\kappa^2\text{-}O,C\text{-}OC_3H_2Me]W(PMe_3)_3(\eta^2\text{–}CH_2PMe_2)$, and its molecular structure is shown in Figure 4. The other complex is most probably formed due to the presence of adventitious oxygen, and is the dimeric compound, $[\mu^2\text{-}\kappa^2,\kappa^2\text{-}(OC_3H_2Me)_2][W(PMe_3)_3O]_2$; Its molecular structure is shown in Figure 5.

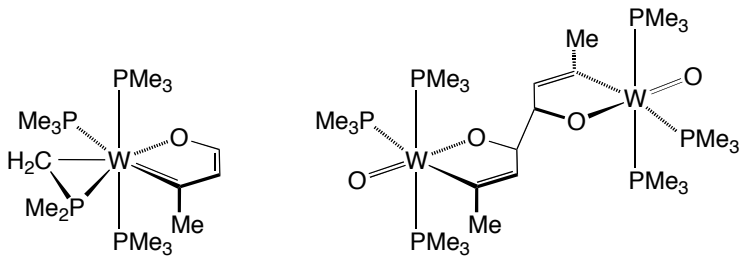

Figure 3. Two compounds isolated from reaction of $W(PMe_3)_4(\eta^2\text{–}CH_2PMe_2)H$ and furan: $[\kappa^2\text{-}O,C\text{-}OC_3H_2Me]W(PMe_3)_3(\eta^2\text{–}CH_2PMe_2)$ (left) and $[\mu^2\text{-}\kappa^2,\kappa^2\text{-}(OC_3H_2Me)_2][W(PMe_3)_3O]_2$ (right).

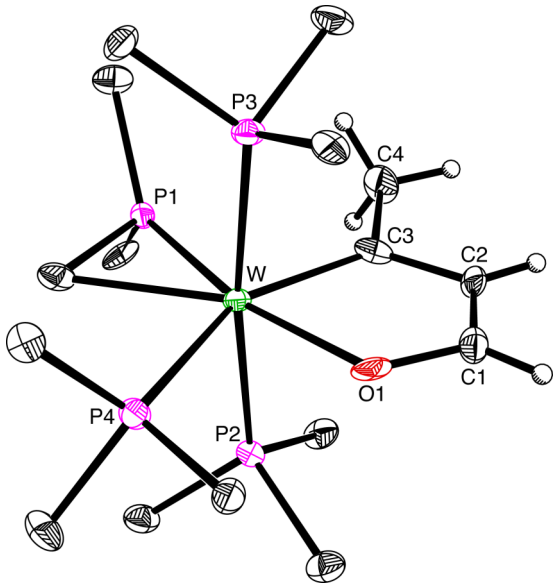

Figure 4. Molecular structure of $[\kappa^2\text{-}O,C\text{-}OC_3H_2Me]W(PMe_3)_3(\eta^2\text{–}CH_2PMe_2)$.

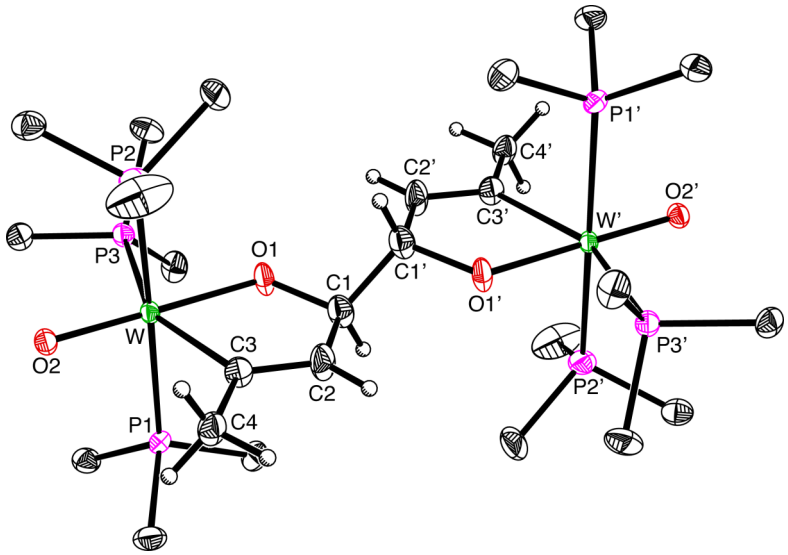

Figure 5. Molecular structure of $[\mu^2\text{-}\kappa^2,\kappa^2\text{-}(OC_3H_2Me)_2][W(PMe_3)_3O]_2$.

The reactivity of $W(PMe_3)_4(\eta^2\text{–}CH_2PMe_2)H$ towards furan in the presence of H_2 (*ca*. 1 atm) was also studied, thereby demonstrating the formation of the furyl complex $W(PMe_3)_4(\kappa^1\text{-}C_\alpha\text{-}C_4H_3O)H_3$ *via* furan α-C–H bond cleavage (Scheme 4). The molecular structure of $W(PMe_3)_4(\kappa^1\text{-}C_\alpha\text{-}C_4H_3O)H_3$ has been determined by X-ray diffraction (Figure 6) and has very similar geometry to that of the thienyl complex, $W(PMe_3)_4(\kappa^1\text{-}C_\alpha\text{-}C_4H_3S)H_3$ (see Chapter 4), as illustrated in Figure 7. Hence, the coordination geometry around the tungsten center is almost identical, while the major difference resides in the larger ring size of the thienyl ligand, compared with that of the furyl ligand (Figure 7).

Previous studies found that an *ansa*-molybdenocene complex reacted with furan to produce the respective C–H activated furyl complex,[18] but DFT calculations indicated that C–O bond cleavage was, in fact, thermodynamically favored compared to C–H bond cleavage; thus, the C–H bond cleaved species observed was due to kinetic factors. In order to ascertain if this was the case in tungsten system described above, DFT calculations were carried out on the two isomeric species, $W(PH_3)_4(\kappa^1\text{-}C_\alpha\text{-}C_4H_3O)H_3$ and $(\kappa^2\text{-}C,O\text{-}C_4H_4O)W(PH_3)_4H_2$,[19] which are products obtained by C–H and C–O bond cleavage, respectively.[20] The results show that $(\kappa^2\text{-}C,O\text{-}C_4H_4O)W(PH_3)_4H_2$ is 9.1 kcal mol^{-1} lower in energy than $W(PH_3)_4(\kappa^1\text{-}C_\alpha\text{-}C_4H_3O)H_3$, thereby indicating that $W(PMe_3)_4(\kappa^1\text{-}C_\alpha\text{-}C_4H_3O)H_3$ is formed due to kinetic factors. It should be noted that, in accord with these results, Chisholm has observed ring opening of furyl compounds at ditungsten centers.[21]

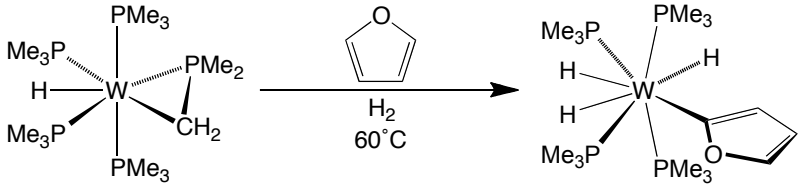

Scheme 4. Reactivity of $W(PMe_3)_4(\eta^2\text{–}CH_2PMe_2)H$ towards furan in the presence of H_2.

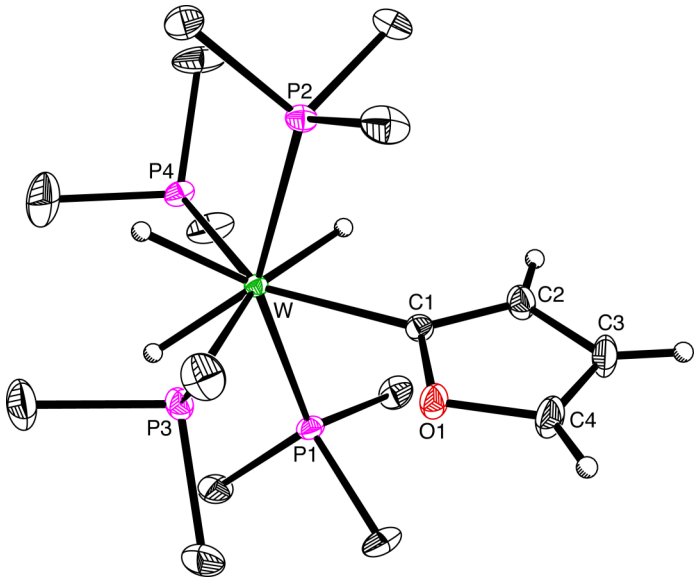

Figure 6. Molecular structure of $W(PMe_3)_4(\kappa^1\text{-}C_\alpha\text{-}C_4H_3O)H_3$.

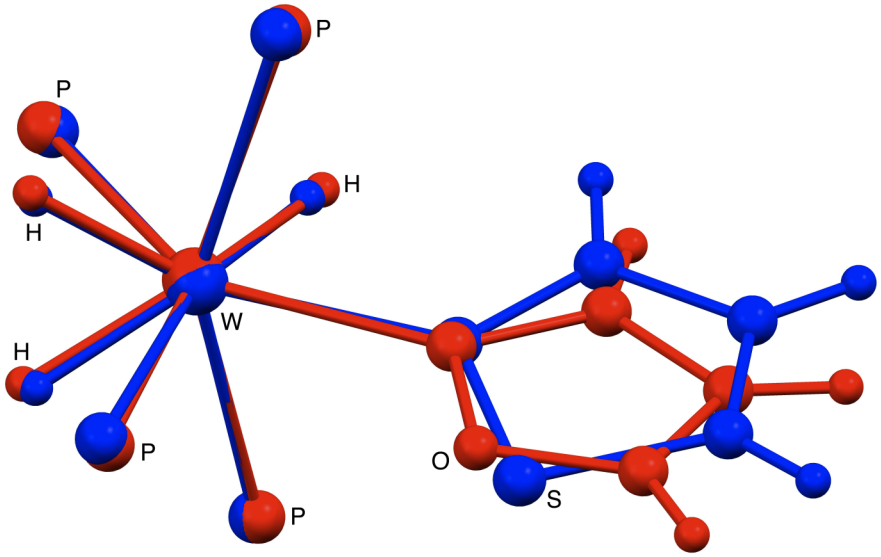

Figure 7. Structural overlay of $W(PMe_3)_4(\kappa^1\text{-}C_\alpha\text{-}C_4H_3\mathbf{O})H_3$ (red) and $W(PMe_3)_4(\kappa^1\text{-}C_\alpha\text{-}C_4H_3\mathbf{S})H_3$ (blue). Methyl groups of the PMe_3 ligands are not shown for clarity.

5.3 Reactivity of tungsten hydrides towards furan

The furyl complex, $W(PMe_3)_4(\kappa^1\text{-}C_\alpha\text{-}C_4H_3O)H_3$, can also be produced from the reactions of several other tungsten compounds with furan, namely $W(PMe_3)_5H_2$, $W(PMe_3)_4H_4$, and $W(PMe_3)_3H_6$. For example, heating a solution of $W(PMe_3)_5H_2$ and

furan in benzene at 60 ˚C results in the formation of $W(PMe_3)_4(\kappa^1\text{-}C_\alpha\text{-}C_4H_3O)H_3$ (Scheme 5), which is similar to the reactivity observed with $W(PMe_3)_5H_2$ and thiophene, which produces $W(PMe_3)_4(\kappa^1\text{-}C_\alpha\text{-}C_4H_3S)H_3$ (Chapter 4). Furthermore, $W(PMe_3)_4(\kappa^1\text{-}C_\alpha\text{-}C_4H_3O)H_3$ can also be synthesized by either (*i*) treatment of $W(PMe_3)_4H_4$ with furan in benzene under photochemical activation[22] or (*ii*) treatment of $W(PMe_3)_3H_6$ with furan in benzene at 60 ˚C, shown in Scheme 5.

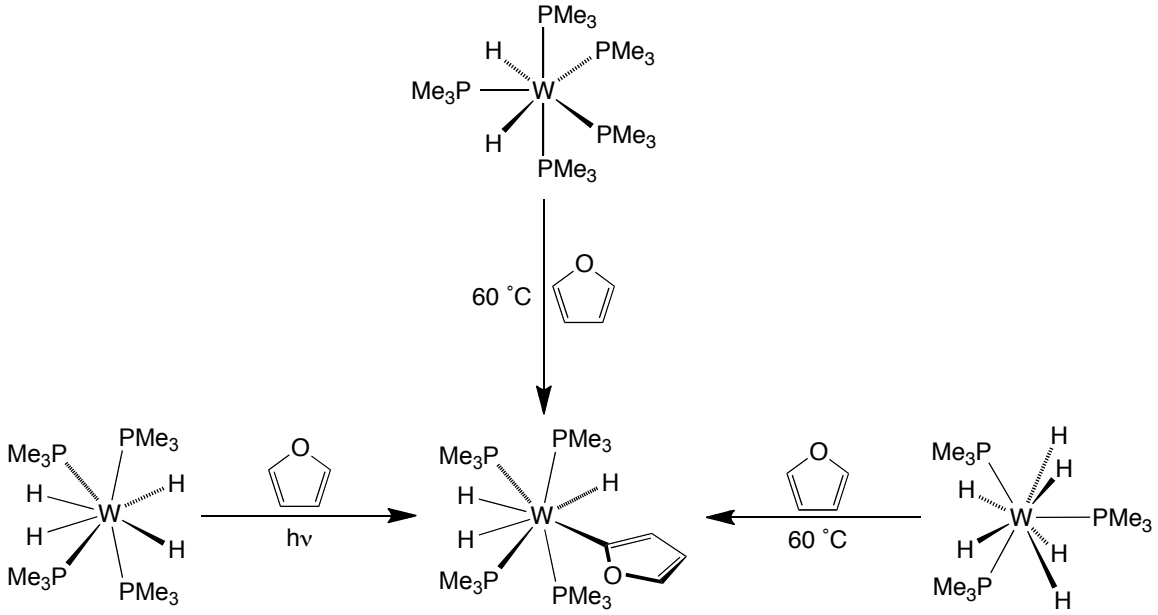

Scheme 5. Reactivity of $W(PMe_3)_5H_2$, $W(PMe_3)_4H_4$, and $W(PMe_3)_3H_6$ towards furan.

It is interesting to note that if the reactions of $W(PMe_3)_4H_4$ or $W(PMe_3)_3H_6$ with furan are performed in d_6-benzene, the only signals in the ^{1}H NMR spectrum that are observed for the furyl compound, $W(PMe_3)_4(\kappa^1\text{-}C_\alpha\text{-}C_4H_3O)H_3$, are those for the PMe_3 ligands, indicating that H/D exchange is occurring. Additionally, when there is an excess of furan in the reaction mixture, the resonances in the ^{1}H NMR spectrum of both the α- and β-sites of furan in solution almost quantitatively disappear, again indicating that deuterium is being incorporated into furan. In contrast, H/D exchange is not observed in reactions between $W(PMe_3)_4(\eta^2\text{–}CH_2PMe_2)H$ or $W(PMe_3)_5H_2$ and furan.

Taking all of these observations into account, we postulate that the active intermediate inducing H/D exchange is the 16-electron tetrahydride complex [$W(PMe_3)_3H_4$] (Table 1) for the following reasons. One, the reactivities of $W(PMe_3)_4(\eta^2$–$CH_2PMe_2)H$ and $W(PMe_3)_5H_2$ with furan are different, thereby indicating that *different* reactive intermediates are being produced. Therefore, while $W(PMe_3)_4(\eta^2$–$CH_2PMe_2)H$ is likely to react *via* [$W(PMe_3)_5$], $W(PMe_3)_5H_2$ presumably proceeds *via* [$W(PMe_3)_4H_2$], rather than the same [$W(PMe_3)_5$] intermediate (Table 1). Two, $W(PMe_3)_5H_2$ does not induce H/D exchange while $W(PMe_3)_4H_4$ does, thereby indicating that *different* intermediates are formed. Thus, while two likely intermediates of $W(PMe_3)_4H_4$ are [$W(PMe_3)_4H_2$] and [$W(PMe_3)_3H_4$] (Table 1), the former can be disregarded because it is the same intermediate that is proposed for $W(PMe_3)_5H_2$. Three, $W(PMe_3)_3H_6$ also induces H/D exchange, and a likely intermediate is [$W(PMe_3)_3H_4$], which is the same proposed for $W(PMe_3)_4H_4$. Although $W(PMe_3)_3H_6$ could also lose a PMe_3 ligand to produce the intermediate [$W(PMe_3)_2H_6$] (Table 1), it is considered to be unlikely because the hexavalent nature of the compound would prevent oxidative addition of a C–D bond of d_6-benzene, although a sigma-bond metathesis process is possible.

Therefore, it is proposed that [$W(PMe_3)_3H_4$] is the active intermediate that is able to undergo reversible oxidative-addition of C–D bonds of d_6-benzene and C–H bonds of furan. This would, therefore, produce d_4-furan and [$W(PMe_3)_3D_4$], which would then form the isotopomer, $W(PMe_3)_4(\kappa^1$-C_α-$C_4D_3O)D_3$, after the reaction is complete.

Table 1. Proposed intermediates of tungsten compounds and their ability to undergo H/D exchange.[a]

	Possible Intermediate(s)		H/D Exchange Observed?
$W(PMe_3)_4(\eta^2$–$CH_2PMe_2)H$	**[$W(PMe_3)_5$]**		no
$W(PMe_3)_5H_2$	[$W(PMe_3)_5$]	**[$W(PMe_3)_4H_2$]**	no
$W(PMe_3)_4H_4$	[$W(PMe_3)_4H_2$]	**[$W(PMe_3)_3H_4$]**	yes
$W(PMe_3)_3H_6$	[$W(PMe_3)_2H_6$]	**[$W(PMe_3)_3H_4$]**	yes

(a) Blue intermediates represent the proposed active intermediate in the reactions with furan in C_6D_6.

5.4 Reactivity of tungsten complexes towards benzofuran

The reactivity of tungsten trimethylphosphine complexes with benzofuran was also studied. Unfortunately, heating a solution of $W(PMe_3)_4(\eta^2\text{–}CH_2PMe_2)H$ in benzene with benzofuran at 60 ˚C is accompanied by a significant amount of decomposition; however, the aryloxide-olefin compound, $(\kappa^1,\eta^2\text{-}CH_2CHC_6H_4O)W(PMe_3)_3(\eta^2\text{–}CH_2PMe_2)$ (Scheme 6), was successfully isolated and its molecular structure is shown in Figure 8. $(\kappa^1,\eta^2\text{-}CH_2CHC_6H_4O)W(PMe_3)_3(\eta^2\text{–}CH_2PMe_2)$ is analogous to the product that is obtained from the reaction between benzothiophene and $W(PMe_3)_4(\eta^2\text{–}CH_2PMe_2)H$, namely $(\kappa^1,\eta^2\text{-}CH_2CHC_6H_4S)W(PMe_3)_3(\eta^2\text{–}CH_2PMe_2)$ (see Chapter 4). If the reaction between $W(PMe_3)_4(\eta^2\text{–}CH_2PMe_2)H$ and benzofuran is carried out in the presence of H_2, two different products are observed (Scheme 6), namely (*i*) the C–H cleaved benzofuryl complex, $W(PMe_3)_4(\kappa^1\text{-}C_\alpha\text{-}CCHOC_6H_4)H_3$ and (*ii*) the aryloxide complex, $W(PMe_3)_4(OC_6H_4Et)H_3$,[23] which presumably results from hydrogenation of the aforementioned C–O bond cleaved product, $(\kappa^1,\eta^2\text{-}CH_2CHC_6H_4O)W(PMe_3)_3(\eta^2\text{–}CH_2PMe_2)$. Both complexes have been structurally characterized by X-ray diffraction and their molecular structures are shown in Figures 9 and 10, respectively, thereby indicating that their geometries are very similar to the respective sulfur compounds, $W(PMe_3)_4(\kappa^1\text{-}C_\alpha\text{-}CCHSC_6H_4)H_3$ and $W(PMe_3)_4(SC_6H_4Et)H_3$ (see Chapter 4).

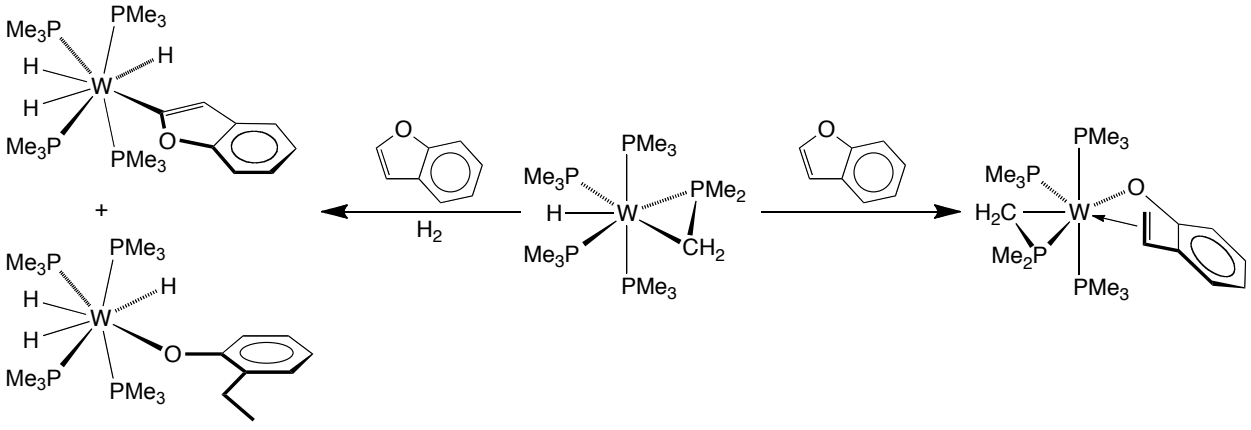

Scheme 6. Reactivity of $W(PMe_3)_4(\eta^2\text{–}CH_2PMe_2)H$ towards benzofuran.

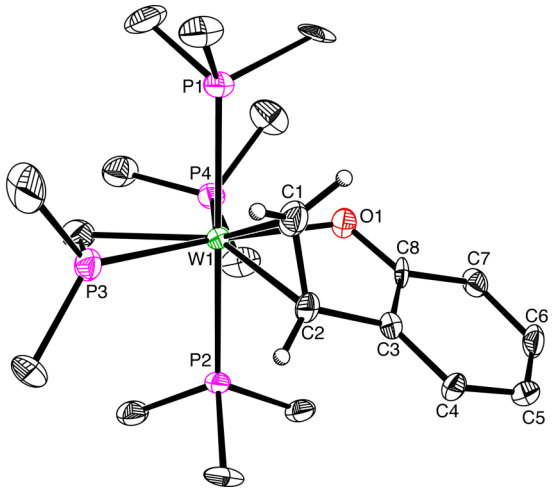

Figure 8. Molecular structure of $(\kappa^1,\eta^2\text{–}CH_2CHC_6H_4O)W(PMe_3)_3(\eta^2\text{–}CH_2PMe_2)$.

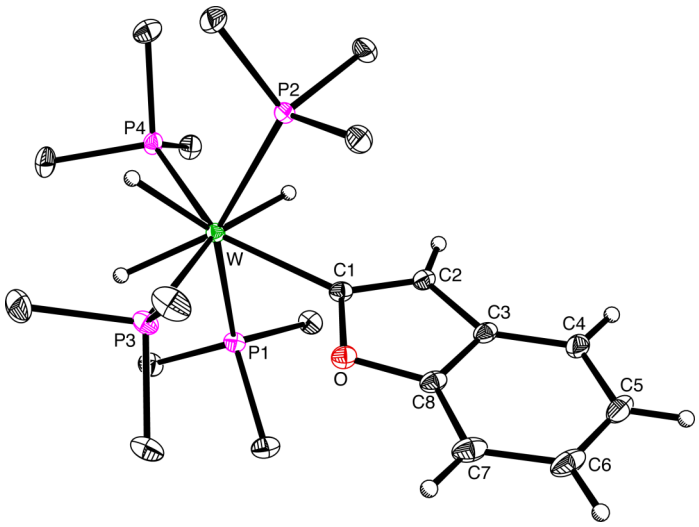

Figure 9. Molecular structure of $W(PMe_3)_4(\kappa^1\text{–}C_\alpha\text{–}CCHOC_6H_4)H_3$.

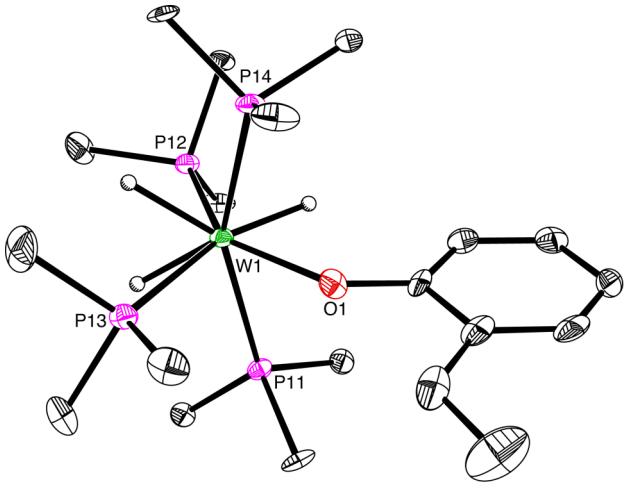

Figure 10. Molecular structure of $W(PMe_3)_4(OC_6H_4Et)H_3$.

The reactivity of the series of tungsten trimethylphosphine hydrides, namely $W(PMe_3)_5H_2$, $W(PMe_3)_4H_4$, and $W(PMe_3)_3H_6$ with benzofuran was also investigated. For example, treatment of $W(PMe_3)_4H_4$ or $W(PMe_3)_3H_6$ with benzofuran also results in the formation of, *inter alia*, $W(PMe_3)_4(\kappa^1\text{-}C_\alpha\text{-}CCHOC_6H_4)H_3$ and $W(PMe_3)_4(OC_6H_4Et)H_3$, although the former requires activation by photolysis (Scheme 7). The best method of synthesis of $W(PMe_3)_4(\kappa^1\text{-}C_\alpha\text{-}CCHOC_6H_4)H_3$ is, however, heating a solution of $W(PMe_3)_5H_2$ and benzofuran in benzene at 60 ˚C, as negligible quantities of $W(PMe_3)_4(OC_6H_4Et)H_3$ are observed (Scheme 8).

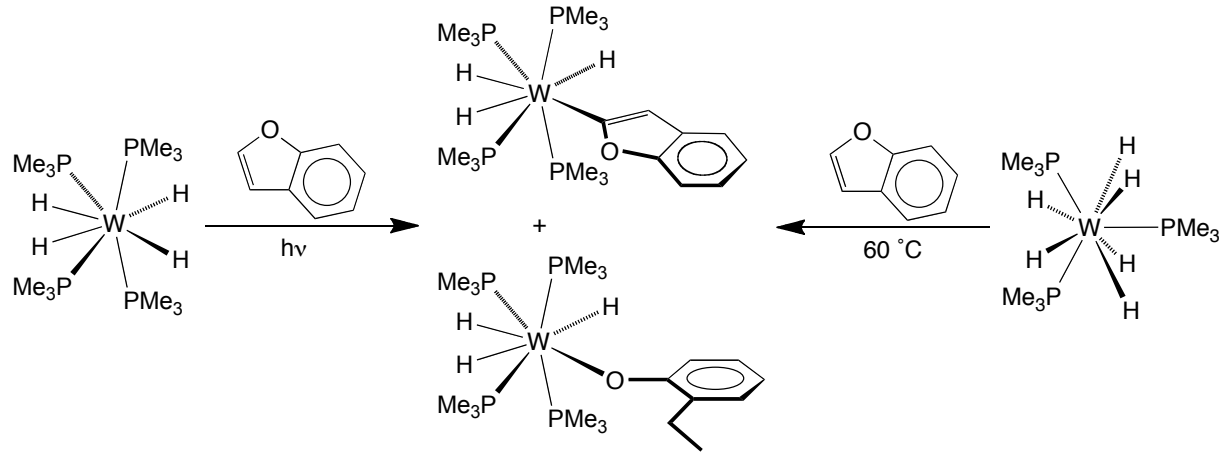

Scheme 7. Reactivity of $W(PMe_3)_4H_4$ and $W(PMe_3)_3H_6$ towards benzofuran.

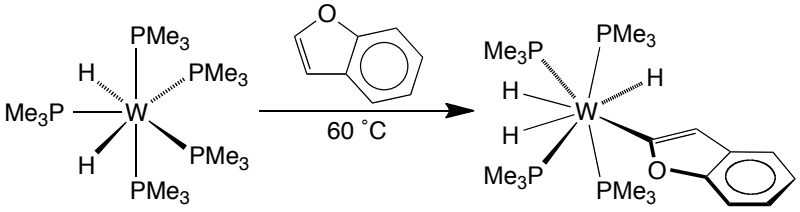

Scheme 8. Reactivity of $W(PMe_3)_5H_2$ towards benzofuran.

5.5 Reactivity of $Mo(PMe_3)_6$ towards furan

The reactivity of $Mo(PMe_3)_6$ towards furan suffered from a significant amount of decomposition when heated at 60 ˚C in d_6-benzene, but two complexes were identified in solution by comparison of the ^1H NMR spectrum of the reaction mixture to that of the

tungsten system, namely (η^5–C_4H_5O)Mo(PMe_3)$_2$(η^2–CH_2PMe_2) and (κ^1,η^2-C_4H_3O)(κ^1-*O*-C_4H_5O)Mo(PMe_3)$_3$ (Scheme 9). Furthermore, the formation of (κ^1,η^2-C_4H_3O)(κ^1-*O*-C_4H_5O)Mo(PMe_3)$_3$ was confirmed by X-ray diffraction (Figure 11). Interestingly, a geometrical isomer of (κ^1,η^2-C_4H_3O)(κ^1-*O*-C_4H_5O)Mo(PMe_3)$_3$ is also formed in the reaction between Mo(PMe_3)$_6$ and furan, in which the (κ^1-*O*-C_4H_5O) ligand has an *E* configuration (Figure 12) rather than the expected *Z* isomer (based on the fact that furan has a *Z* configuration). The molecular structure of the *E* isomer is also shown in Figure 11.[24] Additionally, it is apparent that with the exception of the (κ^1-*O*-C_4H_5O) ligands, the two isomers of (κ^1,η^2-C_4H_3O)(κ^1-*O*-C_4H_5O)Mo(PMe_3)$_3$ are structurally very similar, which is illustrated by the structural overlay in Figure 13.

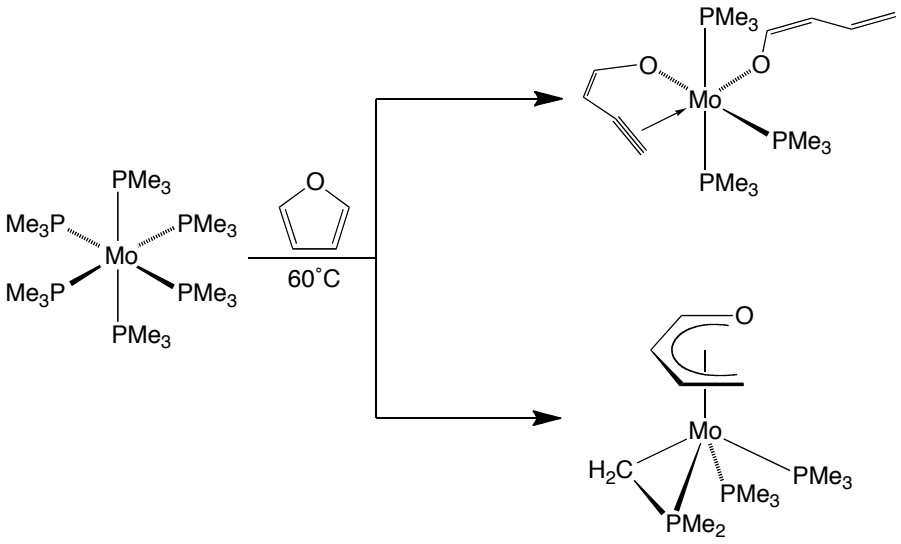

Scheme 9. Reactivity of Mo(PMe_3)$_6$ towards furan.

It is interesting to note that while the reaction between Mo(PMe_3)$_6$ and thiophene allowed for the characterization of the η^5-thiophene complex (η^5–C_4H_4S)Mo(PMe_3)$_3$,[11] there is no evidence for the production of the analogous η^5-furan complex in the reaction between Mo(PMe_3)$_6$ and furan. This is, however, not surprising as π-complexes of furan are not well-known;[25,26] indeed, we are aware of only one report of a furan π-complex, namely [Cp*Ru(η^5-C_4H_4O)]Cl.[27,28]

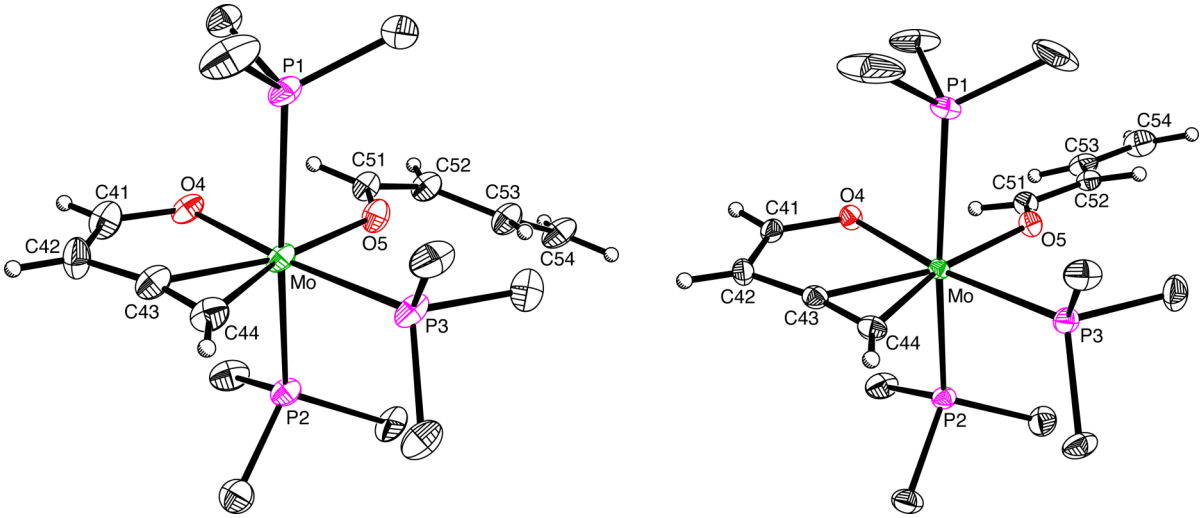

Figure 11. Molecular structures of *Z* (left) and *E* (right) isomers of $(\kappa^1,\eta^2\text{-}C_4H_3O)(\kappa^1\text{-}O\text{-}C_4H_5O)Mo(PMe_3)_3$.

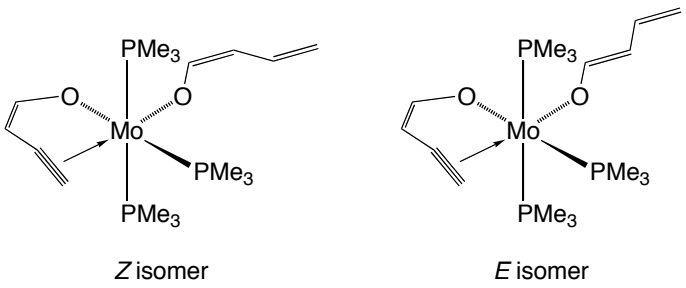

Figure 12. Isomeric forms of $(\kappa^1,\eta^2\text{-}C_4H_3O)(\kappa^1\text{-}O\text{-}C_4H_5O)Mo(PMe_3)_3$.

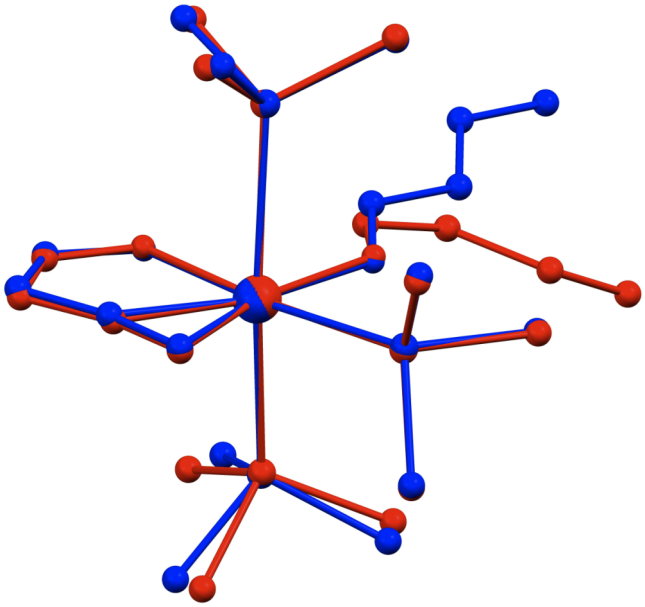

Figure 13. Structural overlay of *Z* (red) and *E* (blue) isomers of $(\kappa^1,\eta^2\text{-}C_4H_3O)(\kappa^1\text{-}O\text{-}C_4H_5O)Mo(PMe_3)_3$.

As an attempt to discover a better synthetic route towards the aforementioned molybdenum compounds, the reactivity of crotonaldehyde towards $Mo(PMe_3)_6$ was explored (Scheme 10). Alas, this reaction was also accompanied by a significant amount of decomposition, and analysis of the ^1H NMR spectrum did not indicate the presence of any $(\eta^5\text{–}C_4H_5O)Mo(PMe_3)_2(\eta^2\text{–}CH_2PMe_2)$ or $(\kappa^1,\eta^2\text{-}C_4H_3O)(\kappa^1\text{-}O\text{-}C_4H_5O)Mo(PMe_3)_3$. However, a new complex of molybdenum, namely $(\eta^4\text{-}OC_4H_6)_2Mo(PMe_3)_2$, was isolated and structurally characterized by X-ray diffraction (Figure 14). Interestingly, there are no transition metal η^4-crotonaldehyde complexes listed in the Cambridge Structural Database,[29] making $(\eta^4\text{-}OC_4H_6)_2Mo(PMe_3)_2$ the first structurally characterized example of this type.[30] It should be noted, however, that there are several structurally characterized κ^1-crotonaldehyde complexes reported,[31] all of which have an *s-trans* conformation.

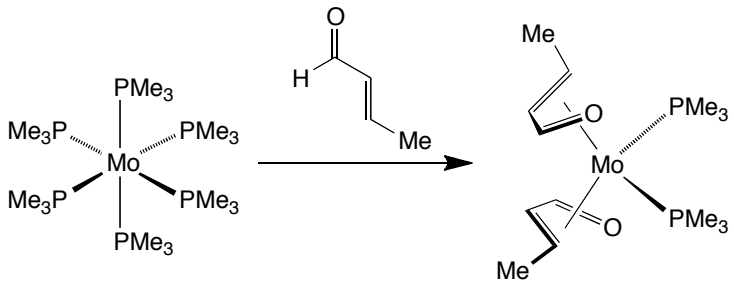

Scheme 10. Reactivity of $Mo(PMe_3)_6$ towards crotonaldehyde.

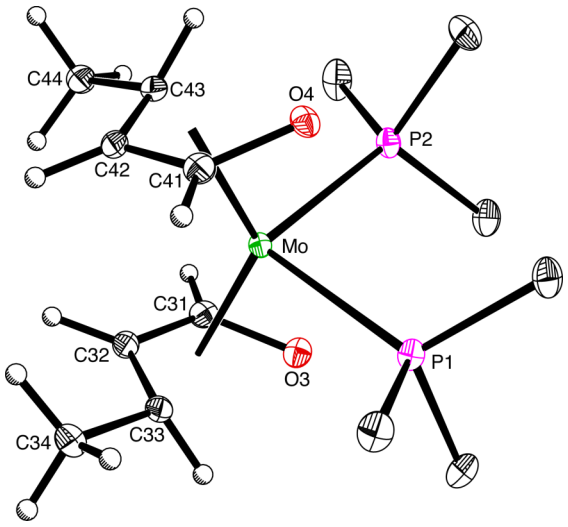

Figure 14. Molecular structure of $(\eta^4\text{-}OC_4H_6)_2Mo(PMe_3)_2$.

The (η^4-OC_4H_6) ligands in (η^4-OC_4H_6)$_2$Mo(PMe_3)$_2$ can be described by two limiting resonance structures, illustrated in Figure 15. In resonance (A), the crotonaldehyde ligand is an L_2 donor (Figure 15) with purely dative bonding from the π-system to empty metal d-orbitals, and would be expected to be dominant in electron-poor complexes. On the other hand, in resonance (B), there is a significant amount of backbonding such the crotonaldehyde ligand is more appropriately described as an LX_2 ligand (Figure 15), and is expected for electron-rich complexes. In this regard, analysis of the crystal structure data of (η^4-OC_4H_6)$_2$Mo(PMe_3)$_2$ indicate a situation intermediate between resonances (A) and (B), in which there is a significant amount of metal-ligand backbonding. Specifically, the relevant C–C bond lengths (*i.e.* not including the C–Me bond) in the (η^4-OC_4H_6) ligands [C31–C32: 1.415(3) Å, C32–C33: 1.421(3) Å, C41–C42: 1.417(3) Å, C42–C43: 1.424(3) Å] are all very similar with a narrow range of 0.009 Å, indicating that there is not a localization of double bond character. For comparison purposes, Templeton has reported the κ^1-crotonaldehyde complex of tungsten, Tp'W(CO)(PhC≡CMe)(κ^1-OC_4H_6) (Tp' = hydrotris(3,5-dimethylpyrazolyl)borate), which has C–C bond lengths that differ by 0.095 Å [1.423(10) Å and 1.328(11) Å] in the (κ^1-OC_4H_6) ligand, clearly indicating the localization of the double bonds in the α,β-unsaturated system.[31a] Moreover, the O–C bond length of 1.232(8) Å in Tp'W(CO)-(PhC≡CMe)(κ^1-OC_4H_6)[31a] is significantly shorter (Δ_{avg} = 0.111 Å) as compared with the C–O bond lengths [O3–C31: 1.344(2) Å, O4–C41: 1.342(2) Å] in (η^4-OC_4H_6)$_2$Mo(PMe_3)$_2$.

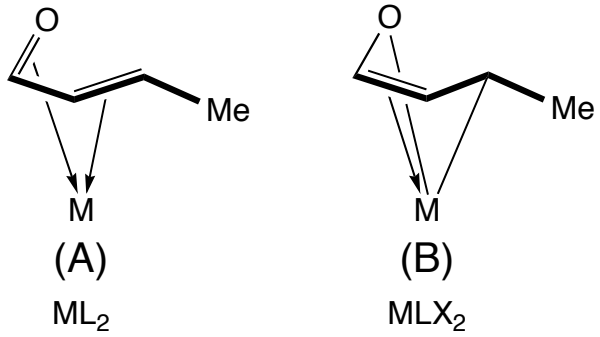

Figure 15. Resonance structures describing the metal-ligand interactions in η^4-crotonaldehyde complexes.

It is relevant to note that the *bis*-butadiene compound $(\eta^4\text{-}C_4H_6)_2Mo(PMe_3)_2$ synthesized by Green[32] is structurally very similar to that of $(\eta^4\text{-}OC_4H_6)_2Mo(PMe_3)_2$, and this is illustrated in Figure 16. Akin to $(\eta^4\text{-}OC_4H_6)_2Mo(PMe_3)_2$, the C–C bond lengths in $(\eta^4\text{-}C_4H_6)_2Mo(PMe_3)_2$ are all very similar [C1–C2: 1.406(5) Å, C2–C3: 1.395(5) Å, C3–C4: 1.413(5) Å, C5–C6: 1.409(5) Å, C6–C7: 1.397(5) Å, C7–C8: 1.413(5) Å], with a narrow range of 0.018 Å, indicating a similar degree of metal-to-ligand backbonding.

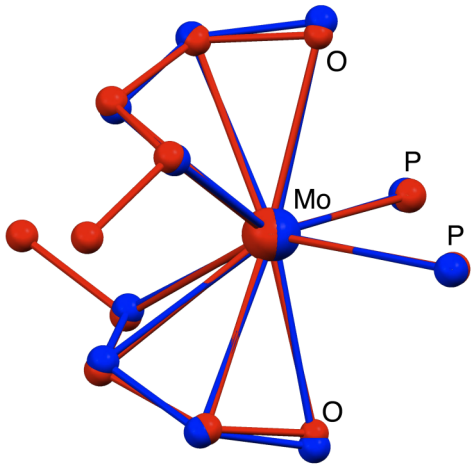

Figure 16. Structural overlay of $(\eta^4\text{-}OC_4H_6)_2Mo(PMe_3)_2$ (red) and $(\eta^4\text{-}C_4H_6)_2Mo(PMe_3)_2$ (blue). Methyl groups of the PMe_3 ligands are not shown for clarity.

5.6 Reactivity of molybdenum hydride complexes towards furan

The reactivity of furan towards molybdenum hydrides was also studied. For example, heating a mixture of $Mo(PMe_3)_6$ and furan in benzene under an atmosphere of H_2 produces, *inter alia*, propene and propane (Scheme 11), as identified by ^1H NMR spectroscopy.[33,34] These observations indicate that the C–O and C–C bonds of furan have been broken. Furthermore, it was determined that the other fragment emanating from furan is CO, as confirmed by obtaining a crystal structure of the metal carbonyl compound, $(\eta^6\text{-}PhH)Mo(PMe_3)_2CO$, shown in Figure 17.[35] It should be noted that $Mo(PMe_3)_6$ converts to $Mo(PMe_3)_4H_4$ under such conditions, such that $Mo(PMe_3)_4H_4$ may be the active reagent causing the furan fragmentation. In this regard, heating

solutions of $Mo(PMe_3)_4H_4$ and furan in benzene also produced propene and propane (Scheme 11).[36] Furan C–C and C–O bond cleavage reactions have been observed previously in a homogenous system,[14] and in addition, the formation of CO from furan has also been observed on molybdenum and palladium surfaces.[37,38]

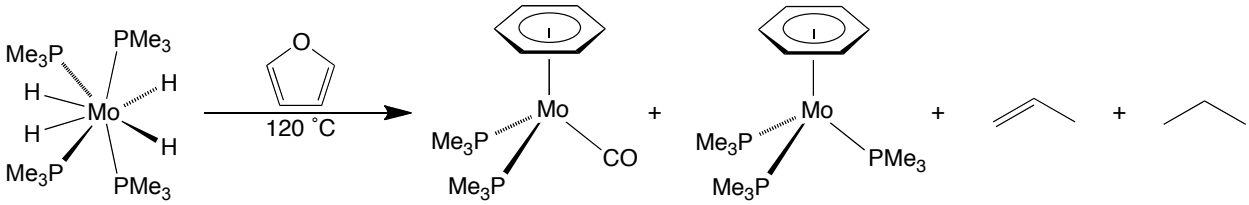

Scheme 11. C–O, C–H, and C–C bond cleavage of furan by molybdenum.

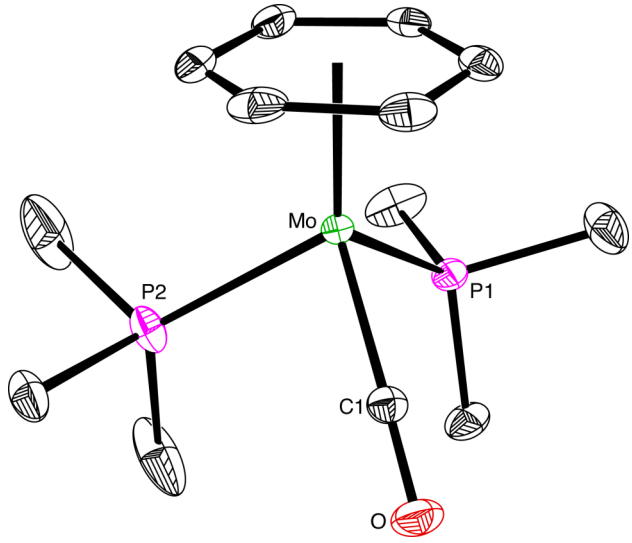

Figure 17. Molecular structure of $(\eta^6\text{-PhH})Mo(PMe_3)_2CO$.

5.7 Structural characterization of molybdenum complexes derived from benzofuran and dibenzofuran

The reactivity of $Mo(PMe_3)_6$ towards benzofuran was also studied. In contrast to the other furan reactions with the abovementioned molybdenum and tungsten compounds, a reaction between $Mo(PMe_3)_6$ and benzofuran occurs immediately at room temperature when the two compounds are mixed in d_6-benzene. Analysis of the ^1H NMR spectrum of the reaction mixture indicates the presence of at least two

paramagnetic compounds. One of these paramagnetic compounds was identified by former graduate student Daniela Buccella[39] as (κ^1,η^2-$CH_2CHC_6H_4O$)Mo(κ^1-C_α-$CCHOC_6H_4$)(PMe_3)$_3$ (Scheme 12), which has two ligands emanating from benzofuran: one ligand is the C–H cleaved benzofuryl unit, (κ^1-C_α-$CCHOC_6H_4$), and the other is the aryloxide-olefin (κ^1,η^2-$CH_2CHC_6H_4O$), both of which were observed as ligands for tungsten (see Section 5.4). Another compound identified by X-ray diffraction, namely (κ^1,η^2-$CH_2CHC_6H_4O$)(κ^1,η^2-$HC(PMe_3)CHC_6H_4O$)Mo(PMe_3)$_2$ (Figure 18), also contains two ligands derived from benzofuran (Scheme 12); both are aryloxide-olefins, except one has a PMe_3 group replacing a hydrogen at the vinyl position. Lastly, (κ^1,η^2-$CH_2CHC_6H_4O$)Mo(PMe_3)$_3$(η^2–CH_2PMe_2), a diamagnetic complex, was isolated (Scheme 12) and structurally characterized (Figure 19), a complex that is analogous to product obtained from the reaction between W(PMe_3)$_4$(η^2–CH_2PMe_2)H and benzofuran, namely (κ^1,η^2-$CH_2CHC_6H_4O$)W(PMe_3)$_3$(η^2–CH_2PMe_2).[40]

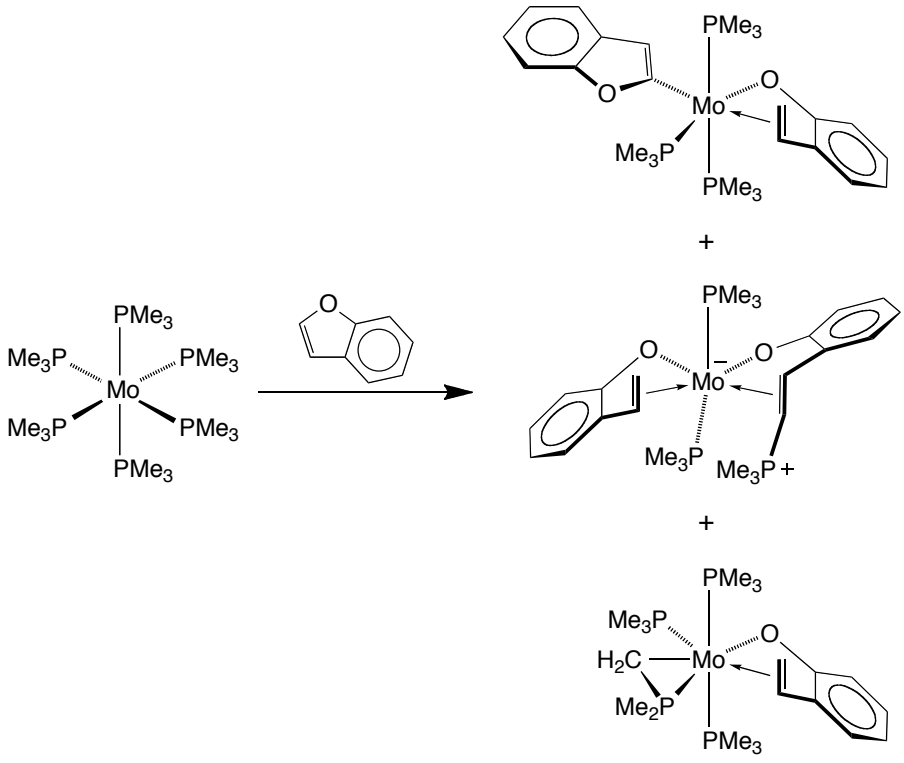

Scheme 12. Reactivity of Mo(PMe_3)$_6$ towards benzofuran.

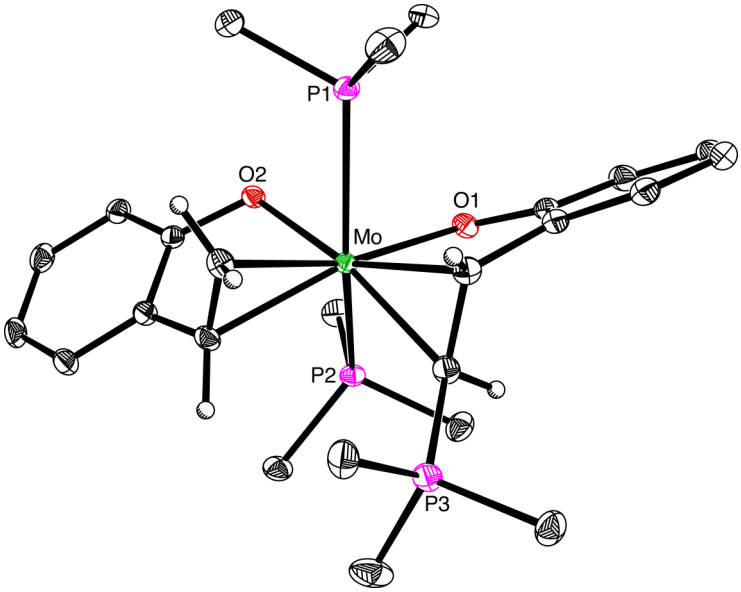

Figure 18. Molecular structure of $(\kappa^1,\eta^2\text{-}CH_2CHC_6H_4O)(\kappa^1,\eta^2\text{-}HC(PMe_3)CHC_6H_4O)Mo(PMe_3)_2$.

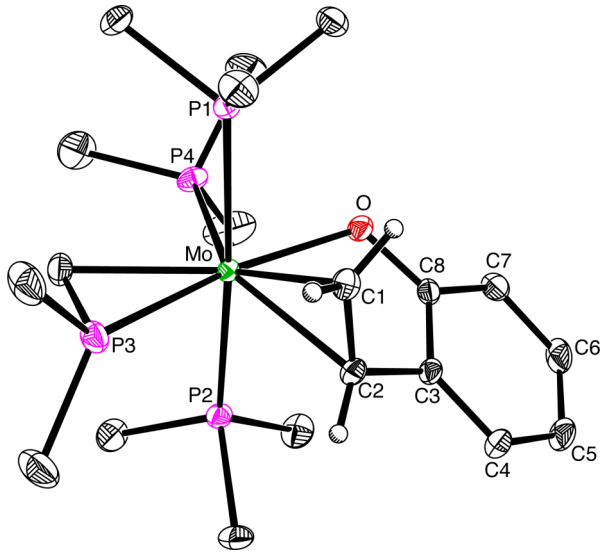

Figure 19. Molecular structure of $(\kappa^1,\eta^2\text{–}CH_2CHC_6H_4O)Mo(PMe_3)_3(\eta^2\text{–}CH_2PMe_2)$.

The reactivity of $Mo(PMe_3)_6$ towards dibenzothiophene was also explored, allowing for the isolation of $(\eta^6\text{-}C_6H_4C_6H_4O)Mo(PMe_3)_3$, which has been structurally characterized by X-ray diffraction (Figure 20). Interestingly, in the Cambridge Structural Database,[29] there are no transition metal dibenzofuran complexes, such that

$(\eta^6\text{-}C_6H_4C_6H_4O)Mo(PMe_3)_3$ is the first structurally characterized transition metal dibenzofuran adduct. It should be noted that a substituted benzodibenzofuran compound with a $[Cr(CO)_3]$ unit coordinated in an η^6 fashion to the carbocyclic ring has been synthesized and structurally characterized.[41]

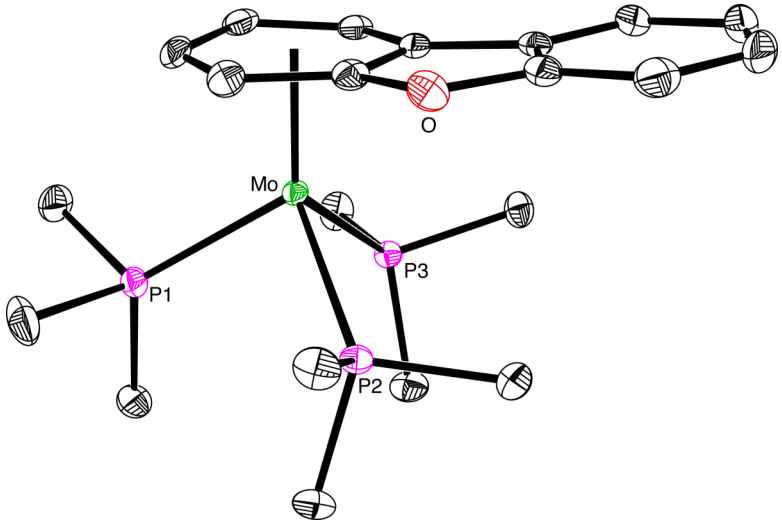

Figure 20. Molecular structure of $(\eta^6\text{-}C_6H_4C_6H_4O)Mo(PMe_3)_3$.

5.8 Reactivity of $W(PMe_3)_4(\eta^2\text{–}CH_2PMe_2)H$ and $Mo(PMe_3)_6$ towards dihydrofurans

The reactivity of dihydrofurans (2,5-dihydrofuran and 2,3-dihydrofuran) towards $W(PMe_3)_4(\eta^2\text{–}CH_2PMe_2)H$ and $Mo(PMe_3)_6$ was also investigated. For example, the dihydrofuryl complex, $W(PMe_3)_4(\kappa^1\text{-}C_\alpha\text{-}C_4H_5O)H_3$ (Figure 22), was isolated by reaction of $W(PMe_3)_4(\eta^2\text{–}CH_2PMe_2)H$ towards 2,3-dihydrofuran in the presence of H_2 at 60°C (Scheme 13). The dihydrofuryl complex, $W(PMe_3)_4(\kappa^1\text{-}C_\alpha\text{-}C_4H_5O)H_3$, is structurally very similar to that of the furyl complex, $W(PMe_3)_4(\kappa^1\text{-}C_\alpha\text{-}C_4H_3O)H_3$, which is illustrated by the structural overlay in Figure 23. Additionally, the reaction of $Mo(PMe_3)_6$ and 2,5-dihydrofuran at room temperature produces the compound $(\eta^5\text{–}C_4H_5O)Mo(PMe_3)_3H$ (Scheme 14), which was characterized by ^1H and $^{31}P\{^1H\}$ NMR spectroscopy.[42] Hence, $(\eta^5\text{–}C_4H_5O)Mo(PMe_3)_3H$ is related to $(\eta^5\text{–}C_4H_5O)Mo(PMe_3)_2(\eta^2\text{–}CH_2PMe_2)$ by formal H_2

addition across the Mo–C bond of the cyclometalated (η^2–CH_2PMe_2) ligand, and this H_2 equivalent presumably emanates from the 2,5-dihydrofuran.[43]

Figure 21. Isomeric forms of dihydrofurans.

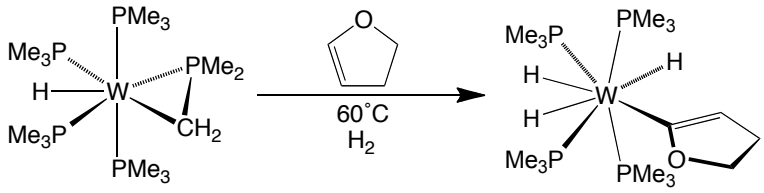

Scheme 13. Reactivity of $W(PMe_3)_4(\eta^2–CH_2PMe_2)H$ towards 2,3-dihydrofuran and H_2.

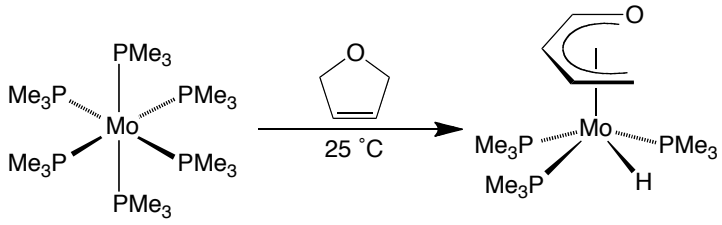

Scheme 14. Reactivity of $Mo(PMe_3)_6$ towards 2,5-dihydrofuran.

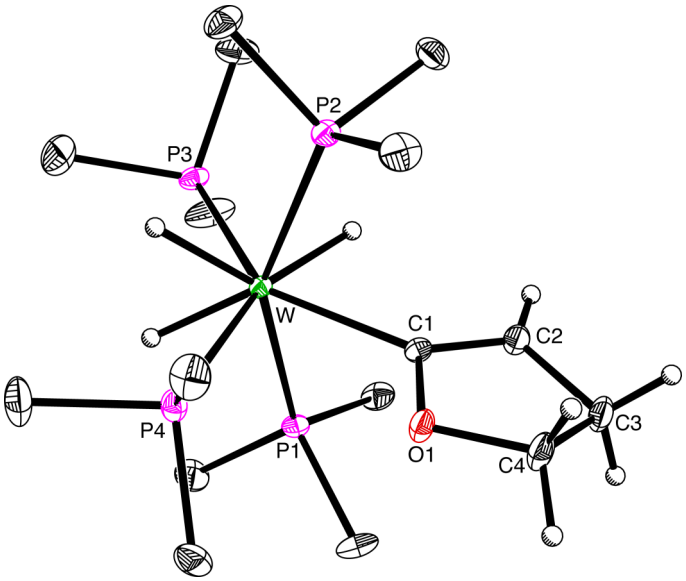

Figure 22. Molecular structure of $W(PMe_3)_4(\kappa^1–C_\alpha–C_4H_5O)H_3$.

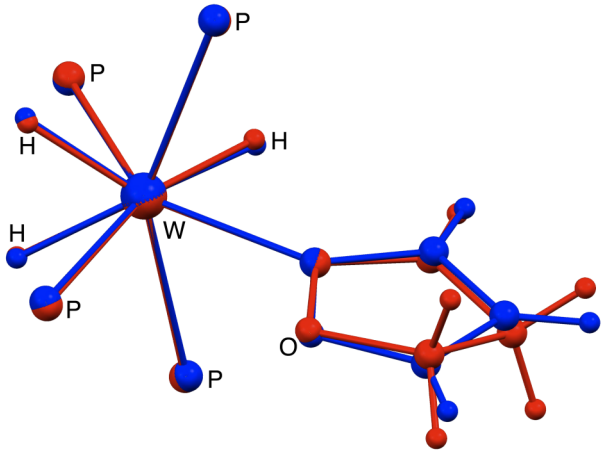

Figure 23. Structural overlay of $W(PMe_3)_4(\kappa^1\text{-}C_\alpha\text{-}C_4H_5O)H_3$ (red) and $W(PMe_3)_4(\kappa^1\text{-}C_\alpha\text{-}C_4H_3O)H_3$ (blue). Methyl groups of the PMe_3 ligands are not shown for clarity.

Lastly, several other interesting reactions of $Mo(PMe_3)_6$ and $W(PMe_3)_4(\eta^2\text{–}CH_2PMe_2)H$ towards dihydrofurans were discovered. Specifically, treatment of (*i*) $Mo(PMe_3)_6$ with either isomer of dihydrofuran resulted in the production of, *inter alia*, propene[33] and $Mo(PMe_3)_5CO$ (Scheme 15) and (*ii*) treatment of $W(PMe_3)_4(\eta^2\text{–}CH_2PMe_2)H$ with either isomer of dihydrofuran resulted in the production of, *inter alia*, propene[33] and $W(PMe_3)_5CO$ (Scheme 16) at 60 ˚C. The carbonyl compounds, $Mo(PMe_3)_5CO$ and $W(PMe_3)_5CO$, were structurally characterized by X-ray diffraction and are shown in Figures 24 and 25, respectively. These observations clearly indicate the ability of molybdenum and tungsten to perform C–O, C–C, and C–H bond activations of oxygenated compounds.

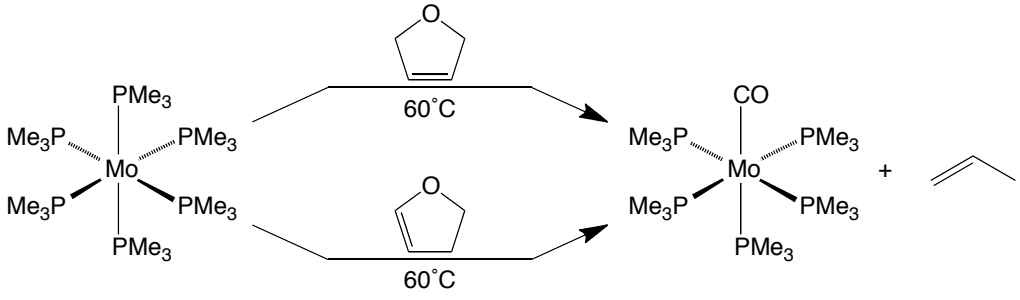

Scheme 15. Reactivity of $Mo(PMe_3)_6$ with dihydrofurans.

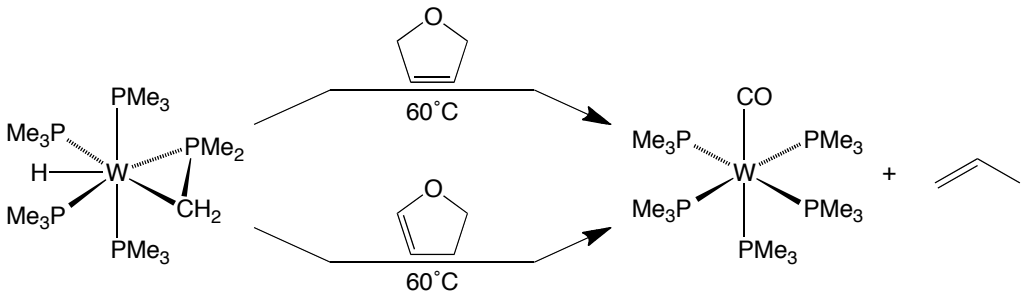

Scheme 16. Reactivity of $W(PMe_3)_4(\eta^2–CH_2PMe_2)H$ towards dihydrofurans.

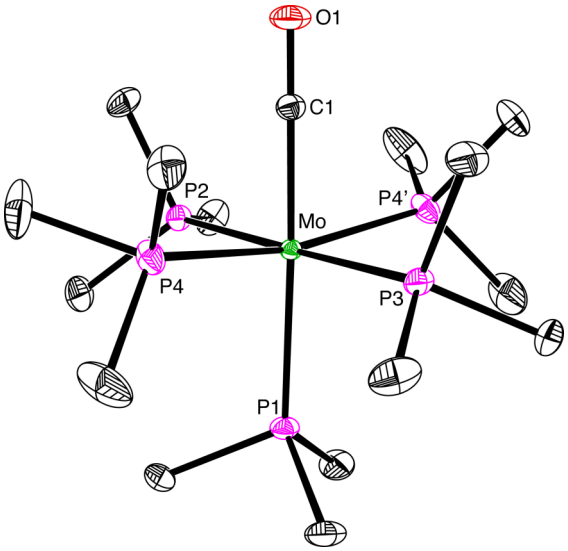

Figure 24. Molecular structure of $Mo(PMe_3)_5CO$.

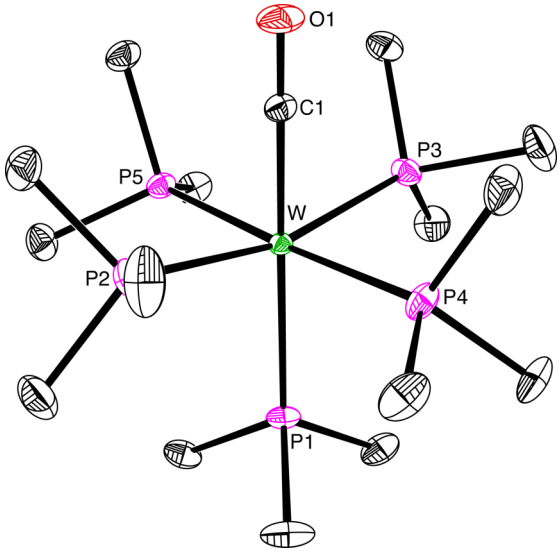

Figure 25. Molecular structure of $W(PMe_3)_5CO$.

5.9 Reactivity of alcohols towards tungsten and molybdenum trimethylphoshpine complexes

The Parkin group has previously examined the reactivity of alcohols with $Mo(PMe_3)_6$,[44,45] and $W(PMe_3)_4(\eta^2\text{–}CH_2PMe_2)H$.[46] Furthermore, Parkin and Green discovered that $W(PMe_3)_4(\eta^2\text{–}CH_2PMe_2)H$ reacts with methanol to produce an η^2-formaldehyde complex *via* dehydrogenation, namely $W(PMe_3)_4(\eta^2\text{-}OCH_2)H_2$,[47] which then reacts with H_2 to produce the methoxy trihydride complex, $W(PMe_3)_4(OMe)H_3$ (Scheme 17).[48,49] We have now crystallographically characterized the formaldehyde compound, and its molecular structure is shown in Figure 26.[50] Similar reactivity between ethanol and $W(PMe_3)_4(\eta^2\text{–}CH_2PMe_2)H$ has been observed (Scheme 17), first producing the η^2-acetaldehyde complex, $W(PMe_3)_4(\eta^2\text{-}OCMeH)H_2$, followed by the hydrogenated ethoxy trihydride complex, $W(PMe_3)_4(OEt)H_3$.[51] Both complexes, namely $W(PMe_3)_4(\eta^2\text{-}OCMeH)H_2$ and $W(PMe_3)_4(OEt)H_3$,[52] have been structurally characterized by X-ray diffraction, and are shown in Figures 26 and 27, respectively.

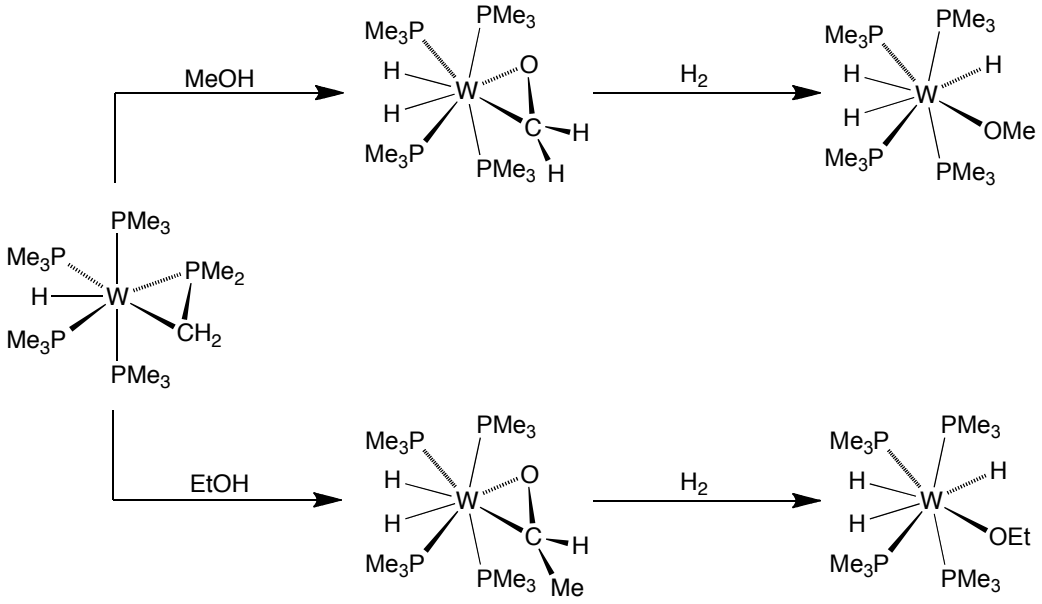

Scheme 17. Reactivity of $W(PMe_3)_4(\eta^2\text{–}CH_2PMe_2)H$ towards methanol and ethanol.

Interestingly, there are no metal acetaldehyde complexes listed in the Cambridge Structural Database,[29] making $W(PMe_3)_4(\eta^2\text{-}OCMeH)H_2$ the first structurally characterized example of this type. It should be noted, however, that there are reports of acetaldehyde complexes in the literature, but their molecular structures were not determined.[53] Lastly, $W(PMe_3)_4(OEt)H_3$ has a similar coordination geometry to that of the related phenoxide complex $W(PMe_3)_4(OPh)H_3$, which has been previously synthesized and structurally characterized by Wilkinson.[49]

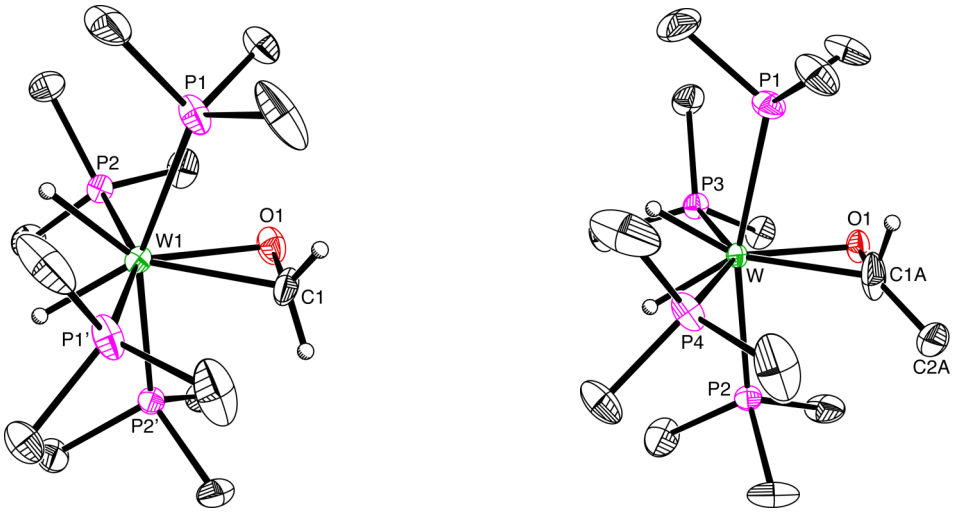

Figure 26. Molecular structures of $W(PMe_3)_4(\eta^2\text{-}OCH_2)H_2$ (left) (disorder between the η^2-OCH_2 unit and the two hydrides not shown) and $W(PMe_3)_4(\eta^2\text{-}OCMeH)H_2$ (right) (only one disordered configuration of the η^2-OCMeH unit shown).

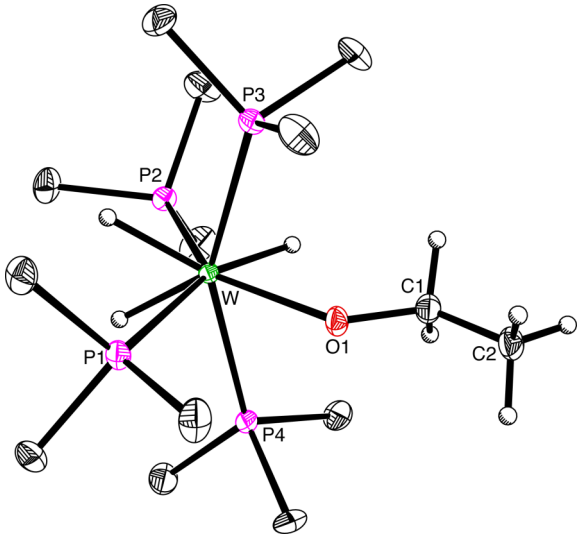

Figure 27. Molecular structure of $W(PMe_3)_4(OEt)H_3$.

5.10 Summary and conclusions

In summary, the reactivity of trimethylphosphine complexes of tungsten and molybdenum towards organic oxygenated compounds has been investigated. Several interesting C–O and C–H bond cleavage reactions have been observed for furan, benzofuran and dihydrofurans, and many of these products have been structurally characterized, giving insight into the type of coordination chemistry that may be observed on the surface of a hydrotreating catalyst. Most interestingly, $Mo(PMe_3)_4H_4$ is capable of deoxygenating furan to produce propene and carbon monoxide, the latter being trapped *in situ* to form the molybdenum carbonyl compound, (η^6-PhH)$Mo(PMe_3)_2CO$.

5.11 Experimental details

5.11.1 General considerations

All manipulations were performed using a combination of glovebox, high vacuum, and Schlenk techniques under an argon atmosphere unless otherwise specified.[54] Solvents were purified and degassed by standard procedures. ^1H NMR spectra were measured on Bruker 300 DRX, Bruker 400 DRX, and Bruker Avance 500 DMX spectrometers. ^1H chemical shifts are reported in ppm relative to $SiMe_4$ ($\delta = 0$) and were referenced internally with respect to the protio solvent impurity (δ 7.16 for C_6D_5H, 2.09 for C_7D_7H, 1.38 for $C_6D_{11}H$, and 7.26 for $CHCl_3$).[55,56] ^{13}C NMR spectra are reported in ppm relative to $SiMe_4$ ($\delta = 0$) and were referenced internally with respect to the solvent (δ 128.06 for C_6D_6).[55] ^{31}P chemical shifts are reported in ppm relative to 85% H_3PO_4 ($\delta = 0$) and were referenced using $P(OMe)_3$ ($\delta = 141.0$) as an external standard.[57] Coupling constants are given in hertz. Infrared spectra were recorded on Nicolet Avatar 370 DTGS spectrometer and are reported in cm^{-1}. Mass spectra were obtained on a Micromass Quadrupole-Time-of-Flight mass spectrometer using fast atom bombardment (FAB).

$Mo(PMe_3)_6$,[58] $Mo(PMe_3)_4H_4$,[59] $W(PMe_3)_4(\eta^2–CH_2PMe_2)H$,[60] $W(PMe_3)_5H_2$,[60] $W(PMe_3)_4H_4$,[60] and were prepared by the literature methods. $W(PMe_3)_3H_6$ was obtained *via* the photochemical reaction of $W(PMe_3)_4H_4$ with H_2.[61] Furan, d_4-furan, benzofuran, and crotonaldehyde were purchased from Aldrich and dried over molecular sieves prior to use. Dibenzofuran was purchased from Aldrich.

5.11.2 X-ray structure determinations

X-ray diffraction data were collected on a Bruker Apex II diffractometer. Crystal data, data collection and refinement parameters are summarized in the Section 5.12, Table 2. The structures were solved using direct methods and standard difference map techniques, and were refined by full-matrix least-squares procedures on F^2 with SHELXTL (Version 6.10).[62]

5.11.3 Computational details

Calculations were carried out using DFT as implemented in the Jaguar 7.5 (release 207) suite of *ab initio* quantum chemistry programs.[63] Geometry optimizations were performed with the B3LYP density functional[64] using the 6-31G** (C, H, P and O) and LACVP (Mo and W) basis sets.[65] The energies of the optimized structures were reevaluated by additional single point calculations on each optimized geometry using cc-pVTZ(-f) correlation consistent triple-ζ basis set for C, H, P, and O and LACV3P for Mo and W.

5.11.4 Synthesis of $(\kappa^1,\eta^2\text{-}C_4H_3O)(\kappa^1\text{-}O\text{-}C_4H_5O)W(PMe_3)_3$

$W(PMe_3)_4(\eta^2–CH_2PMe_2)H$ (25 mg, 0.04 mmol) was added to an NMR tube equipped with a J. Young valve. Furan (ca. 71 μL, 0.98 mmol) was added to a vial with d_6-benzene (*ca*. 0.7 mL) and this solution was then added to the NMR tube and sealed.

Integration of the ^{1}H NMR spectrum of this sample indicated that the ratio of $W(PMe_3)_4(\eta^2\text{–}CH_2PMe_2)H$ to furan was 1 : 22, respectively. The sample was heated at 60˚C for ~6 hours and monitored by ^{1}H NMR spectroscopy, thereby demonstrating conversion to $(\kappa^1,\eta^2\text{-}C_4H_3O)(\kappa^1\text{-}O\text{-}C_4H_5O)W(PMe_3)_3$ as the major product (5 : 1 with respect to minor product, $(\eta^5\text{-}C_4H_5O)W(PMe_3)_2(\eta^2\text{-}CH_2PMe_2)$). The volatile components were removed via lyopholization and the residue dried in vacuo, giving a dark brown powder composed of $(\kappa^1,\eta^2\text{-}C_4H_3O)(\kappa^1\text{-}O\text{-}C_4H_5O)W(PMe_3)_3$, accompanied by ~ 16% $(\eta^5\text{-}C_4H_5O)W(PMe_3)_2(\eta^2\text{-}CH_2PMe_2)$, (12 mg). Based on the ratio of products determined by ^{1}H NMR integration, the yield of $(\kappa^1,\eta^2\text{-}C_4H_3O)(\kappa^1\text{-}O\text{-}C_4H_5O)W(PMe_3)_3$ is 41%. Black X-ray quality crystals of $(\kappa^1,\eta^2\text{-}C_4H_3O)(\kappa^1\text{-}O\text{-}C_4H_5O)W(PMe_3)_3$ were obtained from a pentane solution at –15 ˚C.

^{1}H NMR (C_6D_6) of $(\kappa^1,\eta^2\text{-}C_4H_3O)(\kappa^1\text{-}O\text{-}C_4H_5O)W(PMe_3)_3$: 0.63 [vt, $^2J_{P\text{-}H}$ = 7, 18H of $W(PMe_3)_3$], 1.53 [d, $^2J_{P\text{-}H}$ = 7, 9H of $W(PMe_3)_3$], 4.98 [d, $^3J_{H\text{-}H}$ = 10, 1H of OCHCHCHC$\underline{H}_2$], 5.22 [dd, $^3J_{H\text{-}H}$ = 18, $^2J_{H\text{-}H}$ = 3 1H of OCHCHCHC$\underline{H}_2$], 5.50 [dd, $^3J_{H\text{-}H}$ = 11, $^3J_{H\text{-}H}$ = 5 1H of OCHC$\underline{H}$CHCH$_2$], 7.48 [ddd, $^3J_{H\text{-}H}$ = 18, $^3J_{H\text{-}H}$ = 11, $^3J_{H\text{-}H}$ = 10, 1H of OCHCHC$\underline{H}$CH$_2$], 8.07 [s, 1H of OC$_4\underline{H}_3$], 8.33 [d, $^3J_{H\text{-}H}$ = 5, 1H of OC$\underline{H}$CHCHCH$_2$], 9.25 [d, $J_{P\text{-}H}$ = 8, 1H of OC$_4\underline{H}_3$], 13.04 [d, $J_{P\text{-}H}$ = 12, 1H of OC$_4\underline{H}_3$]. ^{31}P{^{1}H} NMR (C_6D_6) of $(\kappa^1\text{-}O,\eta^2\text{-}C_2\text{-}C_4H_3O)(\kappa^1\text{-}O\text{-}C_4H_5O)W(PMe_3)_3$: -18.6 [s, 2P of $W(PMe_3)_3$], -17.8 [s, 1P of $W(PMe_3)_3$].

5.11.5 Synthesis of $(\eta^5\text{-}C_4H_5O)W(PMe_3)_2(\eta^2\text{-}CH_2PMe_2)$

$W(PMe_3)_4(\eta^2\text{–}CH_2PMe_2)H$ (25 mg, 0.04 mmol) was added to an NMR tube equipped with a J. Young valve. Furan (ca. 6 μL, 0.08 mmol) was added to a vial with d^6-benzene (ca. 0.7 mL) and this solution was then added to the NMR tube. The tube was sealed, frozen in liquid nitrogen and pumped on in vacuo to remove the argon atmosphere. PMe_3 (< 0.1 mL) was then vapor transferred into the NMR tube and sealed. Integration of the ^{1}H NMR spectrum of this sample indicated that the ratio of $W(PMe_3)_4(\eta^2\text{–}$

CH_2PMe_2)H to furan to PMe_3 was 1 : 2 : 15, respectively. The sample was then heated at 60˚C for ~17 hours and monitored by ^{1}H NMR spectroscopy, thereby demonstrating conversion to (η^5-C_4H_5O)W(PMe_3)$_2$(η^2-CH_2PMe_2) as the major product (3 : 1 with respect to minor product, W(PMe_3)$_4H_4$). The volatile components were removed via lyopholization and the residue dried in vacuo, giving a dark red – brown powder composed of (η^5-C_4H_5O)W(PMe_3)$_2$(η^2-CH_2PMe_2), accompanied by ~ 25% W(PMe_3)$_4H_4$, (17 mg). Based on the ratio of products determined by ^{1}H NMR integration, the yield of (η^5-C_4H_5O)W(PMe_3)$_2$(η^2-CH_2PMe_2) is 61%. When crystals of (η^5-C_4H_5O)W(PMe_3)$_2$(η^2-CH_2PMe_2) were trying to be obtained from a pentane solution at –15 ˚C, [κ^2-*O,C*-OC_3H_2Me]W(PMe_3)$_3$(η^2–CH_2PMe_2) and [μ^2-κ^2,κ^2-(OC_3H_2Me)$_2$][W(PMe_3)$_3$O]$_2$ crystallized and their structures were determined by X-ray diffraction.

^{1}H NMR (C_6D_6) of (η^5-C_4H_5O)W(PMe_3)$_2$(η^2-CH_2PMe_2): 0.63 [m, 2H of (η^2-C<u>H$_2$</u>PMe$_2$), *tentative due to impurities*], 0.90 [d, $^2J_{P\text{-}H}$ = 9, 3H of (η^2-CH_2P<u>Me$_2$</u>)], 0.95 [m, 1H of OCHCHCHC<u>H$_2$</u>], 1.22 [d, $^2J_{P\text{-}H}$ = 6, 9H of (P<u>Me$_3$</u>)$_2$], 1.25 [d, $^2J_{P\text{-}H}$ = 10, 3H of (η^2-CH_2P<u>Me$_2$</u>)], 1.35 [d, $^2J_{P\text{-}H}$ = 8, 9H of (P<u>Me$_3$</u>)$_2$], 2.45 [m, 1H of OCHCHCHC<u>H$_2$</u>], 3.27 [m, 1H of OCHCHC<u>H</u>CH_2], 4.62 [m, 1H of OCHC<u>H</u>$CHCH_2$], 6.63 [m, 1H of OC<u>H</u>$CHCHCH_2$]. ^{31}P{^{1}H} NMR (C_6D_6) of (η^5-C_4H_5O)W(PMe_3)$_2$(η^2-CH_2PMe_2): -75.2 [dd, $^2J_{P\text{-}P}$ = 55, $^2J_{P\text{-}P}$ = 3, 1P of W(η^2-CH_2PMe_2)], -25.7 [dd, $^2J_{P\text{-}P}$ = 19, $^2J_{P\text{-}P}$ = 3, 1P of W(PMe_3)$_2$], -16.6 [dd, $^2J_{P\text{-}P}$ = 54, $^2J_{P\text{-}P}$ = 19, 1P of W(PMe_3)$_3$]. Mass Spectrum (FAB+): m/z = 480.02 {M_+}

5.11.6 Reaction between W(PMe_3)$_4$(η^2–CH_2PMe_2)H and d_4–furan in C_6D_6

W(PMe_3)$_4$(η^2–CH_2PMe_2)H (10 mg, 0.02 mmol) was added to an NMR tube equipped with a J. Young valve. C_6D_6 (ca. 0.7 mL) was added followed by d_4-furan. The sample was heated at 60 ˚C for 1 day and monitored by ^{1}H NMR spectroscopy, demonstrating that deuterium incorporation in (η^5-C_4H_5O)W(PMe_3)$_2$(η^2-CH_2PMe_2) was in the CH_2 group of η^5-C_4H_5O.

5.11.7 Reaction between $W(PMe_3)_4(\eta^2–CH_2PMe_2)H$ and d_4–furan in C_6H_6

$W(PMe_3)_4(\eta^2–CH_2PMe_2)H$ (10 mg, 0.02 mmol) was added to an NMR tube equipped with a J. Young valve. C_6H_6 (ca. 0.7 mL) was added followed by d_4-furan. The sample was heated at 60 ˚C for 1 day and monitored by ^2H NMR spectroscopy, demonstrating that hydrogen incorporation in $(\eta^5\text{-}C_4H_5O)W(PMe_3)_2(\eta^2\text{-}CH_2PMe_2)$ was in the CH_2 group of $\eta^5\text{-}C_4H_5O$.

5.11.8 Synthesis of $W(PMe_3)_4(\kappa^1\text{-}C_\alpha\text{-}C_4H_3O)H_3$

$W(PMe_3)_4(\eta^2–CH_2PMe_2)H$ (50 mg, 0.09 mmol) was added to a medium size ampoule. Benzene (3 mL) was added to the ampoule followed by furan (ca. 0.2 mL). The ampoule was sealed, frozen in liquid nitrogen and pumped on in vacuo to remove the argon atmosphere. The solution was allowed to thaw and then was charged with H_2 (ca. 1 atm). The ampoule was then heated at 60˚C for 1.5 days. After this period, the solution was frozen in liquid nitrogen and lyophilized giving a light yellow powder (34 mg). ^1H NMR spectroscopy indicated that 92% converted to $W(PMe_3)_4(\kappa^1\text{-}C_\alpha\text{-}C_4H_3O)H_3$ as the major product, but a small amount of $W(PMe_3)_3H_6$ (8%) was also formed. Based on the ratio of products determined by ^1H NMR integration, the yield of $W(PMe_3)_4(\kappa^1\text{-}C_\alpha\text{-}C_4H_3O)H_3$ is 65%. Colorless X-ray quality crystals of $W(PMe_3)_4(\kappa^1\text{-}C_\alpha\text{-}C_4H_3O)H_3$ were obtained from a pentane solution at –15 ˚C.

^1H NMR (C_6D_6): –3.76 [m, 2H of $W\underline{H}_3$], –1.28 [dt, $^2J_{P\text{-}H}$ = 76, $^2J_{P\text{-}H}$ = 28, 1H of $W\underline{H}_3$], 1.25 [vt, $^3J_{P\text{-}H}$ = 6, 18H of $W(P\underline{Me}_3)_4$], 1.55 [d, $^3J_{P\text{-}H}$ = 8, 9H of $W(P\underline{Me}_3)_4$], 1.60 [d, $^3J_{P\text{-}H}$ = 7, 9H of $W(P\underline{Me}_3)_4$], 6.44 [s, 1H of $OC_4\underline{H}_3$], 6.50 [d, $J_{H\text{-}H}$ = 3, 1H of 1H of $OC_4\underline{H}_3$], 7.80 [d, $J_{H\text{-}H}$ = 2, 1H of 1H of $OC_4\underline{H}_3$]. $^{31}P\{^1H\}$ NMR (C_6D_6): -37.6 [dt, $^2J_{P\text{-}P}$ = 28, $^2J_{P\text{-}P}$ = 20, 1P of $W(PMe_3)_4$], -25.8 [t, $^2J_{P\text{-}P}$ = 19, $^1J_{W\text{-}P}$ = 175, 2P of $W(PMe_3)_4$], -18.8 [dt, $^2J_{P\text{-}P}$ = 28, $^2J_{P\text{-}P}$ = 19, 1P of $W(PMe_3)_4$]. $^{13}C\{^1H\}$ NMR (C_6D_6): 26.2 [vt, $^1J_{P\text{-}C}$ = 24, 6C of $W(P\underline{Me}_3)_4$], 29.1 [d, $^1J_{P\text{-}C}$ = 23, 3C of $W(P\underline{Me}_3)_4$], 32.2 [d, $^1J_{P\text{-}C}$ = 29, 3C of $W(P\underline{Me}_3)_4$], 111.4 [s, 1C of $O\underline{C}_4H_3$], 129.1 [s, 1C

of O$\underline{C}_4H_3$], 144.8 [s, 1C of O$\underline{C}_4H_3$], 1C not observed. Mass Spectrum (FAB+): m/z = 558.2 {M_+}.

5.11.9 Reactivity of $W(PMe_3)_5H_2$ towards furan

A solution of $W(PMe_3)_5H_2$ (5 mg, 0.01 mmol) in d_6-benzene (*ca*. 0.7 mL) was treated with furan (*ca*. 0.01 mL) and added to an NMR tube equipped with a J. Young valve. The solution was heated at 80 ˚C for 3 hours, and analyzed by ^{1}H NMR spectroscopy, thereby demonstrating conversion to $W(PMe_3)_4(\kappa^1\text{-}C_\alpha\text{-}C_4H_3O)H_3$.

5.11.10 Reactivity of $W(PMe_3)_4H_4$ towards furan

(a) A solution of $W(PMe_3)_4H_4$ (5 mg, 0.01 mmol) in benzene (*ca*. 0.7 mL) was treated with furan (*ca*. 0.02 mL) and added to an NMR tube equipped with a J. Young valve. The sample was photolyzed (λ_{max} = 350 nm) for 1.5 hours, lyophilized, and then treated with d_6-benzene (*ca*. 0.7 mL). The sample was analyzed by ^{1}H NMR spectroscopy, thereby demonstrating that $W(PMe_3)_4(\kappa^1\text{-}C_\alpha\text{-}C_4H_3O)H_3$ was produced, in addition to $W(PMe_3)_3H_6$.

(b) A solution of $W(PMe_3)_4H_4$ (5 mg, 0.01 mmol) in d_6-benzene (*ca*. 0.7 mL) was treated with furan (*ca*. 0.02 mL) and added to an NMR tube equipped with a J. Young valve. The sample was photolyzed (λ_{max} = 350 nm) for 1.5 hours, and analyzed by ^{1}H NMR spectroscopy, thereby demonstrating that (*i*) deuterium was incorporated (> 95%) into both the α and β sites of furan, (ii) $W(PMe_3)_4(\kappa^1\text{-}C_\alpha\text{-}C_4D_3O)D_3$ was produced (based on comparison of the PMe_3 resonances of $W(PMe_3)_4(\kappa^1\text{-}C_\alpha\text{-}C_4H_3O)H_3$), and (*iii*) $W(PMe_3)_3(H/D)_6$ was produced.

5.11.11 Reactivity of $W(PMe_3)_3H_6$ towards furan

A solution of $W(PMe_3)_3H_6$ (5 mg, 0.01 mmol) in d_6-benzene (*ca*. 0.7 mL) was treated with furan (*ca*. 0.02 mL) and added to an NMR tube equipped with a J. Young valve. The sample was heated at 60 ˚C for 2 hours, and analyzed by ^{1}H NMR spectroscopy, thereby demonstrating that (*i*) deuterium was incorporated (> 90%) into both the α and β sites of furan, (*ii*) $W(PMe_3)_4(\kappa^1\text{-}C_\alpha\text{-}C_4D_3O)D_3$ was produced (based on comparison of the PMe_3 resonances of $W(PMe_3)_4(\kappa^1\text{-}C_\alpha\text{-}C_4H_3O)H_3$).

5.11.12 Structural characterization of $(\kappa^1,\eta^2\text{–}CH_2CHC_6H_4O)W(PMe_3)_3(\eta^2\text{–}CH_2PMe_2)$

A solution of $W(PMe_3)_4(\eta^2\text{–}CH_2PMe_2)H$ (50 mg, 0.09 mmol) in d_6-benzene (*ca*. 0.7 mL) was treated with benzofuran (*ca*. 0.1 mL) and added to an NMR tube equipped with a J. Young valve. The sample was heated at 60˚C for 1 day, lyophilized, extracted into pentane (1 mL), filtered and then cooled to –15 ˚C, thereby depositing yellow crystals of $(\kappa^1,\eta^2\text{–}CH_2CHC_6H_4O)W(PMe_3)_3(\eta^2\text{–}CH_2PMe_2)$ suitable for X-ray diffraction.

5.11.13 Reaction between $W(PMe_3)_4(\eta^2\text{–}CH_2PMe_2)H$ and benzofuran in the presence of H_2

A solution of $W(PMe_3)_4(\eta^2\text{–}CH_2PMe_2)H$ (10 mg, 0.02 mmol) in d_6-benzene (*ca*. 0.7 mL) was treated with benzofuran (*ca*. 0.02 mL) and added to an NMR tube equipped with a J. Young valve. The sample was then charged with H_2 (*ca*. 1 atm) and heated at 60 ˚C for 1 day. Analysis by ^{1}H NMR spectroscopy demonstrated the production of two major products, namely $W(PMe_3)_4(\kappa^1\text{-}C_\alpha\text{-}CCHOC_6H_4)H_3$ and $W(PMe_3)_4(OC_6H_4Et)H_3$.[23] Although $W(PMe_3)_4(OC_6H_4Et)H_3$ has been previously synthesized,[23] we were able to determine its molecular structure by X-ray diffraction. Yellow crystals of $W(PMe_3)_4(OC_6H_4Et)H_3$ were grown in a solution of pentane at –15 ˚C.

5.11.14 Synthesis of $W(PMe_3)_4(\kappa^1–C_\alpha–CCHOC_6H_4)H_3$

$W(PMe_3)_5H_2$ (50 mg, 0.09 mmol) was added to an NMR tube equipped with a J. Young valve. C_6D_6 (ca. 0.7 mL) was added to the NMR tube, followed by benzofuran (ca. 10 μL, 0.90 mmol). The solution was heated at 60˚C for 9 hours, and monitored by ^1H NMR spectroscopy, demonstrating conversion to $W(PMe_3)_4(\kappa^1\text{-}C_\alpha\text{-}CCHOC_6H_4)H_3$, in addition to a small amount of $W(PMe_3)_4H_4$. After this period, the solution was frozen in liquid nitrogen and lyophilized giving a dark brown oily substance. The thick oil was re-dissolved in benzene, and lyophilized again. This was repeated twice in order to remove all the excess benzofuran, and gave a mustard yellow (powder (47 mg). ^1H NMR spectroscopy indicated that 85% converted to $W(PMe_3)_4(\kappa^1\text{-}C_\alpha\text{-}CCHOC_6H_4)H_3$ as the major product, but a small amount of $W(PMe_3)_4H_4$ (15 %) was also formed. Based on the ratio of products determined by ^1H NMR integration, the yield of $W(PMe_3)_4(\kappa^1\text{-}C_\alpha\text{-}CCHOC_6H_4)H_3$ is 76%. Yellow X-ray quality crystals of $W(PMe_3)_4(\kappa^1\text{-}C_\alpha\text{-}CCHOC_6H_4)H_3$ were obtained from a pentane solution at –15 ˚C. Anal. Calcd.: C, 39.5%, H, 7.3%. Found: C, 39.4%, H, 7.1%.

^1H NMR (C_6D_6) of $W(PMe_3)_4(\kappa^1–C_\alpha–CCHOC_6H_4)H_3$: -3.71 [m, 2H of $W\underline{H}_3$], -1.12 [dt, $^2J_{P\text{-}H} = 73$, $^2J_{P\text{-}H} = 29$, 1H of $W\underline{H}_3$], 1.19 [vt, $^3J_{P\text{-}H} = 6$, 18H of $W(P\underline{Me}_3)_4$], 1.52 [d, $^3J_{P\text{-}H} = 7$, 9H of $W(P\underline{Me}_3)_4$], 1.64 [d, $^3J_{P\text{-}H} = 7$, 9H of $W(P\underline{Me}_3)_4$], 6.88 [t, $^4J_{P\text{-}H} = 3$, 1H of $OC_2\underline{H}C_6H_4$], 7.05 [t, $^3J_{H\text{-}H} = 8$, 1H of $OC_2HC_6\underline{H}_4$], 7.16 [under solvent peak, should be triplet, 1H of $OC_2\underline{H}C_6H_4$], 7.45 [d, $^3J_{H\text{-}H} = 8$, 1H of $OC_2HC_6\underline{H}_4$], 7.53 [d, $^3J_{H\text{-}H} = 7$, 1H of $OC_2HC_6\underline{H}_4$]. $^{31}P\{^1H\}$ NMR (C_6D_6): -37.8 [dt, $^2J_{P\text{-}P} = 26$, $^2J_{P\text{-}P} = 20$, 1P of $W(PMe_3)_4$], -28.1 [t, $^2J_{P\text{-}P} = 19$, $^1J_{W\text{-}P} = 175$, 2P of $W(PMe_3)_4$], -19.9 [dt, $^2J_{P\text{-}P} = 26$, $^2J_{P\text{-}P} = 19$, 1P of $W(PMe_3)_4$]. $^{13}C\{^1H\}$ NMR (C_6D_6): 26.2 [vt, $^1J_{P\text{-}C} = 24$, 6C of $W(P\underline{Me}_3)_4$], 29.1 [d, $^1J_{P\text{-}C} = 23$, 3C of $W(P\underline{Me}_3)_4$], 31.9 [d, $^1J_{P\text{-}C} = 29$, 3C of $W(P\underline{Me}_3)_4$], 108.9 [s, 1C of $OC(CH)\underline{C}_6H_4$, adjacent to ring fusion], 117.6 [s, 1C of $OC(CH)\underline{C}_6H_4$, adjacent to ring fusion], 119.7 [s, 1C of $OC(CH)\underline{C}_6H_4$, meta to ring fusion], 121.2 [s, 1C of $OC(CH)\underline{C}_6H_4$, meta to ring fusion], 126.0 [s, 1C of $OC(\underline{C}H)C_6H_4$],

133.2 [s, 1C of OC(CH)$\underline{C}_6H_4$, ring fusion], 161.0 [s, 1C of OC(CH)$\underline{C}_6H_4$, ring fusion], 196.6 [br, 1C of O$\underline{C}$(CH)C_6H_4, carbon bonded to W], peaks assigned are supported with HSQC and HMBC spectroscopy.

5.11.15 Reactivity of $W(PMe_3)_4H_4$ towards benzofuran

A solution of $W(PMe_3)_4H_4$ (5 mg, 0.01 mmol) in benzene (*ca*. 0.7 mL) was treated with benzofuran (*ca*. 0.02 mL) and added to an NMR tube equipped with a J. Young valve. The sample was photolyzed (λ_{max} = 350 nm) for 1.5 hours, lyophilized, and then treated with d_6-benzene (*ca*. 0.7 mL). The sample was analyzed by ^{1}H NMR spectroscopy, thereby demonstrating that $W(PMe_3)_4(\kappa^1\text{-}C_\alpha\text{-}CCHOC_6H_4)H_3$ and $W(PMe_3)_4(OC_6H_4Et)H_3$ were produced, in addition to $W(PMe_3)_3H_6$.

5.11.16 Reactivity of $W(PMe_3)_3H_6$ towards benzofuran

A solution of $W(PMe_3)_3H_6$ (5 mg, 0.01 mmol) in d_6-benzene (*ca*. 0.7 mL) was treated with benzofuran (*ca*. 0.02 mL) and added to an NMR tube equipped with a J. Young valve. The sample was heated at 60 ˚C for 2 hours, and analyzed by ^{1}H NMR spectroscopy, thereby demonstrating the production of $W(PMe_3)_4(\kappa^1\text{-}C_\alpha\text{-}CCHOC_6H_4)H_3$ and $W(PMe_3)_4(OC_6H_4Et)H_3$.[66]

5.11.17 Reaction Between $Mo(PMe_3)_6$ and Furan

A suspension of $Mo(PMe_3)_6$ (25 mg, 0.04 mmol) in d_6-benzene (*ca*. 0.7 mL) was treated with furan (*ca*. 0.1 mL) and added to an NMR tube equipped with a J. Young valve. The sample was heated at 60 ˚C and monitored by ^{1}H NMR spectroscopy, thereby demonstrating conversion to, *inter alia*, $(\kappa^1,\eta^2\text{-}C_4H_3O)(\kappa^1\text{-}O\text{-}C_4H_5O)Mo(PMe_3)_3$ and $(\eta^5\text{-}C_4H_5O)Mo(PMe_3)_2(\eta^2\text{-}CH_2PMe_2)$.[67] The sample was lyophilized, extracted with pentane (1 mL), filtered and cooled to –15 ˚C, thereby depositing crystals of $(\kappa^1,\eta^2\text{-}C_4H_3O)(\kappa^1\text{-}O\text{-}$

$C_4H_5O)Mo(PMe_3)_3$, which were characterized by X-ray diffraction. The mother liquor was removed from the crystals, filtered and cooled at –15 ˚C, thereby deposited crystals of the *E* isomer of $(\kappa^1,\eta^2\text{-}C_4H_3O)(\kappa^1\text{-}O\text{-}C_4H_5O)Mo(PMe_3)_3$, which was also characterized by X-ray diffraction.

5.11.18 Structural characterization of $(\eta^4\text{-}OC_4H_6)_2Mo(PMe_3)_2$

A suspension of $Mo(PMe_3)_6$ (10 mg, 0.02 mmol) in d_6-benzene (*ca*. 0.7 mL) was treated with crotonaldehyde (*ca*. 0.02 mL) and added to an NMR tube equipped with a J. Young valve. The sample was allowed to sit at room temperature for 1 day, after which period it was lyophilized, extracted into pentane (*ca*. 1 mL), filtered and cooled to –15 ˚C, thereby depositing crystals of $(\eta^4\text{-}OC_4H_6)_2Mo(PMe_3)_2$, which were structurally characterized by X-ray diffraction.

5.11.19 Reaction Between $Mo(PMe_3)_4H_4$ and Furan

$Mo(PMe_3)_4H_4$ (10 mg, 0.02 mmol), d_6-benzene (*ca*. 0.7 mL) and furan (*ca*. 0.1 mL) were added to an NMR tube equipped with a J. Young valve. The sample was heated at 120 ˚C for *ca*. 12 hours, and monitored by ^1H NMR spectroscopy, demonstrating that propene and propane were produced. In addition, the molybdenum containing compounds, $(\eta^6\text{-}PhH)Mo(PMe_3)_3$[68] and $(\eta^6\text{-}PhH)Mo(PMe_3)_2CO$, were also produced. Yellow X-ray quality crystals of $(\eta^6\text{-}PhH)Mo(PMe_3)_2CO$ were obtained by slow evaporation of a pentane solution at –15 ˚C.

5.11.20 Structural characterization of compounds derived from reaction of $Mo(PMe_3)_6$ towards benzofuran

(a) A suspension of $Mo(PMe_3)_6$ (20 mg, 0.04 mmol) in d_6-benzene (*ca*. 0.7 mL) was treated with benzofuran (*ca*. 0.03 mL) and added to an NMR tube equipped with a J.

Young valve. A reaction occurs immediately, based on the color of the mixture and the observation that the suspension turned into a solution, indicating that there was no more $Mo(PMe_3)_6$. Crystals of $(\kappa^1,\eta^2\text{-}CH_2CHC_6H_4O)Mo(\kappa^1\text{-}C_\alpha\text{-}CCHOC_6H_4)(PMe_3)_3$ were obtained by former graduate student Daniela Buccella. Crystals of $(\kappa^1,\eta^2\text{-}CH_2CHC_6H_4O)(\kappa^1,\eta^2\text{-}HC(PMe_3)CHC_6H_4O)Mo(PMe_3)_2$ were obtained from the reaction mixture in benzene, and characterized by X-ray diffraction.

^1H NMR (C_6D_6) of $(\kappa^1,\eta^2CH_2CHC_6H_4O)(\kappa^1,\eta^2\text{-}CHC(PMe_3)CHC_6H_4O)Mo(PMe_3)_2$ (tentative assignment due to paramagnetic nature of compound): –22.9 [9H of PMe_3], –17.9 [9H of PMe_3], 3.4 [9H of PMe_3]. Mass Spectrum of $(\kappa^1,\eta^2\text{-}CH_2CHC_6H_4O)(\kappa^1,\eta^2\text{-}HC(PMe_3)CHC_6H_4O)Mo(PMe_3)_2$ (FAB+): $m/z = 563.16$ $\{M_+\}$, $m/z = 487.13$ $\{M_+ - PMe_3\}$, $m/z = 411.10$ $\{M_+ - 2\ PMe_3\}$.

(b) A suspension of $Mo(PMe_3)_6$ (20 mg, 0.04 mmol) in d_6-benzene (*ca*. 0.7 mL) was treated with benzofuran (*ca*. 0.03 mL) and added to an NMR tube equipped with a J. Young valve. The sample was heated at 60 ˚C for *ca*. 12 hours, after which period the mixture was lyophilized, extracted with pentane (1 mL), filtered and cooled to –15 ˚C, thereby depositing crystals of $(\kappa^1,\eta^2\text{-}CH_2CHC_6H_4O)Mo(PMe_3)_3(\eta^2\text{–}CH_2PMe_2)$, which were characterized by X-ray diffraction.

5.11.21 Structural characterization of $(\eta^6\text{-}C_6H_4C_6H_4O)Mo(PMe_3)_3$

$Mo(PMe_3)_6$ (15 mg, 0.03 mmol) and dibenzofuran (5 mg, 0.03 mmol) were added to an NMR tube equipped with a J. Young valve. The sample was heated at 120 ˚C for *ca*. 16 hours, after which period the volatile components were removed *in vacuo*. The dark solid was then extracted into pentane (*ca*. 2 mL), filtered and allowed to slowly evaporate, thereby depositing purple crystals of $(\eta^6\text{-}C_6H_4C_6H_4O)Mo(PMe_3)_3$, which were structurally characterized by X-ray diffraction.

5.11.22 Structural characterization of $W(PMe_3)_4(\kappa^1–C_\alpha–C_4H_5O)H_3$

A solution of $W(PMe_3)_4(\eta^2–CH_2PMe_2)H$ (50 mg, 0.09 mmol) in d_6-benzene (*ca*. 0.7 mL) was treated with 2,3-dihydrofuran (*ca*. 0.1 mL). The sample was then charged with H_2 and heated at 60 ˚C for *ca*. 12 hours. Analysis by ^1H NMR spectroscopy, indicated the production of a trihydride compound. The sample was lyophilized, extracted with pentane (1 mL), filtered and cooled to –15 ˚C, thereby depositing colorless X-ray quality crystals of $W(PMe_3)_4(\kappa^1\text{-}C_\alpha\text{-}C_4H_5O)H_3$.

^1H NMR (C_6D_6) of $W(PMe_3)_4(\kappa^1\text{-}C_\alpha\text{-}C_4H_5O)H_3$: -4.00 [m, 2H of $W\underline{H}_3$], -1.49 [dtdt, $^2J_{P\text{-}H}$ = 75, $^2J_{P\text{-}H}$ = 29, $^2J_{P\text{-}H}$ = 6, $^2J_{H\text{-}H}$ = 6, 1H of $W\underline{H}_3$], 1.50 [vt, $^3J_{P\text{-}H}$ = 6, 18H of $W(P\underline{Me}_3)_4$], 1.53 [d, $^3J_{P\text{-}H}$ = 8, 9H of $W(P\underline{Me}_3)_4$], 1.56 [d, $^3J_{P\text{-}H}$ = 7, 9H of $W(P\underline{Me}_3)_4$], 2.56 [m, 2H of $OCH_2C\underline{H}_2CHC$], 4.10 [t, $^3J_{H\text{-}H}$ = 10, 2H of $OC\underline{H}_2CH_2CHC$], 5.00 [m, 1H of $OCH_2CH_2C\underline{H}C$], peaks assigned are supported with $^{31}P–^1H$ HMBC spectroscopy and $^1H\{^{31}P\}$ selective heteronuclear decoupling spectroscopy. $^{31}P\{^1H\}$ NMR (C_6D_6) of $W(PMe_3)_4(\kappa^1\text{-}C_\alpha\text{-}C_4H_5O)H_3$: -37.8 [dt, $^2J_{P\text{-}P}$ = 29, $^2J_{P\text{-}P}$ = 21, 1P of $W(PMe_3)_4$], -28.4 [t, $^2J_{P\text{-}P}$ = 21, 2P of $W(PMe_3)_4$], -20.0 [dt, $^2J_{P\text{-}P}$ = 29, $^2J_{P\text{-}P}$ = 20, 1P of $W(PMe_3)_4$]. $^{13}C\{^1H\}$ NMR (C_6D_6) of $W(PMe_3)_4(\kappa^1\text{-}C_\alpha\text{-}C_4H_5O)H_3$: 26.3 [vt, $^1J_{P\text{-}C}$ = 25, 6C of $W(P\underline{Me}_3)_4$], 29.0 [d, $^1J_{P\text{-}C}$ = 23, 3C of $W(P\underline{Me}_3)_4$], 32.1 [d, $^1J_{P\text{-}C}$ = 28, 3C of $W(P\underline{Me}_3)_4$], 33.3 [s, 1C of $OCH_2\underline{C}H_2CHC$], 69.2 [d, $^4J_{P\text{-}C}$ = 3, 1C of $O\underline{C}H_2CH_2CHC$], 116.3 [q, $^3J_{P\text{-}C}$ = 7, 1C of $OCH_2CH_2\underline{C}HC$], 1C not observed, peaks assigned are supported with HSQC spectroscopy.

5.11.23 Reaction between $Mo(PMe_3)_6$ and 2,5-dihydrofuran

(a) A suspension of $Mo(PMe_3)_6$ (10 mg, 0.02 mmol) in d_6-benzene (*ca*. 0.7 mL) was treated with 2,5-dihydrofuran (*ca*. 0.02 mL) and added to an NMR tube equipped with a J. Young valve. The sample was allowed to stand at room temperature, thereby demonstrating conversion to $(\eta^5–C_4H_5O)Mo(PMe_3)_3H$. Ashley Zuzek has recently crystallographically characterized this compound, confirming its structure.

^{1}H NMR (C_6D_6) of (η^5-C_4H_5O)Mo(PMe_3)$_3$H: -8.55 [ddd, $^{2}J_{P\text{-}H}$ = 92, $^{2}J_{P\text{-}H}$ = 61, $^{2}J_{P\text{-}H}$ = 31, 1H of Mo<u>H</u>), 0.80 [br, 1H of η^5-OCHCHCHC<u>H</u>$_2$], 0.97 [d, $^{2}J_{P\text{-}H}$ = 6, 9H of Mo(P<u>Me</u>$_3$)], 1.23 [d, $^{2}J_{P\text{-}H}$ = 6, 9H of Mo(P<u>Me</u>$_3$)], 1.31 [d, $^{2}J_{P\text{-}H}$ = 7, 9H of Mo(P<u>Me</u>$_3$)], 2.53 [m, 1H of η^5-OCHCHCHC<u>H</u>$_2$], 4.22 [m, 1H of η^5-OCHCHC<u>H</u>CH$_2$], 4.74 [d, $^{3}J_{H\text{-}H}$ = 6, 1H of η^5-OCHC<u>H</u>CHCH$_2$], 6.58 [s, 1H of η^5-OC<u>H</u>CHCHCH$_2$]. ^{31}P{^{1}H} NMR (C_6D_6) of (η^5-C_4H_5O)Mo(PMe_3)$_3$H: 3.7 [m, 1P of Mo(<u>P</u>Me$_3$)], 5.0 [m, 1P of Mo(<u>P</u>Me$_3$)], 9.6 [m, 1P of Mo(<u>P</u>Me$_3$)].

(b) A suspension of Mo(PMe_3)$_6$ (10 mg, 0.02 mmol) in d$_6$-benzene (*ca*. 0.7 mL) was treated with 2,5-dihydrofuran (*ca*. 0.02 mL) and added to an NMR tube equipped with a J. Young valve. The sample was heated at 60 ˚C, thereby demonstrating conversion to, *inter alia*, propene, Mo(PMe_3)$_5$CO[69] and (η^5–C_4H_5O)Mo(PMe_3)$_3$H.

^{1}H NMR (C_6D_6) of Mo(PMe_3)$_5$CO: 1.03 [d, $^{2}J_{P\text{-}H}$ = 4, 9H of Mo(P<u>Me</u>$_3$)$_5$], 1.40 [s, 36H of Mo(P<u>Me</u>$_3$)$_5$]. ^{31}P{^{1}H} NMR (C_6D_6) of Mo(PMe_3)$_5$CO: –19.5 [q, $^{2}J_{P\text{-}P}$ = 25, 1P of Mo(PMe_3)$_5$, trans to CO], –4.6 [d, $^{2}J_{P\text{-}P}$ = 25, 4P of Mo(PMe_3)$_5$, cis to CO]

5.11.24 Reaction between Mo(PMe_3)$_6$ and 2,3-dihydrofuran

A suspension of Mo(PMe_3)$_6$ (10 mg, 0.02 mmol) in d$_6$-benzene (*ca*. 0.7 mL) was treated with 2,3-dihydrofuran (*ca*. 0.02 mL) and added to an NMR tube equipped with a J. Young valve. The sample was heated at 60 ˚C, thereby demonstrating conversion to, *inter alia*, propene and Mo(PMe_3)$_5$CO.

5.11.25 Reaction between W(PMe_3)$_4$(η^2–CH_2PMe_2)H and 2,5-dihydrofuran

A solution of W(PMe_3)$_4$(η^2–CH_2PMe_2)H (10 mg, 0.02 mmol) in d$_6$-benzene (*ca*. 0.7 mL) was treated with 2,5-dihydrofuran (*ca*. 0.02 mL) and added to an NMR tube equipped with a J. Young valve. The sample was heated at 60 ˚C, thereby demonstrating

conversion to, *inter alia*, propene and $W(PMe_3)_5CO$, which was identified by X-ray crystallography.

5.11.26 Reaction between $W(PMe_3)_4(\eta^2–CH_2PMe_2)H$ and 2,3-dihydrofuran

A solution of $W(PMe_3)_4(\eta^2–CH_2PMe_2)H$ (10 mg, 0.02 mmol) in d_6-benzene (*ca*. 0.7 mL) was treated with 2,3-dihydrofuran (*ca*. 0.02 mL) and added to an NMR tube equipped with a J. Young valve. The sample was heated at 60 ˚C, thereby demonstrating conversion to, *inter alia*, propene and $W(PMe_3)_5CO$.

5.11.27 Structural characterization of $W(PMe_3)_4(\eta^2\text{-}OCH_2)H_2$

A solution of $W(PMe_3)_4(\eta^2–CH_2PMe_2)H$ (25 mg, 0.04 mmol) in d_6-benzene (*ca*. 0.7 mL) was treated with MeOH (*ca*. 0.1 mL) and was added to an NMR tube equipped with a J. Young valve. Analysis by ^1H NMR demonstrated immediate conversion to $W(PMe_3)_4(\eta^2\text{-}OCH_2)H_2$. The sample was lyophilized, extracted into pentane (*ca*. 1 mL), filtered and cooled to –15 ˚C, thereby depositing crystals of $W(PMe_3)_4(\eta^2\text{-}OCH_2)H_2$, which were structurally characterized by X-ray diffraction.

5.11.28 Structural characterization of $W(PMe_3)_4(\eta^2\text{-}OCMeH)H_2$

A solution of $W(PMe_3)_4(\eta^2–CH_2PMe_2)H$ (25 mg, 0.04 mmol) in pentane (*ca*. 1 mL) was treated with EtOH (*ca*. 0.1 mL) and immediately cooled to –15 ˚C. After several days, pink crystals of $W(PMe_3)_4(\eta^2\text{-}OCMeH)H_2$•EtOH, which were very sensitive to air, were deposited and structurally characterized by X-ray diffraction.

5.11.29 Structural characterization of $W(PMe_3)_4(OEt)H_3$

A solution of $W(PMe_3)_4(\eta^2–CH_2PMe_2)H$ (25 mg, 0.04 mmol) in d_6-benzene (*ca*. 0.7 mL) was treated with EtOH (*ca*. 0.1 mL) and added to an NMR tube equipped with a J.

Young valve. The sample was then charged with H_2 (*ca*. 1 atm) and allowed to stand at room temperature. After 1 day, analysis by ^1H NMR demonstrated conversion to $W(PMe_3)_4(OEt)H_3$. The sample was lyophilized, extracted into pentane (*ca*. 1 mL), filtered and cooled to –15 ˚C, thereby depositing crystals of $W(PMe_3)_4(OEt)H_3$, which were structurally characterized by X-ray diffraction.

5.12 Crystallographic data

Table 2. Crystal, intensity collection and refinement data.

	$(\eta^2\text{-}OCH_2)W(PMe_3)_4H_2$	$(\eta^2\text{-}OCMeH)W(PMe_3)_4H_2$
lattice	Monoclinic	Orthorhombic
formula	$C_{13}H_{40}OP_4W$	$C_{16}H_{48}O_2P_4W$
formula weight	520.18	580.27
space group	*P2/c*	*Pbca*
a / Å	16.4151(14)	17.4301(13)
b / Å	9.5486(8)	16.5047(12)
c / Å	15.6711(13)	17.8724(13)
α / °	90	90
β / °	117.7910(10)	90
γ / °	90	90
V / Å^3	2173.0(3)	5141.5(7)
Z	4	8
temperature (K)	125(2)	125(2)
radiation (λ, Å)	0.71073	0.71073
ρ (calcd.) g cm^{-3}	1.590	1.499
μ (Mo Kα), mm^{-1}	5.605	4.749
θ max, deg.	32.67	30.65
no. of data collected	36770	78495
no. of data	7659	7936
no. of parameters	216	273
R_1 [$I > 2\sigma(I)$]	0.0251	0.0245
wR_2 [$I > 2\sigma(I)$]	0.0512	0.0470
R_1 [all data]	0.0367	0.0516
wR_2 [all data]	0.545	0.0566
GOF	1.030	1.298

Table 2 (cont). Crystal, intensity collection and refinement data.

	$W(PMe_3)_4(OEt)H_3$	$(\kappa^1,\eta^2\text{-}C_4H_3O)(\kappa^1\text{-}O\text{-}C_4H_5O)W(PMe_3)_3$
lattice	Orthorhombic	Monoclinic
formula	$C_{14}H_{44}OP_4W$	$C_{17}H_{35}O_2P_3W$
formula weight	536.22	548.21
space group	*Pna2(1)*	*Cc*
a / Å	12.0173(4)	9.0469(16)
b / Å	14.4460(5)	16.395(3)
c / Å	13.5266(13)	15.243(3)
α / °	90	90
β / °	90	90.608(3)
γ / °	90	90
V / Å^3	2348.39(13)	2260.8(7)
Z	4	4
temperature (K)	125(2)	125(2)
radiation (λ, Å)	0.71073	0.71073
ρ (calcd.) g cm^{-3}	1.517	1.611
μ (Mo Kα), mm^{-1}	5.188	5.328
θ max, deg.	32.73	30.50
no. of data collected	38946	12495
no. of data	8240	6420
no. of parameters	205	222
R_1 [$I > 2\sigma(I)$]	0.0145	0.0329
wR_2 [$I > 2\sigma(I)$]	0.0356	0.0646
R_1 [all data]	0.0158	0.0413
wR_2 [all data]	0.0362	0.0672
GOF	1.038	1.011

Table 2 (cont). Crystal, intensity collection and refinement data.

	$W(PMe_3)_4(\kappa^1\text{-}C_\alpha\text{-}C_4H_3O)H_3$	$[\kappa^2\text{-}O,C\text{-}OC_3H_2Me]W(PMe_3)_3(\eta^2\text{-}CH_2PMe_2)$
lattice	Monoclinic	Triclinic
formula	$C_{16}H_{42}OP_4W$	$C_{16}H_{40}OP_4W$
formula weight	558.23	556.21
space group	$P2_1/n$	$P\text{-}1$
a / Å	9.3202(4)	9.045(2)
b / Å	16.1649(7)	9.228(2)
c / Å	16.1521(7)	15.499(4)
α / °	90	85.153(4)
β / °	91.0740(10)	87.990(4)
γ / °	90	62.047(4)
V / Å^3	2433.05(18)	1138.6(5)
Z	4	2
temperature (K)	125(2)	125(2)
radiation (λ, Å)	0.71073	0.71073
ρ (calcd.) g cm^{-3}	1.524	1.622
μ (Mo Kα), mm^{-1}	5.011	5.354
θ max, deg.	30.51	26.39
no. of data collected	38590	17729
no. of data	7432	4658
no. of parameters	223	212
R_1 [$I > 2\sigma(I)$]	0.0144	0.0547
wR_2 [$I > 2\sigma(I)$]	0.0345	0.1244
R_1 [all data]	0.0176	0.0655
wR_2 [all data]	0.0357	0.1302
GOF	1.026	1.041

Table 2 (cont). Crystal, intensity collection and refinement data.

	[μ^2-κ^2,κ^2-$(OC_3H_2Me)_2$][$W(PMe_3)_3O]_2$	**(κ^1,η^2-$CH_2CHC_6H_4O$)$W(PMe_3)_3$(η^2-CH_2PMe_2)**
lattice	Triclinic	Orthorhombic
formula	$C_{26}H_{64}O_4P_6W_2$	$C_{20}H_{42}OP_4W$
formula weight	994.29	606.27
space group	*P-1*	*Pbca*
a / Å	9.5478(17)	19.829(11)
b / Å	9.6423(17)	18.770(10)
c / Å	12.211(2)	27.142(15)
α / °	103.736(2)	90
β / °	93.439(3)	90
γ / °	110.804(2)	90
V / Å^3	1007.8(3)	10102(10)
Z	1	16
temperature (K)	125(2)	200(2)
radiation (λ, Å)	0.71073	0.71073
ρ (calcd.) g cm^{-3}	1.638	1.594
μ (Mo Kα), mm^{-1}	5.966	4.835
θ max, deg.	30.55	26.37
no. of data collected	27162	114893
no. of data	6123	10318
no. of parameters	183	491
R_1 [$I > 2\sigma(I)$]	0.0392	0.0675
wR_2 [$I > 2\sigma(I)$]	0.0790	0.0980
R_1 [all data]	0.0464	0.1910
wR_2 [all data]	0.0816	0.1155
GOF	1.038	1.666

Table 2 (cont). Crystal, intensity collection and refinement data.

	$W(PMe_3)_4(\kappa^1\text{-}C_\alpha\text{-}CCHOC_6H_4)H_3$	$W(PMe_3)_4(OC_6H_4Et)H_3$
lattice	Monoclinic	Monoclinic
formula	$C_{20}H_{44}OP_4W$	$C_{22.50}H_{54}OP_4W$
formula weight	608.28	648.39
space group	$P2_1/n$	$P2_1/c$
a/Å	9.2779(9)	13.916(2)
b/Å	10.6718(11)	33.829(5)
c/Å	26.780(3)	26.420(4)
α/°	90	90
β/°	95.2870(10)	103.779(3)
γ/°	90	90
V/Å^3	2640.2(5)	12080(3)
Z	4	16
temperature (K)	125(2)	125(2)
radiation (λ, Å)	0.71073	0.71073
ρ (calcd.) g cm^{-3}	1.530	1.426
μ (Mo Kα), mm^{-1}	4.625	4.048
θ max, deg.	30.51	28.35
no. of data collected	41622	197346
no. of data	8055	30062
no. of parameters	259	1058
R_1 [$I > 2\sigma(I)$]	0.0186	0.0663
wR_2 [$I > 2\sigma(I)$]	0.0417	0.1557
R_1 [all data]	0.0223	0.1095
wR_2 [all data]	0.0428	0.1785
GOF	1.033	1.015

Table 2 (cont). Crystal, intensity collection and refinement data.

	$W(PMe_3)_4(\kappa^1\text{-}C_\alpha\text{-}C_4H_5O)H_3$	$(\kappa^1,\eta^2\text{-}C_4H_3O)(\kappa^1\text{-}O\text{-}C_4H_5O)W(PMe_3)_3$ (*Z* isomer)
lattice	Monoclinic	Monoclinic
formula	$C_{16}H_{44}OP_4W$	$C_{17}H_{35}MoO_2P_3$
formula weight	560.24	460.30
space group	$P2_1/n$	Cc
a/Å	9.2152(11)	9.012(2)
b/Å	16.296(2)	16.437(4)
c/Å	16.257(2)	15.277(3)
α/°	90	90
β/°	91.266(2)	90.655(3)
γ/°	90	90
V/Å^3	2440.7(5)	2262.8(9)
Z	4	4
temperature (K)	125(2)	125(2)
radiation (λ, Å)	0.71073	0.71073
ρ (calcd.) g cm^{-3}	1.525	1.351
μ (Mo Kα), mm^{-1}	4.996	0.798
θ max, deg.	31.51	26.47
no. of data collected	40990	24899
no. of data	8119	2344
no. of parameters	223	221
R_1 [$I > 2\sigma(I)$]	0.0206	0.0579
wR_2 [$I > 2\sigma(I)$]	0.0421	0.1404
R_1 [all data]	0.0296	0.0669
wR_2 [all data]	0.0449	0.1446
GOF	1.017	1.116

Table 2 (cont). Crystal, intensity collection and refinement data.

	(κ^1,η^2-C_4H_3O)(κ^1-*O*-C_4H_5O)$W(PMe_3)_3$ (*E* isomer)	**$Mo(PMe_3)_5CO$**
lattice	Monoclinic	Monoclinic
formula	$C_{17}H_{35}MoO_2P_3$	$C_{16}H_{45}MoOP_5$
formula weight	460.30	504.31
space group	$P2_1/c$	$P2_1/n$
a/Å	16.0739(14)	9.5943(13)
b/Å	8.9595(8)	16.209(2)
c/Å	16.3513(14)	16.505(2)
α/°	90	90
β/°	96.5260(10)	90.426(2)
γ/°	90	90
V/Å^3	2339.6(4)	2566.7(6)
Z	4	4
temperature (K)	125(2)	125(2)
radiation (λ, Å)	0.71073	0.71073
ρ (calcd.) g cm^{-3}	1.307	1.305
μ (Mo Kα), mm^{-1}	0.771	0.825
θ max, deg.	31.56	32.71
no. of data collected	39015	43593
no. of data	7777	8949
no. of parameters	244	224
R_1 [$I > 2\sigma(I)$]	0.0468	0.0457
wR_2 [$I > 2\sigma(I)$]	0.0809	0.1057
R_1 [all data]	0.1011	0.0700
wR_2 [all data]	0.0960	0.1196
GOF	1.002	1.043

Table 2 (cont). Crystal, intensity collection and refinement data.

	$Mo(PMe_3)_5CO$	**$(\eta^6\text{-PhH})Mo(PMe_3)_2CO$**
lattice	Orthorhombic	Monoclinic
formula	$C_{16}H_{45}MoOP_5$	$C_{13}H_{24}MoOP_2$
formula weight	504.31	354.20
space group	*Pnma*	$P2_1/c$
a/Å	21.915(4)	15.091(2)
b/Å	11.966(2)	9.4093(14)
c/Å	9.5783(19)	12.4116(19)
α/°	90	90
β/°	90	113.750(2)
γ/°	90	90
V/Å^3	2511.7(9)	1613.1(4)
Z	4	4
temperature (K)	125(2)	125(2)
radiation (λ, Å)	0.71073	0.71073
ρ (calcd.) g cm^{-3}	1.334	1.458
μ (Mo Kα), mm^{-1}	0.843	0.996
θ max, deg.	32.72	31.93
no. of data collected	41959	26974
no. of data	4677	5515
no. of parameters	153	160
R_1 [$I > 2\sigma(I)$]	0.0222	0.0358
wR_2 [$I > 2\sigma(I)$]	0.0525	0.0720
R_1 [all data]	0.0281	0.0624
wR_2 [all data]	0.0557	0.0808
GOF	1.045	1.004

Table 2 (cont). Crystal, intensity collection and refinement data.

	(κ^1,η^2-$CH_2CHC_6H_4O$) $Mo(PMe_3)_3(\eta^2$-CH_2PMe_2)	**(κ^1,η^2-$CH_2CHC_6H_4O$)(κ^1,η^2-$HC(PMe_3)CHC_6H_4O$)$Mo(PMe_3)_2$**
lattice	Triclinic	Monoclinic
formula	$C_{20}H_{42}MoOP_4$	$C_{28}H_{43}MoO_2P_3$
formula weight	518.36	600.47
space group	*P-1*	$P2_1/n$
a / Å	9.566(5)	9.2268(13)
b / Å	9.918(5)	26.978(4)
c / Å	14.383(7)	12.1568(17)
α / °	76.904(7)	90
β / °	85.410(7)	100.856(2)
γ / °	71.723(7)	90
V / Å^3	1261.9(10)	2971.9(7)
Z	2	4
temperature (K)	200(2)	125(2)
radiation (λ, Å)	0.71073	0.71073
ρ (calcd.) g cm^{-3}	1.364	1.342
μ (Mo Kα), mm^{-1}	0.781	0.625
θ max, deg.	30.53	32.77
no. of data collected	20418	50718
no. of data	7670	10467
no. of parameters	256	336
R_1 [$I > 2\sigma(I)$]	0.0503	0.0411
wR_2 [$I > 2\sigma(I)$]	0.1038	0.0915
R_1 [all data]	0.0921	0.0549
wR_2 [all data]	0.1171	0.0958
GOF	1.018	1.042

Table 2 (cont). Crystal, intensity collection and refinement data.

	$(\eta^4\text{-}OC_4H_6)_2Mo(PMe_3)_2$	$(\eta^6\text{-}C_6H_4C_6H_4O)Mo(PMe_3)_3$
lattice	Monoclinic	Triclinic
formula	$C_{14}H_{30}MoO_2P_2$	$C_{21}H_{35}MoOP_3$
formula weight	388.26	492.34
space group	$P2_1/n$	$P\text{-}1$
a/Å	10.6896(16)	8.5830(6)
b/Å	10.5998(16)	9.7259(7)
c/Å	15.882(2)	14.2710(11)
α/°	90	82.8430(10)
β/°	92.792(2)	86.7470(10)
γ/°	90	88.0610(10)
V/Å^3	1797.4(5)	1179.69(15)
Z	4	2
temperature (K)	125(2)	150(2)
radiation (λ, Å)	0.71073	0.71073
ρ (calcd.) g cm^{-3}	1.435	1.386
μ (Mo Kα), mm^{-1}	0.905	0.767
θ max, deg.	30.51	32.02
no. of data collected	26640	20518
no. of data	5476	7972
no. of parameters	180	244
R_1 [$I > 2\sigma(I)$]	0.0273	0.0312
wR_2 [$I > 2\sigma(I)$]	0.0556	0.0663
R_1 [all data]	0.0382	0.0419
wR_2 [all data]	0.0601	0.0705
GOF	1.008	1.029

Table 2 (cont). Crystal, intensity collection and refinement data.

	$W(PMe_3)_5CO$
lattice	Monoclinic
formula	$C_{16}H_{45}OP_5W$
formula weight	592.22
space group	$P2_1/n$
a / Å	9.587(2)
b / Å	16.179(4)
c / Å	16.496(4)
α / °	90
β / °	90.572(3)
γ / °	90
V / Å^3	2558.6(10)
Z	4
temperature (K)	125(2)
radiation (λ, Å)	0.71073
ρ (calcd.) g cm^{-3}	1.537
μ (Mo Kα), mm^{-1}	4.830
θ max, deg.	32.03
no. of data collected	43792
no. of data	8810
no. of parameters	224
R_1 [$I > 2\sigma(I)$]	0.0322
wR_2 [$I > 2\sigma(I)$]	0.0697
R_1 [all data]	0.0504
wR_2 [all data]	0.0775
GOF	1.038

5.13 References and notes

(1) Sanchez-Delgado, R. A. *Organometallic Modelling of the Hydrodesulfurization and Hydrodenitrogenation Reactions*, Kluwer Academic Publishers, Boston, 2002.

(2) Topsøe, H.; Clausen, B. S.; Masoth, F. E. *Catalysis Science and Technology*, Volume 11, Anderson, J. R. and Boudart, M. (Eds) Springer-Verlag, New York, 1996.

(3) Furimsky, E. *Catal. Rev. Sci. Eng.* **1983**, 421-458.

(4) Angelici, R. J. *Polyhedron* **1997**, 3073-3088.

(5) Sánchez-Delgado, R. A. Comprehensive Organometallic Chemistry III, Volume 1, Chapter 27; Crabtree, R. H. and Mingos, D. M. P. (Eds), Elsevier, Oxford, 2006.

(6) Furimsky, E. *Appl. Catal., A* **2000**, 147-190.

(7) Sattler, A.; Janak, K. E.; Parkin, G. *Inorg. Chim. Acta* **2011**, *369*, 197-202.

(8) Sattler, A.; Parkin, G. *J. Am. Chem. Soc.* **2011**, *133*, 3748-3751.

(9) Sattler, A.; Zhu, G.; Parkin, G. *J. Am. Chem. Soc.* **2009**, 7828-7838.

(10) Sattler, A.; Parkin, G. *Nature* **2010**, *463*, 523-526.

(11) Janak, K. E.; Tanski, J. M.; Churchill, D. G.; Parkin, G. *J. Am. Chem. Soc.* **2002**, 4182-4183.

(12) Buccella, D.; Janak, K. E.; Parkin, G. *J. Am. Chem. Soc.* **2008**, 16187-16189.

(13) Zhu, G.; Pang, K.; Parkin, G. *J. Am. Chem. Soc.* **2008**, 1564-1565.

(14) Baudry, D.; Daran, J.-C.; Dromzee, Y.; Ephritikhine, M.; Felkin, H.; Jeannin, Y.; Zakrzewski, J. *J. Chem. Soc., Chem. Commun.* **1983**, 813-814.

(15) The α-site is the carbon adjacent to oxygen and the β-site is next to the α-site.

(16) (a) Ringelberg, S. N.; Meetsma, A.; Troyanov, S. I.; Hessen, B.; Teuben, J. H. *Organometallics* **2002,** *21*, 1759-1765.

(b) Arndt, S.; Spaniol, T. P.; Okuda, J. *Organometallics* **2003,** *22*, 775-781.

(c) Hitzbleck, J.; Okuda, J. *Organometallics* **2007,** *26*, 3227-3235.

(17) See section 5.11.3 for details.

(18) Churchill, D. G.; Bridgewater, B. M.; Zhu, G.; Pang, K.; Parkin, G. *Polyhedron* **2006**, 499-512.

(19) (κ^2-*C,O*–C_4H_4O) is a 6-membered metallacycle, analogous to (κ^2-*C,S*–C_4H_4S) in (κ^2-*C,S*–C_4H_4S)Mo(PMe_3)$_4$ (see Chapter 4).

(20) Calculations were performed for a computationally simpler system in which the methyl groups of PMe_3 were placed by hydrogen atoms.

(21) Chisholm, M. H.; Haubrich, S. T.; Huffman, J. C.; Streib, W. E. *J. Am. Chem. Soc.* **1997**, 1634-1647.

(22) W(PMe_3)$_3H_6$ is also produced in the reaction.

(23) W(PMe_3)$_4$(OC_6H_4Et)H_3 has previously been synthesized by reaction of W(PMe_3)$_4$(η^2–CH_2PMe_2)H with *o*-ethylphenol, with subsequent hydrogenation. See reference 46.

(24) Density functional calculations on the two isomeric species indicate that the E isomer is less than 1 kcal mol^{-1} lower in energy.

(25) Basolo, F.; Kershner, D. L. *Coord. Chem. Rev.* **1987**, 279-292.

(26) For a review of organometallic compounds of furan and thiophene, see: Sadimenko, A. P. *Adv. Heterocycl. Chem.* **2001**, 1-64.

(27) Chaudret, B.; Jalon, F. A. *J. Chem. Soc., Chem. Commun.* **1988**, 711-713.

(28) The authors do not have a crystal structure of [Cp*Ru(η^5-C_4H_4O)]Cl and base the molecular assignment solely on ^{1}H NMR spectroscopic data. Additionally, in the article, the compound is written as [Cp*Ru(η^6-C_5H_4O)]Cl, but this is presumably a typo and not the actual compound.

(29) Cambridge Structural Database (Version 5.32). *3D Search and Research Using the Cambridge Structural Database*, Allen, F. H.; Kennard, O. *Chemical Design Automation News* **1993**, *8* (1), pp 1 & 31-37.

(30) For related transition metal α,β-unsaturated compounds, see:

(a) Zhang, W. Y.; Jakiela, D. J.; Maul, A.; Knors, C.; Lauher, J. W.; Helquist, P.; Enders, D. *J. Am. Chem. Soc.* **1988,** *110*, 4652-4660.

(b) Feng, Q.; Krautscheid, H.; Rauchfuss, T. B.; Skaugset, A. E.; Venturelli, A. *Organometallics* **1995,** *14*, 297-304.

(31) (a) Schuster, D. M.; White, P. S.; Templeton, J. L. *Organometallics* **2000,** *19*, 1540-1548.

(b) Hsieh, V.; De Crisci, A. G.; Lough, A. J.; Fekl, U. *Organometallics* **2007,** *26*, 938-944.

(c) Saito, S.; Nagahara, T.; Shiozawa, M.; Nakadai, M.; Yamamoto, H. *J. Am. Chem. Soc.* **2003,** *125*, 6200-6210.

(32) (a) Cloke, F. G. N.; Cox, K. P.; Green, M. L. H.; Bashkin, J.; Prout, K. *J. Chem. Soc., Chem. Commun.* **1982**, 393-394.

(b) Brookhart, M.; Cox, K. P.; Cloke, F. G. N.; Green, J. C.; Green, M. L. H.; Hare, P. M.; Bashkin, J.; Derome, A. E.; Grebenik, P. D. *J. Chem. Soc., Dalton Trans.* **1985**, 423-433.

(33) Propene was identified by comparison to the ^{1}H NMR spectrum of an authentic sample. However, because the reaction produces many compounds, the propene is present in a mixture and the methyl resonance is obscured by other signals from other compounds. Therefore, only the [H_2C=CH] fragment was compared making this assignment tentative.

(34) Propane was also identified by comparison of the ^{1}H NMR spectrum of an authentic sample but assignment is also tentative because it is present in a mixture of compounds.

(35) (η^6-PhH)Mo(PMe_3)$_2$CO is likely produced from reaction of the *in situ* produced (η^6-PhH)Mo(PMe_3)$_3$ and CO. For synthesis of (η^6-PhH)Mo(PMe_3)$_3$, see reference 68.

(36) Heating solutions of Mo(PMe_3)$_4H_4$ and propene in benzene (120 ˚C) resulted in the formation of propane.

(37) Watson, P. R.; Tinseth, G. R. *J. Am. Chem. Soc.* **1991**, 8549-8550.

(38) Caldwell, T. E.; Abdelrehim, I. M.; Land, D. P. *J. Am. Chem. Soc.* **1996**, 907-908.

(39) Now Professor Daniela Buccella of New York University.

(40) For previous C–O bond cleavage of benzofuran, see:

(a) Zhang, X.; Watson, E. J.; Dullaghan, C. A.; Gorun, S. M.; Sweigart, D. A. *Angew. Chem. Int. Ed.* **1999**, 2206-2208.

(b) Edelman, M. C.; Maholland, M. K.; Baldwin, R. M.; Cowley, S. W. *J. Catal.* **1988**, 243-253.

(41) Jahr, H. C.; Nieger, M.; Dötz, K. H. *J. Organomet. Chem.* **2002,** *641*, 185-194.

(42) The molecular structure of $(\eta^5\text{–}C_4H_5O)Mo(PMe_3)_3H$ was determined afterward by Ashley Zuzek.

(43) Initial studies indicate that the isomeric 2,3-dihydrofuran does not react with $Mo(PMe_3)_6$ under similar conditions to give $(\eta^5\text{–}C_4H_5O)Mo(PMe_3)_3H$.

(44) Hascall, T.; Murphy, V. J.; Janak, K. E.; Parkin, G. *J. Organomet. Chem.* **2002**, *652*, 37-49.

(45) Hascall, T.; Murphy, V. J.; Parkin, G. *Organometallics* **1996**, *15*, 3910-3912.

(46) Rabinovich, D.; Zelman, R.; Parkin, G. *J. Am. Chem. Soc.* **1992**, 4611-4621

(47) For a review on aldehyde ligands, see: Huang, Y.-H.; Gladysz, J. A. *J. Chem. Educ.* **1988**, *65*, 298-303.

(48) Green, M. L. H.; Parkin, G.; Moynihan, K. J.; Prout, K. *J. Chem. Soc., Chem Commun.* **1984**, 1540.

(49) $W(PMe_3)_4(OMe)H_3$ was first synthesized by Wilkinson. See: Chiu, K. W.; Jones, R. A.; Wilkinson, G.; Galas, A. M. R.; Hursthouse, M. B.; Malik, K. M. A. *J. Chem. Soc., Dalton Trans.* **1981**, 1204-1211.

(50) The molybdenum congener, namely $Mo(PMe_3)_4(\eta^2\text{-}OCH_2)H_2$, has been structurally characterized. See reference 44.

(51) The reaction of $W(PMe_3)_4(\eta^2\text{–}CH_2PMe_2)H$ with ethanol will produce the $W(PMe_3)_4(OEt)H_3$ in the absence of H_2. However, the production of $W(PMe_3)_4(OEt)H_3$ is significantly accelerated in the presence of H_2.

(52) For a related tungsten ethoxide complex, see: Carlson-Day, K. M.; Eglin, J. L.; Valente, E. J.; Zubkowski, J. D. *Inorg. Chim. Acta* **1999,** *284*, 300-303.

(53) (a) Meiere, S. H.; Harman, W. D. *Organometallics* **2001,** *20*, 3876-3883.

(b) Graham, P. M.; Mocella, C. J.; Sabat, M.; Harman, W. D. *Organometallics* **2005,** *24*, 911-919.

(54) (a) McNally, J. P.; Leong, V. S.; Cooper, N. J. in *Experimental Organometallic Chemistry*, Wayda, A. L.; Darensbourg, M. Y., Eds.; American Chemical Society: Washington, DC, 1987; Chapter 2, pp 6-23.

(b) Burger, B.J.; Bercaw, J. E. in *Experimental Organometallic Chemistry*; Wayda, A. L.; Darensbourg, M. Y., Eds.; American Chemical Society: Washington, DC, 1987; Chapter 4, pp 79-98.

(c) Shriver, D. F.; Drezdzon, M. A.; *The Manipulation of Air-Sensitive Compounds*, 2nd Edition; Wiley-Interscience: New York, 1986.

(55) Gottlieb, H. E.; Kotlyar, V.; Nudelman, A. *J. Org. Chem.* **1997**, *62*, 7512-7515.

(56) Cambridge Isotope Laboratories, Inc., NMR Solvent Data Chart (www.isotope.com/cil/products/images/nmrchart.pdf).

(57) "Nuclear Magnetic Resonance Spectroscopy" Nelson, J. H. Prentice Hall, New Jersey (2003), p 79.

(58) Murphy, V. J.; Parkin, G. *J. Am. Chem. Soc.* **1995**, *117*, 3522-3528.

(59) Lyons, D.; Wilkinson, G. *J. Chem. Soc. Dalton Trans.* **1985**, 587-590.

(60) Green, M. L. H.; Parkin, G.; Chen, M.; Prout, K. *J. Chem. Soc., Dalton Trans.* **1986**, 2227–2236.

(61) Parkin, G. *Rev. Inorg. Chem.* **1985**, *7*, 251-297.

(62) (a) Sheldrick, G. M. SHELXTL, An Integrated System for Solving, Refining and Displaying Crystal Structures from Diffraction Data; University of Göttingen, Göttingen, Federal Republic of Germany, 1981.

(b) Sheldrick, G. M. *Acta Cryst.* **2008**, *A64*, 112-122.

(63) Jaguar 7.5, Schrödinger, LLC, New York, NY 2008.

(64) (a) Becke, A. D. *J. Chem. Phys.* **1993**, *98*, 5648-5652.

(b) Becke, A. D. *Phys. Rev. A* **1988**, *38*, 3098-3100.

(c) Lee, C. T.; Yang, W. T.; Parr, R. G. *Phys. Rev. B* **1988**, *37*, 785-789.

(d) Vosko, S. H.; Wilk, L.; Nusair, M. *Can. J. Phys.* **1980**, *58*, 1200-1211.

(e) Slater, J. C. *Quantum Theory of Molecules and Solids, Vol. 4: The Self-Consistent Field for Molecules and Solids*; McGraw-Hill: New York, 1974.

(65) (a) Hay, P. J.; Wadt, W. R. *J. Chem. Phys.* **1985**, *82*, 270-283.

(b) Wadt, W. R.; Hay, P. J. *J. Chem. Phys.* **1985**, *82*, 284-298.

(c) Hay, P. J.; Wadt, W. R. *J. Chem. Phys.* **1985**, *82*, 299-310.

(66) The compounds contain deuterium, and as such, exist as a mixture of isotopologues.

(67) The assignment of $(\eta^5\text{-}C_4H_5O)Mo(PMe_3)_2(\eta^2\text{-}CH_2PMe_2)$ is based on the similarity to the tungsten compound, $(\eta^5\text{-}C_4H_5O)W(PMe_3)_2(\eta^2\text{-}CH_2PMe_2)$.

(68) For synthesis of $(\eta^6\text{-}PhH)Mo(PMe_3)_3$, see: Zhu, G.; Janak, K. E.; Figueroa, J. S.; Parkin, G. *J. Am. Chem. Soc.* **2006**, 128, 5452-5461.

(69) Mathieu, R.; Poilblanc, R. *Inorg. Chem.* **1972,** *11*, 1858-1861.

CHAPTER 6

Synthesis of the first transition metal complexes that feature a [*CCC*] X_3-donor pincer ligand

Table of Contents

Reproduced in part from:

Sattler, A.; Ruccolo, S.; Parkin, G. *Dalton Trans.* **2011**, *40*, 7777–7782.

Sattler, A.; Parkin, G. *J. Am. Chem. Soc.* **2012**, *134*, 2355–2366.

6.1 Introduction

Ligand design is of fundamental interest in synthetic inorganic chemistry,[1] and those which bind to a metal with a κ^3–tridentate meridional (*i.e.* T-shaped) motif (Figure 1) have been termed "pincer" ligands. Pincer ligands are an important class of ligands that have received much attention in areas such as *(i)* fundamental chemical transformations involving bond activation, *(ii)* catalysis, *(iii)* sensors, *(iv)* switches and *(v)* supramolecular chemistry.[2] A large array of such ligands are known and, in many cases, the backbone features 6-membered aromatic rings that either contain the central **A** donor (Figure 1, II) or serve as a linker to the lateral **B** donors (Figure 1, III). This type of arrangement enforces planarity with respect to the coordination sphere around the metal center, especially when two 5-membered chelate rings are formed. One of the reasons for the widespread applications of pincer ligands is that it is possible to vary the steric and electronic nature of the ligand. Thus, tuning the ligand system can effectively modulate the properties of the metal center. In this regard, pincer ligands are known for each of the L_3, L_2X, LX_2 and X_3 Covalent Bond Classifications,[3] which provides a clear indication of the electronic variations that may be achieved within this system of ligands.[2] Furthermore, pincer ligands may incorporate a variety of donor atoms, of which [*NCN*] and [*PCP*] are common examples.[2]

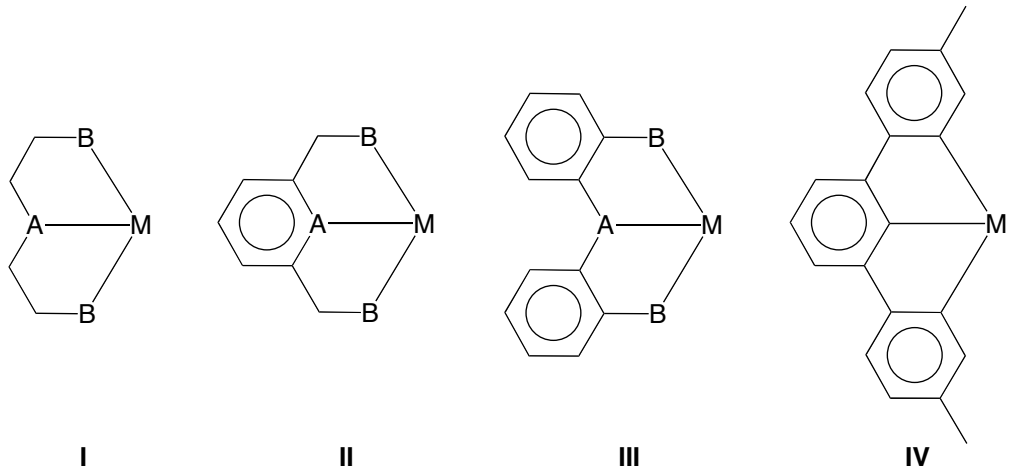

Figure 1. Pincer Ligand Motifs.

Notably absent from the large collection of known pincer ligands for transition metals, however, are those that feature a planar [*CCC*] X_3-donor array,[4,5,6] an observation that may reflect synthetic difficulties. We rationalized that access to an X_3-donor [*CCC*] pincer ligand could be achieved by cyclometalation of a terphenyl derivative.[7,8] In this regard, organometallic compounds containing κ^1-*m*-terphenyl ligands ([Ar^{Ph_2}]) (Figure 2) have received considerable attention over the past several decades due to the steric protection provided by the flanking aryl rings, common examples of which are [Ar^{Mes_2}] and [Ar^{Dipp_2}] (Figure 2).[9] Indeed, structurally characterized compounds of the generic formula [κ^1-*m*-terphenyl]M are known for almost half of the metals in groups 3 through 12, including: Sc,[10] Y,[10,11] Ti,[12] Cr,[13] Mn,[13d,14] Fe,[13d,14a-f,15] Co,[13d,14b-d,16] Cu,[17] Ag,[17a,18] Au,[19] Zn,[20] Cd,[20a,21] Hg,[20a,22] as depicted in Figure 3. This chapter describes the synthesis of the first terphenyl ([Ar^{Tol_2}]) (Figure 2) complex of tantalum and its subsequent cyclometalation chemistry that allows the synthesis of the first transition metal complex with a [*CCC*] X_3-donor pincer ligand.

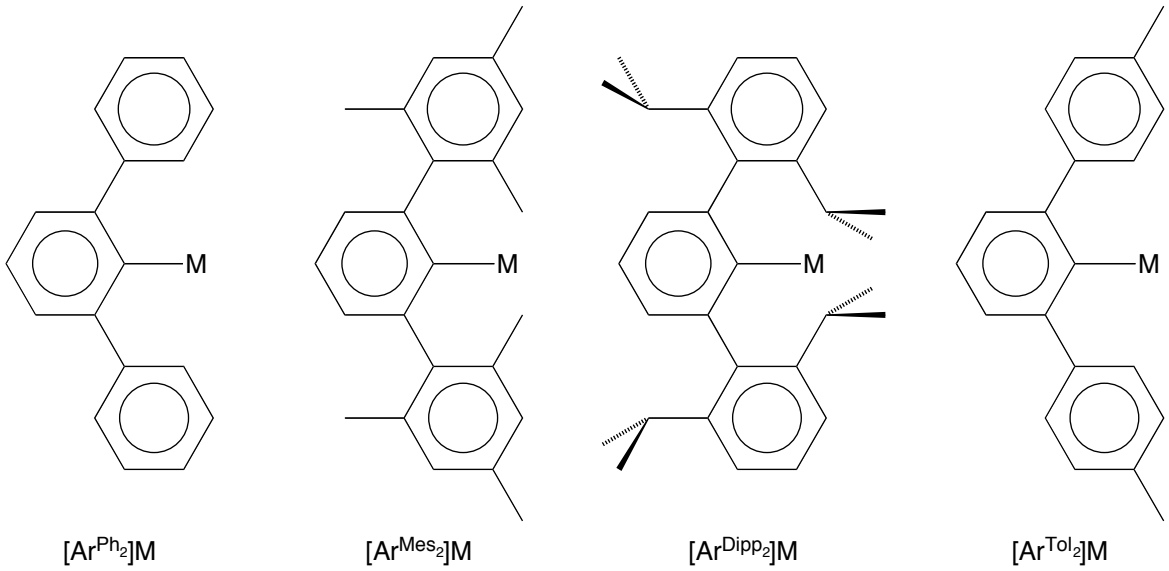

Figure 2. Examples of [κ^1-*m*-terphenyl] ligands and their common abbreviations.

3	4	5	6	7	8	9	10	11	12
Sc	Ti	V	Cr	Mn	Fe	Co	Ni	Cu	Zn
Y	Zr	Nb	Mo	Tc	Ru	Rh	Pd	Ag	Cd
Lu	Hf	Ta	W	Re	Os	Ir	Pt	Au	Hg

Figure 3. [κ^1-*m*-terphenyl]M compounds of groups 3 through 12 (blue = compounds structurally characterized by X-ray diffraction, red = compounds not yet known by X-ray diffraction).

6.2 Trimethyldichlorotantalum: $TaMe_3Cl_2$

In 1964, Juvinall reported the first synthesis of a σ-bonded alkyl compound of tantalum, namely trimethyldichlorotantalum, $TaMe_3Cl_2$,[23,24] in the reaction of $TaCl_5$ and Me_2Zn (Scheme 1).[25] $TaMe_3Cl_2$ has proven to be a valuable synthetic precursor for a large variety of d^0 tantalum compounds.[26] Moreover, $TaMe_3Cl_2$ has been the subject of several studies, including gas phase electron diffraction,[27] photoelectron spectroscopy,[28] and density functional theory (DFT) calculations.[28] Despite this interest, however, the molecular structure of $TaMe_3Cl_2$ has not been determined by X-ray diffraction.

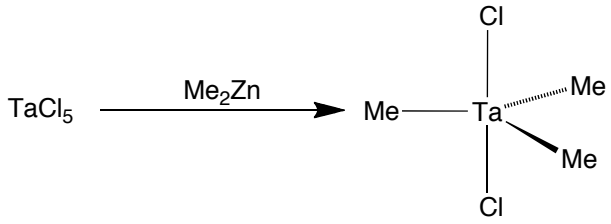

Scheme 1. Synthesis of $TaMe_3Cl_2$

We suspect that a possible reason for the absence of a single crystal X-ray diffraction study on $TaMe_3Cl_2$ is its thermal instability and its high reactivity towards air and water.[23] We were, however, able to obtain pale yellow X-ray quality crystals of $TaMe_3Cl_2$ by either (*i*) cooling a saturated solution of $TaMe_3Cl_2$ in pentane at –15 °C[29] or (*ii*) by subliming the product of the reaction between $TaCl_5$ and Me_2Zn into a vessel

maintained at 0 ˚C. The molecular structure is shown in Figure 4, and reveals a well-defined trigonal bipyramidal geometry with axial chloride ligands and Cl–Ta–C and C–Ta–C bond angles of 90˚ and 120˚, respectively. The derived bond lengths (Table 1) are similar to those of the gas phase molecular structure of $TaMe_3Cl_2$ as determined by electron diffraction.[27] Additionally, the axial placement of the more electronegative chloride ligands in $TaMe_3Cl_2$ is in accord with Hoffman's analysis of five-coordinate transition metal compounds.[30]

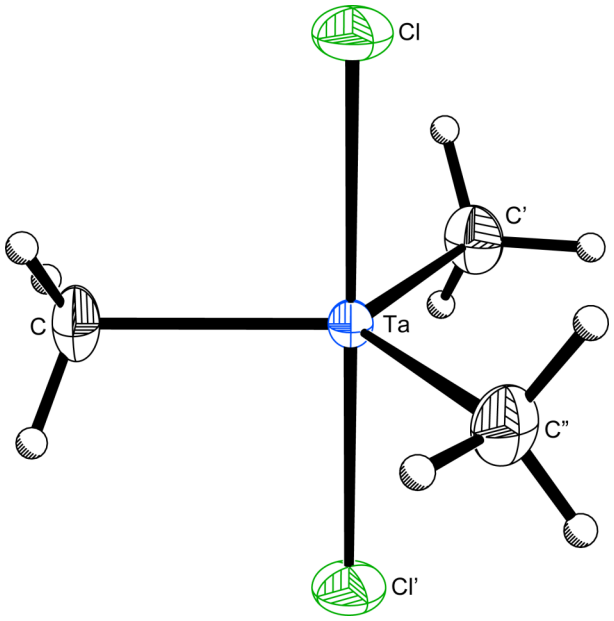

Figure 4: Molecular Structure of $TaMe_3Cl_2$ (the hydrogen atoms are placed in idealized positions and only one of the disordered configurations is shown).

Table 1. Comparison of Ta–Me and Ta–Cl bond lengths of $TaMe_3Cl_2$ in the solid state and gas phase.

	***d*(Ta–Me)/Å**	***d*(Ta–Cl)/Å**	**reference**
solid state	2.117(5)	2.312(2)	29
gas phase	2.158(5)	2.317(3)	27

Although five-coordinate tantalum compounds are known to adopt idealized structures that are trigonal bipyramidal and square pyramidal,[31,32] there are no $TaMe_3X_2$

derivatives listed in the Cambridge Structural Database[33] that possesses a trigonal bipyramidal geometry with bond angles of 90˚, 120˚ and 180˚. It should be noted, however, that the idealized bond angles for $TaMe_3Cl_2$ are dictated by the fact that the tantalum atom resides on a site of $\bar{6}m2$ symmetry in space group $P6_3/mmc$. Conversely, if the tantalum were to be slightly displaced from the plane of the three methyl groups towards one of the chloride ligands, the X–Ta–X bond angles would not be exactly 90˚ and 120˚. In such a case, the molecule would be statistically disordered about the $\bar{6}m2$ site. Although the shape of the thermal ellipsoid of the tantalum or other atoms provides no indication for such disorder, it is not unprecedented for disorder of this type to go unrecognized;[34] as such, the possibility exists that the coordination environment of $TaMe_3Cl_2$ is not rigorously trigonal bipyramidal, but is only approximately so. In this regard, DFT calculations predict a slight distortion, with C–Ta–Cl bond angles of 88˚ and 92˚ rather than 90˚.[28,35,36] In contrast to the trigonal bipyramidal nature of $TaMe_3Cl_2$, it is interesting to note that the pentamethyl complex, $TaMe_5$, adopts a structure that is better described as a square-pyramid.[37]

For comparison, the metrical data for other structurally characterized $TaMe_3X_2$ compounds are summarized in Table 2, and are largely restricted to complexes in which X is an oxygen donor ligand. Specific examples include the aryloxide derivatives $TaMe_3(OAr)_2$ synthesized by Rothwell[38] and an enolate derivative, $TaMe_3[OC(Ad)Ar]_2$, synthesized by Cummins.[26p] Each of these complexes adopts a trigonal bipyramidal geometry, as does the mixed siloxide-chloride derivative $TaMe_3[OSi(o\text{-}Tol)_3]Cl$.[39] In addition to these methyl compounds, other five-coordinate organotantalum compounds that adopt trigonal bipyramidal geometries include $Ta(CH_2\text{-}p\text{-}Tol)_3F_2$,[40] $Ta(CH_2\text{-}p\text{-}Tol)_3(OC_6Ph_2H_3)_2$,[41] and $Ta(CH_2SiMe_3)_3(OC_6Ph_2Pr^i{}_2H)_2$.[42] In line with $TaMe_3Cl_2$, the more electronegative ligands in complexes above also occupy the axial sites.[30] Conversely, $[\kappa^2\text{-}PhAs(CH_2SiMe_2NPh)_2]TaMe_3$ is better described as a square-pyramid, but contains a bidentate ligand.[26b]

Table 2. Metrical data for $TaMe_3X_2$ compounds.

	***d*(Ta–C)/Å**	**X–Ta–X/°**	**reference**
$TaMe_3Cl_2$	2.117(5)	180	this work
$TaMe_3(OC_6H_3Bu^t_2)_2$	2.136(10), 2.138(10), 2.248(10)	164.1(2)	38
$TaMe_3(OC_6H_2Bu^t_2OMe)_2$	2.150(8), 2.169(8), 2.219(8)	167.2(2)	38b
$TaMe_3[OSi(o\text{-}Tol)_3]Cl$	2.107(7), 2.143(8), 2.169(8),	177.8(2)	39
$TaMe_3[OC(Ad)Ar]_2$	2.137(5), 2.139(4), 2.150(5)	175.76(10)	26p
$TaMe_5$	$2.073(14)_{apical}$, $2.150(7)_{basal}$	–	37
$[\kappa^2\text{-}PhAs(CH_2SiMe_2NPh)_2]TaMe_3$	2.176(2), 2.189(2), 2.223(2)	111.44(7)	26b

6.3 Synthesis and molecular structure of $Ta(PMe_3)_2Me_3Cl_2$

In view of the fact that $TaMe_3Cl_2$ has a formal 10-electron configuration, it is known to be capable of forming adducts with Lewis bases, such as pyridine and dimethoxyethane.[43] However, only one such adduct has been structurally characterized by X–ray diffraction, namely $Ta(bipy)Me_3Cl_2$ (bipy = 2,2′-bipyridine), which features a bidentate ligand.[44] Therefore, it is noteworthy that a pale yellow solution of $TaMe_3Cl_2$ in pentane reacts immediately with trimethylphosphine to deposit the bright yellow, crystalline, seven-coordinate complex, $Ta(PMe_3)_2Me_3Cl_2$ (Scheme 2), which has been structurally characterized by X-ray diffraction (Figure 5).[45]

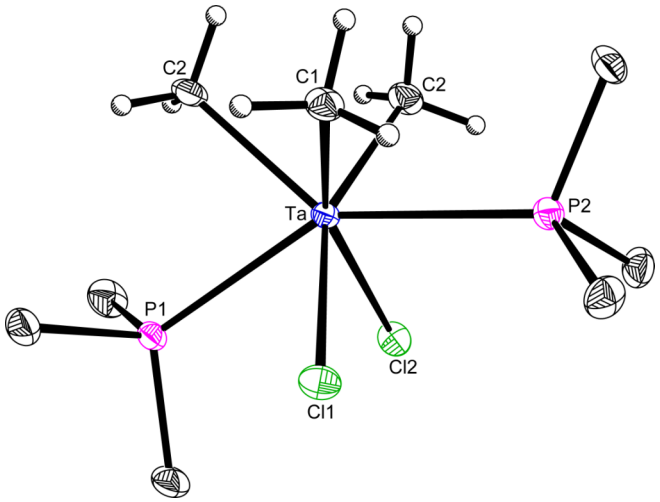

Figure 5. Molecular Structure of $Ta(PMe_3)_2Me_3Cl_2$.

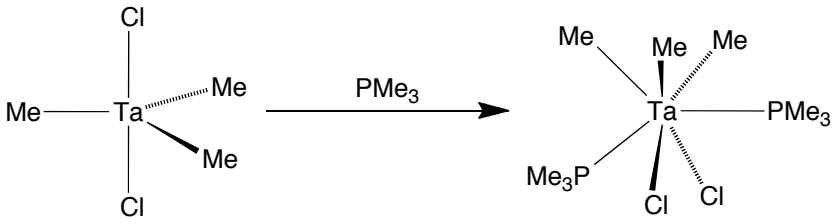

Scheme 2. Synthesis of $Ta(PMe_3)_2Me_3Cl_2$.

Comparison of the molecular structures of $TaMe_3Cl_2$ and $Ta(PMe_3)_2Me_3Cl_2$ (Table 3) indicates that coordination of the two PMe_3 ligands results in a distinct lengthening of both the Ta–Me and Ta–Cl bond lengths. Thus, the average Ta–Me bond length in $Ta(PMe_3)_2Me_3Cl_2$ (2.23 Å) is 0.11 Å longer than that in $TaMe_3Cl_2$ (2.12 Å) and the average Ta–Cl bond length in $Ta(PMe_3)_2Me_3Cl_2$ (2.45 Å) is 0.14 Å longer than that in $TaMe_3Cl_2$ (2.31 Å). The Ta–P bond lengths [2.6711(7) Å and 2.6758(7) Å] are comparable to the mean value for trimethylphosphine tantalum compounds listed in the Cambridge Structural Database (2.61 Å).[33]

Table 3. Comparison of Ta–Me and Ta–Cl bond lengths of $TaMe_3Cl_2$ and $Ta(PMe_3)_2Me_3Cl_2$.

	***d*(Ta–Me)/Å**	***d*(Ta–Cl)/Å**
$TaMe_3Cl_2$	2.117(5)	2.312(2)
$Ta(PMe_3)_2Me_3Cl_2$	2.219(3), 2.233(2), 2.240(3)	2.4501(7), 2.4588(6)

Seven-coordinate structures are often described as being based on one of three idealized high symmetry structures, namely *(i)* a pentagonal bipyramid (D_{5h}, 1:5:1), *(ii)* a capped octahedron (C_{3v}, 1:3:3), and *(iii)* a capped trigonal prism (C_{2v}, 1:4:2), as illustrated in Figure 6.[46] In addition to these high symmetry geometries, there is also a lower symmetry alternative, namely a tetragonal base-trigonal cap geometry, also known as a 4:3 piano stool, (C_s, 4:3) (Figure 6).[46,47] Although compounds that feature a 4:3 piano stool are not as common as those that are described as pentagonal bipyramidal, capped

octahedral and capped trigonal prismatic, a variety of such complexes is known, as originally highlighted by Lippard.[48,49]

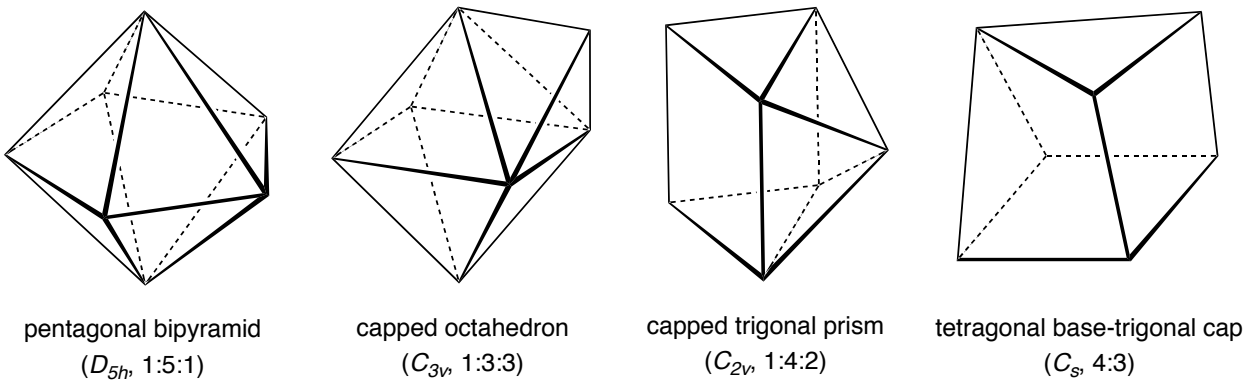

Figure 6. Idealized geometries of seven-coordinate compounds.

Of these idealized seven-coordinate geometries, the molecular structure of $Ta(PMe_3)_2Me_3Cl_2$ bears little relationship to that of the pentagonal bipyramid,[50] but can be approximately represented as either *(i)* a capped octahedron, in which a methyl group [C2] caps the trigonal face comprising a PMe_3 and two methyl groups [P1,C1,C3], *(ii)* a capped trigonal prism in which [P2] of a PMe_3 ligand caps a quadrilateral face that comprises two methyl groups and two chloride ligands [C1,C3,Cl1,Cl2], or *(iii)* a 4:3 piano stool in which the combination of the two PMe_3 and two Cl ligands form the tetragonal base (albeit not in the same plane) and the three methyl groups form the trigonal cap. Views of $Ta(PMe_3)_2Me_3Cl_2$ that illustrate these different possibilities are shown in Figure 7.

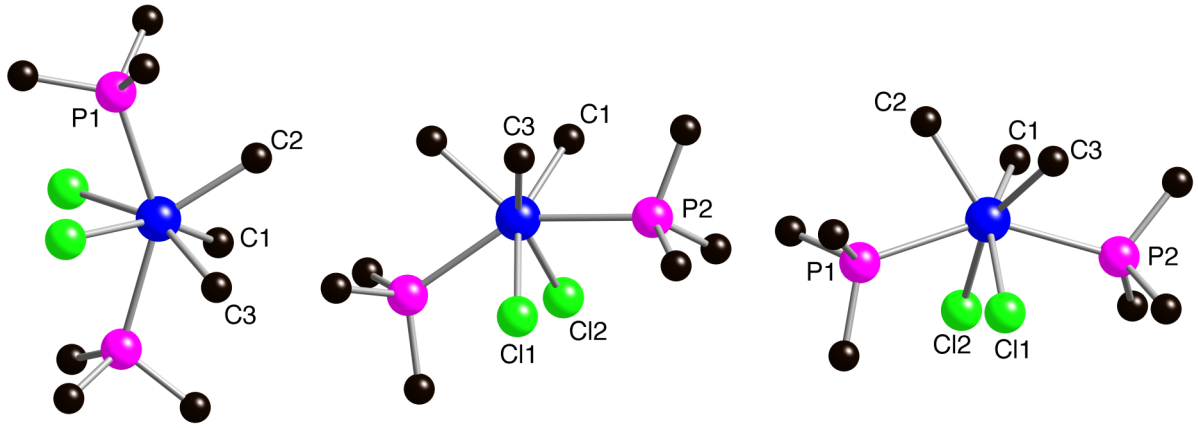

Figure 7. Views of $Ta(PMe_3)_2Me_3Cl_2$ that illustrate the possible capped octahedron (left), capped trigonal prism (center) and 4:3 piano stool (right) structural representations. For the capped octahedron, C2 caps the [P1,C1,C3] trigonal face; for the capped trigonal prism, P2 caps the [C1,C3,Cl1,Cl2] quadrilateral face; while for the 4:3 piano stool, [P1,P2,Cl1,Cl2] forms the tetragonal base and [C1,C2,C3] forms the trigonal cap.

With respect to these alternatives, the molecular structure of $Mo(PEt_3)_2(CO)_3Cl_2$,[51] a seven-coordinate compound that also possesses two PR_3 ligands and two chloride ligands has been described as possessing a capped octahedral structure. For $Ta(PMe_3)_2Me_3Cl_2$, however, the capped octahedral description is not particularly satisfactory because, neglecting the capping [C2] methyl group, the remaining six-coordinate fragment is grossly distorted from that of an octahedral geometry. For example, the P–Ta–P bond angle [146.85(2)˚] deviates substantially from linearity. On this basis, the capped trigonal prism would be the better description.

The notion that $Ta(PMe_3)_2Me_3Cl_2$ is best described as capped trigonal prism is supported by consideration of the interligand bond angles. Specifically, a simple method that has been employed for identifying the best description for a seven-coordinate complex involves listing the 21 interligand bond angles in order of decreasing size and comparing the values with those for idealized geometries.[48c] The bond angles for the various geometries are listed in Table 4, from which it is apparent that the average deviation in angle between the calculated and observed structures

increases in the sequence: capped trigonal prism (3.2°) < 4:3 piano stool (4.4°) < capped octahedron (5.8°) < pentagonal bipyramid (10.9°).

Interestingly, while the molecular structure of the bipyridyl analogue, $Ta(bipy)Me_3Cl_2$,[44] is also described as a distorted capped trigonal prism (Figure 8), the detailed structure is very different from that of $Ta(PMe_3)_2Me_3Cl_2$. Specifically, whereas the structure of $Ta(PMe_3)_2Me_3Cl_2$ is based on a PMe_3 ligand capping a quadrilateral face that comprises two methyl groups and two chloride ligands, the structure of $Ta(bipy)Me_3Cl_2$ is based on a chloride ligand capping a quadrilateral face composed of a methyl group, a chloride ligand and the two nitrogen atoms of the bipy ligand.[44] The distinctly different structures of $Ta(PMe_3)_2Me_3Cl_2$ and $Ta(bipy)Me_3Cl_2$ is undoubtedly a consequence of the fact that the bipy ligand coordinates with a small N–Ta–N bond angle [68.2(8)°]. In contrast, the seven-coordinate tantalum trimethyl compound [κ^4-N_2P_2-$PhP(CH_2SiMe_2NSiMe_2CH_2)_2PPh]TaMe_3$ has also been described as possessing a capped trigonal prismatic geometry (Figure 8),[26k] but one that is much more similar to that of $Ta(PMe_3)_2Me_3Cl_2$ than to $Ta(bipy)Me_3Cl_2$. For example, the P–Ta–P bond angle of $PhP(CH_2SiMe_2NSiMe_2CH_2)_2PPh]TaMe_3$ [143.00(3)°] is comparable to that of $Ta(PMe_3)_2Me_3Cl_2$ [146.85(2)°] and for both complexes a phosphorus donor serves to cap the quadrilateral face.

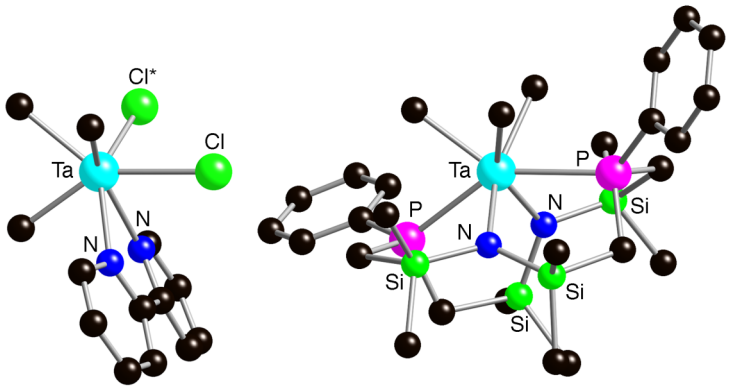

Figure 8. Different capped trigonal prism structures of $Ta(bipy)Me_3Cl_2$ (left, reference 44) and [κ^4-N_2P_2-$PhP(CH_2SiMe_2NSiMe_2CH_2)_2PPh]TaMe_3$ (right, reference 26k), of which the latter is similar to that of $Ta(PMe_3)_2Me_3Cl_2$. The Cl ligand marked with an asterisk (Cl*) is disordered with a methyl group.

Table 4. X–Ta–Y bond angles (°) for $Ta(PMe_3)_2Me_3Cl_2$ and comparison with the values for idealized seven-coordinate geometries.[a]

Angle#	Exp	PB[b]	CO[b]	CTP[b]	4:3[b]	|Exp–PB|	|Exp–CO|	|Exp–CTP|	|Exp–4:3|
1	156.5	180.0	160.0	164.0	170.0	23.5	3.5	7.5	13.5
2	154.3	144.0	160.0	164.0	153.6	10.3	5.7	9.7	0.7
3	146.9	144.0	160.0	144.2	153.6	2.9	13.1	2.7	6.7
4	138.2	144.0	130.0	144.2	130.8	5.8	8.2	6.0	7.4
5	126.1	144.0	130.0	119.0	130.8	17.9	3.9	7.1	4.7
6	125.4	144.0	130.0	119.0	120.0	18.6	4.6	6.4	5.4
7	124.8	90.0	108.9	118.8	120.0	34.8	15.9	6.0	4.8
8	120.1	90.0	108.9	118.8	108.8	30.1	11.2	1.3	11.3
9	98.7	90.0	108.9	99.0	108.8	8.7	10.2	0.3	10.1
10	88.7	90.0	83.1	99.0	89.4	1.3	5.6	10.3	0.7
11	81.9	90.0	83.1	83.7	89.4	8.1	1.2	1.8	7.5
12	81.8	90.0	83.1	83.7	83.1	8.2	1.3	1.9	1.3
13	80.8	90.0	82.0	80.3	83.1	9.2	1.2	0.5	2.3
14	80.4	90.0	82.0	80.3	83.1	9.6	1.6	0.1	2.7
15	78.2	90.0	82.0	78.8	75.5	11.8	3.8	0.6	2.7
16	77.8	90.0	82.0	78.6	75.5	12.2	4.2	0.8	2.3
17	76.3	72.0	82.0	75.2	75.5	4.3	5.7	1.1	0.8
18	75.6	72.0	82.0	75.2	75.5	3.6	6.4	0.4	0.1
19	74.9	72.0	70.0	75.0	73.3	2.9	4.9	0.1	1.6
20	74.7	72.0	70.0	75.0	73.3	2.7	4.7	0.3	1.4
21	74.5	72.0	70.0	71.5	70.0	2.5	4.5	3.0	4.5
Σ|Exp – ideal|						229.0	121.4	67.9	92.5
Σ|Exp – ideal| (average)						10.9	5.8	3.2	4.4

(a) Abbreviations: Exp (experimental), PB (pentagonal bipyramid), CO (capped octahedron), CTP (capped trigonal prism) and 4:3 (4:3 piano stool).

(b) Values for idealized structures are taken from reference 48c.

6.4 ^{1}H NMR spectroscopic features of $Ta(PMe_3)_2Me_3Cl_2$

The ^{1}H NMR spectroscopic features of $Ta(PMe_3)_2Me_3Cl_2$ have also been analyzed. For example, at room temperature, the ^{1}H NMR spectrum in d_8-toluene consists of two signals in the ratio 1:2, namely a singlet at 1.38 attributable to the tantalum methyl groups and a doublet at 1.22 attributable to the PMe_3 groups (Figure 9). Thus, while the X-ray diffraction study of $Ta(PMe_3)_2Me_3Cl_2$ indicates that there are two sets of chemically inequivalent tantalum methyl groups in the ratio 2:1, ^{1}H NMR spectroscopic studies indicate that the molecule is fluxional such that the tantalum methyl groups are observed as a singlet at room temperature (Figure 9). The absence of $J_{P\text{-}H}$ coupling for

the tantalum methyl groups at room temperature implies that $Ta(PMe_3)_2Me_3Cl_2$ undergoes facile and reversible dissociation of PMe_3.[52] Lowering the temperature to –30 ˚C, however, causes the rate of PMe_3 dissociation to become sufficiently slow that phosphorus coupling is observed and the signal attributable to the tantalum methyl groups becomes a 1:2:1 triplet while the signal due to the PMe_3 ligands become a virtual triplet (Figure 9). Upon further lowering of the temperature to –70 ˚C, the triplet attributable to the tantalum methyl groups starts to broaden, presumably indicative of the onset of decoalescence into a 2:1 set of chemically inequivalent methyl groups. Fluxionality of seven-coordinate trimethyl tantalum compounds has been previously reported. For example, 2:1 ratios for the methyl groups have been observed by Arnold for $[\kappa^2\text{-TolC(NSiMe}_3)_2]_2TaMe_3$[26d] and for $[\kappa^4\text{-}N_2P_2\text{-PhP(CH}_2SiMe_2NSiMe_2CH_2)_2PPh]TaMe_3$ by Fryzuk,[26k] although the 2:1 ratio for the latter remains broad at temperatures as low as –93 ˚C.

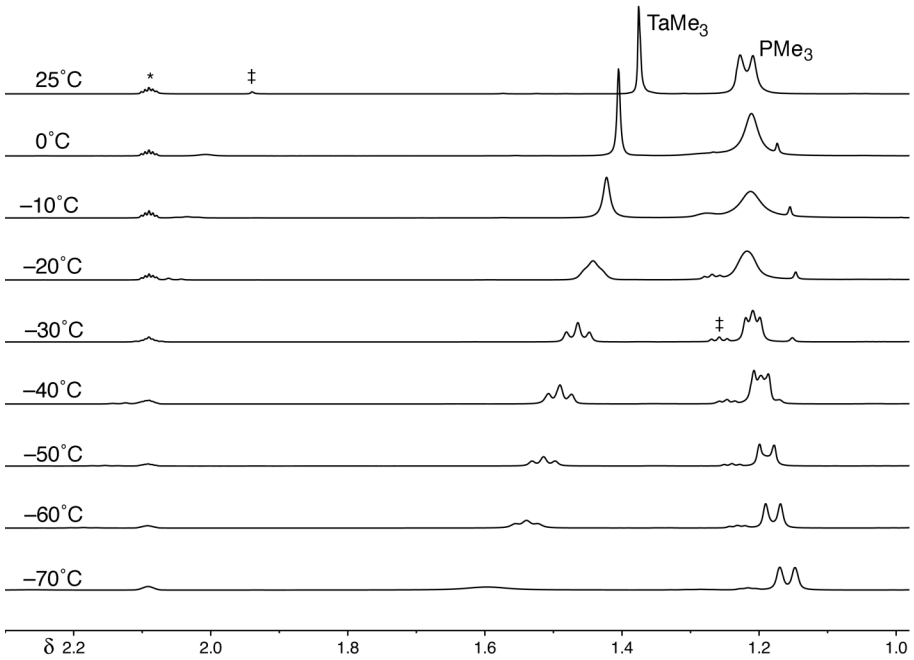

Figure 9. Variable temperature ^1H NMR spectra of $Ta(PMe_3)_2Me_3Cl_2$ in d_8-toluene (*). The presence of a small quantity of a compound tentatively identified as $Ta(PMe_3)_2Me_2Cl_3$ (*ca.* 3 %) is indicated by the signals marked (‡). While the Ta–Me signal of $Ta(PMe_3)_2Me_2Cl_3$ is evident at room temperature, the PMe_3 signal is only observed at low temperature.

6.5 Reactivity of $TaMe_3Cl_2$ with $[Ar^{Tol_2}]Li$

Treatment of $TaMe_3Cl_2$ with $[Ar^{Tol_2}]Li$ results in an immediate reaction, from which $[Ar^{Tol_2}]TaMe_3Cl$ can be isolated (Scheme 3). $[Ar^{Tol_2}]TaMe_3Cl$, however, exhibits limited stability in solution and converts to, *inter alia*, $[Ar^{Tol_2}]TaMe_2Cl_2$. It is postulated that the mechanism for the decomposition of $[Ar^{Tol_2}]TaMe_3Cl$ to $[Ar^{Tol_2}]TaMe_2Cl_2$ is *via* a redistribution process, which produces $[Ar^{Tol_2}]TaMe_2Cl_2$ and $[[Ar^{Tol_2}]TaMe_4]$, the latter of which is unstable and decomposes to give the α-hydrogen eliminated products methane and $[Ar^{Tol_2}]H$, both of which are observed by ^1H NMR spectroscopy.[53] In accord with this behavior, Schrock demonstrated that treatment of $TaNp_3Cl_2$ (Np = neopentyl) with NpLi (2 equivalents) produces the neopentylidene complex, $TaNp_3(=CHCMe_3)$, instead of the pentaalkyl complex, $TaNp_5$, a process that is proposed to occur *via* α-hydrogen abstraction.[54] Additionally, Schrock has also reported that the pentaalkyls, $TaMe_5$ and $TaBn_5$ (Bn = benzyl), decompose by an α-hydrogen atom abstraction mechanism.[55]

The molecular structures of both $[Ar^{Tol_2}]TaMe_3Cl$ and $[Ar^{Tol_2}]TaMe_2Cl_2$ have been determined by X–ray diffraction (Figures 10 and 11, respectively), thereby demonstrating that while $[Ar^{Tol_2}]TaMe_2Cl_2$ is an approximate trigonal bipyramid (with axial Cl substituents), the structure of $[Ar^{Tol_2}]TaMe_3Cl$ is distorted towards a square pyramidal geometry. The most interesting structural features of $[Ar^{Tol_2}]TaMe_3Cl$ and $[Ar^{Tol_2}]TaMe_2Cl_2$, however, pertains to the fact that the tantalum atom in each of these complexes is displaced substantially from the plane of the aryl ligand.[56] Specifically, the $Ta–C_{ipso}–C_{para}$ angles in $[Ar^{Tol_2}]TaMe_3Cl$ (145.1°) and $[Ar^{Tol_2}]TaMe_2Cl_2$ (157.1°) deviate considerably from 180°, as illustrated by the views in Figures 10 and 11.

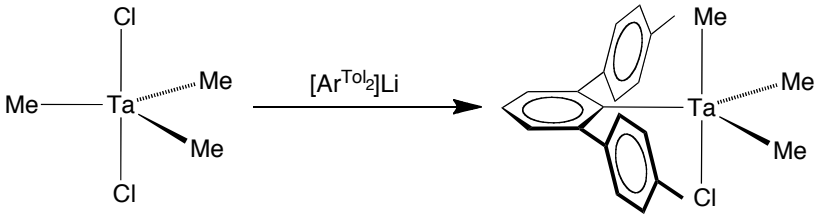

Scheme 3. Synthesis of $[Ar^{Tol_2}]TaMe_3Cl$.

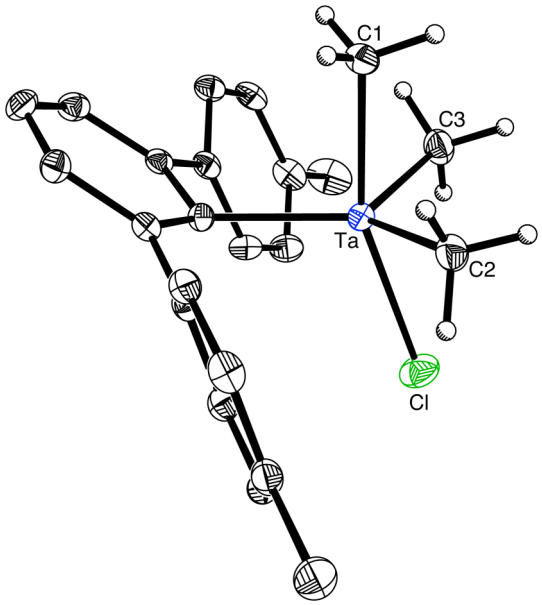

Figure 10. Molecular structure of $[Ar^{Tol_2}]TaMe_3Cl$.

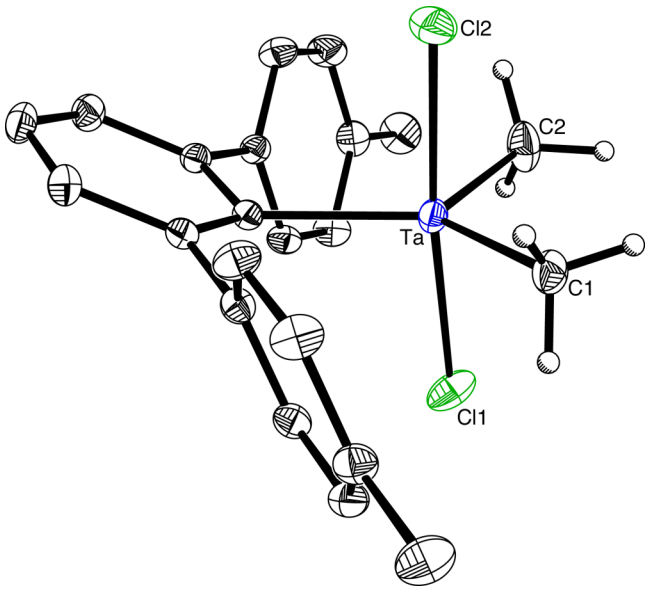

Figure 11. Molecular structure of $[Ar^{Tol_2}]TaMe_2Cl_2$.

Since tantalum phenyl compounds do not exhibit distortions of this magnitude,[33,57,58] the unusual displacement of tantalum from the respective aryl planes in [Ar^{Tol2}]TaMe$_3$Cl and [Ar^{Tol2}]TaMe$_2$Cl$_2$ may be attributed to increased steric interactions between the tolyl groups and the equatorial methyl substituents that would result if the tantalum were to reside in the aryl plane. In support of this notion, density functional theory geometry optimization calculations on the phenyl counterparts, PhTaMe$_3$Cl and PhTaMe$_2$Cl$_2$, predict structures in which the tantalum lies in the aryl planes (Figure 12), with Ta–C$_{ipso}$–C$_{para}$ angles of 179.4° and 179.9°, respectively, whereas nonplanar geometries that are in accord with the experimental structures are predicted for [Ar^{Tol2}]TaMe$_3$Cl (153.3°) and [Ar^{Tol2}]TaMe$_2$Cl$_2$ (157.2°). Furthermore, the geometry optimized structure of PhTaMe$_3$Cl reproduces the distortion towards a square pyramidal geometry that is observed for [Ar^{Tol2}]TaMe$_3$Cl, thereby suggesting that the square pyramidal distortion is not due to steric factors.

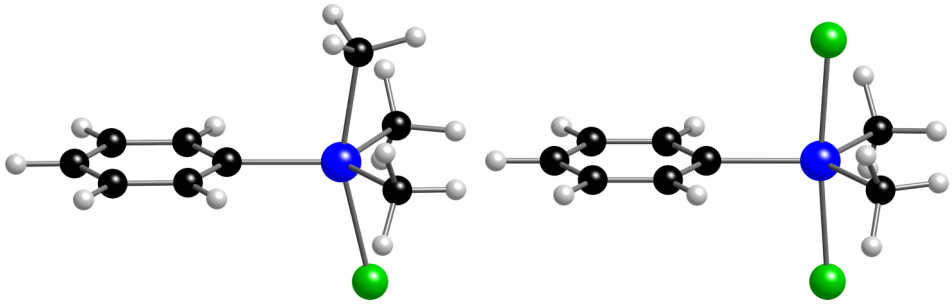

Figure 12. Geometry optimized structures of PhTaMe$_3$Cl (left) and PhTaMe$_2$Cl$_2$ (right).

It is also relevant to note that κ^1-terphenyl compounds do not typically exhibit a displacement of the metal from the aryl plane.[59] For example, the Yb–C$_{ipso}$–C$_{para}$ angle in five-coordinate [Ar^{Nap2}]Yb(THF)$_2$Cl$_2$ and [Ar^{Mes2}]Yb(THF)$_2$Cl$_2$ are 180.0° and 172.4°, respectively.[60,61] Likewise, six coordinate [Ar^{Mes2}]Yb(THF)$_3$Cl$_2$ exhibits a normal coordination mode with a Yb–C$_{ipso}$–C$_{para}$ angle of 176.3°.[61] Distortions of the type observed for [Ar^{Tol2}]TaMe$_3$Cl and [Ar^{Tol2}]TaMe$_2$Cl$_2$ have, nevertheless, been observed in

compounds that feature *two* terphenyl ligands, as illustrated by $[Ar^{Ph2}]_2Yb(THF)_2$, which has Yb–C_{ipso}–C_{para} angles of 147.6˚ and 161.9˚,[62] and $[Ar^{Ph2}]_2Eu(THF)_2$, which has Eu–C_{ipso}–C_{para} angles of 145.4˚ and 159.9˚.[63,64] Additionally, a *bis*-terphenyl complex of tantalum, namely $[Ar^{Tol2}]_2Ta(NMe_2)_3$, has also been synthesized (see Chapter 7) and exhibits similar distortions in one of the $[Ar^{Tol2}]$ ligands, having Ta–C_{ipso}–C_{para} angles of 154.5˚ and 177.3˚.

6.6 Synthesis and structural characterization of tantalum complexes that feature a [*CCC*] X_3-donor pincer ligand

While the reaction of $TaMe_3Cl_2$ with $[Ar^{Tol2}]Li$ produced $[Ar^{Tol2}]TaMe_3Cl$, treatment of a bright yellow solution of $Ta(PMe_3)_2Me_3Cl_2$ in benzene with $[Ar^{Tol2}]Li$ produces the [*CCC*] X_3-donor pincer complex $[\kappa^3\text{-}Ar^{Tol'2}]Ta(PMe_3)_2MeCl$ (Tol′ = C_6H_3Me), as illustrated in Scheme 4.[65,66] Additionally, $[\kappa^3\text{-}Ar^{Tol'2}]Ta(PMe_3)_2MeCl$ can also be synthesized by treating $[Ar^{Tol2}]TaMe_3Cl$ with PMe_3; thus, cyclometalation of the $[Ar^{Tol2}]$ ligand occurs in the presence of PMe_3. In this regard, the ability of PMe_3 to induce alkane elimination in Ta(V) compounds by α-H abstraction has been previously noted.[67]

Solutions of $[\kappa^3\text{-}Ar^{Tol'2}]Ta(PMe_3)_2MeCl$ undergo ligand redistribution with the formation of $[\kappa^3\text{-}Ar^{Tol'2}]Ta(PMe_3)_2Me_2$ and $[\kappa^3\text{-}Ar^{Tol'2}]Ta(PMe_3)_2Cl_2$. In order to try and isolate pure $[\kappa^3\text{-}Ar^{Tol'2}]Ta(PMe_3)_2Me_2$, $[\kappa^3\text{-}Ar^{Tol'2}]Ta(PMe_3)_2MeCl$ was treated with Me_2Zn; however, this resulted in the formation of an equilibrium mixture of $[\kappa^3\text{-}Ar^{Tol'2}]Ta(PMe_3)_2Me_2$ and $[\kappa^3\text{-}Ar^{Tol'2}]Ta(PMe_3)_2MeCl$. Contrasting Me_2Zn, addition of MeLi to $[\kappa^3\text{-}Ar^{Tol'2}]Ta(PMe_3)_2MeCl$ caused overalkylation, forming an anionic complex, tentatively identified as $[\kappa^3\text{-}Ar^{Tol'2}]Ta(PMe_3)Me_3]^-Li^+$.[68] Fortunately, the Grignard reagent MeMgBr irreversibly alkylated $[\kappa^3\text{-}Ar^{Tol'2}]Ta(PMe_3)_2MeCl$ once, producing $[\kappa^3\text{-}Ar^{Tol'2}]Ta(PMe_3)_2Me_2$ in good yield (Scheme 5).

In view of the fact that Me_2Zn only formed equilibrium mixtures of [κ^3-$Ar^{Tol'2}$]Ta(PMe_3)$_2$$Me_2$ and [κ^3-$Ar^{Tol'2}$]Ta(PMe_3)$_2$MeCl, it was postulated that a suitable reagent towards the synthesis of the dichloride complex, [κ^3-$Ar^{Tol'2}$]Ta(PMe_3)$_2$$Cl_2$ is $ZnCl_2$. Indeed, addition of a suspension of anhydrous $ZnCl_2$ in Et_2O to [κ^3-$Ar^{Tol'2}$]Ta(PMe_3)$_2$MeCl allows for the isolation of [κ^3-$Ar^{Tol'2}$]Ta(PMe_3)$_2$$Cl_2$ (Scheme 5).[69] It should also be noted that the redistribution reaction was confirmed to be an equilibrium; thus, treatment of [κ^3-$Ar^{Tol'2}$]Ta(PMe_3)$_2$$Me_2$ with [κ^3-$Ar^{Tol'2}$]Ta(PMe_3)$_2$$Cl_2$ produces the methylchloride complex, [κ^3-$Ar^{Tol'2}$]Ta(PMe_3)$_2$MeCl.

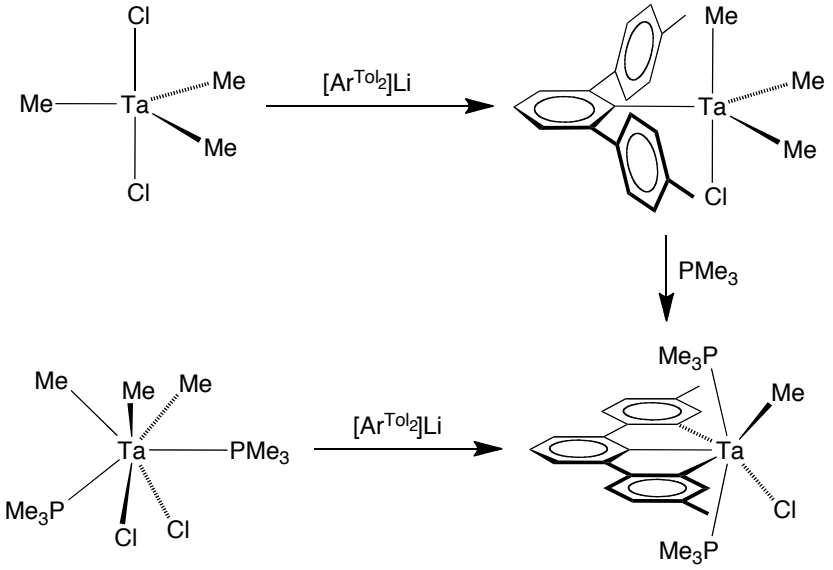

Scheme 4. Synthesis of [κ^3-$Ar^{Tol'2}$]Ta(PMe_3)$_2$MeCl.

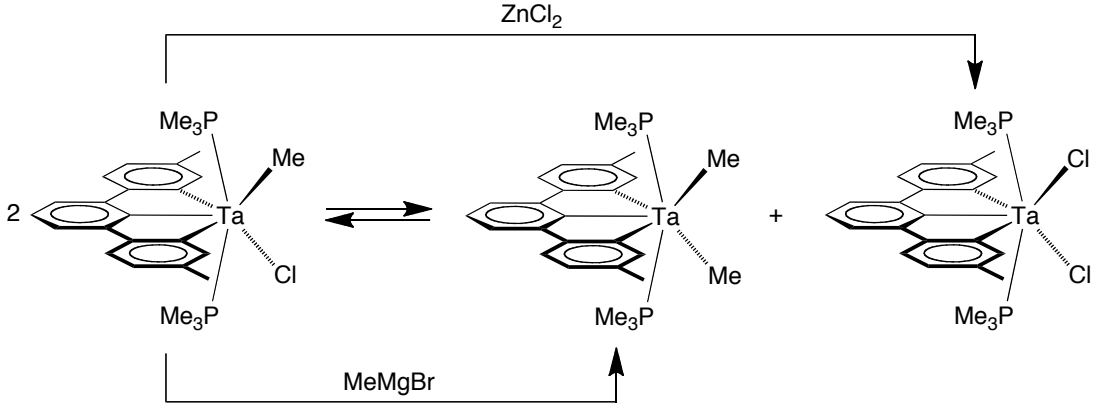

Scheme 5. Redistribution of [κ^3-$Ar^{Tol'2}$]Ta(PMe_3)$_2$MeCl and syntheses of [κ^3-$Ar^{Tol'2}$]Ta(PMe_3)$_2$$Me_2$ and [κ^3-$Ar^{Tol'2}$]Ta(PMe_3)$_2$$Cl_2$.

The molecular structures of [κ^3-Ar$^{Tol'2}$]Ta(PMe$_3$)$_2$MeCl, [κ^3-Ar$^{Tol'2}$]Ta(PMe$_3$)$_2$Me$_2$, and [κ^3-Ar$^{Tol'2}$]Ta(PMe$_3$)$_2$Cl$_2$ have been determined by X–ray diffraction and demonstrate the κ^3-planar binding mode of the pincer ligand, as illustrated in Figures 13 – 15, respectively. [κ^3-Ar$^{Tol'2}$]Ta(PMe$_3$)$_2$MeCl is shown from two different views in Figure 16, in order to show the *pseudo* T-shape geometry of the tantalum center and the high degree of planarity of the [κ^3-Ar$^{Tol'2}$] ligand. The two PMe$_3$ ligands bind in such a manner that the P–Ta–P plane is approximately orthogonal to the plane of the pincer ligand, while the methyl and chloride ligands are oriented such that the X–Ta–Y plane (X = Me, Cl; Y = Me, Cl) approximately bisects the P–Ta–P and pincer planes. As such, [κ^3-Ar$^{Tol'2}$]Ta(PMe$_3$)$_2$Me$_2$ and [κ^3-Ar$^{Tol'2}$]Ta(PMe$_3$)$_2$Cl$_2$ possess molecular C_2 symmetry.

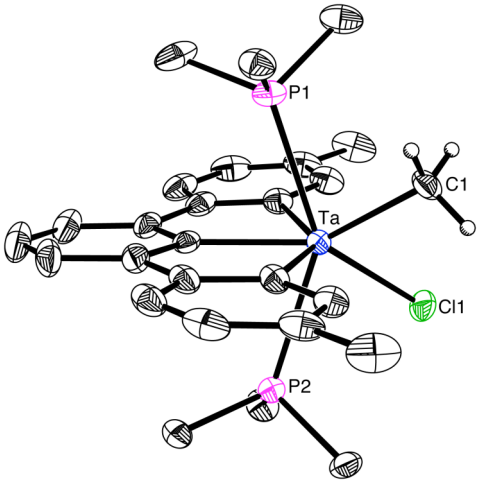

Figure 13. Molecular structure of [κ^3-Ar$^{Tol'2}$]Ta(PMe$_3$)$_2$MeCl.

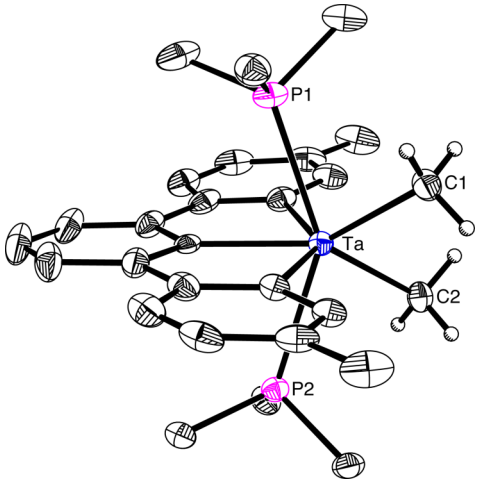

Figure 14. Molecular structure of [κ^3-Ar$^{Tol'2}$]Ta(PMe$_3$)$_2$Me$_2$.

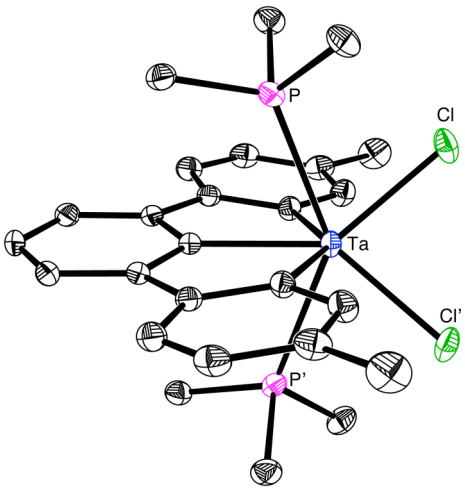

Figure 15. Molecular structure of $[\kappa^3\text{-}Ar^{Tol'_2}]Ta(PMe_3)_2Cl_2$.

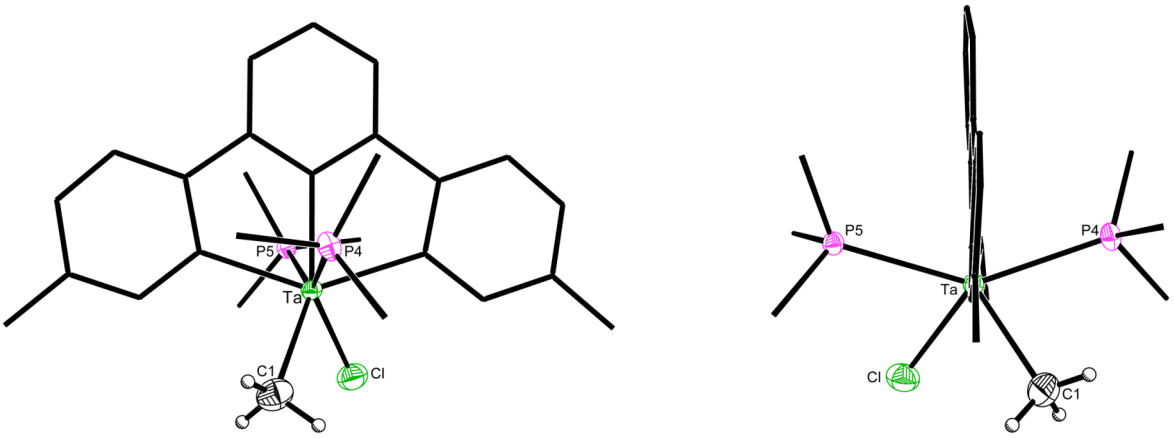

Figure 16. Views of $[\kappa^3\text{-}Ar^{Tol'_2}]Ta(PMe_3)_2MeCl$ showing *pseudo* T-shape geometry of tantalum (left) and the high degree of planarity of the $[\kappa^3\text{-}Ar^{Tol'_2}]$ ligand (right).

With respect to the binding of the pincer ligand, the three Ta–Ar bond lengths in each complex are very similar (Table 5) and are comparable to the Ta–$[Ar^{Tol_2}]$ bond lengths in both $[Ar^{Tol_2}]TaMe_3Cl$ and $[Ar^{Tol_2}]TaMe_2Cl_2$. Furthermore, these values are comparable to the mean bond length of 2.23 Å for structurally characterized tantalum phenyl compounds listed in the Cambridge Structural Database.[33] In view of the similarity in bond lengths, it would appear that there is little strain associated with the κ^3-coordination mode, a notion that is endorsed by the fact that the Ta–C–C angles in the pincer complexes are also close to the idealized value of 120° (Figure 17).

Table 5. Ta–C bond lengths pertaining to coordination of [$Ar^{Tol}{}_2$] and [κ^3-$Ar^{Tol'}{}_2$] ligands.[a]

	$Ta–C_{cent}$/Å	$Ta–C_{lat\#1}$/Å	$Ta–C_{lat\#2}$/Å
[κ^3-$Ar^{Tol'}{}_2$]$Ta(PMe_3)_2Me_2$	2.200(5)	2.230(5)	2.243(5)
[κ^3-$Ar^{Tol'}{}_2$]$Ta(PMe_3)_2Cl_2$	2.227(4)	2.207(3)	2.207(3)
[κ^3-$Ar^{Tol'}{}_2$]$Ta(PMe_3)_2MeCl$	2.190(3)	2.230(3)	2.227(3)
[κ^3-$Ar^{Tol'}{}_2$]$Ta(PMe_3)_2(\eta^6$-$C_6H_6)$	2.243(2)	2.356(2)	2.362(2)
[$Ar^{Tol}{}_2$]$TaMe_3Cl$	2.116(3)	–	–
[$Ar^{Tol}{}_2$]$TaMe_2Cl_2$	2.139(2)	–	–

(a) cent = central carbon, lat = lateral carbon.

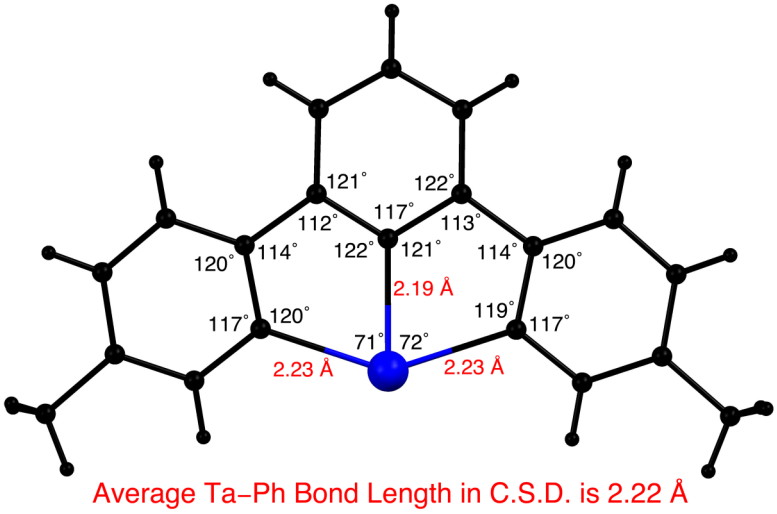

Figure 17. Bond lengths and angles in [κ^3-$Ar^{Tol'}{}_2$]$Ta(PMe_3)_2MeCl$.

6.7 NMR spectroscopic properties of [κ^3-$Ar^{Tol'}{}_2$]$Ta(PMe_3)_2Me_2$

The NMR spectroscopic properties of the dimethyl complex [κ^3-$Ar^{Tol'}{}_2$]$Ta(PMe_3)_2Me_2$ (Figure 18) are particularly interesting. For example, while the $^{31}P\{^1H\}$ NMR spectrum of [κ^3-$Ar^{Tol'}{}_2$]$Ta(PMe_3)_2Me_2$ is a singlet, indicative of chemically equivalent PMe_3 ligands, the $^{13}C\{^1H\}$ NMR signal for the PMe_3 ligands has the appearance of an approximate doublet of triplets (Figure 19), rather than either a doublet (as observed for [κ^3-$Ar^{Tol'}{}_2$]$Ta(PMe_3)_2Cl_2$, *vide infra*) or a virtual triplet.[70] In addition, the $^{13}C\{^1H\}$ NMR signal of the tantalum methyl groups does not appear as

either a binomial 1:2:1 triplet or a doublet of doublets due to coupling to the two phosphorus nuclei, but rather appears as a non-binomial triplet with an intensity ratio of 1:13.7:1 (Figure 20, left). On the other hand, the corresponding $^{13}C\{^1H\}$ NMR signal for the isotopically enriched isotopologue $[\kappa^3\text{-}Ar^{Tol'_2}]Ta(PMe_3)_2(^{13}CH_3)_2$ exhibits an irregular five line pattern (Figure 20, right), as does the $^{31}P\{^1H\}$ NMR spectrum of $[\kappa^3\text{-}Ar^{Tol'_2}]Ta(PMe_3)_2(^{13}CH_3)_2$ (Figure 21, right).[71]

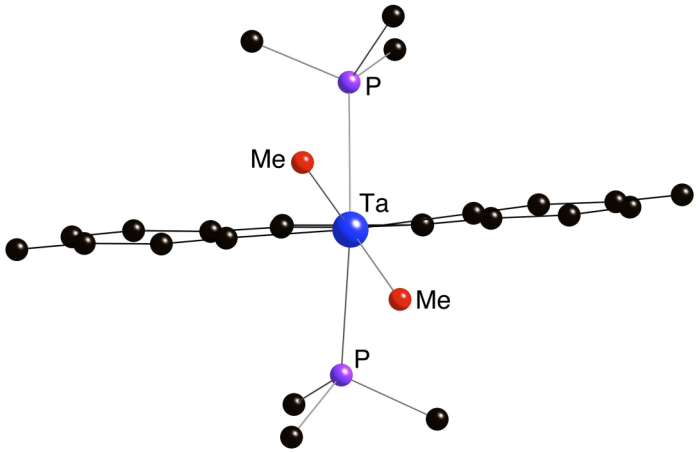

Figure 18. Molecular structure of $[\kappa^3\text{-}Ar^{Tol'_2}]Ta(PMe_3)_2Me_2$ showing C_2 symmetry.

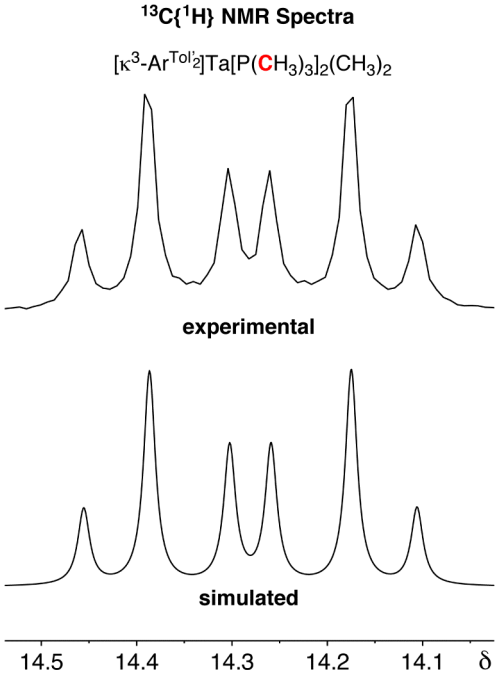

Figure 19. $^{13}C\{^1H\}$ NMR signal for the PMe_3 ligands of $[\kappa^3\text{-}Ar^{Tol'_2}]Ta(PMe_3)_2Me_2$.

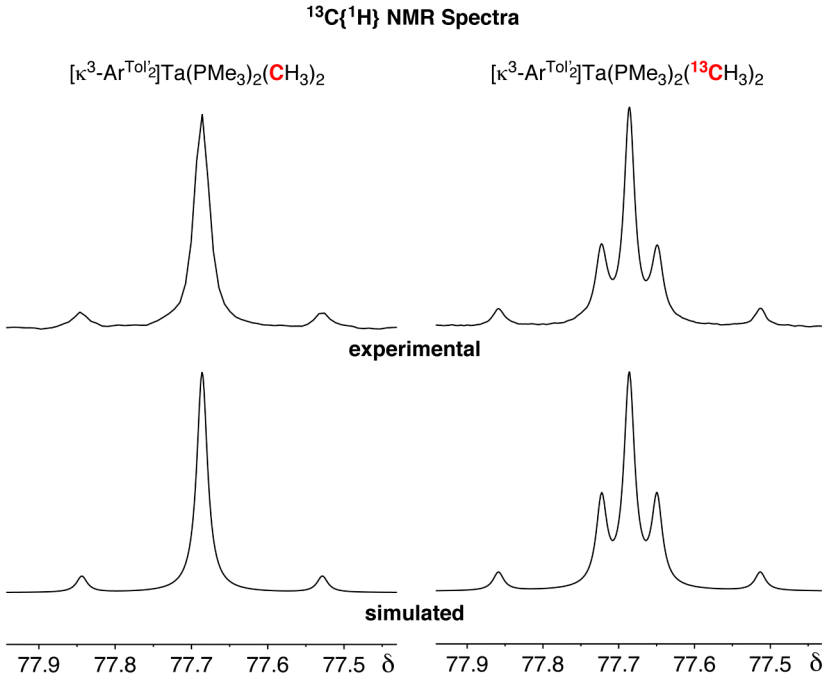

Figure 20. $^{13}C\{^{1}H\}$ NMR signals for the tantalum methyl ligands of natural abundance [κ^3-$Ar^{Tol'}{}_2$]Ta$(PMe_3)_2Me_2$ (left) and ^{13}C labeled [κ^3-$Ar^{Tol'}{}_2$]Ta$(PMe_3)_2(^{13}CH_3)_2$ (right).

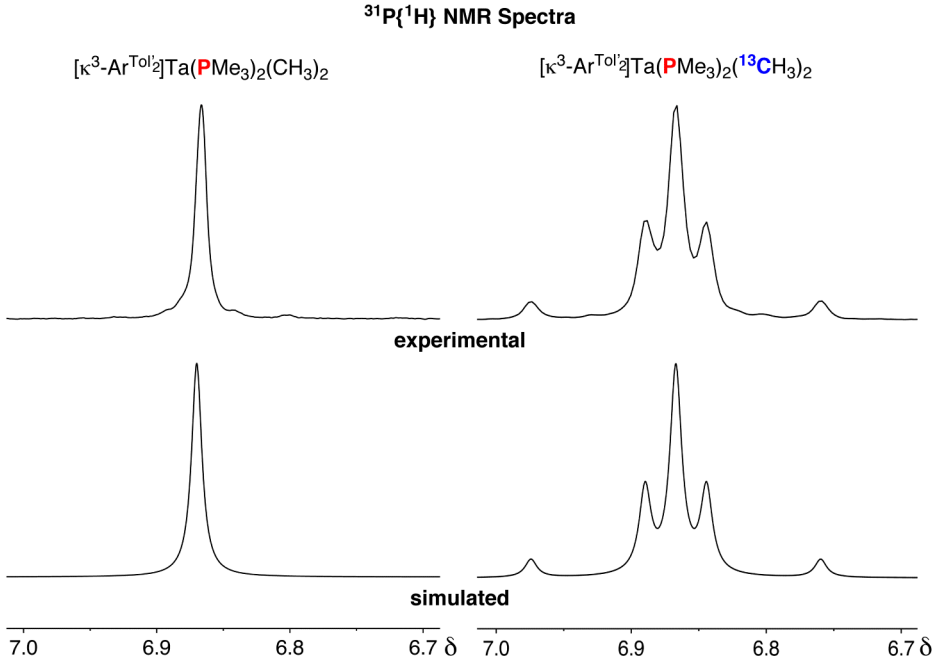

Figure 21. $^{31}P\{^{1}H\}$ NMR signals for natural abundance [κ^3-$Ar^{Tol'}{}_2$]Ta$(PMe_3)_2Me_2$ (left) and ^{13}C labelled [κ^3-$Ar^{Tol'}{}_2$]Ta$(PMe_3)_2(^{13}CH_3)_2$ (right).

The various spectra have been analyzed in detail and the unusual features of the tantalum methyl region of the $^{13}C\{^1H\}$ NMR spectrum are associated with the fact that the two $^2J_{PC}$ coupling constants have an equal magnitude but are of opposite sign. In this regard, the tantalum methyl groups of natural abundance $[\kappa^3\text{-}Ar^{Tol'_2}]Ta(PMe_3)_2Me_2$ are a component of an AA'X spin system (where A = phosphorus and X = carbon), such that the $^{13}C\{^1H\}$ NMR spectrum would be composed of a maximum of five lines (Figure 22a).[72,73] The overall appearance of the AA'X spectrum, however, depends on the values of J_{AX}, $J_{A'X}$, and $J_{AA'}$. For example, it is well established that such spectra have a first order appearance (*i.e.* a 1:2:1 virtual triplet for X) if $|J_{AA'}| >> |J_{AX}|, |J_{A'X}|$; under such conditions the line spacing is the average coupling constant, *i.e.* $\frac{1}{2}(J_{AX} + J_{A'X})$. The observation of a triplet does not, however, require that $|J_{AA'}|$ is significantly larger than $|J_{AX}|$ and $|J_{A'X}|$. Specifically, a triplet may also be observed if $J_{AX} = -J_{A'X}$, regardless of the magnitude of $|J_{AA'}|$. However, for such a situation, the intensity ratio of the triplet is not 1:2:1, and the line spacing does not correspond to a single coupling constant, but is rather $[(J_{AA'}^2 + J_{AX}^2)]^{1/2}$.[72] Thus, the observation of a non-binomial triplet for the tantalum methyl groups in the $^{13}C\{^1H\}$ NMR spectrum of natural abundance $[\kappa^3\text{-}Ar^{Tol'_2}]Ta(PMe_3)_2Me_2$ (Figure 20, upper left) is a consequence of the two $^2J_{PC}$ coupling constants having equal, but opposite, values, as illustrated by the simulation for $^2J_{PP} = |13.7|$ and $^2J_{PC} = \pm 8.0$ Hz (Figure 20, lower left). More complicated patterns are observed if $|J_{AX}| \neq |J_{A'X}|$, and the sensitivity of the X spectrum as a function of varying $J_{A'X}$ is illustrated in Figure 23. On the basis of this simulation, it is evident that one could encounter situations where the signal has the approximate appearance of a binomial triplet (*e.g.* $J_{AX'} = 6$ or 10), but the derived coupling constant would be erroneous.

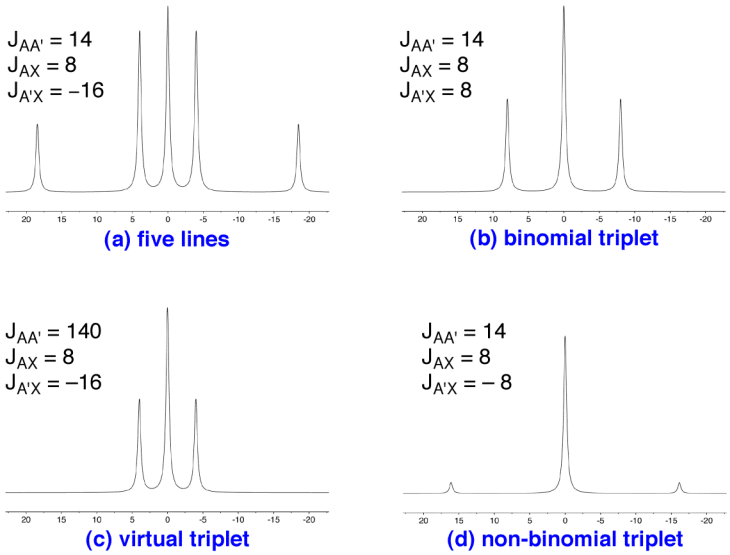

Figure 22: AA′X spectra for different sets of coupling constants (Hz): (a) a five line pattern, (b) a binomial triplet pattern, when $J_{AX} = J_{A'X}$ (*i.e.* A_2X spectra, line spacing = $|J_{AX}|$), (c) a virtual triplet pattern, when $J_{AA'} >> |J_{AX}|, |J_{A'X}|$ (line spacing = ½(J_{AX} + $J_{A'X}$), (d) a non-binomial triplet pattern, when $J_{AX} = -J_{A'X}$ (line spacing = $[(J_{AA'})^2 + (J_{AX})^2]^{½}$).

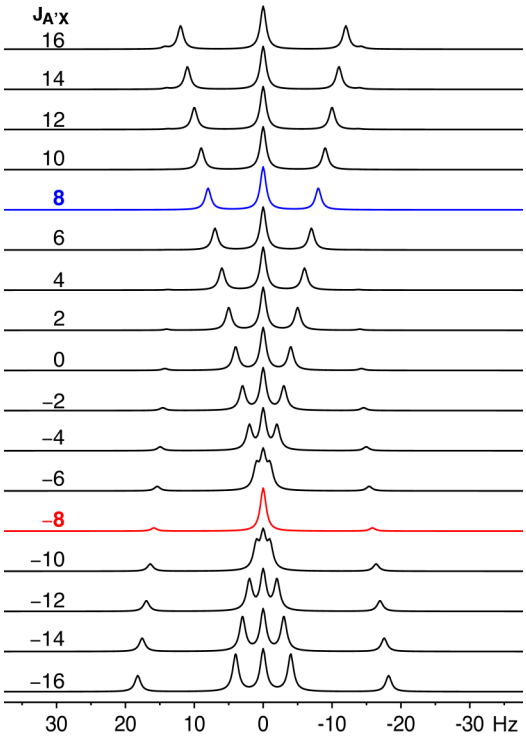

Figure 23. AA′X simulation (X spectrum) as a function of $J_{A'X}$ for fixed $J_{AA'}$ (13.7 Hz) and J_{AX} (8.0 Hz). A non-binomial 1:13.7:1 triplet results when $J_{A'X}$ = –8.0 Hz (red), as compared to a binomial 1:2:1 triplet when $J_{A'X}$ = 8.0 Hz (blue); A = phosphorus and X = carbon.

The tantalum methyl region of the $^{13}C\{^1H\}$ NMR spectrum of isotopically enriched $[\kappa^3\text{-}Ar^{Tol'_2}]Ta(PMe_3)_2(^{13}CH_3)_2$ is a 5 line pattern with an intensity ratio 1:4.7:11.4:4.7:1 (Figure 20, right). The latter spectrum is more complicated than that of the natural abundance version (Figure 20, left) because the spin system is now AA'XX',[74] rather than AA'X. An AA'XX' spectrum gives a maximum of 10 lines for each set of nuclei, but this reduces to five lines if $J_{AX} = -J_{A'X}$ and $J_{AA'}$ (or $J_{XX'}$) = 0.[73] Accordingly, the $^{13}C\{^1H\}$ and $^{31}P\{^1H\}$ NMR spectra of $[\kappa^3\text{-}Ar^{Tol'_2}]Ta(PMe_3)_2(^{13}CH_3)_2$ may be simulated satisfactorily with the parameters $^2J_{PP} = |13.7|$ Hz, $^2J_{PC} = 8.0$ Hz and –8.0 Hz, and $^2J_{CC} = 0.0$ Hz.[75,76]

As indicated above, the unusual appearance of the tantalum methyl signals in the $^{13}C\{^1H\}$ NMR spectra is a consequence of the two $^2J_{PC}$ coupling constants being of equal magnitude but opposite sign. In this regard, it is well known that $^2J_{XY}$ coupling constants in metal complexes vary with interligand bond angles. For example, the magnitude of $^2J_{PP}$ in metal phosphine compounds is often used to assign a *trans versus cis* stereochemistry by virtue of the fact that *trans* $^2J_{PP}$ coupling constants are generally larger in magnitude than *cis* coupling constants; furthermore, the former are positive and the latter negative.[77] By comparison, there are fewer studies pertaining to $^2J_{CC}$ coupling constants, but it has been observed that *cis* $^2J_{CC}$ coupling constants may be an order of magnitude smaller than *trans* coupling constants, and are often not observed.[78] In view of this angular dependence of $^2J_{PP}$ and $^2J_{CC}$ coupling constants, it is not unreasonable that the substantially different P–Ta–C angles [75.1(1)° and 135.1(1)°] for $[\kappa^3\text{-}Ar^{Tol'_2}]Ta(PMe_3)_2Me_2$ would give rise to significantly different $^2J_{PC}$ coupling constants.

Returning to the observation of a singlet in the $^{31}P\{^1H\}$ NMR spectrum of $[\kappa^3\text{-}Ar^{Tol'_2}]Ta(PMe_3)_2Me_2$, but the appearance of an approximate doublet of triplets for the PMe_3 groups in the $^{13}C\{^1H\}$ NMR spectrum (Figure 19), the latter is reconciled by the fact that the presence of a single ^{13}C nucleus causes the phosphorus atoms of the two PMe_3 ligands to become chemically inequivalent due to a secondary isotope effect.[79,80]

As such, the $^{13}C\{^{1}H\}$ NMR signal for the PMe_3 ligands corresponds to an ABX spin system[81] and the observed spectrum can be simulated by $\Delta\delta_{PP}$ = 0.022 ppm,[82] $^{2}J_{PP}$ = |13.7| Hz, $^{1}J_{PC}$ = |21.4| and $^{3}J_{PC}$ = 0.0 Hz.[83,84] The impact of $\Delta\delta_{PP}$ on the appearance of the spectrum is illustrated by the simulation shown in Figure 24 in which $^{2}J_{PP}$ (13.7 Hz), $^{1}J_{PC}$ (21.4 Hz) and $^{3}J_{PC}$ (0.0 Hz) are fixed. Further evidence for a secondary isotope effect causing the phosphorus nuclei to become chemically inequivalent was obtained by treating $[\kappa^3\text{-}Ar^{Tol'2}]Ta(PMe_3)_2MeCl$ with $(^{13}CH_3)MgI\bullet(Et_2O)_{1.5}$, which gave a statistical mixture of isotopologues, namely $[\kappa^3\text{-}Ar^{Tol'2}]Ta(PMe_3)_2(^{12}CH_3)_2$ (25 %), $[\kappa^3\text{-}Ar^{Tol'2}]Ta(PMe_3)_2(^{13}CH_3)_2$ (25 %), and $[\kappa^3\text{-}Ar^{Tol'2}]Ta(PMe_3)_2(^{12}CH_3)(^{13}CH_3)$ (50 %). Specifically, analysis of the $^{31}P\{^{1}H\}$ (Figure 25) and $^{13}C\{^{1}H\}$ (Figure 26) spectra indicate that the isotopologues have slightly different chemical shifts, based on the asymmetry of the signals.

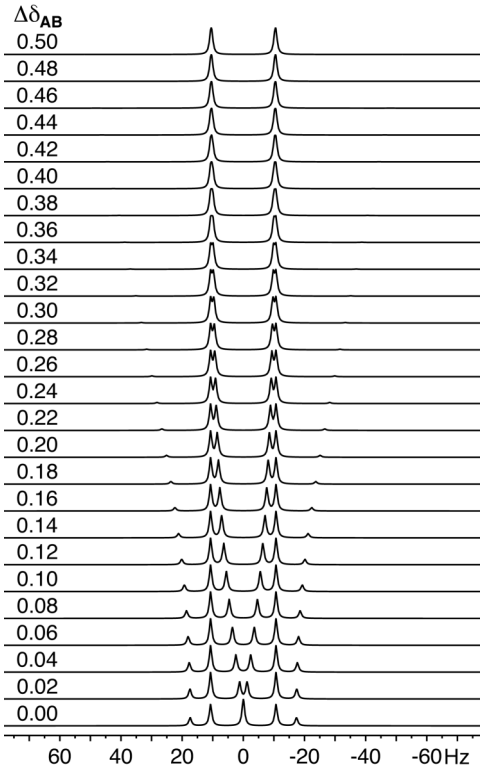

Figure 24. ABX simulation (X spectrum) as a function of $\Delta\delta_{AB}$ for fixed J_{AB} (13.7 Hz), J_{AX} (21.4 Hz) and J_{BX} (0.0 Hz); A = phosphorus, B = phosphorus and X = carbon.

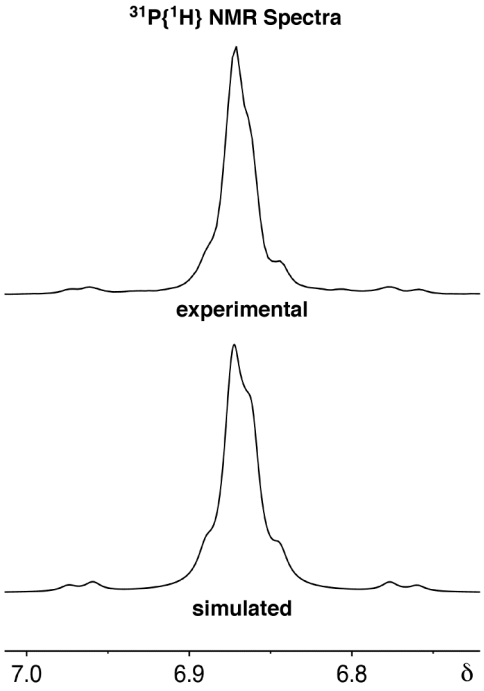

Figure 25. $^{31}P\{^{1}H\}$ NMR signals for the tantalum methyl ligands of $[\kappa^3\text{-}Ar^{Tol'_2}]Ta(PMe_3)_2Me_2$, as a mixture of isotopologues.

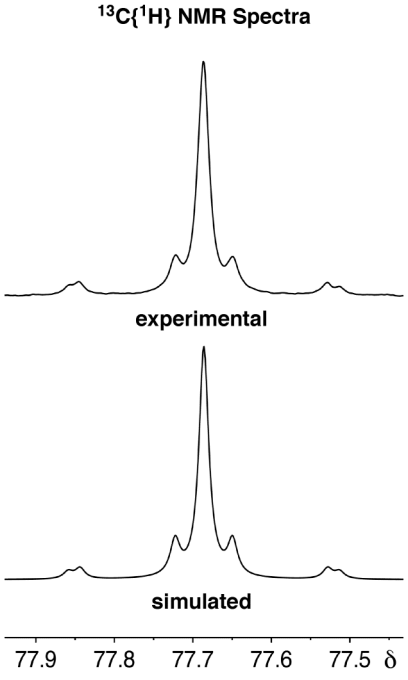

Figure 26. $^{13}C\{^{1}H\}$ NMR signals for the tantalum methyl ligands of $[\kappa^3\text{-}Ar^{Tol'_2}]Ta(PMe_3)_2Me_2$, as a mixture of isotopologues.

It is interesting to note that, in contrast to $[\kappa^3\text{-Ar}^{\text{Tol}'}_2]\text{Ta}(\text{PMe}_3)_2\text{Me}_2$, the corresponding $^{13}\text{C}\{^1\text{H}\}$ NMR spectrum of the dichloride $[\kappa^3\text{-Ar}^{\text{Tol}'}_2]\text{Ta}(\text{PMe}_3)_2\text{Cl}_2$ has the appearance of a doublet for the PMe_3 ligands (Figure 27). Despite its appearance, however, the spectrum may be simulated with the parameters $\Delta\delta_{PP} = 0.022$ ppm,[85] $^2J_{PP} = |3.0|$ Hz, $^1J_{PC} = |27.8|$ and $^3J_{PC} = 0.0$ Hz (Figure 27). The fact that it appears as a doublet, rather than a complex 6 line pattern similar to that for $[\kappa^3\text{-Ar}^{\text{Tol}'}_2]\text{Ta}(\text{PMe}_3)_2\text{Me}_2$, may be attributed to the smaller (but non-zero) value of $^2J_{PP}$, which is presumably a consequence of the fact that the P–Ta–P angle of $[\kappa^3\text{-Ar}^{\text{Tol}'}_2]\text{Ta}(\text{PMe}_3)_2\text{Cl}_2$ [139.49(3)°] is smaller than that of $[\kappa^3\text{-Ar}^{\text{Tol}'}_2]\text{Ta}(\text{PMe}_3)_2\text{Me}_2$ [144.77(4)°].[77] In this regard, the sensitivity of the appearance of the $^{13}\text{C}\{^1\text{H}\}$ NMR spectrum to $^2J_{PP}$ is illustrated by the simulation shown in Figure 28, for which $\Delta\delta_{PP}$ (0.022 ppm), $^1J_{PC}$ (21.4 Hz) and $^3J_{PC}$ (0.0 Hz) are fixed with values for $[\kappa^3\text{-Ar}^{\text{Tol}'}_2]\text{Ta}(\text{PMe}_3)_2\text{Me}_2$.

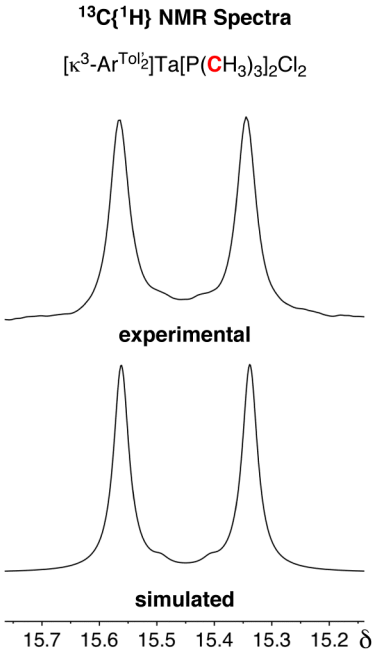

Figure 27. $^{13}\text{C}\{^1\text{H}\}$ NMR signal for the PMe_3 ligands of $[\kappa^3\text{-Ar}^{\text{Tol}'}_2]\text{Ta}(\text{PMe}_3)_2\text{Cl}_2$.

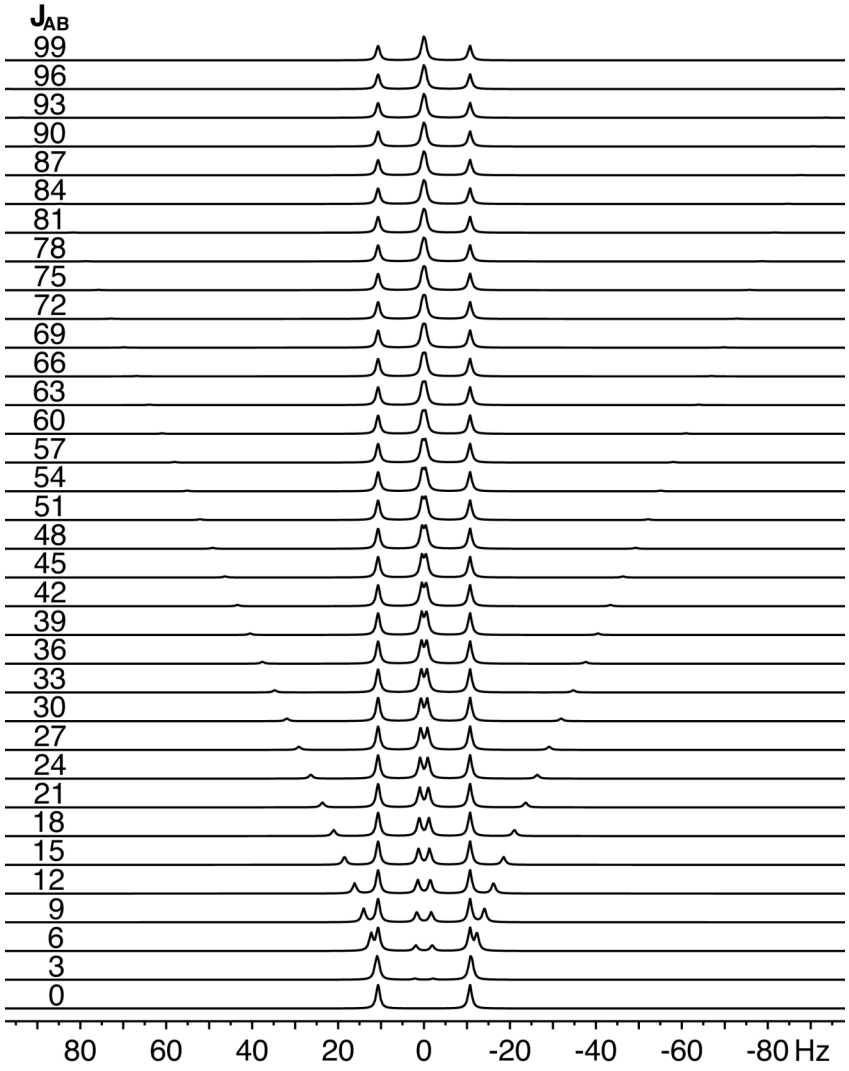

Figure 28. ABX simulation (X spectrum) as a function of J_{AB} for fixed $\Delta\delta_{AB}$ (0.022 ppm), J_{AX} (21.4 Hz) and J_{BX} (0.0 Hz); A = phosphorus, B = phosphorus, X = carbon.

Finally, the ^{1}H NMR spectrum of $[\kappa^3\text{-Ar}^{\text{Tol'}_2}]\text{Ta}(\text{PMe}_3)_2\text{Me}_2$ also exhibits some interesting features. For example, while irradiation typically results in spectral simplification, irradiation at the proton frequency of the PMe_3 ligands results in the appearance of *additional* coupling in the ^{1}H NMR signal for the tantalum methyl groups of $[\kappa^3\text{-Ar}^{\text{Tol'}_2}]\text{Ta}(\text{PMe}_3)_2\text{Me}_2$. Specifically, upon irradiation, the doublet takes on the appearance of a "filled-in" doublet (Figure 29). A similar "filled-in" doublet pattern is also observed for the tantalum methyl groups of the $[\kappa^3\text{-Ar}^{\text{Tol'}_2}]\text{Ta}[\text{P}(\text{CD}_3)_3]_2\text{Me}_2$

isotopologue (Figure 29) and so it is evident that the simpler "doublet" appearance of the non-irradiated spectrum is a result of a small $^{5}J_{HH}$ coupling between the PMe_3 and TaMe hydrogen atoms, which serves to broaden the features of the "filled-in" doublet. A summary of the coupling constants is shown in Table 6.

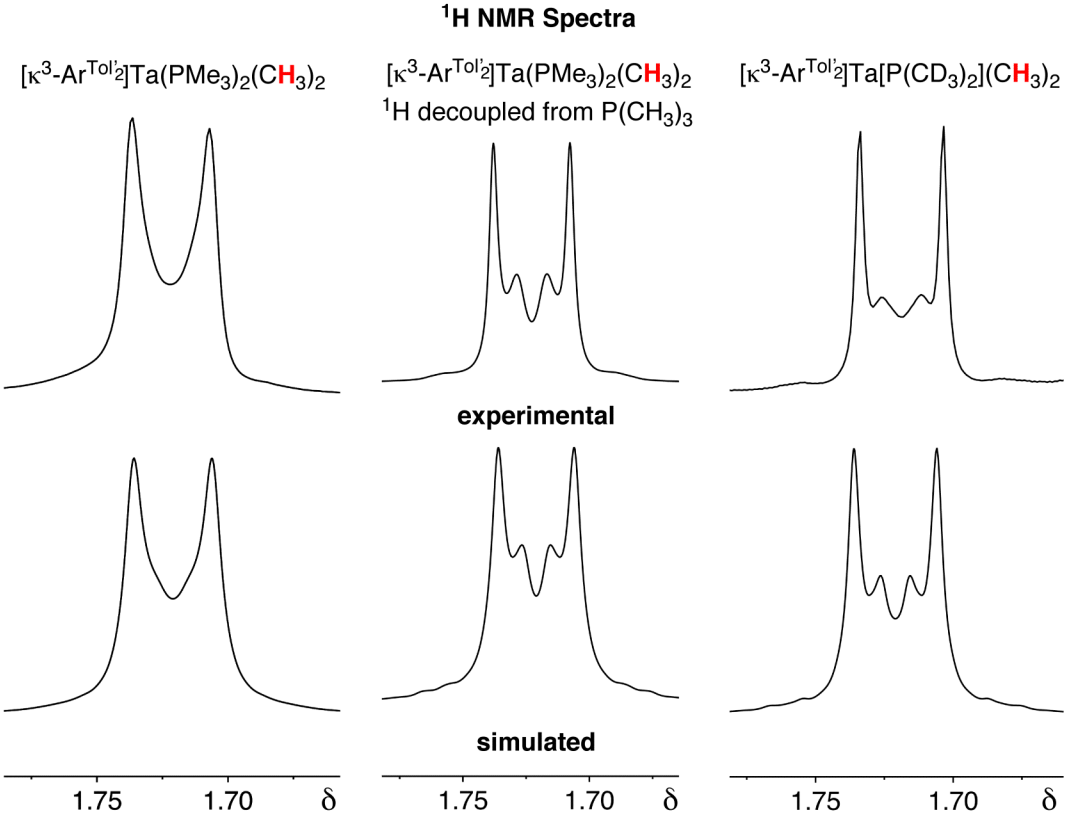

Figure 29. ^{1}H NMR signals for the tantalum methyl groups of [κ^3-Ar$^{Tol'2}$]Ta(PMe$_3$)$_2$Me$_2$ (left), [κ^3-Ar$^{Tol'2}$]Ta(PMe$_3$)$_2$Me$_2$ upon selective decoupling of the ^{1}H signals of the PMe_3 ligands (center) and the isotopologue [κ^3-Ar$^{Tol'2}$]Ta[P(CD$_3$)$_3$]$_2$Me$_2$ (right).

Table 6. Coupling Constant Data for $[\kappa^3\text{-}Ar^{Tol'_2}]Ta(PMe_3)_2Me_2$ for spectra obtained on a 400.13 MHz (^1H) NMR spectrometer.

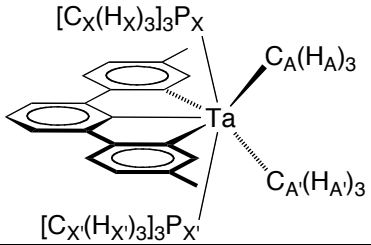

	C_A	$C_{A'}$	C_X	$C_{X'}$	P_X	$P_{X'}$	H_A	$H_{A'}$	H_X	$H_{X'}$
C_A	-[a]									
$C_{A'}$	0	-[a]								
C_X	-[a]	-[a]	-[a]							
$C_{X'}$	-[a]	-[a]	-[a]	-[a]						
P_X	8.0[b]	–8.0[b]	21.4[c]	0	-[a]					
$P_{X'}$	–8.0[b]	8.0[b]	0	21.4[c]	13.7[c]	-[a]				
H_A	116.8[e]	-	-	-	12.21[c]	–0.10[d]	-[a]			
$H_{A'}$	-	116.8[e]	-	-	–0.10[d]	12.21[c]	2.00[d]	-[a]		
H_X	-	-	129.8[e]	-	7.26[d]	0.10[d]	0.10[d]	0.10[d]	-[a]	
$H_{X'}$	-	-	-	129.8[e]	0.10[d]	7.26[d]	0.10[d]	0.10[d]	0[c]	-[a]

(a) A dash (-) indicates that the coupling constant was not included in the simulation.

(b) The signs of the coupling constants may be mutually interchanged with no effect on the simulation.

(c) The simulation does not depend on the sign of these coupling constants.

(d) The J_{HX} coupling constants listed correspond to the final simulations. It should be noted, however, that small variations of these coupling constants give rise to similar simulated spectra.

(e) $^1J_{CH}$ are invariably positive [*Multinuclear NMR* Mason, J. (Ed.) Plenum Press, New York, 1987].

6.8 Mechanism for the formation of $[\kappa^3\text{-}Ar^{Tol'_2}]Ta(PMe_3)_2MeCl$

The mechanism for formation of $[\kappa^3\text{-}Ar^{Tol'_2}]Ta(PMe_3)_2MeCl$ is of interest in view of (*i*) the geometrical constraints, and (*ii*) the several bond cleavages, which are involved in construction of the pincer ligand. One mechanistic possibility for creation of the pincer

ligand from a $[Ar^{Tol}{}_2]Ta(PMe_3)_xMe_3Cl$ species involves a pair of Ar–H/Ta–Me sigma-bond metathesis (SBM) transformations, as illustrated in Scheme 6 (in which the PMe_3 ligands are omitted for clarity). A second possibility involves elimination of methane by an α–H abstraction process to generate a methylidene ($Ta{=}CH_2$) species, that subsequently reacts with the Ar–H bond by a formal 1,2-addition process. For example, it was previously shown that $(ArO)_2TaMe_3$ (Ar = $C_6H_3Bu^t_2$) thermally eliminates methane by a sigma-bond metathesis (SBM) process to give the cyclometalated complex $(ArO)(\kappa^2\text{-}OC_6H_3Bu^tCMe_2CH_2)TaMe_2$, whereas under photochemical conditions $(ArO)_2TaMe_3$ eliminates methane *via* α–H abstraction to give the methylidene complex $(ArO)_2Ta(CH_2)Me$; the latter complex subsequently converts to $(ArO)(\kappa^2\text{-}OC_6H_3Bu^tCMe_2CH_2)TaMe$ by 1,2-addition of a methyl C–H bond.[8,86,87,88] Furthermore, Bercaw has proposed that both sigma-bond metathesis and α–H abstraction processes operate in the elimination of toluene from $Ti[(OC_6H_2\text{-}2\text{-}Bu^t\text{-}4\text{-}Me)_2C_6H_3](CH_2Ph)_2$.[6a]

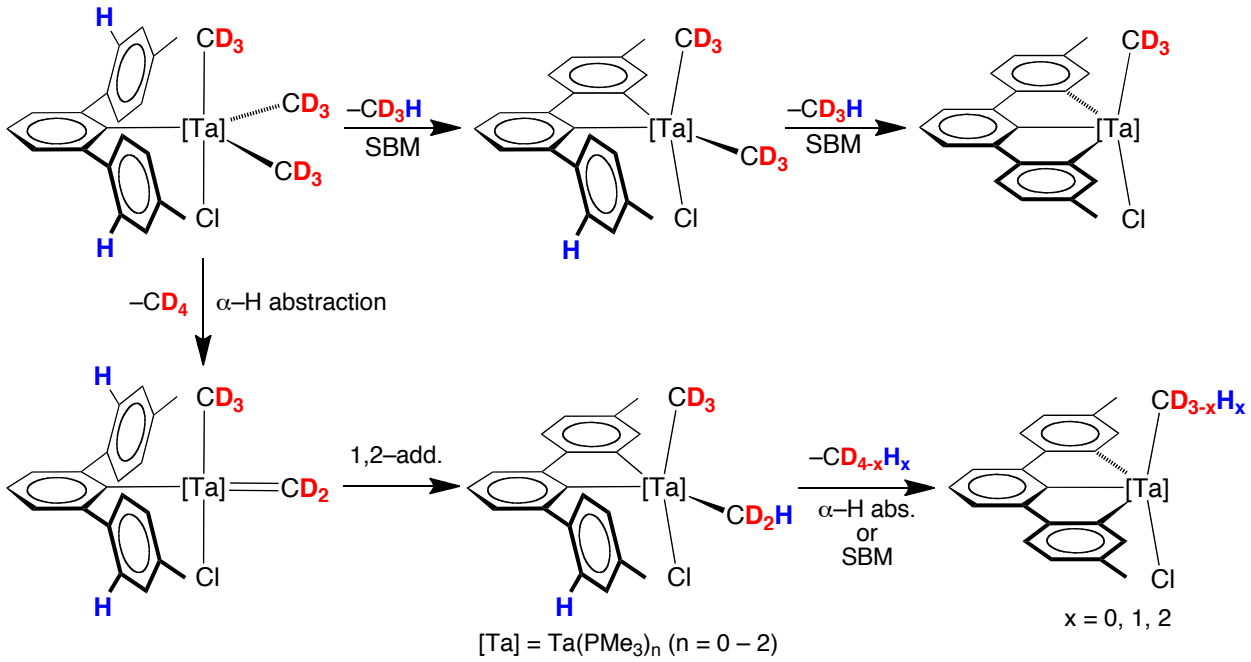

Scheme 6. Sigma-bond metathesis (SBM) and α-hydride abstraction mechanisms for formation of $[\kappa^3\text{-}Ar^{Tol'}{}_2]Ta(PMe_3)_2MeCl$.

In order to distinguish which type of mechanism is occurring in our system, the reaction of the deuterated isotopologue $Ta(PMe_3)_2(CD_3)_3Cl_2$ with $[Ar^{Tol_2}]Li$ was investigated (see Section 6.15.6 for synthesis of $Ta(CD_3)_3Cl_2$ and $Ta(PMe_3)_2(CD_3)_3Cl_2$). Significantly, the reaction selectively generates CD_3H and $[\kappa^3\text{-}Ar^{Tol'_2}]Ta(PMe_3)_2(CD_3)Cl$, both of which are inconsistent with a mechanism that involves α–H abstraction.[89] For example, an α–H abstraction reaction would require both elimination of CD_4[90] and a degree of incorporation of ^1H into the tantalum methyl group (Scheme 6). Conversely, elimination of methane by a sigma-bond metathesis process would liberate only CD_3H and result in no incorporation of ^1H into the TaMe group. Thus, the observations of *(i)* CD_3H formation (coupled with the absence of CD_4) and *(ii)* no ^1H incorporation into the tantalum methyl group, provide convincing evidence that the pincer ligand is created by a pair of Ar–H/Ta–Me sigma-bond metathesis (SBM) transformations.

6.9 Reactions of $[\kappa^3\text{-}Ar^{Tol'_2}]Ta(PMe_3)_2X_2$ (X = Me, Cl) towards small molecules

Initial reactivity studies have been carried out in order to ascertain the ability of the [*CCC*] X_3-donor pincer platform, $[\kappa^3\text{-}Ar^{Tol'_2}]$, to serve as a ligand for small molecule activation chemistry. For example, treatment of $[\kappa^3\text{-}Ar^{Tol'_2}]Ta(PMe_3)_2Cl_2$ with KC_8 in benzene resulted in the formation of $[\kappa^3\text{-}Ar^{Tol'_2}]Ta(PMe_3)_2(\eta^6\text{-}C_6H_6)$ (Scheme 7), presumably a reaction that proceeds *via* the trivalent intermediate $[[\kappa^3\text{-}Ar^{Tol'_2}]Ta(PMe_3)_2]$. $[\kappa^3\text{-}Ar^{Tol'_2}]Ta(PMe_3)_2(\eta^6\text{-}C_6H_6)$ has been structurally characterized by X-ray diffraction, as shown in Figure 30. Despite the fact that the first tantalum benzene complex, $Ta(\eta^6\text{-}C_6H_6)_2$, was reported in 1981,[91] and a variety of other tantalum arene compounds have also been synthesized,[92] there are no structurally characterized tantalum benzene complexes listed in the Cambridge Structural Database.[33,93] A notable feature of $[\kappa^3\text{-}Ar^{Tol'_2}]Ta(PMe_3)_2(\eta^6\text{-}C_6H_6)$ is that the $\eta^6\text{-}C_6H_6$ ligand does not coordinate in a planar symmetric manner, but is puckered, with a fold angle of 17.1° at C1•••C4, such that two

of the Ta–C bonds [Ta–C(1) = 2.317(2) Å and Ta–C(4) = 2.318(2) Å] are 0.15 Å shorter than the average for the other four carbon atoms (2.463 Å).[94] Furthermore, the C–C bond lengths of the benzene ring vary, with C(2)–C(3) and C(5)–C(6) (average of 1.373 Å) being significantly shorter than the bonds to C(1) and C(4) (average of 1.436 Å). The localization of the single and double bonds, together with the variation of the Ta–C bond lengths, suggests that the benzene is better described as an L_2X_2 1,4-cyclohexadienediyl ligand (Figure 31).[3,95,96] As such, [κ^3-$Ar^{Tol'_2}$]Ta(PMe_3)$_2$(η^6-C_6H_6) is better classified as a d^0 ML_4X_5 complex, rather than as a d^2 ML_5X_3 derivative.

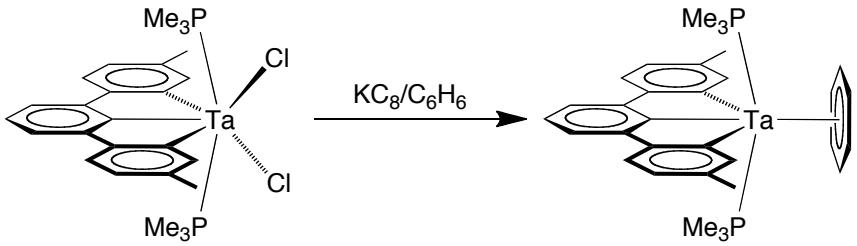

Scheme 7. Synthesis of [κ^3-$Ar^{Tol'_2}$]Ta(PMe_3)$_2$(η^6-C_6H_6).

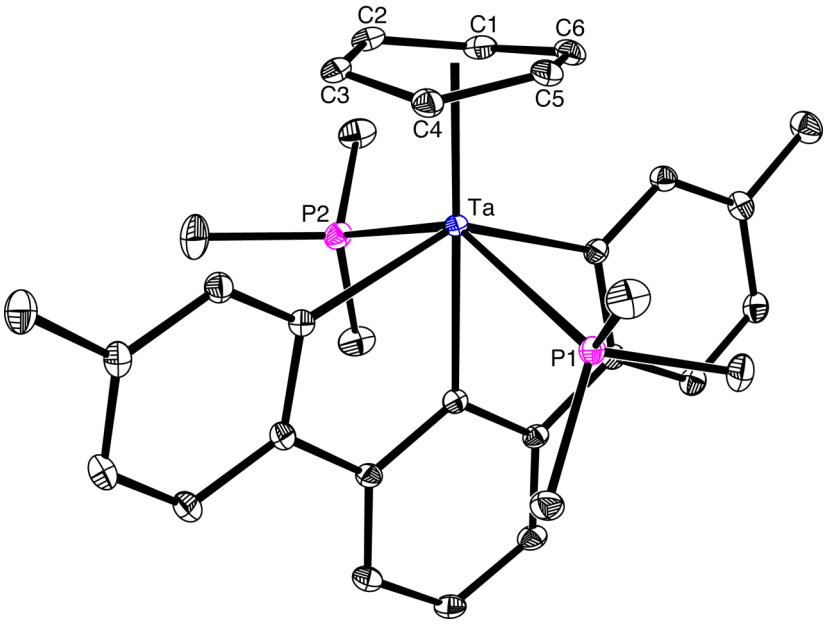

Figure 30. Molecular structure of [κ^3-$Ar^{Tol'_2}$]Ta(PMe_3)$_2$(η^6-C_6H_6).

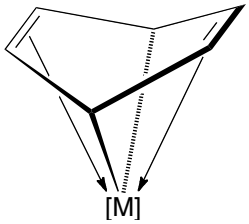

Figure 31. The L_2X_2 1,4-cyclohexadienediyl ligand.

In accord with the formulation as a d^0 Ta 1,4-cyclohexadienediyl derivative, analysis of the Fenske-Hall molecular orbitals[97] indicates that the HOMO of [κ^3-$Ar^{Tol'2}$]Ta(PMe_3)$_2$(η^6-C_6H_6) is a Ta–(η^6-C_6H_6) bonding orbital, rather than a metal based nonbonding orbital that is required for a d^2 description. Specifically, as illustrated in Figure 32, the HOMO represents a δ-interaction between a tantalum d_{xy} orbital[98] and one component of the benzene LUMO e_{2u} set; a molecular orbital diagram for [κ^3-$Ar^{Tol'2}$]Ta(PMe_3)$_2$(η^6-C_6H_6) which illustrates this interaction is shown in Figure 33.

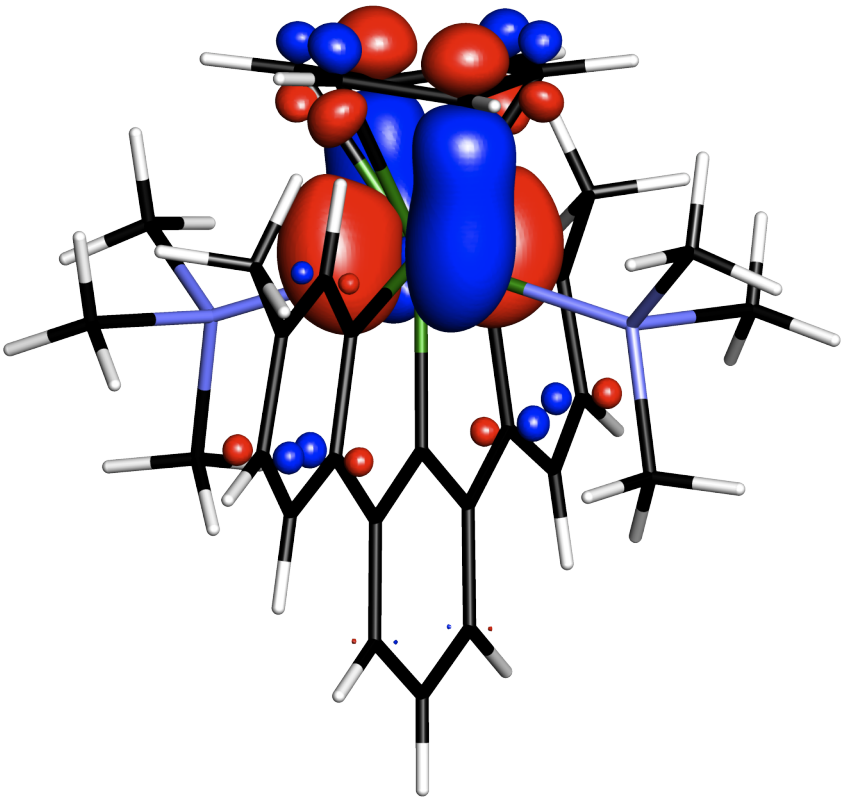

Figure 32. HOMO of [κ^3-$Ar^{Tol'2}$]Ta(PMe_3)$_2$(η^6-C_6H_6).

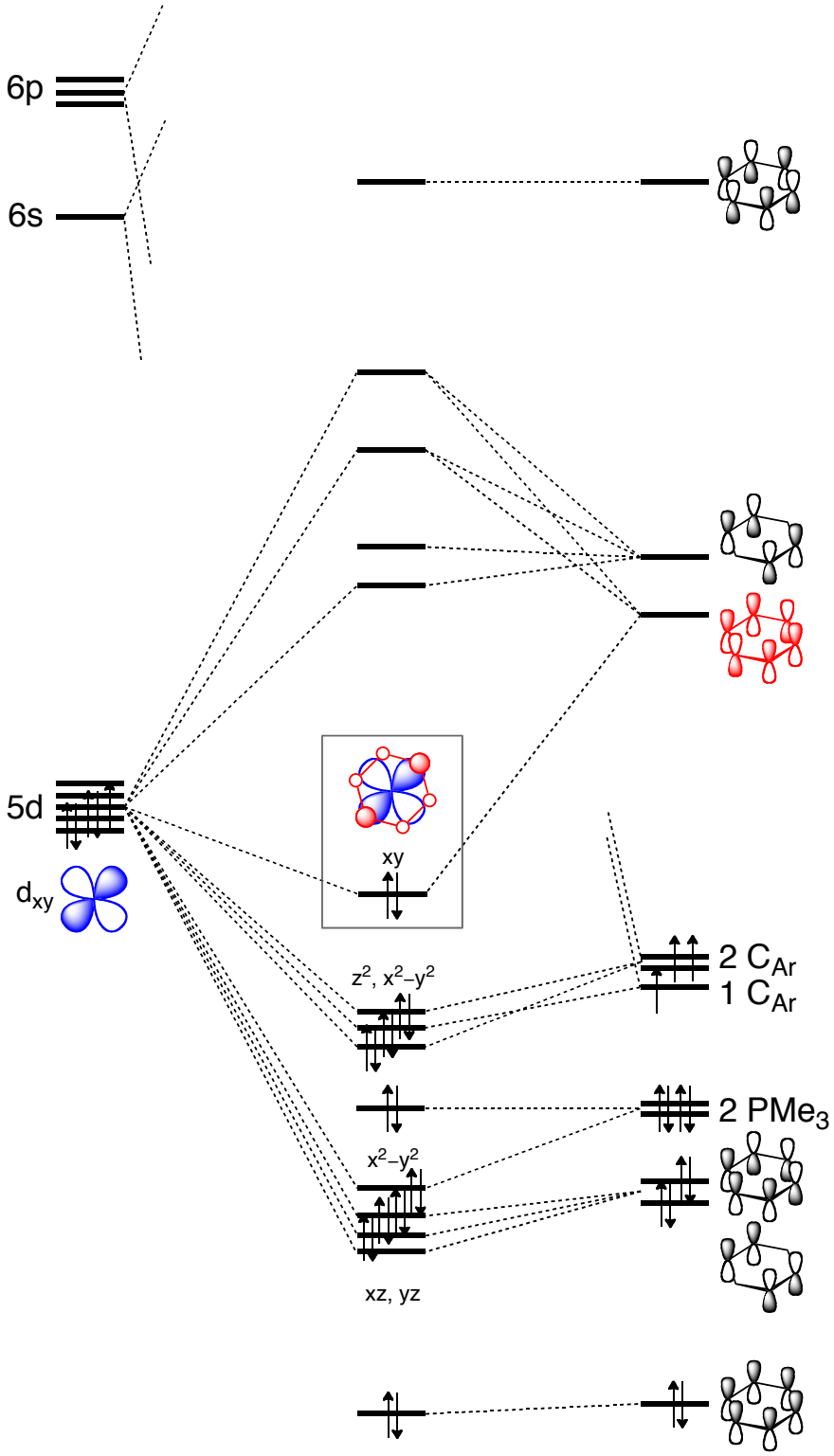

Figure 33. Qualitative molecular orbital diagram for $[\kappa^3\text{-}Ar^{Tol'}{}_2]Ta(PMe_3)_2(\eta^6\text{-}C_6H_6)$, with the δ-interaction between the tantalum d_{xy} orbital (blue) and one component of the benzene LUMO e_{2u} set (red) shown in grey box.

The reactivity of $[\kappa^3\text{-Ar}^{\text{Tol}'_2}]\text{Ta}(\text{PMe}_3)_2\text{Cl}_2$ towards carbon monoxide was also studied, allowing for the isolation of $[\kappa^2,\eta^2\text{-Ar}^{\text{Tol}',\text{Tol}(\text{Me}_3\text{PCO})}]\text{Ta}(\text{PMe}_3)\text{Cl}_2$ and $[\eta^2,\eta^2\text{-Ar}^{\text{Tol}(\text{CO}),\text{Tol}(\text{Me}_3\text{PCO})}]\text{Ta}(\text{PMe}_3)_2\text{Cl}_2$ (Scheme 8);[99,100,101] both complexes have been structurally characterized by X-ray diffraction and their molecular structures are shown in Figures 34 and 35, respectively.

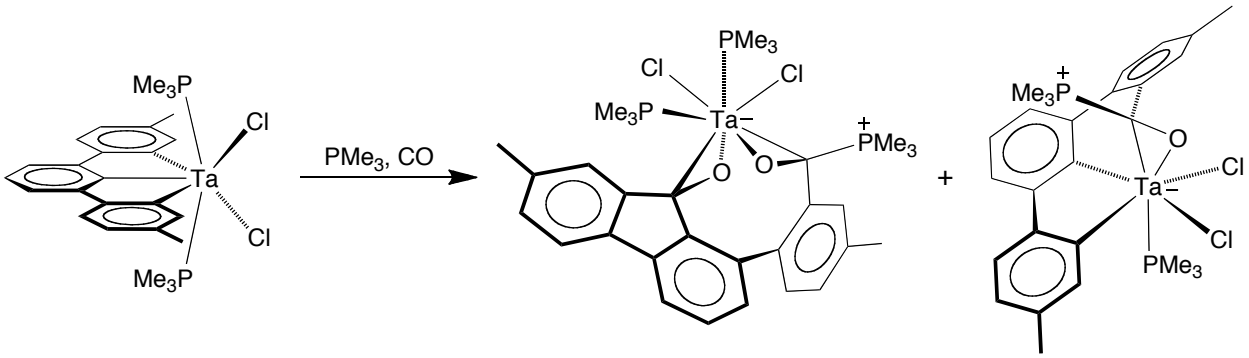

Scheme 8. Reactivity of $[\kappa^3\text{-Ar}^{\text{Tol}'_2}]\text{Ta}(\text{PMe}_3)_2\text{Cl}_2$ with PMe_3 and CO.

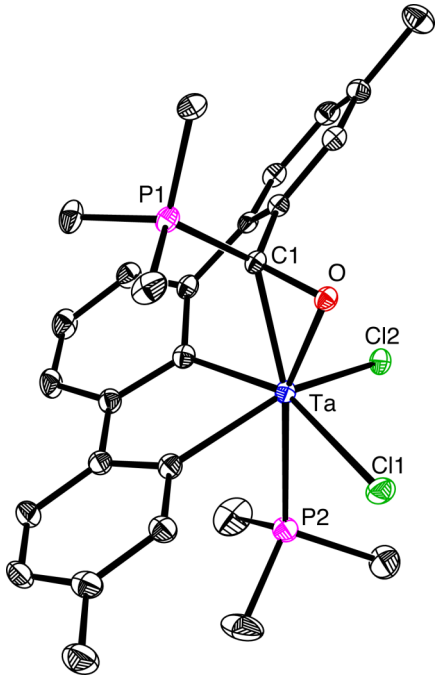

Figure 34. Molecular structure of $[\kappa^2,\eta^2\text{-Ar}^{\text{Tol}',\text{Tol}(\text{Me}_3\text{PCO})}]\text{Ta}(\text{PMe}_3)\text{Cl}_2$.

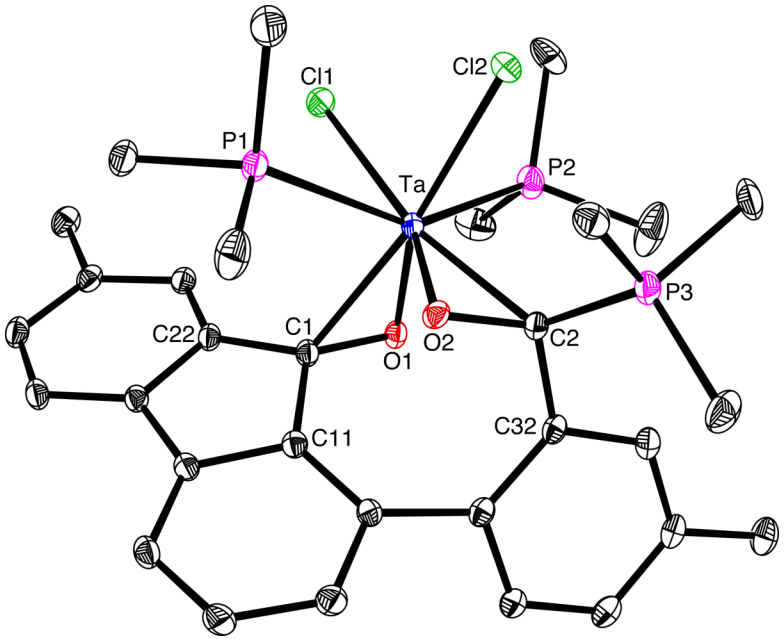

Figure 35. Molecular structure of $[\eta^2,\eta^2\text{-}Ar^{Tol(CO),Tol(Me_3PCO)}]Ta(PMe_3)_2Cl_2$.

Two possible mechanisms for the formation of the insertion products obtained upon addition of CO to $[\kappa^3\text{-}Ar^{Tol'_2}]Ta(PMe_3)_2Cl_2$ (Scheme 8), namely $[\kappa^2,\eta^2\text{-}Ar^{Tol',Tol(Me_3PCO)}]Ta(PMe_3)Cl_2$ and $[\eta^2,\eta^2\text{-}Ar^{Tol(CO),Tol(Me_3PCO)}]Ta(PMe_3)_2Cl_2$, are illustrated in Scheme 9. For example, insertion of CO to one Ta–Tol' bond, followed by attack of PMe_3 on the carbonyl (Scheme 9, right pathway) would give $[\kappa^2,\eta^2\text{-}Ar^{Tol',Tol(Me_3PCO)}]$-$Ta(PMe_3)Cl_2$. The formation of $[\eta^2,\eta^2\text{-}Ar^{Tol(CO),Tol(Me_3PCO)}]Ta(PMe_3)_2Cl_2$ is, however, more complicated. For example, one possibility is that after $[\kappa^2,\eta^2\text{-}Ar^{Tol',Tol(Me_3PCO)}]Ta(PMe_3)Cl_2$ is formed, another CO insertion occurs followed by bond migrations and addition of PMe_3 (Scheme 9, right pathway).[102] Another option is, nevertheless, that after formation of the first acyl intermediate (Scheme 9, top left), the Ta–Ar bond migrates to the carbonyl, which then reacts with another equivalent of CO and PMe_3 to produce $[\eta^2,\eta^2\text{-}Ar^{Tol(CO),Tol(Me_3PCO)}]Ta(PMe_3)_2Cl_2$ (Scheme 9, left pathway).

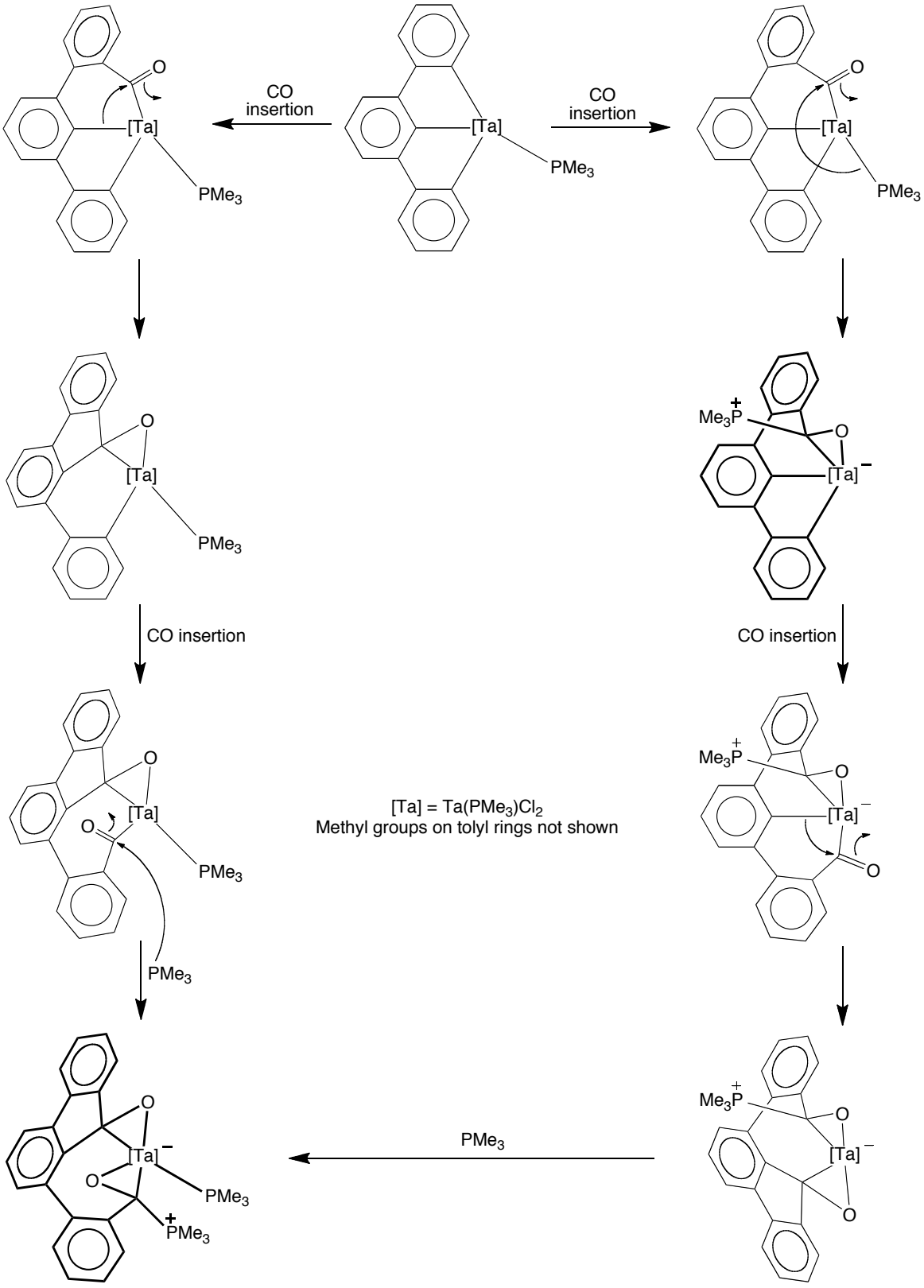

Scheme 9. Possible mechanisms of formation of $[\kappa^2,\eta^2\text{-}Ar^{Tol',Tol(Me_3PCO)}]Ta(PMe_3)Cl_2$ and $[\eta^2,\eta^2\text{-}Ar^{Tol(CO),Tol(Me_3PCO)}]Ta(PMe_3)_2Cl_2$ (isolated products are bolded for clarity).

Another interesting compound was isolated from the reaction of [κ^3-Ar$^{Tol'2}$]Ta(PMe$_3$)$_2$Cl$_2$ towards KC$_8$ in the presence of ethylene, namely [κ^3-Ar$^{Tol'2}$]-Ta(PMe$_3$)$_2$(κ^2-C$_4$H$_8$) (Scheme 10), which has been structurally characterized by X-ray diffraction (Figure 36). [κ^3-Ar$^{Tol'2}$]Ta(PMe$_3$)$_2$(κ^2-C$_4$H$_8$) is formally obtained by the coupling of two ethylene molecules and the tantalum center,[103,104,105] but likely proceeds *via* the production of a metallacyclopropane, followed by a 1,2-insertion of ethylene.[106]

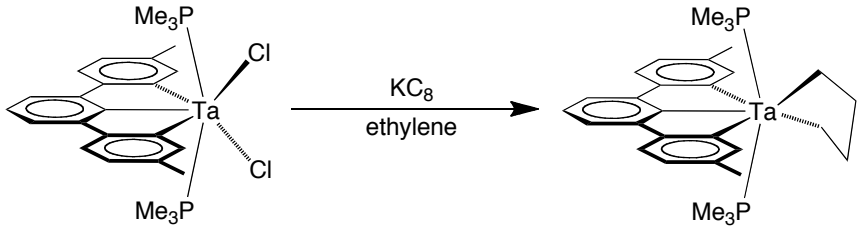

Scheme 10. Reactivity of [κ^3-Ar$^{Tol'2}$]Ta(PMe$_3$)$_2$Cl$_2$ with ethylene and KC$_8$.

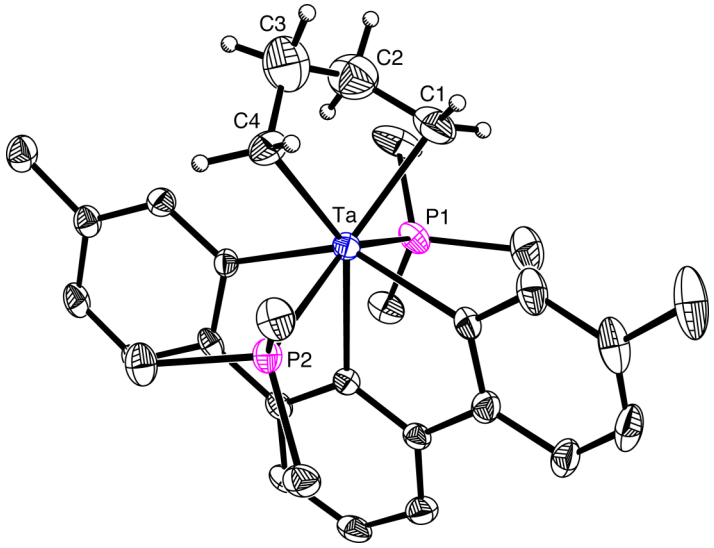

Figure 36. Molecular structure of [κ^3-Ar$^{Tol'2}$]Ta(PMe$_3$)$_2$(κ^2-C$_4$H$_8$).

Another compound was isolated from the reaction of neopentyllithium (NpLi) with [κ^3-Ar$^{Tol'2}$]Ta(PMe$_3$)$_2$MeCl (Scheme 11). Specifically, addition of excess NpLi to [κ^3-Ar$^{Tol'2}$]Ta(PMe$_3$)$_2$MeCl forms the neopentyl neopentylidene complex, [[κ^3-Ar$^{Tol'2}$]Ta(PMe$_3$)Np(=CHCMe$_3$)][LiPMe$_3$], which has been structurally characterized by X-ray diffraction (Figure 37). The most interesting feature of [[κ^3-Ar$^{Tol'2}$]-

$Ta(PMe_3)Np(=CHCMe_3)][LiPMe_3]$ is the presence of the lithium atom that is interacting with the metallacyclopentadiene π-system of the pincer ligand. It should, however, be noted that lithium π-arene complexes are known.[107] For example, a close analogue is the previously synthesized nickel compound, $[CpNi(\kappa^2\text{-}C_{12}H_8)][Li\bullet DME]$, in which the lithium atom is also bound to the metallacyclopentadiene moiety.[107a] Furthermore, a related lithium-tantalum complex , namely $[Cp^*Ta(NAr)_2Cl][LiOEt_2]$ (Ar = 2,6-$C_6H_3Pr^i_2$), has been structurally characterized by Wigley.[108]

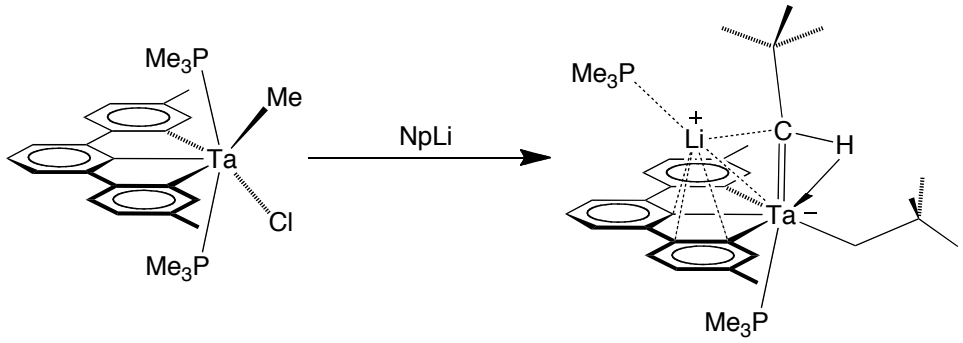

Scheme 11. Reactivity of $[\kappa^3\text{-}Ar^{Tol'_2}]Ta(PMe_3)_2MeCl$ with neopentyllithium.

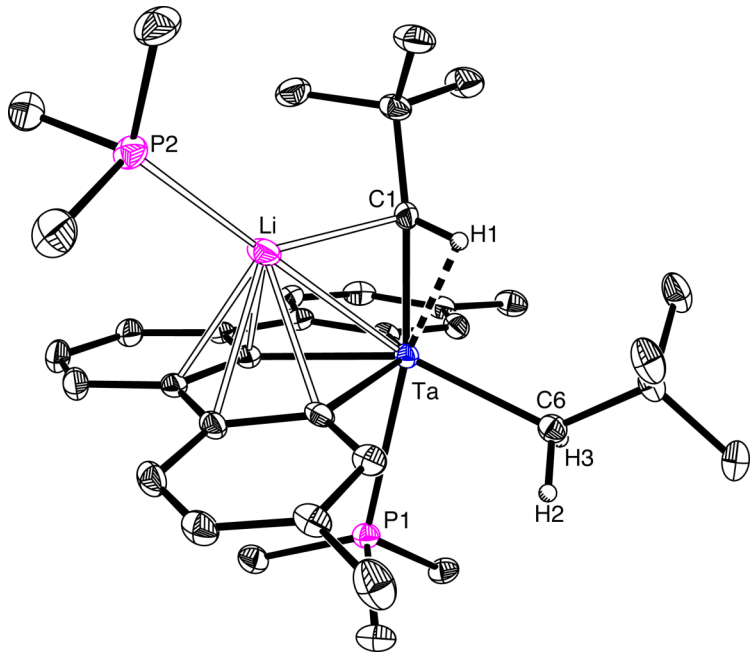

Figure 37. Molecular structure of $[[\kappa^3\text{-}Ar^{Tol'_2}]Ta(PMe_3)Np(=CHCMe_3)][LiPMe_3]$.

6.10 Niobium chemistry

Juvinall also reported the synthesis of the first σ-bonded alkyl complex of niobium, namely $NbMe_3Cl_2$.[23,109,110] Therefore, studies were carried out in order to determine if a niobium complex supported by a [*CCC*] X_3-donor pincer ligand could also be synthesized.

6.11 Molecular structure of $NbMe_3Cl_2$

The crystal structure of $NbMe_3Cl_2$ has been previously described in the literature in the noncentrosymmetric space group *P6₃mc*; this space group was selected based on the authors' DFT calculations that predict a slightly distorted trigonal bipyramid geometry.[35] In view of the almost identical unit cell parameters of $NbMe_3Cl_2$ and $TaMe_3Cl_2$ ($TaMe_3Cl_2$ crystallizes in the centrosymmetric space group *P6₃/mmc*, see Section 6.2), the molecular structure of $NbMe_3Cl_2$ was reinvestigated. Interestingly, it was determined that the structure of $NbMe_3Cl_2$ refined better in the centrosymmetric space group *P6₃/mmc*, compared with the reported noncentrosymmetric space group of *P6₃mc*. Thus, it is proposed that even though DFT calculations predict that $NbMe_3Cl_2$ adopts a slightly distorted trigonal bipyramidal geometry, the best solid-state *crystal structure* description is in space group *P6₃/mmc*, with a rigorous trigonal bipyramidal geometry. The centrosymmetric structure of $NbMe_3Cl_2$ is shown in Figure 38.

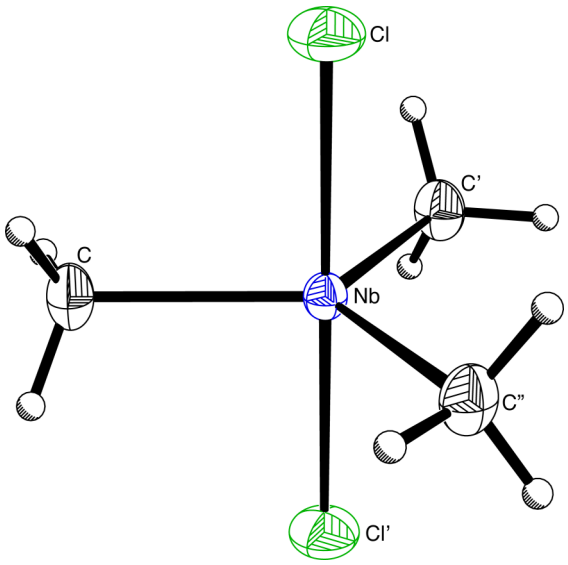

Figure 38. Molecular Structure of $NbMe_3Cl_2$ (the hydrogen atoms are placed in idealized positions and only one of the disordered configurations is shown).

6.12 Reactivity of $NbMe_3Cl_2$

$NbMe_3Cl_2$ is significantly less stable in solution compared with $TaMe_3Cl_2$, making it more difficult to handle. For example, a solution of $NbMe_3Cl_2$ in d_6-benzene produces methane and a fine black precipitate within minutes.[111] In accord with these observations, there are only three compounds, including $NbMe_3Cl_2$, in the Cambridge Structural Database[33] with the [$NbMe_3$] fragment,[35,112] compared with 33 for that of tantalum, *.i.e.* [$TaMe_3$].

Addition of PMe_3 to $NbMe_3Cl_2$ resulted in the formation of a blood red solution, and it was determined that the major product was $Nb(PMe_3)_2Me_3Cl_2$ (Scheme 12).[113] However, there was a significant amount (*ca.* 25 %) of an impurity tentatively identified as $Nb(PMe_3)_2Me_2Cl_3$, most likely due to a redistribution process. The molecular structure of $Nb(PMe_3)_2Me_3Cl_2$ was determined by X-ray diffraction (Figure 39), but unfortunately, also contained a significant amount of the trichloride impurity, $Nb(PMe_3)_2Me_2Cl_3$ (*ca.* 40 %).

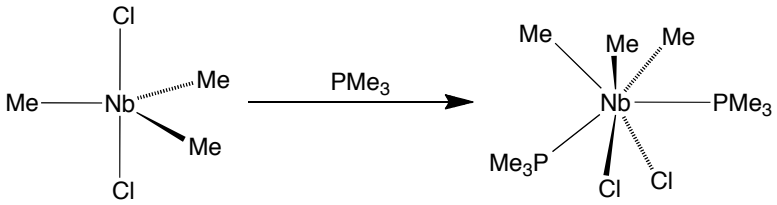

Scheme 12. Synthesis of $Nb(PMe_3)_2Me_3Cl_2$.

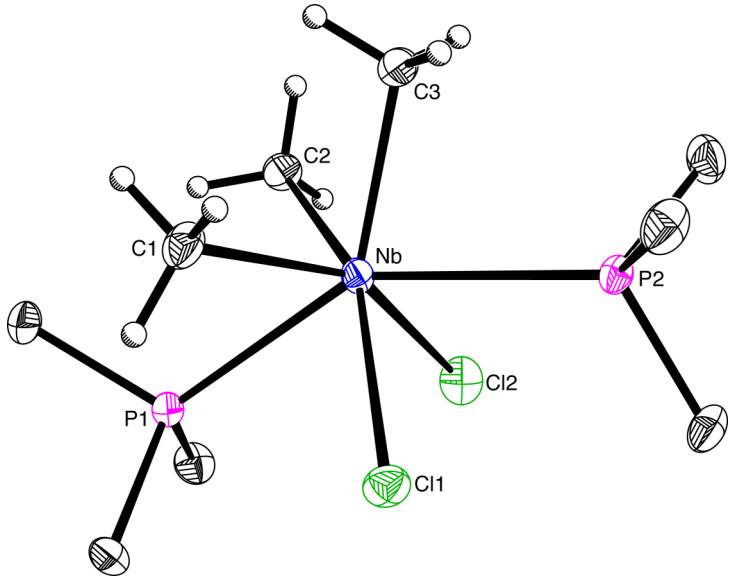

Figure 39. Molecular Structure of $Nb(PMe_3)_2Me_3Cl_2$ (disorder with $Nb(PMe_3)_2Me_2Cl_3$ not shown).

Despite the instability of $NbMe_3Cl_2$ and $Nb(PMe_3)_2Me_3Cl_2$, their reactivity towards $[Ar^{Tol_2}]Li$ was studied. For example, treatment of a solution of $NbMe_3Cl_2$ with $[Ar^{Tol_2}]Li$ allowed for isolation of $[Ar^{Tol_2}]NbMe_2Cl_2$ (Scheme 13),[114,115] which has been structurally characterized by X-ray diffraction (Figure 40).[116] Moreover, treatment of $Nb(PMe_3)_2Me_3Cl_2$ with $[Ar^{Tol_2}]Li$ resulted in the formation of $[\kappa^3\text{-}Ar^{Tol'_2}]Nb(PMe_3)_2MeCl$ (Scheme 14), and its molecular structure is shown in Figure 41.[117] Similar to the tantalum system, $[\kappa^3\text{-}Ar^{Tol'_2}]Nb(PMe_3)_2MeCl$ undergoes a redistribution process in solution, forming $[\kappa^3\text{-}Ar^{Tol'_2}]Nb(PMe_3)_2Me_2$[118] and $[\kappa^3\text{-}Ar^{Tol'_2}]Nb(PMe_3)_2Cl_2$, both of which can be isolated by crystallization after addition of MeMgBr and $ZnCl_2$,[119] respectively

(Scheme 15).[120] The molecular structures of [κ³-Ar$^{Tol'_2}$]Nb(PMe$_3$)$_2$Me$_2$ and [κ³-Ar$^{Tol'_2}$]Nb(PMe$_3$)$_2$Cl$_2$ are shown in Figure 42.

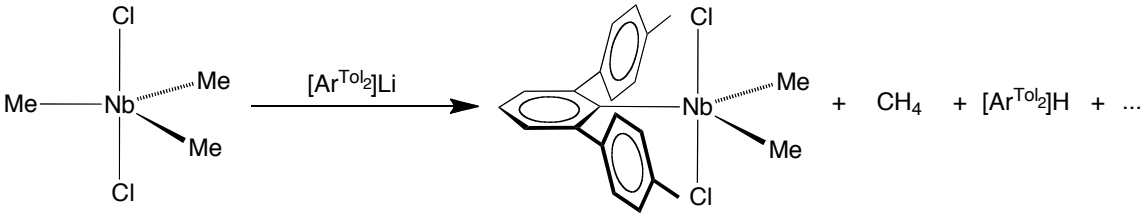

Scheme 13. Reactivity of NbMe$_3$Cl$_2$ with [Ar^{Tol_2}]Li.

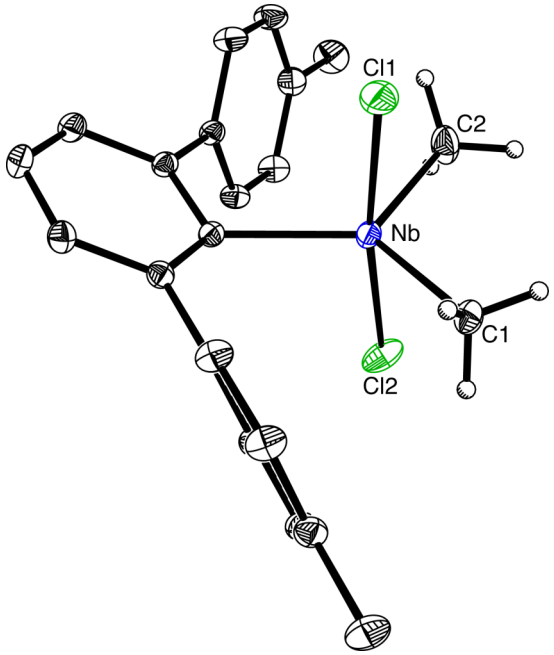

Figure 40. Molecular structure of [Ar^{Tol_2}]NbMe$_2$Cl$_2$.

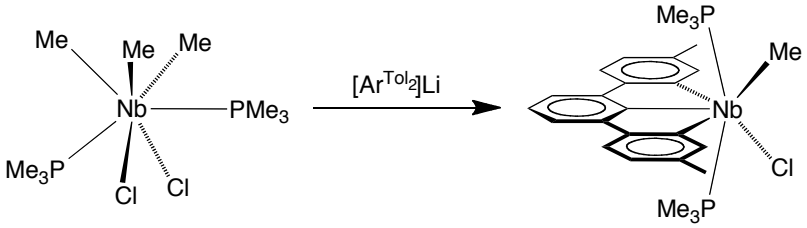

Scheme 14. Production of [κ³-Ar$^{Tol'_2}$]Nb(PMe$_3$)$_2$MeCl.

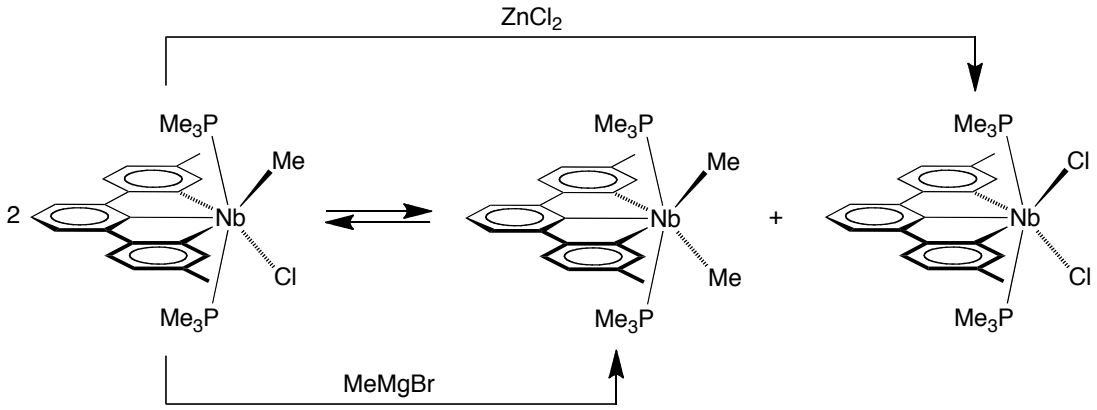

Scheme 15. Production of [κ^3-Ar$^{Tol'2}$]Nb(PMe$_3$)$_2$Me$_2$ and [κ^3-Ar$^{Tol'2}$]Nb(PMe$_3$)$_2$Cl$_2$.

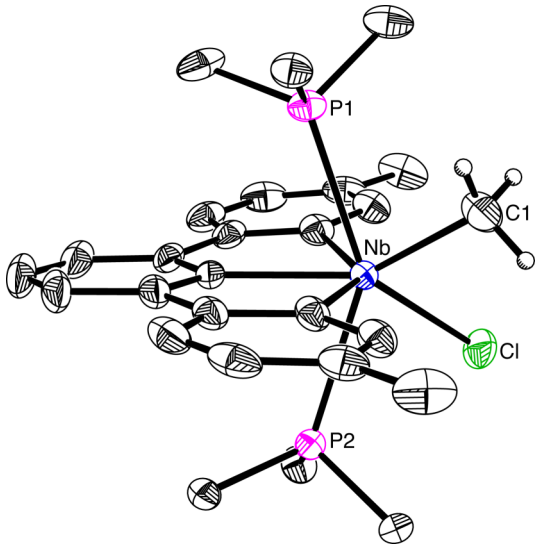

Figure 41. Molecular structure of [κ^3-Ar$^{Tol'2}$]Nb(PMe$_3$)$_2$MeCl (disorder between Me and Cl not shown).

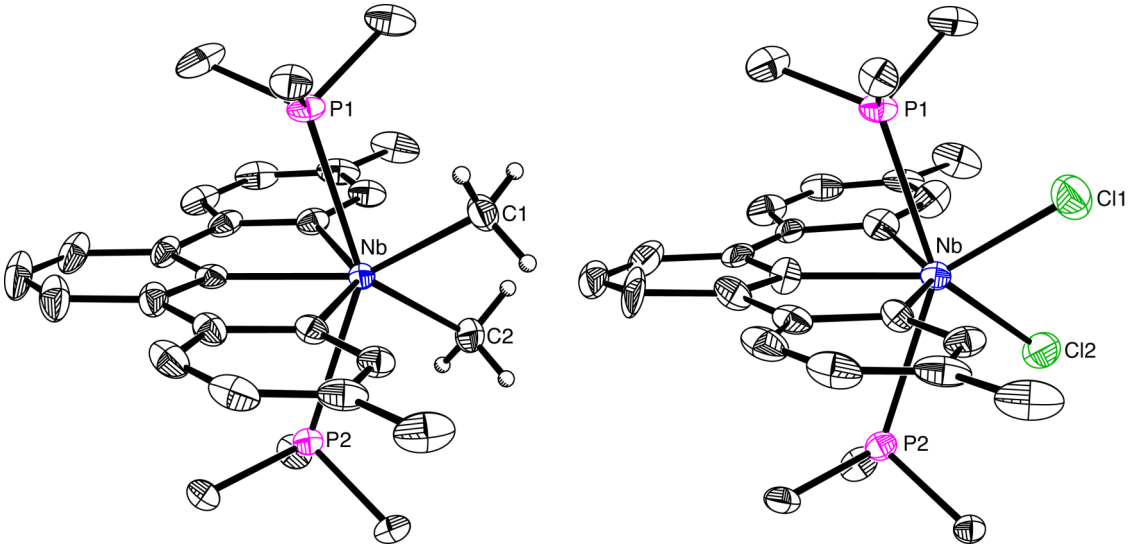

Figure 42. Molecular structure of [κ^3-Ar$^{Tol'2}$]Nb(PMe$_3$)$_2$Me$_2$ (left) and [κ^3-Ar$^{Tol'2}$]Nb(PMe$_3$)$_2$Cl$_2$ (right).

6.13 NMR spectroscopic features of $[\kappa^3\text{-}Ar^{Tol'_2}]Nb(PMe_3)_2Me_2$

It is useful to note that the NMR spectroscopic features of $[\kappa^3\text{-}Ar^{Tol'_2}]Nb(PMe_3)_2Me_2$ are similar to those of $[\kappa^3\text{-}Ar^{Tol'_2}]Ta(PMe_3)_2Me_2$. For example, the methyl signal of $[\kappa^3\text{-}Ar^{Tol'_2}]Nb(PMe_3)_2Me_2$ in the ^1H NMR spectrum is a filled-in doublet (Figure 43), but upon irradiation of the PMe_3 signal, the methyl changes shape significantly, thereby indicating that there is 5-bond H–H coupling constant between the methyl and PMe_3 hydrogens (Figure 43).[121] Furthermore, the $^{13}C\{^1H\}$ NMR spectrum of $[\kappa^3\text{-}Ar^{Tol'_2}]Nb(PMe_3)_2Me_2$ (Figure 44) demonstrates that the signal for the PMe_3 ligands *appears* as a doublet of triplets due to a secondary isotope effect (see above for full explanation with tantalum system).

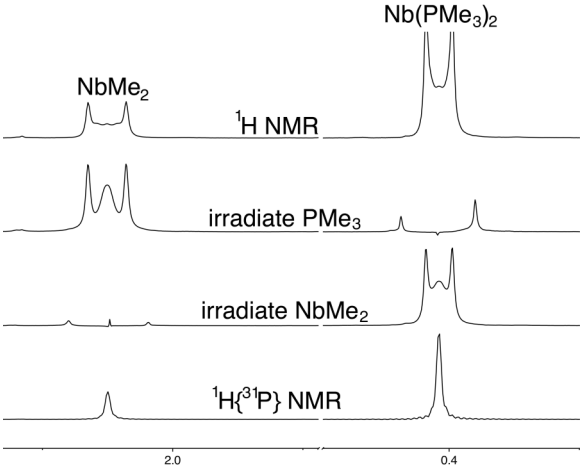

Figure 43. ^1H NMR spectra of $NbMe_2$ and $Nb(PMe_3)_2$ signals of $[\kappa^3\text{-}Ar^{Tol'_2}]Nb(PMe_3)_2Me_2$.

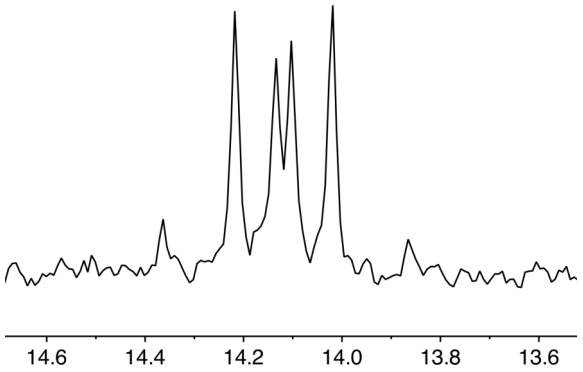

Figure 44. $^{13}C\{^1H\}$ NMR spectrum of $Nb(PMe_3)_2$ signal of $[\kappa^3\text{-}Ar^{Tol'_2}]Nb(PMe_3)_2Me_2$.

6.14 Summary and conclusions

In conclusion, a novel [*CCC*] X_3-donor pincer ligand has been constructed on tantalum and niobium by the PMe_3 induced cyclometalation of a terphenyl ligand. The mechanism for the cyclometalation for the tantalum system involves a pair of sigma-bond metathesis reactions and, as such, it is possible that this approach may provide a general means for obtaining [*CCC*] X_3-donor pincer complexes of other metals, and especially those of the early transition elements for which sigma-bond metathesis reactions are common.

6.15 Experimental details

6.15.1 General considerations

All manipulations were performed using a combination of glovebox, high vacuum, and Schlenk techniques under an argon atmosphere unless otherwise specified.[122] Solvents were purified and degassed by using standard procedures. ^1H NMR spectra were measured on Bruker 300 DRX, Bruker 300 DPX, Bruker 400 Avance III, Bruker 400 Cyber-enabled Avance III, and Bruker 500 DMX spectrometers. ^1H chemical shifts are reported in ppm relative to $SiMe_4$ ($\delta = 0$) and were referenced internally with respect to the protio solvent impurity (δ 7.16 for C_6D_5H and 2.09 for C_7D_7H).[123] ^{13}C NMR spectra are reported in ppm relative to $SiMe_4$ ($\delta = 0$) and were referenced internally with respect to the solvent (δ 128.06 for C_6D_6).[123] ^{31}P chemical shifts are reported in ppm relative to 85% H_3PO_4 ($\delta = 0$) and were referenced using $P(OMe)_3$ ($\delta = 141.0$) as an external standard.[124] Coupling constants are given in hertz. NMR spectroscopic simulations were performed using gNMR 5.1 (Adept Scientific) and MestReNova v7.0.3 (Mestrelab Research S.L. 2001) and final images were produced by MestReNova. $TaCl_5$, PMe_3, $P(CD_3)_3$, $^{13}CH_3I$, CD_3I and Li wire (0.5 – 1.0 % Na) were obtained commercially from Aldrich. $NbCl_5$ and Me_2Zn were obtained commercially from Strem Chemicals. $ZnCl_2$

was obtained from Strem Chemicals and dried with $SOCl_2$ prior to use.[125] Et_2O was dried over $LiAlH_4$ and vacuum transferred into an ampoule containing molecular sieves prior to use.

6.15.2 X-ray structure determinations

X-ray diffraction data were collected on a Bruker Apex II diffractometer. Crystal data, data collection and refinement parameters are summarized in Section 6.16, Table 7. The structures were solved using direct methods and standard difference map techniques, and were refined by full-matrix least-squares procedures on F^2 with SHELXTL (Version 6.10).[126]

6.15.3 Computational details

Calculations were carried out using DFT as implemented in the Jaguar 7.5 (release 207) suite of *ab initio* quantum chemistry programs.[127] Geometry optimizations were performed with the B3LYP density functional[128] using the 6-31G** (C, H, Cl and P) and LACVP (Ta) basis sets.[129] The energies of the optimized structures were reevaluated by additional single point calculations on each optimized geometry using cc-pVTZ(-f) correlation consistent triple-ζ basis set for C, H, Cl, and P and LACV3P for Ta. Molecular orbital analyses were performed with the aid of JIMP2,[97] which employs Fenske-Hall calculations and visualization using MOPLOT.[130]

6.15.4 Synthesis of $TaMe_3Cl_2$

The synthesis of $TaMe_3Cl_2$ was adapted from the literature method.[23] A suspension of $TaCl_5$ (2.0 g, 5.6 mmol) in pentane (25 mL) was treated with a solution of Me_2Zn (0.70 mL, 10.2 mmol) in pentane (5 mL) over a period of 10 minutes. The suspension was stirred for 2 hours, after which period the mixture was filtered. The volatile

components were removed from the filtrate *in vacuo* to give $TaMe_3Cl_2$ as a pale yellow crystalline solid (1.38 g, 83% yield). Pale yellow crystals of $TaMe_3Cl_2$, suitable for X-ray diffraction studies, were obtained by cooling a solution of $TaMe_3Cl_2$ in pentane at –15 ˚C.

6.15.5 Synthesis of $Ta(PMe_3)_2Me_3Cl_2$

A suspension of $TaCl_5$ (1.0 g, 2.8 mmol) in pentane (25 mL) was treated with a solution of Me_2Zn (0.35 mL, 5.1 mmol) in pentane (5 mL) over a period of 10 minutes. The suspension was stirred for 1 hour, after which period the mixture was filtered. The volatile components were removed from the filtrate *in vacuo* to give $TaMe_3Cl_2$ as a pale yellow crystalline solid. The solid was dissolved in cold pentane (10 mL at –78 ˚C) and the pale yellow solution was frozen in a liquid nitrogen bath and treated with PMe_3 (0.7 mL, 6.9 mmol) *via* vapor transfer. The mixture was allowed to warm to room temperature, producing a bright yellow suspension. The suspension was cooled to –78 ˚C for 20 minutes to induce additional crystallization, after which period the bright yellow crystalline $Ta(PMe_3)_2Me_3Cl_2$ was isolated by filtration and dried *in vacuo* (0.86 g, 69% yield). Bright yellow crystals of $Ta(PMe_3)_2Me_3Cl_2$, suitable for X-ray diffraction studies, were obtained by cooling a solution of $Ta(PMe_3)_2Me_3Cl_2$ in pentane at –15 ˚C. Anal. Calcd.: C, 24.1%, H, 6.1%. Found: C, 22.5%, H, 5.6%.

^{1}H NMR (C_6D_6): 1.21 [d, $^2J_{P\text{-}H}$ = 8, 18H of $2PMe_3$], 1.46 [s, 9H of $TaMe_3$] (chemical shift values vary slightly with concentration; values given are for a 0.1 M solution). ^{1}H NMR (d_8-toluene): 1.22 [d, $^2J_{P\text{-}H}$ = 8, 18H of $2PMe_3$], 1.38 [s, 9H of $TaMe_3$]. $^{31}P\{^1H\}$ NMR (C_6D_6): 2.3 [br s, 2P of $2PMe_3$]. $^{13}C\{^1H\}$ NMR (C_6D_6): 13.6 [d, $^1J_{P\text{-}C}$ = 21, 6C of $2PMe_3$], 76.0 [s, 3C of $TaMe_3$].

6.15.6 Synthesis of $Ta(CD_3)_3Cl_2$ and $Ta(PMe_3)_2(CD_3)_3Cl_2$

The synthesis of $Ta(CD_3)_3Cl_2$ was adapted from the literature procedure for $Ta(CH_3)_3Cl_2$.[23c] A solution of CD_3I (2.5 g, 17.2 mmol) in Et_2O (3 mL), cooled to –78 ˚C to minimize evaporation of CD_3I, was added to a suspension of lithium wire (600 mg, 86 mmol, 0.5 – 1.0 % Na, *ca*. 5 mm pieces) in Et_2O (20 mL) at room temperature over a period of 10 minutes. The mixture was stirred for 2 hours at room temperature and filtered. The filtrate was slowly added to a stirred suspension of $ZnCl_2$ (1.41 g, 10.3 mmol, dried with $SOCl_2$) in Et_2O (5 mL) at –78 ˚C. After the addition was complete, the suspension was allowed to warm to 0 ˚C, and stirred for 30 minutes. The *in situ* generated solution of $Zn(CD_3)_2$ in Et_2O was then vapor transferred into a Schlenk tube containing $TaCl_5$ (750 mg, 2.1 mmol) at –196 ˚C. After the transfer was complete, the mixture was allowed to warm to room temperature and stirred for 2 hours. 1,4-Dioxane (0.3 mL, 0.31 g, 3.5 mmol) was added to precipitate $ZnCl_2$•dioxane, which was removed by filtration. The volatile components were removed from the filtrate *in vacuo* and the resulting pale yellow solid was extracted with pentane (50 mL) and filtered. The pentane was removed from the filtrate *in vacuo* to give $Ta(CD_3)_3Cl_2$ (250 mg, 39 % yield). The pale yellow residue of $Ta(CD_3)_3Cl_2$ that could not be removed from the sides of the Schlenk tube was dissolved in pentane (10 mL) and treated with PMe_3 (0.5 mL, 4.9 mmol). The resulting bright yellow suspension was stirred for 20 minutes, after which the volatile components were removed *in vacuo* to give $Ta(PMe_3)_2(CD_3)_3Cl_2$ (200 mg, 21 % yield). The combined yield based on $TaCl_5$ is 60 %.

6.15.7 Synthesis of $Ta[P(CD_3)_3]_2Me_3Cl_2$

A solution of $TaMe_3Cl_2$ (350 mg, 1.18 mmol) in pentane (5 mL) was treated with $P(CD_3)_3$ (250 mg, 2.94 mmol, cooled at –15 ˚C). The resulting bright yellow mixture was shaken

for 10 minutes. After this period, the volatile components were removed *in vacuo* to give $Ta[P(CD_3)_3]_2Me_3Cl_2$ as a bright yellow solid (523 mg, 95 % yield).

6.15.8 Synthesis of $[Ar^{Tol_2}]I$

The synthesis of $[Ar^{Tol_2}]I$ was adapted from literature procedures.[131]

(i) Preparation of p-TolMgBr

A degassed solution of *p*-bromotoluene (50.0 g, 0.292 mol) in THF (50 mL) was added slowly over a period of 4 hours to a stirred mixture of Mg (10.0 g, 0.411 mol) and THF (250 mL). The mixture was stirred for a further 16 hours to generate a solution of the *p*-TolMgBr Grignard reagent.

(ii) Preparation of $[C_6H_3Cl_2]Li$

A solution of 1,3-dichlorobenzene (17.6 g, 0.120 mol) in THF (200 mL) was cooled to -78 ˚C and treated dropwise with a solution of Bu^nLi in hexanes (52.0 mL, 2.5 M, 0.130 mol) over a period of 3 hours, resulting in a yellow-white suspension. The mixture was then stirred for an additional 2 hours at –78 ˚C to generate $[C_6H_3Cl_2]Li$.

(iii) Synthesis of $[Ar^{Tol_2}]I$

The stirred suspension of $[C_6H_3Cl_2]Li$ in THF/hexanes at –78 ˚C [see section (*ii*) above] was treated dropwise with the *p*-TolMgBr Grignard reagent [see section (*i*) above] over a period of 2 hours. After the addition, the mixture was allowed to warm slowly to room temperature and stirred for an additional 12 hours at room temperature, and then refluxed for 1 hour. An aliquot was taken to confirm that the coupling was complete by using ^1H NMR spectroscopy; the aliquot was also used to obtain crystals of $[Ar^{Tol_2}]MgBr(THF)_2$ that were analyzed by X-ray diffraction to confirm the identity of

the product (see Supporting Information), although it should be noted that there is disorder with the chloride derivative. The bulk reaction mixture was then cooled to 0 ˚C and treated slowly with a solution of I_2 (55 g, 0.217 mol) in THF (100 mL) over a period of 20 minutes, and then allowed to warm to room temperature. The mixture was filtered in air through a glass frit to remove the insoluble salts and the filtrate was washed sequentially with aqueous Na_2SO_3 (2 × 200 mL) and H_2O (2 × 100 mL). The aqueous washings were combined and extracted into Et_2O (200 mL). The ether extract was combined with the original organic layer, which was then dried with $MgSO_4$. The volatile components were removed *in vacuo* to give a light yellow sticky solid that was washed with pentane (3 × 50 mL) and then dried *in vacuo* to give [Ar^{Tol_2}]I as a white powder (28.2 g). The pentane washes were combined and cooled to –15 ˚C, thereby depositing crystals that were washed with pentane (2 × 10 mL) to give an additional crop of [Ar^{Tol_2}]I (3.7 g). The combined yield of [Ar^{Tol_2}]I is 31.9 g (yield 69 %). X-ray quality crystals of [Ar^{Tol_2}]I were obtained from a solution in pentane at –15 ˚C. Anal. Calcd.: C, 62.5 %, H, 4.5 %. Found: C, 62.7 %, H, 4.6%.

^{1}H NMR (C_6D_6): 2.14 [s, 6H of Me of Ar^{Tol_2}], 7.03 [m, 5H of Ar^{Tol_2}], 7.11 [d, $^3J_{H\text{-}H}$ = 8, 2H of Ar^{Tol_2}], 7.27 [d, $^3J_{H\text{-}H}$ = 8, 4H of Ar^{Tol_2}]. $^{13}C\{^1H\}$ NMR (C_6D_6): 21.2 [s, 2C of Me of Ar^{Tol_2}], 104.8 [s, 1C of Ar^{Tol_2}], 129.0 [s, 3C of Ar^{Tol_2}], 129.7 [s, 4C of Ar^{Tol_2}], 137.2 [s, 2C of Ar^{Tol_2}], 143.5 [s, 2C of Ar^{Tol_2}], 148.9 [s, 2C of Ar^{Tol_2}].

6.15.9 Synthesis of [Ar^{Tol_2}]Li

A stirred suspension of [Ar^{Tol_2}]I (5.0 g, 0.013 mol) in pentane (50 mL) was cooled to –78 ˚C and treated slowly with a solution of Bu^nLi in hexanes (6.77 mL, 2.5 M, 0.017 mol) over a period of 10 minutes. The mixture was allowed to warm to room temperature over a period of approximately 40 minutes, after which period the volatile components

were removed *in vacuo*. The resulting white waxy solid was washed with pentane (2 × 50 mL) and dried *in vacuo* to give [Ar^{Tol_2}]Li as a fine white powder (3.4 g, 99% yield).

^{1}H NMR (C_6D_6): 2.04 [s, 6H of Me of Ar^{Tol_2}], 6.78 [d, $^3J_{H\text{-}H}$ = 8, 4H of Ar^{Tol_2}], 7.34 [d, $^3J_{H\text{-}H}$ = 8, 4H of Ar^{Tol_2} and 1H of Ar^{Tol_2} located by COSY], 7.43 [d, $^3J_{H\text{-}H}$ = 8, 2H of Ar^{Tol_2}]. $^{13}C\{^1H\}$ NMR (C_6D_6): 20.9 [s, 2C of Me of Ar^{Tol_2}], 124.4 [s, 2C of Ar^{Tol_2}], 126.5 [s, 1C of Ar^{Tol_2}], 126.9 [s, 4C of Ar^{Tol_2}], 131.0 [br s, 4C of Ar^{Tol_2}], 136.4 [s, 2C of Ar^{Tol_2}], 144.7 [s, 2C of Ar^{Tol_2}], 152.1 [s, 2C of Ar^{Tol_2}], 175.4 [s, 1C of Ar^{Tol_2}, not observed, located using 2D HMBC].

6.15.10 Synthesis of [Ar^{Tol_2}]$TaMe_3Cl$

A pale yellow solution of $TaMe_3Cl_2$ (60 mg, 0.20 mmol) in Et_2O (1 mL) at –15 ˚C was treated with a suspension of [Ar^{Tol_2}]Li (60 mg, 0.23 mmol) and Et_2O (2 mL) at –15 ˚C resulting in the immediate formation of a dark brown suspension. The volatile components were removed *in vacuo* resulting in a brown solid that was washed with pentane (3 × 1 mL), and then extracted into benzene (2 × 0.5 mL). The solution was lyophilized to give [Ar^{Tol_2}]$TaMe_3Cl$ as an orange brown powder (22 mg, 21% yield). X-ray quality crystals were obtained from slow evaporation of a solution in pentane at room temperature. Anal. Calcd.: C, 53.24%, H, 5.05%. Found: C, 54.06%, H, 5.04%.

^{1}H NMR (C_6D_6): 0.86 [s, 9H of $Ta\underline{Me}_3$], 2.09 [s, 6H of Me of Ar^{Tol_2}], 7.06 [d, $^3J_{H\text{-}H}$ = 7, 4H of Ar^{Tol_2}], 7.22 [t, $^3J_{H\text{-}H}$ = 8, 1H of Ar^{Tol_2}], 7.31 [d, $^3J_{H\text{-}H}$ = 8, 2H of Ar^{Tol_2}], 7.72 [d, $^3J_{H\text{-}H}$ = 7, 4H of Ar^{Tol_2}]. $^{13}C\{^1H\}$ NMR (C_6D_6): 21.2 [s, 2C of Me of Ar^{Tol_2}], 86.4 [very br, 3C of $Ta\underline{Me}_3$, supported by HSQC spectroscopy], 129.1 [s, 2C of Me of Ar^{Tol_2}], 130.4 [s, 4C of Me of Ar^{Tol_2}], 131.4 [s, 1C of Me of Ar^{Tol_2}], 131.4 [s, 4C of Me of Ar^{Tol_2}], 138.1 [s, 2C of Me of Ar^{Tol_2}], 139.2 [s, 2C of Me of Ar^{Tol_2}], 145.1 [s, 2C of Me of Ar^{Tol_2}], 216.1 [s, 1C of Me of Ar^{Tol_2}].

6.15.11 Decomposition of $[Ar^{Tol_2}]TaMe_3Cl$ to $[Ar^{Tol_2}]TaMe_2Cl_2$

A solution of $[Ar^{Tol_2}]TaMe_3Cl$ in d_6-benzene decomposes at room temperature to produce, *inter alia*, $[Ar^{Tol_2}]TaMe_2Cl_2$ and methane over a period of several days. X-ray quality crystals were obtained from a solution in pentane at –15 ˚C.

^{1}H NMR (C_6D_6): 1.06 [s, 6H of Ta<u>Me</u>$_2$], 2.06 [s, 6H of Me of Ar^{Tol_2}], 6.98 [d, $^3J_{H\text{-}H}$ = 8, 4H of Ar^{Tol_2}], 7.16 [1H of Ar^{Tol_2}, under C_6D_5H signal], 7.22 [d, $^3J_{H\text{-}H}$ = 7, 2H of Ar^{Tol_2}], 7.67 [d, $^3J_{H\text{-}H}$ = 8, 4H of Ar^{Tol_2}].

6.15.12 Synthesis of $[\kappa^3\text{-}Ar^{Tol'_2}]Ta(PMe_3)_2MeCl$

A solution of $Ta(PMe_3)_2Me_3Cl_2$ (50 mg, 0.11 mmol) in d_6-benzene (*ca*. 1 mL) in a vial was treated with $[Ar^{Tol_2}]Li$ (50 mg, 0.19 mmol). After 5 minutes, the mixture was filtered through celite into an NMR tube equipped with a J. Young valve and then allowed to sit at room temperature for 12 hours. After this period, the mixture was lyophilized, washed with pentane (3 × 1 mL), extracted into d_6-benzene (2 × 0.5 mL), and filtered through celite. The filtrate was analyzed by ^{1}H and ^{31}P{^{1}H} NMR spectroscopy, thereby demonstrating the formation of $[\kappa^3\text{-}Ar^{Tol'_2}]Ta(PMe_3)_2MeCl$. The solution was lyophilized to give $[\kappa^3\text{-}Ar^{Tol'_2}]Ta(PMe_3)_2MeCl$ as an orange brown powder (34 mg, 48% yield). X-ray quality crystals were obtained from a solution in pentane at –15 ˚C. It should be noted, however, that the methyl and chloride ligands are disordered. Furthermore, in solution, $[\kappa^3\text{-}Ar^{Tol'_2}]Ta(PMe_3)_2MeCl$ is in equilibrium with $[\kappa\ ^3\text{-}Ar^{Tol'_2}]Ta(PMe_3)_2Cl_2$ and $[\kappa^3\text{-}Ar^{Tol'_2}]Ta(PMe_3)_2Me_2$ ($K \approx 5 \times 10^{-2}$). The disorder was modeled such that the Ta-Me and the Ta-Cl ligands each have a total occupancy of 1. Anal. Calcd.: C, 50.76%, H, 5.68%. Found: C, 50.03%, H, 5.41%.

^{1}H NMR (C_6D_6): 0.42 [d, $^2J_{P\text{-}H}$ = 9, 9H of (P<u>Me</u>$_3$)$_2$], 0.53 [d, $^2J_{P\text{-}H}$ = 9, 9H of (P<u>Me</u>$_3$)$_2$], 2.00 [d, $^3J_{P\text{-}H}$ = 12, 3H of Ta<u>Me</u>], 2.23 [s, 6H of Me of $Ar^{Tol'_2}$], 7.08 [d, $^3J_{H\text{-}H}$ = 7, 2H of $Ar^{Tol'_2}$], 7.36 [t, $^3J_{H\text{-}H}$ = 8, 1H of $Ar^{Tol'_2}$], 7.62 [d, $^3J_{H\text{-}H}$ = 8, 2H of $Ar^{Tol'_2}$], 7.75 [d, $^3J_{H\text{-}H}$ = 7, 2H of

$Ar^{Tol'_2}$], 7.82 [s, 2H of $Ar^{Tol'_2}$]. $^{31}P\{^1H\}$ NMR (C_6D_6): 9.0 [d, $^2J_{P\text{-}P}$ = 10, 1P of ($\underline{P}Me_3)_2$], 17.3 [d, $^2J_{P\text{-}P}$ = 10, 1P of ($\underline{P}Me_3)_2$]. $^{13}C\{^1H\}$ NMR (C_6D_6): 14.5 [d, $^1J_{P\text{-}C}$ = 24, 3C of ($P\underline{Me}_3)_2$], 15.0 [d, $^1J_{P\text{-}C}$ = 25, 3C of ($P\underline{Me}_3)_2$], 21.8 [s, 2C of Me of $Ar^{Tol'_2}$], 75.9 [dd, $^2J_{P\text{-}C}$ = 13, $^2J_{P\text{-}C}$ = 9, 1C of Ta$\underline{Me}$], 119.4 [t, $J_{P\text{-}C}$ = 3, 2C of $Ar^{Tol'_2}$], 121.3 [s, 2C of $Ar^{Tol'_2}$], 128.0 [s, 1C of $Ar^{Tol'_2}$, under C_6D_6, located by HSQC spectroscopy], 129.1 [s, 2C of $Ar^{Tol'_2}$], 133.5 [s, 2C of $Ar^{Tol'_2}$], 139.9 [s, 2C of $Ar^{Tol'_2}$], 152.8 [s, 2C of $Ar^{Tol'_2}$], 156.4 [t, $^2J_{P\text{-}C}$ = 3, 2C of $Ar^{Tol'_2}$], 198.8 [dd, $^2J_{P\text{-}C}$ = 26, $^2J_{P\text{-}C}$ = 19, 1C of $Ar^{Tol'_2}$], 204.8 [dd, $^2J_{P\text{-}C}$ = 11, $^2J_{P\text{-}C}$ = 8, 2C of $Ar^{Tol'_2}$].

6.15.13 Reaction between $Ta(PMe_3)_2(CD_3)_3Cl_2$ and $[Ar^{Tol_2}]Li$

(a) A solution of $Ta(PMe_3)_2(CD_3)_3Cl_2$ (20 mg, 0.04 mmol) in d_6-benzene (*ca*. 0.7 mL) in a vial was treated with $[Ar^{Tol_2}]Li$ (18 mg, 0.07 mmol) and filtered quickly through celite into an NMR tube equipped with a J. Young valve that was closed following the transfer. The solution was analyzed by ^1H NMR spectroscopy, thereby demonstrating the rapid formation of CD_3H. In addition, there were no signals attributable to the methyl groups of $[\kappa^3\text{-}Ar^{Tol'_2}]Ta(PMe_3)_2Me_2$ and $[\kappa^3\text{-}Ar^{Tol'_2}]Ta(PMe_3)_2MeCl$, consistent with the presence of $[\kappa^3\text{-}Ar^{Tol'_2}]Ta(PMe_3)_2(CD_3)_2$ and $[\kappa^3\text{-}Ar^{Tol'_2}]Ta(PMe_3)_2(CD_3)Cl$ isotopologues.

(b) A solution of $Ta(PMe_3)_2(CD_3)_3Cl_2$ (20 mg, 0.04 mmol) in benzene (*ca*. 0.7 mL) in a vial was treated with $[Ar^{Tol_2}]Li$ (18 mg, 0.07 mmol). The vial was capped with a suba seal, shaken for 1 minute and then allowed to stand at room temperature for 30 minutes. The gas above the solution was then collected using a 1 mL gastight microsyringe and injected into the mass spectrometer (Electron Ionization (EI) method, 70 eV ionization energy through gas inlet reservoir; HX110 double focusing mass spectrometer JEOL ltd. Tokyo, Japan). The spectra displayed a signal at m/z = 19 (CD_3H), and no signal at m/z = 20 (CD_4), thereby providing further evidence for the presence of CD_3H, with no

evidence for CD_4. After the first analysis, another 1 mL of gas was collected and the experiment was repeated, giving consistent results.

6.15.14 Reaction between $Ta[P(CD_3)_3]_2Me_3Cl_2$ and $[Ar^{Tol}{}_2]Li$

(a) A solution of $Ta[P(CD_3)_3]_2Me_3Cl_2$ (20 mg, 0.04 mmol) in d_6-benzene (*ca*. 0.7 mL) was treated with $[Ar^{Tol}{}_2]Li$ (18 mg, 0.07 mmol). The mixture was shaken for 1 minute, filtered through celite into an NMR tube equipped with a J. Young valve and allowed to stand at room temperature for 12 hours. The solution was analyzed by ^1H NMR spectroscopy, thereby demonstrating the formation of $[\kappa^3\text{-}Ar^{Tol'}{}_2]Ta[P(CD_3)_3]_2MeCl$.

(b) The above solution of $[\kappa^3\text{-}Ar^{Tol'}{}_2]Ta[P(CD_3)_3]_2MeCl$ was treated with PMe_3 (0.05 mL) and monitored by ^1H NMR spectroscopy, thereby demonstrating $PMe_3/P(CD_3)_3$ exchange over a period of 12 hours.

6.15.15 Conversion of $[Ar^{Tol}{}_2]TaMe_3Cl$ to $[\kappa^3\text{-}Ar^{Tol'}{}_2]Ta(PMe_3)_2MeCl$

A solution of $[Ar^{Tol}{}_2]TaMe_3Cl$ (22 mg, 0.04 mmol) in d_6-benzene in an NMR tube equipped with a J. Young valve was treated with PMe_3 (*ca*. 0.05 mL) *via* vapor transfer. The reaction was monitored by ^1H and $^{31}P\{^1H\}$ NMR spectroscopy, thereby demonstrating the formation of $[\kappa^3\text{-}Ar^{Tol'}{}_2]Ta(PMe_3)_2MeCl$ as the major product, in addition to a small quantity of $Ar^{Tol}{}_2H$ (< 10%). The sample was lyophilized, washed with pentane (2 × 1 mL), and extracted into benzene (2 × 0.5 mL). The solution was lyophilized to give $[\kappa^3\text{-}Ar^{Tol'}{}_2]Ta(PMe_3)_2MeCl$ as an orange powder (17 mg, 63% yield).

6.15.16 Reaction between $[Ar^{Tol}{}_2]Ta(CD_3)_3Cl$ and PMe_3

A solution of $Ta(CD_3)_3Cl_2$ (20 mg, 0.07 mmol) in d_6-benzene (*ca*. 0.7 mL) was treated with $[Ar^{Tol}{}_2]Li$ (18 mg, 0.07 mmol). The mixture was shaken for 1 minute and then filtered

through celite into an NMR tube equipped with a J. Young valve. The sample was analyzed by ^{1}H NMR spectroscopy demonstrating the immediate conversion to, *inter alia*, [Ar$^{Tol}_2$]Ta(CD$_3$)$_3$Cl. PMe$_3$ (0.05 mL) was added *via* vapor transfer and the solution analyzed by ^{1}H NMR spectroscopy, thereby demonstrating the immediate formation of CD$_3$H. In addition, there were no signals attributable to the methyl groups of [κ^3-Ar$^{Tol'}_2$]Ta(PMe$_3$)$_2$Me$_2$ and [κ^3-Ar$^{Tol'}_2$]Ta(PMe$_3$)$_2$MeCl, consistent with the presence of [κ^3-Ar$^{Tol'}_2$]Ta(PMe$_3$)$_2$(CD$_3$)$_2$ and [κ^3-Ar$^{Tol'}_2$]Ta(PMe$_3$)$_2$(CD$_3$)Cl isotopologues.

6.15.17 Synthesis of [κ^3-Ar$^{Tol'}_2$]Ta(PMe$_3$)$_2$Cl$_2$

A solution of [κ^3-Ar$^{Tol'}_2$]Ta(PMe$_3$)$_2$MeCl (25 mg, 0.04 mmol) in d_6-benzene (*ca*. 0.7 mL) in an NMR tube equipped with a J. Young valve was treated with a suspension of ZnCl$_2$ (25 mg, 0.18 mmol) in Et$_2$O (*ca*. 0.1 mL). The sample was lyophilized after 1 hour, extracted into benzene and filtered into an NMR tube. The sample was treated with PMe$_3$ (*ca*. 0.05 mL) and analyzed by ^{1}H NMR spectroscopy, thereby demonstrating the formation of [κ^3-Ar$^{Tol'}_2$]Ta(PMe$_3$)$_2$Cl$_2$. The sample was then lyophilized and the residue obtained was washed with pentane (1 mL), extracted into benzene (2 × 0.7 mL) and lyophilized to give [κ^3-Ar$^{Tol'}_2$]Ta(PMe$_3$)$_2$Cl$_2$ as a red powder (11 mg, 42 %yield). X-ray quality crystals of [κ^3-Ar$^{Tol'}_2$]Ta(PMe$_3$)$_2$Cl$_2$ were obtained from a solution in pentane at –15 ˚C. Anal. Calcd.: C, 47.4%, H, 5.0%. Found: C, 47.6%, H, 4.8%.

^{1}H NMR (C$_6$D$_6$): 0.54 [d, $^2J_{P\text{-}H}$ = 10, 18H of (P$\underline{\text{Me}}_3$)$_2$], 2.16 [s, 6H of Me of Ar$^{Tol'}_2$], 7.08 [d, $^3J_{H\text{-}H}$ = 8, 2H of Ar$^{Tol'}_2$], 7.32 [t, $^3J_{H\text{-}H}$ = 8, 1H of Ar$^{Tol'}_2$], 7.61 [d, $^3J_{H\text{-}H}$ = 8, 2H of Ar$^{Tol'}_2$], 7.70 [d, $^3J_{H\text{-}H}$ = 7, 2H of Ar$^{Tol'}_2$], 8.27 [s, 2H of Ar$^{Tol'}_2$]. ^{31}P{^{1}H} NMR (C$_6$D$_6$): 20.2 [s, 2P of ($\underline{\text{P}}$Me$_3$)$_2$]. ^{13}C{^{1}H} NMR (C$_6$D$_6$): 15.5 [apparent doublet, $^1J_{P\text{-}C}$ = 27.75, $^2J_{P\text{-}P}$ = 3.0, $^3J_{P\text{-}C}$ = 0, $\delta_{P\text{-}P}$ = 0.022 (see below for simulation), 6C of (P$\underline{\text{Me}}_3$)$_2$], 21.7 [s, 2C of Me of Ar$^{Tol'}_2$], 120.3 [s, 2C of Ar$^{Tol'}_2$], 121.2 [s, 2C of Ar$^{Tol'}_2$], 128.0 [s, 1C of Ar$^{Tol'}_2$, under C$_6$D$_6$, located by HSQC spectroscopy], 130.4 [s, 2C of Ar$^{Tol'}_2$], 133.9 [s, 2C of Ar$^{Tol'}_2$], 141.6 [s, 2C of Ar$^{Tol'}_2$],

152.0 [s, 2C of $Ar^{Tol'_2}$], 156.6 [s, 2C of $Ar^{Tol'_2}$], 201.5 [t, $^2J_{P-C}$ = 25, 1C of $Ar^{Tol'_2}$], 206.4 [t, $^2J_{P-C}$ = 9, 2C of $Ar^{Tol'_2}$].

6.15.18 Synthesis of $[\kappa^3\text{-}Ar^{Tol'_2}]Ta(PMe_3)_2Me_2$

(a) A solution of $Ta(PMe_3)_2Me_3Cl_2$ (50mg, 0.11 mmol) in d_6-benzene (*ca*. 1 mL) in a vial was treated with $[Ar^{Tol_2}]Li$ (50mg, 0.19 mmol). After 5 minutes, the mixture was filtered through celite into an NMR tube equipped with a J. Young valve and then allowed to sit at room temperature for 12 hours to generate $[\kappa^3\text{-}Ar^{Tol'_2}]Ta(PMe_3)_2MeCl$. After this period, MeMgBr (20 mg, 0.17 mmol) was added, the tube was shaken, and allowed to sit at room temperature for 4 hours. The mixture was then lyophilized and the residue obtained was washed with pentane (3 × 1 mL) and extracted into benzene (2 × 0.5 mL). The solution was lyophilized to give $[\kappa^3\text{-}Ar^{Tol'_2}]Ta(PMe_3)_2Me_2$ as an orange brown powder (32 mg, 46% yield). X-ray quality crystals of $[\kappa^3\text{-}Ar^{Tol'_2}]Ta(PMe_3)_2Me_2$ were obtained from a solution in pentane at –15 °C.

^{1}H NMR (C_6D_6): 0.46 [m, 18H of $(P\underline{Me}_3)_2$], 1.73 [m, 6H of $Ta\underline{Me}_2$], 2.29 [s, 6H of Me of $Ar^{Tol'_2}$], 7.10 [d, $^3J_{H-H}$ = 8, 2H of $Ar^{Tol'_2}$], 7.37 [t, $^3J_{H-H}$ = 8, 1H of $Ar^{Tol'_2}$], 7.61 [d, $^3J_{H-H}$ = 8, 2H of $Ar^{Tol'_2}$], 7.67 [s, 2H of $Ar^{Tol'_2}$], 7.77 [d, $^3J_{H-H}$ = 8, 2H of $Ar^{Tol'_2}$]. $^{31}P\{^1H\}$ NMR (C_6D_6): 6.9 [s, 2P of $(\underline{P}Me_3)_2$]. $^{13}C\{^1H\}$ NMR (C_6D_6): 14.3 [m, 6C of $(P\underline{Me}_3)_2$], 21.9 [s, 2C of Me of $Ar^{Tol'_2}$], 77.7 [m, 2C of $Ta\underline{Me}_2$], 118.7 [t, J_{P-C} = 3, 2C of $Ar^{Tol'_2}$], 121.3 [s, 2C of $Ar^{Tol'_2}$], 127.6 [t, J_{P-C} = 3, 2C of $Ar^{Tol'_2}$], 128.0 [s, 1C of $Ar^{Tol'_2}$, under C_6D_6, located by HSQC spectroscopy], 133.2 [s, 2C of $Ar^{Tol'_2}$], 138.1 [s, 2C of $Ar^{Tol'_2}$], 153.6 [s, 2C of $Ar^{Tol'_2}$], 156.9 [t, J_{P-C} = 3, 2C of $Ar^{Tol'_2}$], 198.2 [t, $^2J_{P-C}$ = 21, 1C of $Ar^{Tol'_2}$], 206.9 [t, $^2J_{P-C}$ = 8, 2C of $Ar^{Tol'_2}$].

(b) A mixture of $[\kappa^3\text{-}Ar^{Tol'_2}]Ta(PMe_3)_2Cl_2$ (10 mg, 0.02 mmol) and MeMgBr (4 mg, 0.03 mmol) in an NMR tube equipped with a J. Young valve was treated with d_6-benzene (*ca*. 0.7 mL) and Et_2O (*ca*. 0.05 mL). The reaction was monitored by ^{1}H NMR spectroscopy,

thereby demonstrating conversion to [κ^3-Ar$^{Tol'2}$]Ta(PMe$_3$)$_2$Me$_2$ over a period of less than 10 minutes.

6.15.19 Synthesis of (^{13}CH$_3$)MgI•(Et$_2$O)$_{1.5}$

A stirred suspension of Mg turnings (0.85 g, 35.0 mmol) in Et$_2$O (7 mL) was treated with ^{13}CH$_3$I (1.0 g, 7.0 mmol) and stirred for 2 hours at room temperature. After this period, the mixture was filtered and the volatile components were removed from the filtrate *in vacuo* to give (^{13}CH$_3$)MgI•(Et$_2$O)$_{1.5}$ as a white powder (1.20 g, 62% yield).

^{1}H NMR (C$_6$D$_6$): –0.41 [d, ^{1}J$_{C\text{-}H}$ = 105, 3H of ^{13}C<u>H</u>$_3$MgI], 0.78 [t, ^{3}J$_{H\text{-}H}$ = 7, 9H of (Et$_2$O)$_{1.5}$], 3.36 [q, ^{3}J$_{H\text{-}H}$ = 7, 6H of (Et$_2$O)$_{1.5}$]. ^{13}C{^{1}H} NMR (C$_6$D$_6$): –9.2 [s, 1C of ^{13}<u>C</u>H$_3$MgI], 14.1 [s, 3C of (Et$_2$O)$_{1.5}$], 66.7 [s, 3C of (Et$_2$O)$_{1.5}$].

6.15.20 Synthesis of [κ^3-Ar$^{Tol'2}$]Ta(PMe$_3$)$_2$(^{13}CH$_3$)$_2$

A mixture of [κ^3-Ar$^{Tol'2}$]Ta(PMe$_3$)$_2$Cl$_2$ (10 mg, 0.02 mmol) and (^{13}CH$_3$)MgI•(Et$_2$O)$_{1.5}$ (5 mg, 0.02 mmol) in an NMR tube equipped with a J. Young valve was treated with d$_6$-benzene (*ca*. 0.7 mL). The reaction was monitored by ^{1}H NMR spectroscopy, thereby demonstrating conversion to [κ^3-Ar$^{Tol'2}$]Ta(PMe$_3$)$_2$(^{13}CH$_3$)$_2$ over a period of less than 10 minutes. The mixture was lyophilized and the residue was extracted into d_6-benzene for analysis by multinuclear NMR spectroscopy.

Selected ^{1}H NMR (C$_6$D$_6$): 1.72 [dm, ^{1}J$_{C\text{-}H}$ = 117, 6H of Ta(^{13}C<u>H</u>$_3$)$_2$].

6.15.21 Synthesis of [κ^3-Ar$^{Tol'2}$]Ta(PMe$_3$)$_2$(^{13}CH$_3$)$_{2-x}$(Me)$_x$

A mixture of [κ^3-Ar$^{Tol'2}$]Ta(PMe$_3$)$_2$MeCl (10 mg, 0.02 mmol) and (^{13}CH$_3$)MgI•(Et$_2$O)$_{1.5}$ (3 mg, 0.01 mmol) an NMR tube equipped with a J. Young valve was treated with d_6-benzene (*ca*. 0.7 mL). The reaction was monitored by ^{1}H NMR spectroscopy, thereby demonstrating conversion to a mixture of isotopologues, [κ^3-

$Ar^{Tol'_2}]Ta(PMe_3)_2(^{13}CH_3)_{2-x}(Me)_x$ (x = 0, 1, 2), over a period of less than 10 minutes. The mixture was lyophilized and the residue obtained was extracted into d_6-benzene for analysis by multinuclear NMR spectroscopy. Simulation of the $^{13}C\{^1H\}$ and $^{31}P\{^1H\}$ NMR spectra (see supporting information) identified that the mixture of isopologues consisted of $[\kappa^3\text{-}Ar^{Tol'_2}]Ta(PMe_3)_2(^{13}CH_3)_2$ (25 %), $[\kappa^3\text{-}Ar^{Tol'_2}]Ta(PMe_3)_2(^{13}CH_3)(^{12}CH_3)$ (50 %) and $[\kappa^3\text{-}Ar^{Tol'_2}]Ta(PMe_3)_2(^{12}CH_3)_2$ (25 %).

Selected ^1H NMR (C_6D_6) for the mixture of three isotopologues: 1.72 [dm, $^1J_{C\text{-}H}$ = 117, 6H of $Ta(^{13}C\underline{H}_3)_2$]; 1.72 [dm, $^1J_{C\text{-}H}$ = 117, 3H of $Ta(^{13}C\underline{H}_3)Me$], 1.72 [m, 3H of $Ta(^{13}CH_3)\underline{Me}$]; 1.72 [m, 6H of $Ta\underline{Me}_2$].

6.15.22 Synthesis of $[\kappa^3\text{-}Ar^{Tol'_2}]Ta(PMe_3)_2(\eta^6\text{-}C_6H_6)$

A solution of $[\kappa^3\text{-}Ar^{Tol'_2}]Ta(PMe_3)_2Cl_2$ (30 mg, 0.05 mmol) in benzene (*ca*. 1 mL) in a vial equipped with a stir bar was treated with KC_8 (30 mg, 0.22 mmol). The resulting mixture was stirred for 1 hour, filtered, and the filtrate was lyophilized. The sample was extracted into pentane (1 mL), and cooled at –15 ˚C thereby depositing red crystals of $[\kappa^3\text{-}Ar^{Tol'_2}]Ta(PMe_3)_2(\eta^6\text{-}C_6H_6)$ (*ca.* 3 mg), in addition to colorless crystals of $[Ar^{Tol_2}]H$. X-ray quality crystals of $[\kappa^3\text{-}Ar^{Tol'_2}]Ta(PMe_3)_2(\eta^6\text{-}C_6H_6)$ were obtained from a solution in hexane at –15 ˚C.

^1H NMR (C_6D_6): 0.27 [vt, $^2J_{P\text{-}H}$ = 8, 18H of $(P\underline{Me}_3)_2$], 2.44 [s, 6H of Me of $Ar^{Tol'_2}$], 4.10 [t, $J_{P\text{-}H}$ = 2, 6H of $(\eta^6\text{-}C_6\underline{H}_6)$], 7.11 [d, $^3J_{H\text{-}H}$ = 8, 2H of $Ar^{Tol'_2}$], 7.43 [m, 3H of $Ar^{Tol'_2}$], 7.81 [d, $^3J_{H\text{-}H}$ = 8, 2H of $Ar^{Tol'_2}$], 7.93 [d, $^3J_{H\text{-}H}$ = 8, 2H of $Ar^{Tol'_2}$]. $^{31}P\{^1H\}$ NMR (C_6D_6): –29.3 [s, 2P of $(\underline{P}Me_3)_2$]. Selected $^{13}C\{^1H\}$ NMR located by 2D HSQC experiment (C_6D_6): 98.7 [6C of $(\eta^6\text{-}\underline{C}_6H_6)$], 16.2 [6C of $(P\underline{Me}_3)_2$].

6.15.23 Structural characterization of $[\eta^2,\eta^2\text{-}Ar^{Tol(CO),Tol(Me_3PCO)}]Ta(PMe_3)_2Cl_2$ and $[\kappa^2,\eta^2\text{-}Ar^{Tol',Tol(Me_3PCO)}]Ta(PMe_3)Cl_2$

A solution of $[\kappa^3\text{-}Ar^{Tol'_2}]Ta(PMe_3)_2Cl_2$ (10 mg, 0.02 mmol) in d_6-benzene (*ca*. 0.7 mL) was added to an NMR tube equipped with a J. Young valve. The sample was then treated consecutively with PMe_3 (*ca*. 0.01 mL) and CO (1 atm), and allowed to stand at room temperature for *ca*. 2 days. The sample was then lyophilized, extracted with Et_2O (*ca*. 1 mL), filtered into a vial and cooled to –15 ˚C, thereby depositing two different sets of crystals: yellow blocks and purple plates. Both sets were analyzed by X-ray diffraction, thereby identifying that the yellow blocks were $[\eta^2,\eta^2\text{-}Ar^{Tol(CO),Tol(Me_3PCO)}]Ta(PMe_3)_2Cl_2$ and the purple plates were $[\kappa^2,\eta^2\text{-}Ar^{Tol',Tol(Me_3PCO)}]Ta(PMe_3)Cl_2$.

6.15.24 Structural characterization of $[\kappa^3\text{-}Ar^{Tol'_2}]Ta(PMe_3)_2(\kappa^2\text{-}C_4H_8)$

A solution of $[\kappa^3\text{-}Ar^{Tol'_2}]Ta(PMe_3)_2Cl_2$ (20 mg, 0.03 mmol) in benzene (*ca*. 1 mL) was added to an NMR tube equipped with a J. Young valve. KC_8 (20 mg, 0.15 mmol) was then added to the top of the tube, but was not mixed into the solution. The sample was then treated with ethylene (1 atm), allowed to stand at room temperature for *ca*. 10 minutes, after which period the KC_8 was mixed into the solution. The resulting mixture was shaken vigorously, allowed to stand at room temperature for *ca*. 1 day, and then lyophilized. The sample was then extracted into pentane (1 mL), filtered, and cooled at –15 ˚C thereby depositing yellow crystals of $[\kappa^3\text{-}Ar^{Tol'_2}]Ta(PMe_3)_2(\kappa^2\text{-}C_4H_8)$, which were analyzed by X-ray diffraction.

6.15.25 Structural characterization of $[[\kappa^3\text{-}Ar^{Tol'_2}]Ta(PMe_3)Np(=CHCMe_3)][LiPMe_3]$

A solution of $[\kappa^3\text{-}Ar^{Tol'_2}]Ta(PMe_3)_2MeCl$ (10 mg, 0.02 mmol) in d_6-benzene (*ca*. 0.7 mL) was added to an NMR tube equipped with a J. Young valve and treated with NpLi (5 mg, 0.06 mmol). The sample was allowed to stand at room temperature for *ca*. 1 day

and was then lyophilized. The resulting dark powder was extracted with pentane (*ca*. 1 mL), filtered into a vial and cooled to –15 ˚C, thereby depositing yellow crystals [[κ^3-$Ar^{Tol'_2}$]Ta(PMe_3)Np(=$CHCMe_3$)][$LiPMe_3$], which were analyzed by X-ray diffraction.

6.15.26 Synthesis of $NbMe_3Cl_2$

The synthesis of $NbMe_3Cl_2$ was adapted from the literature method.[23] A suspension of $NbCl_5$ (2.0 g, 7.4 mmol) in pentane (20 mL) was treated with a solution of Me_2Zn (1.0 mL, 14.8 mmol) in pentane (5 mL) over a period of 10 minutes. The suspension was stirred for 3 hours, after which period the mixture was filtered. The volatile components were removed from the filtrate *in vacuo* to give $NbMe_3Cl_2$ as a yellow-orange crystalline solid (1.07 g, 69% yield). Crystals of $TaMe_3Cl_2$, suitable for X-ray diffraction studies, were obtained by cooling a solution of $NbMe_3Cl_2$ in pentane at –15 ˚C.

6.15.27 Structural characterization of $Nb(PMe_3)_2Me_3Cl_2$

A solution of $NbMe_3Cl_2$ (200 mg, 0.96 mmol) in pentane (10 mL) was frozen in a liquid nitrogen bath and treated with PMe_3 (0.25 mL, 2.4 mmol) *via* vapor transfer. The mixture was allowed to warm to room temperature, producing a blood red suspension, which was allowed to stand at room temperature for *ca*. 10 minutes. The volatile components were then removed *in vacuo* giving a blood red powder identified. Bright red crystals of $Nb(PMe_3)_2Me_3Cl_2$, suitable for X-ray diffraction studies, were obtained by cooling a solution of $Nb(PMe_3)_2Me_3Cl_2$ in pentane at –15 ˚C.

6.16 Crystallographic data

Table 7. Crystal, intensity collection and refinement data.

	$TaMe_3Cl_2$	$Ta(PMe_3)_2Me_3Cl_2$
lattice	Hexagonal	Monoclinic
formula	$C_3H_9Cl_2Ta$	$C_9H_{27}Cl_2P_2Ta$
formula weight	296.95	449.10
space group	$P6_3/mmc$	$C2/c$
a / Å	7.431(2)	25.613(3)
b / Å	7.431(2)	9.3349(9)
c / Å	8.058(2)	13.9838(14)
α / °	90	90
β / °	90	98.2670(10)
γ / °	120	90
V / Å^3	385.36(19)	3308.7(6)
Z	2	8
temperature (K)	150(2)	170(2)
radiation (λ, Å)	0.71073	0.71073
ρ (calcd.) g cm^{-3}	2.559	1.803
μ (Mo Kα), mm^{-1}	14.841	7.132
θ max, deg.	31.43	31.51
no. of data collected	5998	27366
no. of data	273	5509
no. of parameters	10	137
R_1 [$I > 2\sigma(I)$]	0.0128	0.0207
wR_2 [$I > 2\sigma(I)$]	0.0325	0.0422
R_1 [all data]	0.0141	0.0278
wR_2 [all data]	0.0333	0.0444
GOF	1.245	1.042

Table 7 (cont). Crystal, intensity collection and refinement data.

	[Ar$^{Tol}_2$]I	**[Ar$^{Tol}_2$]TaMe$_3$Cl**
lattice	Orthorhombic	Monoclinic
formula	$C_{20}H_{17}I$	$C_{23}H_{26}ClTa$
formula weight	384.24	518.84
space group	$P2_12_12_1$	$P2_1/n$
a / Å	7.5927(5)	7.0053(8)
b / Å	19.6428(13)	18.055(2)
c / Å	21.5544(14)	16.2693(18)
α / °	90	90
β / °	90	91.585(2)
γ / °	90	90
V / Å^3	3214.7(4)	2057.0(4)
Z	8	4
temperature (K)	125(2)	170(2)
radiation (λ, Å)	0.71073	0.71073
ρ (calcd.) g cm^{-3}	1.588	1.675
μ (Mo Kα), mm^{-1}	1.984	5.476
θ max, deg.	30.51	31.00
no. of data collected	51962	25434
no. of data	9789	6516
no. of parameters	384	231
R_1 [$I > 2\sigma(I)$]	0.0247	0.0322
wR_2 [$I > 2\sigma(I)$]	0.0557	0.0630
R_1 [all data]	0.0287	0.0535
wR_2 [all data]	0.0575	0.0698
GOF	1.037	1.027

Table 7 (cont). Crystal, intensity collection and refinement data.

	$[\kappa^3\text{-}Ar^{Tol'_2}]Ta(PMe_3)_2MeCl$	$[\kappa^3\text{-}Ar^{Tol'_2}]Ta(PMe_3)_2Cl_2$
lattice	Monoclinic	Monoclinic
formula	$C_{27}H_{36}ClP_2Ta$	$C_{26}H_{33}Cl_2P_2Ta$
formula weight	638.90	659.31
space group	*C2/c*	*C2/c*
a / Å	26.179(3)	12.4272(17)
b / Å	13.3008(15)	12.8506(18)
c / Å	16.988(2)	16.636(2)
α / °	90	90
β / °	117.349(2)	102.338(2)
γ / °	90	90
V / Å^3	5254.1(10)	2595.4(6)
Z	8	4
temperature (K)	170(2)	170(2)
radiation (λ, Å)	0.71073	0.71073
ρ (calcd.) g cm^{-3}	1.615	1.687
μ (Mo Kα), mm^{-1}	4.420	4.577
θ max, deg.	31.50	32.02
no. of data collected	43742	22162
no. of data	8756	4492
no. of parameters	297	146
R_1 [$I > 2\sigma(I)$]	0.0320	0.0281
wR_2 [$I > 2\sigma(I)$]	0.0620	0.0557
R_1 [all data]	0.0603	0.0377
wR_2 [all data]	0.0721	0.0592
GOF	1.019	1.038

Table 7 (cont). Crystal, intensity collection and refinement data.

	$[\kappa^3\text{-}Ar^{Tol'_2}]Ta(PMe_3)_2Me_2$	$[Ar^{Tol_2}]TaMe_2Cl_2$
lattice	Monoclinic	Triclinic
formula	$C_{28}H_{39}P_2Ta$	$C_{22}H_{23}Cl_2Ta$
formula weight	618.48	539.25
space group	*C2/c*	*P-1*
a / Å	26.1350(19)	8.8509(9)
b / Å	13.3142(10)	8.9422(9)
c / Å	17.0189(13)	13.5025(13)
α / °	90	82.2550(10)
β / °	116.8610(10)	79.6780(10)
γ / °	90	80.4060(10)
V / Å^3	5283.1(7)	1030.60(18)
Z	8	2
temperature (K)	150(2)	170(2)
radiation (λ, Å)	0.71073	0.71073
ρ (calcd.) g cm^{-3}	1.555	1.738
μ (Mo Kα), mm^{-1}	4.295	5.594
θ max, deg.	30.63	31.51
no. of data collected	41940	17480
no. of data	8097	6764
no. of parameters	290	231
R_1 [$I > 2\sigma(I)$]	0.0410	0.0213
wR_2 [$I > 2\sigma(I)$]	0.0728	0.0475
R_1 [all data]	0.0819	0.0253
wR_2 [all data]	0.0865	0.0488
GOF	1.001	1.056

Table 7 (cont). Crystal, intensity collection and refinement data.

	$[Ar^{Tol}{}_2]MgBr_{0.66}Cl_{0.34}(THF)_2$	$[\kappa^3\text{-}Ar^{Tol'}{}_2]Ta(PMe_3)_2(\eta^6\text{-}C_6H_6)$
lattice	Triclinic	Triclinic
formula	$C_{28}H_{33}Br_{0.66}Cl_{0.34}MgO_2$	$C_{32}H_{39}P_2Ta$
formula weight	490.54	666.52
space group	*P-1*	*P-1*
a / Å	7.8735(9)	9.311(3)
b / Å	8.7919(10)	11.161(4)
c / Å	37.038(4)	14.008(5)
α / °	88.550(2)	90.704(4)
β / °	88.722(2)	97.034(4)
γ / °	89.755(2)	111.539(4)
V / Å^3	2562.4(5)	1341.4(8)
Z	4	2
temperature (K)	125(2)	150(2)
radiation (λ, Å)	0.71073	0.71073
ρ (calcd.) g cm^{-3}	1.272	1.650
μ (Mo Kα), mm^{-1}	1.152	4.236
θ max, deg.	30.64	31.51
no. of data collected	41974	22648
no. of data	15704	8812
no. of parameters	588	324
R_1 [$I > 2\sigma(I)$]	0.0555	0.0177
wR_2 [$I > 2\sigma(I)$]	0.1159	0.0443
R_1 [all data]	0.1009	0.0193
wR_2 [all data]	0.1309	0.0450
GOF	1.015	1.048

Table 7 (cont). Crystal, intensity collection and refinement data.

	$[\eta^2,\eta^2\text{-}Ar^{Tol(CO),Tol(Me_3PCO)}]\text{-}Ta(PMe_3)_2Cl_2$	$[\kappa^2,\eta^2\text{-}Ar^{Tol',Tol(Me_3PCO)}]\text{-}Ta(PMe_3)Cl_2$
lattice	Monoclinic	Monoclinc
formula	$C_{33}H_{47}Cl_2O_{2.5}P_3Ta$	$C_{31}H_{43}Cl_2O_2P_2Ta$
formula weight	828.47	761.44
space group	$P2_1/n$	$C2/c$
a/Å	9.8909(11)	34.016(4)
b/Å	16.0716(17)	11.0628(14)
c/Å	22.022(2)	17.126(2)
α/°	90	90
β/°	98.4210(10)	90.953(2)
γ/°	90	90
V/Å^3	3463.0(7)	6443.9(14)
Z	4	8
temperature (K)	150(2)	150(2)
radiation (λ, Å)	0.71073	0.71073
ρ (calcd.) g cm^{-3}	1.589	1.570
μ (Mo Kα), mm^{-1}	3.497	3.703
θ max, deg.	31.77	31.51
no. of data collected	59006	53688
no. of data	11762	10720
no. of parameters	405	306
R_1 [$I > 2\sigma(I)$]	0.0277	0.0353
wR_2 [$I > 2\sigma(I)$]	0.0555	0.0682
R_1 [all data]	0.0426	0.0580
wR_2 [all data]	0.0609	0.0736
GOF	1.021	1.009

Table 7 (cont). Crystal, intensity collection and refinement data.

	$[\kappa^3\text{-}Ar^{Tol'}{}_2]\text{-}Ta(PMe_3)_2(\kappa^2\text{-}C_4H_8)$	**$[[\kappa^3\text{-}Ar^{Tol'}{}_2]Ta(PMe_3)\text{-}Np(=CHCMe_3)][LiPMe_3]$**
lattice	Triclinic	Triclinic
formula	$C_{30}H_{41}P_2Ta$	$C_{36}H_{54}LiP_2Ta$
formula weight	644.52	736.62
space group	*P-1*	*P-1*
a/Å	9.0763(19)	10.9638(16)
b/Å	10.815(2)	11.2328(17)
c/Å	14.666(3)	15.545(2)
α/°	88.981(3)	85.984(2)
β/°	84.450(3)	88.165(2)
γ/°	69.130(3)	67.073(2)
V/Å^3	1338.6(5)	1758.8(5)
Z	2	2
temperature (K)	150(2)	150(2)
radiation (λ, Å)	0.71073	0.71073
ρ (calcd.) g cm^{-3}	1.599	1.391
μ (Mo Kα), mm^{-1}	4.242	3.237
θ max, deg.	30.25	30.55
no. of data collected	40901	28330
no. of data	7946	10718
no. of parameters	306	385
R_1 [$I > 2\sigma(I)$]	0.0573	0.0365
wR_2 [$I > 2\sigma(I)$]	0.1092	0.0706
R_1 [all data]	0.0896	0.0545
wR_2 [all data]	0.1184	0.0768
GOF	1.049	1.002

Table 7 (cont). Crystal, intensity collection and refinement data.

	$NbMe_3Cl_2$	$Nb(PMe_3)_2Me_3Cl_2$
lattice	Hexagonal	Monoclinic
formula	$C_3H_9Cl_2Nb$	$C_{8.61}H_{25.83}Cl_{2.39}NbP_2$
formula weight	208.91	369.02
space group	$P6_3/mmc$	$C2/c$
a / Å	7.403(4)	25.469(3)
b / Å	7.403(4)	9.3275(11)
c / Å	8.053(4)	13.9866(16)
α / °	90	90
β / °	90	98.302(2)
γ / °	120	90
V / Å^3	382.2(3)	3287.8(7)
Z	2	8
temperature (K)	150(2)	150(2)
radiation (λ, Å)	0.71073	0.71073
ρ (calcd.) g cm^{-3}	1.815	1.491
μ (Mo Kα), mm^{-1}	2.159	1.286
θ max, deg.	32.71	31.50
no. of data collected	6163	27164
no. of data	297	5472
no. of parameters	10	141
R_1 [$I > 2\sigma(I)$]	0.0243	0.0349
wR_2 [$I > 2\sigma(I)$]	0.0670	0.1062
R_1 [all data]	0.0275	0.0395
wR_2 [all data]	0.0680	0.1106
GOF	1.194	1.058

Table 7 (cont). Crystal, intensity collection and refinement data.

	$[Ar^{Tol}_2]NbMe_2Cl_2$	$[\kappa^3\text{-}Ar^{Tol'}_2]Nb(PMe_3)_2MeCl$
lattice	Triclinic	Monoclinic
formula	$C_{22}H_{23}Cl_2Nb$	$C_{27}H_{36}ClNbP_2$
formula weight	451.21	550.86
space group	*P-1*	*C2/c*
a / Å	8.8031(7)	26.157(5)
b / Å	8.9200(8)	13.288(3)
c / Å	13.5091(11)	16.989(18)
α / °	82.3730(10)	90
β / °	79.6980(10)	117.690(3)
γ / °	80.4600(10)	90
V / Å^3	1023.42(15)	5228.4(18)
Z	2	8
temperature (K)	150(2)	150(2)
radiation (λ, Å)	0.71073	0.71073
ρ (calcd.) g cm^{-3}	1.464	1.400
μ (Mo Kα), mm^{-1}	0.851	0.698
θ max, deg.	31.51	29.80
no. of data collected	17270	39816
no. of data	6705	7485
no. of parameters	230	297
R_1 [$I > 2\sigma(I)$]	0.0275	0.0502
wR_2 [$I > 2\sigma(I)$]	0.0709	0.0998
R_1 [all data]	0.0326	0.1107
wR_2 [all data]	0.0746	0.1224
GOF	1.033	1.019

Table 7 (cont). Crystal, intensity collection and refinement data.

	[κ³-Ar$^{Tol'_2}$]Nb(PMe$_3$)$_2$Me$_2$	**[κ³-Ar$^{Tol'_2}$]Nb(PMe$_3$)$_2$Cl$_2$**
lattice	Monoclinic	Monoclinic
formula	$C_{28}H_{39}NbP_2$	$C_{26}H_{33}Cl_2NbP_2$
formula weight	530.44	571.27
space group	*C*2/*c*	*C*2/*c*
a / Å	26.149(5)	26.122(18)
b / Å	13.331(3)	13.281(8)
c / Å	17.027(17)	16.919(10)
α / °	90	90
β / °	117.113(2)	118.994(17)
γ / °	90	90
V / Å^3	5283.3(17)	5134(6)
Z	8	8
temperature (K)	150(2)	150(2)
radiation (λ, Å)	0.71073	0.71073
ρ (calcd.) g cm^{-3}	1.334	1.478
μ (Mo Kα), mm^{-1}	0.590	0.814
θ max, deg.	31.51	30.84
no. of data collected	43629	14564
no. of data	8804	7507
no. of parameters	290	288
R_1 [$I > 2\sigma(I)$]	0.0407	0.0639
wR_2 [$I > 2\sigma(I)$]	0.0973	0.1108
R_1 [all data]	0.0628	0.3407
wR_2 [all data]	0.1114	0.1741
GOF	1.052	0.633

6.17 References and notes

(1) Peters, J.; Thomas, J. C. *Comprehensive Organometallic Chemistry III*, Volume 1, Chapter 2; Crabtree, R. H. and Mingos, D. M. P. (Eds), Elsevier, Oxford, 2006.

(2) (a) Choi, J.; MacArthur, A. H. R.; Brookhart, M.; Goldman, A. S. *Chem. Rev.* **2011**, *111*, 1761-1779.

(b) Albrecht M.; Lindner, M. M. *Dalton Trans.* **2011**, *40*, 8733-8744.

(c) Leis, W.; Mayer, H. A.; Kaska, W. C. *Coord. Chem. Rev.* **2008**, *252*, 1787-1797.

(d) van der Boom, M. E.; Milstein, D. *Chem. Rev.* **2003**, *103*, 1759-1792.

(e) Albrecht, M.; van Koten, G. *Angew. Chem. Int. Ed.* **2001**, *40*, 3750-3781.

(f) Pugh, D.; Danopoulos, A. A. *Coord. Chem. Rev.* **2007**, *251*, 610-641.

(g) Benito-Garagorri, D.; Kirchner, K. *Acc. Chem. Res.* **2008**, *41*, 201-213.

(h) Nishiyama, H. *Chem. Soc. Rev.* **2007**, *36*, 1133-1141.

(i) van der Vlugt, J. I.; Reek, J. N. H. *Angew. Chem. Int. Ed.* **2009**, *48*, 8832-8846.

(j) Liang, L.-C. *Coord. Chem. Rev.* **2006**, *250*, 1152-1177.

(k) van Koten, G. *Pure Appl. Chem.* **1989**, *61*, 1681-1694.

(l) Fryzuk, M. D.; Montgomery, C. D. *Coord. Chem. Rev.* **1989**, *95*, 1-40.

(m) Fryzuk, M. D. *Can. J. Chem.* **1992**, *70*, 2839-2845.

(n) Moughton, A. O.; O'Reilly, R. K. *Macromol. Rapid Commun.* **2010**, *31*, 37-52.

(o) Wieczorek, B.; Dijkstra, H. P.; Egmond, M. R.; Klein Gebbink, R. J. M.; van Koten, G. *J. Organomet. Chem.* **2009**, *694*, 812-822.

(p) *The Chemistry of Pincer Compounds*; Morales-Morales, D., Jensen, C. M., Eds.; Elsevier: Amsterdam, 2007.

(3) (a) Green, M. L. H. *J. Organomet. Chem.* **1995**, *500*, 127-148.

(b) Parkin, G. in *Comprehensive Organometallic Chemistry III*, Volume 1, Chapter 1.01; Crabtree, R. H. and Mingos, D. M. P. (Eds), Elsevier, Oxford, 2006.

(4) For examples of L_2X [*CCC*] pincer ligands, see:

(a) Chianese, A. R.; Mo, A.; Lampland, N. L.; Swartz, R. L.; Bremer, P. T. *Organometallics* **2010**, *29*, 3019-3026.

(b) Lv, K.; Cui, D. *Organometallics* **2008**, *27*, 5438-5440.

(c) Lv, K.; Cui, D. *Organometallics* **2010**, *29*, 2987-2993.

(d) Liu, A.; Zhang, X.; Chen, W. *Organometallics* **2009**, *28*, 4868-4871.

(e) Gründemann, S.; Albrecht, M.; Loch, J. A.; Faller, J. W.; Crabtree, R. H. *Organometallics* **2001**, *20*, 5485-5488.

(f) Cho, J.; Hollis, T. K.; Valente, E. J.; Trate, J. M. *J. Organomet. Chem.* **2011**, *696*, 373-377.

(g) Cho, J.; Hollis, T. K.; Helgert, T. R.; Valente, E. J. *Chem. Commun.* **2008**, 5001-5003.

(h) Bauer, E. B.; Andavan, G. T. S.; Hollis, T. K.; Rubio, R. J.; Cho, J.; Kuchenbeiser, G. R.; Helgert, T. R.; Letko, C. S.; Tham, F. S. *Org. Lett.* **2008**, *10*, 1175-1178.

(i) Andavan, G. T. S.; Bauer, E. B.; Letko, C. S.; Hollis, T. K.; Tham, F. S. *J. Organomet. Chem.* **2005**, *690*, 5938-5947.

(j) Rubio, R. J.; Andavan, G. T. S.; Bauer, E. B.; Hollis, T. K.; Cho, J.; Tham, F. S.; Donnadieu, B. *J. Organomet. Chem.* **2005**, *690*, 5353-5364.

(5) For examples of LX_2 [*CCC*] pincer and related ligands, see:

(a) Stylianides, N.; Danopoulos, A. A.; Pugh, D.; Hancock, F.; Zanotti-Gerosa, A. *Organometallics* **2007**, *26*, 5627-5635.

(b) Navarro, J.; Torres, O.; Martín, M.; Sola, E. *J. Am. Chem. Soc.* **2011**, *133*, 9738-9740.

(6) For some recent illustrations of X_3 pincer ligands that feature other donor arrays, *e.g.* [*OCO*], [*NCN*], and [*ONO*], see:

(a) Golisz, S. R.; Labinger, J. A.; Bercaw, J. E. *Organometallics* **2010**, *29*, 5026–5032.

(b) Kuppuswamy, S.; Ghiviriga, I.; Abboud, K. A.; Veige, A. S. *Organometallics* **2010,** *29*, 6711-6722.

(c) Kuppuswamy, S.; Peloquin, A. J.; Ghiviriga, I.; Abboud, K. A.; Veige, A. S. *Organometallics* **2010,** *29*, 4227-4233.

(d) Sarkar, S.; McGowan, K. P.; Culver, J. A.; Carlson, A. R.; Koller, J.; Peloquin, A. J.; Veige, M. K.; Abboud, K. A.; Veige, A. S. *Inorg. Chem.* **2010,** *49*, 5143-5156.

(e) Nguyen, A. I.; Blackmore, K. J.; Carter, S. M.; Zarkesh, R. A.; Heyduk, A. F. *J. Am. Chem. Soc.* **2009,** *131*, 3307-3316.

(f) Nguyen, A. I.; Zarkesh, R. A.; Lacy, D. C.; Thorson, M. K.; Heyduk, A. F. *Chem. Sci.* **2011,** *2*, 166-169.

(g) Zarkesh, R. A.; Heyduk, A. F. *Organometallics* **2009,** *28*, 6629-6631.

(h) Korobkov, I.; Gorelsky, S.; Gambarotta, S. *J. Am. Chem. Soc.* **2009**, *131*, 10406-10420.

(i) O'Reilly, M.; Falkowski, J. M.; Ramachandran, V.; Pati, M.; Abboud, K. A.; Dalal, N. S.; Gray, T. G.; Veige, A. S. *Inorg. Chem.* **2009**, *48*, 10901-10903.

(j) Sarkar, S.; Carlson, A. R.; Veige, M. K.; Falkowski, J. M.; Abboud, K. A.; Veige, A. S. *J. Am. Chem. Soc.* **2008**, *130*, 1116-1117.

(k) Sarkar, S.; Abboud, K. A.; Veige, A. S. *J. Am. Chem. Soc.* **2008**, *130*, 16128-16129.

(l) Koller, J.; Sarkar, S.; Abboud, K. A.; Veige, A. S. *Organometallics* **2007**, *26*, 5438-5441.

(7) (a) Albrecht, M. *Chem. Rev.* **2010**, *110*, 576-623.

(b) Ryabov, A. D. *Chem. Rev.* **1990**, *90*, 403-424.

(8) For specific examples of cyclometalation in tantalum chemistry, see: Rothwell, I. P. *Acc. Chem. Res.* **1988**, *21*, 153-159.

(9) Rivard, E.; Power, P. P. *Inorg. Chem.* **2007**, *46*, 10047-10064.

(10) Rabe, G. W.; Bérube, C. D.; Yap, G. P. A.; Lam, K.-C.; Concolino, T. E.; Rheingold, A. L. *Inorg. Chem.* **2002**, *41*, 1446-1453.

(11) Rabe, G. W.; Bérube, C. D.; Yap, G. P. A. *Inorg. Chem.* **2001**, *40*, 2682-2685.

(12) Quillian, B.; Wang, Y.; Wei, P.; Robinson, G. H. *Journal of Coordination Chemistry* **2008,** *61*, 137-142.

(13) (a) Ni, C.; Ellis, B. D.; Long, G. J.; Power, P. P. *Chem. Commun.* **2009**, 2332-2334.

(b) Wolf, R.; Brynda, M.; Ni, C.; Long, G. J.; Power, P. P. *J. Am. Chem. Soc.* **2007,** *129*, 6076-6077.

(c) Wolf, R.; Ni, C.; Nguyen, T.; Brynda, M.; Long, G. J.; Sutton, A. D.; Fischer, R. C.; Fettinger, J. C.; Hellman, M.; Pu, L.; Power, P. P. *Inorg. Chem.* **2007,** *46*, 11277-11290.

(d) Ni, C.; Long, G. J.; Grandjean, F.; Power, P. P. *Inorg. Chem.* **2009,** *48*, 11594-11600.

(14) (a) Ni, C.; Ellis, B. D.; Fettinger, J. C.; Long, G. J.; Power, P. P. *Chem. Commun.* **2008**, 1014-1016.

(b) Kays, D. L.; Cowley, A. R. *Chem. Commun.* **2007**, 1053-1055.

(c) Ni, C.; Fettinger, J. C.; Long, G. J.; Power, P. P. *Inorg. Chem.* **2009,** *48*, 2443-2448.

(d) Sutton, A. D.; Ngyuen, T.; Fettinger, J. C.; Olmstead, M. M.; Long, G. J.; Power, P. P. *Inorg. Chem.* **2007,** *46*, 4809-4814.

(e) Ni, C.; Fettinger, J. C.; Long, G. J.; Power, P. P. *Dalton Trans.* **2010,** *39*, 10664-10670.

(f) Ni, C.; Lei, H.; Power, P. P. *Organometallics* **2010,** *29*, 1988-1991.

(g) Ni, C.; Fettinger, J. C.; Power, P. P. *Organometallics* **2009,** *29*, 269-272.

(15) (a) Ni, C.; Long, G. J.; Power, P. P. *Organometallics* **2009,** *28*, 5012-5016.

(b) Ni, C.; Fettinger, J. C.; Long, G. J.; Brynda, M.; Power, P. P. *Chem. Commun.* **2008**, 6045-6047.

(16) (a) Ellison, J. J.; Power, P. P. *J. Organomet. Chem.* **1996,** *526*, 263-267.

(b) Lei, H.; Ellis, B. D.; Ni, C.; Grandjean, F.; Long, G. J.; Power, P. P. *Inorg. Chem.* **2008,** *47*, 10205-10207.

(c) Ni, C.; Stich, T. A.; Long, G. J.; Power, P. P. *Chem. Commun.* **2010,** *46*, 4466-4468.

(17) (a) Lang, H.; Köhler, K.; Rheinwald, G.; Zsolnai, L.; Büchner, M.; Driess, A.; Huttner, G.; Strähle, J. *Organometallics* **1999,** *18*, 598-605.

(b) Groysman, S.; Holm, R. H. *Inorg. Chem.* **2009,** *48*, 621-627.

(c) He, X.; Olmstead, M. M.; Power, P. P. *J. Am. Chem. Soc.* **1992,** *114*, 9668-9670.

(d) Hwang, C.-S.; Power, P. P. *J. Am. Chem. Soc.* **1998,** *120*, 6409-6410.

(e) Hwang, C.-S.; Power, P. P. *Organometallics* **1999,** *18*, 697-700.

(f) Schiemenz, B.; Power, P. P. *Organometallics* **1996,** *15*, 958-964.

(g) Niemeyer, M. *Z. Anorg. Allg. Chem.* **2003,** *629*, 1535-1540.

(h) Niemeyer, M. *Z. Anorg. Allg. Chem.* **2004,** *630*, 252-256.

(18) Hwang, C.-S.; Power, P. P. *J. Organomet. Chem.* **1999,** *589*, 234-238.

(19) Rabe, G. W.; Mitzel, N. W. *Inorg. Chim. Acta* **2001,** *316*, 132-134.

(20) (a) Zhu, Z.; Brynda, M.; Wright, R. J.; Fischer, R. C.; Merrill, W. A.; Rivard, E.; Wolf, R.; Fettinger, J. C.; Olmstead, M. M.; Power, P. P. *J. Am. Chem. Soc.* **2007,** *129*, 10847-10857.

(b) Zhu, Z.; Wright, R. J.; Olmstead, M. M.; Rivard, E.; Brynda, M.; Power, P. P. *Angew. Chem. Int. Ed.* **2006,** *45*, 5807-5810.

(c) Wang, Y.; Quillian, B.; Wannere, C. S.; Wei, P.; Schleyer, P. v. R.; Robinson, G. H. *Organometallics* **2007,** *26*, 3054-3056.

(d) Zhu, Z.; Fettinger, J. C.; Olmstead, M. M.; Power, P. P. *Organometallics* **2009,** *28*, 2091-2095.

(21) Zhu, Z.; Fischer, R. C.; Fettinger, J. C.; Rivard, E.; Brynda, M.; Power, P. P. *J. Am. Chem. Soc.* **2006,** *128*, 15068-15069.

(22) Niemeyer, M.; Power, P. P. *Organometallics* **1997,** *16*, 3258-3260.

(23) Juvinall, G. L. *J. Am. Chem. Soc.* **1964**, *86*, 4202-4203.

(24) The synthesis of $NbMe_3Cl_2$ was also reported in reference 23.

(25) For other syntheses of $TaMe_3Cl_2$, see:

(a) Fowles, G. W. A.; Rice, D. A.; Wilkins, J. D. *J. Chem. Soc., Dalton Trans.* **1973**, 961-965.

(b) Schrock, R. R.; Sharp, P. R. *J. Am. Chem. Soc.* **1978**, *100*, 2389-2399.

(26) (a) Zarkesh, R. A.; Ziller, J. W.; Heyduk, A. F. *Angew. Chem. Int. Ed. Engl.* **2008**, *47*, 4715-4718.

(b) Carmichael, C. D.; Shaver, M. P.; Fryzuk, M. D. *Can. J. Chem.* **2006**, *84*, 1667-1678.

(c) Carmichael, C. D.; Fryzuk, M. D. *Can. J. Chem.* **2010**, *88*, 667-675.

(d) Dawson, D. Y.; Arnold, J. *Organometallics* **1997**, *16*, 1111-1113.

(e) Lavoie, N.; Gorelsky, S. I.; Liu, Z.; Burchell, T. J.; Yap, G. P. A.; Richeson, D. S. *Inorg. Chem.* **2010**, *49*, 5231-5240.

(f) Fryzuk, M. D.; Johnson, S. A.; Patrick, B. O.; Albinati, A.; Mason, S. A.; Koetzle, T. F. *J. Am. Chem. Soc.* **2001**, *123*, 3960-3973.

(g) Gavenonis, J.; Tilley, T. D. *J. Am. Chem. Soc.* **2002**, *124*, 8536-8537.

(h) Spencer, L. P.; Beddie, C.; Hall, M. B.; Fryzuk, M. D. *J. Am. Chem. Soc.* **2006**, *128*, 12531-12543.

(i) LaPointe, R. E.; Wolczanski, P. T.; Van Duyne, G. D. *Organometallics* **1985**, *4*, 1810-1818.

(j) Baxter, S. M.; Wolczanski, P. T. *Organometallics* **1990**, *9*, 2498-2509.

(k) Fryzuk, M. D.; Johnson, S. A.; Rettig, S. J. *Organometallics* **1999**, *18*, 4059-4067.

(l) Ishino, H.; Nagano, T.; Kuwata, S.; Yokobayashi, Y.; Ishii, Y.; Hidai, M. *Organometallics* **2001**, *20*, 188-198.

(m) Araujo, J. P.; Wicht, D. K.; Bonitatebus, P. J., Jr.; Schrock, R. R. *Organometallics* **2001**, *20*, 5682-5689.

(n) Gavenonis, J.; Tilley, T. D. *Organometallics* **2002**, *21*, 5549-5563.

(o) Chirik, P. J.; Zubris, D. L.; Ackerman, L. J.; Henling, L. M.; Day, M. W.; Bercaw, J. E. *Organometallics* **2003**, *22*, 172-187.

(p) Sen Soo, H.; Diaconescu, P. L.; Cummins, C. C. *Organometallics* **2004**, *23*, 498-503.

(q) Shaver, M. P.; Fryzuk, M. D. *Organometallics* **2005**, *24*, 1419-1427.

(r) Agapie, T.; Bercaw, J. E. *Organometallics* **2007**, *26*, 2957-2959.

(s) Agapie, T.; Day, M. W.; Bercaw, J. E. *Organometallics* **2008**, *27*, 6123-6142.

(t) Bazan, G. C.; Rodriguez, G. *Polyhedron* **1995**, *14*, 93-102.

(u) Cloke, F. G. N.; Hitchcock, P. B.; Kuchta, M. C.; Morley-Smith, N. A. *Polyhedron* **2004**, *23*, 2625-2630.

(v) Schaller, C. P.; Wolczanski, P. T. *Inorg. Chem.* **1993**, *32*, 131-144.

(27) Haaland, A.; Verne, H. P.; Volden, H. V.; Pulham, C. R. *J. Mol. Struct.* **1996**, *376*, 151-155.

(28) Downs, A. J.; Green, J. C.; McGrady, G. S.; Munkman, N.; Parkin, R. P. G. *J. Chem. Soc. Dalton Trans.* **2000**, 21-27.

(29) Sattler, A.; Ruccolo, S.; Parkin, G. *Dalton Trans.* **2011**, *40*, 7777–7782.

(30) Rossi, A. R.; Hoffmann, R. *Inorg. Chem.* **1975**, *14*, 365-374.

(31) (a) Muetterties, E. L.; Schunn, R. A. *Q. Rev. Chem. Soc.* **1966**, *20*, 245-299.

(b) Hoskins, B. F.; Whillans, F. D. *Coord. Chem. Rev.* **1972-1973**, *9*, 365-388.

(32) Holloway, C. E.; Melnik, M. *J. Organomet. Chem.* **1986**, *303*, 39-72.

(33) Cambridge Structural Database (Version 5.32). *3D Search and Research Using the Cambridge Structural Database*, Allen, F. H.; Kennard, O. *Chemical Design Automation News* **1993**, *8* (1), pp 1 & 31-37.

(34) (a) Parkin, G. *Chem. Rev.* **1993**, *93*, 887-911.

(b) Parkin, G. *Acc. Chem. Res.* **1992**, *25*, 455-460.

(c) Yoon, K.; Parkin, G.; Rheingold, A. L. *J. Am. Chem. Soc.* **1992**, *114*, 2210-2218.

(d) Yoon, K.; Parkin, G.; Rheingold, A. L. *J. Am. Chem. Soc.* **1991**, *113*, 1437-1438.

(e) Yoon, K.; Parkin, G. *Inorg. Chem.* **1992**, *31*, 1656-1662.

(f) Yoon, K.; Parkin, G. *J. Am. Chem. Soc.* **1991**, *113*, 8414-8418.

(g) Parkin, G. *Encyclopedia of Supramolecular Chemistry*, pp 120-128, Marcel Dekker, New York (2004).

(35) Furthermore, a distortion of this type has been reported for $NbMe_3Cl_2$. See: McGrady, G. S.; Haaland, A.; Verne, H. P.; Volden, H. V.; Downs, A. J.; Shorokhov, D.; Eickerling, G.; Scherer, W. *Chem. Eur. J.* **2005**, *11*, 4921-4934.

(36) We also considered the possibility that the space group could be noncentrosymmetric $P6_3mc$ rather than $P6_3/mmc$, cf. $NbMe_3Cl_2$ (reference 35), but refinement in $P6_3mc$ did not result in an improved structure.

(37) Roessler, B.; Kleinhenz, S.; Seppelt, K. *Chem. Commun.* **2000**, 1039-1040.

(38) (a) Chamberlain, L.; Keddington, J.; Rothwell, I. P.; Huffman, J. C. *Organometallics* **1982**, *1*, 1538-1540.

(b) Chamberlain, L. R.; Rothwell, I. P.; Huffman, J. C. *J. Am. Chem. Soc.* **1986**, *108*, 1502-1509.

(39) Bott, S. G.; Mazid, M. A.; Hursthouse, M. B.; Sullivan, A. C. *J. Chem. Soc. Dalton Trans.* **1991**, 355-359.

(40) Guzyr, O. I.; Schormann, M.; Schimkowiak, J.; Roesky, H. W.; Lehmann, C.; Walawalkar, M. G.; Murugavel, R.; Schmidt, H.-G.; Noltemeyer, M. *Organometallics* **1999**, *18*, 832-836.

(41) Chesnut, R. W.; Jacob, G. G.; Yu, J. S.; Fanwick, P. E.; Rothwell, I. P. *Organometallics* **1991**, *10*, 321-328.

(42) Vilardo, J. S.; Lockwood, M. A.; Hanson, L. G.; Clark, J. R.; Parkin, B. C.; Fanwick, P. E.; Rothwell, I. P. *J. Chem. Soc. Dalton Trans.* **1997**, 3353-3362.

(43) Fowles, G. W. A.; Rice, D. A.; Wilkins, J. D. *J. Chem. Soc. Dalton Trans.* **1974**, 1080-1084.

(44) Drew, M. G. B.; Wilkins, J. D. *J. Chem. Soc. Dalton Trans.* **1973**, 1830-1834.

(45) For other seven-coordinate trimethyltantalum compounds, see: Santini-Scampucci, C.; Wilkinson, G. *J. Chem. Soc. Dalton Trans.* **1976**, 807-811.

(46) (a) Muetterties, E. L.; Wright, C. M. *Q. Rev. Chem. Soc.* **1967**, *21*, 109-194.

(b) Hoffmann, R.; Beier, B. F.; Muetterties, E. L.; Rossi, A. R. *Inorg. Chem.* **1977**, *16*, 511-522.

(c) Drew, M. G. B. *Prog. Inorg. Chem.* **1977**, *23*, 67-210.

(d) Kepert, D. L. *Prog. Inorg. Chem.* **1979**, *25*, 41-144.

(e) Muetterties, E. L.; Guggenberger, L. J. *J. Am. Chem. Soc.* **1974**, *96*, 1748-1756.

(47) An excellent early example is provided by the cyclobutadiene derivative, (η^4-C_4Ph_4)$Fe(CO)_3$. See: Dodge, R. P.; Schomaker, V. *Nature* **1960**, *186*, 798-799.

(48) (a) Dreyer, E. B.; Lam, C. T.; Lippard, S. J. *Inorg. Chem.* **1979**, *18*, 1904-1908.

(b) Szalda, D. J.; Dewan, J. C.; Lippard, S. J. *Inorg. Chem.* **1981**, *20*, 3851-3857.

(c) Dewan, J. C.; Mialki, W. S.; Walton, R. A.; Lippard, S. J. *J. Am. Chem. Soc.* **1982**, *104*, 133-136.

(d) Giandomenico, C. M.; Dewan, J. C.; Lippard, S. J. *J. Am. Chem. Soc.* **1981**, *103*, 1407-1412.

(e) Dewan, J. C.; Roberts, M. M.; Lippard, S. J. *Inorg. Chem.* **1983**, *22*, 1529-1533.

(49) For other examples of complexes with 4:3 piano stool geometries, see:

(a) Brower, D. C.; Winston, P. B.; Tonker, T. L.; Templeton, J. L. *Inorg. Chem.* **1986**, *25*, 2883-2888.

(b) Ambrosius, H. P. M. M.; Bosman, W. P.; Cras, J. A. *J. Organomet. Chem.* **1981**, *215*, 201-213.

(c) Dilsky, S. *J. Organomet. Chem.* **2007**, *692*, 2887-2896.

(d) Ryu, S.; Whang, D.; Kim, J.; Yeo, W.; Kim, K. *J. Chem. Soc. Dalton Trans.* **1993**, 205-209.

(e) Szymanska-Buzar, T.; Gowiak, T. *J. Organomet. Chem.* **1999**, *575*, 98-107.

(f) Yang, C.-H.; Tung, J.-Y.; Liau, B.-C.; Ko, B.-T.; Elango, S.; Chen, J.-H.; Hwang, L.-P. *Polyhedron* **2001**, *20*, 3257-3264.

(50) For an example of a distorted pentagonal bipyrimidal trimethyl tantalum compound, see: Noor, A.; Kretschmer, W.; Kempe, R. *Eur. J. Inorg. Chem.* **2006**, 2683-2689.

(51) Drew, M. G. B.; Wilkins, J. D. *J. Chem. Soc. Dalton Trans.* **1977**, 194-197.

(52) Consistent with this suggestion, the ^{1}H NMR chemical shifts vary slightly with concentration, and are also influenced by additional PMe_3.

(53) Additional evidence for α-hydrogen abstraction is provided by using the isotopologue, $[Ar^{Tol_2}]Ta(CD_3)_3Cl$, which decomposes to give, *inter alia*, $[Ar^{Tol_2}]D$ and CD_4.

(54) Schrock, R. R.; Fellmann, J. D. *J. Am. Chem. Soc.* **1978**, *100*, 3359-3370.

(55) Schrock, R. R. *J. Organomet. Chem.* **1976**, *122*, 209-225.

(56) This displacement is reproduced by density functional theory calculations (B3LYP using 6-31G** (C, H and Cl) and LACVP (Ta) basis sets (Jaguar 7.5, Schrödinger, LLC, New York, NY 2008).

(57) For comparison, the mean displacement for structurally characterized tantalum phenyl compounds listed in the Cambridge Structural Database (Version 5.32) is 174.8°.

(58) See, for example:

(a) Steffey, B. D.; Fanwick, P. E.; Rothwell, I. P. *Polyhedron* **1990**, *9*, 963-968.

(b) Kleinhenz, S.; Schubert, M.; Seppelt, K. *Chem. Ber. Recl.* **1997**, *130*, 903-906.

(59) (a) Zhu, Z.; Brynda, M.; Wright, R. J.; Fischer, R. C.; Merrill, W. A.; Rivard, E.; Wolf, R.; Fettinger, J. C.; Olmstead, M. M.; Power, P. P. *J. Am. Chem. Soc.* **2007**, *129*, 10847-10857.

(b) Wang, Y.; Quillian, B.; Wannere, C. S.; Wei, P.; Schleyer, P. v. R.; Robinson, G. H. *Organometallics* **2007**, *26*, 3054-3056.

(c) Quillian, B.; Wang, Y.; Wei, P.; Robinson, G. H. *New J. Chem.* **2008**, *32*, 774-776.

(d) Ni, C.; Ellis, B. D.; Fettinger, J. C.; Long, G. J.; Power, P. P. *Chem. Commun.* **2008**, 1014-1016.

(60) Rabe, G. W.; Bérube, C. D.; Yap, G. P. A. *Inorg. Chem.* **2001**, *40*, 2682-2685.

(61) Rabe, G. W.; Bérube, C. D.; Yap, G. P. A.; Lam, K.-C.; Concolino, T. E.; Rheingold, A. L. *Inorg. Chem.* **2002**, *41*, 1446-1453.

(62) Niemeyer, M. *Acta Cryst.* **2001**, *E57*, m578-m580.

(63) Heckmann, G.; Niemeyer, M. *J. Am. Chem. Soc.* **2000**, *122*, 4227-4228.

(64) In-plane distortions of terphenyl ligands are also known. For example, $\{[Ar^{Pri_2}]Cr(\mu\text{–}Cl)\}_2$ has $Cr\text{–}C_{ipso}\text{–}C_{ortho}$ angles of 99.9° and 142.0°. See: Sutton, A. D.; Ngyuen, T.; Fettinger, J. C.; Olmstead, M. M.; Long, G. J.; Power, P. P. *Inorg. Chem.* **2007**, 46, 4809-4814.

(65) For construction of an X_3 [*OCO*] pincer ligand on tantalum by elimination of methane, see:

(a) Agapie, T.; Bercaw, J. E. *Organometallics* **2007**, *26*, 2957-2959.

(b) Agapie, T.; Day, M. W.; Bercaw, J. E. *Organometallics* **2008**, *27*, 6123-6142.

(66) Low temperature NMR spectroscopic evidence has been presented for the generation of selenium ate complexes derived from *m*-terphenyl derivatives. However, such complexes have neither been isolated nor structurally characterized by X-ray diffraction. See:

(a) Reich, H. J.; Gudmundsson, B. O.; Dykstra, R. R. *J. Am. Chem. Soc.* **1992**, *114*, 7937-7938.

(b) Reich, H. J.; Gudmundsson, B. O.; Green, D. P.; Bevan, M. J.; Reich, I. L. *Helv. Chim. Acta* **2002**, *85*, 3748-3772.

(67) (a) McLain, S. J.; Wood, C. D.; Messerle, L. W.; Schrock, R. R.; Hollander, F. J.; Youngs, W. J.; Churchill, M. R. *J. Am. Chem. Soc.* **1978**, *100*, 5962-5964.

(b) Fellman, J. D.; Rupprecht, G. A.; Wood, C. D.; Schrock, R. R. *J. Am. Chem. Soc.* **1978**, *100*, 5964-5966.

(c) Schrock, R. R. *Acc. Chem. Res.* **1979**, *12*, 98-104.

(68) $[\kappa^3\text{-}Ar^{Tol'_2}]Ta(PMe_3)Me_3]^-Li^+$ was identified by obtaining a low quality single crystal used for an X-ray diffraction study.

(69) The initial product obtained is tentatively assigned as the mono phosphine complex $[\kappa^3\text{-}Ar^{Tol'_2}]Ta(PMe_3)Cl_2$. Treatment with PMe_3 then converts $[\kappa^3\text{-}Ar^{Tol'_2}]Ta(PMe_3)Cl_2$ to the *bis* PMe_3 complex, $[\kappa^3\text{-}Ar^{Tol'_2}]Ta(PMe_3)_2Cl_2$.

(70) (a) Redfield, D. A.; Cary, L. W.; Nelson, J. H. *Inorg. Chem.* **1975**, *14*, 50-59.

(b) Nelson, J. H. *Concepts Magnetic Res.* **2002**, *14*, 19-78.

(c) Redfield, D. A.; Nelson, J. H.; Cary, L. W. *Inorg. Nucl. Chem. Lett.* **1974**, *10*, 727-733.

(71) A similar five line pattern is also observed in the $^{31}P\{^1H\}$ NMR spectrum of $[\kappa^3\text{-}Ar^{Tol'_2}]Ta(PMe_3)_2(^{13}CH_3)_2$.

(72) (a) Bishop, E. O.; Carey, P. R. *Mol. Phys.* **1970**, *18*, 845-850.

(b) Ault, A. *J. Chem. Educ.* **1970**, *47*, 812-818.

(c) Abraham, R. J.; Bernstein, H. J. *Can. J. Chem.* **1961**, *39*, 216-230.

(73) Bovey, F. A. *Nuclear Magnetic Resonance Spectroscopy*, Academic Press, New York (1969).

(74) (a) Günther, H. *Angew. Chem. Int. Ed.* **1972**, *11*, 861-874.

(b) McFarlane, W.; Rycroft, D. S. *J. Chem. Soc., Farady Trans.* **1974**, 377-385.

(75) The derived value of $^{2}J_{CC} = 0$ for the [Ta($^{13}CH_3$)$_2$] moiety is consistent with the observation that there is no discernible $^{2}J_{CC}$ between the Ta–$^{13}CH_3$ groups of [κ^3-$Ar^{Tol'}{}_2$]Ta(PMe_3)$_2$($^{13}CH_3$)$_2$ and the pincer carbon atoms.

(76) It is worth pointing out that while the 1:4.7:11.4:4.7:1 intensity ratio is in accord with the formulas presented in reference 73, another text (Becker, E. D. *High Resolution NMR. Theory and Chemical Applications*, 3rd Ed., Academic Press, New York, 2000) predicts an incorrect ratio because the intensities of transitions 5 to 12 of the general AA'XX' pattern are listed as twice the correct values.

(77) (a) Baker, M. V.; Field, L. D. *Inorg. Chem.* **1987**, *26*, 2010-2011.

(b) Goodfellow, R. J.; Taylor, B. F. *J. Chem. Soc. Dalton Trans.* **1974**, 1676-1684.

(c) Verkade, J. G. *Coord. Chem. Rev.* **1972**, *9*, 1-106.

(d) Pregosin, P. S.; Kunz, R. W. *NMR Basic Princ. Prog.* **1979**, *15*, 28-34.

(78) (a) Darensbourg, D. J. *J. Organomet. Chem.* **1981**, *209*, C37-C40.

(b) Aime, S.; Osella, D. *J. Chem. Soc. Chem. Commun.* **1981**, 300-302.

(c) Aime, S. *Inorg. Chim. Acta* **1982**, *62*, 51-56.

(d) Hawkes, G. E.; Lian, L. Y.; Randall, E. W.; Sales, K. D.; Aime, S. *J. Chem. Soc.-Dalton Trans.* **1985**, 225-227.

(e) Tachikawa, M.; Richter, S. I.; Shapley, J. R. *J. Organomet. Chem.* **1977**, *128*, C9-C14.

(f) Shapley, J. R.; Stuntz, G. F.; Churchill, M. R.; Hutchinson, J. P. *J. Chem. Soc. Chem. Commun.* **1979**, 219-220.

(79) (a) de Dios, A. C.; Jameson, C. J. *Ann. Rep. NMR. Spectrosc.* **1994**, *29*, 1-69.

(b) Hansen, P. E. *Ann. Rep. NMR Spectrosc.* **1983**, *15*, 105-234.

(80) For related examples, see:

(a) Gross, C. L.; Girolami, G. S. *Organometallics* **1996**, *15*, 5359-5367.

(b) Hughes, R. P.; Zheng, X.; Morse, C. A.; Curnow, O. J.; Lomprey, J. R. *Organometallics* **1998**, *17*, 457-465.

(c) Fox, M. E.; Jackson, M.; Lennon, I. C.; Klosin, J.; Abboud, K. A. *J. Org. Chem.* **2008**, *73*, 775-784.

(d) Braddock, D. C.; Bhuva, R.; Millan, D. S.; Pérez-Fuertes, Y.; Roberts, C. A.; Sheppard, R. N.; Solanki, S.; Stokes, E. S. E.; White, A. J. P. *Org. Lett.* **2007**, *9*, 445-448.

(81) For other examples, see: Hersh, W. H. *J. Chem. Educ.* **1997**, *74*, 1485-1488.

(82) The magnitude of $\Delta\delta_{PP}$ is comparable to the one bond ^{13}C isotope effect on the ^{31}P chemical shift, $^{1}\Delta P(C)$, for other systems (0.022 – 0.025 ppm). See reference 80 and:

(a) Maple, S. R.; Carson, J. E.; Allerhand, A. *J. Am. Chem. Soc.* **1989**, *111*, 7293-7295.

(b) Aime, S.; Harris, R. K. *J. Magn. Reson.* **1974**, *13*, 236-238.

(c) Buchner, W.; Ries, W.; Malisch, W. *Magn. Reson. Chem.* **1990**, *28*, 515-518.

(83) $^{3}J_{PC}$ was fixed to be zero because no $^{3}J_{PC}$ coupling is observed for [κ^3-$Ar^{Tol'_2}$]Ta(PMe_3)$_2$MeCl. Specifically, the chemical inequivalence of the phosphorus nuclei of [κ^3-$Ar^{Tol'_2}$]Ta(PMe_3)$_2$MeCl is sufficiently large ($\Delta\delta_{PP}$ = 8.3 ppm) that the $^{13}C\{^{1}H\}$ signals for the PMe_3 ligands exhibit a first order pattern, *i.e.* two doublets with $^{1}J_{PC}$ coupling constants of 24 and 25 Hz.

(84) The appearance of the simulated spectra do not depend on the signs of either $^{2}J_{PP}$ or $^{1}J_{PC}$.

(85) This value of the secondary isotope effect was not refined but was assumed to be the same as that for [κ^3-$Ar^{Tol'_2}$]Ta$(PMe_3)_2Me_2$. Also see reference 82.

(86) Chamberlain, L. R.; Rothwell, I. P.; Huffman, J. C. *J. Am. Chem. Soc.* **1986**, *108*, 1502-1509.

(87) For related studies, see: Lockwood, M. A.; Clark, J. R.; Parkin, B. C.; Rothwell, I. P. *Chem. Commun.* **1996**, 1973-1974.

(88) Likewise, Bercaw has reported that elimination of toluene from $Cp^*_2Hf(CH_2Ph)_2$ to give the metallated complex $Cp^*_2Hf(\kappa^2$-$CH_2C_6H_4)$ occurs *via* a sequence that primarily involves initial α–H abstraction to generate the benzylidene complex $Cp^*_2Hf{=}CHPh$ that undergoes 1,2-addition of a methyl C–H bond to give $Cp^*(\eta^5,\eta^1$-$C_5Me_4CH_2)HfCH_2Ph$ that subsequently isomerizes to $Cp^*_2Hf(\kappa^2$-$CH_2C_6H_4)$. See: Bulls, A. R.; Schaefer, W. P.; Serfas, M.; Bercaw, J. E. *Organometallics* **1987**, *6*, 1219-1226.

(89) Likewise, addition of PMe_3 to [Ar^{Tol_2}]Ta$(CD_3)_3Cl$ liberates CD_3H and forms [κ^3-$Ar^{Tol'_2}$]Ta$(PMe_3)_2(CD_3)Cl$.

(90) In addition to CD_4, the α–H abstraction pathway would also result in the formation of other methane isotopologues.

(91) (a) Cloke, F. G. N.; Dix, A. N.; Green, J. C.; Perutz, R. N.; Seddon, E. A. *Organometallics* **1983**, *2*, 1150-9.

(b) Cloke, F. G. N.; Green, M. L. H. *J. Chem. Soc., Dalton Trans.* **1981**, 1938-43.

(c) Lyon, J. T.; Andrews, L. *J. Phys. Chem. A* **2005**, *109*, 431-440.

(92) (a) Wigley, D. E.; Gray, S. D. in *Comprehensive Organometallic Chemistry II*, Vol 5, Chapter 2, pp 57-153; Abel, E. W., Stone, F. G. A. and Wilkinson, G. (Eds), Elsevier, Oxford, 1995.

(b) Mashima, K. in *Comprehensive Organometallic Chemistry III*, Volume 5, Chapter 5.03, pp 101-200; Crabtree, R. H. and Mingos, D. M. P. (Eds), Elsevier, Oxford, 2006.

(93) For examples of structurally characterized tantalum complexes that feature other arenes, see:

(a) Bruck, M. A.; Copenhaver, A. S.; Wigley, D. E. *J. Am. Chem. Soc.* **1987,** *109*, 6525-6527.

(b) Wexler, P. A.; Wigley, D. E. *J. Chem. Soc., Chem. Commun.* **1989**, 664-665.

(c) Arney, D. J.; Wexler, P. A.; Wigley, D. E. *Organometallics* **1990,** *9*, 1282-1289.

(d) Wexler, P. A.; Wigley, D. E.; Koerner, J. B.; Albright, T. A. *Organometallics* **1991,** *10*, 2319-2327.

(e) Arney, D. J.; Bruck, M. A.; Wigley, D. E. *Organometallics* **1991,** *10*, 3947-3949.

(f) Smith, D. P.; Strickler, J. R.; Gray, S. D.; Bruck, M. A.; Holmes, R. S.; Wigley, D. E. *Organometallics* **1992,** *11*, 1275-1288.

(g) Arney, D. S. J.; Fox, P. A.; Bruck, M. A.; Wigley, D. E. *Organometallics* **1997,** *16*, 3421-3430.

(94) Puckered arenes with folds in the opposite direction such that the two carbon atoms along the fold are further from the metal are also known. See, for example:

(a) Radonovich, L. J.; Koch, F. J.; Albright, T. A. *Inorg. Chem.* **1980**, *19*, 3373-3379.

(b) Atwood, J. L.; Hunter, W. E.; Rogers, R. D.; Carmona-Guzman, E.; Wilkinson, G. *J. Chem. Soc. Dalton Trans.* **1979**, 1519-1523.

(95) For examples of arene complexes that feature puckered 1,4-cyclohexadienediyl geometries, see reference 93 and:

(a) Churchill, M. R.; Chang, S. W.-Y. *J. Chem. Soc. Chem. Commun.* **1974**, 248-249.

(b) Gardner, T. G.; Girolami, G. S. *Angew. Chem. Int. Ed.* **1988**, *27*, 1693-1695.

(c) Hagadorn, J. R.; Arnold, J. *Angew. Chem. Int. Ed.* **1998,** *37*, 1729-1731.

(d) Graham, T. W.; Kickham, J.; Courtenay, S.; Wei, P.; Stephan, D. W. *Organometallics* **2004,** *23*, 3309-3318.

(e) Kissounko, D.; Epshteyn, A.; Fettinger, J. C.; Sita, L. R. *Organometallics* **2006**, *25*, 531-535.

(f) Otten, E.; Meetsma, A.; Hessen, B. *J. Am. Chem. Soc.* **2007,** *129*, 10100-10101.

(g) Kawaguchi, H.; Matsuo, T. *J. Am. Chem. Soc.* **2003,** *125*, 14254-14255.

(96) For other arene coordination modes see:

(a) Zhu, G.; Figueroa, J. S.; Parkin, G. *J. Am. Chem. Soc.* **2006**, *128*, 5452-5461.

(b) Maslowsky, E. *J. Chem. Educ.* **1993**, *70*, 980-984.

(97) (a) Hall, M. B.; Fenske, R. F. *Inorg. Chem.* **1972**, *11*, 768.

(b) Bursten, B. E.; Jensen, J. R.; Fenske, R. F. *J. Chem. Phys.* **1978**, *68*, 3320.

(c) Manson, J.; Webster, C. E.; Pérez, L. M.; Hall, M. B. http://www.chem.tamu.edu/jimp2/index.html.

(98) The *z*-axis defined as the Ta–$[C_6H_6]_{cent}$ axis, with the *x*- and *y*-axes lying in the TaC_3 and TaP_2 planes, respectively.

(99) For related studies, see:

(a) Arnold, J.; Tilley, T. D.; Rheingold, A. L. *J. Am. Chem. Soc.* **1986,** *108*, 5355-5356.

(b) Arnold, J.; Tilley, T. D.; Rheingold, A. L.; Geib, S. J.; Arif, A. M. *J. Am. Chem. Soc.* **1989,** *111*, 149-164.

(c) Meyer, T. Y.; Garner, L. R.; Baenziger, N. C.; Messerle, L. *Inorg. Chem.* **1990,** *29*, 4045-4050.

(d) Gómez, M.; Gómez-Sal, P.; Jiménez, G.; Martín, A.; Royo, P.; Sánchez-Nieves, J. *Organometallics* **1996,** *15*, 3579-3587.

(e) Gómez, M. *Eur. J. Inorg. Chem.* **2003,** *2003*, 3681-3697.

(f) Rietveld, M. H. P.; Hagen, H.; van de Water, L.; Grove, D. M.; Kooijman, H.; Veldman, N.; Spek, A. L.; van Koten, G. *Organometallics* **1997,** *16*, 168-177.

(100) Both compounds have only been isolated and characterized by X-ray diffraction. ^{1}H NMR spectroscopy indicates that other species are formed, in addition to a dark unidentified precipitate.

(101) It should also be noted that both complexes are produced in the absence of PMe_3, such that other decomposition pathways give access to the additional equivalent of PMe_3 needed to produce $[\eta^2,\eta^2\text{-}Ar^{Tol(CO),Tol(Me_3PCO)}]Ta(PMe_3)_2Cl_2$.

(102) If this is the case, $[\kappa^2,\eta^2\text{-}Ar^{Tol',Tol(Me_3PCO)}]Ta(PMe_3)Cl_2$ will convert to $[\eta^2,\eta^2\text{-}Ar^{Tol(CO),Tol(Me_3PCO)}]Ta(PMe_3)_2Cl_2$ upon addition of PMe_3 and CO.

(103) For examples of olefin coupling by tantalum, see:

(a) McLain, S. J.; Wood, C. D.; Schrock, R. R. *J. Am. Chem. Soc.* **1977,** *99*, 3519-3520.

(b) McLain, S. J.; Schrock, R. R. *J. Am. Chem. Soc.* **1978,** *100*, 1315-1317.

(c) McLain, S. J.; Wood, C. D.; Schrock, R. R. *J. Am. Chem. Soc.* **1979,** *101*, 4558-4570.

(d) Mashima, K.; Tanaka, Y.; Nakamura, A. *J. Organomet. Chem.* **1995,** *502*, 19-23.

(104) For related studies, see:

(a) McGuinness, D. S. *Chem. Rev.* **2010,** *111*, 2321-2341.

(b) Cohen, S. A.; Auburn, P. R.; Bercaw, J. E. *J. Am. Chem. Soc.* **1983,** *105*, 1136-1143.

(c) Cohen, S. A.; Bercaw, J. E. *Organometallics* **1985,** *4*, 1006-1014.

(105) For the only structurally characterized tantalacyclopentane listed in the Cambridge Structural Database, see: Churchill, M. R.; Youngs, W. J. *J. Am. Chem. Soc.* **1979,** *101*, 6462-6463.

(106) It is worthwhile noting that the ability to isolate $[\kappa^3\text{-}Ar^{Tol'_2}]Ta(PMe_3)_2(\kappa^2\text{-}C_4H_8)$ indicates that the reactivity of the intermediate $[[\kappa^3\text{-}Ar^{Tol'_2}]Ta(PMe_3)_2]$ with ethylene is more facile than with the solvent, benzene.

(107) For examples of lithium π-arene complexes, see:

(a) Buchalski, P.; Grabowska, I.; Kaminska, E.; Suwinska, K. *Organometallics*, **2008**, *27*, 2346-2349.

(b) Brooks, J. J.; Rhine, W.; Stucky, G. D. *J. Am. Chem. Soc.* **1972**, *94*, 7346-7351.

(c) Hino, S.; Olmstead, M. M.; Fettinger, J. C.; Power, P. P. *J. Organomet. Chem.* **2005**, *690*, 1638-1644.

(d) Kirillov, E.; Toupet, L.; Lehmann, C. W.; Razavi, A.; Carpentier, J.-F. *Organometallics*, **2003**, *22*, 4467-4479.

(e) Feil, F.; Harder, S. *Eur. J. Inorg. Chem.* **2003**, 3401-3408.

(108) Baldwin, T. C.; Huber, S. R.; Bruck, M. A.; Wigley, D. E. *Inorg. Chem.* **1993**, *32*, 5682-5686.

(109) For additional reactivity studies of $NbCl_5$ with Me_2Zn, see: Fowles, G. W. A.; Rice, D. A.; Wilkins, J. D. *J. C. S. Dalton* **1972**, 2313-2318.

(110) Interestingly, unlike tantalum, there are no other structurally characterized 5-coordinate compounds that have an $NbMe_3$ moiety.

(111) A solution of $TaMe_3Cl_2$ in d_6-benzene also produces methane, but over a period of hours.

(112) For the two other structurally characterized complexes which contain the $[NbMe_3]$ fragment, see:

(a) Kleinhenz, S; Pfennig, V.; Seppelt, K. *Chem. Eur. J.* **1998**, *4*, 1687-1691.

(b) Martinez, G.; Stephan, D. W. *Can. J. Chem.* **2006**, *84*, 1180-1187.

(113) Coordination complexes of $NbMe_3Cl_2$ have been reported, see reference 43.

(114) ^1H NMR of $[Ar^{Tol_2}]NbMe_2Cl_2$ (C_6D_6): 1.84 [s, 6H of $Nb\underline{Me_2}$], 2.07 [s, 6H of Me of Ar^{Tol_2}], 7.00 [d, $^3J_{H\text{-}H} = 8$, 4H of Ar^{Tol_2}], 7.12 [m, 3H of Ar^{Tol_2}], 7.71 [d, $^3J_{H\text{-}H} = 8$, 4H of Ar^{Tol_2}].

(115) Upon addition of [Ar^{Tol_2}]Li, the mixture bubbles rapidly. Analysis of the ^1H NMR spectrum demonstrates the production of methane, in addition to a significant amount of [Ar^{Tol_2}]H.

(116) X-ray quality crystals of [Ar^{Tol_2}]$NbMe_2Cl_2$ were obtained from a solution in pentane at –15 ˚C.

(117) X-ray quality crystals of [κ^3-$Ar^{Tol'_2}$]$Nb(PMe_3)_2MeCl$ were obtained from a solution in pentane at –15 ˚C.

(118) ^1H NMR of [κ^3-$Ar^{Tol'_2}$]$Nb(PMe_3)_2Me_2$ (C_6D_6): 0.41 [m, 18H of $(P\underline{Me}_3)_2$], 2.05 [m, 6H of $Nb\underline{Me}_2$], 2.28 [s, 6H of Me of $Ar^{Tol'_2}$], 7.04 [d, $^3J_{H\text{-}H}$ = 8, 2H of $Ar^{Tol'_2}$], 7.32 [tt, $^3J_{H\text{-}H}$ = 8, $^6J_{P\text{-}H}$ = 2, 1H of $Ar^{Tol'_2}$], 7.50 [s, 2H of $Ar^{Tol'_2}$], 7.52 [d, $^3J_{H\text{-}H}$ = 8, 2H of $Ar^{Tol'_2}$], 7.69 [d, $^3J_{H\text{-}H}$ = 8, 2H of $Ar^{Tol'_2}$]. $^{31}P\{^1H\}$ NMR of [κ^3-$Ar^{Tol'_2}$]$Nb(PMe_3)_2Me_2$ (C_6D_6): 2.9 [br s, 2P of $(\underline{P}Me_3)_2$].

(119) The molecular structure of [κ^3-$Ar^{Tol'_2}$]$Nb(PMe_3)_2Cl_2$ may contain a small amount of [κ^3-$Ar^{Tol'_2}$]$Nb(PMe_3)_2MeCl$ impurity based on the size of the chloride thermal ellipsoids. However, attempts to model this disorder did not result in an improved refinement and was thus ignored.

(120) X-ray quality crystals of [κ^3-$Ar^{Tol'_2}$]$Nb(PMe_3)_2Me_2$ and κ^3-$Ar^{Tol'_2}$]$Nb(PMe_3)_2Cl_2$ were obtained from solutions in pentane at –15 ˚C.

(121) Similar signals are observed for the methyl groups of [κ^3-$Ar^{Tol'_2}$]$Ta(PMe_3)_2Me_2$ (Figure 29).

(122) (a) McNally, J. P.; Leong, V. S.; Cooper, N. J. in *Experimental Organometallic Chemistry*, Wayda, A. L.; Darensbourg, M. Y., Eds.; American Chemical Society: Washington, DC, 1987; Chapter 2, pp 6-23.

(b) Burger, B.J.; Bercaw, J. E. in *Experimental Organometallic Chemistry*; Wayda, A. L.; Darensbourg, M. Y., Eds.; American Chemical Society: Washington, DC, 1987; Chapter 4, pp 79-98.

(c) Shriver, D. F.; Drezdzon, M. A.; *The Manipulation of Air-Sensitive Compounds*, 2nd Edition; Wiley-Interscience: New York, 1986.

(123) Gottlieb, H. E.; Kotlyar, V.; Nudelman, A. *J. Org. Chem.* **1997**, *62*, 7512-7515.

(124) "Nuclear Magnetic Resonance Spectroscopy" Nelson, J. H. Prentice Hall, New Jersey (2003), p 79.

(125) Pray, A. R. *Inorg. Synth.* **1957**, *5*, 153-156.

(126) (a) Sheldrick, G. M. SHELXTL, An Integrated System for Solving, Refining and Displaying Crystal Structures from Diffraction Data; University of Göttingen, Göttingen, Federal Republic of Germany, 1981.

(b) Sheldrick, G. M. *Acta Cryst.* **2008**, *A64*, 112-122.

(127) Jaguar 7.5, Schrödinger, LLC, New York, NY 2008.

(128) (a) Becke, A. D. *J. Chem. Phys.* **1993**, *98*, 5648-5652.

(b) Becke, A. D. *Phys. Rev. A* **1988**, *38*, 3098-3100.

(c) Lee, C. T.; Yang, W.; Parr, R. G. *Phys. Rev. B* **1988**, *37*, 785-789.

(d) Vosko, S. H.; Wilk, L.; Nusair, M. *Can. J. Phys.* **1980**, *58*, 1200-1211.

(e) Slater, J. C. *Quantum Theory of Molecules and Solids, Vol. 4: The Self-Consistent Field for Molecules and Solids*; McGraw-Hill: New York, 1974.

(129) (a) Hay, P. J.; Wadt, W. R. *J. Chem. Phys.* **1985**, *82*, 270-283.

(b) Wadt, W. R.; Hay, P. J. *J. Chem. Phys.* **1985**, *82*, 284-298.

(c) Hay, P. J.; Wadt, W. R. *J. Chem. Phys.* **1985**, *82*, 299-310.

(130) Version 2.0, June 1993; Lichtenberger, D. L. Department of Chemistry, University of Arizona, Tuscon, AZ 85721.

(131) (a) Wright, R. J.; Steiner, J.; Beaini, S.; Power, P. P. *Inorg. Chim. Acta.* **2006**, *359*, 1939-1946.

(b) Saednya, A.; Hart, H. *Synthesis* **1996**, 1455-1458.

CHAPTER 7

Other efforts towards a [*CCC*] X_3-donor pincer ligand

Table of Contents

7.1 Introduction

In Chapter 6, the cyclometalation chemistry of $[Ar^{Tol}{}_2]TaMe_3Cl$ ($[Ar^{Tol}{}_2]$ = 2,6-di-*p*-tolylpheny) was elucidated, towards the synthesis of the first [*CCC*] X_3–donor pincer ligand on a transition metal, namely $[\kappa^3\text{-}Ar^{Tol'}{}_2]Ta(PMe_3)_2MeCl$ (Tol′ = C_6H_3Me). In this chapter, other attempts towards the synthesis of a [*CCC*] X_3–donor pincer on tantalum are described.

7.2 Synthesis of $[Ar^{Tol}{}_2]Ta(NMe_2)_3Cl$

It has been previously reported that dimethylamide ligands of transition metals are capable of hydrogen atom abstraction reactions.[1] In this regard, $[Ta(NMe_2)_3Cl_2]_2$[2,3] was selected as an appropriate starting material for the cyclometalation of a terphenyl ligand. Thus, treatment of $[Ta(NMe_2)_3Cl_2]_2$ with $[Ar^{Tol}{}_2]Li$ gives $[Ar^{Tol}{}_2]Ta(NMe_2)_3Cl$ (Scheme 1), and its molecular structure is shown in Figure 1. $[Ar^{Tol}{}_2]Ta(NMe_2)_3Cl$ is stable in solution over a period of days at room temperature; even upon heating, there was no detectable cyclometalation of the tolyl groups of $[Ar^{Tol}{}_2]$ ligand,[4,5] but instead, decomposition to, *inter alia*, $[Ar^{Tol}{}_2]H$ was observed. Furthermore, attempts to induce elimination of $HNMe_2$ by addition of PMe_3[6] were also unsuccessful, and no reaction was observed at room temperature.

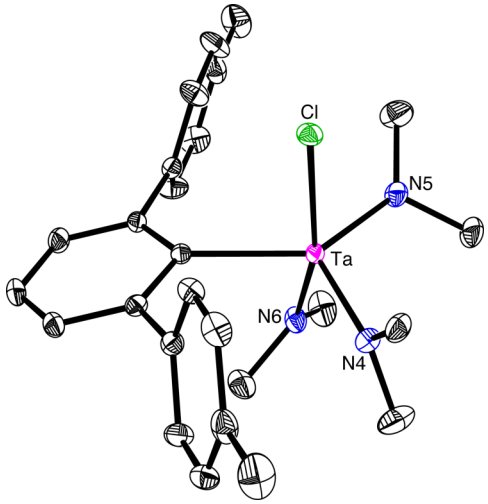

Figure 1. Molecular structure of $[Ar^{Tol}{}_2]Ta(NMe_2)_3Cl$.

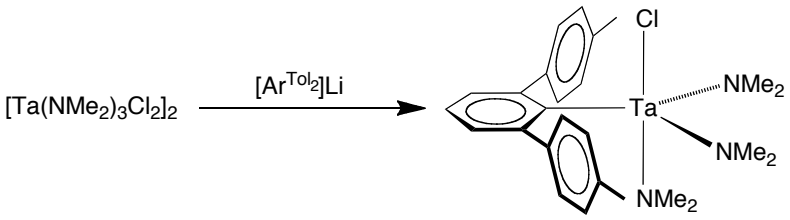

Scheme 1. Synthesis of $[Ar^{Tol_2}]Ta(NMe_2)_3Cl$.

7.3 Functionalization of $[Ar^{Tol_2}]Ta(NMe_2)_3Cl$

It was determined that $[Ar^{Tol_2}]Ta(NMe_2)_3Cl$ could be alkylated upon treatment with the appropriate lithium reagent. For example, treatment of $[Ar^{Tol_2}]Ta(NMe_2)_3Cl$ with RLi (R = Me, Et, Pr^n, Bu^n or Np) produced the tantalum complexes $[Ar^{Tol_2}]Ta(NMe_2)_3R$ (Scheme 2). All of the tantalum alkyl complexes have been structurally characterized by X-ray diffraction, and their molecular structures are shown in Figures 2 – 6.

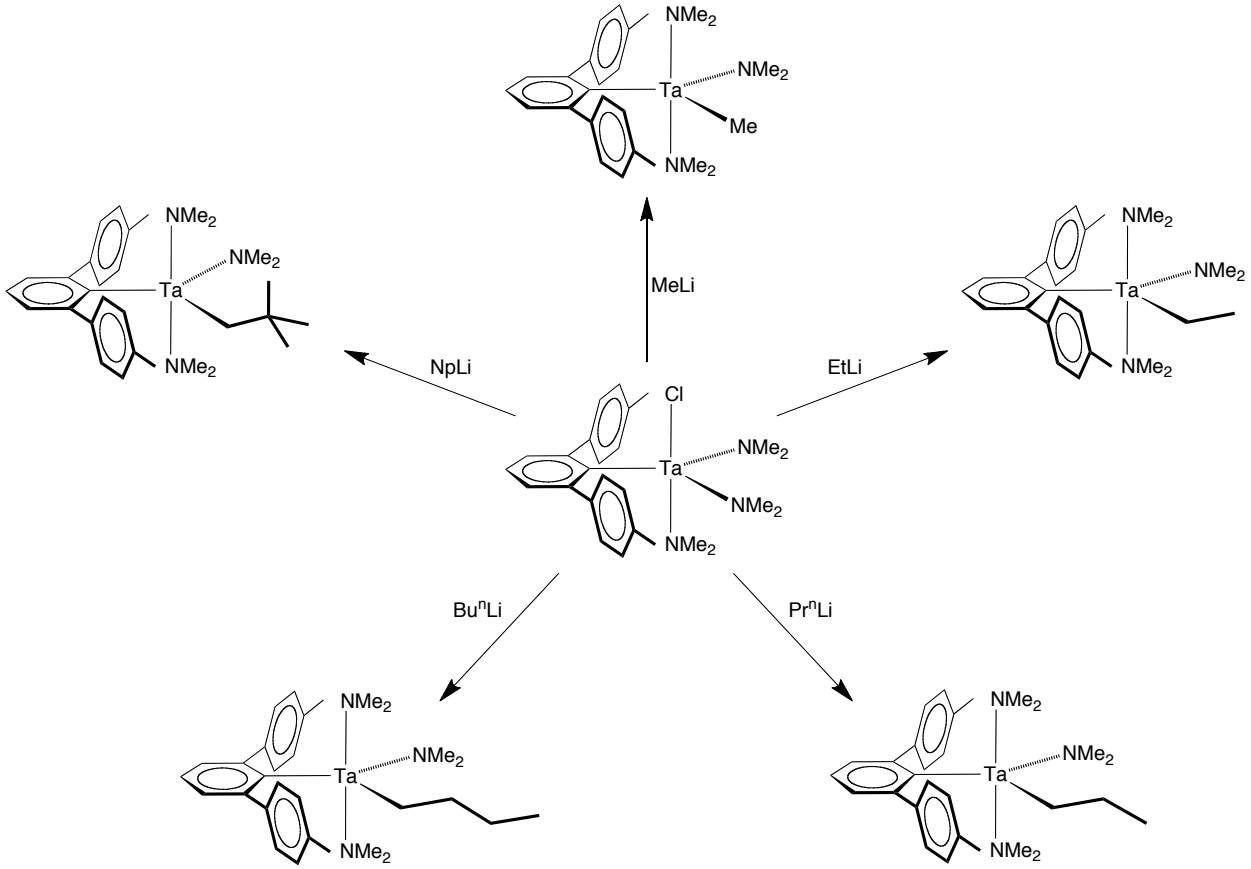

Scheme 2. Alkylation of $[Ar^{Tol_2}]Ta(NMe_2)_3Cl$.

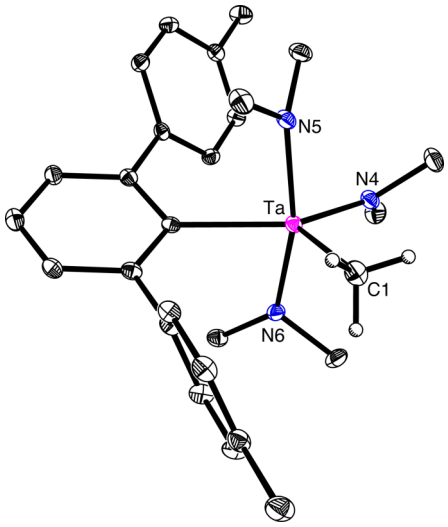

Figure 2. Molecular structure of [Ar^{Tol}_2]Ta(NMe_2)$_3$Me.

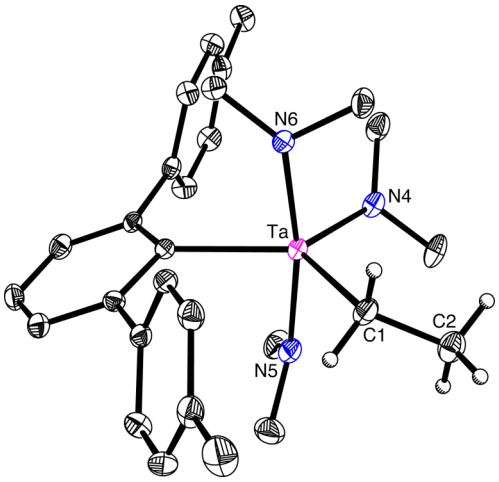

Figure 3. Molecular structure of [Ar^{Tol}_2]Ta(NMe_2)$_3$Et.

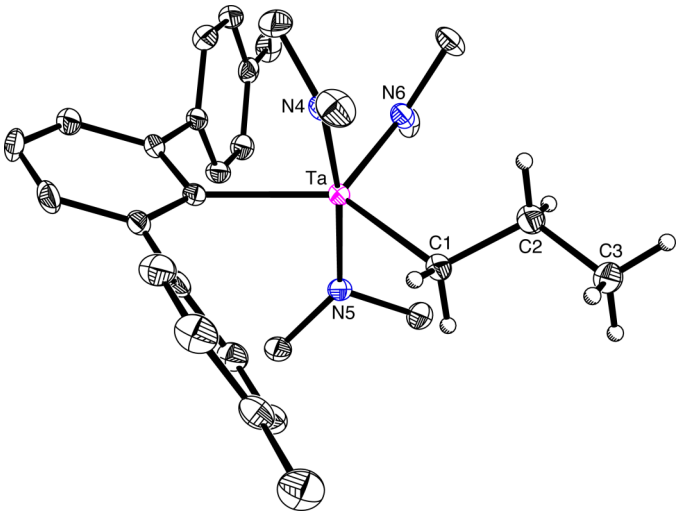

Figure 4. Molecular structure of [Ar^{Tol}_2]Ta(NMe_2)$_3$$Pr^n$.

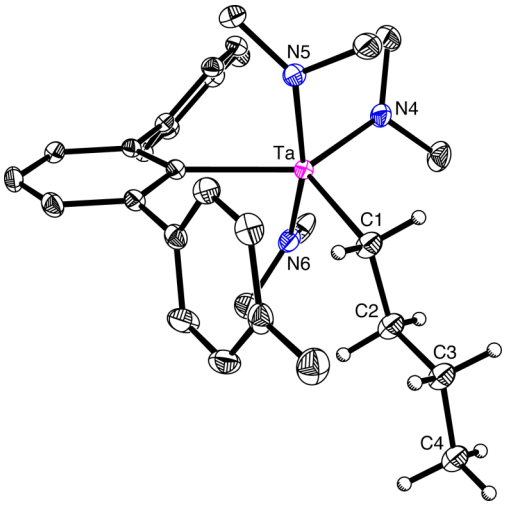

Figure 5. Molecular structure of $[Ar^{Tol}{}_2]Ta(NMe_2)_3Bu^n$.

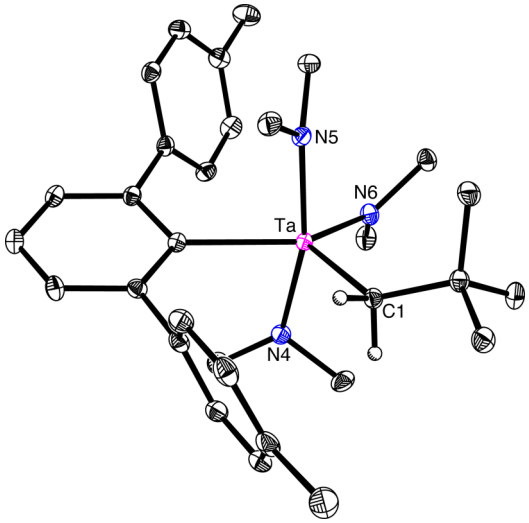

Figure 6. Molecular structure of $[Ar^{Tol}{}_2]Ta(NMe_2)_3Np$.

In addition to the synthesis of the tantalum alkyl complexes, the *bis*-terphenyl complex $[Ar^{Tol}{}_2]_2Ta(NMe_2)_3$ was formed upon treatment of $[Ar^{Tol}{}_2]Ta(NMe_2)_3Cl$ with $[Ar^{Tol}{}_2]Li$ (Scheme 3), and its molecular structure is shown in Figure 7.[7] Interestingly, $[Ar^{Tol}{}_2]_2Ta(NMe_2)_3$ is not stable in solution and decomposes to give the cyclometalated complex $[\kappa^2\text{-}Ar^{Tol,Tol'}]Ta(NMe_2)_3$ (Figure 8) and $[Ar^{Tol}{}_2]H$ over a period of one day at room temperature (Scheme 4). Notable spectroscopic signals of $[\kappa^2\text{-}Ar^{Tol,Tol'}]Ta(NMe_2)_3$ are (*i*) the inequivalent methyl groups of the $[\kappa^2\text{-}Ar^{Tol,Tol'}]$ moiety [$\delta(^1H)$ = 2.19 ppm and 2.38

ppm, δ(^{13}C{^{1}H}) = 21.2 ppm and 21.9 ppm], (*ii*) the asymmetry of the [κ^2-Ar$^{Tol,Tol'}$] moiety, giving 8 signals rather than the typical 4 observed for [Ar$^{Tol}_2$]Ta(NMe$_2$)$_3$X (X = Cl, Me, Et, Pr^n, Bu^n, Np, [Ar$^{Tol}_2$], and BH$_4$) complexes, and (*iii*) the presence of two ^{13}C signals with chemical shifts of approximately 200 (± 10) ppm [δ = 197.7 ppm and 199.6 ppm], distinctive for the aryl carbons bonded to tantalum [Ta–C$_{aryl}$] (see experimental section, 7.12).[8]

Moreover, it was determined that upon heating (100 ˚C) solutions of the tantalum alkyl complexes, [Ar$^{Tol}_2$]Ta(NMe$_2$)$_3$R (R = Me, Et, Pr^n, Bu^n or Np), cyclometalation also occurs, forming [κ^2-Ar$^{Tol,Tol'}$]Ta(NMe$_2$)$_3$, in addition to the respective alkane (Scheme 4).

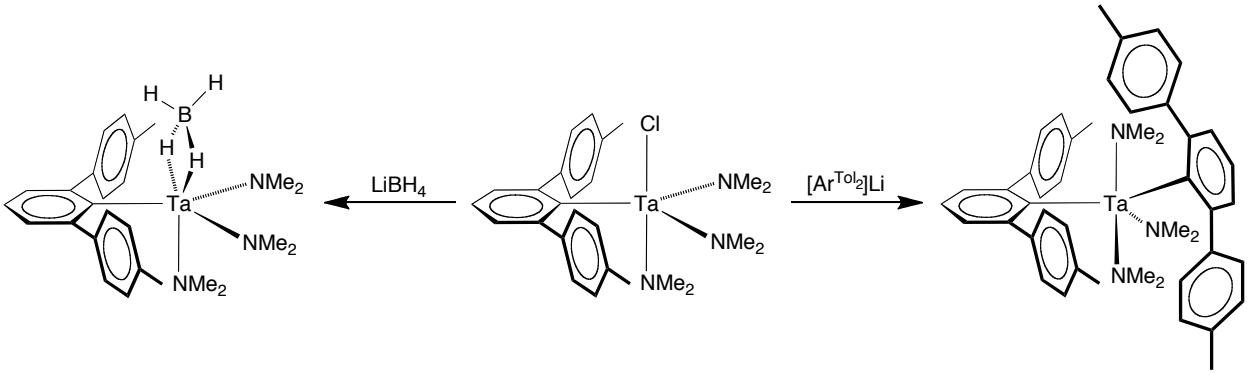

Scheme 3. Synthesis of [Ar$^{Tol}_2$]Ta(NMe$_2$)$_3$(BH$_4$) and [Ar$^{Tol}_2$]$_2$Ta(NMe$_2$)$_3$.

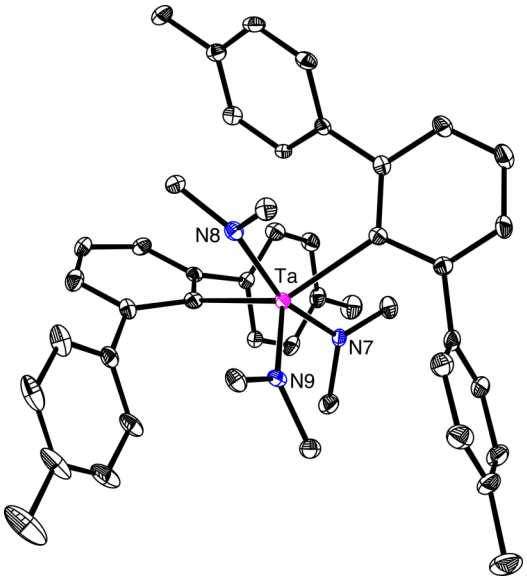

Figure 7. Molecular structure of [Ar$^{Tol}_2$]$_2$Ta(NMe$_2$)$_3$.

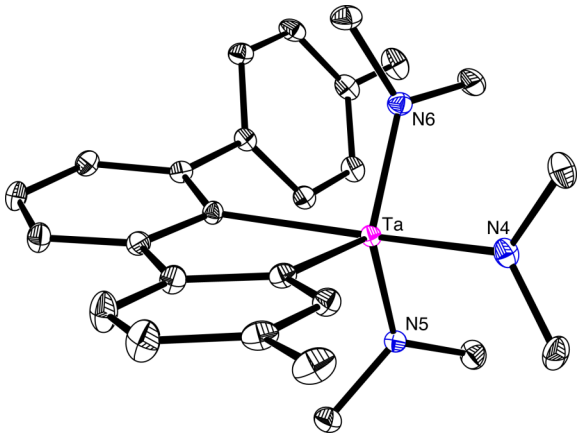

Figure 8. Molecular structure of [κ²-Ar$^{Tol,Tol'}$]Ta(NMe$_2$)$_3$.

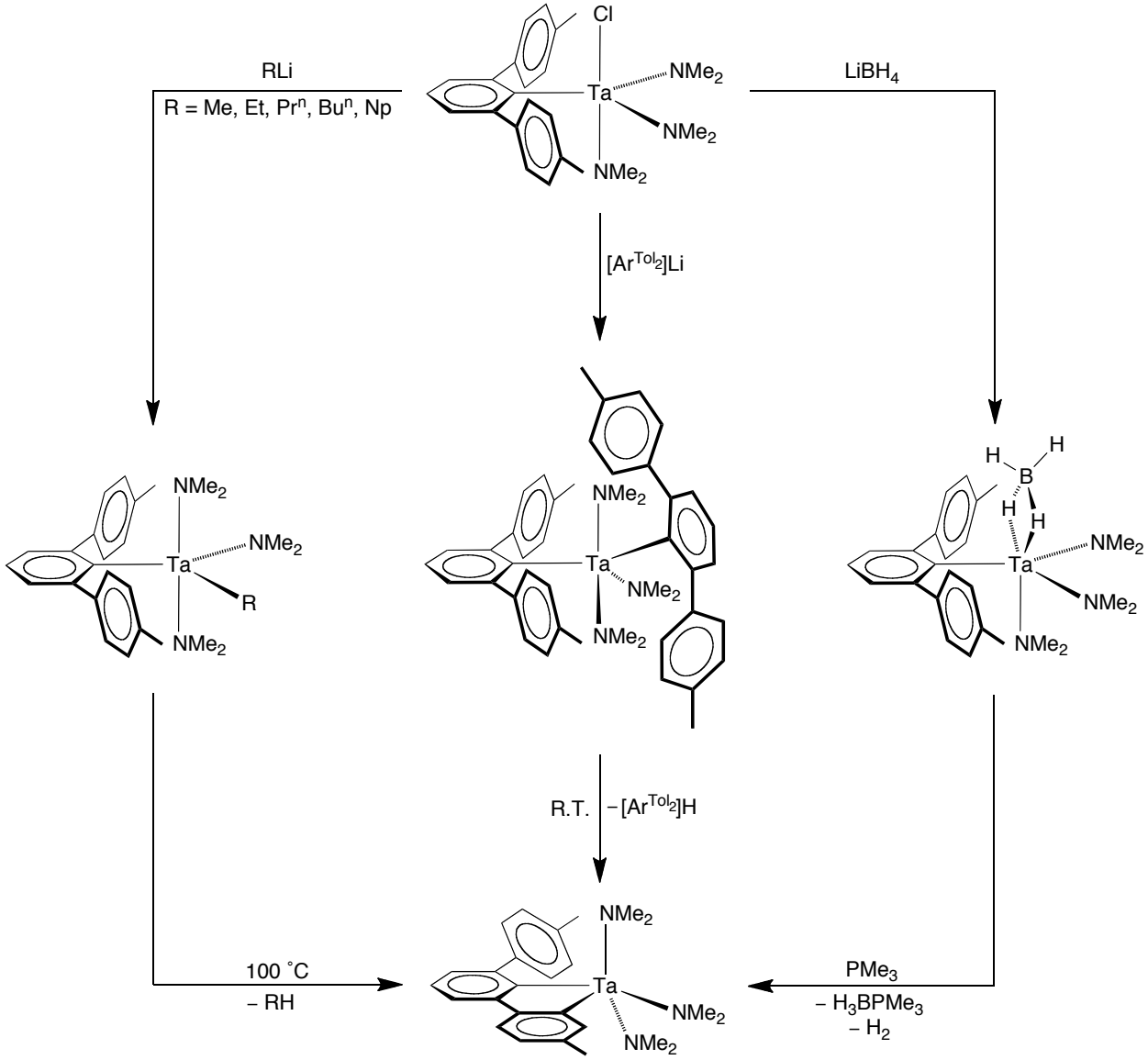

Scheme 4. Reactivity of [Ar$^{Tol}_2$]Ta(NMe$_2$)$_3$Cl and synthetic routes towards [κ²-Ar$^{Tol,Tol'}$]Ta(NMe$_2$)$_3$.

Additionally, the synthesis of a tantalum hydride complex was attempted by addition of $LiBH_4$ to $[Ar^{Tol_2}]Ta(NMe_2)_3Cl$; however, this resulted in the formation of the borohydride complex, $[Ar^{Tol_2}]Ta(NMe_2)_3(BH_4)$ (Scheme 3),[9] which has been structurally characterized by X-ray diffraction (Figure 9). In order to abstract the BH_3 fragment, $[Ar^{Tol_2}]Ta(NMe_2)_3(BH_4)$ was treated with PMe_3. In this regard, $Me_3P{\rightarrow}BH_3$ is formed but the major tantalum product is $[\kappa^2\text{-}Ar^{Tol,Tol'}]Ta(NMe_2)_3$ (Scheme 4). Thus, $[[Ar^{Tol_2}]Ta(NMe_2)_3H]$ is presumably a short-lived intermediate that eliminates H_2 at room temperature *via* cyclometalation.

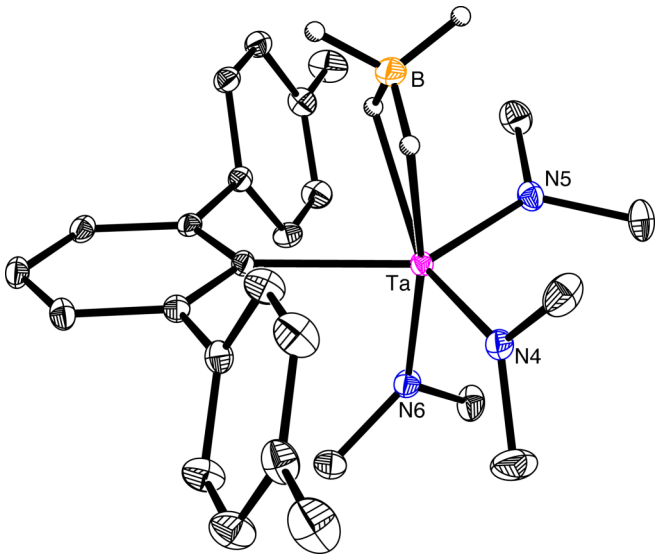

Figure 9. Molecular structure of $[Ar^{Tol_2}]Ta(NMe_2)_3(BH_4)$.

7.4 Synthesis and reactivity of $[Ar^{Tol_2}]Ta(NMe_2)_2Cl_2$

In view of the cyclometalation chemistry observed for the monoalkyl complexes, $[Ar^{Tol_2}]Ta(NMe_2)_3R$, dialkyl complexes were sought after. In this regard, the dichloride complex, $[Ar^{Tol_2}]Ta(NMe_2)_2Cl_2$, can be formed upon treatment of $[Ar^{Tol_2}]Ta(NMe_2)_3Cl$ with Me_3SiCl, which can subsequently be converted to the dialkyl complexes $[Ar^{Tol_2}]Ta(NMe_2)_2R_2$ (R = Me, Et, Pr^n, Bu^n, and Np), after addition of the appropriate alkyllithium reagent (Scheme 5). The molecular structures of $[Ar^{Tol_2}]Ta(NMe_2)_2Cl_2$ and

the dialkyl complexes $[Ar^{Tol_2}]Ta(NMe_2)_2R_2$ (R = Me, Et, Pr^n, Bu^n, and Np) have been determined by X-ray diffraction, and are shown in Figures 10 – 15.[10]

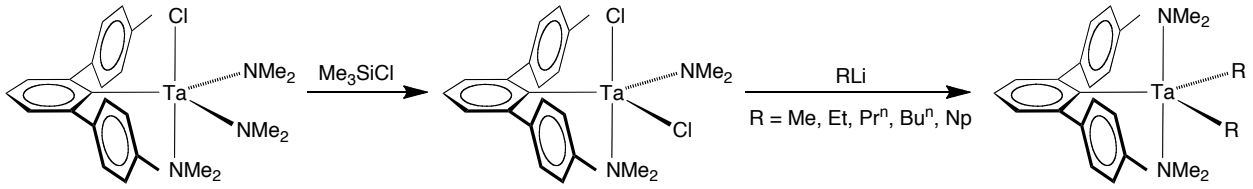

Scheme 5. Synthesis of $[Ar^{Tol_2}]Ta(NMe_2)_2Cl_2$ and reactivity with alkyllithium reagents.

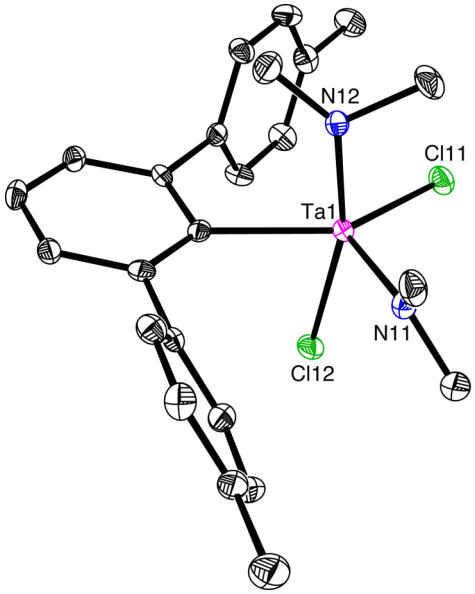

Figure 10. Molecular structure of $[Ar^{Tol_2}]Ta(NMe_2)_2Cl_2$.

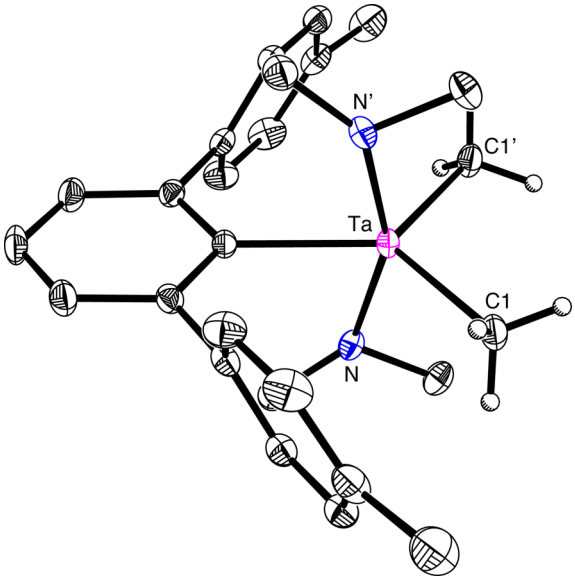

Figure 11. Molecular structure of $[Ar^{Tol_2}]Ta(NMe_2)_2Me_2$.

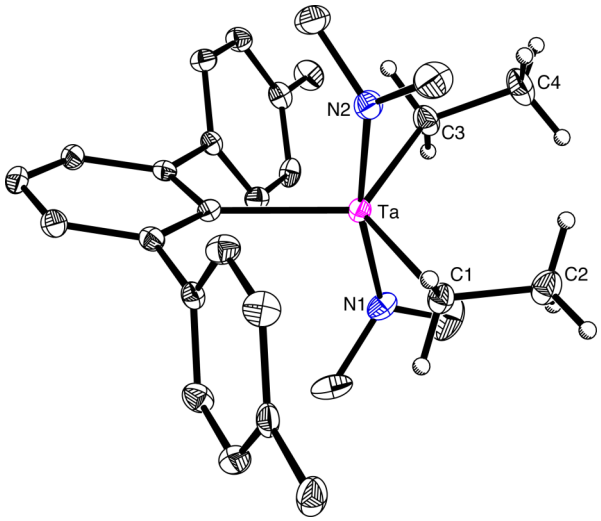

Figure 12. Molecular structure of $[Ar^{Tol}_2]Ta(NMe_2)_2Et_2$.

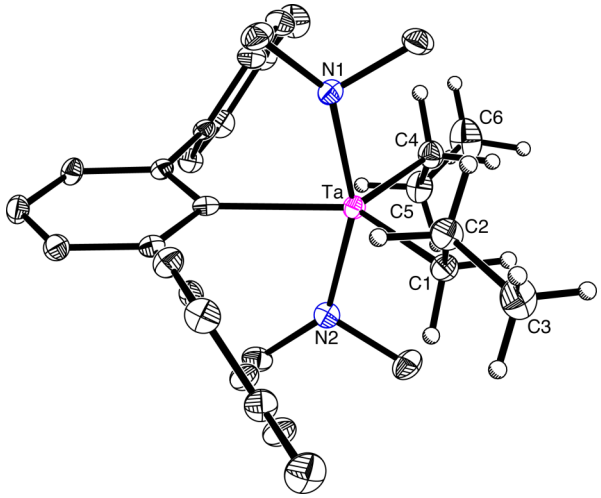

Figure 13. Molecular structure of $[Ar^{Tol}_2]Ta(NMe_2)_2Pr^n_2$.

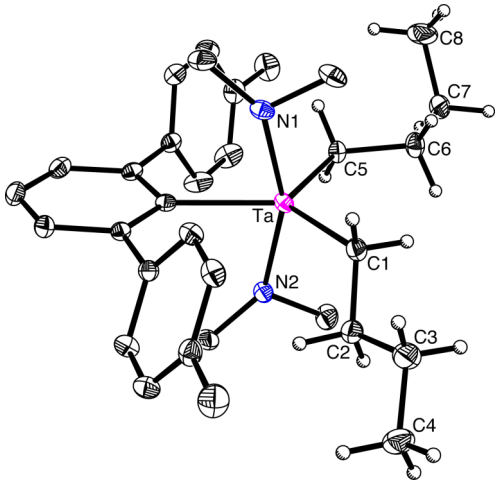

Figure 14. Molecular structure of $[Ar^{Tol}_2]Ta(NMe_2)_2Bu^n_2$.

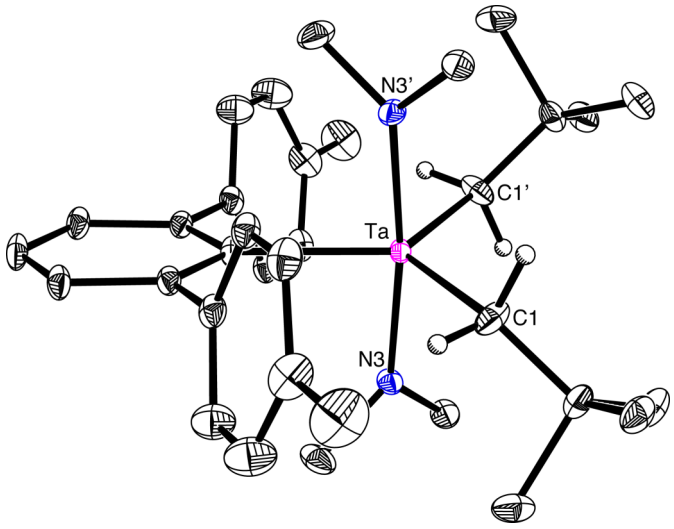

Figure 15. Molecular structure of $[Ar^{Tol}{}_2]Ta(NMe_2)_2Np_2$.

7.5 Reactivity of the dialkyl tantalum complexes, $[Ar^{Tol}{}_2]Ta(NMe_2)_2R_2$

Unfortunately, heating (100 °C) solutions of $[Ar^{Tol}{}_2]Ta(NMe_2)_2R_2$ (R = Me, Et, Pr^n, and Bu^n) did not result in the desired clean formation of $[\kappa^3\text{-}Ar^{Tol'}{}_2]Ta(NMe_2)_2$ and 2 equivalents of alkane (RH). Instead, significant decomposition to, *inter alia*, $[Ar^{Tol}{}_2]H$ was observed. In addition, the formation of $[\kappa^2\text{-}Ar^{Tol,Tol'}]Ta(NMe_2)_3$ was identified by ^1H NMR spectroscopy, signifying the occurrence of a redistribution process. In contrast to the other dialkyls, the *bis*-neopentyl complex, $[Ar^{Tol}{}_2]Ta(NMe_2)_2Np_2$, was unstable in solution at room temperature, and cyclometalates to give $[\kappa^2\text{-}Ar^{Tol,Tol'}]Ta(NMe_2)_2Np$ and neopentane (Scheme 6). The molecular structure of $[\kappa^2\text{-}Ar^{Tol,Tol'}]Ta(NMe_2)_2Np$ has been determined by X-ray diffraction and is shown in Figure 16.

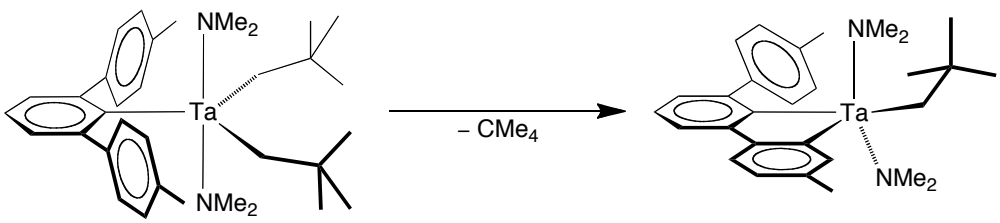

Scheme 6. Room temperature cyclometalation of $[Ar^{Tol}{}_2]Ta(NMe_2)_2Np_2$ to give $[\kappa^2\text{-}Ar^{Tol,Tol'}]Ta(NMe_2)_2Np$ and neopentane.

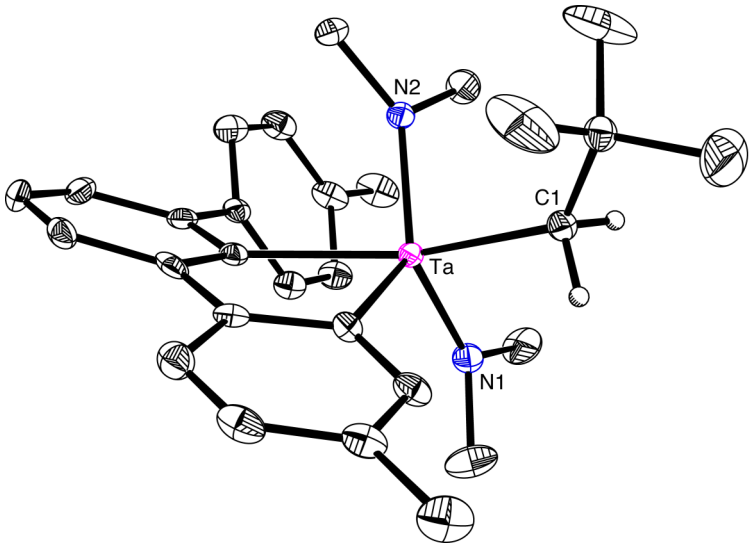

Figure 16. Molecular structure of [κ^2-Ar$^{Tol,Tol'}$]Ta(NMe$_2$)$_2$Np.

Interestingly, when a solution of [κ^2-Ar$^{Tol,Tol'}$]Ta(NMe$_2$)$_2$Np in d$_6$-benzene was heated at 60 ˚C and monitored by ^{1}H NMR spectroscopy, a new major product was observed that still contained a neopentyl (–CH$_2$CMe$_3$) group.[11] The ^{1}H and ^{13}C{^{1}H} NMR spectra of this reaction mixture have been analyzed, and it is postulated that the major product is an isomer of [κ^2-Ar$^{Tol,Tol'}$]Ta(NMe$_2$)$_2$Np, namely [κ^2-Ar*$^{Tol,Tol'}$]Ta(NMe$_2$)$_2$Np (the * signifies the different connectivity of the center arene to tantalum), as shown in Scheme 7.[12,13] It is apparent that this isomerization reaction requires that (*i*) the Ta–Ar bond is broken, (*ii*) a new Ta–Ar* bond is formed, and (*iii*) a hydrogen atom is formally transferred from the *meta* position to the *ipso* position of the central arene.[14]

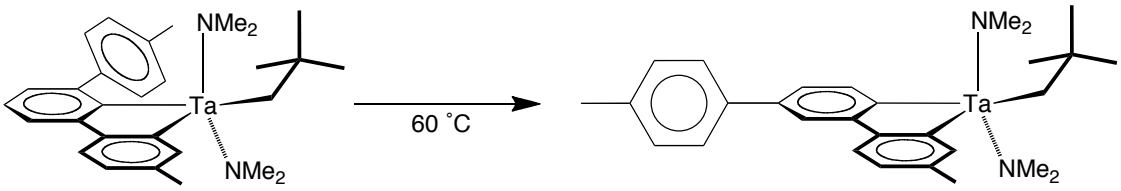

Scheme 7. Isomerization of [κ^2-Ar$^{Tol,Tol'}$]Ta(NMe$_2$)$_2$Np to [κ^2-Ar*$^{Tol,Tol'}$]Ta(NMe$_2$)$_2$Np.

7.6 Spectroscopic characterization of $[\kappa^2\text{-}Ar^{*Tol,Tol'}]Ta(NMe_2)_2Np$

It is useful to first note two important features of the ^{1}H NMR spectrum of the C_2 symmetric $[Ar^{Tol}{}_2]Ta(NMe_2)_2Np_2$, which is shown in Figure 17. These are:

1. The tolyl-methyl groups are *equivalent*.
2. The aromatic region (*i.e.* 6 – 9 ppm) has only 4 signals with a total integration of 11 (as compared with the CMe_3 group normalized to 18), thereby indicating that Tol groups have *not* been cyclometalated.
3. Furthermore, in the $^{13}C\{^1H\}$ NMR spectrum, there is only *one* signal with a chemical shift of approximately 200 (± 10) ppm, *i.e.* 201.6 ppm, thereby indicating that there is only *one* aryl carbon bonded to tantalum.

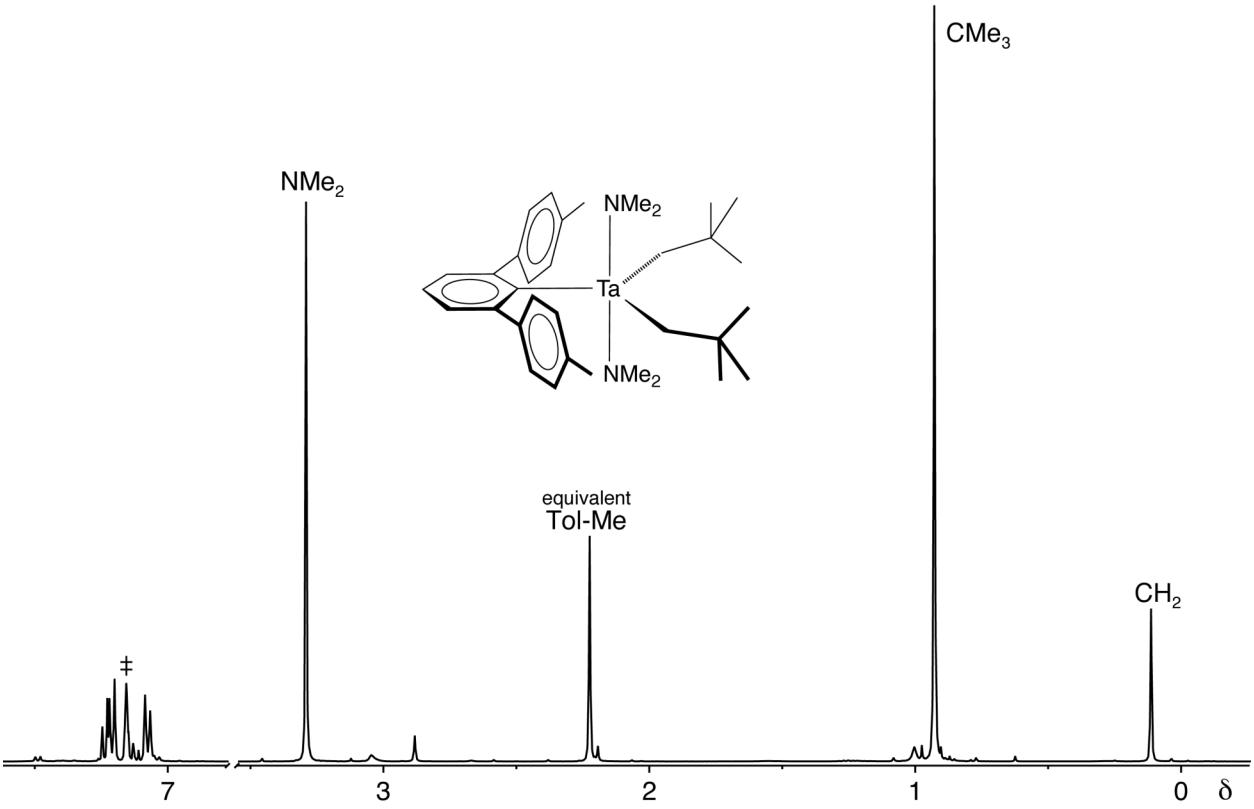

Figure 17. ^{1}H NMR spectrum of $[Ar^{Tol}{}_2]Ta(NMe_2)_2Np_2$ in d_6-benzene (‡).

It is also prudent to analyze the ^{1}H spectrum of [κ^{2}-Ar$^{Tol,Tol'}$]Ta(NMe$_2$)$_2$Np, which is shown in Figure 18. The key observations are:

1. Unlike [Ar$^{Tol}_2$]Ta(NMe$_2$)$_2$Np$_2$, there are two signals for the *inequivalent* tolyl-methyl groups in [κ^{2}-Ar$^{Tol,Tol'}$]Ta(NMe$_2$)$_2$Np.
2. The aromatic region has 8 signals with a total integration of 10 (as compared with the CMe$_3$ group normalized to 9), indicating its *asymmetry* due to cyclometalation.
3. One of these aromatic signals is a singlet (8.24 ppm, marked with an asterisk in Figure 18), representative of an aromatic proton that does not have protons in the respective *ortho* positions, thus lacking the typical ~8 Hz coupling constant.[15]
4. In the ^{13}C{^{1}H} NMR spectrum of [κ^{2}-Ar$^{Tol,Tol'}$]Ta-(NMe$_2$)$_2$Np, there are *two* signals with chemical shifts of approximately 200 (± 10) ppm, *i.e.* 197.7 ppm and 201.5 ppm, thereby indicating the presence of *two* aryl carbons bonded to tantalum.

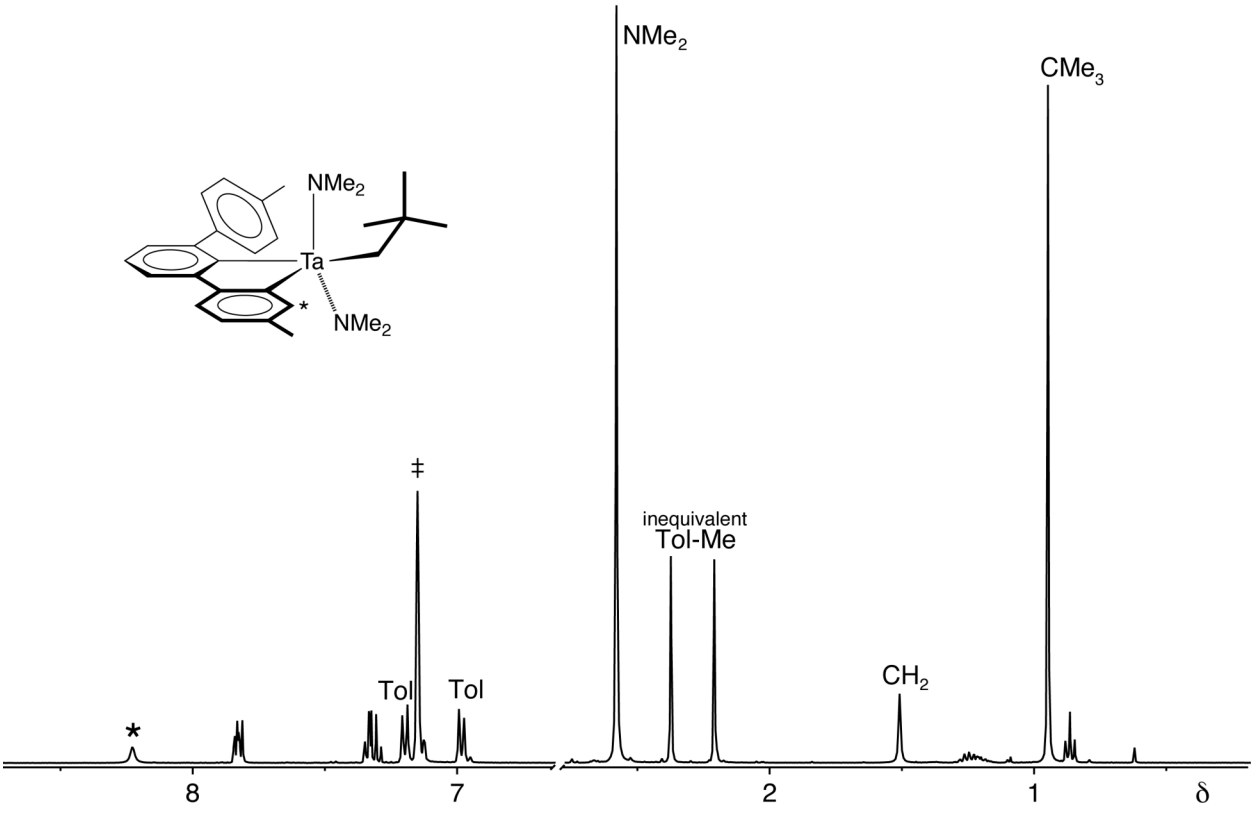

Figure 18. ^{1}H NMR spectrum of [κ^{2}-Ar$^{Tol,Tol'}$]Ta(NMe$_2$)$_2$Np in d$_6$-benzene (‡).

The ^{1}H NMR spectrum of the reaction mixture produced from heating [κ^2-Ar$^{Tol,Tol'}$]Ta(NMe$_2$)$_2$Np is shown in Figure 19, and the major observations that give indication that [κ^2-Ar$^{*Tol,Tol'}$]Ta(NMe$_2$)$_2$Np has been formed are the following:

1. There are two new signals for *inequivalent* tolyl-methyl groups.
2. There is a new set of signals for a neopentyl (–CH$_2$CMe$_3$) group.
3. The aromatic region contains 8 new signals.
4. There are *two* signals, which lack ~8 Hz coupling constants [*i.e.* 7.90 ppm (s) and 8.15 ppm (d, $^{4}J_{H\text{-}H}$ = 1.5 Hz)], indicating that there are *two* protons positioned on the arenes that do not have vicinal protons (marked by an asterisk in Figure 19).
5. In the ^{13}C{^{1}H} NMR spectrum of the reaction mixture (Figure 20), there are *two* new signals with chemical shifts of approximately 200 (± 10) ppm, *i.e.* 199.7 ppm and 201.2 ppm,[16] thereby indicating the presence of *two* aryl carbons bonded to tantalum.

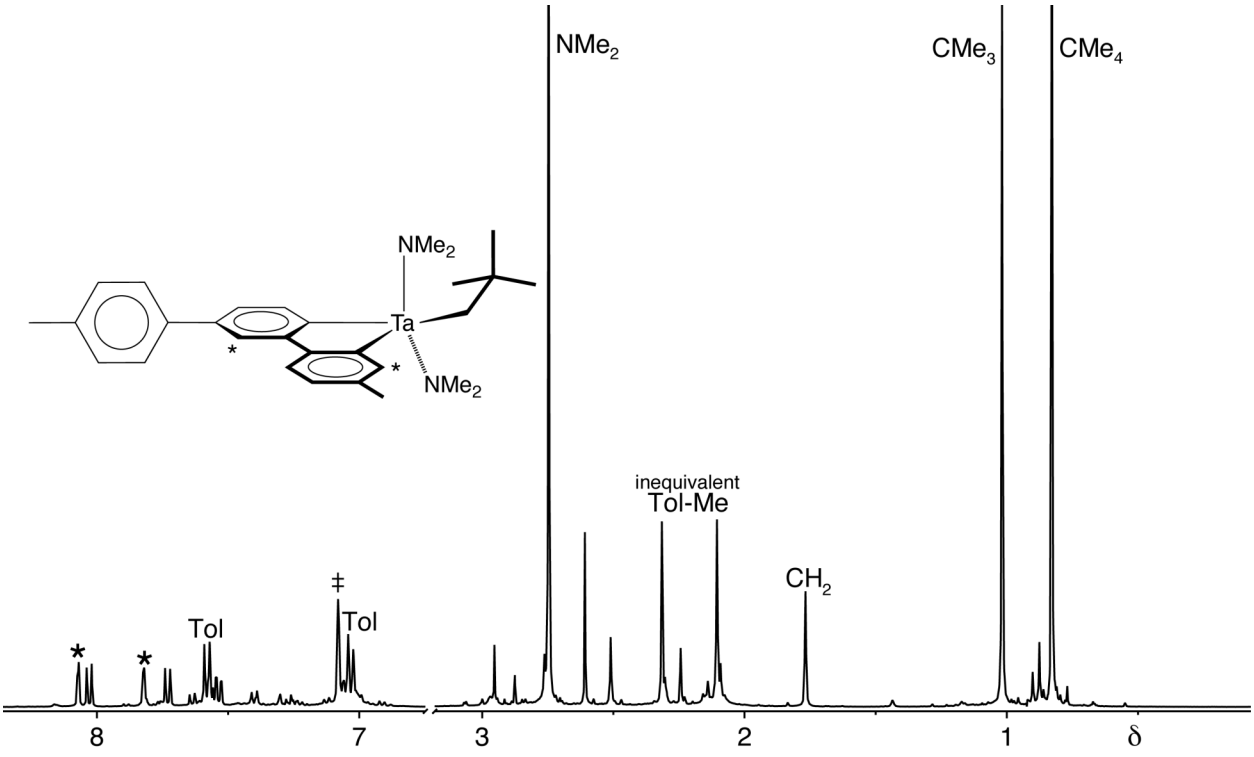

Figure 19. ^{1}H NMR spectrum of [κ^2-Ar$^{*Tol,Tol'}$]Ta(NMe$_2$)$_2$Np in d$_6$-benzene (‡).

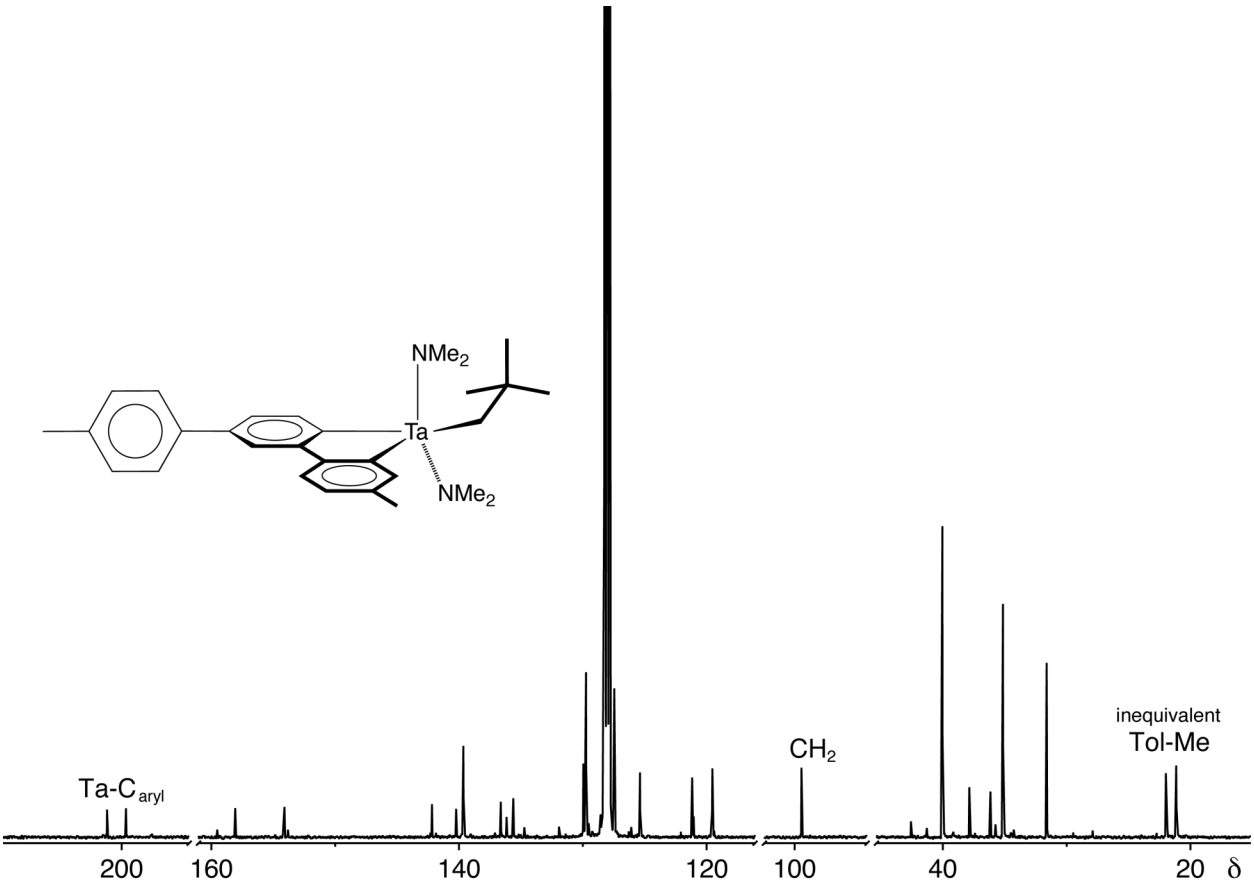

Figure 20. $^{13}C\{^{1}H\}$ NMR spectrum of $[\kappa^2\text{-}Ar^{*Tol,Tol'}]Ta(NMe_2)_2Np$ in d_6-benzene (‡).

7.7 Protolytic cleavage studies

Protolytic cleavage studies were performed in order to obtain supporting data for the structural assignment of $[\kappa^2\text{-}Ar^{*Tol,Tol'}]Ta(NMe_2)_2Np$. In this regard, d_4-MeOD was added to d_6-benzene solutions of (**A**) $[Ar^{Tol_2}]Li$, (**B**) $[\kappa^2\text{-}Ar^{Tol,Tol'}]Ta(NMe_2)_2Np$ and (**C**) $[\kappa^2\text{-}Ar^{*Tol,Tol'}]Ta(NMe_2)_2Np$, to ascertain the positions in which the deuterium ends up after protolytic cleavage. The rational d_x-$[Ar^{Tol_2}]H$ products of these reactions are shown in Scheme 8 and the ^{1}H NMR spectra of the reactions, with peak assignment and integration, are shown in Figure 21.

The protonated ligand, [Ar^{Tol}_2]H, has been characterized by ^{1}H NMR and its peak assignment is shown in Figure 21. In reaction (**A**), signal (**a**) is absent, thereby indicating the presence of deuterium in position (**a**). In reaction (**B**), signal (**a**) is absent but additionally, the integration of the signal that consists of (**b**) and (**d**) integrates to 5 (as compared with the tolyl-methyl groups normalized to 6), indicating that one site of (**d**) has been replaced with deuterium. In reaction (**C**), signal (**a**) is present but the integration of the signal that consists of (**b**) and (**d**) integrates to 4, signifying that one site of (**b**) and one site of (**d**) has been replaced with deuterium atoms.[17] Lastly, reactions (**B**) and (**C**) were also analyzed by ^{2}H NMR spectroscopy and the deuterium signals are in accord for both [κ^2-$Ar^{Tol,Tol'}$]Ta(NMe_2)$_2$Np and [κ^2-$Ar^{*Tol,Tol'}$]Ta(NMe_2)$_2$Np (Figure 22).

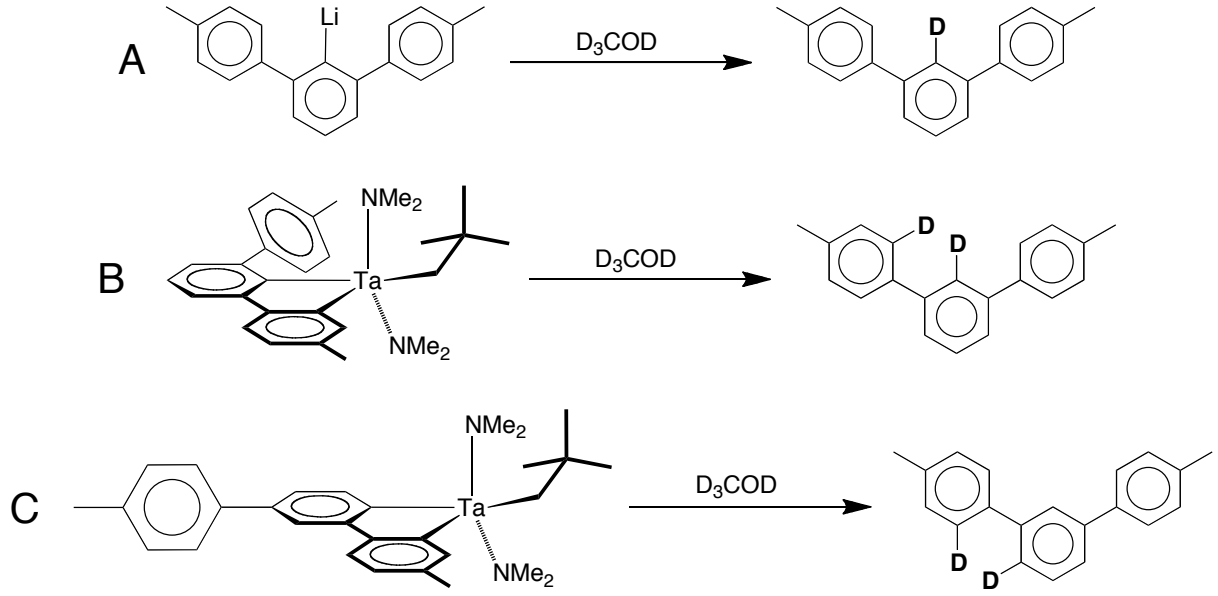

Scheme 8. Proposed deuterium distribution upon treament of (**A**) [Ar^{Tol}_2]Li, (**B**) [κ^2-$Ar^{Tol,Tol'}$]Ta(NMe_2)$_2$Np, and (**C**) [κ^2-$Ar^{*Tol,Tol'}$]Ta(NMe_2)$_2$Np with d_4-MeOD.

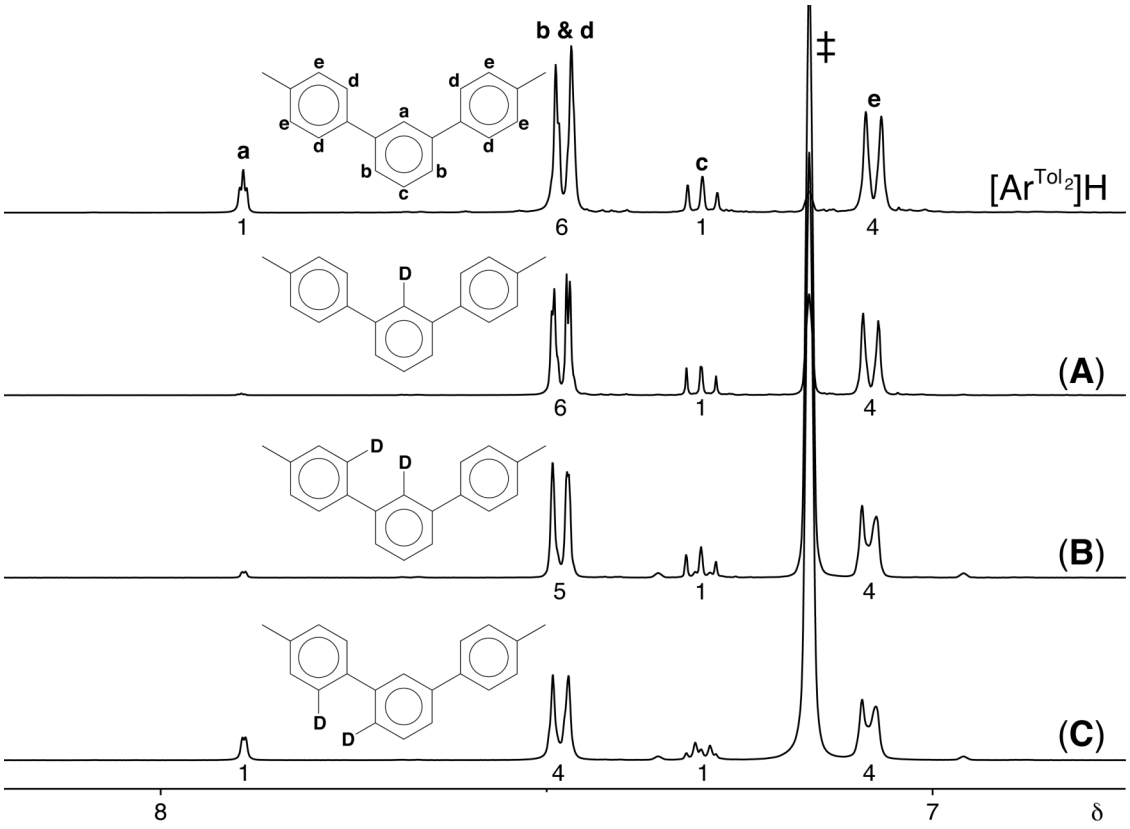

Figure 21. ^{1}H NMR spectra of [Ar$^{Tol}_2$]Li, and reactions (**A**) [Ar$^{Tol}_2$]Li, (**B**) [κ^2-Ar$^{Tol,Tol'}$]Ta(NMe$_2$)$_2$Np, and (**C**) [κ^2-Ar*$^{Tol,Tol'}$]Ta(NMe$_2$)$_2$Np with d$_4$-MeOD in d$_6$-benzene (‡). The peak integration is written below each signal.

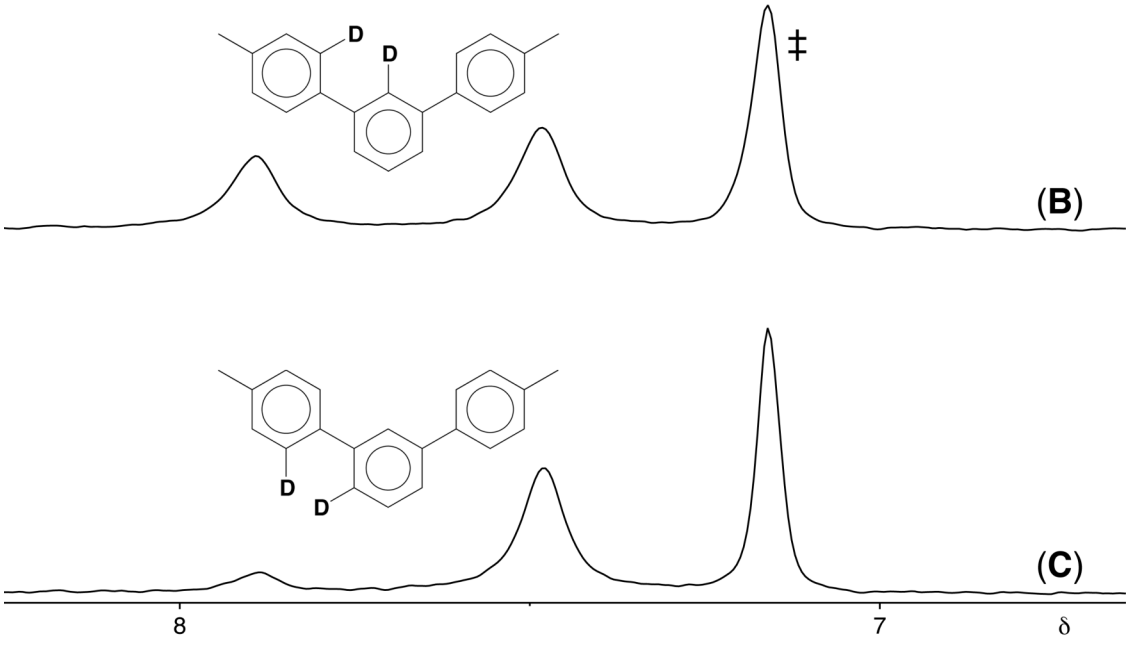

Figure 22. ^{2}H NMR spectra of reactions (**B**) [κ^2-Ar$^{Tol,Tol'}$]Ta(NMe$_2$)$_2$Np, and (**C**) [κ^2-Ar*$^{Tol,Tol'}$]Ta(NMe$_2$)$_2$Np with d$_4$-MeOD in d$_6$-benzene (‡).

7.8 Kinetics of thermolysis of $[Ar^{Tol}{}_2]Ta(NMe_2)_2Np_2$

The kinetics of cyclometalation of $[Ar^{Tol}{}_2]Ta(NMe_2)_2Np_2$ to form $[\kappa^2\text{-}Ar^{Tol,Tol'}]\text{-}Ta(NMe_2)_2Np$, and subsequent isomerization of $[\kappa^2\text{-}Ar^{Tol,Tol'}]Ta(NMe_2)_2Np$ to form $[\kappa^2\text{-}Ar^{*Tol,Tol'}]Ta(NMe_2)_2Np$ was analyzed by using ^{1}H NMR spectroscopy. In this regard, if the reaction is performed at 47 ˚C, the first step (*i.e.* elimination of neopentane from $[Ar^{Tol}{}_2]Ta(NMe_2)_2Np_2$ giving $[\kappa^2\text{-}Ar^{Tol,Tol'}]Ta(NMe_2)_2Np$, Scheme 6), can be monitored without isomerization to $[\kappa^2\text{-}Ar^{*Tol,Tol'}]Ta(NMe_2)_2Np$ occurring (Figure 23). Analysis of the data gives good evidence that the reaction is first order (*i.e.* unimolecular) in $[Ar^{Tol}{}_2]Ta(NMe_2)_2Np_2$ (Figure 24) and the first order rate constant (k_1) is 6.67×10^{-5} s^{-1}, corresponding to a free energy of activation ($\Delta G^{\ddagger}$) of 24.9 kcal mol^{-1} at 47 ˚C.

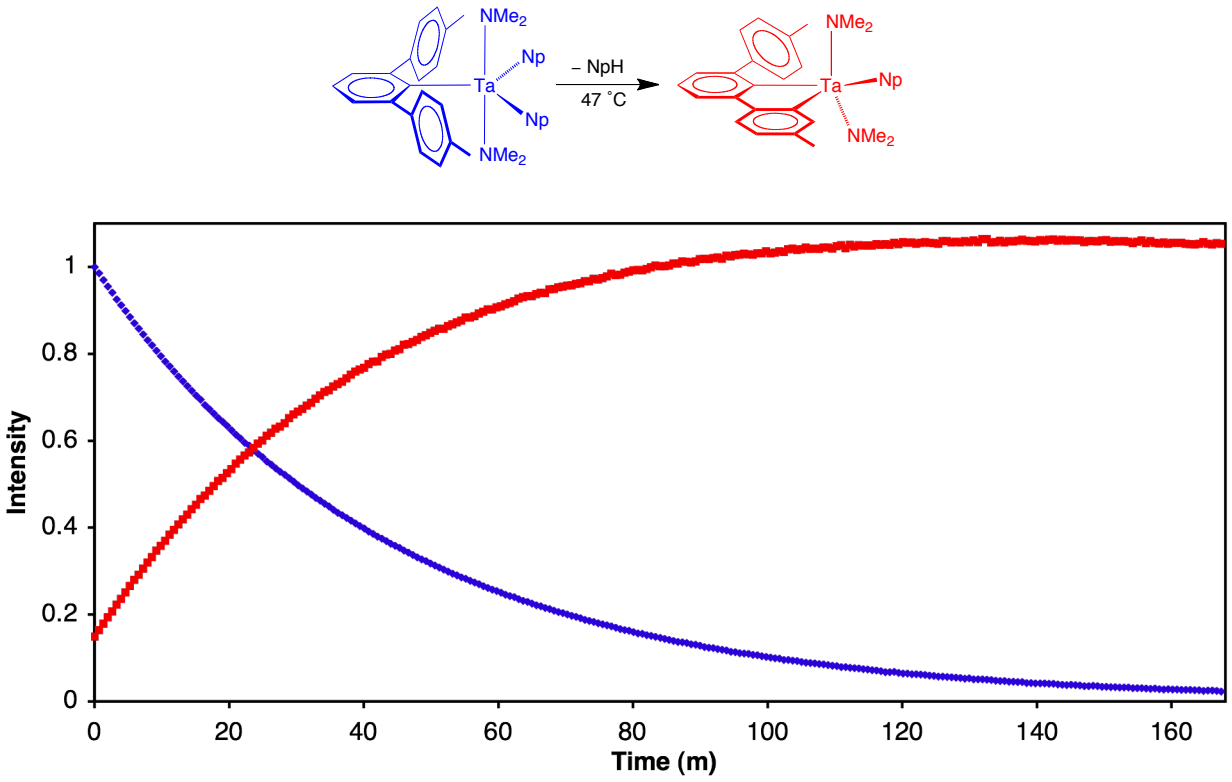

Figure 23. Plot of intensity of $[Ar^{Tol}{}_2]Ta(NMe_2)_2Np_2$ (blue) and $[\kappa^2\text{-}Ar^{Tol,Tol'}]Ta(NMe_2)_2Np$ (red) versus time at 47 ˚C. 256 data points were collected, each point at 0.66 min intervals. The kinetics were measured in the probe of the NMR spectrometer, by monitoring the intensity of the $(NMe_2)_2$ ^{1}H NMR signals for both compounds.

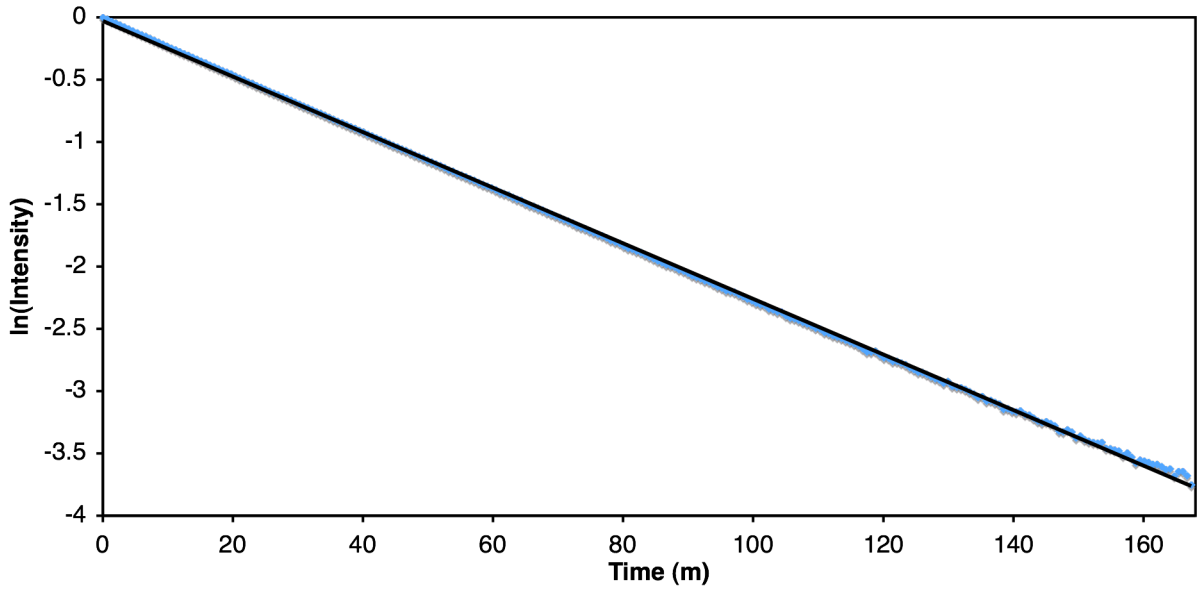

Figure 24. Plot of the natural log of intensity of $[Ar^{Tol_2}]Ta(NMe_2)_2Np_2$ versus time at 47 °C (using the data from Figure 23).

If the thermolysis of $[Ar^{Tol_2}]Ta(NMe_2)_2Np_2$ is performed at higher temperature (67 °C), the kinetics of the cyclometalation and isomerization reaction (*i.e.* $[\kappa^2\text{-}Ar^{Tol,Tol'}]$-$Ta(NMe_2)_2Np$ forming $[\kappa^2\text{-}Ar^{*Tol,Tol'}]Ta(NMe_2)_2Np$, Scheme 7) can be analyzed. As illustrated in (Figure 25), $[Ar^{Tol_2}]Ta(NMe_2)_2Np_2$ (light blue) quickly disappears (within 20 min) with subsequent production of $[\kappa^2\text{-}Ar^{Tol,Tol'}]Ta(NMe_2)_2Np$ (dark blue), which then converts to $[\kappa^2\text{-}Ar^{*Tol,Tol'}]Ta(NMe_2)_2Np$ (red). Analysis of the data gives good evidence that the isomerization reaction is also first order in $[\kappa^2\text{-}Ar^{Tol,Tol'}]Ta(NMe_2)_2Np$ (Figure 26); the first order rate constant (k_1) is 1.15×10^{-4} s^{-1}, corresponding to a free energy of activation ($\Delta G^{\ddagger}$) of 26.1 kcal mol^{-1} at 67 °C.

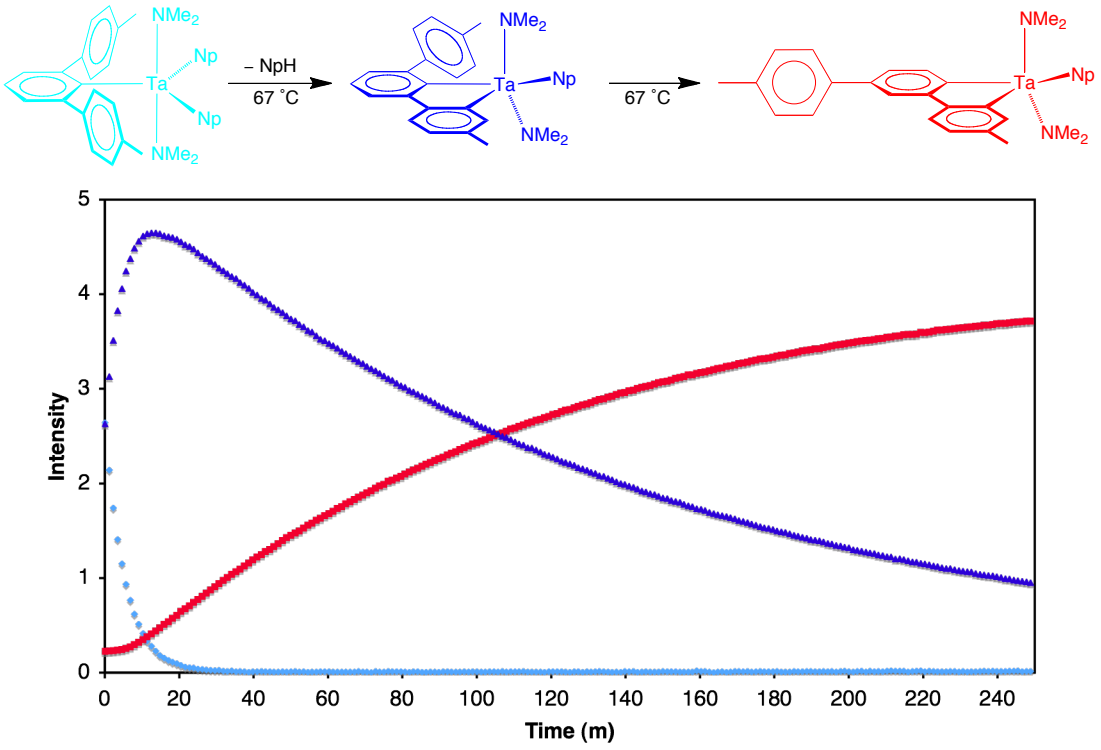

Figure 25. Plot of the intensity of $[Ar^{Tol}_2]Ta(NMe_2)_2Np_2$ (light blue), $[\kappa^2\text{-}Ar^{Tol,Tol'}]Ta(NMe_2)_2Np$ (dark blue), and $[\kappa^2\text{-}Ar^{*Tol,Tol'}]Ta(NMe_2)_2Np$ (red) versus time at 67 °C. 220 data points were collected, each point at 1.14 min intervals. The kinetics were measured in the probe of the NMR spectrometer, by monitoring the intensity of the $(NMe_2)_2$ ^1H NMR signals for the three compounds.

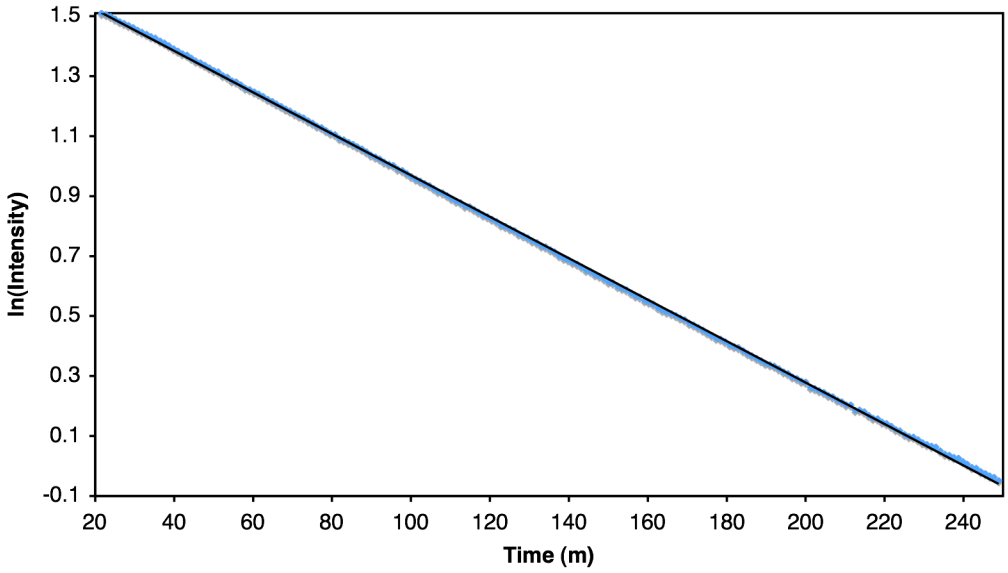

Figure 26. Plot of the natural log of intensity of $[\kappa^2\text{-}Ar^{Tol,Tol'}]Ta(NMe_2)_2Np$ versus time at 67 °C (using the data from Figure 25). The data starts at 20 minutes because this is the time at which $[Ar^{Tol}_2]Ta(NMe_2)_2Np_2$ had all reacted.

7.9 Mechanism of formation of [κ²-Ar*$^{Tol,Tol'}$]Ta(NMe$_2$)$_2$Np

The mechanism of formation of [κ²-Ar*$^{Tol,Tol'}$]Ta(NMe$_2$)$_2$Np is of interest as it requires several bond cleavages and bond formations. One possibility is the formation of a neopentylidene intermediate *via* α-hydride abstraction, followed by a 180° bond rotation, and then a 1,2-addition to form the new Ta–Ar* bond and reform the neopentyl unit (Scheme 9). In this regard, an isotopologue of [Ar$^{Tol}_2$]Ta(NMe$_2$)$_2$Np$_2$, namely d$_4$-[Ar$^{Tol}_2$]Ta(NMe$_2$)$_2$(CD$_2$Bu^t)$_2$, was synthesized in order to ascertain if this mechanism was plausible. Monitoring the thermolysis reaction of d$_4$-[Ar$^{Tol}_2$]Ta-(NMe$_2$)$_2$(CD$_2$Bu^t)$_2$ in d$_6$-benzene by ^{1}H NMR spectroscopy demonstrates the selective formation of d$_2$-[κ²-Ar$^{Tol,Tol'}$]Ta(NMe$_2$)$_2$(CD$_2$Bu^t) followed by d$_2$-[κ²-Ar*$^{Tol,Tol'}$]Ta(NMe$_2$)$_2$-(CD$_2$Bu^t). The formation of d$_2$-[κ²-Ar$^{Tol,Tol'}$]Ta(NMe$_2$)$_2$(CD$_2$Bu^t) indicates that this compound is formed by a sigma-bond metathesis (SBM) mechanism rather than α-hydride abstraction.[18] The formation of d$_2$-[κ²-Ar*$^{Tol,Tol'}$]Ta(NMe$_2$)$_2$(CD$_2$Bu^t),[19] in which there is no hydrogen incorporation into the methylene site of the neopentyl unit, is very informative as it rules out the formation of a neopentylidene intermediate as a plausible mechanism for this reaction (Scheme 9).

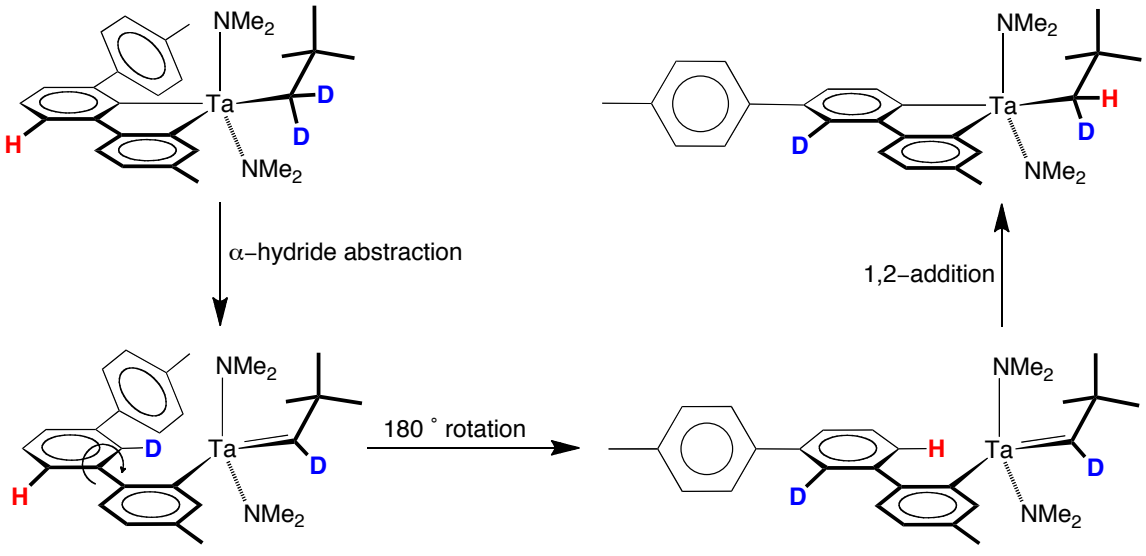

Scheme 9. Possible mechanism of isomerization (ruled out by isotopic labeling experiment).

Another possible mechanistic scenario is one in which an amide ligand (NMe_2) cyclometalates to form a metallaaziridine ring, (η^2-CH_2NMe), transferring a hydrogen to the *ipso* position, followed by bond rotation and 1,2-addition to reform the NMe_2 group (Scheme 10). As illustrated in Scheme 10, the neopentyl group is not participating in this pathway; thus the (CD_2Bu^t) group would not be expected to have protio incorporation. In support of this notion, cyclometalation of dimethylamido ligands on tantalum has been previously observed.[20]

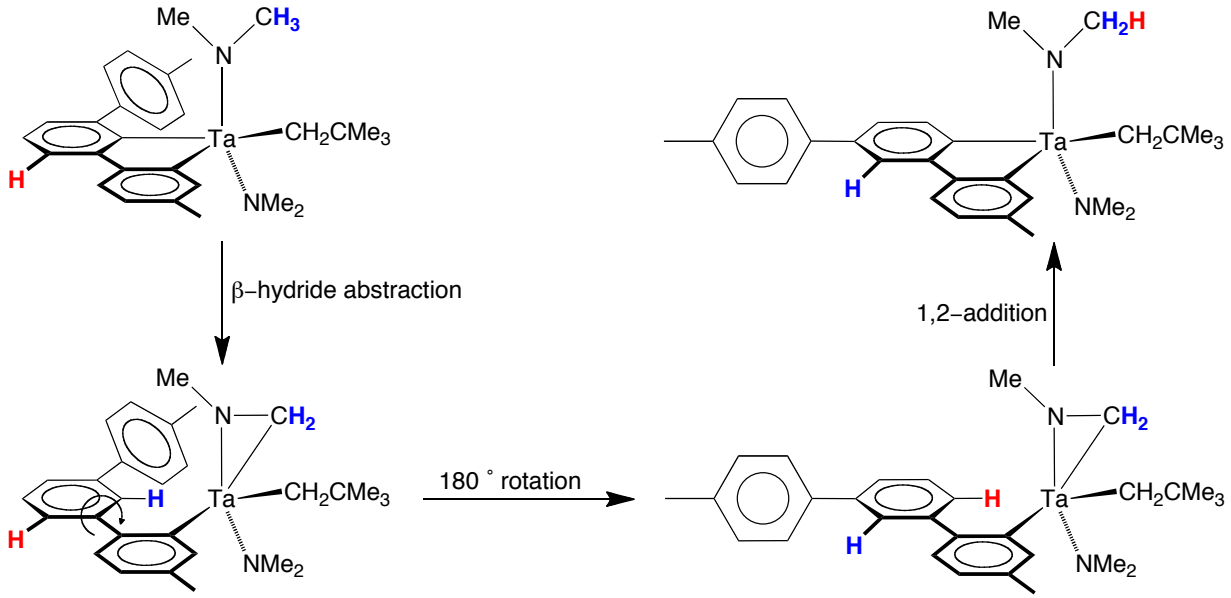

Scheme 10. Possible mechanism of isomerization through a metallaaziridine ring.

7.10 Structural Aspects of {[Ar^{Tol_2}]Ta} Complexes

The molecular structures of the *mono*-alkyl compounds, [Ar^{Tol_2}]Ta(NMe_2)$_3$R (R = Me, Et, Pr^n, Bu^n, and Np) have all been determined by X-ray diffraction. Notably, the Ta–C_{ipso}–C_{para} angles, which are listed in Table 1, have a large range of 18.6˚ (160.7˚ to 179.3˚); however, there is no discernable trend based on steric factors. In fact, the [Ar^{Tol_2}]Ta(NMe_2)$_3$Np (179.3˚) has the most idealized angle (180˚), while [Ar^{Tol_2}]Ta(NMe_2)$_3$$Pr^n$ (160.7˚) has the largest deviation from linearity. In order to understand these differences, density function geometry optimization calculations were

performed on the alkyl derivatives.[21] However, the calculated geometries did not reproduce the Ta–C_{ipso}–C_{para} angles that were determined by X-ray diffraction [$\Delta_{Calculated–Crystal}$ (˚), Table 1], with a calculated range of 5.0 ˚ (163.4˚ to 168.4˚), which is significantly smaller than the experimental range (18.6˚). The largest deviation form linearity for the Ta–C_{ipso}–C_{para} angle is observed in the *bis*-terphenyl complex, $[Ar^{Tol_2}]_2Ta(NMe_2)_3$, having angles of 154.5˚ and 177.3˚.[22] This distortion, however, is reproduced by density function calculations giving indication that the calculations are working properly. Thus, although it is possible that the calculations are erroneous, the deviations from linearity observed in the experimental crystal structures are postulated to be due to crystal packing effects.[23]

Table 1. Ta–C_{ipso}–C_{para} Angles for $[Ar^{Tol_2}]Ta(NMe_2)_3X$.

X =	Crystal (˚)	Calculated (˚)	$\Delta_{Calculated–Cystal}$ (˚)
Cl	162.7	166.7	4.0
Me	174.5	168.4	–6.1
Et	161.0	164.2	3.2
Pr^n	160.7	165.0	4.3
Bu^n	176.9	163.4	–13.5
Np	179.3	164.0	–15.3
$[Ar^{Tol_2}]^a$	177.3, 154.5	176.1, 150.4	–1.2, –4.1
BH_4	174.9	174.6	–0.3

(a) Two $[Ar^{Tol_2}]$ groups in complex.

Is it worth noting that contrary to the *mono*-alkyl complexes, the *di*-alkyl complexes $[Ar^{Tol_2}]Ta(NMe_2)_2R_2$ (R = Me, Et, Pr^n, Bu^n, and Np), which have also been structurally characterized by X-ray diffraction, do not display significant Ta–C_{ipso}–C_{para} angle distortions (Table 2). Instead, they prefer to take a C_2 symmetric geometry, as depicted for $[Ar^{Tol_2}]Ta(NMe_2)_2Me_2$ in Figure 27.

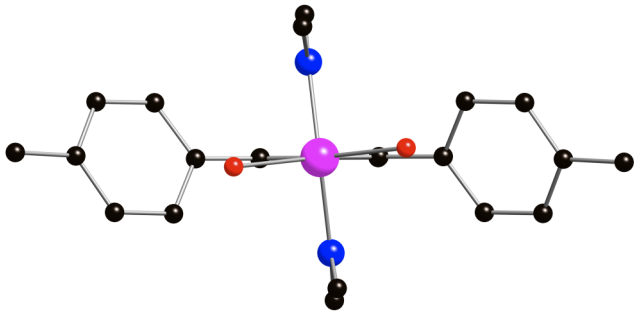

Figure 27. Molecular structures of $[Ar^{Tol}_2]Ta(NMe_2)_2Me_2$ showing C_2 symmetry (Ta–C_{ipso}–C_{para} = C_2 axis, directly into page). [Pink = Tantalum, Blue = Nitrogen, Black = Carbon, Red = Carbon's of $TaMe_2$, Hydrogen atoms not shown for clarity].

Table 2. Ta–C_{ipso}–C_{para} Angles for $[Ar^{Tol}_2]Ta(NMe_2)_2R_2$.

R =	Crystal (°)
Me	180.0
Et	169.2
Pr^n	178.3
Bu^n	176.3
Np[a]	180.0, 177.2

(a) Two independent structures for $[Ar^{Tol}_2]Ta(NMe_2)_2Np_2$ were obtained. Space groups: *C2/c* and *P-1*, respectively.

7.11 Summary and conclusions

In conclusion, a series of new $[Ar^{Tol}_2]$ tantalum complexes supported by dimethylamido ligands have been synthesized and structurally characterized. Several methods were observed to induce cyclometalation of the $[Ar^{Tol}_2]Ta(NMe_2)_3X$ (X = Me, Et, Pr^n, Bu^n, Np, $[Ar^{Tol}_2]$ and BH_4) complexes, thereby forming $[\kappa^2\text{-}Ar^{Tol,Tol'}]Ta(NMe_2)_3$. Additionally, $[Ar^{Tol}_2]Ta(NMe_2)_2Np_2$ eliminates one equivalent of neopentane at room temperature to form $[\kappa^2\text{-}Ar^{Tol,Tol'}]Ta(NMe_2)_2Np$, which subsequently isomerizes to $[\kappa^2\text{-}Ar^{*Tol,Tol'}]Ta(NMe_2)_2Np$.

7.12 Experimental details

7.12.1 General considerations

All manipulations were performed using a combination of glovebox, high vacuum, and Schlenk techniques under an argon atmosphere unless otherwise specified.[24] Solvents were purified and degassed by using standard procedures. ^{1}H NMR spectra were measured on Bruker 300 DRX, Bruker 300 DPX, Bruker 400 Avance III, Bruker 400 Cyber-enabled Avance III, and Bruker 500 DMX spectrometers. ^{1}H chemical shifts are reported in ppm relative to $SiMe_4$ ($\delta = 0$) and were referenced internally with respect to the protio solvent impurity (δ 7.16 for C_6D_5H and 2.09 for C_7D_7H).[25] ^{13}C NMR spectra are reported in ppm relative to $SiMe_4$ ($\delta = 0$) and were referenced internally with respect to the solvent (δ 128.06 for C_6D_6).[25] ^{31}P chemical shifts are reported in ppm relative to 85% H_3PO_4 ($\delta = 0$) and were referenced using $P(OMe)_3$ ($\delta = 141.0$) as an external standard.[26] Coupling constants are given in hertz. NMR spectroscopic simulations were performed using gNMR 5.1 (Adept Scientific) and MestReNova v7.0.3 (Mestrelab Research S.L. 2001) and final images were produced by MestReNova. $TaCl_5$, PMe_3, EtLi (0.5M solution in benzene/cyclohexane 9:1), Li wire (0.5 – 1.0 % Na), MeI, $P(OPh)_3$, and pivaloyl chloride were obtained commercially from Aldrich. $LiAlD_4$ was obtained commercially from Acros Organics. $ZnCl_2$ was obtained commercially from Strem Chemicals and dried with $SOCl_2$ prior to use.[27] Et_2O was dried over $LiAlH_4$ and vacuum transferred into an ampoule containing molecular sieves prior to use. THF was dried over $LiAlH_4$ and vacuum transferred into an ampoule containing molecular sieves prior to use. Me_3SiCl was obtained from Aldrich, dried over CaH_2 prior to use, and vacuum transferred directly into the reaction flask. Pr^nLi,[28] NpLi,[29] and $[Ar^{Tol}_2]Li$[30] were prepared by the literature methods.

7.12.2 X-ray structure determinations

X-ray diffraction data were collected on a Bruker Apex II diffractometer. Crystal data, data collection and refinement parameters are summarized in Section 7.13, Table 3. The structures were solved using direct methods and standard difference map techniques, and were refined by full-matrix least-squares procedures on F^2 with SHELXTL (Version 6.10).[31]

7.12.3 Computational details

Calculations were carried out using DFT as implemented in the Jaguar 7.5 (release 207) suite of *ab initio* quantum chemistry programs.[32] Geometry optimizations were performed with the B3LYP density functional[33] using the 6-31G** (C, H, N, B, and Cl) and LACVP (Ta) basis sets.[34] The energies of the optimized structures were reevaluated by additional single point calculations on each optimized geometry using cc-pVTZ(-f) correlation consistent triple-ζ basis set for C, H, N, B, and Cl and LACV3P for Ta.

7.12.4 Synthesis of $[Ta(NMe_2)_3Cl_2]_2$

The synthesis of $[Ta(NMe_2)_3Cl_2]_2$ was adapted from the literature procedure.[35] In an ampoule, a stirred suspension of $LiNMe_2$ (3.575 g, 0.070 mol) in pentane (100 mL) was treated with $TaCl_5$ (5 g, 0.014 mol). The mixture was stirred while open to argon for 5 hours, after which point the ampoule was sealed and stirred for an additional 2 days. The resulting dark brown suspension was allowed to settle and filtered. [*Caution! Mixture is not filtered to dryness because of previous reports of detonation, see*: Chesnut, R. W.; Rothwell, I. P.; Holl, M. B.; Wolczanski, P. T. *Chem. Eng. News* **1990**, *68*, 2] At this point, instead of isolating the $Ta(NMe_2)_5$,[36] the filtrate was frozen at –196 ˚C, and treated with Me_3SiCl (*ca.* 10 mL, 0.079 mol) *via* vapour transfer. The mixture was allowed to warm to room temperature and stirred for 3 hours, thereby producing an orange brown powder.

The powder was allowed to settle after which point the mother liquor was removed by filtration. The powder was then washed with pentane (1 × 100 mL, 1 × 50 mL), and dried *in vacuo* giving $[Ta(NMe_2)_3Cl_2]_2$ as a light orange brown powder (3.32 g, 62% isolated yield).

7.12.5 Synthesis of $[Ar^{Tol_2}]Ta(NMe_2)_3Cl$

To a stirring suspension of $[Ta(NMe_2)_3Cl_2]_2$ (1.0 g, 1.30 mmol) in Et_2O (15 mL) was added a solution of $[Ar^{Tol_2}]Li$ (760 mg, 2.88 mmol) in Et_2O (10 mL) over a period of 5 minutes. The mixture was then stirred for 30 minutes, after which period the volatiles were removed *in vacuo*. The resulting solid was first washed with pentane (15 mL), and then extracted with pentane (100 mL), filtered and the filtrate pumped down *in vacuo* giving a golden-yellow to brown powder. The powder was then washed with pentane (*ca*. 1 × 5 mL, 1 × 3 mL) and dried *in vacuo* giving $[Ar^{Tol_2}]Ta(NMe_2)_3Cl$ (427 mg, 28% isolated yield). X-ray quality crystals were obtained from a solution in pentane at –15 °C. Anal. Calcd.: C, 51.5%, H, 5.8%, N, 6.9%. Found: C, 51.4%, H, 5.9%, N, 6.8%.

^1H NMR (C_6D_6): 2.17 [s, 6H of Me of Ar^{Tol_2}], 2.86 [s, 18H of $(N\underline{Me}_2)_3$], 7.05 [d, $^3J_{H\text{-}H}$ = 8, 4H of Ar^{Tol_2}], 7.19 [dd, $^3J_{H\text{-}H}$ = 8, $^3J_{H\text{-}H}$ = 7, 1H of Ar^{Tol_2}], 7.30 [d, $^3J_{H\text{-}H}$ = 8, 2H of Ar^{Tol_2}], 7.74 [br s, 4H of Ar^{Tol_2}]. $^{13}C\{^1H\}$ NMR (C_6D_6): 21.1 [s, 2C of Me of Ar^{Tol_2}], 46.9 [s, 6C of $(N\underline{Me}_2)_3$], 126.0 [s, 1C of Ar^{Tol_2}], 128.8 [s, 4C of Ar^{Tol_2}], 130.4 [s, 2C of Ar^{Tol_2}], 130.9 [br s, 4C of Ar^{Tol_2}], 136.0 [s, 2C of Ar^{Tol_2}], 144.7 [s, 2C of Ar^{Tol_2}], 146.5 [s, 2C of Ar^{Tol_2}], 202.5 [s, 1C of Ar^{Tol_2}].

7.12.9 Synthesis of $[Ar^{Tol_2}]Ta(NMe_2)_3Me$

A solution of $[Ar^{Tol_2}]Ta(NMe_2)_3Cl$ (30 mg, 0.05 mmol) and d_6-benzene (*ca*. 0.7 mL) in an NMR tube equipped with a J. Young valve was treated with a suspension of MeLi (10 mg, 0.45 mmol) in Et_2O (*ca*. 0.1 mL). The suspension was analyzed by ^1H NMR

spectroscopy, thereby demonstrating conversion to $[Ar^{Tol_2}]Ta(NMe_2)_3Me$. The mixture was then lyophilized, extracted into pentane (*ca.* 1 mL), filtered through celite and placed at –15 ˚C for 1 day, thereby depositing light yellow crystals of $[Ar^{Tol_2}]Ta(NMe_2)_3Me$. The mother liquor was removed using a pipette, and the crystals were washed with cold (–15 ˚C) pentane (2 × 1 mL), and dried *in vacuo* giving $[Ar^{Tol_2}]Ta(NMe_2)_3Me$ (15 mg, 52% isolated yield). X-ray quality crystals were obtained from a solution in pentane at –15 ˚C. Anal. Calcd.: C, 55.4%, H, 6.5%, N, 7.2%. Found: C, 55.4%, H, 6.6%, N, 7.0%.

^{1}H NMR (C_6D_6): 0.25 [s, 3H of Ta<u>Me</u>], 2.20 [s, 6H of Me of Ar^{Tol_2}], 3.01 [br s, 18H of (N<u>Me</u>$_2$)$_3$], 7.08 [d, $^3J_{H\text{-}H}$ = 8, 4H of Ar^{Tol_2}], 7.20 [t, $^3J_{H\text{-}H}$ = 8, 1H of Ar^{Tol_2}], 7.35 [d, $^3J_{H\text{-}H}$ = 8, 2H of Ar^{Tol_2}], 7.46 [d, $^3J_{H\text{-}H}$ = 8, 4H of Ar^{Tol_2}]. $^{13}C\{^1H\}$ NMR (C_6D_6): 21.2 [s, 2C of Me of Ar^{Tol_2}], 46.6 [s, 6C of (N<u>Me</u>$_2$)$_3$], 53.3 [s, 1C of Ta<u>Me</u>], 125.2 [s, 1C of Ar^{Tol_2}], 129.0 [br s, 4C of Ar^{Tol_2}], 129.8 [s, 4C of Ar^{Tol_2}], 130.4 [s, 2C of Ar^{Tol_2}], 135.8 [very br, 2C of Ar^{Tol_2}], 145.9 [very br, 4C of Ar^{Tol_2}], 200.3 [s, 1C of Ar^{Tol_2}].

7.12.10 Synthesis of $[Ar^{Tol_2}]Ta(NMe_2)_3Et$

$[Ar^{Tol_2}]Ta(NMe_2)_3Cl$ (30 mg, 0.05 mmol), d_6-benzene (*ca.* 0.7 mL), and EtLi (2 mg, 0.05 mmol) were consecutively added to a small vial. The suspension was mixed for 1 minute, filtered through celite and then added to an NMR tube equipped with a J. Young valve. The pale yellow to colorless solution was analyzed by ^{1}H NMR spectroscopy, thereby demonstrating conversion to $[Ar^{Tol_2}]Ta(NMe_2)_3Et$. The mixture was then lyophilized, extracted into pentane (*ca.* 1 mL) and allowed to evaportate slowly at room temperature giving light yellow crystals of $[Ar^{Tol_2}]Ta(NMe_2)_3Et$. The crystals were washed with cold (–15 ˚C) pentane (1 mL), and dried *in vacuo* giving $[Ar^{Tol_2}]Ta(NMe_2)_3Et$ (8 mg, 27% isolated yield). X-ray quality crystals were obtained from a solution in pentane at –15 ˚C.

^{1}H NMR (C_6D_6): 0.42 [q, $^{3}J_{H\text{-}H}$ = 8, 2H of TaC$\underline{H}_2$CH$_3$], 1.77 [t, $^{3}J_{H\text{-}H}$ = 8, 3H of TaCH$_2$C$\underline{H}_3$], 2.20 [s, 6H of Me of Ar$^{Tol}{}_2$], 3.00 [br s, 18H of (N$\underline{Me}_2$)$_3$], 7.08 [d, $^{3}J_{H\text{-}H}$ = 8, 4H of Ar$^{Tol}{}_2$], 7.20 [t, $^{3}J_{H\text{-}H}$ = 8, 1H of Ar$^{Tol}{}_2$], 7.34 [d, $^{3}J_{H\text{-}H}$ = 8, 2H of Ar$^{Tol}{}_2$], 7.46 [d, $^{3}J_{H\text{-}H}$ = 8, 4H of Ar$^{Tol}{}_2$]. ^{13}C{^{1}H} NMR (C_6D_6): 15.2 [s, 1C of TaCH$_2$$\underline{C}H_3$], 21.2 [s, 2C of Me of Ar$^{Tol}{}_2$], 46.8 [s, 6C of (N$\underline{Me}_2$)$_3$], 67.2 [s, 1C of Ta$\underline{C}$H$_2$CH$_3$], 125.1 [s, 1C of Ar$^{Tol}{}_2$], 128.9 [br s, 4C of Ar$^{Tol}{}_2$], 130.0 [br s, 4C of Ar$^{Tol}{}_2$], 130.4 [s, 2C of Ar$^{Tol}{}_2$], 136.2 [very br, 2C of Ar$^{Tol}{}_2$], 146.1 [very br, 4C of Ar$^{Tol}{}_2$], 200.5 [s, 1C of Ar$^{Tol}{}_2$].

7.12.11 Synthesis of [Ar$^{Tol}{}_2$]Ta(NMe$_2$)$_3$Pr^n

[Ar$^{Tol}{}_2$]Ta(NMe$_2$)$_3$Cl (30 mg, 0.05 mmol), d$_6$-benzene (*ca*. 0.7 mL), and Pr^{n}Li (5 mg, 0.10 mmol) were consecutively added to a small vial. The suspension was mixed for 1 minute, filtered through celite and then added to an NMR tube equipped with a J. Young valve. The pale yellow to colorless solution was analyzed by ^{1}H NMR spectroscopy, thereby demonstrating conversion to [Ar$^{Tol}{}_2$]Ta(NMe$_2$)$_3$Pr^n. The mixture was then lyophilized, extracted into pentane (*ca*. 1 mL), filtered and placed at –15 ˚C for *ca*. 1 week, thereby depositing light yellow crystals of [Ar$^{Tol}{}_2$]Ta(NMe$_2$)$_3$Pr^n. The mother liquor was removed using a pipette, and the crystals were washed with cold (–15 ˚C) pentane (1 mL), and dried *in vacuo* giving [Ar$^{Tol}{}_2$]Ta(NMe$_2$)$_3$Pr^n (6 mg, 20% isolated yield). X-ray quality crystals were obtained from a solution in pentane at –15 ˚C. Anal. Calcd.: C, 56.8%, H, 6.9%, N, 6.8%. Found: C, 56.0%, H, 6.7%, N, 5.8%.

^{1}H NMR (C_6D_6): 0.28 [m, 2H of TaC$\underline{H}_2$CH$_2$CH$_3$], 0.93 [t, $^{3}J_{H\text{-}H}$ = 7, 3H of TaCH$_2$CH$_2$C$\underline{H}_3$], 1.80 [m, 2H of TaCH$_2$C$\underline{H}_2$CH$_3$], 2.22 [s, 6H of Me of Ar$^{Tol}{}_2$], 3.00 [br s, 18H of (N$\underline{Me}_2$)$_3$], 7.08 [d, $^{3}J_{H\text{-}H}$ = 8, 4H of Ar$^{Tol}{}_2$], 7.20 [t, $^{3}J_{H\text{-}H}$ = 8, 1H of Ar$^{Tol}{}_2$], 7.35 [d, $^{3}J_{H\text{-}H}$ = 8, 2H of Ar$^{Tol}{}_2$], 7.46 [d, $^{3}J_{H\text{-}H}$ = 8, 4H of Ar$^{Tol}{}_2$]. ^{13}C{^{1}H} NMR (C_6D_6): 21.2 [s, 2C of Me of Ar$^{Tol}{}_2$], 22.3 [s, 1C of TaCH$_2$CH$_2$$\underline{C}H_3$], 24.6 [s, 1C of TaCH$_2$$\underline{C}H_2CH_3$], 46.8 [s, 6C of (N$\underline{Me}_2$)$_3$], 79.6 [s, 1C of Ta$\underline{C}H_2CH_2CH_3$], 125.1 [s, 1C of Ar$^{Tol}{}_2$], 128.9 [br s, 4C of Ar$^{Tol}{}_2$],

130.0 [br s, 4C of Ar^{Tol_2}], 130.3 [s, 2C of Ar^{Tol_2}], 136.2 [very br, 2C of Ar^{Tol_2}], 146.1 [very br, 4C of Ar^{Tol_2}], 200.9 [s, 1C of Ar^{Tol_2}].

7.12.12 Synthesis of $[Ar^{Tol_2}]Ta(NMe_2)_3Bu^n$

$[Ar^{Tol_2}]Ta(NMe_2)_3Cl$ (30 mg, 0.05 mmol), d_6-benzene (*ca*. 1 mL) and Bu^nLi (3 mg, 0.05 mmol, in 0.2 mL d_6-benzene) were consecutively added to a small vial. The suspension was mixed for 1 minute, filtered through celite and then added to an NMR tube equipped with a J. Young valve. The pale yellow to colorless solution and analyzed by ^1H NMR spectroscopy, thereby demonstrating conversion to $[Ar^{Tol_2}]Ta(NMe_2)_3Bu^n$. The mixture was then lyophilized, extracted into pentane (*ca*. 1 mL), filtered and placed at –15 ˚C for *ca*. 1 week and allowed to evaporate slowly, thereby forming light yellow crystals of $[Ar^{Tol_2}]Ta(NMe_2)_3Bu^n$ on the side of the vial wall. The crystals were dried *in vacuo* giving $[Ar^{Tol_2}]Ta(NMe_2)_3Bu^n$ (9 mg, 29% isolated yield). X-ray quality crystals were obtained from a solution in pentane at –15 ˚C.

^1H NMR (C_6D_6): 0.25 [m, 2H of $TaC\underline{H}_2CH_2CH_2CH_3$], 0.91 [t, $^3J_{H-H}$ = 7, 3H of $TaCH_2CH_2CH_2C\underline{H}_3$], 1.23 [m, 2H of $TaCH_2CH_2C\underline{H}_2CH_3$], 1.76 [m, 2H of $TaCH_2C\underline{H}_2CH_2CH_3$], 2.22 [s, 6H of Me of Ar^{Tol_2}], 3.01 [br s, 18H of $(N\underline{Me}_2)_3$], 7.08 [d, $^3J_{H-H}$ = 8, 4H of Ar^{Tol_2}], 7.20 [t, $^3J_{H-H}$ = 8, 1H of Ar^{Tol_2}], 7.35 [d, $^3J_{H-H}$ = 8, 2H of Ar^{Tol_2}], 7.47 [d, $^3J_{H-H}$ = 8, 4H of Ar^{Tol_2}]. $^{13}C\{^1H\}$ NMR (C_6D_6): 13.7 [s, 1C of $TaCH_2CH_2CH_2\underline{C}H_3$], 21.2 [s, 2C of Me of Ar^{Tol_2}], 30.4 [s, 1C of $TaCH_2CH_2\underline{C}H_2CH_3$], 33.1 [s, 1C of $TaCH_2\underline{C}H_2CH_2CH_3$], 46.8 [s, 6C of $(N\underline{Me}_2)_3$], 79.3 [s, 1C of $Ta\underline{C}H_2CH_2CH_2CH_3$], 125.1 [s, 1C of Ar^{Tol_2}], 128.9 [br s, 4C of Ar^{Tol_2}], 130.1 [br s, 4C of Ar^{Tol_2}], 130.3 [s, 2C of Ar^{Tol_2}], 136.1 [very br, 2C of Ar^{Tol_2}], 146.0 [very br, 4C of Ar^{Tol_2}], 200.8 [s, 1C of Ar^{Tol_2}].

7.12.13 Synthesis of $[Ar^{Tol_2}]Ta(NMe_2)_3Np$

$[Ar^{Tol_2}]Ta(NMe_2)_3Cl$ (30 mg, 0.05 mmol), d_6-benzene (*ca*. 0.7 mL), and NpLi (5 mg, 0.06 mmol) were consecutively added to a small vial. The suspension was mixed for 1 minute, filtered through celite and then added to an NMR tube equipped with a J. Young valve. The pale yellow to colorless solution was analyzed by ^1H NMR spectroscopy, thereby demonstrating conversion to $[Ar^{Tol_2}]Ta(NMe_2)_3Np$. The mixture was then lyophilized, extracted into pentane (*ca*. 1 mL), filtered and placed at –15 ˚C for *ca*. 1 week, thereby depositing light yellow crystals of $[Ar^{Tol_2}]Ta(NMe_2)_3Np$. The mother liquor was removed using a pipette, and the crystals were washed with cold (–15 ˚C) pentane (2 × 1 mL), and dried *in vacuo* giving $[Ar^{Tol_2}]Ta(NMe_2)_3Np$ (10 mg, 31% isolated yield). X-ray quality crystals were obtained from a solution in pentane at –15 ˚C. Anal. Calcd.: C, 58.0%, H, 7.2%, N, 6.6%. Found: C, 57.5%, H, 6.7%, N, 6.2%.

^1H NMR (C_6D_6): 0.04 [s, 2H of $TaC\underline{H}_2CMe_3$], 0.98 [s, 9H of $TaCH_2C\underline{Me}_3$], 2.23 [s, 6H of Me of Ar^{Tol_2}], 3.05 [br s, 18H of $(N\underline{Me}_2)_3$], 7.07 [br, 4H of Ar^{Tol_2}], 7.21 [t, $^3J_{H\text{-}H} = 8$, 1H of Ar^{Tol_2}], 7.40 [br, 4H of Ar^{Tol_2}], 7.52 [br, 2H of Ar^{Tol_2}]. $^{13}C\{^1H\}$ NMR (C_6D_6): 21.2 [s, 2C of Me of Ar^{Tol_2}], 34.3 [s, 1C of $TaCH_2C\underline{Me}_3$], 37.7 [s, 1C of $TaCH_2\underline{C}Me_3$], 46.8 [s, 6C of $(N\underline{Me}_2)_3$], 98.7 [s, 1C of $Ta\underline{C}H_2CMe_3$], 124.7 [s, 1C of Ar^{Tol_2}], 129.2 [br s, 4C of Ar^{Tol_2}], 129.8 [br s, 4C of Ar^{Tol_2}], 130.8 [br s, 2C of Ar^{Tol_2}], 135.3 [br s, 1C of Ar^{Tol_2}], 136.7 [br s, 1C of Ar^{Tol_2}], 143.8 [br s, 1C of Ar^{Tol_2}], 144.8 [br s, 1C of Ar^{Tol_2}], 145.6 [br s, 1C of Ar^{Tol_2}], 146.8 [br s, 1C of Ar^{Tol_2}], 201.3 [s, 1C of Ar^{Tol_2}].

7.12.14 Synthesis of $[Ar^{Tol_2}]_2Ta(NMe_2)_3$

A solution of $[Ar^{Tol_2}]Ta(NMe_2)_3Cl$ (25 mg, 0.04 mmol) in d_6-benzene (*ca*. 0.7 mL) in a small vial was treated with $[Ar^{Tol_2}]Li$ [15 mg, 0.06 mmol]. The reaction mixture was stirred (*ca*. 1 min), filtered into an NMR tube equipped with a J. Young and monitored by ^1H NMR spectscopy, thereby demonstrating that all of the $[Ar^{Tol_2}]Ta(NMe_2)_3Cl$ had

reacted. The sample was then lyophilized, extracted with pentane (*ca*. 1 mL), filtered, and crystallized at –15 ˚C for 1 week, thereby depositing yellow crystals of $[Ar^{Tol_2}]_2Ta(NMe_2)_3$• ½ C_5H_{12}. The mother liquor was removed using a pipette, and the crystals were washed with cold pentane (–15 ˚C) (2 × 1 mL), giving $[Ar^{Tol_2}]_2Ta(NMe_2)_3$• ½ C_5H_{12} (14 mg, 39% isolated yield). X-ray quality crystals were obtained from a solution in pentane at –15 ˚C. Anal. Calcd.: C, 66.7%, H, 6.3%, N, 5.1%. Found: C, 65.6%, H, 6.3%, N, 4.5%.

^{1}H NMR (C_6D_6): 2.19 [s, 12H of Me of Ar^{Tol_2}], 2.51 [s, 18H of $(N\underline{Me}_2)_3$], 7.08 [d, $^3J_{H-H}$ = 7, 8H of Ar^{Tol_2}], 7.10 [t, $^3J_{H-H}$ = 8, 2H of Ar^{Tol_2}], 7.24 [d, $^3J_{H-H}$ = 7, 4H of Ar^{Tol_2}], 7.40 [d, $^3J_{H-H}$ = 7, 8H of Ar^{Tol_2}]. $^{13}C\{^1H\}$ NMR (C_6D_6): 21.1 [s, 4C of Me of Ar^{Tol_2}], 47.0 [s, 6C of $(N\underline{Me}_2)_3$], 125.4 [s, 2C of Ar^{Tol_2}], 128.4 [s, 8C of Ar^{Tol_2}], 130.1 [s, 8C of Ar^{Tol_2}], 131.3 [s, 4C of Ar^{Tol_2}], 134.9 [s, 4C of Ar^{Tol_2}], 147.8 [s, 4C of Ar^{Tol_2}], 152.2 [s, 4C of Ar^{Tol_2}], 199.2 [s, 2C of Ar^{Tol_2}].

7.12.15 Synthesis of $[Ar^{Tol_2}]Ta(NMe_2)_3(BH_4)$

$[Ar^{Tol_2}]Ta(NMe_2)_3Cl$ (50 mg, 0.08 mmol) and $LiBH_4$ (3 mg, 0.14 mmol) was added to an NMR tube equipped with a J. Young valve and was treated with Et_2O (*ca*. 0.5 mL). After 30 minutes, the volatiles were removed *in vacuo*, and the off white solid was extracted with pentane (2 mL), filtered, and placed at –15 ˚C for 1 day, thereby depositing colorless crystals of $[Ar^{Tol_2}]Ta(NMe_2)_3(BH_4)$. The mother liquor was removed using a pipette, and the crystals were washed with cold (–15 ˚C) pentane (2 × 1 mL), and dried *in vacuo* giving $[Ar^{Tol_2}]Ta(NMe_2)_3(BH_4)$ (13 mg, 27% isolated yield). X-ray quality crystals were obtained from a solution in pentane at –15 ˚C. Anal. Calcd.: C, 53.3%, H, 6.7%, N, 7.2%. Found: C, 51.7%, H, 6.2%, N, 6.9%.

^{1}H NMR (C_6D_6): 2.17 [s, 6H of Me of Ar^{Tol_2}], 2.92 [s, 18H of $(N\underline{Me}_2)_3$], 3.28 [very br, 4H of $Ta(B\underline{H}_4)$], 7.03 [d, $^3J_{H-H}$ = 8, 4H of Ar^{Tol_2}], 7.20 [dd, $^3J_{H-H}$ = 8, $^3J_{H-H}$ = 7, 1H of Ar^{Tol_2}],

7.31 [d, $^3J_{H-H}$ = 8, 2H of Ar^{Tol}_2], 7.48 [d, $^3J_{H-H}$ = 8, 4H of Ar^{Tol}_2]. $^{13}C\{^1H\}$ NMR (C_6D_6): 21.1 [s, 2C of Me of Ar^{Tol}_2], 48.9 [s, 6C of $(N\underline{Me}_2)_3$], 125.9 [s, 1C of Ar^{Tol}_2], 128.6 [s, 4C of Ar^{Tol}_2], 130.1 [s, 2C of Ar^{Tol}_2], 130.8 [br s, 4C of Ar^{Tol}_2], 135.5 [s, 2C of Ar^{Tol}_2], 145.7 [s, 2C of Ar^{Tol}_2], 148.0 [s, 2C of Ar^{Tol}_2], 198.4 [s, 1C of Ar^{Tol}_2]. ^{11}B NMR (C_6D_6): –8.4 [br, 1B of $Ta(\underline{B}H_4)$].

7.12.16 Synthesis of $[\kappa^2\text{-}Ar^{Tol,Tol'}]Ta(NMe_2)_3$

$[Ar^{Tol}_2]Ta(NMe_2)_3Cl$ (50 mg, 0.08 mmol), d_6-benzene (*ca*. 0.7 mL), and NpLi (7 mg, 0.09 mmol) were consecutively added to a small vial. The suspension was mixed for 1 minute, and then filtered through celite into an NMR tube equipped with a J. Young valve. The solution was analyzed by ^1H NMR spectroscopy, thereby demonstrating conversion to $[Ar^{Tol}_2]Ta(NMe_2)_3Np$. The sample was then heated at 100 °C for 2 hours, thereby demonstrating conversion to $[\kappa^2\text{-}Ar^{Tol,Tol'}]Ta(NMe_2)_3$ and neopentane. The mixture was then lyophilized, extracted into pentane, filtered and evaporated giving $[\kappa^2\text{-}Ar^{Tol,Tol'}]Ta(NMe_2)_3$, which contained a small amount (*ca*. 10%) $[Ar^{Tol}_2]H$ (27 mg total, *ca*. 55% yield of $[\kappa^2\text{-}Ar^{Tol,Tol'}]Ta(NMe_2)_3$). X-ray quality crystals were obtained from a solution in pentane at –15 °C.

^1H NMR (C_6D_6): 2.19 [s, 3H of Me of $Ar^{Tol,Tol'}$], 2.38 [s, 3H of Me of $Ar^{Tol,Tol'}$], 3.03 [s, 18H of $(N\underline{Me}_2)_3$], 7.11 [d, $^3J_{H-H}$ = 8, 2H of $Ar^{\underline{Tol},Tol'}$], 7.16 [m, 1H of $\underline{Ar}^{Tol,Tol'}$, under C_6D_5H signal, located by 2D COSY and homonuclear decoupling], 7.63 [dd, $^3J_{H-H}$ = 7, $^4J_{H-H}$ = 2, 1H of $Ar^{Tol,\underline{Tol'}}$], 7.68 [m, 3H of $\underline{Ar}^{\underline{Tol},Tol'}$], 7.85 [d, $^3J_{H-H}$ = 7, 1H of $Ar^{Tol,\underline{Tol'}}$], 7.90 [d, $^3J_{H-H}$ = 8, 1H of $\underline{Ar}^{Tol,Tol'}$], 8.24 [d, $^4J_{H-H}$ = 2, 1H of $Ar^{Tol,\underline{Tol'}}$]. $^{13}C\{^1H\}$ NMR (C_6D_6): 21.2 [s, 1C of Me of $Ar^{Tol,Tol'}$], 21.9 [s, 1C of Me of $Ar^{Tol,Tol'}$], 42.6 [s, 6C of $(N\underline{Me}_2)_3$], 119.6 [s, 1C of $Ar^{Tol,Tol'}$], 121.2 [s, 1C of $Ar^{Tol,Tol'}$], 125.5 [s, 1C of $Ar^{Tol,Tol'}$], 127.5 [s, 2C of $Ar^{Tol,Tol'}$], 129.7 [s, 2C of $Ar^{Tol,Tol'}$], 129.9 [s, 1C of $Ar^{Tol,Tol'}$], 135.7 [s, 1C of $Ar^{Tol,Tol'}$], 136.5 [s, 1C of $Ar^{Tol,Tol'}$], 139.8 [s, 2C of $Ar^{Tol,Tol'}$], 140.4 [s, 1C of $Ar^{Tol,Tol'}$], 142.2 [s, 1C of $Ar^{Tol,Tol'}$], 154.2 [s, 1C of $Ar^{Tol,Tol'}$], 158.3 [s, 1C of $Ar^{Tol,Tol'}$], 197.7 [s, 1C of $Ar^{Tol,Tol'}$], 199.6 [s, 1C of $Ar^{Tol,Tol'}$].

7.12.17 Production of $[\kappa^2\text{-}Ar^{Tol,Tol'}]Ta(NMe_2)_3$ *via* Cyclometalation

In the reactions (i – vi, not including vii) below, the major products (> 75%) are $[\kappa^2\text{-}Ar^{Tol,Tol'}]Ta(NMe_2)_3$ *and the eliminated XH [X = Me, Et, Pr, Bu, Np,* $[Ar^{Tol}{}_2]$*, H]. In reaction vii, a significant amount of* $[Ar^{Tol}{}_2]H$ *(ca. 50%) is produced instead of the* $[\kappa^2\text{-}Ar^{Tol,Tol'}]Ta(NMe_2)_3$*,* $Me_3P{\rightarrow}BH_3$ *and* H_2*.*

(*i*) $[Ar^{Tol}{}_2]Ta(NMe_2)_3Me$ (5 mg, 0.01 mmol) and d_6-benzene (*ca*. 0.7 mL) were added to an NMR tube equipped with a J. Young valve. The sample was heated at 100 ˚C for 1 day, thereby demonstrating the formation of, *inter alia*, $[\kappa^2\text{-}Ar^{Tol,Tol'}]Ta(NMe_2)_3$ and methane.

(*ii*) $[Ar^{Tol}{}_2]Ta(NMe_2)_3Et$ (5 mg, 0.01 mmol) and d_6-benzene (*ca*. 0.7 mL) were added to an NMR tube equipped with a J. Young valve. The sample was heated at 100 ˚C for 3 hours, thereby demonstrating the formation of, *inter alia*, $[\kappa^2\text{-}Ar^{Tol,Tol'}]Ta(NMe_2)_3$ and ethane.

(*iii*) $[Ar^{Tol}{}_2]Ta(NMe_2)_3Pr^n$ (5 mg, 0.01 mmol) and d_6-benzene (*ca*. 0.7 mL) were added to an NMR tube equipped with a J. Young valve. The sample was heated at 100 ˚C for 3 hours, thereby demonstrating the formation of, *inter alia*, $[\kappa^2\text{-}Ar^{Tol,Tol'}]Ta(NMe_2)_3$ and propane.

(*iv*) $[Ar^{Tol}{}_2]Ta(NMe_2)_3Bu^n$ (5 mg, 0.01 mmol) and d_6-benzene (*ca*. 0.7 mL) were added to an NMR tube equipped with a J. Young valve. The sample was heated at 100 ˚C for 3 hours, thereby demonstrating the formation of, *inter alia*, $[\kappa^2\text{-}Ar^{Tol,Tol'}]Ta(NMe_2)_3$ and *n*-butane.

(*v*) $[Ar^{Tol_2}]Ta(NMe_2)_3Np$ (5 mg, 0.01 mmol) and d_6-benzene (*ca*. 0.7 mL) were added to an NMR tube equipped with a J. Young valve. The sample was heated at 100 ˚C for 2 hours, thereby demonstrating the formation of, *inter alia*, $[\kappa^2\text{-}Ar^{Tol,Tol'}]Ta(NMe_2)_3$ and neopentane.

(*vi*) $[Ar^{Tol_2}]_2Ta(NMe_2)_3$ (10 mg, 0.01 mmol) and d_6-benzene (*ca*. 0.7 mL) were added to an NMR tube equipped with a J. Young valve. The sample was allowed to stand at 22 ˚C for 1 day, thereby demonstrating the formation of, *inter alia*, $[\kappa^2\text{-}Ar^{Tol,Tol'}]Ta(NMe_2)_3$ and $[Ar^{Tol_2}]H$.

(*vii*) $[Ar^{Tol_2}]Ta(NMe_2)_3(BH_4)$ (10 mg, 0.02 mmol) and d_6-benzene (*ca*. 0.7 mL) were added to an NMR tube equipped with a J. Young valve. The sample was treated with PMe_3 (*ca*. 0.05 mL) and allowed to stand at 22 ˚C for 1 day, thereby demonstrating the formation of, *inter alia*, $[\kappa^2\text{-}Ar^{Tol,Tol'}]Ta(NMe_2)_3$, $Me_3P{\rightarrow}BH_3$ and H_2.

7.12.18 Treatment of $[Ar^{Tol_2}]Ta(NMe_2)_3X$ (X = Cl, Me, Et, Pr^n, Bu^n, and Np) with PMe_3

$[Ar^{Tol_2}]Ta(NMe_2)_3X$ (5 mg, 0.01 mmol, X = Cl, Me, Et, Pr^n, Bu^n, and Np) and d_6-benzene were added to an NMR tube equipped with a J. Young valve. The sample was then treated with PMe_3 (*ca*. 0.05 mL) and monitored by ^1H NMR spectroscopy, thereby demonstrating that there was no observable formation of $[\kappa^2\text{-}Ar^{Tol,Tol'}]Ta(NMe_2)_3$ over a period of 1 day at room temperature.

7.12.19 Synthesis of $[Ar^{Tol_2}]Ta(NMe_2)_2Cl_2$

$[Ar^{Tol_2}]Ta(NMe_2)_3Cl$ (100 mg, 0.17 mmol) and d_6-benzene (*ca*. 1 mL) were added to an NMR tube equipped with a J. Young valve. Me_3SiCl (*ca*. 0.7 mL) was the vapor transferred into the NMR tube, shaken for 1 minute, and allowed to stand at room

temperature for 10 minutes. The sample was analyzed by ^{1}H NMR spectroscopy, thereby demonstrating conversion to [Ar^{Tol_2}]Ta(NMe$_2$)$_2$Cl$_2$ and Me$_3$SiNMe$_2$. The volatiles were removed *in vacuo* leaving a yellow oily residue, which was extracted with pentane (5 × 1 mL), filtered into 5 separate small vials, and cooled to –15 ˚C, thereby depositing yellow crystals of [Ar^{Tol_2}]Ta(NMe$_2$)$_2$Cl$_2$. The mother liquor was removed from each vial using a pipette, and the crystals were washed with cold (–15 ˚C) pentane (1 mL each), combined and dried *in vacuo* giving [Ar^{Tol_2}]Ta(NMe$_2$)$_2$Cl$_2$ (30 mg). Additionally, the yellow solid left over after the pentane extractions was extracted into benzene, filtered and lyophilized giving an additional batch of [Ar^{Tol_2}]Ta(NMe$_2$)$_2$Cl$_2$ (23 mg). The total isolated yield is 54% (53 mg). X-ray quality crystals formed on the wall of the NMR tube after the benzene solution was pumped down. Anal. Calcd.: C, 48.3%, H, 4.9%, N, 4.7%. Found: C, 49.1%, H, 4.5%, N, 4.2%.

^{1}H NMR (C_6D_6): 2.18 [s, 6H of Me of Ar^{Tol_2}], 2.94 [s, 12H of (N$\underline{Me}_2$)$_2$], 7.07 [d, $^3J_{H\text{-}H}$ = 8, 4H of Ar^{Tol_2}], 7.16 [m, 1H of Ar^{Tol_2}], 7.29 [d, $^3J_{H\text{-}H}$ = 7, 2H of Ar^{Tol_2}], 7.72 [br d, $^3J_{H\text{-}H}$ = 7, 4H of Ar^{Tol_2}]. ^{13}C{^{1}H} NMR (C_6D_6): 21.3 [s, 2C of Me of Ar^{Tol_2}], 47.7 [s, 4C of (N$\underline{Me}_2$)$_2$], 128.3 [s, 1C of Ar^{Tol_2}, under C_6D_6 signal, located by HSQC], 129.3 [s, 4C of Ar^{Tol_2}], 130.4 [s, 2C of Ar^{Tol_2}], 131.4 [s, 4C of Ar^{Tol_2}], 137.5 [s, 2C of Ar^{Tol_2}], 139.4 [br s, 2C of Ar^{Tol_2}], 144.4 [s, 2C of Ar^{Tol_2}], 201.4 [s, 1C of Ar^{Tol_2}].

7.12.20 Synthesis of [Ar^{Tol_2}]Ta(NMe$_2$)$_2$Me$_2$

A solution of [Ar^{Tol_2}]Ta(NMe$_2$)$_2$Cl$_2$ (20 mg, 0.03 mmol) and d_6-benzene (*ca*. 0.7 mL) in an NMR tube equipped with a J. Young valve was treated with a suspension of MeLi (10 mg, 0.45 mmol) in Et$_2$O (*ca*. 0.2 mL) and mixture for *ca*. 1 hour. The suspension was analyzed by ^{1}H NMR spectroscopy, thereby demonstrating conversion to [Ar^{Tol_2}]Ta(NMe$_2$)$_2$Me$_2$. The sample was lyophilized, extracted into d_6-benzene, and analyzed by ^{1}H NMR spectroscopy demonstrating that the sample consisted of

$[Ar^{Tol_2}]Ta(NMe_2)_2Me_2$ as the major product, in addition to $[Ar^{Tol_2}]H$ (< 5%). The sample was then lyophilized giving $[Ar^{Tol_2}]Ta(NMe_2)_2Me_2$ (12 mg, 65% yield) as a light brown powder. X-ray quality crystals were obtained from a solution in pentane at –15 ˚C.

^1H NMR (C_6D_6): –0.41 [s, 6H of Ta<u>Me</u>$_2$], 2.15 [s, 6H of Me of Ar^{Tol_2}], 2.89 [s, 12H of (N<u>Me</u>$_2$)$_2$], 6.99 [d, $^3J_{H\text{-}H}$ = 8, 4H of Ar^{Tol_2}], 7.22 [m, 1H of Ar^{Tol_2}], 7.28 [m, 6H of Ar^{Tol_2}]. $^{13}C\{^1H\}$ NMR (C_6D_6): 21.2 [s, 2C of Me of Ar^{Tol_2}], 43.0 [s, 4C of (N<u>Me</u>$_2$)$_2$], 56.1 [s, 2C of Ta<u>Me</u>$_2$], 125.1 [s, 1C of Ar^{Tol_2}], 128.8 [s, 4C of Ar^{Tol_2}], 129.6 [s, 4C of Ar^{Tol_2}], 130.5 [s, 2C of Ar^{Tol_2}], 136.4 [s, 2C of Ar^{Tol_2}], 141.0 [s, 2C of Ar^{Tol_2}], 143.6 [s, 2C of Ar^{Tol_2}], 195.6 [s, 1C of Ar^{Tol_2}].

7.12.21 Isolation of $[Ar^{Tol_2}]Ta(NMe_2)_2MeCl$

During the synthesis of $[Ar^{Tol_2}]Ta(NMe_2)_2Me_2$, if less than 2 equivalent of MeLi was added or if the sample was not mixture for a long enough period, a mixture of $[Ar^{Tol_2}]Ta(NMe_2)_2Me_2$ and $[Ar^{Tol_2}]Ta(NMe_2)_2MeCl$ was observed. Additionally, we were able to crystallize $[Ar^{Tol_2}]Ta(NMe_2)_2MeCl$ allowing for its molecular structure to be determined. X-ray quality crystals were obtained from a solution in pentane at –15 ˚C.

^1H NMR (C_6D_6) – *tentative because mixture*: 0.20 [s, 3H of Ta<u>Me</u>], 2.14 [s, 6H of Me of Ar^{Tol_2}], 2.74 [br s, 12H of (N<u>Me</u>$_2$)$_2$], 7.05 [d, $^3J_{H\text{-}H}$ = 7, 4H of Ar^{Tol_2}], 7.18 [m, 1H of Ar^{Tol_2}], 7.28 [m, 2H of Ar^{Tol_2}], 7.80 [d, $^3J_{H\text{-}H}$ = 7, 4H of Ar^{Tol_2}].

7.12.22 Synthesis of $[Ar^{Tol_2}]Ta(NMe_2)_2Et_2$

$[Ar^{Tol_2}]Ta(NMe_2)_2Cl_2$ (15 mg, 0.03 mmol), d_6-benzene (*ca*. 0.7 mL), and EtLi (3 mg, 0.08 mmol) were consecutively added to a small vial. The suspension was mixed for 1 minute, filtered through celite, and then added to NMR tube equipped with a J. Young valve. The solution was analyzed by ^1H NMR spectroscopy, thereby demonstrating conversion to $[Ar^{Tol_2}]Ta(NMe_2)_2Et_2$ (which may be used for further reactions directly

when appropriate). The mixture was then lyophilized, extracted into pentane (*ca*. 1 mL) and allowed to evaportate slowly at –15 ˚C giving light yellow crystals of $[Ar^{Tol_2}]Ta(NMe_2)_2Et_2$. X-ray quality crystals were obtained from a solution in pentane at –15 ˚C.

^1H NMR (C_6D_6): 0.15 [q, $^3J_{H-H}$ = 8, 4H of $Ta(C\underline{H}_2CH_3)_2$], 1.32 [t, $^3J_{H-H}$ = 8, 6H of $Ta(CH_2C\underline{H}_3)_2$], 2.18 [s, 6H of Me of Ar^{Tol_2}], 2.99 [s, 12H of $(N\underline{Me}_2)_2$], 7.05 [d, $^3J_{H-H}$ = 8, 4H of Ar^{Tol_2}], 7.18 [m, 1H of Ar^{Tol_2}], 7.25 [d, $^3J_{H-H}$ = 7, 2H of Ar^{Tol_2}], 7.32 [d, $^3J_{H-H}$ = 8, 4H of Ar^{Tol_2}]. $^{13}C\{^1H\}$ NMR (C_6D_6): 13.6 [s, 2C of $Ta(CH_2\underline{C}H_3)_2$], 21.2 [s, 2C of Me of Ar^{Tol_2}], 43.4 [s, 4C of $(N\underline{Me}_2)_2$], 71.1 [s, 2C of $Ta(\underline{C}H_2CH_3)_2$], 126.0 [s, 1C of Ar^{Tol_2}], 128.8 [s, 4C of Ar^{Tol_2}], 130.1 [s, 4C of Ar^{Tol_2}], 130.4 [s, 2C of Ar^{Tol_2}], 136.5 [s, 2C of Ar^{Tol_2}], 142.0 [s, 2C of Ar^{Tol_2}], 145.3 [s, 2C of Ar^{Tol_2}], 197.8 [s, 1C of Ar^{Tol_2}].

7.12.23 Synthesis of $[Ar^{Tol_2}]Ta(NMe_2)_2Pr^n_2$

$[Ar^{Tol_2}]Ta(NMe_2)_2Cl_2$ (15 mg, 0.03 mmol), d_6-benzene (*ca*. 0.7 mL), and Pr^nLi (3 mg, 0.06 mmol) were consecutively added to a small vial. The suspension was mixed for 1 minute, filtered through celite, and then added to NMR tube equipped with a J. Young valve. The solution was analyzed by ^1H NMR spectroscopy, thereby demonstrating conversion to $[Ar^{Tol_2}]Ta(NMe_2)_2Pr^n_2$ (which may be used for further reactions directly when appropriate). The mixture was then lyophilized, extracted into pentane (*ca*. 1 mL) and allowed to evaportate slowly at –15 ˚C giving light yellow crystals of $[Ar^{Tol_2}]Ta(NMe_2)_2Pr^n_2$. X-ray quality crystals were obtained from a solution in pentane at –15 ˚C.

^1H NMR (C_6D_6): 0.04 [m, 4H of $Ta(C\underline{H}_2CH_2CH_3)_2$], 0.80 [t, $^3J_{H-H}$ = 7, 6H of $Ta(CH_2CH_2C\underline{H}_3)_2$], 1.32 [m, 4H of $Ta(CH_2C\underline{H}_2CH_3)_2$], 2.21 [s, 6H of Me of Ar^{Tol_2}], 2.97 [s, 12H of $(N\underline{Me}_2)_2$], 7.02 [d, $^3J_{H-H}$ = 8, 4H of Ar^{Tol_2}], 7.19 [t, $^3J_{H-H}$ = 7, 1H of Ar^{Tol_2}], 7.26 [d, $^3J_{H-H}$ = 7, 2H of Ar^{Tol_2}], 7.30 [d, $^3J_{H-H}$ = 8, 4H of Ar^{Tol_2}]. $^{13}C\{^1H\}$ NMR (C_6D_6): 21.2 [s, 2C of Me of

Ar^{Tol_2}], 22.0 [s, 2C of $Ta(CH_2CH_2\underline{C}H_3)_2$], 23.1 [s, 2C of $Ta(CH_2\underline{C}H_2CH_3)_2$], 43.5 [s, 4C of $(N\underline{Me}_2)_2$], 83.1 [s, 2C of $Ta(\underline{C}H_2CH_2H_3)_2$], 125.6 [s, 1C of Ar^{Tol_2}], 128.8 [s, 4C of Ar^{Tol_2}], 129.9 [s, 4C of Ar^{Tol_2}], 130.4 [s, 2C of Ar^{Tol_2}], 136.5 [s, 2C of Ar^{Tol_2}], 141.9 [s, 2C of Ar^{Tol_2}], 144.7 [s, 2C of Ar^{Tol_2}], 197.6 [s, 1C of Ar^{Tol_2}].

7.12.24 Synthesis of $[Ar^{Tol_2}]Ta(NMe_2)_2Bu^n_2$

$[Ar^{Tol_2}]Ta(NMe_2)_2Cl_2$ (10 mg, 0.03 mmol), d_6-benzene (*ca*. 0.7 mL), and Bu^nLi (2 mg, 0.03 mmol) were consecutively added to a small vial. The suspension was mixed for 1 minute, filtered through celite, and then added to NMR tube equipped with a J. Young valve. The solution was analyzed by ^1H NMR spectroscopy, thereby demonstrating conversion to $[Ar^{Tol_2}]Ta(NMe_2)_2Bu^n_2$ (which may be used for further reactions directly when appropriate). The mixture was then lyophilized, extracted into pentane (*ca*. 1 mL) and allowed to evaportate slowly at –15 ˚C giving light yellow crystals of $[Ar^{Tol_2}]Ta(NMe_2)_2Pr^n_2$. X-ray quality crystals were obtained from a solution in pentane at –15 ˚C. X-ray quality crystals were obtained from a solution in pentane at –15 ˚C.

^1H NMR (C_6D_6): 0.04 [m, 4H of $Ta(C\underline{H}_2CH_2CH_2CH_3)_2$], 0.83 [t, $^3J_{H\text{-}H}$ = 7, 6H of $Ta(CH_2CH_2CH_2C\underline{H}_3)_2$], 1.10 [sextet, $^3J_{H\text{-}H}$ = 7, 4H of $Ta(CH_2CH_2C\underline{H}_2CH_3)_2$], 1.28 [m, 4H of $Ta(CH_2C\underline{H}_2CH_2CH_3)_2$], 2.21 [s, 6H of Me of Ar^{Tol_2}], 2.99 [s, 12H of $(N\underline{Me}_2)_2$], 7.03 [d, $^3J_{H\text{-}H}$ = 8, 4H of Ar^{Tol_2}], 7.19 [m, $^3J_{H\text{-}H}$ = 7, 1H of Ar^{Tol_2}], 7.26 [m, $^3J_{H\text{-}H}$ = 7, 2H of Ar^{Tol_2}], 7.31 [d, $^3J_{H\text{-}H}$ = 8, 4H of Ar^{Tol_2}]. $^{13}C\{^1H\}$ NMR (C_6D_6): 13.8 [s, 2C of $Ta(CH_2CH_2CH_2\underline{C}H_3)_2$], 21.2 [s, 2C of Me of Ar^{Tol_2}], 30.1 [s, 2C of $Ta(CH_2CH_2\underline{C}H_2CH_3)_2$], 31.6 [s, 2C of $Ta(CH_2\underline{C}H_2CH_2CH_3)_2$], 43.4 [s, 4C of $(N\underline{Me}_2)_2$], 79.5 [s, 2C of $Ta(\underline{C}H_2CH_2CH_2CH_3)_2$], 125.6 [s, 1C of Ar^{Tol_2}], 128.8 [s, 4C of Ar^{Tol_2}], 130.0 [s, 4C of Ar^{Tol_2}], 130.4 [s, 2C of Ar^{Tol_2}], 136.5 [s, 2C of Ar^{Tol_2}], 142.0 [s, 2C of Ar^{Tol_2}], 144.8 [s, 2C of Ar^{Tol_2}], 200.8 [s, 1C of Ar^{Tol_2}].

7.12.25 Synthesis of $[Ar^{Tol_2}]Ta(NMe_2)_2Np_2$

A suspension of $[Ar^{Tol_2}]Ta(NMe_2)_2Cl_2$ (60 mg, 0.10 mmol) in pentane (*ca*. 2 mL) was added to NpLi (19 mg, 0.24 mmol) and stirred for *ca*. 5 minutes until all the yellow solid ($[Ar^{Tol_2}]Ta(NMe_2)_2Cl_2$) was gone. The mixture was the filtered through celite and the filtrate was cooled at –15 ˚C for 1 day, thereby depositing yellow crystals of $[Ar^{Tol_2}]Ta(NMe_2)_2Np_2$. The mother liquor was removed using a pipette, and the crystals were washed with cold (–15 ˚C) pentane (2 × 0.5 mL), giving $[Ar^{Tol_2}]Ta(NMe_2)_2Np_2$ (27 mg, 40% isolated yield). X-ray quality crystals were obtained from a solution in pentane at –15 ˚C. Anal. Calcd.: C, 61.07%, H, 7.69%, N, 4.19%. Found: C, 60.86%, H, 7.65%, N, 4.19%.

^{1}H NMR (C_6D_6): 0.12 [s, 4H of $Ta(C\underline{H}_2CMe_3)_2$], 0.93 [s, 18H of $Ta(CH_2C\underline{Me}_3)_2$], 2.23 [s, 6H of Me of Ar^{Tol_2}], 3.30 [s, 12H of $(N\underline{Me}_2)_2$], 7.08 [d, $^3J_{H\text{-}H}$ = 8, 4H of Ar^{Tol_2}], 7.13 [m, 1H of Ar^{Tol_2}], 7.23 [m, 6H of Ar^{Tol_2}]. $^{13}C\{^1H\}$ NMR (C_6D_6): 21.2 [s, 2C of Me of Ar^{Tol_2}], 34.8 [s, 6C of $Ta(CH_2C\underline{Me}_3)_2$], 38.5 [s, 2C of $Ta(CH_2\underline{C}Me_3)_2$], 47.7 [s, 4C of $(N\underline{Me}_2)_2$], 111.5 [s, 2C of $Ta(\underline{C}H_2CMe_3)_2$], 125.9 [s, 1C of Ar^{Tol_2}], 129.0 [s, 4C of Ar^{Tol_2}], 130.3 [s, 4C of Ar^{Tol_2}], 130.4 [s, 2C of Ar^{Tol_2}], 136.5 [s, 2C of Ar^{Tol_2}], 143.9 [s, 2C of Ar^{Tol_2}], 146.2 [s, 2C of Ar^{Tol_2}], 201.6 [s, 1C of Ar^{Tol_2}].

7.12.26 Synthesis of $[\kappa^2\text{-}Ar^{Tol,Tol'}]Ta(NMe_2)_2Np$

(a) A solution of $[Ar^{Tol_2}]Ta(NMe_2)_2Np_2$ (10 mg, 0.02 mmol) in d_6-benzene was added to an NMR tube equipped with a J. Young valve and allowed to stand at room temperature for 2 days. Analysis by ^{1}H NMR spectroscopy demonstrated conversion to, *inter alia*, $[\kappa^2\text{-}Ar^{Tol,Tol'}]Ta(NMe_2)_2Np$ (*ca*. 90%) and NpH. The mixture was then lyophilized, extracted into pentane (1 mL) and cooled to –15 ˚C, thereby depositing yellow crystals of $[\kappa^2\text{-}Ar^{Tol,Tol'}]Ta(NMe_2)_2Np$, which were used for X-ray diffraction studies.

(b) A solution of $[Ar^{Tol}{}_2]Ta(NMe_2)_2Np_2$ (5 mg, 0.01 mmol) in pentane was allowed to stand at room temperature for 2 days in a sealed vial. After this period, the mixture was filtered, and cooled to –15 ˚C, thereby depositing yellow crystals of $[\kappa^2\text{-}Ar^{Tol,Tol'}]Ta(NMe_2)_2Np$. The mother liquor was removed using a pipette, and the crystals were washed with cold (–15 ˚C) pentane (0.5 mL), giving $[\kappa^2\text{-}Ar^{Tol,Tol'}]Ta(NMe_2)_2Np$ (2 mg, 45% isolated yield).

^{1}H NMR (C_6D_6): 0.96 [s, 9H of $TaCH_2C\underline{Me}_3$], 1.52 [s, 2H of $TaC\underline{H}_2CMe_3$], 2.22 [s, 3H of Me of $Ar^{Tol,Tol'}$], 2.38 [s, 3H of Me of $Ar^{Tol,Tol'}$], 2.59 [s, 12H of $(N\underline{Me}_2)_2$], 6.99 [d, $^3J_{H\text{-}H}$ = 8, 2H of $Ar^{\underline{Tol},Tol'}$], 7.16 [m, 1H of $\underline{Ar}^{Tol,Tol'}$, under C_6D_5H signal, located by 2D COSY], 7.21 [d, $^3J_{H\text{-}H}$ = 8, 2H of $Ar^{\underline{Tol},Tol'}$], 7.33 [m, 2H of $Ar^{Tol,Tol'}$], 7.83 [d, $^3J_{H\text{-}H}$ = 8, 1H of $Ar^{Tol,Tol'}$], 7.84 [dd, $^3J_{H\text{-}H}$ = 7, $^4J_{H\text{-}H}$ = 2, 1H of $Ar^{Tol,Tol'}$], 8.24 [br s, 1H of $Ar^{Tol,\underline{Tol'}}$]. $^{13}C\{^1H\}$ NMR (C_6D_6): 21.1 [s, 1C of Me of $Ar^{Tol,Tol'}$], 21.9 [s, 1C of Me of $Ar^{Tol,Tol'}$], 35.7 [s, 3C of $TaCH_2C\underline{Me}_3$], 37.4 [s, 1C of $TaCH_2\underline{C}Me_3$], 39.1 [br s, 4C of $(N\underline{Me}_2)_2$], 96.2 [very br s, 1C of $Ta\underline{C}H_2CMe_3$], 119.4 [s, 1C of $Ar^{Tol,Tol'}$], 122.1 [s, 1C of $Ar^{Tol,Tol'}$], 128.7 [s, 2C of $Ar^{Tol,Tol'}$, tentative because very close to C_6D_6 signal, assignment supported by 2D HSQC and HMBC spectroscopy], 128.7 [s, 2C of $Ar^{Tol,Tol'}$], 129.5 [s, 2C of $Ar^{Tol,Tol'}$], 130.0 [s, 1C of $Ar^{Tol,Tol'}$], 135.0 [s, 1C of $Ar^{Tol,Tol'}$], 135.2 [s, 1C of $Ar^{Tol,Tol'}$], 141.9 [s, 1C of $Ar^{Tol,Tol'}$], 145.3 [s, 1C of $Ar^{Tol,Tol'}$], 152.2 [s, 1C of $Ar^{Tol,Tol'}$], 154.3 [s, 1C of $Ar^{Tol,Tol'}$], 154.9 [s, 1C of $Ar^{Tol,Tol'}$], 197.7 [very br s, 1C of $Ar^{Tol,Tol'}$, confirmed by 2D HMBC spectroscopy], 201.5 [s, 1C of $Ar^{Tol,Tol'}$].

7.12.27 Kinetics of elimination of neopentane from $[Ar^{Tol}{}_2]Ta(NMe_2)_2Np_2$

A solution of $[Ar^{Tol}{}_2]Ta(NMe_2)_2Np_2$ (10 mg, 0.02 mmol) in d_6-benzene was added to an NMR tube equipped with a J. Young valve. The kinetics of the conversion of $[Ar^{Tol}{}_2]Ta(NMe_2)_2Np_2$ to $[\kappa^2\text{-}Ar^{Tol,Tol'}]Ta(NMe_2)_2Np$ and neopentane was measured at 47 ˚C by monitoring the intensity of the $(NMe_2)_2$ groups for both compounds in the probe of the NMR spectrometer.

7.12.28 Isomerization of [κ²-Ar$^{Tol,Tol'}$]Ta(NMe$_2$)$_2$Np to [κ²-Ar*$^{Tol,Tol'}$]Ta(NMe$_2$)$_2$Np

A solution of [Ar$^{Tol}_2$]Ta(NMe$_2$)$_2$Np$_2$ (10 mg, 0.02 mmol) in d$_6$-benzene was added to an NMR tube equipped with a J. Young valve and heated at 80 ˚C for *ca*. 6 hours. Analysis by ^{1}H NMR spectroscopy demonstrated conversion to, *inter alia*, [κ²-Ar*$^{Tol,Tol'}$]Ta(NMe$_2$)$_2$Np (assignment is tentative, see above for analysis).

^{1}H NMR (C$_6$D$_6$) (assignment is tentative because obtained as a mixture of compounds; 2D COSY experiment was also conducted to assist with assignment): 1.10 [s, 9H of TaCH$_2$C<u>Me</u>$_3$], 1.85 [s, 2H of TaC<u>H</u>$_2$CMe$_3$], 2.18 [s, 3H of Me of Ar$^{Tol,Tol'}$], 2.39 [s, 3H of Me of Ar$^{Tol,Tol'}$], 2.83 [s, 12H of (N<u>Me</u>$_2$)$_2$], 7.11 [d, $^3J_{H-H}$ = 8, 1H of Ar$^{Tol,Tol'}$ and 2H of Ar$^{\underline{Tol},Tol'}$], 7.62 [dd, $^3J_{H-H}$ = 8, $^4J_{H-H}$ = 2, 1H of Ar$^{\underline{Tol},Tol'}$], 7.66 [d, $^3J_{H-H}$ = 8, 2H of Ar$^{\underline{Tol},Tol'}$], 7.81 [d, $^3J_{H-H}$ = 8, 1H of Ar$^{Tol,Tol'}$], 7.90 [s, 1H of Ar$^{Tol,Tol'}$], 8.11 [d, $^3J_{H-H}$ = 8, 1H of Ar$^{Tol,Tol'}$], 8.15 [d, $^4J_{H-H}$ = 2, 1H of Ar$^{Tol,Tol'}$]. ^{13}C{^{1}H} NMR (C$_6$D$_6$) (assignment is tentative because obtained as a mixture of compounds; 2D HSQC and 2D HMBC experiments was also conducted to assist with assignment): 21.1 [s, 1C of Me of Ar$^{Tol,Tol'}$], 22.0 [s, 1C of Me of Ar$^{Tol,Tol'}$], 35.1 [s, 3C of TaCH$_2$C<u>Me</u>$_3$], 37.9 [s, 1C of TaCH$_2$<u>C</u>Me$_3$], 40.0 [s, 4C of (N<u>Me</u>$_2$)$_2$], 99.5 [s, 1C of Ta<u>C</u>H$_2$CMe$_3$], 119.5 [s, 1C of Ar$^{Tol,Tol'}$], 121.2 [s, 1C of Ar$^{Tol,Tol'}$], 125.4 [s, 1C of Ar$^{Tol,Tol'}$], 127.5 [s, 2C of Ar$^{Tol,Tol'}$], 129.7 [s, 2C of Ar$^{Tol,Tol'}$], 130.0 [s, 1C of Ar$^{Tol,Tol'}$], 135.6 [s, 1C of Ar$^{Tol,Tol'}$], 136.6 [s, 1C of Ar$^{Tol,Tol'}$], 139.7 [s, 2C of Ar$^{Tol,Tol'}$], 140.2 [s, 1C of Ar$^{Tol,Tol'}$], 142.2 [s, 1C of Ar$^{Tol,Tol'}$], 154.1 [s, 1C of Ar$^{Tol,Tol'}$], 158.1 [s, 1C of Ar$^{Tol,Tol'}$], 199.7 [s, 1C of Ar$^{Tol,Tol'}$], 201.2 [s, 1C of Ar$^{Tol,Tol'}$].

7.12.29 Kinetics of conversion of [Ar$^{Tol}_2$]Ta(NMe$_2$)$_2$Np$_2$ to [κ²-Ar$^{Tol,Tol'}$]Ta(NMe$_2$)$_2$Np and subsequent isomerizaton to [κ²-Ar*$^{Tol,Tol'}$]Ta(NMe$_2$)$_2$Np

A solution of [Ar$^{Tol}_2$]Ta(NMe$_2$)$_2$Np$_2$ (10 mg, 0.02 mmol) in d$_6$-benzene was added to an NMR tube equipped with a J. Young valve. The kinetics of the conversion of [Ar$^{Tol}_2$]Ta(NMe$_2$)$_2$Np$_2$ to [κ²-Ar$^{Tol,Tol'}$]Ta(NMe$_2$)$_2$Np and neopentane and then

isomerization to [κ^2-Ar*$^{Tol,Tol'}$]Ta(NMe_2)$_2$Np was measured at 67 ˚C by monitoring the intensity of the (NMe_2)$_2$ groups for all three compounds in the probe of the NMR spectrometer.

7.12.30 Synthesis of d_2-Me_3CCD_2OH

The synthesis of d_2-Me_3CCD_2OH was adapted from the literature method.[37] $LiAlD_4$ (2.0 g, 47.6 mmol) and Et_2O (40 mL) were added to a Schlenk tube equipped with a magnetic stir bar and the suspension was cooled to 0 ˚C in a ice bath. The suspension was treated slowly with a solution of pivaloyl chloride (11 mL, 89.4 mmol) and Et_2O (10 mL) over a period of 30 minutes. The suspension was stirred at 0 ˚C for 1 hour, and then allowed to warm to room temperature and stirred for an addition 16 hours. After this period, ice water (30 mL) was added slowly the Schlenk, and then the mixture was poured into a 10% H_2SO_4 aqueous solution (100 mL) in air. The organic layer was separated, and the aqueous layer was extracted with Et_2O (3 × 100 mL). The organic extracts were combined with the original organic layer and the volatile components were removed by using a rotavap. The thick oil obtained was distilled under vacuum at 44 ˚C, with the collection flask being cooled at –78 ˚C, giving a white solid. Analysis by ^{1}H and ^{2}H NMR spectroscopy demonstrated production of d_2-Me_3CCD_2OH (5.35 g, 66% yield).

^{1}H NMR ($CDCl_3$): 0.91 [s, 9H of $\underline{Me}_3CCD_2OH$], 1.34 [s, 1H of $Me_3CCD_2O\underline{H}$], 3.28 [t, $^2J_{D\text{-}H}$ = 2, < 1% impurity of $Me_3CC\underline{H}DOH$]. ^{2}H NMR ($CDCl_3$): 3.28 [s, 2D of $Me_3CC\underline{D}_2OH$].

7.12.31 Synthesis of d_2-Me_3CCD_2I

The synthesis of d_2-Me_3CCD_2I was adapted from the literature method.[38] To a two-neck round bottom flask (250 mL) equipped with a magnetic stir bar and reflux condenser was added d_2-Me_3CCD_2OH (5.2 g, 57.7 mmol, see above), $P(OPh)_3$ (16.6 mL, 63.5 mmol),

and MeI (5.4 mL, 8.65 mmol) consecutively. The mixture was then heated in oil bath, starting at 75 ˚C and gradually raising the temperature to 130 ˚C over a period of *ca*. 6 hours, and then heated for an additional 5 hours at 130 ˚C causing the mixture to turn brown. After this period, the mixture was allowed to cool to room temperature, and was then distilled under vacuum at room temperature, with the collection flask being cooled at –78 ˚C, giving a colorless liquid. Analysis by ^{1}H and ^{2}H NMR spectroscopy demonstrated production of d_2-Me_3CCD_2I (5.32 g, 46% yield), which contained a small amount of MeI (*ca*. 5%).

^{1}H NMR ($CDCl_3$): 1.07 [s, 9H of $\underline{Me}_3CCD_2I$], 3.15 [t, $^{2}J_{D\text{-}H}$ = 1, < 1% impurity of $Me_3C\underline{H}DI$]. ^{2}H NMR ($CDCl_3$): 3.17 [s, 2D of $Me_3C\underline{D}_2I$].

7.12.32 Synthesis of d_2-Me_3CCD_2Li

The synthesis of d_2-Me_3CCD_2Li was adapted from the literature method.[39] A stirring, degassed solution of d_2-Me_3CCD_2I (1.0 g, 5.0 mmol) in Et_2O (10 mL) was cooled to –78 ˚C and treated with Bu^tLi (7.0 mL, 1.7M in pentane, 11.9 mmol). The solution was stirred at –78 ˚C for 1 hour, then allowed to warm to room temperature and stirred for an additional 4 hours. After this period, the volatiles removed *in vacuo*, extracted into pentane (10 mL), and filtered through a celite. The volatile components from the filtrate were removed *in vacuo*, and the off-white sticky solid residue obtained was sublimed at 150 ˚C given d_2-Me_3CCD_2Li as a white solid (95 mg, 24% yield).[40]

7.12.33 Synthesis of d_4-$[Ar^{Tol_2}]Ta(NMe_2)_2(CD_2Bu^t)_2$

A suspension of $[Ar^{Tol_2}]Ta(NMe_2)_2Cl_2$ (30 mg, 0.05 mmol) in pentane (*ca*. 2 mL) was added to d_2-Me_3CCD_2Li (12 mg, 0.15 mmol) and stirred for *ca*. 5 minutes until all the yellow solid ($[Ar^{Tol_2}]Ta(NMe_2)_2Cl_2$) was gone. The mixture was the filtered through celite and the filtrate was cooled at –15 ˚C for several days, thereby depositing yellow

crystals of d_4-[Ar^{Tol_2}]Ta(NMe_2)$_2$(CD_2Bu^t)$_2$. The mother liquor was removed using a pipette, and the crystals were washed with cold (–15 ˚C) pentane (3 × 0.5 mL), giving d_4-[Ar^{Tol_2}]Ta(NMe_2)$_2$(CD_2Bu^t)$_2$ (5 mg, 15% isolated yield). This sample was then dissolved in d_6-benzene and monitored by ^{1}H NMR spectroscopy to inquire towards the fate of the deuterium in the CD_2CMe_3 groups.

^{1}H NMR (C_6D_6): 0.93 [s, 18H of Ta($CD_2C\underline{Me}_3$)$_2$], 2.23 [s, 6H of Me of Ar^{Tol_2}], 3.30 [s, 12H of ($N\underline{Me}_2$)$_3$], 7.08 [d, $^3J_{H\text{-}H}$ = 8, 4H of Ar^{Tol_2}], 7.13 [m, 1H of Ar^{Tol_2}], 7.23 [m, 6H of Ar^{Tol_2}]. ^{2}H NMR (C_6D_6): 0.03 [s, 4D of Ta($C\underline{D}_2CMe_3$)$_2$],

7.13 Crystallographic data

Table 3. Crystal, intensity collection and refinement data.

	$[Ar^{Tol_2}]Ta(NMe_2)_3Cl$	$[Ar^{Tol_2}]_2Ta(NMe_2)_3$
lattice	Orthorhombic	Monoclinic
formula	$C_{26}H_{35}ClN_3Ta$	$C_{48.50}H_{58}N_3Ta$
formula weight	605.97	863.93
space group	$P2_12_12_1$	Cc
a/Å	9.6031(13)	14.278(2)
b/Å	14.944(2)	25.977(4)
c/Å	17.795(2)	11.9948(18)
α/°	90	90
β/°	90	100.324(2)
γ/°	90	90
V/Å^3	2553.7(6)	4377.0(11)
Z	4	4
temperature (K)	125(2)	125(2)
radiation (λ, Å)	0.71073	0.71073
ρ (calcd.) g cm^{-3}	1.576	1.311
μ (Mo Kα), mm^{-1}	4.426	2.545
θ max, deg.	32.70	30.60
no. of data collected	44550	35193
no. of data	9023	13362
no. of parameters	289	482
R_1 [$I > 2\sigma(I)$]	0.0248	0.0513
wR_2 [$I > 2\sigma(I)$]	0.0544	0.0915
R_1 [all data]	0.0276	0.0778
wR_2 [all data]	0.0555	0.1004
GOF	1.036	1.003

Table 3 (cont). Crystal, intensity collection and refinement data.

	[Ar$^{Tol}_2$]Ta(NMe$_2$)$_3$Me	**[Ar$^{Tol}_2$]Ta(NMe$_2$)$_3$Et**
lattice	Monoclinic	Monoclinic
formula	$C_{27}H_{38}N_3Ta$	$C_{28}H_{40}N_3Ta$
formula weight	585.55	599.58
space group	$P2_1/c$	$P2_1/n$
a / Å	15.093(3)	8.2335(16)
b / Å	11.3005(19)	14.005(3)
c / Å	16.072(3)	22.975(5)
α / °	90	90
β / °	111.135(2)	92.520(3)
γ / °	90	90
V / Å^3	2556.8(8)	2646.7(9)
Z	4	4
temperature (K)	125(2)	125(2)
radiation (λ, Å)	0.71073	0.71073
ρ (calcd.) g cm^{-3}	1.521	1.505
μ (Mo Kα), mm^{-1}	4.317	4.172
θ max, deg.	31.25	30.58
no. of data collected	42458	41984
no. of data	8326	8119
no. of parameters	300	298
R_1 [$I > 2\sigma(I)$]	0.0284	0.0372
wR_2 [$I > 2\sigma(I)$]	0.0541	0.0673
R_1 [all data]	0.0439	0.0651
wR_2 [all data]	0.0594	0.0760
GOF	1.012	1.008

Table 3 (cont). Crystal, intensity collection and refinement data.

	$[Ar^{Tol}_2]Ta(NMe_2)_3Pr^n$	$[Ar^{Tol}_2]Ta(NMe_2)_3Bu^n$
lattice	Monoclinic	Triclinic
formula	$C_{29}H_{42}N_3Ta$	$C_{30}H_{44}N_3Ta$
formula weight	613.61	627.63
space group	$P2_1/c$	*P-1*
a / Å	18.3491(16)	9.2501(19)
b / Å	8.2356(7)	11.644(2)
c / Å	18.4468(17)	13.988(3)
α / °	90	91.261(3)
β / °	98.9770(10)	101.672(3)
γ / °	90	105.295(3)
V / Å^3	2753.5(4)	1418.7(5)
Z	4	2
temperature (K)	150(2)	150(2)
radiation (λ, Å)	0.71073	0.71073
ρ (calcd.) g cm^{-3}	1.480	1.469
μ (Mo Kα), mm^{-1}	4.012	3.895
θ max, deg.	32.64	30.68
no. of data collected	46017	22814
no. of data	9648	8713
no. of parameters	307	303
R_1 [$I > 2\sigma(I)$]	0.0395	0.0253
wR_2 [$I > 2\sigma(I)$]	0.0713	0.0528
R_1 [all data]	0.0720	0.0332
wR_2 [all data]	0.0797	0.0562
GOF	1.029	1.055

Table 3 (cont). Crystal, intensity collection and refinement data.

	$[Ar^{Tol_2}]Ta(NMe_2)_3Np$	$[Ar^{Tol_2}]Ta(NMe_2)_3Me$
lattice	Triclinic	Triclinic
formula	$C_{31}H_{46}N_3Ta$	$C_{27}H_{38}N_3Ta$
formula weight	641.66	585.55
space group	*P-1*	*P-1*
a / Å	9.8935(19)	7.8601(7)
b / Å	11.596(2)	11.6184(11)
c / Å	13.552(3)	15.1169(14)
α / °	91.385(3)	100.6700(10)
β / °	106.725(3)	102.1860(10)
γ / °	98.740(3)	103.2760(10)
V / Å^3	1467.8(5)	1273.1(2)
Z	2	2
temperature (K)	125(2)	150(2)
radiation (λ, Å)	0.71073	0.71073
ρ (calcd.) g cm^{-3}	1.452	1.527
μ (Mo Kα), mm^{-1}	3.767	4.335
θ max, deg.	30.51	31.00
no. of data collected	23766	21333
no. of data	8898	8051
no. of parameters	327	289
R_1 [$I > 2\sigma(I)$]	0.0250	0.0422
wR_2 [$I > 2\sigma(I)$]	0.0544	0.0625
R_1 [all data]	0.0301	0.0657
wR_2 [all data]	0.0564	0.0691
GOF	1.024	1.012

Table 3 (cont). Crystal, intensity collection and refinement data.

	$[Ar^{Tol_2}]Ta(NMe_2)_3(BH_4)$	$[\kappa^2\text{-}Ar^{Tol_2}]Ta(NMe_2)_3$
lattice	Triclinic	Monoclinic
formula	$C_{26}H_{39}BN_3Ta$	$C_{26}H_{34}N_3Ta$
formula weight	585.36	569.51
space group	*P-1*	$P2_1/n$
a / Å	8.1186(7)	12.652(3)
b / Å	11.0365(9)	12.661(3)
c / Å	16.5384(17)	15.517(4)
α / °	107.4530(10)	90
β / °	93.6850(10)	102.655(4)
γ / °	108.7840(10)	90
V / Å^3	1316.9(2)	2425.4(10)
Z	2	4
temperature (K)	125(2)	125(2)
radiation (λ, Å)	0.71073	0.71073
ρ (calcd.) g cm^{-3}	1.476	1.560
μ (Mo Kα), mm^{-1}	4.190	4.548
θ max, deg.	31.51	30.51
no. of data collected	22254	37750
no. of data	8635	7401
no. of parameters	301	279
R_1 [$I > 2\sigma(I)$]	0.0190	0.0304
wR_2 [$I > 2\sigma(I)$]	0.0480	0.0611
R_1 [all data]	0.0205	0.0484
wR_2 [all data]	0.0487	0.0672
GOF	1.050	1.025

Table 3 (cont). Crystal, intensity collection and refinement data.

	$[\kappa^2\text{-}Ar^{Tol_2}]Ta(NMe_2)_3$	$[Ar^{Tol_2}]Ta(NMe_2)_2Cl_2$
lattice	Triclinic	Triclinic
formula	$C_{26}H_{34}N_3Ta$	$C_{24}H_{29}Cl_2N_2Ta$
formula weight	569.51	597.34
space group	*P-1*	*P-1*
a / Å	9.6625(16)	7.6995(7)
b / Å	10.9602(18)	16.9002(16)
c / Å	12.279(2)	19.9505(19)
α / °	96.318(2)	109.2150(10)
β / °	91.912(2)	93.4150(10)
γ / °	107.030(2)	101.0120(10)
V / Å^3	1232.8(4)	2385.2(4)
Z	2	4
temperature (K)	125(2)	125(2)
radiation (λ, Å)	0.71073	0.71073
ρ (calcd.) g cm^{-3}	1.534	1.663
μ (Mo Kα), mm^{-1}	4.474	4.845
θ max, deg.	32.03	30.63
no. of data collected	21374	38779
no. of data	8346	14573
no. of parameters	279	535
R_1 [$I > 2\sigma(I)$]	0.0264	0.0440
wR_2 [$I > 2\sigma(I)$]	0.0503	0.0733
R_1 [all data]	0.0342	0.0833
wR_2 [all data]	0.0524	0.0824
GOF	1.008	1.029

Table 3 (cont). Crystal, intensity collection and refinement data.

	$[Ar^{Tol_2}]Ta(NMe_2)_2Me_2$	$[Ar^{Tol_2}]Ta(NMe_2)_2Et_2$
lattice	Monoclinic	Monoclinic
formula	$C_{26}H_{35}N_2Ta$	$C_{28}H_{39}N_2Ta$
formula weight	556.51	584.56
space group	*C2/c*	*P-1*
a / Å	13.4946(13)	8.3648(12)
b / Å	9.9492(10)	11.9259(16)
c / Å	18.1475(18)	14.1706(19)
α / °	90	81.000(2)
β / °	101.9400(10)	74.040(2)
γ / °	90	72.405(2)
V / Å^3	2383.8(4)	1291.4(3)
Z	4	2
temperature (K)	150(2)	150(2)
radiation (λ, Å)	0.71073	0.71073
ρ (calcd.) g cm^{-3}	1.551	1.503
μ (Mo Kα), mm^{-1}	4.625	4.272
θ max, deg.	30.56	31.51
no. of data collected	18758	22280
no. of data	3651	8524
no. of parameters	137	288
R_1 [$I > 2\sigma(I)$]	0.0176	0.0403
wR_2 [$I > 2\sigma(I)$]	0.0384	0.0651
R_1 [all data]	0.0206	0.0588
wR_2 [all data]	0.0394	0.0705
GOF	1.040	1.004

Table 3 (cont). Crystal, intensity collection and refinement data.

	$[Ar^{Tol_2}]Ta(NMe_2)_2Pr^n_2$	$[Ar^{Tol_2}]Ta(NMe_2)_2Bu^n_2$
lattice	Triclinic	Triclinic
formula	$C_{30}H_{43}N_2Ta$	$C_{32}H_{47}N_2Ta$
formula weight	612.61	640.67
space group	*P-1*	*P-1*
a / Å	9.268(9)	9.566(4)
b / Å	10.540(10)	10.824(4)
c / Å	14.868(14)	15.350(6)
α / °	101.431(13)	76.545(5)
β / °	93.462(13)	83.679(5)
γ / °	99.112(14)	80.275(5)
V / Å^3	1399(2)	1519.3(10)
Z	2	2
temperature (K)	150(2)	150(2)
radiation (λ, Å)	0.71073	0.71073
ρ (calcd.) g cm^{-3}	1.454	1.400
μ (Mo Kα), mm^{-1}	3.946	3.638
θ max, deg.	31.00	31.51
no. of data collected	17149	25861
no. of data	8752	9993
no. of parameters	306	360
R_1 [$I > 2\sigma(I)$]	0.0387	0.0279
wR_2 [$I > 2\sigma(I)$]	0.1054	0.0550
R_1 [all data]	0.0457	0.0387
wR_2 [all data]	0.1101	0.0586
GOF	1.014	1.025

Table 3 (cont). Crystal, intensity collection and refinement data.

	[Ar$^{Tol}_2$]Ta(NMe$_2$)$_2$Np$_2$	**[Ar$^{Tol}_2$]Ta(NMe$_2$)$_2$Np$_2$**
lattice	Triclinic	Monoclinic
formula	$C_{34}H_{51}N_2Ta$	$C_{34}H_{51}N_2Ta$
formula weight	668.72	668.72
space group	*P-1*	*C2/c*
a / Å	11.397(3)	10.8942(6)
b / Å	12.209(3)	22.6287(13)
c / Å	12.874(3)	13.2647(8)
α / °	84.030(3)	90
β / °	85.101(4)	92.7990(10
γ / °	63.744(3)	90
V / Å^3	1596.4(6)	3266.1
Z	2	4
temperature (K)	125(2)	250(2)
radiation (λ, Å)	0.71073	0.71073
ρ (calcd.) g cm^{-3}	1.391	1.360
μ (Mo Kα), mm^{-1}	3.466	3.388
θ max, deg.	30.72	31.00
no. of data collected	23037	26846
no. of data	9787	5210
no. of parameters	346	200
R_1 [$I > 2\sigma(I)$]	0.0320	0.0263
wR_2 [$I > 2\sigma(I)$]	0.0609	0.0622
R_1 [all data]	0.0439	0.0343
wR_2 [all data]	0.0646	0.0653
GOF	1.008	1.142

Table 3 (cont). Crystal, intensity collection and refinement data.

	[Ar$^{Tol}_2$]Ta(NMe$_2$)$_2$MeCl	**[κ^2-Ar$^{Tol}_2$]Ta(NMe$_2$)$_2$Np**
lattice	Triclinic	Orthorhombic
formula	$C_{25}H_{32}ClN_2Ta$	$C_{29}H_{39}N_2Ta$
formula weight	576.93	596.57
space group	*P-1*	$P2_12_12_1$
a / Å	12.256(4)	9.5686(16)
b / Å	13.518(4)	12.125(2)
c / Å	17.546(5)	22.251(4)
α / °	99.364(4)	90
β / °	105.030(4)	90
γ / °	115.011(4)	90
V / Å^3	2417.9(13)	2581.4(7)
Z	4	4
temperature (K)	150(2)	150(2)
radiation (λ, Å)	0.71073	0.71073
ρ (calcd.) g cm^{-3}	1.585	1.535
μ (Mo Kα), mm^{-1}	4.669	4.276
θ max, deg.	31.56	30.03
no. of data collected	41007	40852
no. of data	15890	7558
no. of parameters	537	299
R_1 [$I > 2\sigma(I)$]	0.0370	0.0375
wR_2 [$I > 2\sigma(I)$]	0.0620	0.0602
R_1 [all data]	0.0725	0.0534
wR_2 [all data]	0.0713	0.0653
GOF	1.005	1.015

7.14 References and notes

(1) For examples of H-atom abstraction reactions by [Ta(NMe_2)] moieties, see:

(a) Tanski, J. M.; Parkin, G. *Inorg. Chem.* **2003,** *42*, 264-266.

(b) Spencer, L. P.; Beddie, C.; Hall, M. B.; Fryzuk, M. D. *J. Am. Chem. Soc.* **2006,** *128*, 12531-12543.

(2) Chisholm, M. H.; Huffman, J. C.; Tan, L. S. *Inorg. Chem.* **1981,** *20*, 1859-1866.

(3) For previous uses of $[Ta(NMe_2)_3Cl_2]_2$, see:

(a) Cai, H.; Yu, X.; Chen, T.; Chen, X.-T.; You, X.-Z.; Xue, Z. *Can. J. Chem.* **2003,** *81*, 1398-1405.

(b) Qiu, H.; Chen, S. J.; Xue, Z. L. *Inorg. Chem.* **2007,** *46*, 6178-6181.

(c) Qiu, H.; Chen, S. J.; Wang, C. S.; Wu, Y. D.; Guzei, I. A.; Chen, X. T.; Xue, Z. L. *Inorg. Chem.* **2009,** *48*, 3073-3079.

(d) Wu, Z. Z.; Diminnie, J. B.; Xue, Z. L. *J. Am. Chem. Soc.* **1999,** *121*, 4300-4301.

(e) Chen, S. J.; Zhang, X. H.; Yu, X. H.; Qiu, H.; Yap, G. P. A.; Guzei, I. A.; Lin, Z. Y.; Wu, Y. D.; Xue, Z. L. *J. Am. Chem. Soc.* **2007,** *129*, 14408-14421.

(f) Wu, Z. Z.; Cai, H.; Yu, X. H.; Blanton, J. R.; Diminnie, J. B.; Pan, H. J.; Xue, Z. L. *Organometallics* **2002,** *21*, 3973-3978.

(g) Qiu, H.; Cai, H.; Woods, J. B.; Wu, Z. Z.; Chen, T. N.; Yu, X. H.; Xue, Z. L. *Organometallics* **2005,** *24*, 4190-4197.

(h) Chen, S. J.; Cai, H.; Xue, Z. L. *Organometallics* **2009,** *28*, 167-171.

(i) Chen, T. N.; Xu, C. Y.; Baum, T. H.; Stauf, G. T.; Roeder, J. F.; DiPasquale, A. G.; Rheingold, A. L. *Chem. Mater.* **2010,** *22*, 27-35.

(j) See reference 1b.

(4) (a) Albrecht, M. *Chem. Rev.* **2010**, *110*, 576-623.

(b) Ryabov, A. D. *Chem. Rev.* **1990**, *90*, 403-424.

(5) For specific examples of cyclometalation in tantalum chemistry, see: Rothwell, I. P. *Acc. Chem. Res.* **1988**, *21*, 153-159.

(6) The ability of PMe_3 to induce alkane elimination in Ta(V) compounds by α-H elimination is also precedented. See, for example:

(a) McLain, S. J.; Wood, C. D.; Messerle, L. W.; Schrock, R. R.; Hollander, F. J.; Youngs, W. J.; Churchill, M. R. *J. Am. Chem. Soc.* **1978**, *100*, 5962-5964.

(b) Fellman, J. D.; Rupprecht, G. A.; Wood, C. D.; Schrock, R. R. *J. Am. Chem. Soc.* **1978**, *100*, 5964-5966.

(c) Schrock, R. R. *Acc. Chem. Res.* **1979**, *12*, 98-104.

(7) $[Ar^{Tol_2}]_2Ta(NMe_2)_3$ can also be synthesized from $[Ta(NMe_2)_3Cl_2]_2$ and excess $[Ar^{Tol_2}]Li$. It is important to note that in order to produce the *mono*-terphenyl without producing the *bis*-terphenyl, $[Ar^{Tol_2}]Li$ should be added slowly to $[Ta(NMe_2)_3Cl_2]_2$, due to the low solubility of $[Ta(NMe_2)_3Cl_2]_2$ (slow addition of $[Ar^{Tol_2}]Li$ allows for the solid $[Ta(NMe_2)_3Cl_2]_2$ to dissolve). Treatment of a 1:1 solution of $[Ta(NMe_2)_3Cl_2]_2$ and $[Ar^{Tol_2}]Ta(NMe_2)_3Cl$ in d_6-benzene with only 1 equivalent of $[Ar^{Tol_2}]Li$ forms only the *mono*-terphenyl complex, $[Ar^{Tol_2}]Ta(NMe_2)_3Cl$, thereby indicating that the rate of the first arylation is significantly faster than the second.

(8) ^{13}C chemical shifts of 200 (± 10) ppm for Ta–C_{aryl} have been previously observed. See:

(a) Agapie, T.; Bercaw, J. E. *Organometallics* **2007**, *26*, 2957-2959.

(b) Agapie, T.; Day, M. W.; Bercaw, J. E. *Organometallics* **2008**, *27*, 6123-6142.

(c) Chapter 6.

(9) For other tantalum borohydride complexes, see:

(a) Luetkens, M. L.; Huffman, J. C.; Sattelberger, A. P. *J. Am. Chem. Soc.* **1985**, *107*, 3361-3363.

(b) Cotton, F. A.; Murillo, C. A.; Wang, X. *J. Am. Chem. Soc.* **1998,** *120*, 9594-9599.

(10) The molecular structure of $[Ar^{Tol_2}]Ta(NMe_2)_2MeCl$ has also been determined by X-ray diffraction.

(11) There were several products observed by using ^1H NMR spectroscopy, in addition to an unidentified precipitate. Thus, it is possible that $[\kappa^3\text{-}Ar^{Tol'_2}]Ta(NMe_2)_2$ is formed in low yields, but has not been identified.

(12) It should be noted that $[\kappa^2\text{-}Ar^{*Tol,Tol'}]Ta(NMe_2)_2Np$ has not been isolated and its assignment is, therefore, tentative.

(13) DFT calculations predict that the ΔH of the isomerization reaction is –5.6 kcal mol^{-1}. Interestingly, the ΔH for the elimination of neopentane from $[\kappa^2\text{-}Ar^{Tol,Tol'}]Ta(NMe_2)_2Np$ to form the theoretical pincer ligand complex, $[\kappa^3\text{-}Ar^{Tol'_2}]Ta(NMe_2)_2$, is –22.7 kcal mol^{-1}, thereby indicating that the absence of its formation is due to kinetic factors.

(14) The *ipso* position of the Ar unit is defined by the position to which the Ta atom is bonded to in $[Ar^{Tol_2}]Ta(NMe_2)_2Np_2$.

(15) Typically, this type of proton is observed as either a singlet or a doublet with a small *meta* coupling constant (*ca.* $^{4}J_{H\text{-}H}$ = 1.5 Hz).

(16) 2D ^{1}H-^{1}H COSY, ^{1}H-^{13}C HSQC and ^{1}H-^{13}C HMBC NMR experiments were also conducted to assist in the molecular assignment.

(17) Furthermore, in accord with deuterium residing in position (**b**) in reaction (**C**), the shape of signal (**c**) is distinctly different, compared with the other spectra, due to the replacement of hydrogen with deuterium and their different three bond coupling constants ($^{3}J_{H\text{-}H(D)}$).

(18) If an α-hydride abstraction were to occur, the formation of the neopentylidene (=CDBu^{t}) and D_3CBu^{t} would be expected, followed by a 1,2-addition to give d_1-[κ^2-$Ar^{Tol,Tol'}$]Ta(NMe_2)$_2$(CDHBu^{t}). The absence of the methylene signal in the ^{1}H NMR spectrum thus discards this as the operating mechanism.

(19) Additionally, all 8 signals of [κ^2-$Ar^{*Tol,Tol'}$] (*i.e.* no deuterium incorporation) are observed in the ^{1}H NMR spectrum of the reaction mixture.

(20) (a) Mayer, J. M.; Curtis, C. J.; Bercaw, J. E. *J. Am. Chem. Soc.* **1983,** *105*, 2651-2660.

(b) Eisenberger, P.; Ayinla, R. O.; Lauzon, J. M. P.; Schafer, L. L. *Angew. Chem. Int. Ed.* **2009,** *48*, 8361-8365.

(c) Zhang, F.; Song, H.; Zi, G. *Dalton Trans.* **2011,** *40*, 1547-1566.

(21) B3LYP using 6-31G** (C, H, and N) and LACVP (Ta) basis sets (Jaguar 7.5, Schrödinger, LLC, New York, NY 2008). See supporting information for all geometry optimized structures.

(22) Other *bis*-terphenyl complexes display large distortions; *i.e.*, [Ar^{Ph2}]$_2$Yb(THF)$_2$, which has Yb–C_{ipso}–C_{para} angles of 147.6˚ and 161.9˚, and [Ar^{Ph2}]$_2$Eu(THF)$_2$, which has Eu–C_{ipso}–C_{para} angles of 145.4˚ and 159.9˚. See:

(a) Niemeyer, M. *Acta Cryst.* **2001**, *E57*, m578-m580.

(b) Heckmann, G.; Niemeyer, M. *J. Am. Chem. Soc.* **2000**, *122*, 4227-4228.

(23) Ta–C_{ipso}–C_{para} angles that deviate substantially from 180˚ have been previously observed in [Ar^{Tol_2}]$TaMe_3Cl$ (145.1˚) and [Ar^{Tol_2}]$TaMe_2Cl_2$ (157.1˚), which is postulated to be due to steric interactions between the tolyl rings and the equatorial substituents (See Chapter 6).

(24) (a) McNally, J. P.; Leong, V. S.; Cooper, N. J. in *Experimental Organometallic Chemistry*, Wayda, A. L.; Darensbourg, M. Y., Eds.; American Chemical Society: Washington, DC, 1987; Chapter 2, pp 6-23.

(b) Burger, B.J.; Bercaw, J. E. in *Experimental Organometallic Chemistry*; Wayda, A. L.; Darensbourg, M. Y., Eds.; American Chemical Society: Washington, DC, 1987; Chapter 4, pp 79-98.

(c) Shriver, D. F.; Drezdzon, M. A.; *The Manipulation of Air-Sensitive Compounds*, 2nd Edition; Wiley-Interscience: New York, 1986.

(25) Gottlieb, H. E.; Kotlyar, V.; Nudelman, A. *J. Org. Chem.* **1997**, *62*, 7512-7515.

(26) "Nuclear Magnetic Resonance Spectroscopy" Nelson, J. H. Prentice Hall, New Jersey (2003), p 79.

(27) Pray, A. R. *Inorg. Synth.* **1957**, *5*, 153-156.

(28) Smith-Bryce, D.; Turner, E. E. *J. Chem. Soc.* **1953**, 861-867.

(29) Schrock, R. R.; Fellmann, J. D. *J. Am. Chem. Soc.* **1978**, *100*, 3359-3370.

(30) Sattler, A.; Parkin, G. *J. Am. Chem. Soc.* **2012**, *143*, 2355-2366.

(31) (a) Sheldrick, G. M. SHELXTL, An Integrated System for Solving, Refining and Displaying Crystal Structures from Diffraction Data; University of Göttingen, Göttingen, Federal Republic of Germany, 1981.

(b) Sheldrick, G. M. *Acta Cryst.* **2008**, *A64*, 112-122.

(32) Jaguar 7.5, Schrödinger, LLC, New York, NY 2008.

(33) (a) Becke, A. D. *J. Chem. Phys.* **1993**, *98*, 5648-5652.

(b) Becke, A. D. *Phys. Rev. A* **1988**, *38*, 3098-3100.

(c) Lee, C. T.; Yang, W.; Parr, R. G. *Phys. Rev. B* **1988**, *37*, 785-789.

(d) Vosko, S. H.; Wilk, L.; Nusair, M. *Can. J. Phys.* **1980**, *58*, 1200-1211.

(e) Slater, J. C. *Quantum Theory of Molecules and Solids, Vol. 4: The Self-Consistent Field for Molecules and Solids*; McGraw-Hill: New York, 1974.

(34) (a) Hay, P. J.; Wadt, W. R. *J. Chem. Phys.* **1985**, *82*, 270-283.

(b) Wadt, W. R.; Hay, P. J. *J. Chem. Phys.* **1985**, *82*, 284-298.

(c) Hay, P. J.; Wadt, W. R. *J. Chem. Phys.* **1985**, *82*, 299-310.

(35) Chisholm, M. H.; Huffman, J. C.; Tan, L.-S. *Inorg. Chem.* **1981**, *20*, 1859-1866.

(36) For synthesis of $Ta(NMe_2)_5$, see:

(a) Bradley, D. C.; Thomas, I. M. *Can. J. Chem.* **1962,** *40*, 1355-1360.

(b) Bradley, D. C.; Thomas, I. M. *Proceedings of the Chemical Society of London* **1959**, 225-226.

(37) Nystrom, R. F.; Brown, W. G. *J. Am. Chem. Soc.* **1947**, *69*, 1197-1199.

(38) Rydon, H. N. *Organic Syntheses* **1971**, *51*, 44-47 [*Coll. Vol. 6* (**1988**), 830-833].

(39) (a) Negishi, E.-i.; Swanson, D. R.; Rousset, C. J. *J. Org. Chem.* **1990**, *55*, 5406-5409.

(b) Bailey, W. F.; Punzalan, E. R. *J. Org. Chem.* **1990**, *55*, 5404-5406.

(40) ^{1}H NMR spectroscopy indicates that there is an impurity present. The material was used unpurified because of the ability to isolate pure d_4-[$Ar^{Tol}{}_2$]Ta(NMe_2)$_2$-(CD_2Bu^t)$_2$ by crystallization.

Aaron Sattler

Curriculum Vitae

604 west 115th Street, Apartment 6A, New York, NY 10025
as3222@columbia.edu
914.438.6364

Education

- **Columbia University, Graduate School of Arts and Sciences (2007 – Present)**
  M.A. in Chemistry **(2009)**
  M.Phil. in Chemistry **(2011)**
  Ph.D. in Chemistry **(2012)**
  Area of Concentration: Inorganic/Organometallic Chemistry
- **State University of New York – Binghamton University (2003 – 2007)**
  B.S. with Honors in Chemistry, *Summa Cum Laude* **(2007)**
  Distinguished Independent Work – Honors Thesis **(2007)**
  Areas of Concentration: Inorganic Chemistry, Physical Chemistry. Major GPA: 4.0/4.0

Awards and Honors

- **Hammett Award (2012)**
  Columbia University
- **Presidential Teaching Award Finalist (2011)**
  Columbia University
- **Presidential Teaching Award Finalist (2010)**
  Columbia University
- **The Jack Miller Award for Excellence in Teaching (2009)**
  Columbia University
- **Presidential Teaching Award Finalist (2009)**
  Columbia University
- **National Science Foundation (NSF) Graduate Research Fellowship Honorable Mention (2009)**
  Columbia University
- **Binghamton Section of the American Chemical Society Outstanding Graduating Senior Award (2007)**
  Binghamton University
- **Graduated Summa Cum Laude (2007)**
  Binghamton University
- **Graduated with Honors (2007)**
  Binghamton University – Distinguished Independent Work in Chemistry
- **Phi Beta Kappa National Honor Society (2006)**
  Binghamton University
- **Phi Eta Sigma National Honor Society (2004)**
  Binghamton University
- **Dean's List (7 Semesters out of possible 7) (2003 – 2006)**
  Binghamton University
- **State of New York Attorney General Triple "C" Award (2003)**
  Ardsley High School
- **AP Scholar (2003)**
  Ardsley High School

Research Experience

- **Graduate Research (Prof. Gerard Parkin) (2008 – Present)**
  1. Modeling aspects of hydrodesulfurization (HDS) and hydrodenitrogenation (HDN) by using molybdenum and tungsten trimethylphosphine complexes. This includes using X-ray diffraction to gain

insight into the binding modes of sulfur and nitrogen heterocycles with these metal centers as well as probing which modes promote hydrogenation of the aromatic systems.
2. Synthesis, structure and reactivity of tantalum and niobium terphenyl complexes; development of a [*CCC*] X_3–donor pincer ligand system by cyclometalation.

- **Undergraduate Research (Prof. Wayne E. Jones Jr.) (2005 – 2007)**
  1. Synthesis of conjugated fluorescent polymers serving as chemosensors for toxic transition metal cations listed by the Environmental Protection Agency.
  2. Inorganic synthesis of self-assembled monolayers and *in-situ* deposition of conducting polymers in order to enhance conductivity of thin films.
- **Summer Research at Memorial Sloan Kettering (Dr. Raju Chaganti) (2005)**
  Research concerning the VHL gene and kidney cancer, DNA sequencing, gel electrophoresis, and PCR (polymerase chain reaction) to determine which mutations affected the effectiveness of chemotherapies.

Teaching Experience

- **Teaching Assistant**
  Structural Methods in Inorganic Chemistry with Prof. Gerard Parkin **(Spring 2011)**
  Columbia University
- **Teaching Assistant**
  General Chemistry I with Prof. Gerard Parkin **(Fall 2009)**
  Columbia University
- **Teaching Assistant**
  General Chemistry I with Prof. Gerard Parkin **(Fall 2008)**
  Columbia University
- **Teaching Assistant**
  General Chemistry II with Dr. Stacey Brydges **(Spring 2008)**
  Columbia University
- **Teaching Assistant**
  General Chemistry I with Prof. Gerard Parkin **(Fall 2007)**
  Columbia University
- **Teaching Assistant**
  Introduction to Physical Chemistry with Prof. James Dix **(Fall 2006)**
  Binghamton University

Publications

1. **Aaron Sattler**, Guang Zhu, and Gerard Parkin "Multiple Modes for Coordination of Phenazine to Molybdenum: Ring Fusion Promotes Access to η^4-Coordination, Oxidative Addition of Dihydrogen and Hydrogenation of Aromatic Nitrogen Compounds." *J. Am. Chem. Soc.* **2009**, *131*, 7828 – 7838.
2. **Aaron Sattler** and Gerard Parkin "Cleaving carbon-carbon bonds by inserting tungsten into unstrained aromatic rings." *Nature* **2010**, *463*, 523 – 526.
3. Noah J. Tremblay, Alon A. Gorodetsky, Marshall P. Cox, Theanne Schiros, Bumjung Kim, Rachel Steiner, Zachary Bullard, **Aaron Sattler**, Woo-Young So, Yoshimitsu Itoh, Michael F. Toney, Hirohito Ogasawara, Arthur P. Ramirez, Ioannis Kymissis, Michael L. Steigerwald, and Colin Nuckolls "Photovoltaic Universal Joints: Ball-and-Socket Interfaces in Molecular Photovoltaic Cells." *ChemPhysChem* **2010**, *11*, 799 – 803.
4. Olaf Zeika, Yongjun Li, Steffen Jockusch, Gerard Parkin, **Aaron Sattler**, Wesley Sattler, and Nicholas J. Turro "Synthesis of Polynitroxides Based on Nucleophilic Aromatic Substitution." *Org. Lett.* **2010**, *12*, 3696 – 3699.
5. Ahmed Al-Harbi, Wesley Sattler, **Aaron Sattler**, and Gerard Parkin "Synthesis and structural characterization of tris(2-oxo-1-*tert*-butylimidazolyl) and tris(2-oxo-1-methylbenzimidazolyl)hydroborato complexes: a new class of tripodal oxygen donor ligand." *Chem. Commun.* **2011**, *47*, 3123 – 3125.
6. **Aaron Sattler**, Kevin E. Janak, and Gerard Parkin "Modeling aspects of hydrodesulfurization by

molybdenum hydride compounds: Desulfurization of thiophene and benzothiophene and C–S bond cleavage of dibenzothiophene." *Inorg. Chim. Acta* **2011**, *369*, 197 – 202.

7. **Aaron Sattler** and Gerard Parkin "Carbon–Sulfur Bond Cleavage and Hydrodesulfurization of Thiophenes by Tungsten." *J. Am. Chem. Soc.* **2011**, *133*, 3748 – 3751.
8. Chien-Yang Chiu, Bumjung Kim, Alon A. Gorodetsky, Wesley Sattler, Sujun Wei, **Aaron Sattler**, Michael Steigerwald and Colin Nuckolls "Shape-shifting in contorted dibenzotetrathienocoronenes." *Chem. Sci.* **2011**, *2*, 1480 – 1486.
9. **Aaron Sattler**, Serge Ruccolo and Gerard Parkin "Structural Characterization of $TaMe_3Cl_2$ and $Ta(PMe_3)_2Me_3Cl_2$, a Pair of Five and Seven-Coordinate d^0 Tantalum Methyl Compounds." *Dalton Trans.* **2011**, *40*, 7777 – 7782.
10. **Aaron Sattler** and Gerard Parkin "Formation of a Cationic Alkylidene Complex *via* Formal Hydride Abstraction: Synthesis and Structural Characterization of $[W(PMe_3)_4(\eta^2\text{–}CHPMe_2)H]X$ (X = Br, I)" *Chem. Commun.* **2011**, *47*, 12828 – 12830.
11. **Aaron Sattler** and Gerard Parkin "A New Class of Transition Metal Pincer Ligand: Tantalum Complexes that Feature a [*CCC*] X_3–Donor Array Derived from a Terphenyl Ligand" *J. Am. Chem. Soc.* **2012**, *134*, 2355 – 2366.
12. Jeffrey S. Meisner, Danielle F. Sedbrook, Markrete Krikorian, Jun Chen, **Aaron Sattler**, Matthew E. Carnes, Christopher B. Murray, Michael Steigerwald and Colin Nuckolls "Functionalizing molecular wires: a tunable class of α,ω-diphenyl-μ,ν-dicyano-oligoenes" *Chem. Sci.* **2012**, *3*, 1007 – 1014.
13. Alberto Martínez, Teresia Carreon, Eva Iniguez, Atilio Anzellotti, Antonio Sánchez, Marina Tyan, **Aaron Sattler**, Linda Herrera, Rosa A. Maldonado and Roberto A. Sánchez-Delgado "Searching for New Chemotherapies for Tropical Diseases: Ruthenium-Clotrimazole Complexes Display High *in vitro* Activity Against *Leishmania major* and *Trypanosoma cruzi* and Low Toxicity Toward Normal Mammalian Cells." *J. Med. Chem.* **2012**, *55*, 3867 – 3877.

Presentations

- **Aaron Sattler**, Wesley Sattler and Wayne R. Jones Jr. "Conjugated Fluorescent Polymer Chemosensors Based on the Dipyridilquinoxaline Receptor Unit." ACS-NERM 2006 Conference, *Undergraduate Poster Session.* Binghamton, NY, USA. **10/6/2006**. **(POSTER)**
- **Aaron Sattler** and Daniel S. Treitler: Thursday Night Organic Problem Session. Columbia University, Department of Chemistry, New York, NY, USA. **5/5/2011**.
- **Aaron Sattler** and Gerard Parkin "Synthesis, Structure and Reactivity of Tantalum Terphenyl Complexes; Development of a [*CCC*] X_3–Donor Pincer Ligand." Gordon Research Conference, Organometallic Chemistry. Salve Regina University, Newport, RI, USA. **7/10/2011**. **(POSTER)**
- **Aaron Sattler** "The Development of a [*CCC*] X_3–Donor Pincer Ligand." Chemical Synthesis Student Symposium. Columbia University, Department of Chemistry, New York, NY, USA. **10/21/2011**.
- **Aaron Sattler** "Highly Reactive Early Transition Metal Chemistry." Awards Ceremony, Hammett Award Talk. Columbia University, Department of Chemistry, New York, NY, USA. **4/24/2012**.
- **Aaron Sattler** "Chemistry of Highly Reactive Group 5 and 6 Transition Metal Compounds." Thesis Dissertation. Columbia University, Department of Chemistry, New York, NY, USA. **7/23/2012**.

Leadership and Mentoring

- Volunteer for the Columbia Secondary School Science Day **(2012)**
- Volunteer for the Women in Science at Columbia, Girls' Science Day **(2011)**
- Volunteer for the Columbia Secondary School Science Day **(2011)**
- Research Mentor for Undergraduate Student: *Kaylyn Shen* **(Fall 2010 – Spring 2011)**
- Volunteer for the Women in Science at Columbia, Girls' Science Day **(2010)**
- Volunteer for the Columbia Secondary School Science Day **(2010)**
- Volunteer for the Women in Science at Columbia, Girls' Science Day **(2009)**

- Volunteer for the Columbia Secondary School Science Day **(2009)**
- Research Mentor for Undergraduate Student: *Diana Bryk* **(Spring 2009)**
- Volunteer for the Columbia Secondary School Science Day **(2008)**
- Volunteer for the Columbia Secondary School Bridge-to-School Day **(2008)**
- Volunteer for the Women in Science at Columbia, Girls' Science Day **(2008)**
- Volunteer for the Johns Hopkins University Center for Talented Youth Academic Program "Pathways to College" program. **(2008)**
- Research Experience for Undergraduates (REU) Mentor: *Philip May* **(Summer 2008)**

Technical Skills

- Single Crystal X-Ray Diffraction
- Organic and inorganic synthesis (including air and water sensitive compounds)
- Homonuclear and Heteronuclear Nuclear Magnetic Resonance (NMR) Spectroscopy
- UV-Visible Spectroscopy (UV-Vis)
- Infrared Spectroscopy (IR)
- DFT Calculations (Jaguar 7.5, Schrödinger)
- Website Design:
  Creator of the Parkin Group Website**:** *http://www.columbia.edu/cu/chemistry/groups/parkin/*
  Creator of the Buccella Group Website: *http://www.nyu.edu/fas/dept/chemistry/buccellagroup/*

Other Contributions

Papers in which I have been acknowledged for performing single crystal X-ray analysis

1. Dai, M.; Danishefsky, S. J. *Tetrahedron Lett.* **2008**, *49*, 6610 – 6612.
2. Wang, Z.; Min, S.-J.; Danishefsky, S. J. *J. Am. Chem. Soc.* **2009**, *131*, 10848 – 10849.
3. Bou-Hamdan, F. R.; Leighton, J. L. *Angew. Chem. Int. Ed.* **2009**, *48*, 2403 – 2406.
4. Snyder, S. A.; Treitler, D. S. *Angew. Chem. Int. Ed.* **2009**, *48*, 7899 – 7903.
5. Zhang, Y.; Danishefsky, S. J. *J. Am. Chem. Soc.* **2010**, *132*, 9567 – 9569.
6. Tambar, U. K.; Lee, S. K.; Leighton, J. L. *J. Am. Chem. Soc.* **2010**, *132*, 10248 – 10250.
7. Li, X.; Danishefsky, S. J. *J. Am. Chem. Soc.* **2010**, *132*, 11004 – 11005.
8. Snyder, S. A.; Treitler, D. S.; Brucks, A. P. *J. Am. Chem. Soc.* **2010**, *132*, 14303 – 14314.
9. Lee, J. H.; Zhang, Y.; Danishefsky, S. J. *J. Am. Chem. Soc.* **2010**, *132*, 14330 – 14333.
10. Snyder, S. A.; Treitler, D. S.; Schall, A. *Tetrahedron* **2010**, *66*, 4796 – 4804.
11. Snyder, S. A.; Sherwood, T. C.; Ross, A. G. *Angew. Chem. Int. Ed.* **2010**, *49*, 5146 – 5150.
12. Yurkerwich, K.; Parkin, G. *J. Cluster Science* **2010**, *21*, 225 – 234.
13. Peng, F.; Danishefsky, S. J. *Tetrahedron Lett.* **2011**, *52*, 2104 – 2106.
14. Zhang, Y.; Lee, J. H.; Danishefsky, S. J. *J. Am. Chem. Soc.* **2011**, *133*, 752 – 755.
15. Snyder, S. A.; Wespe, D. A.; von Hof, J. M. *J. Am. Chem. Soc.* **2011**, *133*, 8850 – 8853.
16. Snyder, S. A.; Treitler, D. S.; Brucks, A. P.; Sattler, W. *J. Am. Chem. Soc.* **2011**, *133*, 15898 – 15901.
17. Snyder, S. A.; Brill, Z. G. *Org. Lett.* **2011**, *13*, 5524 – 5527.
18. Snyder, S. A.; Wright, N. E.; Pflueger, J. J.; Breazzano, S. P. *Angew. Chem. Int. Ed.* **2011**, *50*, 8629 – 8633.
19. Bandar, J. S.; Lambert, T. H. *J. Am. Chem. Soc.* **2012**, *134*, 5552 – 5555.
20. Snyder, S. A.; Thomas, S. B.; Mayer, A. C.; Breazzano, S. P. *Angew. Chem. Int. Ed.* **2012**, *51*, 4080-4084.
21. Peng, F.; Dai, M.; Angeles, A. R.; Danishefsky, S. J. *Chem. Sci.* **2012**, in press, DOI: 10.1039/c2sc20868g.